Functional characterization of potential drug targets in *Schistosoma mansoni* and evaluation of disulfiram and Schl-32.028 as promising anti-schistosomal compounds

Inaugural-Dissertation

zur Erlangung des Doktorgrads der Naturwissenschaften

-doctor rerum naturalium-

im Fachbereich Biologie und Chemie der

Justus-Liebig-Universität Gießen

Mandy Beutler

(M. Sc. Biologie)

aus Saalfeld/Saale

Oktober, 2022

Die vorliegende Arbeit wurde am Institut für Parasitologie,
des Fachbereichs Veterinärmedizin der Justus-Liebig-Universität Gießen
im Rahmen eines LOEWE-Zentrum-geförderten Projekts,
DRUID (Projekt B4, Laufzeit: 01.01.2018-31.12.2021) angefertigt.

Dekan des Fachbereichs Biologie und Chemie: Prof. Dr. Thomas Wilke

Erster Gutachter: Prof. Dr. Albrecht Bindereif
                    Fachbereich Biologie & Chemie, Institut für Biochemie
                    Justus-Liebig-Universität Giessen

Zweiter Gutachter: Prof. Dr. Christoph G. Grevelding
                    Fachbereich Veterinärmedizin, Institut für Parasitologie
                    Justus-Liebig-Universität Giessen

Eingereicht am: 25.10.2022

Abstract

As a neglected tropical disease (NTD), schistosomiasis has a tremendous impact on humans and animals worldwide. Praziquantel (PZQ), an effective drug to kill adult schistosomes, has been used since the 1970s, and there is evidence of emerging resistance. There are several ways to expand the range of drugs against this disease. One is "drug repurposing", which is the use of existing drugs for other applications than those originally approved. Studies on the Abl kinase inhibitor imatinib (Glivec, STI571) showed tremendous effects on adult *S. mansoni in vitro*, which could not be confirmed in a mouse infection model because of the binding capacities of α-1 acid glycoprotein (AGP) and serum albumin protein to imatinib. However, in the research group of Prof. C. G. Grevelding, an aldehyde dehydrogenase (Aldh) was found in the tegument of males. Since the tegument is a naturally occurring surface of the parasite for the host immune system, it seems worthwhile to target its components. As first *in vitro* studies revealed an influence of the Aldh inhibitor disulfiram (DSF) on adult worms, its impact was investigated in detail. Doses $\geq 25\,\mu\mathrm{M}$ showed effects on pairing stability, attachment ability, motility, and oviposition but also on the tegument structure and the gonads of both genders. Furthermore, stem cell proliferation was negatively affected. The effects of DSF alone were enhanced by concomitant treatment with copper, comparable to the DSF metabolite copper bis(diethyldithiocarbamate). Co-administration of DSF, copper, and copper chelators resulted in a dose-dependent reversal of the toxic effects of DSF/Cu with bathocuproinedisulfonic acid (BCPD) but not with ethylenediamine tetraacetic acid (EDTA). These results suggest that DSF has high anti-schistosomal potential, which might be copper-dependent. The synthesized DSF derivative Schl-32.028, provided by a cooperation partner (working group of Prof. M. Schlitzer, Philipps-University Marburg) was also analyzed for its anti-schistosomal potential. Schl-32.028 impaired worm viability, altered stem cell proliferation, and induced oxidative stress-related genes in females.

Another part of this work comprised the cloning and expression of two Aldhs (SmAldh1 and SmAldh2), two Abelson-like (Abl) kinases (SmAbl1 and SmAbl2), and the Src/Abl hybrid kinase SmTK6 for enzyme characterization. To this end, the respective sequences were cloned into expression vectors and tested for expression in different *E. coli* strains. In contrast to *E. coli* pLysS, both SmAldhs and SmTK6 were successfully expressed as full-length proteins in *E. coli* LOBSTR-RIL, whereas no full-length protein of either SmAbl was detected. Instead, the tyrosine kinase (TK) domains (TKDs) of SmAbl1 and SmAbl2 were successfully expressed in *E. coli* LOBSTR-RIL. Since strong protein signals were detected in the pellet fractions, protein solubility enhancement analysis was performed. To this end, both SmAldhs and SmTK6 were cloned for expression as fusion proteins with maltose-binding protein (MBP) and expressed in *E. coli* LOBSTR-RIL. Solubility of MBP:SmAldh1 and MBP:SmTK6 seemed to increase slightly upon fusion, while this was not the case for MBP:SmAldh2. Finally, it was tested whether full-length proteins or truncated versions (TKDs) of SmAbl kinases can be expressed in HEK293-6E (EBNA1) cells, which failed. Since SmAldh1 was expressed in sufficient quantities, enzyme activity tests were established together with the working group of Prof. P. Czermak (University of Applied Sciences Mittelhessen, Giessen). Enzyme assays demonstrated enzyme activity, which was increased after addition of calcium (Ca^{2+}) or magnesium (Mg^{2+}).

Functional analyses of Sm*aldh1* and Sm*aldh2* were performed parallel to the enzyme characterization. Both Sm*aldh* transcripts were transcribed in adult worms as determined by quantitative real-time polymerase chain reaction (qRT-PCR) analyses, and whole mount *in situ* hybridization (WISH) revealed a broad transcript distribution in both genders. During ribonucleic acid (RNA) interference (RNAi) observation periods between 14 - 21 days (d), physiological, morphological and cell-biological parameters were monitored such as pairing stability and egg production, morphological changes of tissues including the gonads, stem cell proliferation, and the transcription of selected genes potentially involved in oxidative stress response, cell cycle, apoptosis, as well as stem cell activity, respectively. The knock down of Sm*aldh1* and Sm*aldh2* showed no clear effects of the observed parameters except Sm*aldh2*, which caused an ovary phenotype. Double-knock down of both Sm*aldhs* also had no clear effect. Since Aldhs are involved in oxidative stress response, their possible involvement in the reaction towards the stressor H_2O_2 was investigated. For this, *S. mansoni* couples were treated with either Sm*aldh1* or Sm*aldh2* double-stranded RNA (dsRNA) and exposed to H_2O_2 for an additional 3 d period. The attachment capacity was slightly lowered in the RNAi

treatment groups of Sm*aldh1*, while it was increased after Sm*aldh2* knock down. While the stress-related gene transcript levels of Sm*gpx* and Sm*sod* were downregulated in females after both treatment combinations, both genes and additionally Sm*sodex* were upregulated in males only after Sm*aldh1* knock down. These data suggested a possible role of SmAldhs in stress-response pathways, but this needs further validation. Further RNAi experiments against Sm*abl1* appeared to impede differentiation of immature oocytes, as their number increased, while the number of mature oocytes decreased. Knock down of Sm*abl2* induced the formation of cell-free spaces in the ovaries of females and in the testes of males. A double knock down of Sm*abl1* and Sm*abl2* combined the observed phenotypes in the gonads. When Sm*tk6* was knocked down, the number of immature oocytes increased and mature oocytes appeared partly granulated, whereas male testes showed cell-free spaces. Upregulation of Sm*tk6* was observed after knock down of both Sm*abls*, while in turn the transcripts of both Sm*abls* were upregulated after knock down of Sm*tk6*. This suggests that these kinases could have redundant functions.

Zusammenfassung

Die Bilharziose ist eine vernachlässigte Tropenkrankheit (NTD) und hat weltweit enorme Auswirkungen Mensch und Tier. Praziquantel (PZQ) ist ein wirksames Medikament zur Bekämpfung adulter Schistosomen und wird seit den 1970er Jahren eingesetzt. Dabei gibt es zunehmend Hinweise auf mögliche Resistenzen. Es gibt mehrere Möglichkeiten, die Palette der Medikamente gegen diese Krankheit zu erweitern. Eine davon ist das so genannte "drug repurposing", d. h. die Verwendung vorhandener Medikamente für andere als die ursprünglich zugelassenen Zwecke. Studien über den Abl-Kinase-Hemmer Imatinib (Glivec, STI571) zeigten *in vitro* eine enorme Wirkung auf adulte *S. mansoni*, die in einem Mausinfektionsmodell aufgrund der Bindungskapazitäten von Imatinib durch saures α-1-Glykoprotein und Serumalbumin nicht bestätigt werden konnte. In der Arbeitsgruppe von Prof. C. G. Grevelding wurde eine Aldehyddehydrogenase (Aldh) im Tegument der Männchen gefunden. Da das Tegument eine natürlich vorkommende Oberfläche des Parasiten für das Wirtsimmunsystem darstellt, erscheint es lohnenswert, seine Bestandteile als potentielle Zielstrukturen für Medikamente zu erforschen. Da erste *in vitro*-Studien Auswirkungen von Disulfiram (DSF), einem Aldh-Inhibitor, auf adulte Würmer zeigten, sollten die Effekte von DSF im Detail untersucht werden. Dosen $\geq 25\,\mu M$ zeigten Auswirkungen auf die Paarungsstabilität, die Ansaugfähigkeit, die Motilität und die Eiablage. Aber auch Auswirkungen auf die Tegumentstruktur und die Gonaden beider Geschlechter, einschließlich der Störung der Stammzellproliferation, wurden beobachtet. Die Wirkung von DSF wurde durch die gleichzeitige Behandlung mit Kupfer verstärkt, vergleichbar mit dem DSF-Metaboliten Kupfer bis(diethyldithiocarbamat). Die gleichzeitige Verabreichung von DSF, Kupfer und Kupferchelatoren führte hingegen zu einer Dosis-abhängigen Umkehrung der toxischen Wirkungen von DSF/Cu mit Bathocuproindisulfonsäure (BCPD), aber nicht mit Ethylendiamin-Tetraessigsäure (EDTA). Diese Ergebnisse legen nahe, dass DSF antischistosomal wirkt und dieser Effekt möglicherweise von Kupfer abhängt. Das synthetisierte DSF-Derivat Schl-32.028, das ein Kooperationspartner (Arbeitsgruppe von

Prof. M. Schlitzer, Philipps-Universität, Marburg, Deutschland) zur Verfügung stellte, wurde ebenfalls auf sein toxisches Potenzial untersucht. Dabei wurde festgestellt, dass Schl-32.028 die Vitalität der Würmer beeinträchtigte, die Stammzellproliferation veränderte und Gene, die mit oxidativem Stress zusammenhängen, in Weibchen induzierte.

Ein weiterer Teil dieser Arbeit umfasste die Klonierung und Expression zweier Aldhs (SmAldh1 und SmAldh2), zweier Abelson-like (Abl)-Kinasen (SmAbl1 und SmAbl2) und der Src/Abl-Hybridkinase SmTK6 zur Enzymcharakterisierung. Zu diesem Zweck wurden die entsprechenden Sequenzen in Expressionsvektoren kloniert und auf ihre Expression in verschiedenen *E. coli*-Stämmen getestet. Im Gegensatz zu *E. coli* pLysS, wurden sowohl die SmAldhs als auch SmTK6 erfolgreich als Volllängen-Proteine in *E. coli* LOBSTR-RIL exprimiert, während von keinem der beiden SmAbl ein Protein in voller Länge nachgewiesen wurde. Stattdessen wurden die Tyrosinkinase-Domänen (TKDs) von SmAbl1 und SmAbl2 erfolgreich in *E. coli* LOBSTR-RIL exprimiert. Da in den Pelletfraktionen starke Proteinsignale nachgewiesen wurden, erfolgte eine Analyse zur Erhöhung der Proteinlöslichkeit. Dazu wurden sowohl die SmAldhs als auch SmTK6 zur Expression als Fusionsproteine mit dem Maltose-bindenden Protein (MBP) kloniert und in *E. coli* LOBSTR-RIL exprimiert. Die Löslichkeit von MBP:SmAldh1 und MBP:SmTK6 schien sich nach der Fusion leicht zu erhöhen, während dies bei MBP:SmAldh2 nicht der Fall war. Schließlich wurde getestet, ob Proteine in voller Länge oder verkürzte Versionen (TKDs) der SmAbl-Kinasen in HEK293-6E (EBNA1)-Zellen exprimiert werden können, was nicht gelang. Da SmAldh1 in ausreichender Menge exprimiert wurde, wurde in Kooperation mit der Arbeitsgruppe von P. Czermak (Fachhochschule Mittelhessen, Giessen) ein Enzymassay etabliert. Entsprechende Versuche zeigten Enzymaktivität, die nach Zugabe von Kalzium (Ca^{2+}) oder Magnesium (Mg^{2+}) erhöht werden konnte. Darüber hinaus wurde gezeigt, dass SmAldh1 durch DSF und ausgewählte Verbindungen der Malaria-Venture-Box gehemmt wird.

Parallel zur Enzymcharakterisierung wurden funktionelle Analysen von Sm*aldh*1 und Sm*aldh*2 durchgeführt. Beide Sm*aldh*-Transkripte wurden mittels qRT-PCR-Analysen in adulten Würmern nachgewiesen und „whole mount" *in situ*-Hybridisierung (WISH) zeigte ein breites Verteilungsmuster der Transkripte. Während der Beobachtungszeiträume von RNA-Interferenz (RNAi)-Versuchen (14 bis 21 Tage) wurden physiologische, morphologische und zellbiologische Parameter wie Paarungsstabilität und Eiproduktion, morphologische Veränderungen von Geweben einschließlich der Gonaden, Stammzellproliferation und die Transkription ausgewählter Gene, die möglicherweise

X

an der Reaktion auf oxidativen Stress, am Zellzyklus, an der Apoptose und an der Stammzellaktivität beteiligt sind, analysiert. Der Knock down von Sm*aldh1* und Sm*aldh2* zeigte keine eindeutigen Auswirkungen auf die beobachteten Parameter, mit Ausnahme von Sm*aldh2*, wo ein Ovar-Phänotyp verursacht wurde. Der Doppel-Knock down beider Sm*aldhs* zeigte ebenfalls keine eindeutigen Veränderungen. Da Aldhs an der oxidativen Stressantwort beteiligt sind, wurde ihre mögliche Beteiligung an dieser Reaktion auf den Stressor H_2O_2 untersucht. Zu diesem Zweck wurden *S. mansoni*-Paare mit Sm*aldh1* oder Sm*aldh2* doppelsträngiger RNA (dsRNA) behandelt und für weitere 3 Tage dem H_2O_2 ausgesetzt. Die Ansaugkapazität war in den RNAi-Behandlungsgruppen von Sm*aldh1* leicht vermindert, während sie nach dem Knock down von Sm*aldh2* erhöht war. Während die Gentranskription von Sm*gpx* und Sm*sod* bei den Weibchen nach beiden Behandlungskombinationen herabreguliert war, waren beide Gene und zusätzlich Sm*sodex* nur bei den Männchen nach der Sm*aldh1*-Knock down-Behandlung hochreguliert. Diese Daten deuten auf eine mögliche Rolle von SmAldhs in den Stressreaktionswegen hin, was jedoch noch weiter validiert werden muss. Zusätzliche RNAi-Experimente gegen Sm*abl1* schien die Differenzierung immaturer Eizellen zu behindern, da ihre Zahl zunahm, während die Zahl maturer Eizellen abnahm. Der Knock down von Sm*abl2* führte zur Bildung von zellfreien Räumen in den Ovaren der Weibchen und in den Testes der Männchen. Als Sm*tk6* über RNAi herunterreguliert wurde, nahm die Zahl der immaturen Eizellen zu, und die maturen Eizellen erschienen teilweise granuliert, während die Testes der Männchen zellfreie Räume aufwiesen. Eine Hochregulierung von Sm*tk6* wurde nach dem Knock down beider Sm*abls* beobachtet, während die Transkripte beider Sm*abls* nach dem Knock down von Sm*tk6* hochreguliert waren. Dies deutet darauf hin, dass diese Kinasen redundante Funktionen ausüben könnten.

Contents

List of figures

List of tables

List of equations

Abbreviations and units

General abbreviations

aa	Amino acid
Abi-1	Abelson interactor 1
Abl	Abelson-like
ACK	Activated CDC42-associated kinase
ActRIIb	Activin receptor IIb
AGC	Protein kinase families A, G, and C
AGP	α-1 acid glycoprotein
Aldh	Aldehyde dehydrogenase
A-MuLV	Abelson murine lymphosarcoma virus
Amp	Ampicillin
APS	Ammonium peroxodisulfate
AR	Aldose reductase
At	*Arabidopsis thaliana*
ApE	A plasmid editor
aPK	Atypical protein kinase
ATP	Adenosinetriphosphate
β-Int1	β integrin receptor 1
BAK	BCL-2 homologous antagonist/killer

BAX	BCL-2 associated X protein
BCIP	4-toluidine salt
BCL-2	B-cell lymphoma-2
BCPD	Bathocuproinedisulfonic acid
BCR-Abl	Fusionprotein: breakpoint cluster region to Abl
B. glabrata	*Biomphalaria glabrata*
BEVS	Baculo virus expression system
Blastp	Basic local alignment search tool - protein
bs	Bi sex
bsF/M	Bi sex female/male
BSA	Bovine serum albumin
Ca^{2+}	Calcium
$CaCl_2$	Calcium chloride
Cam	Chloramphenicol
CAMK	Ca^{2+}/calmodulin-dependent kinases
Cat	Catalase
CDD	Conserved domain database
CDK	Cyclin-dependent kinase
cDNA	Complementary DNA
Ce	*Caenorhabditis elegans*
CK1	Casein kinase 1
CLK	CDK-like kinases
CLSM	Confocal laser scanning microscopy
CMGC	Protein kinase families CDK, MAPK, GSK, and CLK
CO_2	Carbon dioxide
COS	Carbonyl sulfide
Cs	*Clonorchis sinensis*

CS_2	Carbon disulfide
CSC	Cancer stem cell
CSK	C-terminal Src kinase
CTK	Cytoplasmatic tyrosine kinase
$Cu^{+/2+}$	Copper (I/II)
$CuCl_2$	Copper chloride
CuET	Copper bis(diethyldithiocarbamate)
Cu/Zn-SOD	Copper/zinc-dependent super oxide dismutase
dATP	Deoxyadenosinetriphosphate
dCTP	Deoxycytidinetriphosphate
ddH_2O	Double destilled water
DDR1	Discoidin domain receptor 1
DEA	Diethylamine
DEAB	N,N-diethylaminobenzaldehyde
DEPC	Diethyl pyrocarbonate
DETC	Diethyldithiocarbamate
dH_2O	Destilled water
Dia	Diaphanous
DIG	Digoxygenin
DIG-AP	Digoxigenin-alkaline phosphatase
DIG-dUTP	Digoxygenin-uridinetriphosphate
Dm	*Drosophila melanogaster*
DMF	Dimethyl formamide
DMSO	Dimethyl sulfoxide
DNA	Deoxyribonucleic acid
dNTP	Deoxyribonucleotidetriphosphate
dsDNA	Double-stranded DNA

DSF	Disulfiram
DSF/Cu	DSF and copper
dsRNA	Double-stranded RNA
DTT	Dithiothreitol
dTTP	Deoxythymidinetriphosphate
ECM	Extracellular matrix
EDTA	Ethylenediamine tetraacetic acid
EdU	5-ethinyl-2'-deoxyuridine
e.g.	*Exempli gratia*
EMT	Epithelial-mesenchymal transition
ePK	Eukaryotic protein kinase
ϵPKC	ϵ protein kinase C
ER	Endoplasmatic reticulum
ERα	Estrogen receptor α
ERK	Extracellular signal- regulated kinase
et al.	*Et alii*
FAK	Focal adhesion kinase
FCS	Fetal calve serum
FDA	Food and Drug Administration
Fes	Feline *sarcoma*
Fh	*Fasciola hepatica*
FHL2	Four-and-a-half-LIM-only protein 2
GSC	Germ stem cell
GST	Glutathione S-transferase
dGTP	Deoxyguanosinetriphosphate
GPx	Glutathione peroxidase
GSK	Glycogen synthase kinase

XXXIV

gv	Genome version
GVBD	Germinal vesicle break down
H_2O_2	Hydrogen peroxide
HCl	Hydrochloric acid
HEPES	2-4-(2-hydroxyethyl)-1-piperazinyl ethane sulfonic acid
4-HNE	4-hydroxy-2-nonenal
hpRNA	Hairpin RNA
HRP	Horse raddish peroxidase
Hs	*Homo sapiens*
HSA	Human serum albumin
HSA-IC$_{50}$	HSA-adjusted half-maximal inhibitory concentration
IC$_{50}$	half-maximal inhibitory concentration
IDT	Integrated DNA Technologies
ILK	Integrin-linked kinase
IMAC	Immobilized metal affinity chromatography
IPTG	Isopropyl-β-D-thiogalactopyranoside
JAK	Janus kinase
Kan	Kanamycin
KCl	Potassium chloride
Letm1	Leucine zipper-EF-hand-containing transmembrane protein 1
LiCl	Lithium chloride
MAPK	Mitogen-activated protein kinase
MBP	Maltose binding protein
Me-DETC	Methyl diethyldithiocarbamate
Me-DTC	Methyl diethylthiocarbamate
MEK1	Mitogen-activated protein kinase kinase-1
Mg^{2+}	Magnesium

MgCl$_2$	Magnesium chloride
MgSO$_4$	Magnesium sulfate
Mm	*Mus musculus*
MnCl$_2$	Manganese chloride
MOMP	Mitochondrial outer membrane permeabilization
MOPS	3-morpholinopropane sulfonic acid
MW	Molecular weight
NaCl	Sodium chloride
NAD	Nicotinamide adenine dinucleotide
NAD(P)	Nicotinamide adenine dinucleotide phosphate
NaOH	Sodium hydoxide
NBT	Nitro blue tetrazolium
NCK2	Non-catalytic region of tyrosine kinase adaptor protein 2
NEJ	Newly excysted juvenile
Ni-NTA	Nickel-nitrilotriacetic acid
NSCLC	Non-small cell lung cancer cell
NPL4	Nuclear protein localization 4
NRPS	Non-ribosomal peptide synthetase
nt	Nucleotide
NTD	Neglected tropical disease
NQO	NAD(P)H:quinone oxidoreductase
OXA	Oxamniquine
p	Part
p53	Tumor protein p53
PAT	Potassium antimony tartrate
PBS	Phosphate-buffered saline
PBSTx	PBS/Triton X-100

PCR	Polymerase chain reaction
PEG	Polyethylene glycol
PEI	Polyethylenimine
PFA	Formaldehyde
PINCH	Particularly interesting new cysteine-histidine-rich protein
PTK	Protein tyrosine kinase
PTM	Post-translational modification
PVA	Polyvinyl alcohol
PZQ	Praziquantel
qRT-PCR	Quantitative real-time PCR
RA	Retinoic acid
RAR	Retinoic acid receptor
Ras	Rat *sarcoma*
Rho	Rat *sarcoma* homolog
Rn	*Rattus norvegicus*
RNA	Ribonucleic acid
RNAi	RNA interference
RbCl	Rubidium chloride
RGC	Receptor guanylyl cyclase
rNTP	Ribonucleotidetriphosphate
ROS	Reactive oxygen species
RT	Room temperature
RTK	Receptor tyrosine kinase
RXR	Retinoid x receptor
SDS	Sodium dodecyl sulfate
SDS-PAGE	Sodium dodecyl sulfate–polyacrylamide gel electrophoresis
SEC	Size exclusion chromatography

SEM	Scanning electron microscopy
Sh	*Schistosoma haematobium*
SH	Src homology
Sirt3	Sirtuin deacetylase 3
Sj	*Schistosoma japonicum*
SMAD	Suppressor of mothers against decapentaplegic
Src	*Sarcoma*
Ste	Protein kinase group Ste
Stem	Standard error of mean
Stm	Streptomycin
Smed	*Schmidtea mediterranea*
Sm	*Schistosoma mansoni*
SOD	Superoxide dismutase
SODex	Extracellular superoxide dismutase
ss	Single sex
SSC	Saline-sodium citrate
ss/dsDNA	Single-stranded/double-stranded DNA
ssF/M	Single sex female/male
Sult	Sulfotransferase
SUMO	Small ubiquitin-like modifiers
SYK	Spleen tyrosine kinase
TβRI/II	Transforming growth factor β receptor I/II
TAC	Total antioxidant capacity
TAE	Tris/acetate/EDTA
TBS	Tris-buffered saline
TBST	Tris-buffered saline/Tween
TEMED	Tetramethyl ethylenediamine

TGFβ	Transforming growth factor β
TK	Tyrosine kinase
TKD	Tyrosine kinase domain
TKI	Tyrosine kinase inhibitor
TKL	Tyrosine kinase-like
TNT	Tris/NaCl/Tween
Tricaine	Ethyl 3-aminobenzoate methanesulfonate
Tris	Tris(hydroxymethyl)-aminomethane
TRPM	Transient receptor potential melastatin channel
UTP	Uridinetriphosphate
UTR	Untranslated region
vs	Versus
VKR	Venus kinase receptor
WBR	Worm burden reduction
WISH	Whole mount *in situ* hybridization
X-gal	5-bromo-4-chloro-3-indolyl-β-D-galactopyranoside
YopH	*Yersinia* tyrosine phosphatase
Zn, Zn^{2+}	Zinc

Units

%	Percent
‰	Permille
Å	Ångström
A	Ampere
bp	Base pair(s)

°C	Degree Celsius
CV	Column volume
d	Day(s)
h	Hour(s)
kDa	Kilo Dalton
kb	Kilo base pairs
kV	Kilo Volt
l	Litre
M	Molar
mg	Milligram
min	Minute(s)
ml	Millilitre
mm	Millimetre
mM	Millimolar
nm	Nanometre
nM	Nanomolar
OD	Optical density
RPKM	Reads per kilobase million
rpm	Revolutions per minute
s	Second(s)
v/v	Volume per volume
w/v	Weight per volume
μg	Microgram
μl	Microlitre
μM	Micromolar
xg	Times gravitation

XL

Amino acids

A	Ala	Alanine
C	Cys	Cysteine
D	Asp	Aspartartic acid
E	Glu	Glutamic acid
F	Phe	Phenylalanine
G	Gly	Glycine
H	His	Histidine
I	Ile	Isoleucine
K	Lys	Lysine
L	Leu	Leucine
M	Met	Methionine
N	Asn	Asparagine
P	Pro	Proline
Q	Gln	Glutamine
R	Arg	Arginine
S	Ser	Serine
T	Thr	Threonine
V	Val	Valine
W	Trp	Tryptophan
Y	Tyr	Tyrosine

1 Introduction

1.1 Schistosomiasis

1.1.1 The life cycle of schistosomes

Different species of the genus *Schistosoma* (phylum plathyhelminthes, flat worms) cause the infectious disease schistosomiasis or bilharziasis (named after its discoverer Theodor Bilharz) (Di Bella *et al.*, 2018). Schistosomiasis has been classified as a neglected tropical disease (NTD), and it mainly affects people in poor countries with poor access to health care (Hotez and Kamath, 2009; Molyneux, 2013). This disease is common in the subtropical and tropical climates of Asia, South America, and sub-Saharan Africa and has been reported in 78 countries, with an estimation of more than 236.6 million people who required preventive treatment in 2019 (WHO, 2022). Recently, outbreaks of urogenital schistosomiasis have been reported in Corsica (France) (Boissier *et al.*, 2016) and Almeria (Spain) (Salas-Coronas *et al.*, 2021), which indicates that the disease can spread also to moderate climate zones.

In humans, 6 major species cause intestinal (*S. mansoni*, *S. japonicum*, *S. mekongi*, *S. guineensis*, and related *S. intercalatum*) and urogenital (*S. haematobium*) schistosomiasis (WHO, 2022). Schistosomiasis is not only an important human disease, it also affects a wide range of animals (non-human primates, rodents, cattle, sheep, pigs, antelopes, buffaloes, dogs, etc.) (Standley *et al.*, 2012), which leads to socio-economic problems (Adeyemo *et al.*, 2022; Molla *et al.*, 2022).

Schistosomes are the only trematodes that are dioecious, and they have an unique reproduction biology (Moné and Boissier, 2004). Eggs of schistosomes (**Figure 1.1**, ①), excreted by feces (most species) or urine (*S. haematobium*) to freshwater, contain

miracidia, which hatch from the eggs and infect the intermediate host (*Biomphalaria spp. (B. ssp.)* for *S. mansoni*) (LoVerde, 2019). Inside the intermediate host, miracidia transform into sporocysts and reproduce asexually. Finally, cercariae emerge from sporocysts and leave the snail to reach the surrounding water. Cercariae possess a bifurcated tail that allows active movement towards their definitive (vertebrate) hosts. Cercariae penetrate the host's skin. Once inside the skin, they change their morphology (loss of their tail, formation of a double-layered membrane called tegument) and are called schistosomula, which represent the juvenile worm stage. After about a day, schistosomula migrate through the dermis and reach the blood vessels to migrate to the lung capillaries, where they develop further for 3 - 10 d, before they migrate to the liver. Here, they complete their development and mate. Following pairing, schistosome couples migrate to their final destinations; adult *S. mansoni* and *S. japonicum* reside in the mesenteric veins, while *S. haematobium* resides in the vesical vein plexus of the urogenital system (LoVerde, 2019). The adult male forms a cavity (gynaecophoric canal), in which the female worm resides for a constant, life-long pairing contact. This is a prerequisite for the sexual development of the female, which includes the final differentiation of the female gonads (ovary and vitellarium), and subsequently for egg production (Kunz, 2001; LoVerde and Chen, 1991; Popiel and Basch, 1984; Popiel *et al.*, 1984; Popiel, 1986).

Recently, Chen *et al.* (2022) demonstrated that the stimulus for female development is dependent on a non-ribosomal peptide synthetase (SmNRPS) of paired males. SmNRPS generates a β-alanyl-tryptamine dipeptide that is released by ciliated sensory neurons into the gynaecophoric canal. This dipeptide induces molecular pathways for maturation of female reproductive organs followed by egg laying (Chen *et al.*, 2022). *S. mansoni* couples produce an average of 300 eggs per day (Cheever *et al.*, 1994; Moore and Sandground, 1956). The eggs secrete antigenic substances that promote passaging the eggs from the blood vessel via epithelia into the intestinal lumen (or urinary bladder for *S. haematobium*), and the subsequent excretion with feces (or urine in case of *S. haematobium*) (LoVerde, 2019). Migrating schistosomula cause early acute phase symptoms such as cough, myalgia, and fever, which transits with further development and egg production into late phase (chronic) symptoms such as abdominal pain, (bloody) diarrhea, pulmonary arterial hypertension, hepatomegaly, and in case of *S. haematobium* infections, haematuria and bladder cancer (Da Silva *et al.*, 2005; Ross *et al.*, 2007; Sibomana *et al.*, 2020).
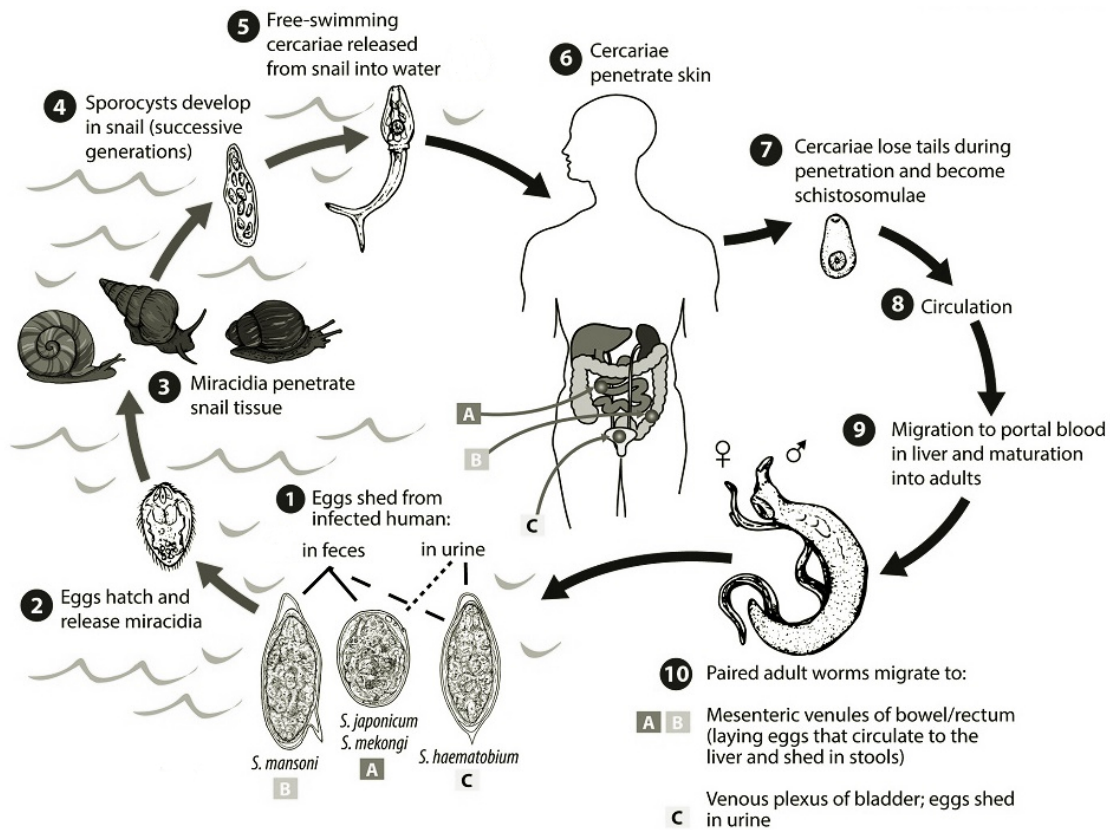
Figure 1.1: The life cycle of human schistosomes
Depicted are the different life stages in the life cycle of schistosomes. For further explanation, see text. Image modified from CDC - Centers for Disease Control and Prevention, DPDx (2019).

1.1.2 Treatment for schistosomiasis

In the early 1900s, potassium antimony tartrate (PAT), a substance that induces vomiting (Weiss and Hatcher, 1923), was proposed as a drug in tropical medicine for the treatment of trypanosomiasis (Low, 1916). When *Trypanosoma*-infected mice were treated with PAT, the protozoa were successfully removed from the blood, and first experiments on humans suffering from trypanosomiasis were carried out with the same success (Low, 1916). From 1913, PAT was even used to treat leishmaniasis (Low, 1916). In 1918, PAT was used to treat schistosomiasis caused by *S. haematobium* (Christopherson, 1918). Over 40 years later, starting in the 1960s, more drugs became available such as amoscante, oltripaz, lucanthone, hycanthone, niridazole, metrifonate, and oxamniquine (OXA) (Cioli *et al.*, 1995) until the discovery of PZQ (sold under the name Biltricide)

in the late 1970s (Seubert *et al.*, 1977). With PZQ being active against *S. mansoni, S. japonicum, S. haematobium, S. intercalatum,* and *S. mekongi* (Ishizaki *et al.*, 1979; Katz *et al.*, 1979; Lorette *et al.*, 1983; McMahon and Kolstrup, 1979; Utzinger *et al.*, 2003; Webbe and James, 1977), PZQ became the drug of choice for the necessity to control schistosomiasis. With a few side effects towards humans such as fever, headaches, nausea, and vomiting, PZQ is considered as a safe drug (Erko *et al.*, 2012). The previous mentioned drugs became obsolete due to toxic effects on the central nervous system and liver (Aruleba *et al.*, 2019; Cioli *et al.*, 1995), except PZQ and OXA.

OXA is a pro-drug that is converted by a sulfotransferase (Sult) to its sulfated active form (Cioli *et al.*, 1985, 1992; Pica-Mattoccia *et al.*, 1993), and it is effective against *S. mansoni* (Foster *et al.*, 1973; Pica-Mattoccia *et al.*, 1997; Valentim *et al.*, 2013) but not against *S. haematobium* or *S. japonicum* (Pica-Mattoccia *et al.*, 1997; Rugel *et al.*, 2020). One explanation for this phenomenon is that OXA does not fit properly into the binding pockets of SjSult and ShSult. Therefore, activation is not sufficient to provide toxic levels for parasite killing (Rugel *et al.*, 2020). Side effects such as headaches, dizziness, drowsiness, nausea, vomiting, diarrhea, and abdominal discomfort are considered mild and the drug safe (Mäder *et al.*, 2018). OXA was listed as alternative drug when PZQ failed to eliminate schistosomiasis (WHO, 2021).

PZQ has been called an enigmatic drug because its direct mechanism of action other than alteration of intracellular Ca^{2+} homeostasis was unknown (Day *et al.*, 1992). In presence of Ca^{2+}, PZQ leads to paralysis, vesicle formation in the tegument, and exposure of antigens to the host's immune system (Andrews and Harder, 1989; Blair *et al.*, 1992; Reimers *et al.*, 2015; Xiao *et al.*, 1984). Recently, one target of PZQ was validated in *S. mansoni*, it is the transient receptor potential melastatin channel (SmTRPM$_{PZQ}$) (Park *et al.*, 2019; Park and Marchant, 2020). TRPMs form channels with high selectivity for various cations (Kraft and Harteneck, 2005), and SmTRPM$_{PZQ}$ appears to be associated with Ca^{2+} transport. There is evidence that *S. mansoni* has become less susceptible to PZQ in some endemic areas (Ismail *et al.*, 1996; Le Clec'h *et al.*, 2021; Liang *et al.*, 2002; Stelma *et al.*, 1997). Analysis of the PZQ-sensitive SmTRPM$_{PZQ}$ and the PZQ-insensitive *Fasciola hepatica* FhTRPM$_{PZQ}$, followed by mutational analysis of the protein, revealed that PZQ insensitivity is mediated by a change of Asn1388 to Thr1388 (Park *et al.*, 2021). In addition, nonsense mutations resulting in truncated versions of SmTRPM$_{PZQ}$ lacking a PZQ-binding site modulate PZQ resistance in *S. mansoni* (Le Clec'h *et al.*, 2021).

The possibility of resistance development and the fact that PZQ fails to affect

schistosomula (Gönnert and Andrews, 1977; Pica-Mattoccia and Cioli, 2004; Sabah *et al.*, 1986; Xiao *et al.*, 1987) explains the need of repeated treatment in endemic areas. Indeed, laboratory studies provided evidence that schistosomes can acquire drug-specific resistance in only a few passages when exposed to PZQ (Fallon and Doenhoff, 1994). Artificially induced PZQ-resistance was also demonstrated for *S. japonicum* (Li *et al.*, 2011). Additionally, there were cases reported, where PZQ compared to OXA showed a lower efficiency to clear worm burden in humans from endemic *S. mansoni* areas (Stelma *et al.*, 1997). Therefore, relying on only one drug keeps the world prone to the development of drug resistance.

1.2 Strategies for the development of new anti-parasitic drugs

Drug repurposing (or repositioning) is a strategy for adding new applications to already known drugs other than those approved. Andrews *et al.* (2014) reviewed repurposed drugs approved for malaria, leishmaniasis, trypanosomiasis and toxoplasmosis. As anti-malarian drug, artemisinin-derivatives were developed and repurposed as anti-schistosomal drugs against the juvenile stage of *S. japonicum* (Xiao, 2005).

Considering that new drugs are estimated to cost up to 2.6 billion $ to develop (Dimasi *et al.*, 2016) and take an average of 13.5 years from discovery to approval (Sun *et al.*, 2022), drug repurposing appears to be a cost-effective and low-risk approach to reduce investment by saving on development costs. Although there is an enormous number of enzymes in an organism, the number of druggable targets is restricted. About one fifth of the Food and Drug Administration (FDA)-approved drugs from 1989 - 2000 have either unknown targets or no distinct molecular target underlying their action (Overington *et al.*, 2006; Santos *et al.*, 2017). For pathogens, 189 targets were listed by Santos *et al.* (2017), which were targeted by 220 drugs.

To develop anti-parasitic drugs, another strategy is to screen compound libraries *in silico*, followed by tests *in vitro* and validation *in vivo* (Beutler, Harnischfeger *et al.*, 2022, manuscript in preparation; Do Nascimento *et al.*, 2020; Gallinger *et al.*, 2022; Pasche *et al.*, 2019; Rodrigues and Schneider, 2015; Rognan, 2017). This strategy has already been successfully applied for anti-parasitic compounds (Gamo *et al.*, 2010; Moine *et al.*, 2015).

Another strategy is target-based drug design (Egner *et al.*, 2005). Here, the structure

of a drug-target molecule is modified as a lead to enhance its effects or specificity (Verma and Prabhakar, 2015). Collaborators at the department of pharmaceutical chemistry (working group of Prof. M. Schlitzer), sought new drug targets in *S. mansoni*, defining inhibitors of aldose reductase (AR) and aldehyde dehydrogenase (Aldh) as good starting points for the development of compounds with anti-schistosomal properties targeting detoxifying enzymes (Blohm *et al.*, 2016; Mäder *et al.*, 2016; Peter Ventura *et al.*, 2019; Rennar *et al.*, 2022). One of their developed compound - Schl-32.028 (Mäder, 2016) - came into focus in this work (**Figure 1.2**).
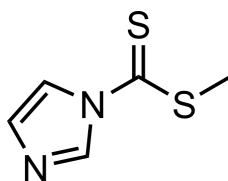
Figure 1.2: Structure of Schl-32.028

1.3 Disulfiram

Approaches to find new drugs against disease-inducing pathogens are the identification of new druggable targets or drug repurposing. One promising candidate for repurposing is DSF (sold under the name Antabuse), which already came into focus as alternative drug treatment for cancer (Cen *et al.*, 2004; Fasehee *et al.*, 2016; Kannappan *et al.*, 2021; Morrison *et al.*, 2010), obesity (Meggyesy *et al.*, 2020), anxiety (Saitoh *et al.*, 2022), and parasitic diseases (Castillo-Villanueva *et al.*, 2017; Peniche *et al.*, 2015; Shirley *et al.*, 2021).

DSF was originally introduced to accelerate the vulcanization of rubber. After exposure, workers reported in the 1930's to become susceptible to alcohol ingestion (Suh *et al.*, 2006). Soon after this observation, Hald and Jacobsen (1948) found that mitochondrial Aldh2, which is involved in the conversion of ethanol to acetic acid, was inhibited by DSF. This results in the accumulation of acetaldehyde, which causes the side effects of alcohol consumption. Thereafter, DSF was approved by the FDA as treatment for alcoholism in 1951. Despite some known late-onset neurotoxicity (neuropathy) (Boukriche *et al.*, 2000; Watson *et al.*, 1980), DSF has long been considered as a safe drug but not recommended for patients with coronary artery disease, heart failure, or

a history of liver disease (Johansson, 1992; Kragh, 2008; Stokes and Abdijadid, 2022). DSF was produced for the last time in 2011 and lost its approval in Germany in 2013, but can be ordered and imported from other countries (Deutsche Hauptstelle für Suchtfragen e.V., 2019; Mutschler and Grosshans, 2016).

After oral ingestion, most DSF molecules are reduced to diethyldithiocarbamate (DETC or DDC) in the stomach (**Figure 1.3**) (Johansson, 1992; Meraz-Torres *et al.*, 2020). On one hand, DSF as well as DETC are absorbed by the upper gastrointestinal tract, while not absorbed DETC (10 - 15 %) is excreted with the feces. On the other hand, DETC in an acidic environment (as it is in the stomach) is further degraded into carbon disulfide (CS_2) and diethylamine (DEA), which is excreted with urine. Oxidation of CS_2 leads to carbonyl sulfide (COS) and can be further oxidized to carbon dioxide (CO_2), which is exhaled. In addition, free DETC is glucuronidized and excreted with the urine. DETC chelates metal ions, such as copper (or zinc) and forms copper bis(diethyldithiocarbamate) (CuET). Remaining non-reduced DSF and CuET molecules are absorbed via the upper gastrointestinal tract (Meraz-Torres *et al.*, 2020). In the blood, DSF and CuET are reduced to their monomer DETC via the endogenous thiols of the glutathione reductase system of erythrocytes and form mixed disulfides with free thiol groups of other proteins (especially albumin). Via S-methyltransferase, DETC becomes methylated to form methyl diethyldithiocarbamate (Me-DETC), which is further oxidized in the liver into methyl diethylthiocarbamate (Me-DTC). Me-DTC can be further oxidized to corresponding Me-DTC sulfoxide or Me-DTC sulfone by cytochrome P450 monooxygenases. Me-DETC sulfoxide and Me-DTC sulfone metabolites form covalent cysteine adducts with Aldh and lead to its inhibition (Johansson, 1992; Meraz-Torres *et al.*, 2020).
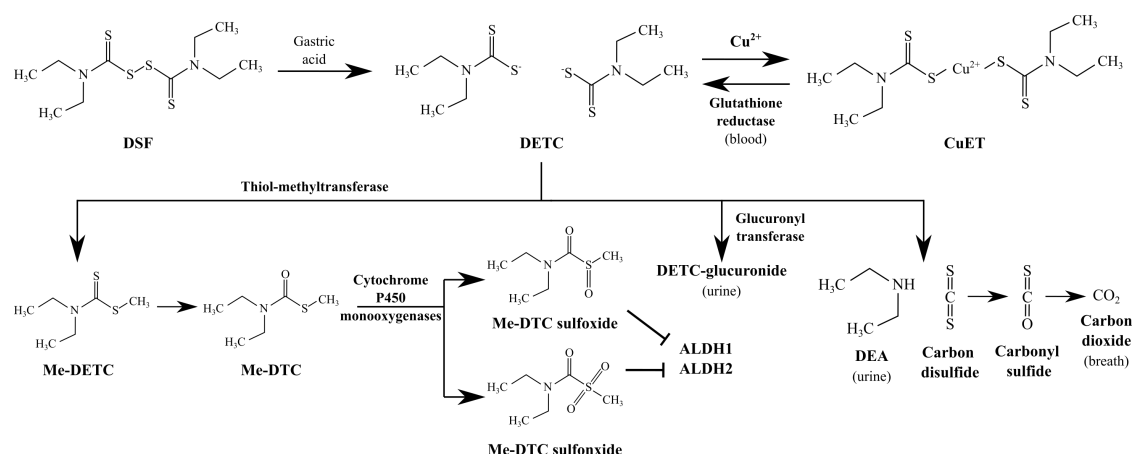
Figure 1.3: Metabolism of DSF
Shown are the major metabolic steps during DSF metabolism. DSF is reduced to diethyldithiocarbamate (DETC) in the stomach and chelates copper (Cu^{2+}) to form copper bis(diethyldithiocarbamate) (CuET). CuET is absorbed and enters the blood stream, where the glutathione reductase system of red blood cells reduces CuET into DETC again. DETC is conjugated with glucuronic acid and excreted by the urine as DETC-glucuronide, or degraded to diethylamine (DEA) and carbon disulfide, which is further oxidized to carbon dioxide (CO_2). DEA and CO_2 are excreted by urine or exhaled. Remaining DETC in converted by S-methyltransferase to methyl diethyldithiocarbamate (Me-DETC), which is further converted into methyl diethylthiocarbamate (Me-DTC). Me-DTC is further oxidized by cytochrom P450 monooxygenases to Me-DTC sulfoxide or Me-DTC sulfonoxide. Both Me-DTC sulfoxide and Me-DTC sulfonoxide, respectively, inhibit Aldh1 and Aldh2. The image was modified after Johansson (1992) and Meraz-Torres *et al.* (2020).

1.4 Aldehyde dehydrogenases

1.4.1 Structural features and mode of action

Aldhs are nicotinamide adenine dinucleotide (phosphate) (NAD(P))-dependent enzymes that form a superfamily consisting of 24 families (Islam and Ghosh, 2022). As suggested by Vasiliou *et al.* (1999), within families, subfamilies are distinguished (represented by letters) and proteins of each subfamily are represented by Arabic numbers, *exempli gratia* (e.g.), subfamily of human (*Homo sapiens*; Hs) Aldh1A (HsAldh1A) consists of three members, HsAldh1A1, HsAldh1A2, and HsAldh1A3. Members of one family should have $\leq 40\%$ amino acid (aa) identity to that from another family, while members of the same subfamily should have $\geq 60\%$ aa identity (Vasiliou *et al.*, 1999). Typically,

Aldhs have a molecular weight of 50 - 60 kilo Dalton (kDa) and function as homodimers, homotetramers, or homohexamers (Shortall *et al.*, 2021). Aldh members catalyze the oxidation of endogenously and exogenously produced aldehydes to their respective carboxylic acids (**Figure 1.4**) and possess an esterase function, which was also reviewed in Koppaka *et al.* (2012).

Aldehyde   Carboxylic acid
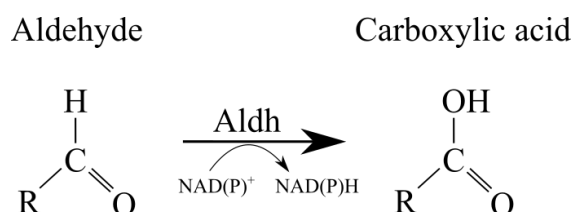
Figure 1.4: Scheme of aldehyde conversion catalyzed by Aldh
An aldehyde is converted into the corresponding carboxylic acid by reduction of $NAD(P)^+$ to $NAD(P)H$. R = any functional moiety/carbon-containing substituent.

Among Aldhs from different species, the Aldh domain is conserved harboring a catalytic site, a binding domain for a co-substrate ($NAD(P)^+$), and a multimerization domain (Liu *et al.*, 1997; Perozich *et al.*, 1999; Steinmetz *et al.*, 1997). The mechanism of activity (**Figure 1.5**) can be described in five steps (Koppaka *et al.*, 2012):

1) activation of Cys302 (HsAldh2 numeration). Here, Glu286 acts as a general base and abstracts a proton of a water molecule, which in turn abstracts a proton of Cys302, which is in close proximity. Simultaneously, a $NAD(P)^+$ molecule binds the co-factor site by Van Der Waals forces and hydrogen bonds (Lys192 und Glu399).

2) nucleophilic attack of Cys302 on the electrophilic carbonyl carbon of the aldehyde mediated by Cys302's thiolate group.

3) formation of a thioacyl-enzyme intermediate with simultaneous hydride transfer to $NAD(P)^+$.

4) hydrolysis of the thioester. Again, Glu268 acts as general base and abstracts a proton of the water molecule, which subsequently attacks the carbonyl carbon of the thioacyl-enzyme complex. This if followed by the release of the acid product from the tetrahedal intermediate and the liberation of the reduced co-factor.

5) regeneration of the enzyme by $NAD(P)^+$ binding.
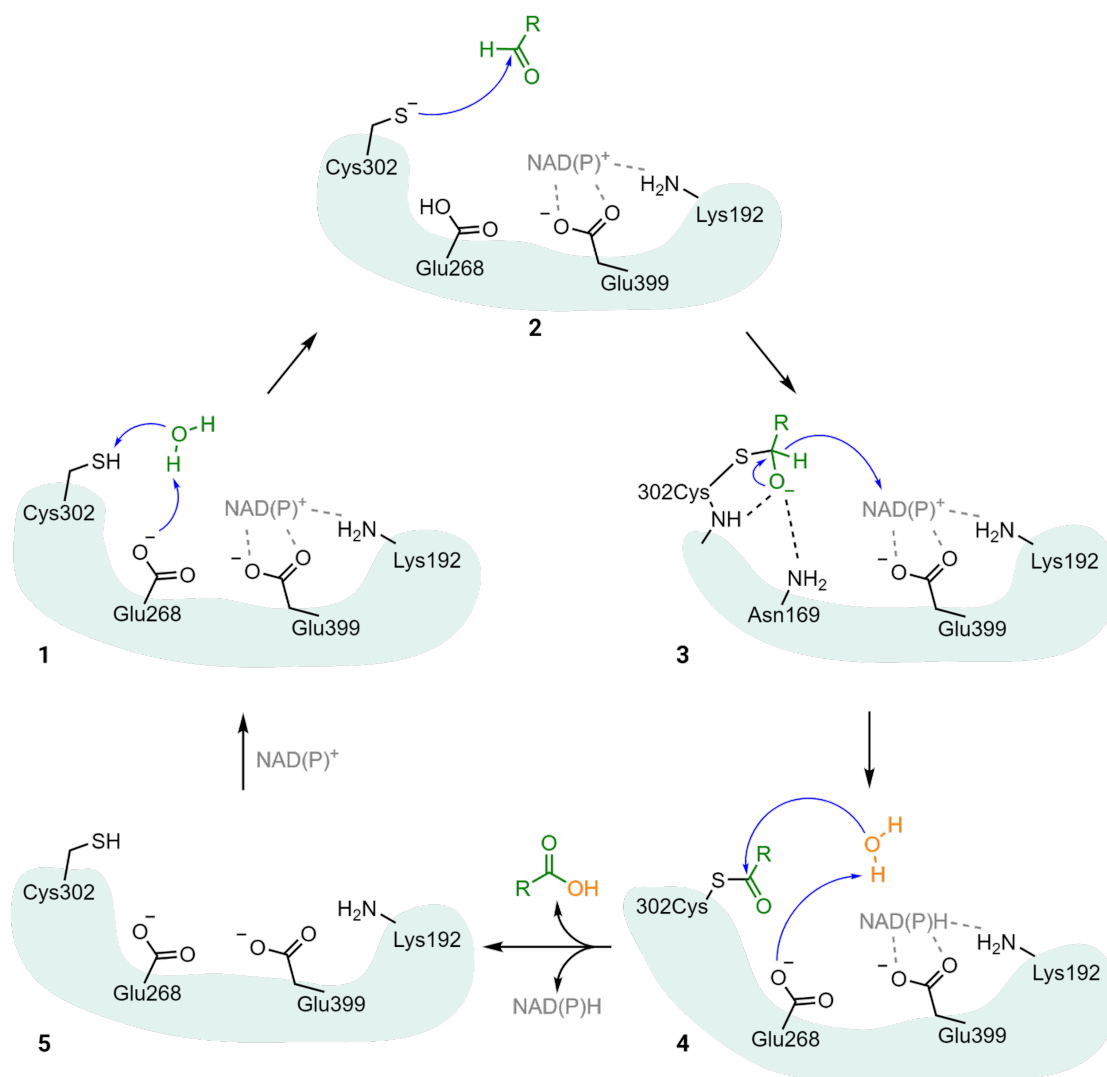
Figure 1.5: Mechanism of aldehyde oxidation by Aldh
1) activation of Cys302, 2) nucleophilic attack of the thiolate on the aldehyde, 3) stabilization of the tetrahedral intermediate and hydride transfer to NAD(P)$^+$, 4) hydrolysis of the thioester, 5) dissociation of the reduced co-factor and carboxylic acid, and regeneration of the enzyme. Image courtesy of Dr. rer. nat. T. L. Gallinger, modified after Koppaka *et al.* (2012).

1.4.2 The roles of Aldhs in diseases

Aldhs oxidize a broad spectrum of aldehydes originated from the biotransformation of endogenous compounds such as amino acids, carbohydrates, neurotransmitters, and lipids (glutamate γ-semialdehyde, γ-aminobutyric acid, 4-hydroxy-2-nonenal (4-HNE)

and malondialdehyde) but also from exogenous sources such as xenobiotics and drugs (ethanol, cancer drugs cyclophosphamide and ifosfamide as aldehyde precursors) as well as from food additives, smog, cigarette smoke, and motor vehicle exhaust (citral, benzaldehyde, formaldehyde, acetaldehyde, and acrolein) (Marchitti *et al.*, 2008). Aldehydes are strongly electrophilic and form adducts with various enzymes and nucleic acids resulting in impaired cellular homeostasis, enzyme inactivation, deoxyribonucleic acid (DNA) damage, and cell death (Marchitti *et al.*, 2008). Therefore, Aldhs play an important role in detoxification processes but also in embryogenesis, neural functions, and regulatory as well as metabolic roles in cancer (Koppaka *et al.*, 2012).

Constitutively active members of the Aldh superfamily occur in several tissues such as the liver, kidney, uterus, brain, and eye, while some cells induce Aldh expression only after stress (Koppaka *et al.*, 2012). Aldhs have been found in several subcellular locations such as mitochondria, nucleus, cytosol, and the endoplasmatic reticulum (ER) (Marchitti *et al.*, 2008).

Aldh dysfunction is associated with a variety of diseases (Marchitti *et al.*, 2007; Shortall *et al.*, 2021). Among these is alcohol sensitivity caused by altered Aldh2. Aldh2 is a part of the alcohol detoxifying pathway in which ethanol is oxidized to acetaldehyde by alcohol dehydrogenase, which is subsequently oxidized by Aldh2 to acetic acid (Marchitti *et al.*, 2008). A single nucleotide polymorphism (E487 $\rightarrow$ K487) results in Aldh2*2 (Shortall *et al.*, 2021). Normally, Aldh2 functions as a homotetramer. If only one monomer is mutated (Aldh2*2), the whole complex shows altered NAD binding and loses catalytic activity. This finally leads to an accumulation of the cytotoxic acetaldehydes (Shortall *et al.*, 2021).

Aldh1 converts retinal into retinoic acid (RA) (Duester, 2000; Huang *et al.*, 2009), which regulates cell differentiation, proliferation, and apoptosis (Tomita *et al.*, 2016). Improper functions of Aldh1A family members are associated with disrupted embryonic development, cataract formation, and Parkinson's and Alzheimer's disease (Shortall *et al.*, 2021). Aldh3A1 contributes to cataract formation if its function has been compromised (Lassen *et al.*, 2007). Mutations of Aldh3A2 (an ER-bound Aldh-converting fatty aldehydes to fatty acids) result in the Sjögren Larsson syndrome (scaling skin, speech abnormalities, intellectual disability, and spasticity) (Shortall *et al.*, 2021). Aldh7A1 is engaged in lysine catabolism, and its dysfunction results in a seizure causing disorder named pyridoxine-related epilepsy (Shortall *et al.*, 2021).

1.4.3 Aldhs and their roles in human stem cells

Aldhs regulate differentiation and proliferation (Muzio *et al.,* 2012). High Aldh levels have been found in some human hematopoietic progenitor cells, neural cells, myogenic cells, mammary cells, intestinal crypt cells, and prostate cells. The expression of Aldh is more pronounced in neural embryonic tissues (less differentiated) than in adult tissues (differentiated), and a part of the cells isolated from mouse brain tissue with high Aldh content (Aldh$^+$) were found to be multipotent, self-renewing, and capable of generating new neurospheres and neuroepithelial stem-like cells in culture. Mammary Aldh$^+$ epithelial cells highly express Aldh1 and are able to self-renew and generate luminal and myoepithelial cells. Murine prostate basal epithelium cells highly express Aldh1A1 and showed increased prostate tissue formation after *in vivo* transplantation (Muzio *et al.,* 2012).

Increased Aldh activity was also found in acute myeloid leukemia and various types of stem cells in solid cancers such as breast, colon, prostate, lung, liver, pancreas, and ovarian cancers (Clark and Palle, 2016). These cells are typical named cancer stem cells (CSCs), and they are chemoresistant and radiation-resistant due to various mechanisms. Upon drug treatment, the formation of reactive oxygen species (ROS) is triggered, inducing structural alterations in DNA and proteins and interfering with cytoplasmic and nuclear signal transduction pathways leading to cell death of tumor cells (Clark and Palle, 2016; Wiseman and Halliwell, 1996). However, CSCs possess a higher activity of DNA-damage response factors and Aldh expression (Abdullah and Chow, 2013; Clark and Palle, 2016).

Aldhs confer chemoresistance by detoxification of anti-cancer drugs such as the metabolized cyclophosphamide product aldophosphamide, which is otherwise decomposed into phosphoramide mustard (cross-links DNA) and acrolein (responsible for hemorrhagic cystitis) (Emadi *et al.,* 2009). Additionally, Aldhs detoxify by-products of lipid peroxidation (4-HNE) mediated by ROS, thereby preventing ROS propagation through accumulation of reactive aldehydes and ROS-induced cell death through mitochondrial disruption (Benedetti *et al.,* 1980; Ryter *et al.,* 2007). In particular, Aldh1A1 was proposed as a stem cell marker (Ginestier *et al.,* 2007; Huang *et al.,* 2009).

CSCs also express high levels of B-cell lymphoma-2 (BCL-2) protein, which promote anti-apoptotic cellular responses (Yip and Reed, 2008). Moreover, CSCs possess adenosinetriphosphate (ATP)-binding cassette-containing drug efflux transporters such as P-glycoprotein and breast cancer resistance protein, which confers chemoresistance

by preventing accumulation of drugs inside cells (Doyle *et al.*, 1998; Juliano and Ling, 1976; Sugawara, 1990). After drug treatment, differentiated tumor cells die, while quiescent CSCs divide and begin to differentiate into normal tumor cells resulting in tumor recurrence and metastasis (Clark and Palle, 2016).

1.4.4 Stem cells in *S. mansoni*

Planarians are free-living members of the class turbellaria (phylum platyhelminthes) and possess pluripotent stem cell-like cells called neoblasts. These unique stem cells enable planarians to regenerate tissue or an entire organism after injury (Newmark and Sánchez Alvarado, 2002). The representative *Dendrocoelum lacteum* has limited regenerative ability, whereas *Dugesia japonica* and *Schmidtea mediterranea* show high regenerative abilities (whole organism) (Newmark and Sánchez Alvarado, 2002). Neoblast-like cells are also present in parasitic tapeworms such as *Echinococcus multilocularis* (Brehm, 2009). In addition, germ cells and neoblasts have been found in *S. mansoni* somatic tissue (Collins *et al.*, 2013) and likely contribute to *in vivo* longevity (Wendt and Collins, 2016).

S. mansoni adults are likely unable to regenerate dissected tissue but may initiate their repair, as seen after treatment with sub-curative doses of PZQ (Wendt and Collins, 2016). Wang *et al.* (2018)) showed that in larval *S. mansoni* there are germinal stem cells (κ cells) that produce δ cells (soma) that give rise to φ cells (associated with transitory larval structures such as the sporocyst epidermis (tegument) and the cercariae tail). When the cercariae enter the host, their expression changes in κ and δ cells (now δ' cells, which serve as a source of somatic stem cells). κ cells give rise to ϵ cells (located in the gonadal primordia and posterior growth zone), which express either Sm*eledh* to form somatic tissue, or additionally Sm*nanos1* to form the germline. Gonadal stem cell self-renewal and differentiation in *S. mansoni* males is controlled by SmEledh (inhibits differentiation), SmBoule (promotes differentiation), and SmOC-1 (inhibits self-renewal). Boule and OC-1 are also conserved in *S. mediterranea*, wheras Eled seems to be specific for schistosomes (Li *et al.*, 2021; Wang *et al.*, 2018).

Although Aldhs are present in normal mammalian and tumor stem cells (Clark and Palle, 2016; Muzio *et al.*, 2012) and serve as human stem cell markers, they have not been proposed as stem cell markers in *S. mansoni*. Nonetheless, it seems likely that Aldhs

affect stem cell activity also in *S. mansoni*. Together with their potential detoxifying potential, Aldhs are therefore interesting targets for further analyses.

1.5 Kinases

1.5.1 Classification and structure

Kinases are involved in many metabolic and developmental processes such as cytoskeleton reorganization, cell proliferation, endocytosis, metabolism, transcription, survival, and stress responses (Manning *et al.*, 2002a; Pendergast, 2002; Roskoski, 2015). Kinases are among the largest superfamilies in the human genome and comprise 518 genes, thus representing approximately 1.7 % of human genes (Manning *et al.*, 2002b). Most kinases (478) belong to one superfamily (**Figure 1.6**), the eukaryotic protein kinases (ePKs), and were categorized as follows: PTKs (protein tyrosine kinases), TKL (tyrosine kinase-like), Ste (Ste20, Ste11, and Ste7 related, named after yeast sterile), CK1 (casein kinase 1), AGC (protein kinase A, protein kinase G, and protein kinase C related), CAMK (Ca^{2+}/calmodulin-dependent kinases), CMGC (cyclin-dependent kinases (CDKs), mitogen-activated protein kinase (MAPK), glycogen synthase kinase (GSK), CDK-like related), RGC (receptor guanylyl cyclase). The remaining 40 kinases were grouped together as atypical protein kinases (aPKs) or "others" (Manning *et al.*, 2002b).

PTKs can be further subdivided into receptor tyrosine kinases (RTKs), which consist of 20 subfamilies (58 kinases), and 32 cytoplasmatic tyrosine kinases (CTKs) (Lemmon and Schlessinger, 2010; Roskoski, 2015) consisting of 10 subfamilies: Abl, ACK (activated CDC42-associated kinase), CSK (C-terminal Src kinase), FAK (focal adhesion kinase), Fes (feline sarcoma), FRK (Fyn related kinase), JAK (Janus kinase), Src (*sarcoma*), SYK (spleen tyrosine kinase), and TEC (Blume-Jensen and Hunter, 2001). In addition to aPKs and ePKs, there are approximately 20 lipid kinases (Fabbro *et al.*, 2012).

Typical for kinases are catalytic kinase domains that are approximately 250 - 300 aa in size and highly conserved (Hanks *et al.*, 1988; Manning *et al.*, 2002b). Further domains mediate protein-protein interactions or serve as regulatory units (Buljan *et al.*,

2020; Fasolo *et al.*, 2011; Pawson and Nash, 2003; Rauch *et al.*, 2011). Kinases function as phosphotransferases, mediating the transfer of a phosphoryl group from ATP to their substrate molecule (Matte *et al.*, 1998). This post-translational modification triggers different events such as protein-protein interactions, activation or inactivation of proteins, and signal transduction (Duan and Walther, 2015; Fang *et al.*, 2000; Nishi *et al.*, 2011; Woo *et al.*, 2010).
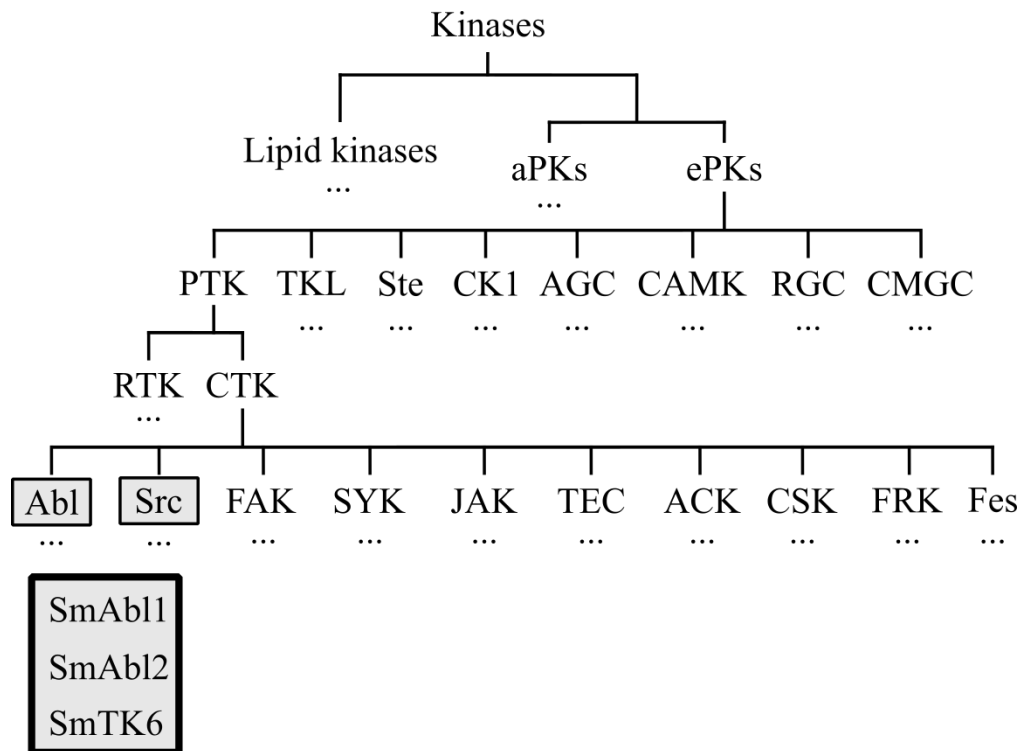
Figure 1.6: Classification of the kinases to be studied
Both SmAbl kinases (SmAbl1 and SmAbl2) and the Src/Abl hybrid kinase SmTK6 belong to the cytosolic tyrosine kinases. For more details see text. Dots (...) indicate further groups/members.

1.5.2 Kinases in *S. mansoni*

Starting in the early 1990's some effort was made to elucidate signaling molecules in *S. mansoni* (Bahia *et al.*, 2006). Among others, the following molecules were identified: small GTP-binding proteins (Kampkötter *et al.*, 1999; Loeffler and Bennett, 1996; Osman *et al.*, 1999), the Src kinase SmTK5 (Fyn subfamily) (Kapp *et al.*, 2001), SYK kinase SmTK4 (Beckmann *et al.*, 2010; Knobloch *et al.*, 2002), Src kinase SmTK3

(Kapp *et al.,* 2004), two transforming growth factor β receptors, type I and type II (SmTβRI/II) (Davies *et al.,* 1998; Forrester *et al.,* 2004), two venus kinase receptors (SmVKRs) (Gouignard *et al.,* 2012; Vicogne *et al.,* 2003), two Abl kinases (Beckmann and Grevelding, 2010), and the Src/Abl hybrid kinase SmTK6 (Beckmann *et al.,* 2011). Most of these molecules have been localized within the gonads and/or vitellarium. Based on inhibitor studies and/or RNAi approaches, they were proposed to play important roles during reproductive organ development and egg production. Inhibition of some of these kinases in *in vitro*-cultured schistosomes showed effects on the reproductive organs. When the TβRI kinase inhibitor TRIKI was applied, mitotic activity was reduced and accordingly less eggs were produced (Knobloch *et al.,* 2007). Moreover, application of the Src kinase inhibitor Herbimycin A resulted in a reduction in the egg-laying capacity of the females including an increase of deformation of eggs of up to 40 % (Knobloch *et al.,* 2006).

Elucidating kinase signaling is complex. In addition to inhibitor treatments, RNAi, germinal vesicle break down (GVBD) assays, yeast-two-hybrid screenings, and coimmunoprecipitation methods were used to elucidate that SmVKR1 interacts in a kinase complex with SmTK3, SmTK4, and SmTK6 (Beckmann *et al.,* 2010, 2011). It was further demonstrated that this complex modulates gametogenesis and oogenesis as well as the formation of eggs in *S. mansoni* females (Vanderstraete *et al.,* 2014). Furthermore, interactions were shown between SmVKR1 and Smβ-integrin 1 (Smβ-Int1), which were connected through three scaffold proteins, SmNCK2 (non-catalytic region of tyrosine kinase adaptor protein 2), SmPINCH (particularly interesting new cysteine-histidine-rich protein), and SmILK (integrin-linked kinase). Functional analyses indicated that this complex may regulate apoptosis mediated by the pro-apoptotic BCL-2 family members, BCL-2 homologous antagonist/killer (SmBAK) and BCL-2 associated X protein (SmBAX), in primary oocytes upon pairing (Gelmedin *et al.,* 2017).

Furthermore, Quack *et al.* (2009) found that a diaphanous homolog (SmDia) interacts with a rat *sarcoma* (Ras) homologue (SmRho1) and the Src kinase SmTK3, which could connect the Src kinase pathway (SmVKR1 complex) with G-protein coupled receptor signaling via Rho GTPases to modulate cytoskeleton reorganization. Gene transcripts of Sm*dia* and Sm*rho1* were found in vitelline cells, oocytes, and testes (Quack *et al.,* 2009) as was Sm*tk3* (Kapp *et al.,* 2004). This demonstrates that maintaining the reproductive organs and differentiation is orchestrated by many signaling pathways including kinases (Grevelding *et al.,* 2018) with some crosstalk activities to other signaling pathways.

1.5.3 The SmAbl kinases

In 1970, Abelson and Rabstein (1970) investigated the oncogenicity of Abelson murine lymphosarcoma virus (A-MuLV) that led to the induction of solid lymphoid tumors in mice. Using parts of A-MuLV for hybridization studies, Abl kinases were identified in humans, rats, Chinese hamsters, rabbits, and chickens (Goff *et al.*, 1980). In later studies, Abl variants fused to the breakpoint cluster region (BCR-Abl) in Philadelphia chromosomes were discovered and associated with human leukemia (Wong and Witte, 2004).

In humans, two paralogs (HsAbl1 and HsAbl2) were identified (Kruh *et al.*, 1986). They consist of two N-terminally Src homology (SH) domains (SH3 and SH2), a C-terminal tyrosine kinase domain (TKD) and additionally varying actin, microtubule, or DNA binding domains (Colicelli, 2010). The SH3 domain mediates protein binding to proline-rich substrates, while SH2 accesses the phosphorylation state of that substrate (Wong and Witte, 2004). Moreover, both SH domains contribute to inhibition of Abl kinases. SH3 binds to the linker region between SH2 domain and the TKD and SH2 binds to the TKD linker region, preventing ATP binding. Additional isoforms of the kinases can be generated through alternative splicing. Isoforms 1b and 2b get myristoylated at Gly2. This modification contributes to an inactive conformation of the kinases by binding to a hydrophobic pocket of the kinase domain (Wong and Witte, 2004). Phosphorylation events in the activation loop (Tyr412) or linker region between SH2 and TKD (Tyr245) may lead to its activation, as well as binding events of SH3 or SH2 ligands (Hantschel and Superti-Furga, 2006).

In 2010, Beckmann and Grevelding (2010) described the existence of two SmAbl homologs in *S. mansoni* and predicted their SH3-SH2-TKD structures. Inhibition of these kinases by imatinib was expected, as 18/21 conserved residues in HsAbl interacting with imatinib were conserved in SmAbl1, and 20/21 in SmAbl2 (Beckmann and Grevelding, 2010). Moreover, inhibition of the SmAbl kinases by imatinib was demonstrated by GVBD assays and *in silico* docking of a homology model (Buro *et al.*, 2014). Transcript analyses by *in situ* hybridization revealed Sm*abl* transcripts in the ovary, testes, and ootype, as well as weakly in the gastrodermis and parenchyma of both genders. Application of imatinib on *S. mansoni in vitro* revealed strong effects on worm vitality, the ovarian structure (oocytes were less close arranged and appeared apoptotic), testes (lobes appeared shrunken and less elongated sperm were detected in the seminal vesicle), and gastrodermis (appeared detached from the parenchyma and collapsed)

with 100 µM after 24 h (Beckmann and Grevelding, 2010). These observations fit the locations of transcripts.

1.5.4 The Src/Abl hybrid SmTK6

SmTK6 was found to be a hybrid kinase with Src and Abl motifs (Beckmann *et al.*, 2011). It does possess the Abl typical SH3-SH2-TK cassette (Colicelli, 2010) and one of two conserved Tyr in the N-terminal TKD part (presence of Tyr312, absence of Tyr416) (Beckmann *et al.*, 2011). SmTK6 does not possess a myristoylation motif although there is a Gly at position 2. Furthermore, the elongated C-terminus as present in Abl kinases is absent in SmTK6. Instead, SmTK6 shares a Src-typical Tyr residue at the C-terminus (Tyr562) but lacks another Src-typical regulatory Tyr in the TKD, where a Ser residue occurs at position 447 instead.

A phylogenetic analysis positioned SmTK6 as intermediate between Src and Abl kinases (Beckmann *et al.*, 2011). Moreover, analysis of the TKDs of SmTK6 with Abl and Src kinases conducted with Clustal Ω showed that SmTK6 shares more similarity with Abl than Src kinases (Beckmann and Grevelding, 2010; Beckmann *et al.*, 2011). The hybrid character was confirmed by GVBD assays using the Abl kinase inhibitor imatinib and the Src kinase inhibitor Herbimycin A on the SmTK6 TKD. Both inhibitors showed inhibition with higher doses as compared to the control TKDs of Src kinase SmTK3 and Abl kinase SmAbl1 (Beckmann *et al.*, 2011).

Beckmann *et al.* (2010) localized Sm*tk6* transcripts in parenchyma and gonads of both genders. Corresponding with this, interactions and complex formation of SmTK6 with SmTK3, SmTK4, and SmVKR1 was detected by yeast-two-hybrid screenings (Beckmann *et al.*, 2010, 2011), suggesting roles in the cytoskeleton organization in the gonads (Quack *et al.*, 2009) and survival of primary oocytes in female *S. mansoni* (Gelmedin *et al.*, 2017).

1.6 Aims of this work

Schistosomiasis is a NTD that affects humans and animals. Although several drugs had been available in recent decades, many were withdrawn from the market because of

toxic side effects. The only remaining drug for treating schistosomiasis is PZQ, which is effective against the six major human parasite species and also against schistosomes of infected animals. Therefore, new targets and drugs are needed, an area of research in which this study was positioned. One aim of this work was to investigate the impact of the Aldh inhibitor DSF on adult *S. mansoni* and to analyze whether DSF or its copper metabolite CuET may cause different effects.

To this end, experiments with DSF alone, DSF in combination with copper, its copper metabolite CuET, and DSF with copper and copper chelating agents were planned. The effects on *S. mansoni* couples will be assessed by bright-field microscopy to evaluate their viability parameters (mating status, attachment capacity, motility, and egg production), confocal laser scanning microscopy (CLSM) to analyze morphological changes, and 5-ethinyl-2'-deoxyuridine (EdU) incorporation assays to analyze stem cell-associated effects. In addition, changes in tegument structure will be analyzed by scanning electron microscopy (SEM) after DSF treatment, and transcript levels of selected genes (likely involved in oxidative stress response, cell cycle, and apoptosis, as well as stem cell markers) determined by qRT-PCR. Moreover, the effect of the DSF derivative Schl-32.028 on adult *S. mansoni* couples should be investigated.

As a further aim of this study, two SmAldhs, two SmAbl kinases, and the Src/Abl hybrid kinase SmTK6 should be functionally investigated to evaluate their potential as drug targets. Here, investigations on the Aldhs will be given preference, as one of them was detected by the working group of Prof. C. G. Grevelding in the stripped tegument fraction of adult *S. mansoni* worms. Analyses will require cloning of the target sequences and validation of the sequences against the available *S. mansoni* genome version 7 (gv7). For functional analysis, RNAi will be applied on adult worms, and the effects investigated at the physiological, morphological, and cell-biological level. The effects of H_2O_2 on adult worms after previous Sm*aldh* knock down will be analyzed as well as Sm*aldh* transcript localization. The relative expression of each gene will be determined for pairing-experienced and pairing-unexperienced worms. In addition, the coding sequences of all genes will be cloned into expression vectors suitable for protein production in bacteria (*E. coli*) and a mammalian expression system (HEK293-6E (EBNA1) cells). After successful protein expression, proteins will be purified and characterized biochemically. Here, Aldh was again in focus, which required the establishment of an enzyme assay for inhibitor binding analyses.

2 Material

2.1 Equipment and consumables

The equipment corresponded to that of a molecular biology laboratory. Special equipment and consumables are listed in **Table 2.1**.

Table 2.1: Equipment and consumables

Name	Reference
Centrifuges and accessories	
Bottles (Polypropylene), 250 ml	HeroLab
Bottles (Fluoroethylenepropylene), 250 ml	Nalgene
Cooling centrifuge Avanti JXN-26	Beckmann Coulter
Rotor JLA-16.250	Beckmann Coulter
Rotor JA-25.50	Beckmann Coulter
Tubes (Polypropylene), 50 ml	HeroLab
Vacuum centrifuge Hetovac VR-1	Heto Lab Equipment
Chromatography system	
ÄKTA Start instrument	GE Healthcare
HisTrap HP, 1 ml	GE Healthcare
Bio-scale mini bio-gel P-6 desalting cartridge, 5 ml	Bio-Rad
Crosslinker	
UV Stratalinker 2400	Stratagene
Filter	
Bottle top filter, 0.45 µm	Sarstedt
Sterile PES syringe filter, 0.2 µm	Thermo Fisher Scientific

Continued on the next page

Table 2.1 – *Continued from previous page*

Name	Reference
Hand-held counter	
Hand-held counter	Carl Roth
Heating plate	
XH-2002 slides warmer	Premiere
Imager	
ChemiDoc MP	Bio-Rad
Gel iX20	INTAS Science Imaging Instruments
Incubators	
CO_2 incubator Galaxy S+	RS Biotech
Shaking incubator 3032	GFL
Microscopy	
Conductive carbon adhesive pads, 12 mm	Plano
Confocal laser scanning microscope TCS SP5 vis	Leica Microsystems
Critcal point dryer CPD030	BAL-TEC AG
High precision cover slips	Menzel
Inverse laboratory microscope DM IL LED	Leica Microsystems
Objective HCX PL APO 20x0.7	Leica Microsystems
Objective HCX PL APO 63x1.3	Leica Microsystems
Pen sample plates	Plano
Scanning electron microscope Gemini DSM 982	Carl Zeiss Microscopy
Sputter system SCD004	BAL-TEC AG
Mortar and pestle	
Polyethylene pestle	Science Services
Porcelain mortar and pestle	Rosenthal
Photometry	
BioSpectrometer basic	Eppendorf
Cytation 3 plate reader	BioTek
µCuvette G1.0	Eppendorf
Microplate, 96-well, black quartz glass	Hellma

Continued on the next page

Table 2.1 – *Continued from previous page*

Name	Reference
Power supply unit	
PowerPac basic power supply	Bio-Rad
Polymerase chain reaction (PCR)	
Loading rack RotoCycler 72	VWR
Cycler C1000 thermal cycler	Bio-Rad
Cycler Rotor-Gene Q MDx	Qiagen
Hood Aura PCR	BioAir
Rotor-Gene 0.1 ml tube strips	Kisker Biotech
Protein expression	
DURAN chicane flask (1 l)	Carl Roth
Reaction tubes	
Canonical tubes, 50 ml and 15 ml	Sarstedt
Protein low-bind canonical tube, 50 ml	Eppendorf
Protein low-bind reaction tube, 2 ml and 1.5 ml	Eppendorf
RNA Analysis	
2100 Bioanalyzer instrument	Agilent Technologies
SDS-polyacrylamide gel electrophoresis (SDS-PAGE)	
Mini-Protean tetra handcast system	Bio-Rad
10-well comb	Bio-Rad
Transferring inserts	
Incubation baskets, 100 µm	CEM
Netwell inserts, 15 mm, 74 µm	Science Service
Tweezers	
EMS ultra fine tweezers	Science Service
Spring steel tweezers, pointed, 105 mm	Carl Roth
Ultrasonic homogenizer	
Sonifier SFX150 cell disruptor	Branson Ultrasonics
Vortexer	
MS 3 basic vortexer	IKA

Table 2.1 – *Continued from previous page*

Name	Reference
Well plates	
6-, 12-, 24-, and 48-well plates	Greiner Bio-One
Western blot	
Blot paper MN 218 B	Macherey-Nagel
Trans-Blot Turbo Transfer system	Bio-Rad
Whatman Protran nitrocellulose membrane, 0.45 µm	GE Healthcare

2.2 Chemicals and ready-to-use reagents

Chemicals and ready-to-use reagents used in this work are listed in **Table 2.2**.

Table 2.2: Chemicals and ready-to-use reagents

Name	Reference
Acetaldehyde	Carl Roth
Acetic acid	Carl Roth
Agar agar	Carl Roth
Agarose	Carl Roth
Ammonium acetate (7.5 M)	Sigma-Aldrich
Ammonium peroxodisulfate (APS)	Sigma-Aldrich
Ampicillin (amp)	Sigma-Aldrich
Antibiotic-antimycotic solution	C C Pro
Bathocuproinedisulfonic acid disodium salt	Sigma-Aldrich
Bovine serum albumin (BSA)	Sigma-Aldrich
5-bromo-4-chloro-3-indolyl–β-D-galactopyranoside (X-gal)	Carl Roth
5-bromo-4-chloro-3-indolylphosphate (50 mg ml^{-1}; BCIP)	Roche
Bromphenol blue	Carl Roth
Calcium chloride (CaCl$_2$)	Carl Roth
Canada balsam	Sigma-Aldrich

Continued on the next page

Table 2.2 – *Continued from previous page*

Name	Reference
Certistain carmine red	Merck
Chloramphenicol (cam)	Sigma-Aldrich
Chloroform	Fisher Bioreagents
10x CutSmart buffer	New England Biolabs
Copper chloride ($CuCl_2$)	Fluka
Copper diethyldithiocarbamate (CuET)	Sigma-Aldrich
Deionized formamide	Thermo Fisher Scientific
Dextran sulfate	Sigma-Aldrich
Diethyl pyrocarbonate (DEPC)	Carl Roth
Dimethyl formamide (DMF)	Sigma-Aldrich
Dimethyl sulfoxide (DMSO)	Sigma-Aldrich
Disulfiram	Sigma-Aldrich
Disodium hydrogen phosphate	Carl Roth
Dithiothreitol (DTT)	Carl Roth
Deoxynukleosidetriphosphate (dNTP) solution set	Solis BioDyne
ECL prime western blot detection reagent	GE Healthcare
Ethanol	Carl Roth
Ethylenediamine tetraacetic acid disodium salt dihydrate	Carl Roth
Ethyl 3-aminobenzoate methanesulfonate (Tricaine)	Sigma-Aldrich
Fetal calf serum (FCS)	Sigma-Aldrich
FluorCare	Carl Roth
Formaldehyde solution (37 %; PFA)	Carl Roth
Formamide	Thermo Fisher Scientific
FreeStyle F17 expression medium	Thermo Fisher Scientific
GelRed nucleic acid gel stain	Biotium
Glacial acetic acid	Carl Roth
Glucose	Carl Roth
Glutaraldehyde	Carl Roth
Glycerol	Carl Roth

Table 2.2 – *Continued from previous page*

Name	Reference
Glycine	Carl Roth
Heparine sodium-250000	Ratiopharm
High-purity water (designated as PCR-water)	Carl Roth
Horse serum, heat-inactivated	Sigma-Aldrich
Hydrochloric acid (37 %; HCl)	Carl Roth
Hydrogen peroxide (30 %; H_2O_2)	Carl Roth
2-4-(2-hydroxyethyl)-1-piperazinyl ethane sulfonic acid (HEPES)	Carl Roth
Imidazole	Carl Roth
Isoflurane	CP Pharma
Isopropanol	Carl Roth
Isopropyl-β-D-thiogalactopyranoside (IPTG)	Carl Roth
Kanamycin (kan)	Sigma-Aldrich
Ketamine ($100\,mg\,ml^{-1}$)	CP Pharma
Lithium chloride (LiCl)	Carl Roth
Magnesium chloride ($MgCl_2$)	Carl Roth
Manganese chloride ($MnCl_2$)	Carl Roth
Methanol	Carl Roth
M199 powder and ready-to-use solution	Gibco
Milk powder	Carl Roth
3-morpholinopropane sulfonic acid (MOPS)	Carl Roth
Nail polish	Maybelline New York
Nicotinamide adenine dinucleotide (NAD^+)	Sigma-Aldrich
Nitro blue tetrazolium ($100\,mg\,ml^{-1}$; NBT)	Roche
Orange G	Carl Roth
Osmiumtetroxide (4 %)	Serva
Phenol	Sigma-Aldrich
Phenol/chloroform/isoamyl alcohol (25:24:1)	Sigma-Aldrich
Polyethylene glycol 8000 (PEG)	Fisher BioReagents
Polyethylenimine (PEI), linear, MW 25000, transfection grade	Polysciences
Polyvinyl alcohol, 30-70 kDa (PVA)	Sigma Aldrich

Continued on the next page

Table 2.2 – *Continued from previous page*

Name	Reference
Ponceau S	Serva
Potassium acetate	Carl Roth
Potassium carbonate	Carl Roth
Potassium chloride (KCl)	Carl Roth
Potassium dihydrogen phosphate	Carl Roth
Sodium acetate	Carl Roth
5x Q5 reaction buffer	New England Biolabs
10x reaction buffer BD	Solis BioDyne
Ribonucleotidetriphosphate (rNTP) mix	New England Biolabs
RNase AWAY	Molecular BioProducts
Rotiphorese Gel 30	Carl Roth
Rubidium chloride (RbCl)	Carl Roth
SIGMAFAST protease inhibitor tablets	Sigma-Aldrich
Sodium cacodylate trihydrate	Sigma-Aldrich
Sodium chloride (NaCl)	Carl Roth
Sodium dodecyl sulfate (SDS)	Serva
Sodium hydrogen carbonate	Carl Roth
Sodium hydroxide (NaOH)	Carl Roth
Sodium hypochlorite	Carl Roth
Spermidine	Sigma-Aldrich
Streptomycin (stm)	Carl Roth
Sucrose	Sigma-Aldrich
Tetramethyl ethylenediamine (TEMED)	Carl Roth
5x transfer buffer	Bio-Rad
10x transcription buffer	Roche
Trichloroethanol	Carl Roth
Tris(hydroxymethyl)aminomethane (Tris)	Carl Roth
Trisodium citrate 2-hydrate	Carl Roth
Triton X-100	Sigma-Aldrich
Tween20	Carl Roth
Xylavet ($20\,\mathrm{mg\,ml^{-1}}$)	CP Pharma
Yeast t-RNA	Carl Roth

2.3 Buffers and solutions

Buffers and solutions used in this work are listed in **Table 2.3**.

Table 2.3: Buffers and solutions

Name	Composition	Application
Acetaldehyde		
Prepare freshly	1 M Acetaldehyde	Activity assay
	Add double distilled water (ddH$_2$O)	
Acetic acid		
Store at room temperature (RT)	1 % (v/v) Acetic acid	Western blot
	Add ddH$_2$O	
Acidic ethanol		
Store at RT	70 % (v/v) Ethanol	Carmine red staining
	2.5 % (v/v) HCl (37 %)	
	Add ddH$_2$O	
AFA		
Store at RT	2 % (v/v) Acetic acid	Carmine red staining
	1.1 % (v/v) PFA	
	66.7 % (v/v) Ethanol	
	Add DEPC-water	
Antibody solution I		
Prepare freshly	1 ‰ (v/v) Anti-6x His-tag	Western blot
Store at −20 °C	3 % (w/v) BSA	
	Add TBST	
Antibody solution II		
Prepare freshly	0.025 ‰ (v/v) Goat anti-mouse IgG (H+L)-horse raddish peroxidase (HRP) conjugate	Western blot
	3 % (w/v) BSA	
	Add TBST	

Continued on the next page

Table 2.3 – *Continued from previous page*

Name	Composition	Application
Antibody solution III		
Prepare freshly	0.05 ‰ (v/v) Anti-digoxigenin (DIG)-alkaline phosphatase (Anti-DIG-AP) conjugate Add colorimetric block solution	WISH
AP buffer		
Store at 4 °C	100 mM Tris (pH 9.5) 100 mM NaCl 50 mM MgCl$_2$ 0.1 % (v/v) Tween20 Add PVA	WISH
10 % APS		
Store at −20 °C	10 % (w/v) APS Add ddH$_2$O	SDS-PAGE
Bleaching solution		
Prepare freshly	5 % (v/v) Deionized formamide 0.5x SSC 1.2 % (v/v) H$_2$O$_2$ Add DEPC-water	EdU staining, WISH
Blocking solution		
Prepare freshly	5 % (w/v) Milk powder Add TBST	Western blot
CaCl$_2$		
Store at −20 °C	0.5 mM CaCl$_2$ Add 100 mM Tris (pH 7.4)	Activity assay
Cacodylate buffer		
Store at 4 °C	0.2 M Sodium cacodylate trihydrate Add ddH$_2$O	SEM
Canada balsam		
Prepare freshly	66.6 % (v/v) Canada balsam Add xylol	Carmine red staining

Continued on the next page

Table 2.3 – *Continued from previous page*

Name	Composition	Application
Carmine red solution		
Store at RT	2.5 % (w/v) Carmine red	Carmine red
	2.5 % (v/v) HCl (37 %)	staining
	92.5 % (v/v) Ethanol (90 %)	
	Add ddH$_2$O	
Colorimetric block solution		
Store at −20 °C	7.5 % (v/v) Horse serum	WISH
	Add TNT buffer	
Coomassie staining solution		
Store at RT	5 % (w/v) Coomassie brilliant blue R250	SDS-gel staining
Filter	0.3 % (v/v) HCl (37 %)	
	Add ddH$_2$O	
DEPC-water		
Store at RT	0.1 % (v/v) DEPC	Working with
	Add ddH$_2$O	RNA
Developing buffer		
Prepare freshly	450 µg ml^{-1} NBT	WISH
	175 µg ml^{-1} BCIP	
	Add AP buffer	
10x DNA loading buffer		
Store at 4 °C	25 % (v/v) Glycerol	Agarose gel
	0.2 % (w/v) Orange G	electrophoresis
	Add TAE buffer	
DIG-dNTP mix		
Store at −20 °C	10 mM Deoxyadenosinetriphosphate (dATP)	WISH
	10 mM Deoxyguanosinetriphosphate (dGTP)	
	10 mM Deoxycytidintriphosphate (dCTP)	
	7 mM Deoxyridinetriphosphate (dUTP)	
	3.5 mM DIG-dUTP	
	Add DEPC-water	

Continued on the next page

Table 2.3 – *Continued from previous page*

Name	Composition	Application
dNTP mix		
Store at −20 °C	10 mM dATP	PCR
	10 mM dCTP	
	10 mM dGTP	
	10 mM Deoxythymidinetriphosphate (dTTP)	
DTT		
Prepare freshly	120 mM DTT	Activity assay
	Add 100 mM Tris (pH 7.4)	
Elution buffer		
Store at 4 °C	300 mM Imidazole	Protein
pH 7.4	100 mM Tris	expression
	Add ddH$_2$O	
70 % Ethanol		
Store at RT	70 % (v/v) Ethanol	Carmine red
	Add DEPC-water	staining, works
		with RNA
90 % Ethanol		
Store at RT	90 % (v/v) Ethanol	Carmine red
	Add DEPC-water	staining
4 % Formaldehyde		
Prepare freshly	4 % (v/v) PFA	EdU staining,
	Add PBSTx	WISH
Fixing solution I		
Prepare freshly	2.5 % (v/v) Glutaraldehyde	SEM
	1 % (v/v) PFA	
	3 % (w/v) Sucrose	
	0.1 M (v/v) Cacodylate buffer	
	Add ddH$_2$O	

Continued on the next page

Table 2.3 – *Continued from previous page*

Name	Composition	Application
Fixing solution II		
Prepare freshly	1 % (v/v) Osmiumtetroxide	SEM
	0.1 M (v/v) Cacodylate buffer	
	Add ddH$_2$O	
GelRed		
Store at RT	2.5 % (v/v) GelRed	Agarose gel
	Add ddH$_2$O	electrophoresis
Glycerol		
Store at RT	80 % (v/v) Glycerol	WISH
	Add PBS	
Heparine		
Store at −20 °C	25 000 U ml^{-1} Heparine sodium	Perfusion
	Add ddH$_2$O	medium
HEPES buffer		
Store at RT	1 M HEPES	Additive for
pH 7.4	Add ddH$_2$O	medium
Filter sterile		
Hoechst 33342		
Store at −20 °C	10 mg ml^{-1} Hoechst 33342	Hoechst staining
	Add ddH$_2$O	
Hybridization buffer		
Store at−20 °C	50 % (v/v) Deionized formamide	WISH
	10 % (w/v) Dextran sulfate	
	5 x SSC	
	1 mg ml^{-1} Yeast t-RNA	
	1 % (v/v) Tween20	
	Add DEPC-water	
LiCl		
Store at −20 °C	7.5 M LiCl	RNA
	Add DEPC-water	precipitation

Continued on the next page

Table 2.3 – *Continued from previous page*

Name	Composition	Application
MgCl$_2$		
Store at −20 °C	0.6 M MgCl$_2$	Activity assay,
	Add DEPC-water or	WISH
	Add 100 mM Tris (pH 7.4)	
50 % Methanol		
Prepare freshly	50 % (v/v) Methanol	EdU staining,
	Add PBSTx	WISH
5 % Milk		
Prepare freshly	5 % (w/v) Milk powder	Western blot
	Add TBST	
NAD$^+$		
Prepare freshly	10 mM NAD$^+$	Activity assay
	Add 100 mM Tris (pH 7.4)	
Narcotics		
Prepare freshly	1.9 % (v/v) Ketamine	Perfusion
2 − 3 ml per	6.2 % (v/v) Xylavet	
hamster	Add 0.9 % NaCl	
10x PBS (phosphate buffered saline)		
Store at RT	1.37 M NaCl	WISH, washing
pH 7.0 - 7.2	27 mM KCl	of *S. mansoni*
	100 mM Disodium hydrogen phosphate	
	17.5 mM Potassium dihydrogen phosphate	
	Add DEPC-water	
PBSTx (PBS/Triton X-100)		
Store at RT	0.3 % (v/v) Triton X-100	EdU staining,
	Add PBS	WISH
PEG solution		
Store at 4 °C	20 % (w/v) PEG 8000	DNA clean up
Filter sterile	20 mM MgCl$_2$	
	Add ddH$_2$O	

Continued on the next page

Table 2.3 – *Continued from previous page*

Name	Composition	Application
10x Ponceau S		
Store at RT	1 % (w/v) Ponceau S	Western blot
	10 % (v/v) Acetic acid	
	Add ddH$_2$O	
Prehybridization buffer		
Store at −20 °C	50 % (v/v) Deionized formamide	WISH
	5x SSC	
	1 mg ml^{-1} Yeast t-RNA	
	1 % (v/v) Tween20	
	Add DEPC-water	
Proteinase K		
Prepare freshly	6 µg µl^{-1} Proteinase K	EdU staining
	Add PBSTx	
PVA		
Store at RT	10 % (w/v) PVA	WISH
Filter sterile	DEPC-water	
RNase A		
Store at −20 °C	20 mg ml^{-1} RNase A	Protein
	Add ddH$_2$O	expression
rNTP mix		
Store at −20 °C	25 mM ATP	dsRNA synthesis
	25 mM GTP	
	25 mM CTP	
	25 mM UTP	
10x running buffer		
Store at RT	25 mM Tris	SDS-PAGE
	192 mM Glycine	
	1 % (w/v) SDS	
	Add ddH$_2$O	

Continued on the next page

Table 2.3 – *Continued from previous page*

Name	Composition	Application
Sodium acetate		
Store at RT pH 5.2	3 M Sodium acetate	WISH
NaCl		
Store at RT	0.9 % (w/v) NaCl Add ddH$_2$O	Perfusion
5x SDS-sample buffer		
Store at −20 °C	62.5 mM Tris 20 % (v/v) Glycerol 2 % (w/v) SDS 0.025 % (w/v) Bromphenol blue 5 % (w/v) DTT Add ddH$_2$O	SDS-PAGE
4x Separating gel buffer		
Store at RT pH 8.8	1.5 M Tris 0.4 % (w/v) SDS Add ddH$_2$O	SDS-PAGE
Snail water		
Store at RT	0.3 % (v/v) Snail water solution I 0.2 % (v/v) Snail water solution II 0.04 % (v/v) Snail water solution III	Culture of *Biomphalaria* glabrata (*B. glabrata*)
Snail water solution I		
Store at RT	1 M CaCl$_2$ 0.35 M MgCl$_2$ Add ddH$_2$O	Culture of *B. glabrata*
Snail water solution II		
Store at RT	21.71 M Potassium carbonate 273.78 M Sodium hydrogen carbonate Add ddH$_2$O	Culture of *B. glabrata*

Continued on the next page

Table 2.3 – *Continued from previous page*

Name	Composition	Application
Snail water solution III		
Store at RT	0.6 M NaOH	Culture of
	Add ddH$_2$O	*B. glabrata*
20x SSC (saline-sodium citrate)		
Store at −20 °C	3 M NaCl	WISH
pH 7.0	0.3 M Trisodium citrate 2-hydrate	
	Add DEPC-water	
2x SSC + 0.1 % Triton X-100		
Store at −20 °C	2x SSC	WISH
	0.1 % (v/v) Triton X-100	
	Add DEPC-water	
0.2x SSC + 0.1 % Triton X-100		
Store at −20 °C	0.2x SSC	WISH
	0.1 % (v/v) Triton X-100	
	Add DEPC-water	
4x stacking gel buffer		
Store at RT	0.5 M Tris	SDS-PAGE
pH 6.8	0.4 % (w/v) SDS	
	Add ddH$_2$O	
Storage solution		
Prepare freshly	0.1 % (v/v) PFA	SEM
	0.1 M (v/v) Cacodylate buffer	
	Add ddH$_2$O	
50x TAE (Tris/acetate/EDTA) buffer		
Store at RT	50 mM EDTA	Agarose gel
pH 8.0	2 M Tris	electrophoresis
	1 M Glacial acetic acid	
	Add ddH$_2$O	

Continued on the next page

Table 2.3 – *Continued from previous page*

Name	Composition	Application
10x TBS (Tris-buffered saline)		
Store at RT	0.2 M Tris	Western blot
pH 7.4	1.5 M NaCl	
	Add ddH$_2$O	
TBST (TBS/Tween) buffer		
Store at RT	0.1 % (v/v) Tween20	Western blot
	Add TBS	
TNT (Tris/NaCl/Tween) buffer		
Store at RT	0.1 M Tris	WISH
pH 7.5	150 mM NaCl	
	0.1 % (v/v) Tween20	
	Add DEPC-water	
Transformation buffer I		
Store at 4 °C	100 mM RbCl	Generation of
pH 5.8	50 mM MnCl$_2$	competent cells
Filter sterile	10 mM CaCl$_2$	
	30 mM Potassium acetate	
	15 % (v/v) Glycerol	
	Add ddH$_2$O	
Transformation buffer II		
Store at 4 °C	10 mM MOPS	Generation of
pH 6.8	10 mM RbCl	competent cells
Filter sterile	75 mM CaCl$_2$	
	15 % (v/v) Glycerol	
	Add ddH$_2$O	
10x transcription buffer		
Store at −20 °C	0.4 M Tris (pH 8.0)	Synthesis of
	0.1 M MgCl$_2$	dsRNA and
	20 mM Spermidine	riboprobes
	0.1 mM DTT	
	Add DEPC-water	

Continued on the next page

Table 2.3 – *Continued from previous page*

Name	Composition	Application
Tricaine		
Prepare freshly	0.25 % Tricaine	Separation of *S.*
	Add PBS	*mansoni* couples
Tris buffer		
Store at 4 °C	100 mM Tris	Protein
pH 7.4	Add ddH$_2$O	expression
Filter sterile		
Wash buffer		
Store at −20 °C	25 % Deionized formamide	WISH
	3.5x SSC	
	0.5 % (v/v) Tween20	
	0.05 % (v/v) Triton X-100	
	Add DEPC-water	
Yeast t-RNA		
Store at −20 °C	1 % (w/v) Yeast t-RNA	WISH
	Add deionized formamide	

2.4 Medium and additives

The media and additives prepared in this work are listed in **Table 2.4**.

Table 2.4: Medium and additives

Name	Solvent	Working concentration
Agar agar	LB Medium	1 - 2 %
Amp	ddH$_2$O	100 µg ml^{-1}
Cam	Ethanol	50 µg ml^{-1}
IPTG	ddH$_2$O	200 µM
Kan	ddH$_2$O	50 µg ml^{-1}

Continued on the next page

Table 2.4 – *Continued from previous page*

Name	Solvent	Working concentration
LB Medium	ddH$_2$O	20 % (w/v)
Stm	ddH$_2$O	50 µg ml^{-1}
X-gal	DMF	50 µg ml^{-1}
Perfusion medium		
M199 (powder)		1 % (w/v)
HEPES buffer (pH 7.4)		12.5 mM
Tris buffer (pH 7.4)		20 mM
Glucose		0.1 % (w/v)
Heparine		0.01 % (v/v)
Add ddH$_2$O		
Medium for *in vitro* culture (M199 (3+))		
Antibiotic-antimycotic solution		1 %
HEPES buffer (pH 7.4)		1 %
FCS		10 %
Add M199 (ready-to-use)		

2.5 Kits

Kits used in this work are listed in **Table 2.5**.

Table 2.5: Kits

Name	Reference
cDNA synthesis	
ProtoScript II First Strand cDNA Synthesis Kit	New England Biolabs
QuantiTect Reverse Transcription Kit	Qiagen
Cloning	
NEBuilder HiFi DNA Assembly Master Mix	New England Biolabs
PCR Cloning Kit	Qiagen

Continued on the next page

Table 2.5 – *Continued from previous page*

Name	Reference
Determination of protein concentration	
Pierce BCA Protein Assay Kit	Thermo Fisher Scientific
DNA extraction	
Monarch DNA Cleanup and Gel Extraction Kit	New England Biolabs
EdU staining	
Click-iT plus EdU Cell Proliferation Kit for Imaging	Invitrogen
Plasmid preparation	
NucleoSpin Plasmid EasyPure	Macherey-Nagel
RNA analysis	
Agilent RNA 6000 Nano Kit	Agilent Technologies
RNA isolation	
Monarch total RNA Miniprep Kit	New England Biolabs

2.6 Antibodies

Antibodies used in this work are listed in **Table 2.6**.

Table 2.6: Antibodies

Name	Reference
Anti-6x His-tag, monoclonal from mouse	Sigma-Aldrich
Anti-DIG-AP conjugate	Roche
Goat anti-mouse IgG (H+L)-HRP conjugate	Bio-Rad

2.7 Standards

The standards used in this work for estimating nucleic acid and protein sizes are listed in **Table 2.7**.

Table 2.7: Standards

Name	Reference
Agarose gel electrophoresis	
HyperLadder 50 bp	Meridian Bioscience
HyperLadder 1 kb	Meridian Bioscience
SDS-PAGE	
Spectra multicolored broad range protein ladder	New England Biolabs
Unstained protein standard, broad range (10 - 200 kDa)	New England Biolabs
VisiBlot standard I	SERVA

2.8 Enzymes

Enzymes used in this work are listed in **Table 2.8**.

Table 2.8: Enzymes

Name	Reference
Cloning	
*Ahd*I (10 Units (U) μl^{-1})	New England Biolabs
*Bam*HI (20 U μl^{-1})	New England Biolabs
*Cla*I (10 U μl^{-1})	New England Biolabs
*Nco*I (10 U μl^{-1})	New England Biolabs
*Nde*I (10 U μl^{-1})	New England Biolabs
*Not*I (20 U μl^{-1})	New England Biolabs
Quick-CIP (5 U μl^{-1})	New England Biolabs
*Sal*I (10 U μl^{-1})	New England Biolabs

Continued on the next page

Table 2.8 – *Continued from previous page*

Name	Reference
T4 DNA ligase (40 U µl^{-1})	New England Biolabs
*Xho*I (20 U µl^{-1})	New England Biolabs
*Xma*I (20 U µl^{-1})	New England Biolabs
*Xmn*I (20 U µl^{-1})	New England Biolabs
dsRNA Synthesis	
T7 RNA polymerase, self-made	Collins Lab (University of Texas, Southwestern Medical Center Dallas)
General purposes	
Inorganic pyrophosphatase (0.1 U µl^{-1})	New England Biolabs
DNase I (2 U µl^{-1})	New England Biolabs
Proteinase K (20 mg ml^{-1})	Roche
RNase A (10 U µl^{-1})	Sigma-Aldrich
RNase H (5 U µl^{-1})	Sigma-Aldrich
PCR	
FirePol DNA polymerase (5 U µl^{-1})	Solis BioDyne
Q5 High-Fidelity DNA polymerase (2 U µl^{-1})	New England Biolabs
PerfeCTa SYBR Green SuperMix	Quantabio
WISH	
RNase inhibitor (40 U µl^{-1})	New England Biolabs
Proteinase K (20 mg ml^{-1})	Ambion
SP6 RNA polymerase (20 U µl^{-1})	New England Biolabs
T3 RNA polymerase (20 U µl^{-1})	New England Biolabs

2.9 Plasmids

Plasmids used in this work are summarized in **Table 2.9**, and the recombinant plasmids created in this work are summarized in **Table 2.10**.

Table 2.9: Plasmids

Name	Properties	Reference	Application
pCDFD Duet-1	Co-expression plasmid with *Yersinia* tyrosine phosphatase (YopH), stm[R]	Provided by Prof. D. Rauh[a]	Expression in *E. coli*
pDrive	LacZ α-peptide, amp[R], kan[R]	Qiagen	Cloning
pET30a+	His-tag, S-tag, thrombin and enterokinase cleavage site, kan[R]	Provided by Prof. K. Becker[b]	Expression in *E. coli*
pMal-c5X	*malE* gene (coding for maltose binding protein (MBP), N-terminal), factor Xa cleavage site, amp[R]	Provided by Prof. M. Göttfert[c]	Expression in *E. coli*
pJC53.2	SP6, T3, and T7 promotor, T7 terminator, amp[R], cam[R], kan[R]	Collins *et al.*, 2010	WISH probe synthesis
pTT22SSP4	Tobacco Etch virus cleavage site, secretion signal, amp[R]	Provided by Prof. F. H. Falcone[d]	Expression in HEK293-6E (EBNA1) cells
pTT28	secretion signal, amp[R]	Provided by Prof. F. H. Falcone[d]	Expression in HEK293-6E (EBNA1) cells
pTTo/GFPq	GFP expression, amp[R]	Provided by Prof. F. H. Falcone[d]	Expression in HEK293-6E (EBNA1) cells

[R] Resistance

[a] Drug Discovery Hub Dortmund, Technical University Dortmund

[b] Interdisciplinary Research Center, Institute of Biochemistry and Molecular Biology, Justus-Liebig-University Giessen

[c] Institute for Genetics, Technical University Dresden

[d] Biomedical Research Center Seltersberg, Institute of Parasitology, Justus-Liebig-University Giessen

Table 2.10: Cloned recombinant plasmids

Name (clone number)	Insert (bases)	Reference
pDrive-Sm*abl1*p1 (133)	Sm*abl1* part1 (1 - 2,407)	this work
pDrive-Sm*abl1*p2 (159)	Sm*abl1* part2 (2,391 - 5,169)	this work
pDrive-Sm*abl1*D (232)	Sm*abl1* fragment 2 (1,366 - 3,945)	this work
pDrive-Sm*abl1*E (228)	Sm*abl1* fragment 3 (3,032 - 5,169)	this work
pDrive-Sm*abl2*p1 (145)	Sm*abl2* part1 (1 - 2,062)	this work
pDrive-Sm*abl2*p2 (155)	Sm*abl2* part2 (2,050 - 3,927)	this work
pDrive-Sm*abl2*A (211)	Sm*abl2* fragment 2 (2,050 - 3,454)	this work
pDrive-Sm*abl2*B (215)	Sm*abl2* fragment 3 (2,357 - 3,927)	this work
pDrive-Sm*tk6* (158)	Sm*tk6* full-length	this work
pET30+ 022[a]	Sm*aldh2* full-length	A. Blohm[c]
pET30+ 050[b]	Sm*aldh1* full-length	A. Blohm[c]
pET30a-Sm*abl1* (437)	Sm*abl1* full-length	this work
pET30a-Sm*abl1*-TKD (615)	Sm*abl1* TKD (1,312 - 2,106)	this work
pET30a-Sm*abl2* (444)	Sm*abl1* full-length	this work
pET30a-Sm*abl2*-TKD (612)	Sm*abl1* TKD (828 - 1,614)	this work
pET30a-Sm*tk6* (464)	Sm*tk6* full-length	this work
pMal-c5X-Sm*aldh1* (531)	Sm*aldh1* full-length	this work
pMal-c5X-Sm*aldh2* (476)	Sm*aldh2* full-length	this work
pMal-c5X-Sm*tk6* (515)	Sm*tk6* full-length	this work
pTT22SSP4-Sm*abl1* (640)	Sm*abl1* full-length	this work
pTT22SSP4-Sm*abl2* (636)	Sm*abl2* full-length	this work
pTT28-Sm*abl1*-TKD (643)	Sm*abl1* TKD (1,312 - 2,106)	this work
pTT28-Sm*abl2*-TKD (698)	Sm*abl2* TKD (828 - 1,614)	this work
pJC53.2-Sm*aldh1*-3'UTR (766)	Sm*aldh1* coding sequence and 3' UTR (1,411 - 1,583)	this work
pJC53.2-Sm*aldh2* (540)	part of Sm*aldh2* coding sequence (1,103 - 1,531)	this work

[a] renamed as pET30a-Sm*aldh2*

[b] renamed as pET30a-Sm*aldh1*

[c] former group member of Prof. C. G. Grevelding, Justus-Liebig-University Giessen

2.10 Cells

Cells used in this work are listed in **Table 2.11**. For cloning purposes, *Escherichia coli* (*E. coli*, Theodor Escherich, 1919) strain DH5α was preferred due to its high plasmid-DNA yield (Taylor *et al.*, 1993). *E. coli* strains BL21(DE) pLysS and LOBSTR-RIL will be referred to as *E. coli* pLysS and *E. coli* LOBSTR-RIL.

Table 2.11: Cells

Cells	Properties	Reference
HEK293-6E (EBNA1)	Cell line for enhanced protein expression, transfected with EBNA1t (with deleted region 101-324 = EBNA1t)	Medical Research Council (Canada)
E. coli DH5α	Cell strain used for cloning, dlacZ ΔM15 Δ(lacZYA-argF) U169 recA1 endA1 hsdR17(rK$^-$mK$^+$) supE44 thi-1 gyrA96 relA1	Thermo Fisher Scientific, (Chen *et al.*, 2018)
E. coli BL21(DE3) pLysS	Cell strain used for tight control of protein expression, F– *ompT hsdSB*(r$_B^-$ m$_B^-$) *dcm gal* λ(DE3) cam^R pLysS	Promega (Studier and Moffatt, 1986)
E. coli BL21(DE3) LOBSTR-RIL	Cell strain used for enhanced protein expression, *fhuA2* [*lon*] *ompT gal* [*dcm*] Δ*hsdS* Δ*ArnA* Δ*SlyD* cam^R extra copies of *argU*, *ileY*, and *leuW* t-RNA genes	KeraFast (Anderson *et al.*, 2013)

2.11 Primers

All used primers were synthesized by Integrated DNA Technologies (IDT) (Leuven, Belgium) and listed in the following tables. Primers for cloning and sequencing purposes, with the aim for protein expression are listed in **Table 2.12**, with the aim to generate riboprobe templates for WISH - **Table 2.13**, to analyze gene transcript regulation - **Table**

2.14 and for dsRNA synthesis - **Table 2.15**. A list of all used gene identifiers (Smp numbers) is provided in **Table A.1** (see appendix).

Table 2.12: Primers for cloning and sequencing

Primer	Sequence 5' → 3'
Sm*aldh1*: cloning	
#190	CAA TAA CAA CAA CCT CGG GAT CGA GGG AAG GAT GAC GAA GAC ATA TCG TCT TCC C
#191	GAC GAT ATC GCG GCC GCC TCA GTG GTG GTG GTG GTG GTG AGA GTT CTT TACT GAA ATT GG
Sm*aldh1*: sequencing	
AB33	ACC CAG CGC ATA AAC ATG GA
AB34	CCA GCC ACA CAA CAT TGT CC
AB35	ATG TGT GGC ATT TGC ACG TT
Sm*aldh2*: cloning	
#148	CAA CAA CCT CGG GAT CGA GGG AAG GAT GGT CTT CCT GTA TTC TG
#149	CCC ATG GAC ATA TGT TAA TGG TGA TGG TGA TGG TGT GAA TTC TTC TGA AGT ATC C
Sm*aldh2*: sequencing	
#154	CTG CTG TCT TCA TTA CCA CTG
#155	TTT GTG GAC AAA TTA TAC CG
#156	ATA TTT GGA CCT GTA ATG C
Sm*abl1*: cloning	
#31	ATG GGA GGA TAT AAT AGT AAA CTG AC
#32	TCG GTC GAC TTG ATT CAG TTG C
#33	GAA TCA AGT CGA CCG AAT CCA G
#34	TTG CTA GCT TAA ACT TTG CCA AAT AC
#82	TTA AAC TTT GCC AAA TAC ATG AGT GG
#91	GTT TAA CTT TAA GAA GGA GAT ATA CAT ATG GGA GGA TAT AAT AGT AAA CTG
#92	GTG GTG GTG GTG CTC GAG TGC GGC CGC TCA GTG GTG GTG GTG GTG GTG AAC TTT GCC AAA TAC ATG AGT GG

Continued on the next page

Table 2.12 – *Continued from previous page*

Primer	Sequence 5' → 3'
#95	GAT GCC CAG AAG CAG TTT ATT C
#96	GTG CCT CCC CCA CCT CAT TCA TC
#215	ATG TGG GAA ATT GAT AGG TCC
#216	ATA CAT TTG TTC CAG TTC CGC ATG
#217	CTT TAA GAA GGA GAT ATA CAT ATG TGG GAA ATT GAT AGG TCC
#218	GGT GCT CGA GTG CGG CCT TAA TGA TGA TGA TGA TGG TGA TAC ATT TGT TCC AGT TCC
#241	TGG GAA ATT GAT AGG TCC GAA AT
#246	TCA GCT GAG TCT TGG AAT TGC CTG GGA AAT TGA TAG GTC CGA AAT
#247	TCA CCC GTG GTG GTG ATG GTG GTG ATG GTG ATA CAT TTG TTC CAG TTC CGC
#248	ACC GGT GCT GGA TCC GGA GCT AGT CAC CCG TGG TGG TGA TGG TGG
#251	GAA CCT GTA CTT TCA GGG CGC TAT GGG AGG ATA TAA TAG TAA ACT G
#252	TCG AGG TCG GGG GAT CTC AGT GGT GGT GGT GGT GGT GAA CTT TGC CAA ATA CAT G

Sm*abl1*: sequencing

#47	CAG CTT GTC TTG AGA CAG CAC
#48	CGT ATC AAA TAA GGG CCC TG
#49	CAT TCA GAT TAA CAT CTT GTT TCA G
#50[a]	TAT GGT GAT GTA TAT GAA GCT G
#51[a]	GAA TAA ACT GCT TCT GGG CAT C
#52	CCT GGA GTT GAA TTG CAT GAT G
#53	GGA ATT TTA GAA ACT ATG GAA GCT GG
#54[a]	CAT CTT ATC AAC CGA ATT CAC AC
#55[a]	GAT GAA TGA GGT GGG GGA GG
#56	CAT TTA CTT ATC ACC AAT CAC AAC C
#57	CAT CAT CTC CTT CAC CAC CAC
#58	ATC CAT CGC GTC TGA CTC TC

Continued on the next page

Table 2.12 – *Continued from previous page*

Primer	Sequence 5' → 3'
Sm*abl2*: cloning	
#7	CAG TGC CAT CAG TTA TGA GTA G
#25	ATG GGC GCA CAA CAC ACA AAG
#26	TGG CAG ATC TTT TTC AGC AGT AC
#27	AAA GAT CTG CCA TTT ACA AAC TCA GGA TCT
#28	TTG CGG CCG CTC AAG TGA AAA CTG
#83	TCA AGT GAA AAC TGT AGC GCT TC
#93	GTT TAA CTT TAA GAA GGA GAT ATA CAT ATG GGC GCA CAA CAC ACA AAG G
#97	AGA TCC TGA GTT TGT AAA TGG CAG ATC TTT TTC AGC AGT AC
#98	CAG TGC CAT CAG TTA TGA GTA G
#99	CTA CTC ATA ACT GAT GGC ACT G
#94	GTG GTG GTG GTG CTC GAG TGC GGC CGC TCA GTG GTG GTG GTG GTG GTG AGT GAA AAC TGT AGC
#211	GAG ATA GAT CGA ACC GAA ATA GTT AT
#212	CAT AGA TTC CAA TTG ATT CAA TAT ATC AG
#213	CTT TAA GAA GGA GAT ATA CAT ATG GAG ATA GAT CGA ACC GA
#214	GGT GCT CGA GTG CGG CCT TAA TGA TGA TGA TGA TGG TGC ATA GAT CCA ATT GAT TC
#248	ACC GGT GCT GGA TCC GGA GCT AGT CAC CCG TGG TGG TGA TGG TGG
#249	TCA GCT GAG TCT TGG AAT TGC CGA GAT AGA TCG AAC CGA AAT AG
#250	TCA CCC GTG GTG GTG ATG GTG GTG ATG GTG CAT AGA TTC CAA TTG ATT C
#253	GAG AAC CTG TAC TTT CAG GGC GCC ATG GGC GCA CAA CAC ACA AAG G
#254	GGT CGA GGT CGG GGG ATC TCA GTG GTG GTG GTG GTG GTG AGT GAA AAC TGT AGC GCT TC

Continued on the next page

Table 2.12 – *Continued from previous page*

Primer	Sequence 5' → 3'
Sm*abl2*: sequencing	
#59	ATG TAC AAG GTC AGA GAC TGA TG
#60	CGT TAT GAA GGA CAG ATT TGG C
#61	GTT CAT AAA CTG GTT CAG GGC
#62	TGC AAC CTA TGG GAA AAC ACC
#63	TGT AAT CGG TTT CTG CTG AGA TG
#64	CTA AGC CAA ATG TTC ATC CTA CC
#65[a]	AGC GGA GGA AGG AGA GGA AG
#66	GTG TTC CAC CAA CAA AAT ACC AC
Sm*tk6*: cloning	
#38	ATG GGA ATT TGT TTG TGT CTT CAA AGG
#38	CTA ATT ATC TAA ATA TTG AGC TTC TGT G
#104	GTT TAA CTT TAA GAA GGA GAT ATA CAT ATG GGA ATT TGT TTG TGT CTT CAA AGG
#105	GTG CTC GAG TGC GGC CGC TCA GTG GTG GTG GTG GTG GTG ATT ATC TAA ATA TTG AGC TTC
Sm*tk6*: sequencing	
#43	CGG AGT CAT AAT GTC GAA CAG
#44	GGA ACA TAC CTT ATT AGA CC
#45	CAC CGA GAT TTA CGC GCA G
#46	ATG GCA CAG ATT GCT AGT GG

Primers provided by **AB:** A. Blohm (a former group member)

[a] also used for cloning

Table 2.13: **Primers to clone sequences and generate riboprobe templates for WISH**

Primer	Sequence 5'→3'	Product length
Sm*aldh1*-3' UTR		
#360	GAA GCA CTG GAT GGG TAC TTA C	173
#361	ACT TAT GCA ATA TAT TTA CTA CTG ACG	

Continued on the next page

Table 2.13 – *Continued from previous page*

Primer	Sequence 5'→3'	Product length
#396	CTA AAG GGA GAC CGA AGC ACT GGA T	203
#397	CTA TAG AAG TGA CCT TAC TTA TGC AAT ATA TTT ACT	
Sm*aldh2*		
#128	GTC CAC AAG TTG ATG AAC ACC	472
#129	TTC TTC TGA AGT ATC CGT GTG G	
T7_ex-tended[a]	CCT AAT ACG ACT CAC TAT AGG GAG	

[a] Primer provided by Collins Lab

Table 2.14: Primers to analyze gene expression

Primer	Sequence 5' → 3'
Sm*abl1*	
#266	CTG GTA TGG CGT ATT TAG AAG C
#267	GGG AAT TTA GCA CCA TTA CGA G
Sm*abl2*	
#296	CGA ATG CTT TGT CCT GAA GGT T
#297	TCT TCC ATT GTA GAA TTA GTT GGC
Sm*aldh1*	
#270	TAT CTC ATT CAC CGG GAG TAC
#271	CTT CAT GAG CAA CTT CTG AAG C
Sm*aldh2*	
#284	AAT CAA AGA AGC CGG ATT CCC A
#285	ACC AAT CAA TCG TCC AAC AGC T
Sm*ar*	
#306	TGG CTG TGA AGA AAG CTC TAG
#307	AGG GCG GAA AAA AGT ATT CCAC

Continued on the next page

Table 2.14 – *Continued from previous page*

Primer	Sequence 5' → 3'
Sm*bax*	
SiH234	CAA GCT CTA ATT GGT CGT CTT ATA
SiH235	ATG AAC AAT ACC ACA ATT CGT GAC
Sm*bcl-2*	
SiH236	TCT TCA TGA TGG TTG GTC TGG A
SiH237	CCG ACA AGA GCA GCT AAA CC
Sm*gpx*	
#162	GAA GTT CGT GAC TGA GAA GTA C
#163	GGT TGT CCT TGA CGA TCT ACA
Sm*letm1*	
SiH192	CGT GGA ATG CGT TCA GTT GG
SiH193	GAA GCT GAT GGA GGT AAT TGAG
Sm*nanos1*	
SiH72	ACT TGT CCA TTA TGC GGT GCT
SiH73	GGT TCC AAC AAA CCA GCT TCA
Sm*nanos2*	
JK17	GCC GTG TTA TGA CCT CTG G
JK18	GAC GAT CTG GAG ACT CTG G
Sm*npl4*	
#188	GAG AAT CGT GAG TGT TTA GGT C
#189	GAT CTT CAT TTA ATT TAC CTT CAG AG
Sm*p53*	
SiH326	ACC GAA AAA GCT ATA CAC CGA C
SiH327	CTT AGC ATA CAA ATT TGT CCA TCC
Sm*sod*	
SiH49	TCG TCA TGT TGG TGA CCT GG
SiH50	GCC TAA ATC ATC TTC ATT TTC ATG G
Sm*sodex*	
SiH53	GAT CTG TGT CAG GTT TGC CG
SiH55	ATG TTG ACC CAC ATA ATG ATT TCC

Table 2.14 – *Continued from previous page*

Primer	Sequence 5' → 3'
Sm*tk6*	
#311	ACA TAC CTT ATT AGA CCT AGT TCG
#312	TTC GGG AAG GTC GTG CGA AT

Primers provided by **JK:** M. Sc. J. Kellershohn (a former group member), **SiH:** PD S. Häberlein, Institute of Parasitology, Justus-Liebig-University Giessen

Table 2.15: Primers for dsRNA synthesis

Primer	Sequence 5'→3'
Sm*aldh1*	
#122	TAA TAC GAC TCA CTA TAG GGA GAT ATC TGA TAC TAT ACA AGT CCA C
#123	TAA TAC GAC TCA CTA TAG GGA GAT CGT TTG TAA GTA CCC ATC CAG
Sm*aldh2*	
#124	TAA TAC GAC TCA CTA TAG GGA GAG TCC ACA AGT TGA TGA ACA CC
#125	TAA TAC GAC TCA CTA TAG GGA GAT TCT TCT GAA GTA TCC GTG TGG
Sm*abl1*	
#136	TAA TAC GAC TCA CTA TAG GGA GAA ACA ATT CTC TAC AAT ACC ACC TC
#138	TAA TAC GAC TCA CTA TAG GGA GAT ATC TGT TAT TGC TTT TGA ATG GAA G
Sm*abl2*	
#139	TAA TAC GAC TCA CTA TAG GGA GAG TAC TGA TGA GTT TGG TAC TGC
#141	TAA TAC GAC TCA CTA TAG GGA GAG GAC AAA TTG ATC TGG TCA GG

Continued on the next page

Table 2.15 – *Continued from previous page*

Primer	Sequence 5'→3'
Sm*tk6*	
#133	TAA TAC GAC TCA CTA TAG GGA GAG AAT GGT TCA GTT GAA GTA GCA G
#135	TAA TAC GAC TCA CTA TAG GGA GAA CCA AAC GAC CAT ACA TCA GAC

3 Methods

3.1 Databases and software

Databases and online software tools used in this work are listed in **Table 3.1**, and used software in **Table 3.2**. The sequence alignments presented in this thesis were created with TEXShade for LaTeX (Beitz, 2000).

Table 3.1: Databases and online software tools

Software URL

Analyses of RNA sequences for WISH probes

http://rna.tbi.univie.ac.at/cgi-bin/RNAWebSuite/RNAfold.cgi (RNAfold webserver; structural RNA analyses; Zuker and Stiegler, 1981)

Codon usage analyses

http://gcua.schoedl.de/ (Graphical Codon Usage Analyser)

Primer analyses

http://biotools.nubic.northwestern.edu/OligoCalc.html (Oligo Calc; primer temperature adjustment; Kibbe *et al*., 2007)

https://eu.idtdna.com/pages (OligoAnalyzer tool; structural primer analyses; IDT)

Post-translational modification (PTM) prediction analyses

http://pail.biocuckoo.org/online.php (GPS-PAIL; acetylation; Li *et al*., 2006)

https://web.expasy.org/myristoylator/ (Myristoylator; myristoylation; Bologna *et al*., 2004)

http://www.csspalm.biocuckoo.org/online.php (CSS-Palm; palmitoylation; Ren *et al*., 2008)

Continued on the next page

Table 3.1 – *Continued from previous page*

Software URL

http://gps.biocuckoo.cn/online.php (GPS; phosphorylation; Wang *et al.*, 2020)

Protein sequences and analyses

https://www.uniprot.org/ (UniProt; The Uniprot Consortium, 2021)

https://www.ncbi.nlm.nih.gov/Structure/cdd/wrpsb.cgi (Conserved domain database (CDD); Lu *et al.*, 2020)

https://blast.ncbi.nlm.nih.gov/Blast.cgi?PAGE=Proteins (Basic local alignment search tool - protein (blastp); Altschul *et al.*, 1990)

***Schistosoma* single-cell transcriptome atlas**

www.collinslab.org/schistocyte/ (Transcript distribution in *S. mansoni*; Wendt *et al.*, 2020)

***Schistosoma* genome analyses**

https://www.ncbi.nlm.nih.gov/nucleotide/ (NCBI nucleotide; Benson *et al.*, 2013)

https://parasite.wormbase.org/Schistosoma_mansoni_prjea36577/Info/Index (WormBase ParaSite; Howe *et al.*, 2016, 2017)

www.schisto.xyz/ (*S. mansoni* gene expression atlas; Lu *et al.*, 2016, 2017)

Sequence alignment

www.ebi.ac.uk/Tools/msa/clustalo/ (Clustal Ω; Sievers and Higgins, 2018)

Table 3.2: Software

Name	Reference
DNA sequence analysis	
A Plasmid Editor (ApE) v3.0.3	Davis and Jorgensen, 2022
Gel documentation	
GelDoc System v.0.2.18	INTAS Science Imaging Instruments
ChemiDoc MP	Bio-Rad

Continued on the next page

Table 3.2 – *Continued from previous page*

Software	Reference
Microscopy	
Leica Application Suite Advanced Fluorescence v2.7.3.9723	Leica Microsystems
Leica Application Suit X v3.7.3.23245	Leica Microsystems
DSM 982 Operating Software v2.3s	Carl Zeiss Microscopy
Pedigree analysis	
MEGA v10.2.5	Kumar *et al.*, 2018
Picture editing	
DOG v2.0	Ren *et al.*, 2009
InkScape v1.02	Free Software Foundation
qRT-PCR	
Q-Rex v1.0.2	Qiagen
Q-Rex Gene expression Plugin v2.0.0.4	Qiagen
RNA analysis	
Bioanalyzer vC.01.069	Agilent Technologies
Statistical analysis	
GraphPad Prism v8	GraphPad Software

3.2 Phylogenetic and protein analysis

For phylogenetic analysis of Smp_022960 (SmAldh2) and Smp_312440 (SmAldh1), Aldh aa sequences of various species (**Table 3.3**) were used. Pedigree analysis was done using the program MEGA X (**Table 3.2**). The parameters were set for the Maximum Likelihood method using the Dayhoff matrix-based model (Schwarz and Dayhoff, 1979). Initial trees for the heuristic search were obtained automatically by applying Neighbor-Join and BioNJ algorithms to a matrix of pairwise distances estimated using the Dayhoff model, and then selecting the topology with superior log likelihood value. The tree with the highest log likelihood (-12163.28) was selected. There were a total of 538 positions in the final data set. The tree was drawn to scale, with branch lengths measured in

the number of substitutions per site. Aa sequences of SmAldh1, SmAldh2, SmAbl1, SmAbl2, and SmTK6 were analyzed for their occurring domains using the CDD (**Table 3.1**) and visualized with the programs DOG v2.0 and InkScape v1.02 (**Table 3.2**). PTMs (acetylation, myristoylation, palmitoylation, and phosphorylation) were predicted using the online tools summarized in **Table 3.1**.

Table 3.3: Aldh proteins used for pedigree analysis

Species	Protein	UniProt identifier
Arabidopsis thaliana (*A. thaliana*, At)	AtAldh1A1	Q56YU0
Caenorhabditis elegans (*C. elegans*, Ce)	CeAldh1A	Q8IG19
	CeAldh1B	Q20780
	CeAldh2	Q9TXM0
Clonorchis sinensis (*C. sinensis*, Cs)	CsAldh1A1	A0A419Q324
	CsAldh2	A0A419PBV4
Danio rerio (*D. rerio*, Dr)	DrAldh1A	Q90Y03
	DrAldh2	Q8QGQ2
Drosophila melanogaster (*D. melanogaster*, Dm)	DmAldh1M1	Q9VB96
	DmAldh1A10	Q9VLC5
Fasciola hepatica (*F. hepatica*, Fh)	FhAldh1	maker-scaffold10x_208_ pilon-snap-gene-0.16[a]
	FhAldh2	maker-scaffold10x_80_ pilon-snap-gene-0.189[a]
Homo sapiens (*H. sapiens*, Hs)	HsAldh1A1	P00352
	HsAldh1A2	O94788
	HsAldh1A3	P47895
	HsAldh1B1	P30837
	HsAldh2	P05091
Mus musculus (*M. musculus*, Mm)	MmAldh1A1	P24549
	MmAldh2	P47738
Rattus norvegicus (*R. norvegicus*, Rn)	RnAldh1A1	P51647
	RnAldh2	P11884
S. mansoni	Smp_022960	sequenced in this work
	Smp_312440	sequenced in this work

Continued on the next page

Table 3.3 – *Continued from previous page*

Species	Protein	UniProt identifier
Schmidtea mediterranea (*S. mediterranea*, Smed)	SmedAldh2-like	A0A5P8I4K9

[a] WormBase ParaSite identifier

3.3 Statistical analysis and image processing

Statistical analyses were conducted in GraphPad Prism v8 (**Table 3.2**) using a paired t-test with 95 % confidence level with two-tailed p-value, where $p < 0.05$ was represented by (*), $p < 0.01$ was represented by (**), and $p < 0.001$ was represented by (***). Physiological parameteres were analyzed using treatment vs control groups. Analyses of qRT-PCRs was done using treatment vs control groups, where control levels were set as 1. Graphs were created in GraphPad Prism v8, too, showing individual values and means as bars with standard error of mean (StEM). Graphs were exported from GraphPad Prism v8 as enhanced metafiles and arranged using InkScape v1.02 (**Table 3.2**). Illustrations of protein domains were created using DOG v2.0 (**Table 3.2**) and exported as vector images. Images obtained by CLSM and bright field microscopy were also compiled using InkScape v1.02. Images obtained by SEM were edited in InkScape v1.02 by removing backgrounds as follows: areas representing worms were outlined with the Bézier Curve tool, then cut out and placed on a neutral background.

3.4 Maintenance of a laboratory cycle of *S. mansoni*

The institute of parasitology (Prof. C. G. Grevelding) has established the life cycle of the parasite *S. mansoni* (Liberian strain isolate obtained from Bayer AG (Monheim) (Gönnert 1955; Grevelding 1995). Schistosome species possess a heteroxenic life cycle. In the laboratory, as intermediate host the snail *B. glabrata* (Thomas Say, 1818; Mitta *et al.*, 2012) was used to provide the infectious stages (cercariae) for the final host, the Syrian golden hamster (*Mesocricetus auratus* (*M. auratus*), George R. Waterhouse,

1839). Livers of infected hamsters were used for extraction of eggs and hatching of miracidia, the infectious stage for the intermediate host. After infection, the snails excreted cercariae, which were used for infection of the hamsters to generate schistosomes. The animal experiments were performed in accordance with the European Convention for the Protection of Vertebrate Animals used for Experimental and other Scientific Purposes (ETS number 123; revised appendix A) and approved by the regional council (Regierungspräsidium Giessen, V54-19 c 20 - 15 h 02 GI18/10 Nr. A 26/2018).

3.4.1 Husbandry of *B. glabrata*

Snail hosts were kept in aquaria with a mixture of commercially available water (Rossbacher) and autoclaved tap water (2:1) in climate chambers at 26 °C. In the aquaria, areas for young snails were separated using nets. They were fed with cucumber and fish food (Tetramin flakes, once a week). The snails were exposed to a day/night rhythm with 16 hours (h) of light and 8 h of darkness. At a size of 6 mm they were infected with miracidia.

3.4.2 Infection of *B. glabrata* with miracidia

Single snails were transferred into a 12-well plate filled with 2 ml snail water containing $10 - 15$ miracidia (bi sex (bs) infection) or a single miracidium (single sex (ss) infection). After 12 h incubation, they were placed in separated aquaria and kept as previously described (see section 3.4.1). After 21 d, snails were transferred into a dark incubation chamber to avoid early release of cercariae. After additional 7 - 14 d, snails were illuminated to induce cercarial shedding and to collect cercariae.

3.4.3 Isolation of cercariae

Infected snails were transferred into wells of a 12-well plate filled with 2 ml snail water and exposed to light. Since cercariae are positive phototactic, they migrate towards the light stimulus. After 2 - 3 h, the number of cercariae was determined and cercariae used

for infection of the final host. To determine the gender of released cercariae, a PCR targeting the W1 region was performed (Grevelding *et al.*, 1997).

3.4.4 Infection of *M. auratus* with cercariae

Animals were either purchased from Janvier Labs (Le Genest-Saint-Isle, France) or provided by the central animal breeding facility (Zentrale Versuchstierhaltung, Justus-Liebig-University Giessen). Hamsters (6 - 8 week old) were bathed in 37 °C warm snail water for 45 minutes (min) to soften their skin for a higher infection efficiency (Dettman *et al.*, 1989). Afterwards, the water was renewed and 1,750 cercariae of mixed or 2,500 cercariae of only one gender added. After 45 min incubation in the infectious water, hamsters were transferred to their cages and held for 46 d (bs infection) or 67 d (ss infection) before perfusion was performed.

3.4.5 Recovery of *S. mansoni* from the final host

Animals were anesthetized with isoflurane in a glass chamber before a mixture of xylazine and ketamine was injected intraperitoneally for further anesthesia and muscle relaxation. After 5 min incubation time, hamsters were sprayed with 70 % ethanol for decontamination before the abdomen was opened. The perfusion procedure was modified after Duvall and DeWitt (1967) and Smithers and Terry (1965). The portal vein of vertically fixed hamsters was opened with a cannula. Afterwards, the left ventricle was pierced and 37 °C pre-warmed perfusion medium was pumped trough a tube into the body. Worms were flushed out of the portal vein and collected on a gaze-net before they were transferred with a fine brush into 6 cm petri dishes with pre-warmed medium. Afterwards, they were sorted by their pairing status (couples, single males or females) into 3 cm petri dishes with pre-warmed medium.

3.4.6 Isolation of miracidia

To obtain miracidia, livers of hamsters were collected after worm recovery and homogenized in PBS. The mixture was centrifuged at 400 xg for 5 min and 4 °C. The resulting pellet was washed twice with 0.9 % NaCl, resuspended in warm snail water, and transferred into a flask with side arm. The flask was filled with tap water to the brim, covered with a wooden box to expose only the side arm to light. Miracidia hatched from eggs and accumulated in the light-exposed region from were they were collected to infect the intermediate host.

3.5 *In vitro* culture of *S. mansoni*

Worms recovered from hamsters were cultured in 5 ml medium per 3 cm petri dish in an incubator at 37 °C and 5 % CO_2. For RNA isolation and fixation for WISH, worms were used the same day as they were recovered. *In vitro* experiments were started one day after perfusion to assure adaption of the worms to the medium and cultivation conditions.

3.5.1 Scoring of *S. mansoni*

To determine the viability of schistosomes following dsRNA or substance treatments, worm motility was scored with values ranging from 0 - 4 (0 represents the total absence of movement, 1 represents only gut movements or occasional movements of head and tail, 2 represents reduced motility, 3 represents normal activity, and 4 represents hyper activity). This scoring system was modified after Ramirez *et al.* (2007). Furthermore, the attachment of worms to the petri dish, the pairing status (either coupled or separated), and oviposition were determined next to morphological changes. Worms were scored with an inverse laboratory microscope (**Table 2.1**).

3.5.2 dsRNA treatment of *S. mansoni*

For *in vitro* experiments, worms were kept one day in the 3 cm petri dish to adapt to *in vitro* culture conditions before they were transferred into 6-well plates filled with pre-warmed 5 ml M199 (3+). Ten couples were transferred into each well and the respective dsRNA added. For knock down approaches, gene-specific dsRNA ranging from 450 - 500 nucleotides (nt) was synthesized (see section 3.10) and $2.5\,\text{mg}\,\text{ml}^{-1}$ or $12.5\,\text{mg}\,\text{ml}^{-1}$ applied while DEPC-water served as a control. The duration for dsRNA applications was 2 - 3 weeks. Depending on the length of the experiment, worms were scored daily or every 3 d. After scoring, worms were transferred into wells containing fresh medium and dsRNA.

3.5.3 Substance treatment of *S. mansoni*

The experimental setup was essentially as described in the previous section (see section 3.5.2). As controls served the solvents for substances, either water or DMSO (0.2 % final concentration). Substances were prepared as stocks for addition of 10 µl to assure a 0.2 % final DMSO concentration in 5 ml M199 (3+). Treatment was done at the beginning of the experiment, and scoring of worms was done every 24 h for up to 3 d. The duration for substance treatments was 3 d.

3.5.4 Separation of *S. mansoni* couples

For all the following analyses of worms (microscopy, RNA isolation), couples were separated. Therefore, tricaine (0.25 % (w/v)) was added to each well, and the plate incubated at 130 revolutions per minute (rpm) for 3 minutes (min) until the couples were separated. Males and females were collected into 1.5 - 2 ml reaction tubes and washed with PBS. The supernatant was discarded and worms fixed or frozen in protection buffer for RNA isolation.

3.6 Staining methods

3.6.1 Carmine red staining of *S. mansoni*

Carmine red staining was performed as described by Beckmann *et al.* (2010), in accordance to Neves *et al.* (2005).

Preparation of the carmine red solution

Carmine red powder was pounded with a pestle in a mortar and transferred into a beaker with 90 % ethanol. Remaining powder was rinsed with 90 % ethanol. The mixture was placed on a magnetic stirrer, where it was heated to 90 °C and dissolved while continuous stirring for about 1 h. At the end, the solution was filtered and the volume adjusted with 90 % ethanol.

Fixation of samples and staining with carmine red

The worm samples were transferred into 1.5 ml tubes, and the medium was discarded before AFA solution was added. The samples were fixed at RT over night and stored at 4 °C until use. For staining, worms were transferred into a netwell insert for 12-well plates and carmine red solution added. After 30 min incubation, they were destained in acidic ethanol for 5 - 10 min. Afterwards, they were dehydrated in an ascending ethanol series (80 %, 90 %, and 100 %) for 5 min each. The worms were transferred to slides and fixed in Canada balsam (2:1 in xylol diluted). For microscopy, a CLSM (**Table 2.1**) was used. The samples were excited with an argon laser at 488 nm, while pictures were taken with a resolution of 1024 x 1024, a pinhole of 1 airy unit, and a line average of 4 - 8. In all CLSM analysis, about 10 worms of each sex were imaged.

3.6.2 Preparation of *S. mansoni* for SEM

Couples were separated as described in section 3.5.4 and fixed in 2 ml fixing solution I at 4 °C and 130 rpm for 24 h. The samples were stored at 4 °C in 0.1 % PFA in cacodylate buffer until further use.

Samples were incubated in fixing solution II for 1 h at RT followed by a 5 min washing step with 0.1 M cacodylate buffer. Afterwards, samples were placed on a molecular sieve, transferred into a small metal tube, and washed twice for 20 min with ultra-pure water at 130 rpm on ice. For dehydration of the samples, they were incubated in an ascending ethanol series (30 %, 50 %, 70 %) each 20 min shaking on ice and stored at 4 °C over night. The next day, dehydration continued in 80 %, 90 %, 96 %, 99.8 %, and 100 % ethanol for each 30 min shaking on ice.

The vessels with the samples were transferred into a critical point dryer and cooled to 4 °C. Thereafter, the chamber was filled several times with CO_2 to displace the ethanol. Eventually, the temperature was raised to the critical point to convert CO_2 into the gaseous phase. Dried samples were transferred to small pen sample plates, which were previously coated with conductive carbon adhesive pads. Afterwards, the samples were transferred into the sputter system and argon gas was introduced. The pressure was lowered to 5×10^{-2} bar, and samples were covered with a thin layer of gold (2 - 10 nm) at 25 mA for 30 seconds (s). The prepared samples (10 females and males) were stored at RT in a desiccator until microscopy. The used settings for microscopy are listed in **Table 3.4**.

Table 3.4: Settings for SEM

Parameter	Value
Aperture	3
Working distance	$3 - 4$ mm
Resolution	1024 x 1024
Scanning speed	4
Voltage	3 kV
Magnification	50 - 5000 x

3.6.3 Staining of proliferating cells with EdU

To perform an EdU-assay, the Click-iT plus EdU Cell Proliferation Kit for Imaging (Invitrogen) was used. EdU was added to a well 24 h before fixation of worms. The couples (10 per condition) were separated (see section 3.5.4) and transferred into 2 ml tubes. The supernatant was removed and 4 % PFA in PBSTx added before incubation at RT over night. The next day, worms were washed with PBSTx for 3 min and dehydrated in 50 % methanol in PBSTx for 10 min followed by incubation in 100 % methanol for 10 min. For storage, fresh 100 % methanol was added and samples stored at −20 °C until further use.

To rehydrate and permeabilize the worms, all steps were carried out in 500 µl at RT and 130 rpm if not stated otherwise. Samples were transferred into small incubation baskets and placed into a well of a 48-well plate. Samples were rehydrated by incubation in 50 % methanol in PBSTx for 10 min, followed by an other incubation step in PBSTx for 10 min. To permeabilize for staining, worms were incubated with proteinase K for 30 min. Afterwards, an additional fixing step with 4 % PFA in PBSTx followed for 10 min. Eventually, worms were washed twice with PBSTx for 5 min.

Click-iT reaction and Hoechst 33342 staining

The following steps were performed in the absence of light in 500 µl at RT and 130 rpm. For each sample, one Click-iT reaction was prepared freshly according to the manufacturer's protocol and 500 µl added before incubation for 30 min. To remove the solution, samples were washed in PBS twice before total DNA was stained with Hoechst33342.

To stain total DNA, Hoechst 33342 (diluted 1:1000 in PBSTx) was added and samples were incubated at 4 °C and 80 rpm over night. The next day, Hoechst staining solution was removed and samples were washed twice in PBS before the worms were fixed in FluorCare on a slide. The cover glass was fixed with translucent nail polish and the slide stored protected from light at 4 °C until microscopy.

3.6.4 WISH

The protocol for WISH was modified after Collins and Collins (2017), based on King and Newmark (2013) and Pearson *et al.* (2009).

Yeast t-RNA clean up for *in situ* solutions

Yeast t-RNA was gradually poured into 600 ml DEPC-water and mixed. Over 2 - 3 d, the yeast t-RNA was dissolved at 55 °C with continuous stirring until the solution cleared. The solution was evenly distributed among 6 centrifuge bottles (250 ml each) and the same volume phenol added. Afterwards, the mixture was centrifuged at 4,750 rpm and 4 °C for 10 min. The cloudy, upper phase was carefully transferred into 50 ml canonical tubes, the rest discarded and the bottles rinsed with DEPC-water, before the solution was transferred back into the bottles. The same volume of phenol/chloroform/isoamyl alcohol was added and centrifuged as before. Again, the upper clear to slightly brown phase was transferred into new 50 ml canonical tubes, the bottles rinsed and the solution transferred back into the bottles. The same volume of chloroform was added, mixed and centrifuged as before. The clear phase was transferred into 50 ml canonical tubes and could be stored at 4 °C if required.

The cleared yeast t-RNA was quantified before evenly distribution among 50 ml canonical tubes. To precipitate, 2.5 times the volume of 100 % ethanol and 0.1 times the volume of 3 M sodium acetate (pH 5.2) were added and mixed before the tubes were stored at −20 °C over night. The next day, the solution was centrifuged at 18,000 xg and 4 °C for 30 min. The supernatant was discarded and the pellets rinsed with 25 ml of 70 % ethanol. After 1 h incubation, the supernatant was discarded, the pellets dried and merged in 2 canonical tubes (50 ml each). They were resuspended in deionized formamide with slight agitation (100 rpm) at 52 °C for several h before merging the solution in a bottle. The t-RNA was quantified and the volume adjusted to the desired concentration with deionized formamide. Eventually, the solution was aliquoted and stored at −20 °C.

Synthesis of riboprobes for hybridization

To generate RNA probes, respective sequences were cloned into the plasmid pJC53.2 (**Table 2.9**) and subsequently amplified by PCR with T7_extended primers (**Table 3.8** and **Table 3.9 A**). The resulting PCR products were electrophoretically separated (see section 3.9) and extracted (see section 3.8.8). To remove impurities, the DNA was cleaned with ammonium acetate. Therefore, one part 7.5 M ammonium acetate and 4 parts of 100 % ethanol were added and the mixture incubated at −20 °C over night. The next day, the DNA was centrifuged at 4 °C and 18,000 xg for 30 min. The supernatant was discarded, the pellet washed with 70 % ethanol followed by centrifugation at 4 °C and 18,000 xg for 10 min. The supernatant was discarded and the pellet resuspended in DEPC-water.

In vitro transcription (**Table 3.5**) was carried out for at least 16 h at 28 °C following DNase I treatment (2 U, at 37 °C for 20 min). To precipitate the RNA, 3 µl 7.5 M LiCl and 50 µl 100 % ethanol were added and incubated at −20 °C over night. The next day, samples were centrifuged and washed as previously described and the pellet resuspended in 20 µl DEPC-water. For each riboprobe, the concentration was determined photometrically, and 100 - 200 ng of the RNA were electrophoretically separated to check the length. Subsequently, the riboprobes were stored at −80 °C until use.

Table 3.5: ***In vitro* transcription reaction mixture to generate probes for WISH**

Component	Volume
10x transcription buffer	2 µl
DIG-dNTP mix	2 µl
RNase inhibitor (40 U µl^{-1})	0.6 µl
RNA polymerase (T3 or SP6, 20 U µl^{-1})	1 µl
100 - 500 ng T7-based PCR product	x µl
DEPC-water	Add 20 µl

Fixation of *S. mansoni* for WISH

All steps were carried out at RT and 130 rpm unless stated otherwise. Couples were separated, transferred into 15 ml canonical tubes, and incubated in 10 ml 0.6 M $MgCl_2$ for 1 min. Afterwards, $MgCl_2$ was replaced with 4 % PFA in PBSTx. After 4 h incubation, worms were washed twice in 10 ml PBSTx and dehydrated in 10 ml 50 % methanol in PBSTx followed by 100 % methanol for 10 min each. Fixed worms were stored at −20 °C until use.

Hybridization

The worms were rehydrated in 50 % methanol in PBSTx and PBSTx for 10 min, respectively. Next, they were bleached under bright light for 1 h. After bleaching, they were washed twice with 10 ml PBSTx and incubated with proteinase K in PBSTx (45 µg ml^{-1} for males and 15 µg ml^{-1} for females) for 45 min. Treated worms were post fixed with 10 ml 4 % PFA in PBSTx for 15 min and washed with 50 % pre-hybridization buffer for 10 min.

The following steps were carried out in 300 µl total volume at 130 rpm and 55 °C. About 4 - 5 worms were transferred into small incubation baskets and incubated in a 48-well plate with pre-hybridization buffer for 2 h. The probe was diluted with hybridization buffer to 5 nM, heated to 78 °C and cooled to 55 °C before adding into a new well and transferring the basket into the respective well. At each basket transfer, excess liquid was removed by dripping baskets on a tissue. Hybridization was performed for at least 16 h.

Colorimetric detection of transcripts

Incubation was carried out at 55 °C and 130 rpm for 30 min unless stated otherwise. The next day, worms were washed twice with washing buffer, twice with 2x SSC/0.1 % (v/v) Triton-X100 (pH 7.0), once with 0.2x SSC/0.1 % (v/v) Triton-X100 (pH 7.0), and once with 0.1x SSC/0.1 % (v/v) Triton-X100 (pH 7.0). Afterwards, they were incubated twice for 10 min each in TNT buffer at RT before the baskets were transferred into colorimetric

blocking solution and incubated at RT for 2 h. Eventually, they were incubated in antibody solution at 4 °C over night. The next day, the worms were incubated in TNT buffer at RT (5 min, 10 min, followed by 6x 20 min each). Subsequently, they were transferred from the baskets into a well of a 24-well plate filled with 400 µl developing buffer and incubated at RT and 130 rpm until color development. Development was stopped by changing development buffer with PBSTx. After 5 min, the worms were transferred into fresh PBSTx and incubated 5 min followed by incubation in 100 % ethanol for 15 min. Ethanol was removed and a few drops PBSTx added. Three minutes later, worms were transferred into 80 % glycerol in PBS for at least 1 h. For documentation, they were embedded in 80 % glycerol in PBS on a slide and imaged with an inverse microscope (**Table 2.1**).

3.7 Working with cells

3.7.1 Preparation of agar plates

LB medium and 1.5 % agar agar were autoclaved, cooled to 40 °C, and specific antibiotics added (**Table 2.4**) to allow selection for plasmid-carrying colonies. Approximately 10 ml prepared medium were poured sterile into 10 cm petri dishes and cooled for 20 min. Prepared plates were stored up to one month at 4 °C.

3.7.2 Cultivation of *E. coli* and preparation of glycerol stocks

E. coli were cultured at 37 °C either on agar plates or in liquid LB medium with appropriate antibiotics (**Table 2.4**). For cultivation on agar plates, approximately 150 µl of a liquid *E. coli* culture were transferred onto an agar plate containing the appropriate antibiotics and distributed evenly on the plate until dry. The plate was stored up-side down in an incubator at 37 °C over night.

For a liquid culture of *E. coli*, 20 ml LB medium containing appropriate antibiotics were inoculated with a single colony-forming unit from an agar plate and incubated

at 37 °C and 170 rpm over night. Starting from this pre-culture, the main culture was inoculated to an optical density (OD_{600}) of 0.1 and cultured as before.

For long-term storage of bacteria, glycerol stocks were prepared. Therefore, 500 µl liquid culture were mixed with 500 µl glycerol and incubated at RT for 30 min before the bacteria were stored at −80 °C.

3.7.3 Generation of competent *E. coli* cells

A 100 µl aliquot of competent cells was thawed on ice. To inoculate 50 ml LB medium in a 100 ml flask, 5 µl were used. The culture was grown at 170 rpm and 37 °C over night. Pre-warmed 200 ml LB medium in a 500 ml flask were inoculated with 2 ml over night culture. Cell growth was monitored to an OD_{600} of 0.5. The cells were stored on ice for 5 min, transferred into a centrifuge bottle, and centrifuged at 4,000 xg and 4 °C for 5 min. The supernatant was decanted, and cells resuspended in cold transformation buffer I. After 90 min incubation on ice, the cells were centrifuged as before. The supernatant was decanted and 8 ml of cold transformation buffer II was added. After resuspension, the cells were aliquoted (100 µl in 1.5 ml Eppendorf tubes) and frozen in liquid nitrogen. Competent cells were stored at −80 °C. Cell growth was checked on LB agar plates with or without antibiotics.

3.7.4 Transformation of *E. coli*

Chemically competent cells were thawed on ice for 10 min. Meanwhile, the plasmid or the ligation reaction mixture for cloning was pre-cooled on ice as well. Approximately 10 - 50 ng of already sequenced plasmid or, for cloning, the whole ligation reaction mixture was added to the bacteria and gently mixed by pipetting. After 30 min incubation on ice, the tube was incubated at 42 °C for 30 - 60 s and placed back on ice, before 700 µl LB medium were added and cells incubated at 37 °C and 170 rpm for 1 h. Subsequently, cells were pelleted gently at 1,000 xg for 1 min, 500 µl supernatant discarded, and cells resuspended gently and transferred onto an agar plate with antibiotics, where they were evenly distributed. Finally, agar plates were placed into an incubator and cultured at 37 °C over night.

3.7.5 Blue white selection of *E. coli*

E. coli DH5α cells transformed with pDrive (**Table 2.9**) were plated on LB plates containing X-gal, IPTG, and amp. This allowed a blue white selection based on the complementation of the β-galactosidase enzyme by a fragment of the α-peptide (Ullmann *et al.*, 1967), which allows hydrolyzation of X-gal to 5-bromo-4-chloro-3-hydroxyindole, which then dimerizes and forms the insoluble blue pigment 5,5'-dibromo-4,4'-dichloro-indigo after oxidation (Kiernan, 2007; Messing *et al.*, 1977). To minimize the number of false positives, a colony was picked from the transformation plate and plated again on a LB plate with X-gal, IPTG, and amp. If grown colonies were still white, a single colony was picked, transferred onto a LB/amp plate, cultured, and stored at 4 °C until analysis ended and preparation of a glycerol stock was done.

3.7.6 Plasmid preparation from *E. coli*

For plasmid preparation, 4 ml of an over night culture (see section 3.7.2) were pelleted at 13,000 xg for 1 min at RT. Plasmid preparation was performed using the NucleoSpin Plasmid EasyPure Kit (Macherey-Nagel) according to the manufacturer's protocol. DNA was eluted twice in 100 µl PCR-water and concentrated using a vacuum centrifuge.

3.7.7 Cultivation and transfection of HEK293-6E (EBNA1) cells

The following steps were carried out under sterile conditions. HEK293-6E (EBNA1) cells were cultured in 25 ml F17 medium (125 ml flask), and cultured in an incubator at 37 °C, 120 rpm and 5 % CO_2. The culture was divided when the cells reached a density of approximately 2×10^6 cells ml^{-1}. Transfection was carried out as described by L'Abbé *et al.* (2018) with a 3:1 ratio of PEI:DNA diluted in F17 medium. Plasmid pTTo/GFPq (**Table 2.9**) was used as a control to analyze transfection success by expression of GFP. Before transient transfection, about 2×10^6 cells ml^{-1} were seeded in each well of a 6-well plate with 2 ml F17 medium. The transfection mixture was then added dropwise while gently swirling.

3.8 Gene technology methods

3.8.1 Isolation of total RNA

For RNA isolation, the Monarch total RNA Miniprep Kit (New England Biolabs) was used.

To isolate total RNA from *S. mansoni* couples, they were separated and washed in PBS before stored in 100 µl protection buffer of the Monarch total RNA Miniprep Kit and frozen in liquid nitrogen until use. For RNA isolation, samples were thawed on ice and processed as the manufacturer suggested. Elution of total RNA was carried out in 50 µl DEPC-water, afterwards the flow through was reloaded onto the column and centrifuged again.

To analyze target transcripts within the expression cells during protein expression, 2 ml culture were collected 2 and 4 h after induction of protein expression and centrifuged at 8,000 xg for 1 min. The pellet was stored in protection buffer of the Monarch total RNA Miniprep Kit at −20 °C over night. The next day, cells were disrupted as the protocol suggested and elution carried out as described before.

3.8.2 Synthesis of cDNA

To generate complementary DNA (cDNA) for cloning purposes, the ProtoScript II First Strand cDNA Synthesis Kit (New England Biolabs) was used. For one reaction, 1 µg total RNA, 2 µl oligo(dT)$_{20}$ Primer (50 µM), 1.5 µl dNTP mix (10 mM) were added with DEPC-water to a volume of 10 µl and incubated at 65 °C for 5 min. After denaturation of RNA, 4 µl 5x ProtoScript II buffer, 2 µl DTT (0.1 mM), 1 µl ProtoScript II M-MuLV reverse transcriptase (200 U µl^{-1}) and 0.2 µl RNase inhibitor (40 U µl^{-1}) were added with DEPC-water to a final volume of 20 µl. Reverse transcription was carried out at 48 °C for 60 min, followed by an inactivation step at 65 °C for 20 min. The RNA template was removed by addition of 1 µl RNase H (5 U µl^{-1}) at 37 °C for 20 min, followed by an additional inactivation step as described previously. The cDNA was stored at −20 °C until use.

To generate cDNA used in qRT-PCR as template, 20 ng of total RNA was used for one reaction with the QuantiTect Reverse Transcription Kit (Qiagen). To this end, total RNA was pre-diluted to $5 \, \text{ng} \, \text{µl}^{-1}$ to set up a master mix for removal of genomic DNA according to the manufacturer's protocol. In the following step, random hexamer primers, the reverse transcription buffer, and the reverse transcriptase enzyme were added. For analysis of transcript occurrence after induction of protein expression in *E. coli* LOBSTR-RIL, primer pairs #31/#32 (Sm*abl1*p1), #33/#34 (Sm*abl1*p2), #25/#26 (Sm*abl2*p1), and #27/#28 (Sm*abl2*p2) were used for the cDNA synthesis reactions, respectively. The whole reaction mixture was incubated at 42 °C for 30 min and the reaction stopped at 95 °C for 3 min.

3.8.3 Concentration of nucleic acids

From *E. coli* isolated plasmids, PCR products and digested plasmids, which were both extracted from an agarose gel, were concentrated in a vacuum centrifuge. Therefore, the starting volume of 200 µl was reduced to approximately 20 - 30 µl in 1 h at 50 °C.

3.8.4 Determination of concentration and analysis of nucleic acids

To determine the concentration and to analyze the integrity of RNA, the Agilent Bioanalyzer (Agilent Technologies) in combination with the RNA 6000 Nano Kit (Agilent Technologies) was used according to the manufacturer's protocol. The concentration of DNA was quantified photometrically and by agarose gel electrophoresis. The latter was used when PCR products were not cleaned up (dsRNA synthesis). The concentration was estimated by comparison of the PCR product intensities to the marker.

3.8.5 Primer design for qRT-PCR

Primers designed for qRT-PCR were 18 - 25 nt in size, had preferably a G/C content of 50 %, and a salt-adjusted melting temperature of 60 ± 0.5 °C. To analyze these properties

the online tool OligoCalc (**Table 3.1**) was used. For analyses of primer dimerization and hairpin formation, IDT's online tool OligoAnalyzer (**Table 3.1**) was used.

3.8.6 Preparation of primer stocks

Primers were dissolved in PCR-water as 100 µM stock solutions. Primer pellets were incubated at 37 °C for 30 min with 300 rpm. Afterwards, temperature was raised to 65 °C followed by an additional incubation step for 15 min while shaking. For working solutions, primers were diluted with PCR-water to 10 µM and stored at −20 °C.

3.8.7 PCR

PCR is a method, in which a polymerase amplifies a gene segment upon addition of dNTPs and synthesized primers (Mullis, 1990). This method was used to amplify:

    a) protein-coding gene sequences for cloning

    b) gene segments of isolated plasmids to check for correctly cloned plasmids

    c) templates for the synthesis of dsRNA

    d) templates for the synthesis of RNA probes for WISH

    e) transcripts of target genes in protein-expressing *E. coli* cells and substance-treated *S. mansoni* worms

Standard PCRs were carried out with FirePol DNA polymerase, which was used for b) and e) (**Table 3.6** and **Table 3.7**). Q5 High-Fidelity DNA polymerase was used for a), c), and d) (reaction mixture and cycling conditions are shown in **Table 3.8** and **Table 3.9**, where cycling condition A was applied for a) and d), and cycling condition B for c)). Another application of PCR is qRT-PCR. In this method, the fluorescent dye SYBR Green I binds double-stranded DNA (dsDNA) generated during each PCR cycle. The dye was excited at 480 nm, and emission was detected at 520 nm, which subsequently allowed quantification of DNA in real time (Morrison *et al.*, 1998; Zipper *et al.*, 2004). qRT-PCR was applied at point e) to analyze transcript levels in treated worms.

Table 3.6: PCR reaction mixture for FirePol DNA Polymerase

Component	Volume
PCR-water	17.75 µl
10x reaction buffer BD	2.5 µl
MgCl$_2$ (25 mM)	2.5 µl
dNTP mix (10 mM)	0.5 µl
Primer forward (10 µM)	0.75 µl
Primer reverse (10 µM)	0.75 µl
FirePol DNA polymerase (5 U µl^{-1})	0.25 µl
Sum	25 µl

Table 3.7: PCR cycling conditions for FirePol DNA polymerase

Temperature	Time	
95 °C	3 min	
95 °C	30 s	
x °C^a	30 s	} 35x
72 °C	1 min/kb	
72 °C	5 min	

^{a} x = temperature was specified according to used primers

Table 3.8: PCR reaction mixture for Q5 High-Fidelity DNA polymerase

Component	Volume
PCR-water	15.75 µl
5x Q5 buffer	5 µl
dNTP mix (10 mM)	0.5 µl
Primer forward (10 µM)^a	1.25 µl
Primer reverse (10 µM)	1.25 µl
Template cDNA^a	1 µl
Q5 High-Fidelity DNA polymerase (5 U µl^{-1})	0.25 µl
Sum	25 µl

^{a} To generate PCR products with T7 promotor for WISH: in total 3 µl Primer T7_extended ($\hat{=}$ forward/reverse, 10 µM) and 4 µl pJC53.2-based template ($\approx$ 1 ng µl^{-1})

Table 3.9: PCR cycling conditions for Q5 High-Fidelity DNA polymerase
A: Conditions to generate templates for cloning and WISH probes, **B:** conditions for dsRNA synthesis.

A			B		
Temperature	**Time**		**Temperature**	**Time**	
95 °C	3 min		95 °C	3 min	
95 °C	15 s		95 °C	8 s	
x °C^a	30 s	35x	60 °C	30 s	5x
72 °C	30 s/kb		72 °C	30 s/kb	
72 °C	5 min		95 °C	8 s	
			65 °C	30 s	30x
			72 °C	30 s/kb	
			72 °C	5 min	

^{a} x = temperature was specified according to used primers, 64 °C to generate PCR products with T7 promotor for WISH

Colony PCR

After blue-white selection, a colony PCR was performed to check whether a white colony was carrying the cloned insert. For colony PCR, a single colony was picked with a pipette tip and transferred into a PCR tube. A prepared master mix for standard PCR (**Table 3.6**) with insert-specific primers was added and PCR according to **Table 3.7** performed.

qRT-PCR

For determination of primer efficiency, PCR was performed with specific primers (**Table 2.14**) to generate a template for qRT-PCR. After excision of the product from an 2 % agarose gel, the amplicon DNA was extracted using the Monarch DNA Cleanup and Gel Extraction Kit (New England Biolabs) (see section 3.8.8). Primers were positively evaluated when the specific product was detected, and when the water control showed no primer dimer. After determining the concentration by photometry, the starting amount for a dilution series was calculated using **Equation 3.1** to determine the molecular weight (MW) of the linear amplicon (MW$_{la}$).

$$\text{MW}_{la} = \frac{\text{Length}_{la} \text{ x G/C content [\%] x MW}_{G/C}}{100} + \frac{\text{Length}_{la} \text{ x A/T content [\%] x MW}_{A/T}}{100} + 2\,\text{MW}_{\text{H}_2\text{O}} - 2\,\text{MW}_{\text{HPO}_3}$$

(3.1)

The average MW of a G/C ($\text{MW}_{G/C}$) base pair (bp) is 618.39 g mol^{-1} and 617.41 g mol^{-1} for a A/T ($\text{MW}_{A/T}$) bp. The MW of one H_2O (MW_{H2O}) is 18 g mol^{-1} and 80 g mol^{-1} for one HPO_3 (MW_{HPO3}).

Based on the MW of the amplicon, the amount of copies per µl was calculated and a dilution series (10^5, 10^4, 10^3, 10^2, and 10^1 amplicons) created, which served as template for qRT-PCR. The reaction mixture and cycling conditions are listed in **Table 3.10** and **Table 3.11**. A primer pair was considered as suitable for use if the resulting efficiency value (calculated by the Q-Rex Gene expression Plugin v2.0.0.4) ranged between 0.9 and 1.1.

Table 3.10: Reaction mixture for qRT-PCR

Component	Volume
2x PerfeCTa SYBR Green SuperMix	10 µl
Primer mix (forward + reverse, each 10 µM)	0.8 µl
PCR-water	4.2 µl
Template cDNA (equivalent to 0.05 ng µl^{-1} total RNA)	5 µl
Sum	20 µl

Table 3.11: qRT-PCR cycling conditions

Temperature	Time	
95 °C	3 min	
95 °C	10 s	
60 °C	15 s	} 45 x
72 °C	20 s	
60 - 95 °C[a]	20 s	

[a] melt curve: +1 °C increase each cycle

The same reaction setup and cycling conditions applied for analyses of transcript levels of target genes after knock down or substance treatment of *S. mansoni*. The relative transcript levels were determined by the method proposed by Pfaffl (2001) as shown in **Equation 3.2**, where Sm*letm1* served as reference gene (Lu *et al.*, 2017; Häberlein *et al.*, 2019). In this equation, E_{target} represents the averaged qRT-PCR efficiency of the target gene transcripts, $E_{Smletm1}$ represents the averaged qRT-PCR efficiency of the reference gene transcripts (Sm*letm1*), ΔCt_{target} represents the Ct deviation of the control minus the sample Ct of the target gene transcripts, $\Delta Ct_{Smletm1}$ represents the Ct deviation of the control minus the sample Ct of the reference gene transcripts Sm*letm1*.

$$\text{Relative gene expression (fold change)} = \frac{\left(E_{target}\right)^{\Delta Ct_{target}(\text{control - sample})}}{\left(E_{Smletm1}\right)^{\Delta Ct_{Smletm1}(\text{control - sample})}} \tag{3.2}$$

To determine the relative gene expression level of the selected genes, the relative gene expression ratio was calculated using Sm*letm1* as the reference gene for each biological replicate and multiplied by an arbitrary factor, f = 2000 (**Equation 3.3**). Afterwards, the values were transferred to GraphPad Prism to generate graphs with means and StEMs.

$$\text{Relative gene transcript levels} = \frac{\left(E_{target}\right)^{Ct_{target}}}{\left(E_{Smletm1}\right)^{Ct_{Smletm1}}} \cdot f \tag{3.3}$$

3.8.8 Purification of nucleic acids

PCR products or digested plasmids were separated on an agarose gel by electrophoresis (see section 3.9). Respective bands were excised and the DNA inside the gel piece extracted using the Monarch DNA Cleanup and Gel Extraction Kit (New England Biolabs) according to the manufacturer's protocol. Elution was carried out twice in 100 µl PCR-water and DNA was concentrated as described in section 3.8.3. When PCR products represented a single band on an agarose gel, the PCR reaction mixture

was transferred into 1.5 ml reaction tubes, where the same volume PEG solution was added, mixed and incubated for 30 min at RT before centrifugation at 18,000 xg for 30 min. The supernatant was discarded, and the pellet washed with 70 % ethanol before the centrifugation step was repeated. The DNA was resuspended in 50 µl PCR-water and the concentration determined (see section 3.8.4).

3.8.9 Enzymatic cleavage of DNA

Plasmid DNA and PCR amplicons were enzymatically cleaved prior to ligation reactions or to prevent a super-coiled plasmid structure during PCR. The DNA was mixed with CutSmart buffer and the respective enzyme added before incubation at 37 °C for 30 min. Additionally, in reaction mixtures containing plasmid DNA, 5 U Quick-CIP was used to dephosphorylate the ends. Afterwards, the DNA was analyzed by agarose gel electrophoresis (see section 3.9) and cleaned up (see section 3.8.8).

Table 3.12: Overview of digested plasmids for downstream applications

Plasmid	Enzymes	Application
pET30a+	*Nde*I, *Not*I	Cloning
pMal-c5X	*Nde*I, *Xmn*I	Cloning
pTT28	*Nhe*I	Cloning
pTT22SSP4	*Nhe*I, *Bam*HI	Cloning
pJC53.2	*Ahd*I	Cloning

3.8.10 Cloning of cDNA

For cloning purposes, isolated total RNA was reverse transcribed into cDNA using the ProtoScript II First Strand Synthesis Kit (New England Biolabs) (see section 3.8.2), and used as template in PCR to amplify the target sequences.

In order to clone protein-coding sequences, primers were designed that either covered the entire sequence (Sm*tk6*) or partial segments (Sm*abl1* and Sm*abl2*). Available gene sequences of the Puerto Rican strain (Berriman *et al.*, 2009) were used as templates

for primer design. The respective PCR fragments were separated by agarose gel elec-trophoresis (see section 3.9) according to size and extracted from the gel (see section 3.8.8). After concentration determination (see section 3.8.4), cloning was performed into plasmid pDrive (**Table 2.9**) according to the instructions of the PCR Cloning Kit (Qiagen). After validation of the inserted sequence by sequencing (see section 3.8.11), these generated plasmids served as templates for further PCRs to sub-clone the sequences into the respective plasmids (**Table 2.10**).

For sub-cloning of sequences, primers were created for the respective gene, which in addition to the target sequence also had a homology region of about 20 nt to the target plasmid sequence. The PCR fragment thus amplified was cloned into the previously digested plasmid (**Table 3.12**) using NEBuilder HiFi DNA Assembly Master Mix (New England Biolabs) according to the manufacturer's instructions. To determine the start and end of the SmAbl-TKDs, sequences were analyzed online using CDD (**Table 3.1**). A start codon was added for expression in *E. coli*.

To clone gene sequences that served as riboprobe-templates for WISH, selected gene sequence sections were analyzed using the RNAfold webserver (**Table 3.1**) to minimize formation of secondary structures. To target an unique region of the Sm*aldh1* gene transcript, the 3' untranslated region (UTR) was chosen for probe synthesis. Primers were designed, and sequences cloned as previously described into plasmid pJC53.2 (**Table 2.9**).

3.8.11 Sequencing of DNA

Isolated plasmids and PCR products were sequenced by the company Microsynth Seqlab GmbH (Balgach, Switzerland). Samples were prepared according to the company's protocol. Analyses of sequencing data was done with ApE (**Table 3.2**).

3.9 Agarose gel electrophoresis

Agarose gel electrophoresis was used for separating nucleic acids and to estimate concentrations. The gels were analyzed and documented under UV light with a GEL iX20 imager (**Table 2.1**). To prepare agarose gels, agarose (1 - 2 %) was dissolved and melted in TAE buffer. The solution was mixed with GelRed nucleic acid gel stain (1:1,000) and poured in a plastic gel tray. While cooling, the samples were prepared by addition of DNA loading dye. After cooling, gels were transferred into a chamber filled with TAE buffer and loaded with the prepared samples. For comparison of band intensity and fragment length, HyperLadder 50 bp or HyperLadder 1 kb were used. The samples were separated at $130 - 150 \, \text{V}$.

3.10 dsRNA Synthesis

A previously amplified PCR product served as the starting product for the dsRNA synthesis. For this purpose, the desired gene sequence was cloned (see section 3.8.10) and subsequently amplified (**Table 2.15**, **Table 3.8**, and **Table 3.9 B**). The generated PCR product was checked for the expected length by agarose gel electrophoresis and the concentration was estimated by comparison to the HyperLadder size standard. Approximately $5 \, \mu\text{g}$ PCR product was used for an *in vitro* transcription reaction (**Table 3.13**, mixture modified after Collins *et al*., 2010). The reaction was carried out for approximately $16 \, \text{h}$ at $37 \, \text{°C}$, followed by a DNaseI treatment (10 U, $37 \, \text{°C}$) for $30 \, \text{min}$. After addition of $50 \, \mu\text{l}$ $7.5 \, \text{M}$ LiCl, the mixture was incubated at $-20 \, \text{°C}$ over night. The next day, it was centrifuged for $30 \, \text{min}$ at $4 \, \text{°C}$ and 18,000 xg. The RNA pellet was washed with ice cold ($-20 \, \text{°C}$) 70 % ethanol and centrifuged again (10 min, $4 \, \text{°C}$, 18,000 xg). The supernatant was removed, the RNA resuspended in DEPC-water and incubated for $3 \, \text{min}$ at $72 \, \text{°C}$. Subsequently, the concentration was determined photometrically, and the synthesis confirmed by agarose gel electrophoresis. The dsRNA thus produced was used at concentrations of $2.5 \, \mu\text{g} \, \text{ml}^{-1}$ and $12.5 \, \mu\text{g} \, \text{ml}^{-1}$ in knock down approaches (see section 3.5.2).

Table 3.13: *In vitro* transcription reaction mixture for dsRNA synthesis

Component	Volume
PCR product ($\approx 5\,\mu g$)	x µl
10 x transcription buffer	10 µl
rNTP mix	20 µl
T7 RNA polymerase (10 µg)	x µl
Inorganic pyrophosphatase ($0.1\,U\,\mu l^{-1}$)	1 µl
DEPC-water	Add 100 µl

3.11 Protein biochemical methods

3.11.1 Protein expression in HEK293-6E (EBNA1) cells

Transfection of plasmid DNA and expression of protein was done as described in section 3.7.7. Every 24 h, 250 µl of supernatant (approximately 5×10^5 cells) was collected and centrifuged at 1,000 xg for 5 min. SDS-sample buffer was added to the pellet as well as the supernatant and stored at $-20\,°C$ until analysis.

3.11.2 Protein expression in *E. coli*

Protein expression in *E. coli* was performed as published by Harnischfeger, Beutler *et al.* (2021). For initial analysis of protein expression, a protein expression kinetic was performed. Therefore, a pre-culture was prepared as described in section 3.7.2. Fifty ml LB medium were inoculated with the pre-culture to an OD_{600} of 0.1 and cultured as before. Cell growth was monitored until the OD_{600} reached 0.6 - 0.8. At this point, protein expression was induced by addition of IPTG to a final concentration of 200 µM and a sample (1 ml) taken. The culture was placed on a shaker (170 rpm at RT). Samples were taken every hour and centrifuged at 8,000 xg for 1 min. After 4 - 6 h, the sampling was stopped and the cells stored at $-20\,°C$ until analysis.

A main culture was grown for protein expression used for downstream applications. As described in section 3.7.2, a pre-culture was cultured over night to inoculate the main culture (total volume of 400 ml in a 1 l flask). Induction of protein expression was carried out as before, and cells harvested at 8,000 xg and 4 °C for 15 min in 250 ml centrifuge bottles after 4 h of incubation. The pellet weight was noted and pellets stored at −20 °C over night.

3.11.3 Lysis of bacterial cells

Cells were thawed on ice and resuspended in 100 mM Tris buffer (pH 7.4). Per g pellet, 100,000 U lysozyme, 10 U DNase I, 10 U RNase A, and a fourth of a SIGMAFAST protease inhibitor cocktail tablet were added before the mixture was transferred into a 50 ml centrifuge tube and incubated at 100 rpm and 4 °C for 1 h. Cells were ultrasonically lysed 3 times for 1 min each by pulsing 1 s on/off with 60 % power. Afterwards, the cells were pelleted at 18,000 xg and 4 °C for 30 min. The supernatant was filtered through a PES filter into a protein low-bind canonical tube.

3.11.4 Immobilized metal affinity chromatography

To purify His-tagged proteins, immobilized metal affinity chromatography (IMAC) was used. His-rich and His-tagged proteins bind to the column matrix (e.g., nickel-nitrilotriacetic acid (Ni-NTA)), whereas proteins poor in His are washed away (Rodriguez *et al.*, 2020). To elute bound proteins imidazole was used.

For purification of His-tagged proteins, the ÄKTA Start system was used. To prevent air bubbles from blocking the tubes, all used buffers and solutions were filtered and degassed beforehand, and equilibrated to RT if necessary. To prepare the HisTrap HP column, it was assembled to the ÄKTA Start instrument and flushed with 10 column volumes (CV) ddH$_2$O, followed by equilibration with 10 CV 100 mM Tris buffer (pH 7.4). All of the crude protein extract was pumped onto the column with a flow rate of 1 ml min^{-1}, followed by a washing step with 8 CV 100 mM Tris buffer (pH 7.4) to wash out unbound proteins. For elution of the proteins, a gradient with increasing imidazole concentration was applied (elution buffer, 4 CV − 50 mM, 4 CV − 100 mM, 8 CV −

300 mM). The flow through was collected in protein low-bind tubes as 2 ml fractions each. Afterwards, the column was washed with 10 CV 100 mM Tris buffer (pH 7.4), before it was flushed with ddH$_2$O and stored in 20 % ethanol at 4 °C.

3.11.5 Size exclusion chromatography

Size exclusion chromatography (SEC) was used for rebuffering of purified protein. To this end, protein was centrifuged at 13,000 xg at 4 °C for 5 min and the supernatant transferred into a new tube, if required. Meanwhile, the desalting column was prepared by equilibration with 100 mM Tris buffer (pH 7.4). Up to 1.4 ml of sample was loaded at one time, before the column was flushed with 1 CV buffer. The flow through was collected in protein low-bind tubes as 500 µl fractions. The column was then washed again with 1 CV 100 mM Tris buffer (pH 7.4) before another sample was rebuffered or the system rinsed with ddH$_2$O and 20 % ethanol for storage.

3.11.6 Determination of protein concentration

To determine protein concentration, the Pierce BCA Protein Assay Kit (Thermo Fisher Scientific) was used according to the manufacturer's protocol using BSA as a standard.

3.11.7 SDS-polyacrylamide gel electrophoresis

Separation of proteins was performed by SDS-PAGE. This method is based on the masking effect of SDS, where all proteins get negatively charged. This allows separation by MW in an electric field (Laemmli, 1970).

At the beginning, glass plates and frames were cleaned with destilled water (dH$_2$O) and assembled. Fresh prepared solution for 12 % separating gels (**Table 3.14**) was pipetted between the glass plates and covered with isopropanol. Forty five minutes later, the isopropanol was removed and fresh prepared solution for the 5 % stacking gel was pipetted on top of the polymerized separating gel. The comb was added air bubble-free.

After 30 min, the gel was used for gel electrophoresis or stored at 4 °C (wrapped in moist tissues for up to 2 weeks). To perform SDS-PAGE, SDS-sample buffer was added to the protein samples and incubated for 5 min at 95 °C. The gel pockets were loaded with the prepared samples and a marker (**Table 2.7**). Samples were separated at 200 V in running buffer for approximately 50 min before the gel was removed and analyzed using the ChemiDoc MP device (application: stain-free gel) or stained with Coomassie staining solution.

Gels without trichloroethanol were prepared for Coomassie staining. To this end, they were rinsed with dH_2O, placed in a container with dH_2O, and heated in a microwave for 40 s at 700 W before they were incubated with slight agitation for 2 min. The water was replaced with Coomassie staining solution and again heated as before. Incubation was carried out with slight agitation for 15 min. Staining solution was used up to 2 times. To destain the gels, dH_2O was added and heated as before and incubated with slight agitation for 10 min. This step was repeated until the desired discoloration was achieved. Gels were then documented by a scanner. Stain-free gels were rinsed with dH_2O, placed on the tray of the ChemiDoc MP device and analyzed by the stain-free application mode.

Table 3.14: Composition of separating and stacking gel for SDS-PAGE

Component	12 % Separating gel	5 % Stacking gel
Rotiphorese Gel 30	6 ml	0.65 ml
ddH$_2$O	5.25 ml	3.05 ml
4x separating gel buffer	3.75 ml	-
4x stacking gel buffer	-	1.25 ml
10 % APS	75 µl	25 µl
TEMED	7.5 µl	5 µl
Trichloroethanol[a]	75 µl	25 µl

[a] only for preparation of stain-free SDS-gels

3.11.8 Western blot

Western blot was carried out using the Trans-Blot turbo transfer system. Here, blotting was done in only 7 min. The nitrocellulose membrane and 12 blot paper sheets were equilibrated in transfer buffer while the SDS-gel was rinsed with ddH_2O. The transfer

chamber was equipped with 6 blot paper sheets, the membrane, the SDS-gel and 6 blot paper sheets. To avoid air bubbles, the stack was rolled at the end. The chamber was assembled, excess buffer poured off, and the device started. Proteins were transferred using the standard protocol (7 min, 2.5 A constant, up to 25 V). To analyze transfer success, the membrane was stained with Ponceau S. The membrane was transferred into a plastic container with Ponceau S and incubated at 100 rpm for 2 - 3 min. After staining, Ponceau S was removed and 1 % acetic acid added. Incubation was carried out with agitation until a clear background appeared. Finally, the membrane was documented with the ChemiDoc MP device.

The following steps were carried out at 130 rpm and RT, if not stated otherwise. Blocking solution was added to the membrane and incubated for 1 h followed by 3 times washing in TBST for 10 min each. Afterwards, the membrane was incubated in antibody solution I at 4 °C over night. The next day, 3 washing steps with TBST for 10 min each were carried out, before the antibody solution II was added and incubated for 1 h. Subsequently, the membrane was washed again 3 times with TBST as before. Development of the blot was done with ECL prime western blot detection reagent. Both solution were mixed 1:1 and evenly distributed on the membrane. After $1 - 2$ min, the solution was removed and the signal detected with the ChemiDoc MP device (application: blots - chemiluminescence, automatic exposure, pictures taken every 10 s for 2 min).

3.12 Enzyme activity assay of SmAldh1

The predominantly expressed and purified enzyme (see sections 3.11.1 - 3.11.5) was used to determine its activity by an enzyme assay, which was established in corporation with the working group of Prof. P. Czermak as part of this thesis (Harnischfeger, Beutler *et al.*, 2021). In a standard reaction, 167 nM SmAldh1, 10 mM DTT, 33.3 µM NAD^+ and 33.3 µM acetaldehyde was used. All components were solved in 100 mM Tris (pH 7.4) except acetaldehyde (ddH_2O). To analyze the influence of ions on the activity, $MgCl_2$ or $CaCl_2$ was added to the mixture. The reaction was carried out in 150 µl in a 96-well quartz plate.

One U of the enzyme was defined as the conversion of 1 nM NADH per minute as shown in **Equation 3.4**, where ΔC represents the change in NADH concentration (nM),

V represents the total reaction volume (l), and ΔT represents the change in time (min). The specific enzyme activity was calculated considering the amount of protein M (mg) used.

$$U\,mg^{-1}[nM\,min^{-1}] = \frac{\Delta C * V}{\Delta T * M_{(SmAldh1)}} \tag{3.4}$$

4 Results

4.1 Substance treatments to unravel the toxicity of DSF in adult *S. mansoni* couples

DSF is a well-known Aldh inhibitor (Hald and Jacobsen, 1948), which has been proven to also inhibit activity of recombinantly expressed SmAldh1 (Beutler, Harnischfeger *et al*., 2022, manuscript in preparation). DSF attracted attention not only as an Aldh inhibitor but also as a proposed anti-parasitic agent against protozoa such as *Giardia lamblia*, *Leishmania sp.* or *Plasmodium falciparum* (Castillo-Villanueva *et al.,* 2017; Khouri *et al.,* 2010; Scheibel *et al.,* 1979). In addition, efficacy against multicellular parasites such as the nematode *Trichuris muris* was also demonstrated (Hill and Fetterer, 1997).

Therefore, the effect of DSF on adult schistosomes was investigated. To determine a possible mechanism of its activity, DSF alone or combinations with $CuCl_2$ and/or copper chelating agents (BCPD and EDTA) as well as the DSF-copper metabolite CuET were examined. In addition, the anti-schistosomal efficiency of a developed DSF-derived substance called Schl-32.028 from a collaboration partner (Prof. M. Schlitzer) was examined, too. Following substance administration, worm fitness was evaluated every 24 h for 3 d. Furthermore, effects on worm morphology and cell proliferation were analyzed using CLSM and an EdU assay, respectively. Finally, transcript profiles of a set of selected genes associated to oxidative stress response (Sm*aldh1*, Sm*aldh2*, Sm*ar*, glutathione peroxidase (Sm*gpx*), superoxide dismutase (Sm*sod*), and extracellular superoxide dismutase (Sm*sodex*)), cell cycle (nuclear protein localization protein 4 (Sm*npl4*) and tumor protein p53 (Sm*p53*)), stem cells (Sm*nanos1* and Sm*nanos2*), or apoptosis (Sm*bax* and Sm*bcl-2*) were determined.

4.1.1 High concentrations of DSF showed tremendous effects on paired *S. mansoni in vitro*

Initially, DSF concentrations ranging from 1 - 200 µM were administered to adult *S. mansoni* couples. Physiological parameters (number of couples, number of attached couples, motility, and number of normal and abnormal eggs) were determined regularly. DMSO, the solvent of DSF, served as control. The focus of the results was on the values obtained after 72 h, where the statistical analysis was performed. To give an overview, all observed time points are presented.

DSF displayed dose-dependent effects on the fitness of the worms. The lowest DSF concentration tested (1 µM) had no impact on the number of couples (**Figure 4.1 A**), while at 10 and 25 µM approximately 50 % of the couples were separated after 72 h. Administration of 100 µM DSF and more resulted in significant separation of all couples after 72 h. Analysis of the attachment capacity of couples showed no effect at 1 µM DSF, whereas 10 µM led to a significant loss of 50 % pairing-stability and 25 µM led to a complete loss of attachment capacity after 72 h (**Figure 4.1 B**). Worm motility was significantly reduced to a score of 2 with DSF concentrations $\leq$ 100 µM after 72 h (**Figure 4.1 C**). Movements were even further reduced (score of 1) with 200 µM DSF. A reduction of about one third of normally formed eggs was observed with 1 µM DSF and a significant reduction to about one fourth with 10 µM DSF (**Figure 4.1 D**). The effects were even stronger with 25 µM DSF and did not change at higher concentrations. The number of abnormally formed eggs remained lower compared to the controls at all tested concentrations, with lowest numbers at $\geq$ 50 µM DSF (**Figure 4.1 E**).

Applications below 100 µM DSF already showed tegument changes. Compared to the untreated controls (**Figure 4.2 A**), constrictions occurred in the female body, while blebbing was observed in both genders at 100 µM DSF (**Figure 4.2 B**), whereas detachment of the tegument was observed in both genders with 200 µM (**Figure 4.2 C**).
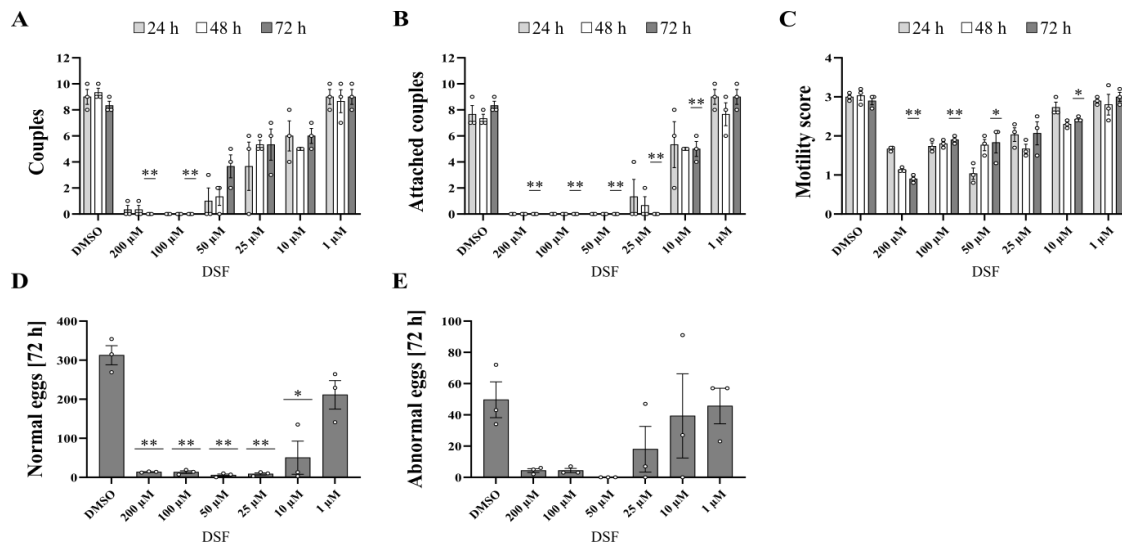
Figure 4.1: Screening of physiological parameters following DSF treatment
A: number of couples, **B:** attachment of couples, **C:** motility score, and egg numbers for **D:** normal and **E:** abnormal eggs during treatment with DSF, n = 3. Each point represents a measurement (average for motility score) of one experiment with 10 couples each. Columns represent means with StEM. Statistical analysis (two-tailed t-test) was performed with values obtained after 72 h (treatment vs DMSO), p < 0.05 (*), p < 0.01 (**).

Figure 4.2: Bright-field microscopy of *S. mansoni* couples following DSF treatment
Couples were treated with **A:** DMSO, which served as control, **B:** 100 µM DSF, and **C:** 200 µM DSF. After 72 h, body constrictions of females (**B**) and the formation of blebs as well as detachment of the tegument in both genders were observed as indicated by arrowheads. Bl = bleb, Co = constriction, dTg = detached tegument, scale bars represent 500 µm.

For a more detailed analysis of the tegument, DSF-treated worms (10, 25, and 50 µM) were fixed for SEM (**Figure 4.3**). Administration of 10 µM DSF caused swellings in females and destruction of tubercles as well as sloughing of the tegument in males (**Figure 4.3 B**) when compared to the controls (**Figure 4.3 A**). With 25 µM DSF, the tegument exhibited damage in the form of sloughing and blebbing in females, while destruction of spines on the tubercles and formation of vesicles were observed in males (**Figure 4.3 C**). The previously observed damages were also observed after administration of 50 µM DSF (**Figure 4.3 D**).

CLSM analysis of treated worms revealed morphological changes in the gonads and tegument of both genders (**Figure 4.4**). No alterations were observed in organs such as ovary, vitellarium, testis, and gut after administration of 10 µM DSF (**Figure 4.4 B**) compared to the controls (**Figure 4.4 A**). A distinct disaggregation within the ovaries, including the granulation of mature oocytes, and tegument detachment were observed in females with 25 µM DSF (**Figure 4.4 C**). In addition, the number of vitelline cells appeared reduced as cell-free spaces were observed within the vitelloducts (not shown). With the same concentration, the testes lost their integrity, and destruction of the tegument in the form of blebbing was observed. The observed effects were even stronger with 50 µM DSF in the ovaries of females, where not only the immature parts of the ovary, but also the mature parts appeared disrupted (**Figure 4.4 D**). The testes were disintegrated with 50 µM DSF, as was also observed with 25 µM, whereas the seminal vesicles contained less spermatozoa.

As a next step, proliferation of cells inside the gonads was analyzed with an EdU assay. DSF showed a dose-dependent effect on proliferating cells in ovaries and testes. The worms treated with 10 µM DSF (**Figure 4.5 B**) seemed not to be affected by the treatment, showing signals of EdU-positive cells comparable to those of the control worms (**Figure 4.5 A**). At a higher dose (25 µM DSF), the signals decreased considerably and few signals were observed (**Figure 4.5 C**), while at 50 µM DSF, almost no signals were detected (**Figure 4.5 D**).

Finally, the effects of DSF on gene expression were determined by qRT-PCR analysis after administration of 10 and 25 µM. For Sm*aldh1*, no alterations in females were observed at both DSF concentrations, while in males a slight downregulation with 25 µM DSF was observed (**Figure 4.6 A** and **F**). For Sm*aldh2*, no noteworthy regulation was noticed. Sm*ar* tended to be upregulated in females with both DSF concentrations

(about 1.2-fold at 10 µM and 1.3-fold at 25 µM DSF). Gene expression of Sm*gpx* was increased by more than half in males after 10 µM (157 %) and 25 µM DSF (185 %), whereas in females a slight upregulation was observed only with 25 µM DSF (**Figure 4.6 B** and **G**). The transcript levels of Sm*sod* were slightly affected in females with 10 µM DSF, while Sm*sodex* was upregulated in females and males after administration of 25 µM DSF. Gene expression of Sm*npl4* was not affected by DSF, whereas Sm*p53* expression was upregulated about 1.6-fold in males with 25 µM DSF (**Figure 4.6 C** and **H**). Sm*bax* and Sm*bcl-2* transcript levels were slightly upregulated by 10 µM DSF in females and Sm*bax* by 25 µM in males (**Figure 4.6 D** and **I**). Transcript abundance of Sm*nanos1* was decreased by about two thirds in females with 25 µM DSF and reduced by one third in males at both concentrations (69 % and 68 %, respectively). In contrast, Sm*nanos2* was upregulated in males at both DSF concentrations, whereas Sm*nanos2* expression was unaffected in females (**Figure 4.6 E** and **J**).
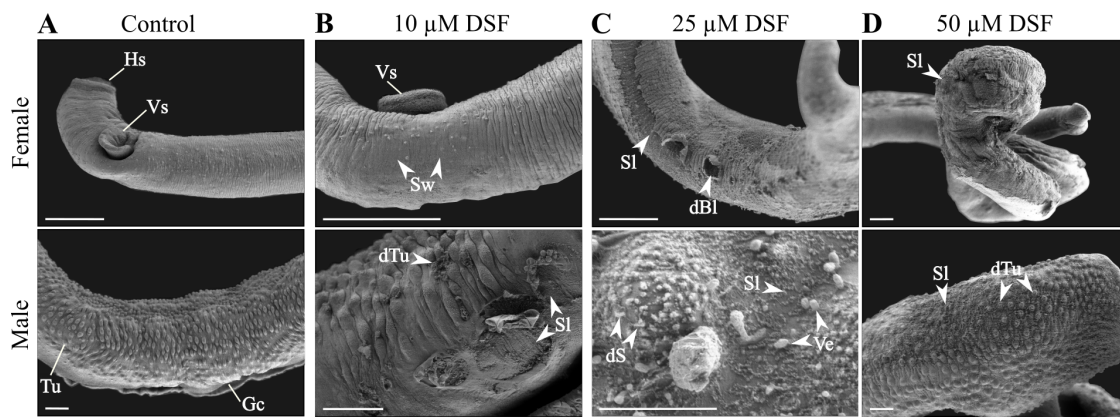
Figure 4.3: SEM-based analyses of the tegument of adult *S. mansoni* following DSF treatment

Couples were treated with **A:** DMSO, which served as control, **B:** 10 µM DSF, **C:** 25 µM DSF, and **D:** 50 µM DSF. Worms were separated and fixed after 72 h. Morphological changes such as swellings, sloughing, destruction of tubercles including the malformation of spines, and vesicle formation are marked by arrowheads. Bl = bleb, dS = deformed spine, Gc = gynaecophoric canal, Hs = head sucker, dBl = destroyed bleb, dTu = destroyed tubercle, Sl = sloughing, Sw = swelling, Tu = tubercle, Ve = vesicle, Vs = ventral sucker. Scale bars represent 50 µm (except C, bottom: 10 µm).

Female   Male
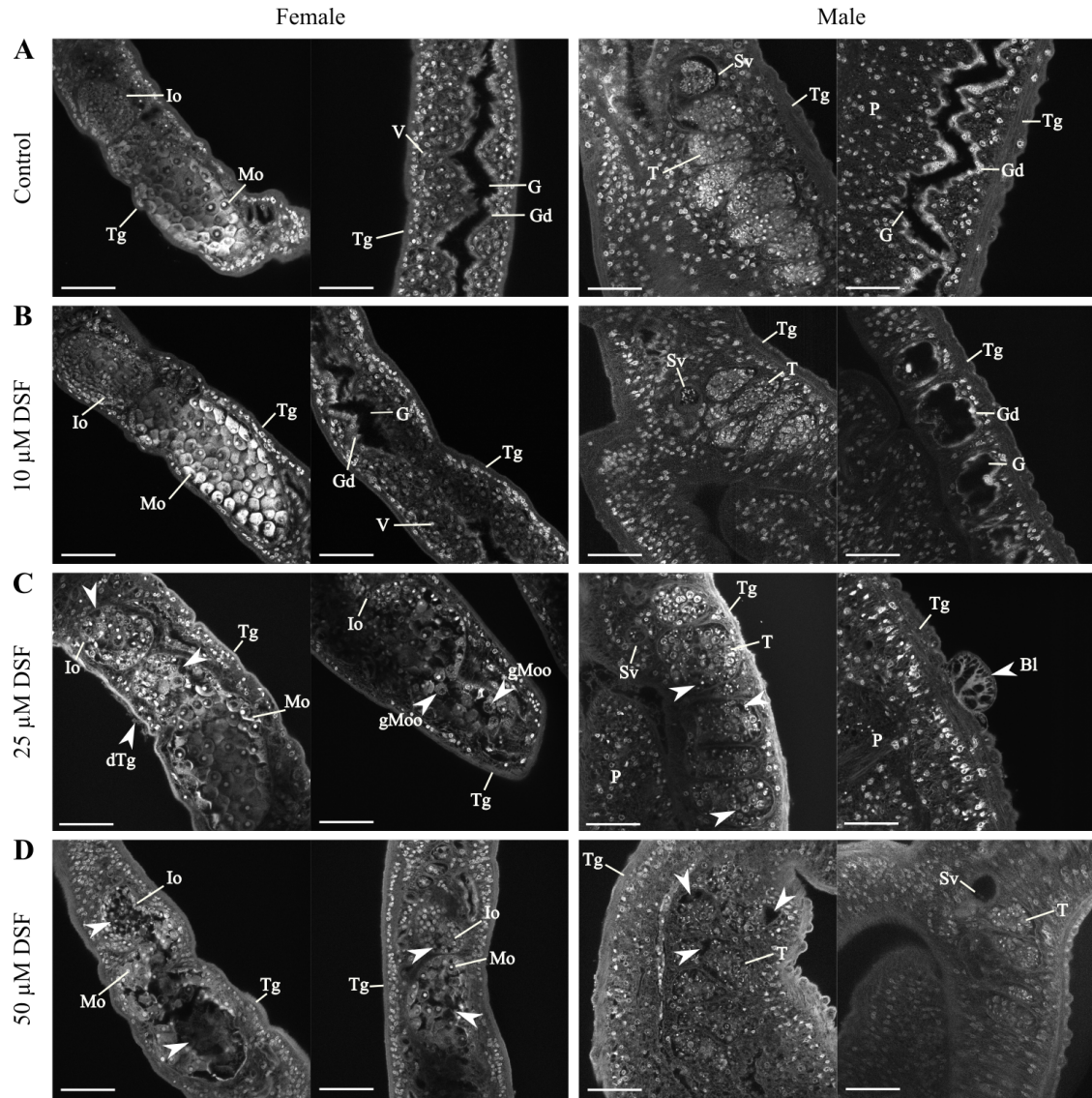
Figure 4.4: Influence of DSF on the morphology of adult *S. mansoni* couples

Couples were treated with **A:** DMSO (solvent of DSF), **B:** 10 µM DSF, **C:** 25 µM DSF, and **D:** 50 µM DSF. The worms were cultured *in vitro* for 72 h before separation and fixation. Shown are representative examples of female and male worms. Morphological changes such as blebs, detachment of the tegument, granulated mature oocytes, and a loss of tissue integrity of the gonads (ovary and testis) were observed (indicated by arrowheads). Bl = bleb, dTg = detached tegument, gMoo = granulated mature oocyte, Io = part of the ovary containing immature oocytes, Mo = part of the ovary containing mature oocytes, P = parenchyma, Sv = seminal vesicle, T = testis, Tg = tegument, V = vitelline cell. Scale bars represent 50 µm.
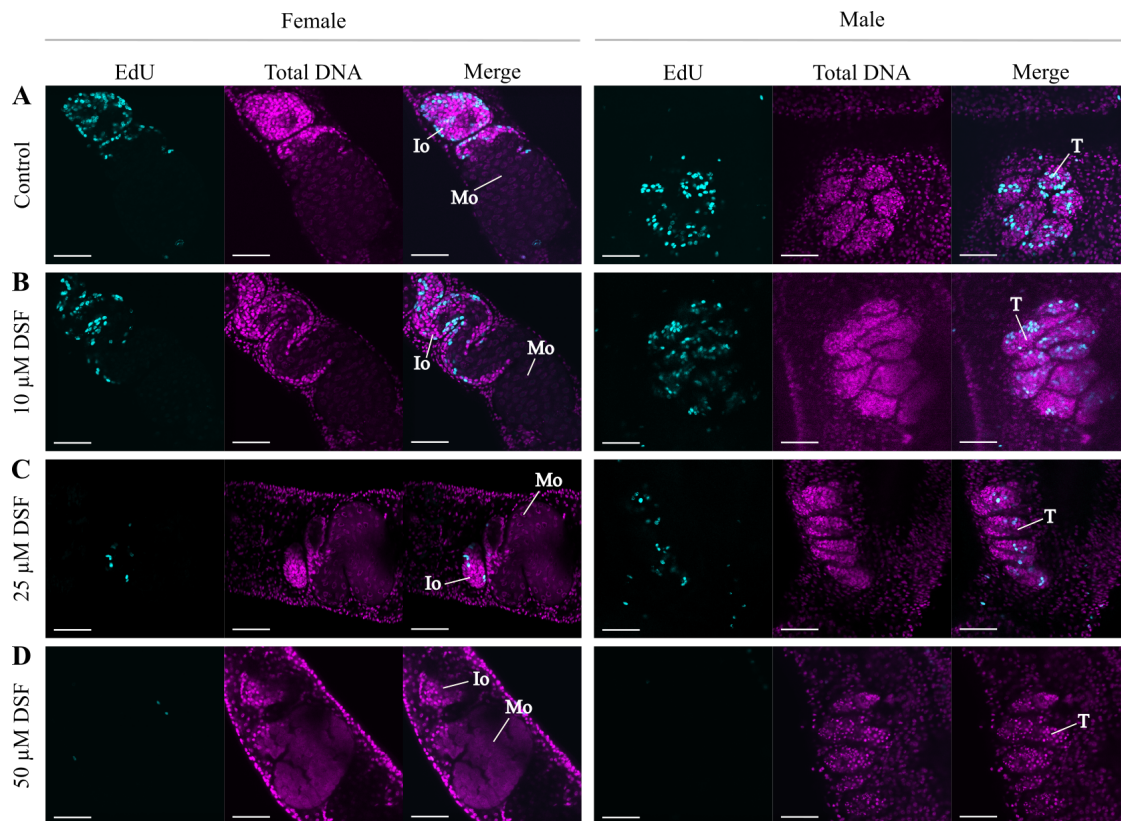
Figure 4.5: Influence of DSF on proliferation in adult *S. mansoni* couples
Schistosome couples were treated with **A:** the solvent of DSF (DMSO), **B:** 10 µM DSF, **C:** 25 µM DSF, **D:** 50 µM DSF, and cultured for 72 h. EdU was added 24 h prior separation of the couples for fixation of females and males. EdU-positive cells are shown in cyan and the total DNA in magenta. With 25 µM DSF, a reduction of signals in ovaries and testes was observed (**C**). The signals were further reduced with 50 µM DSF (**D**). Io = part of the ovary containing immature oocytes, Mo = part of the ovary containing mature oocytes, T = testis. Scale bars represent 50 µm.
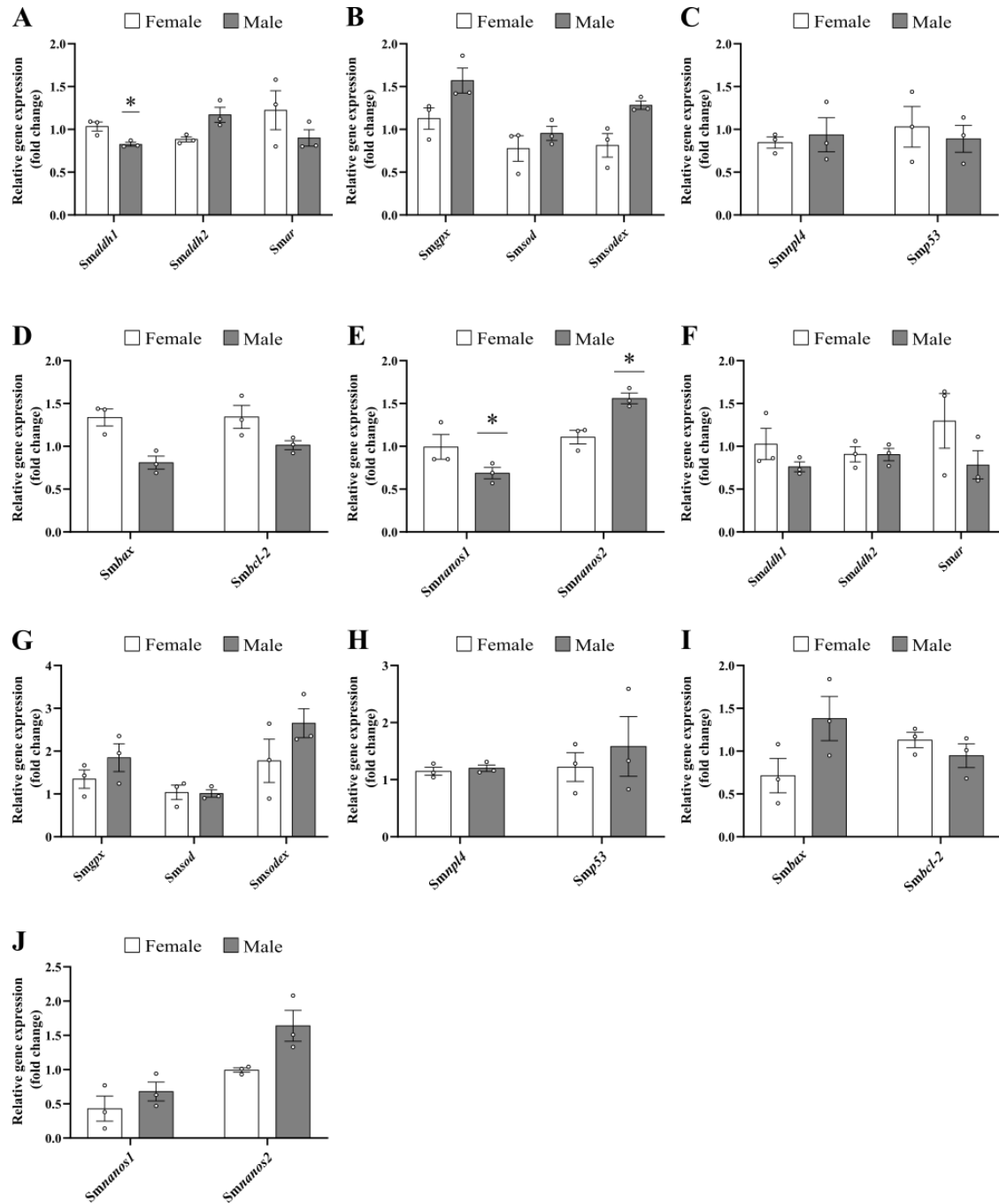
Figure 4.6: qRT-PCR analyses of selected genes following DSF treatment

For this analyses, 10 couples each were treated with **A** - **E:** 10 µM DSF and **F** - **J:** 25 µM DSF. Gene expression of oxidative stress-responsive genes Sm*aldh1*, Sm*aldh2*, Sm*ar* (**A**, **F**), Sm*gpx*, Sm*sod*, and Sm*sodex* (**B**, **G**), cell cycle-associated genes Sm*npl4* and Sm*p53* (**C**, **H**), apoptosis-related genes Sm*bax* and Sm*bcl-2* (**D**, **I**), and stem cell-associated genes Sm*nanos1* and Sm*nanos2* (**E**, **J**) were analyzed. Each data point represents one experiment. Columns represent means with StEM (n = 3). Statistical analysis (two-tailed t-test) was performed using treatment vs control (not shown), p < 0.05 (*).

4.1.2 DSF in combination with copper potentiated toxicity against schistosomes comparable to CuET

After ingestion by humans, DSF is rapidly reduced to the unstable DETC, which itself rapidly dissociates into CS_2 and DEA. Alternatively, DETC forms a stable complex with copper (CuET) (Johansson, 1992; Meraz-Torres *et al.*, 2020). It has been shown that DSF and copper spontaneously form CuET in medium (Skrott *et al.*, 2019). In addition, CuET has been shown to be selectively toxic to cancer cells (Li *et al.*, 2018b; Morrison *et al.*, 2010; Skrott *et al.*, 2019). On this basis, the aim was to verify whether the previously shown effects of DSF were due to the formation of CuET, and whether this could be the toxic substance for schistosomes. Hence, *in vitro* culture experiments were performed in combination with DSF and a copper source ($CuCl_2$) and compared with the effects of CuET alone. The combination of DSF and copper is also referred to as DSF/Cu. Copper was added constantly as 1 µM $CuCl_2$, while concentrations of DSF and CuET ranged between 0.1 - 50 µM. When high concentrations of DSF and $CuCl_2$ were added, a brown precipitate formed rapidly, but dissipated after swirling to distribute all substances evenly in the well.

First, physiological parameters were assessed after addition of DSF/Cu or CuET during an observation period of 72 h (**Figure 4.7**). The solvent for DSF and CuET, DMSO, and 1 µM $CuCl_2$ were included as controls and showed no significant effect on the worms. Combination treatment of DSF/Cu displayed tremendous effects on the pairing stability of worms (**Figure 4.7 A**). At 1 µM DSF, separation of 100 % of the couples occurred after 24 h, which was also observed at higher DSF concentrations. Administration of 5 µM CuET and higher led to the same result (**Figure 4.7 F**), whereas a negligible number of couples remained in the culture with 1 µM CuET. The effect of CuET decreased at lower concentrations. At 0.25 µM, the number of couples was comparable to those in the control group. The number of attached couples decreased to 0 in the combination treatment groups after 24 h (**Figure 4.7 B**), which was also observed for CuET administrations above 1 µM (**Figure 4.7 G**). Lowering the CuET concentration to 0.5 µM displayed a detachment rate of almost 100 % after 72 h, whereas even lower concentrations showed lowered or no effects. The motility score was significantly reduced to 1 at all administered DSF concentrations after 24 h, decreasing further at concentrations above 1 µM DSF (**Figure 4.7 C**). For CuET, a dose-dependent effect on motility was observed (**Figure 4.7 H**). Doses greater than 0.5 µM completely abolished motility after 72 h. The numbers of normal and abnormal formed eggs were almost 0

after treatment with 1 µM DSF after 72 h (**Figure 4.7 D** and **E**). The number of normal eggs was significantly reduced by half at 0.25 and 0.1 µM, while higher concentrations resulted in complete reduction (**Figure 4.7 I**). In contrast, the numbers of abnormally formed eggs were nearly doubled at concentrations below 1 µM (**Figure 4.7 J**).
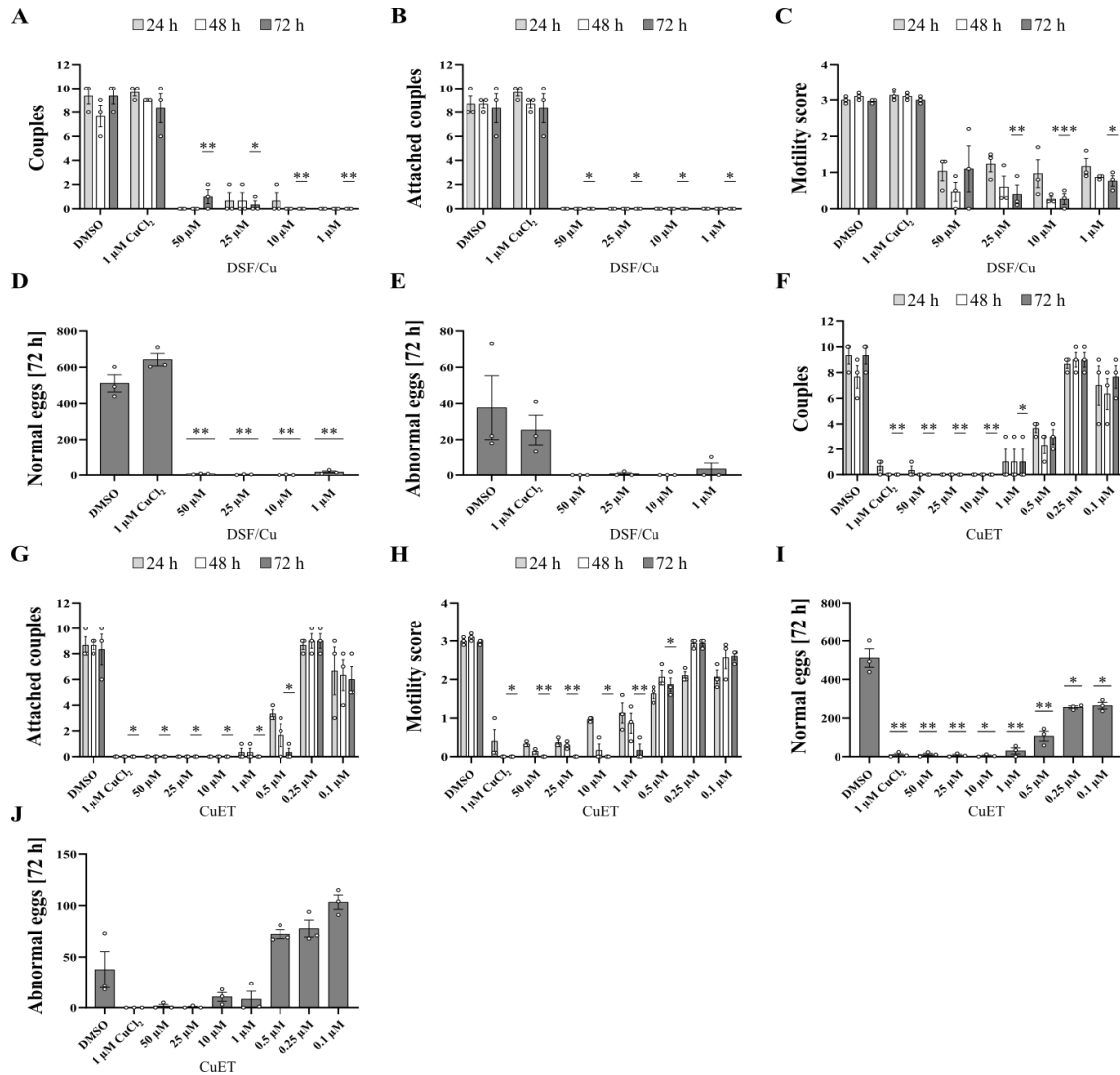
Figure 4.7: Screening of physiological parameters following treatment with DSF in combination with 1 µM CuCl$_2$ or CuET alone

Parameters were assessed during treatment of *S. mansoni* couples with **A** - **E:** varying DSF concentrations (1 - 50 µM DSF) in combination with 1 µM CuCl$_2$ and **E** - **J:** varying CuET concentrations (0.1 - 50 µM). The number of couples (**A**, **F**), attachment of couples (**B**, **G**), motility score (**C**, **H**), and egg count for normally formed eggs (**D**, **I**) and abnormally formed eggs (**E**, **J**), n = 3. Each point represents a measurement (average for motility score) of one experiment with 10 couples each. Columns represent means with StEM. Statistical analysis (two-tailed t-test) was performed using values after 72 h (treatment vs DMSO), p < 0.05 (*), p < 0.01 (**), p < 0.001 (***).

As observed by bright-field microscopy, worms treated with 1 µM DSF and 1 µM CuCl$_2$ (**Figure 4.8 B**) revealed severe tegumental damages in both genders when compared with the controls (**Figure 4.8 A**). Next to the separation of couples, the female and

male worms developed blebs at the tegument, which occurred more frequent with higher DSF concentrations. A change of the tegument was also observed when couples were treated with 5 µM CuET (**Figure 4.8 C**). Next to formation of blebs, detachment of the tegument occurred. These alterations were not observed when couples were treated with lower CuET doses (0.5 and 1 µM, data not shown).
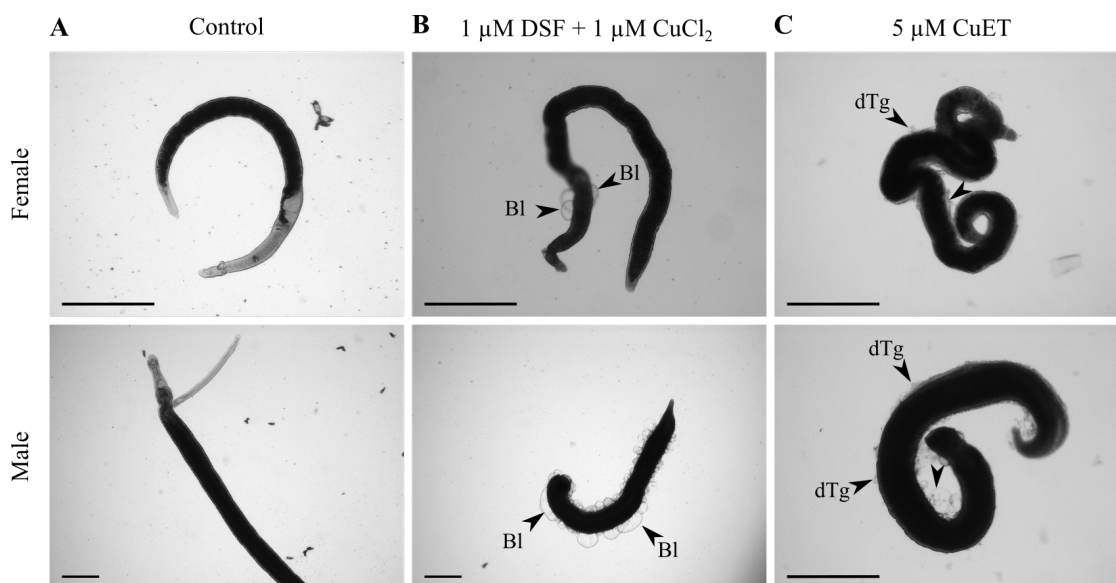
Figure 4.8: Bright-field microscopy of *S. mansoni* couples following DSF/Cu and CuET treatment
S. mansoni couples were treated with **A:** DMSO (control), **B:** 1 µM DSF and 1 µM CuCl$_2$, **C:** 5 µM CuET, and cultured for 72 h. Morphological changes such as the formation of blebs and detachment of the tegument in both genders are indicated by arrowheads. Bl = bleb, dTg = detached tegument. Scale bars represent 500 µm.

For further analysis of morphological alterations, worms were stained with carmine red and fixed for CLSM. Control worms were treated with DMSO, which was the solvent for DSF and CuET (**Figure 4.9 A**). Worms treated with 1 µM DSF and 1 µM CuCl$_2$ showed no alterations in their gonads, whereas detachment of the tegument was clearly recognizable in males (**Figure 4.9 B**). When the concentration of DSF was raised to 10 µM, ovaries and testes appeared lose and disintegrated, while cavities were observed in the vitellaria of females, next to tegument disruptions in both genders (**Figure 4.9 C**). Administration of 0.5 µM CuET did not affect the worm's morphology (data not shown). With 1 µM CuET, the integrity of the worm's gonads appeared to be disrupted without damaging the tegument (**Figure 4.9 D**). Ovarian and testicular dysfunction was more

advanced in 5 µM CuET with formation of cavities in the immature and mature part of the ovaries and formation of cavities within the testes (**Figure 4.9 E**). Again, disintegrated vitellaria were observed in females and, additionally, disruption of tubercles in males.

Finally, analysis of effects on proliferating cells was performed by the EdU assay. Whereas the controls (**Figure 4.10 A**) showed signals of EdU-positive cells inside the ovaries (immature parts) and testes, treatment with the lowest DSF concentration (1 µM) in addition with 1 µM $CuCl_2$ appeared to abolish cell proliferation in the gonads of both genders as no EdU signals were observed (**Figure 4.10 B**). After administration of 0.5 µM CuET (**Figure 4.10 C**), signals occurred that were comparable with the controls, whereas the frequency of EdU-positive cells decreased with 1 µM and completely abolished after administration of 5 µM CuET (**Figure 4.10 D** and **E**).
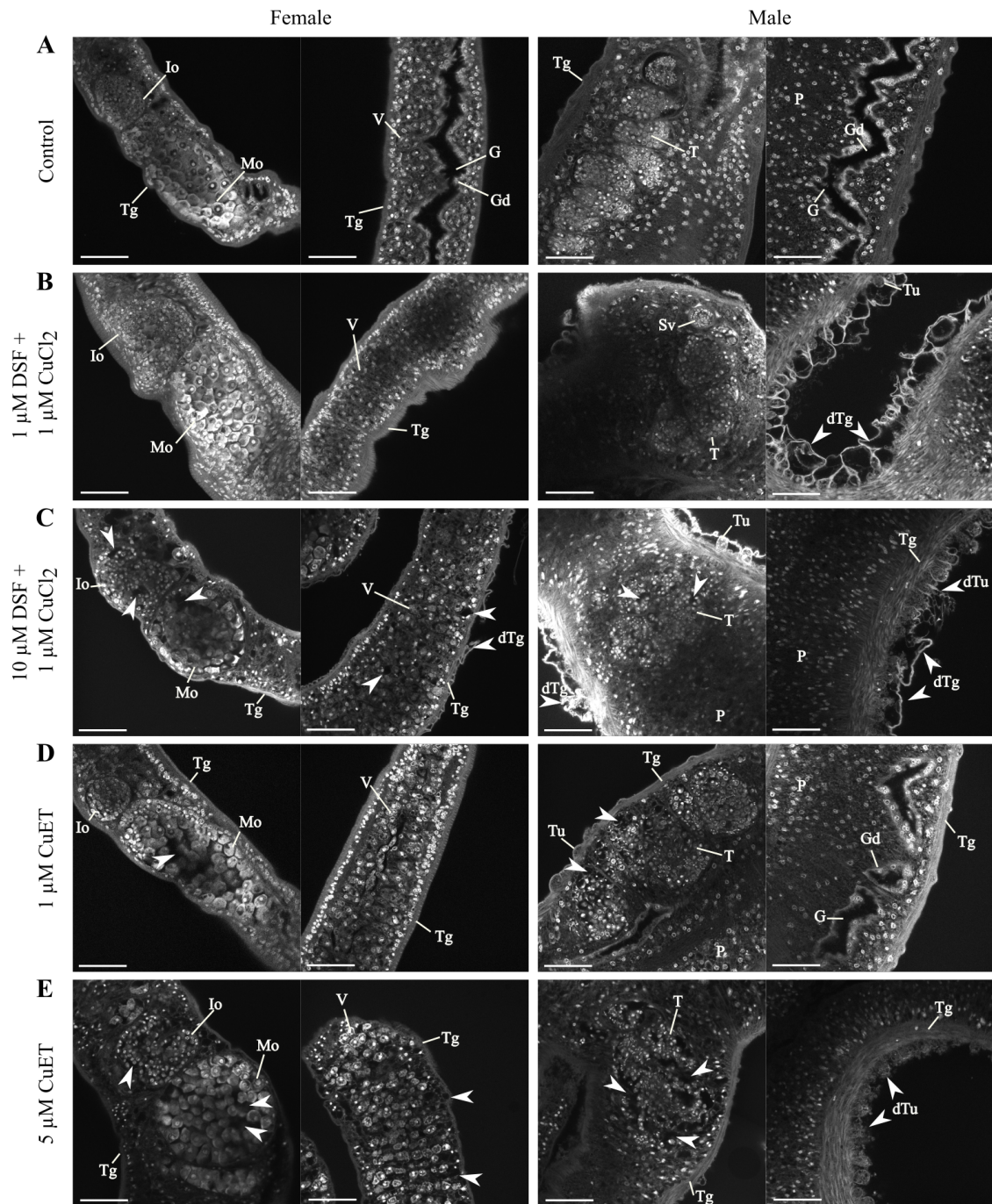
Figure 4.9: Influence of DSF/Cu and CuET on the morphology of adult *S. mansoni* couples Couples were treated with **A:** DMSO (control), **B:** 1 µM DSF and 1 µM CuCl$_2$, **C:** 10 µM DSF and 1 µM CuCl$_2$, **D:** 1 µM CuET, and **E:** 5 µM CuET before fixation after 72 h. Shown are representative examples of female and male worms. Morphological changes such as the destruction of tubercles, detachment of the tegument, and loss of tissue integrity (ovary, vitellarium, and testis) were observed (indicated by arrowheads). dTg = detached tegument, dTu = destroyed tubercle, G = gut, Gd = gastrodermis, Io = part of the ovary containing immature oocytes, Mo = part of the ovary containing mature oocytes, P = parenchyma, Sv = seminal vesicle, T = testis, Tg = tegument, Tu = tubercle, V = vitelline cell. Scale bars represent 50 µm.
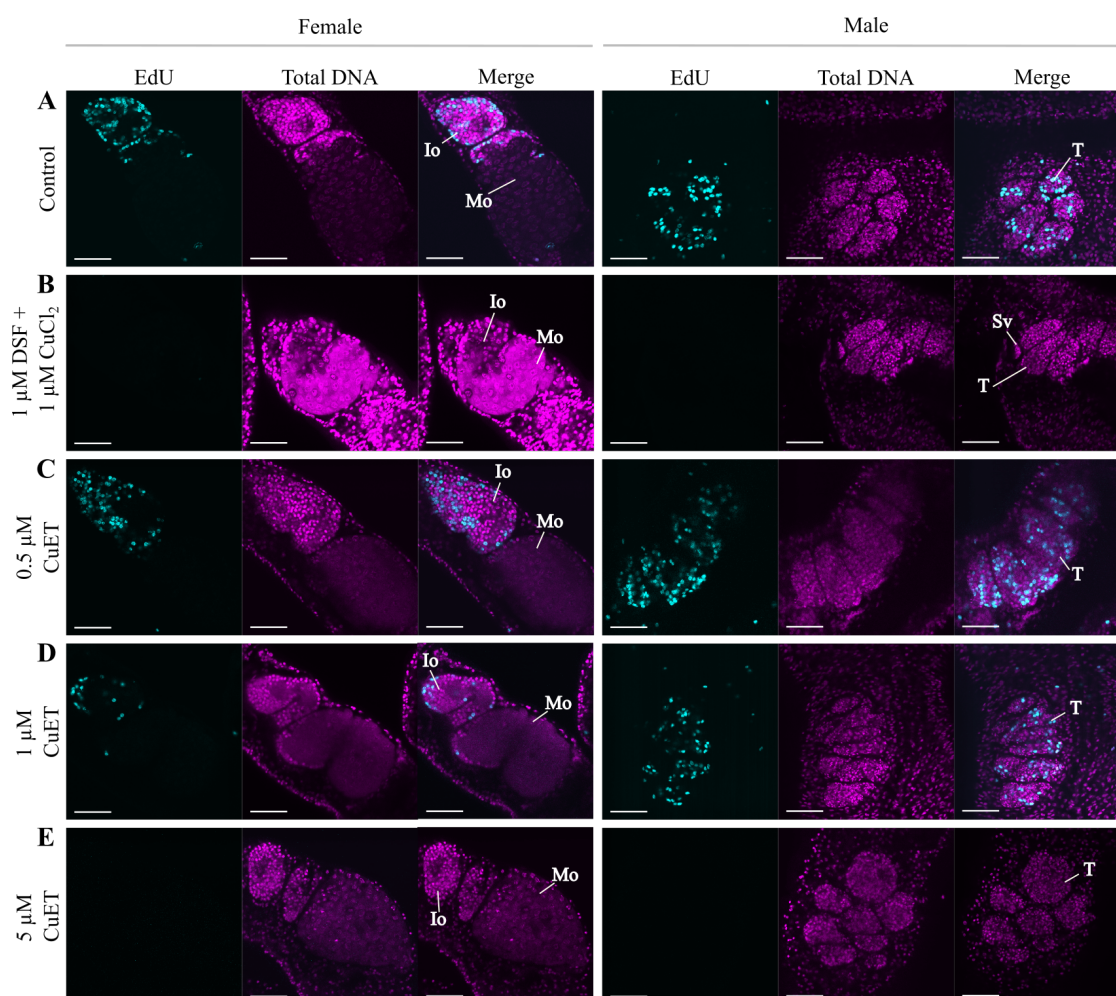
Figure 4.10: Influence of DSF and CuET on proliferation in adult *S. mansoni* couples
Schistosome couples were treated with **A:** the solvent of DSF and CuET (DMSO), **B:** 1 µM DSF and 1 µM CuCl$_2$, **C:** 0.5 µM CuET, **D:** 1 µM CuET, **E:** 5 µM CuET, and cultured for 72 h. EdU was added 24 h prior separation of the couples for fixation of females and males. EdU-positive cells are shown in cyan and the total DNA in magenta. Io = part of the ovary containing immature oocytes, Mo = part of the ovary containing mature oocytes, Sv = seminal vesicle, T = testis. Scale bars represent 50 µm.

4.1.3 The toxic effects of DSF/Cu were partly reversed by chelators

The potential for copper to enhance the toxicity of DSF was highlighted in the previous section (see section 4.1.2). Next, attempts were made to investigate whether the observed toxicity of DSF in combination with copper could be reversed by copper chelators such

as EDTA and BCPD. The ability of BCPD to reverse the copper-mediated toxicity of DSF has been previously investigated and confirmed by others on human cancer cell lines by *in vitro* studies (Brar *et al.*, 2004; Morrison *et al.*, 2010; Skrott *et al.*, 2019).

Application of 0.5 mM BCPD and DSF or DSF/Cu showed dose-dependent effects on worm physiology

Initially, the effects of 0.5 mM BCPD and DSF with and without 1 µM $CuCl_2$ were investigated. The amounts of BCPD and copper were kept constant, only the amount of DSF varied. Pairing stability and worm's attachment capacity were affected in a dose-dependent manner. The numbers of couples were lowest in both treatment approaches at highest DSF concentrations (**Figure 4.11 A** and **F**). The number of couples increased slightly towards the end of the observation period. Triple treatment of BCPD and DSF/Cu resulted in a slightly lower number of couples compared to those of the double treatment groups (0.5 mM BCPD and DSF). For both treatment approaches, the number of attached couples was lowest at the highest DSF concentration and increased as the DSF dose decreased (**Figure 4.11 B** and **G**). Motility was mainly affected with 50 µM DSF (score = 2) but increased to normal movements at DSF concentrations below 10 µM in the double treatment approach (**Figure 4.11 C**). In contrast, normal movements were observed only at 1 µM DSF in the triple treatment group (**Figure 4.11 H**). In both treatment approaches, the numbers of normal eggs were comparable to those of the controls only with 1 µM DSF, whereas administration of 10 µM DSF resulted in a significant reduction to less than one quarter (**Figure 4.11 D** and **I**). The numbers of abnormal eggs were lowest at higher DSF concentrations (25 and 50 µM) but increased at 1 µM DSF in both treatment approaches (**Figure 4.11 E** and **J**). In summary, the combination of 0.5 mM BCPD and DSF/Cu had a slightly stronger effect on worm physiology than the approach without 1 µM $CuCl_2$. No morphological changes were observed during scoring of the worms.

For further analysis, worms were fixed and carmine-stained following treatments after 72 h. The solvent of DSF (DMSO) served as control (**Figure 4.12 A**). Comparison of 0.5 mM BCPD with the control revealed no alterations of the morphology of worm organs (**Figure 4.12 B**). Neither 0.5 mM BCPD and 50 µM DSF nor 0.5 mM BCPD and 50 µM DSF and 1 µM $CuCl_2$ displayed morphological changes of the organs (**Figure 4.12 C** and **D**).
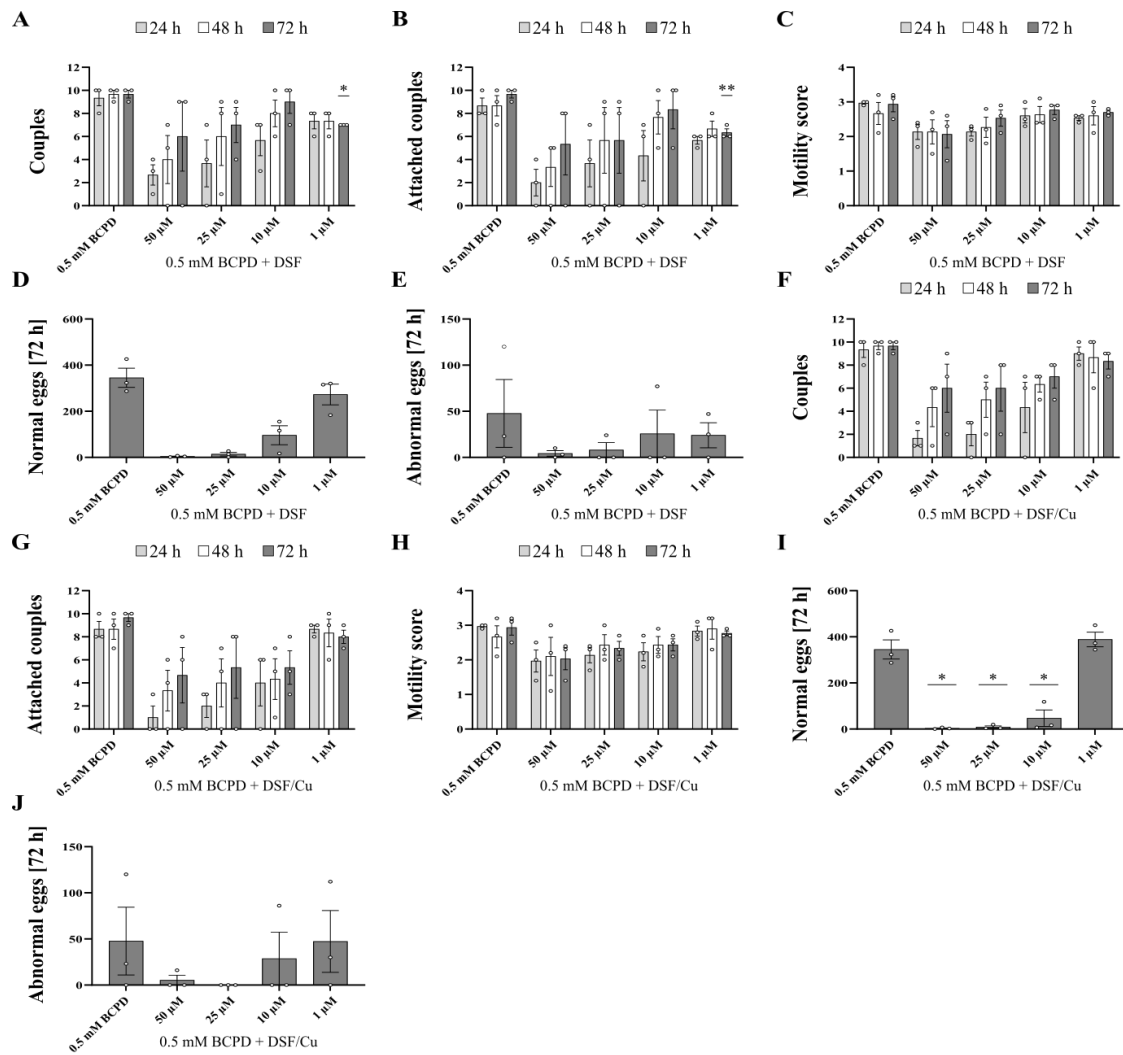
Figure 4.11: Screening of physiological parameters following treatment with 0.5 mM BCPD and DSF or DSF/Cu

S. mansoni couples were treated with **A** - **E:** 0.5 mM BCPD and varying DSF concentrations (1 - 50 µM) and **F** - **J:** 0.5 mM BCPD, 1 µM CuCl$_2$, and varying DSF concentrations (1 - 50 µM). Shown are the assessed number of couples (**A**, **F**), the attachment of couples (**B**, **G**), the motility score (**C**, **H**), and egg count for normal (**D**, **I**) and abnormal eggs (**E**, **J**), n = 3. Each point represents one experiment (average for motility score) with 10 couples each. Columns represent means with StEM. Statistical analysis (two-tailed t-test) was performed using values after 72 h (treatment vs 0.5 mM BCPD), $p < 0.05$ (*), $p < 0.01$ (**).
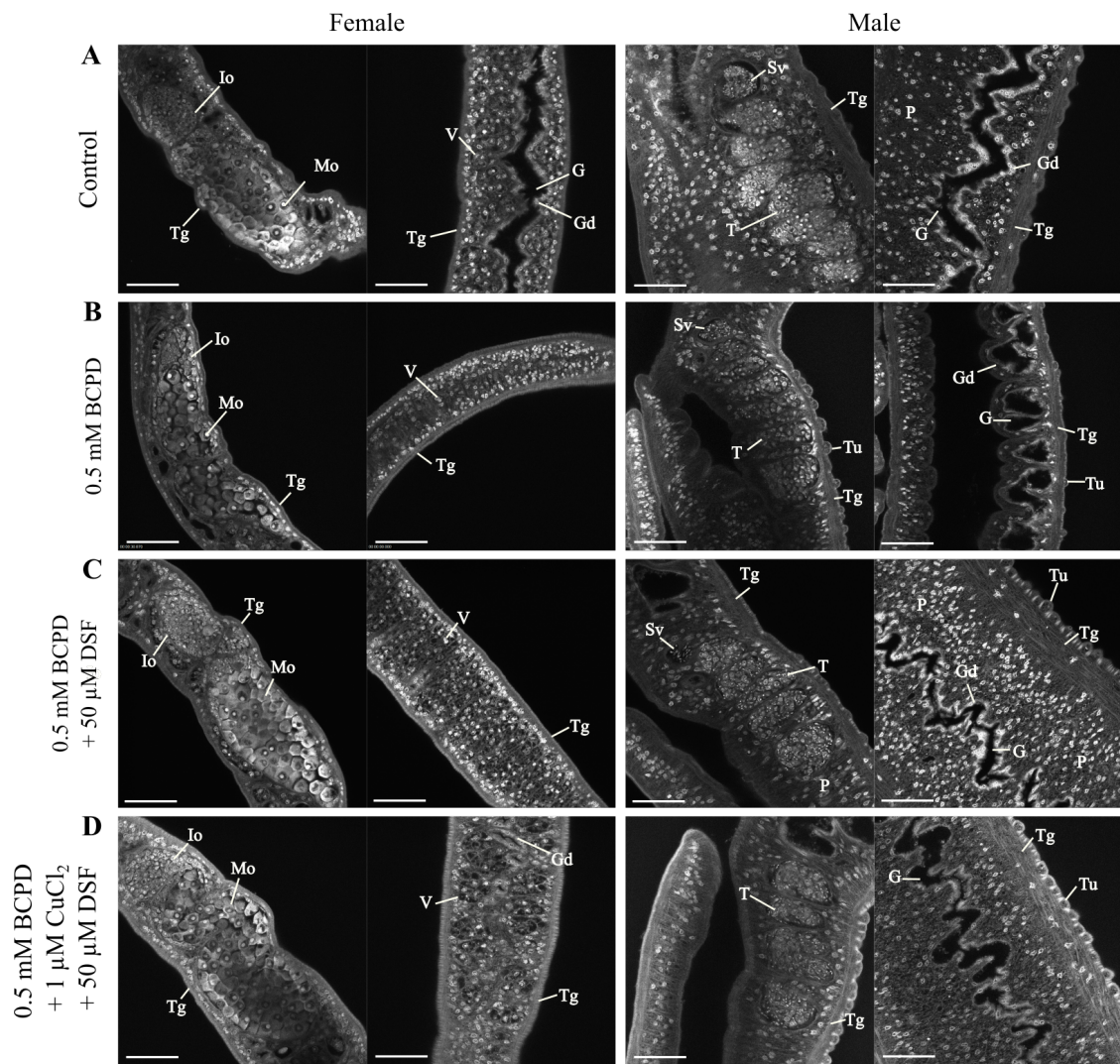
Figure 4.12: Influence of 0.5 mM BCPD and DSF or DSF/Cu on the morphology of adult
***S. mansoni* couples**
Couples were treated with **A:** DMSO, **B:** 0.5 mM BCPD, **C:** 0.5 mM BCPD and 50 µM DSF, and **D:** 0.5 mM BCPD, 1 µM CuCl$_2$, and 50 µM DSF. Worms were separated before analysis after 72 h. No morphological changes were observed. G = gut, Gd = gastrodermis, Io = part of the ovary containing immature oocytes, Mo = part of the ovary containing mature oocytes, P = parenchyma, Sv = seminal vesicle, T = testis, Tg = tegument, Tu = tubercle, V = vitelline cell. Scale bars represent 50 µm.

To investigate the effect of 0.5 mM BCPD and 50 µM DSF with or without 1 µM CuCl$_2$ on cell proliferation in female ovaries and male testes, EdU assays were performed. In the control (**Figure 4.13 A**) signals of EdU-positive cells were observed within the immature parts of ovaries (oogonia) and in testes (spermatogonia). Treatment with 0.5 mM BCPD displayed no changes compared with the control (**Figure 4.13 B**). Some

immature oocytes as well as some spermatogonia appeared EdU-positive comparable with those observed in the DMSO and 0.5 mM BCPD treatment groups (**Figure 4.13 C** and **D**).
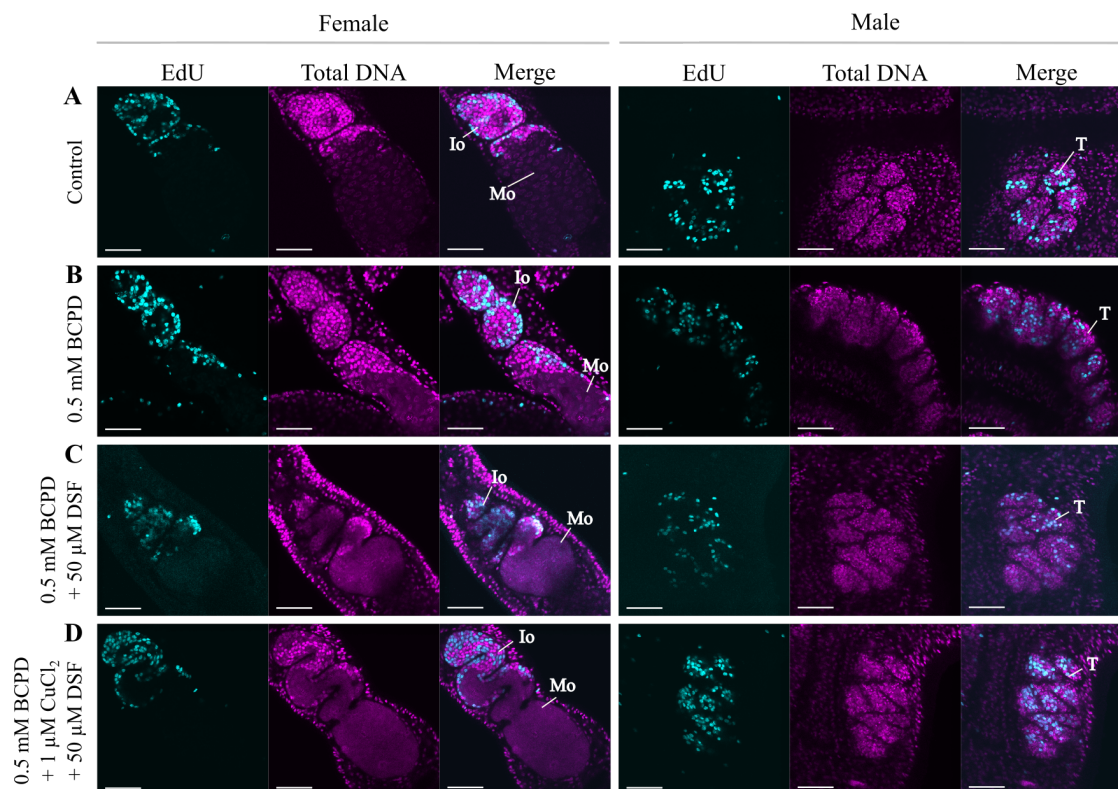
Figure 4.13: Influence of 0.5 mM BCPD and DSF or DSF/Cu on proliferation in adult
***S. mansoni* couples**
Couples were treated with **A:** DMSO, **B:** 0.5 mM BCPD, **C:** 0.5 mM BCPD and 50 µM DSF, and **D:** 0.5 mM BCPD, 1 µM CuCl$_2$, and 50 µM DSF. EdU was added 24 h prior separation of the couples for fixation of females and males. EdU-positive cells are shown in cyan and the total DNA in magenta. The signals of all treatment conditions were comparable to those of the control group. Io = part of the ovary containing immature oocytes, Mo = part of the ovary containing mature oocytes, T = testis. Scale bars represent 50 µm.

Application of 2 mM BCPD and DSF or DSF/Cu showed no negative effects on worm physiology

As shown previously (see section 4.1.3), 0.5 mM BCPD added to the *S. mansoni* culture was able to reverse some of the negative effects of DSF and DSF/Cu. Here, an approach with a higher amount of BCPD (2 mM) was performed to analyze the overall potential

of BCPD to prevent formation of CuET when DSF/Cu was applied on *S. mansoni* couples.

The pairing stability of the worms was comparable between the experimental approaches with and without 1 μM CuCl$_2$ with about 20 % fewer couples than in the control (2 mM BCPD) after 72 h, whereas the number of couples was slightly lower in the treatment groups with 1 μM CuCl$_2$ after 24 h (**Figure 4.14 A** and **F**). The attachment rate increased over time and was dose-dependent in both treatment approaches, with 50 μM DSF displaying the lowest number of attached couples (**Figure 4.14 B** and **G**). Worm motility was reduced at the highest DSF concentration (50 μM), with a slightly higher decrease in the group, which was additionally treated with 1 μM CuCl$_2$ (**Figure 4.14 C** and **H**). The number of normal eggs was reduced by about half at 1 μM DSF, and almost no eggs were observed with 10 μM DSF and higher concentrations in both treatment approaches after 72 h (**Figure 4.14 D** and **I**). When 2 mM BCPD and DSF were administered, only a low number of abnormal eggs was found, whereas in the groups additionally treated with 1 μM CuCl$_2$ no abnormally formed eggs were found (**Figure 4.14 E** and **J**). Overall, the combination of 2 mM BCPD and DSF/Cu appeared to have only a slightly stronger effect on worm physiology than the approach without 1 μM CuCl$_2$.

During the scoring period, no morphological changes were observed on the worms. To analyze whether the treatments affected the internal structures of the worms, a CLSM-based analysis of carmine-stained worms was performed. Control worms were treated with DMSO (**Figure 4.15 A**). 2 mM BCPD alone showed no effects on worm organs when compared with the control (**Figure 4.15 B**). Analysis of worms treated with 2 mM BCPD and 50 μM DSF (**Figure 4.15 C**) and additionally with 1 μM CuCl$_2$ (**Figure 4.15 D**) revealed no effects on gonads, vitellaria, or guts of worms.

Finally, a potential influence on cell proliferation was investigated using an EdU assay. Application of 2 mM BCPD showed signals in the ovaries and testes comparable to those in the controls (**Figure 4.16 A** and **B**). The same applied, when couples treated with 2 mM BCPD and 50 μM DSF (**Figure 4.16 C**) and 2 mM BCPD, 1 μM CuCl$_2$ and 50 μM DSF (**Figure 4.16 D**) were used for EdU-assays. Signals were obtained in immature oocytes of ovaries and spermatogonia of testes. No negative effects on cell proliferation was observed.
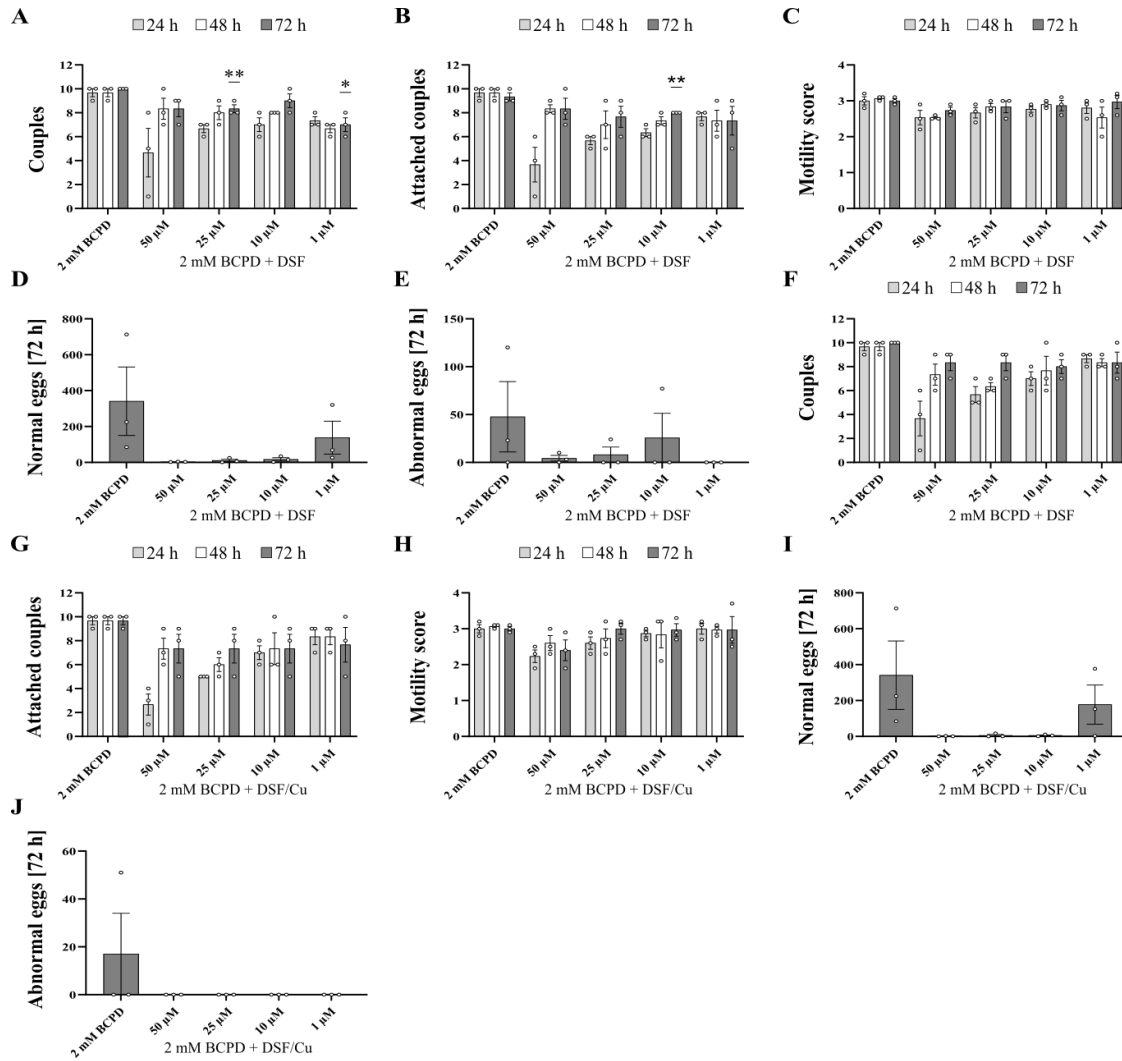
Figure 4.14: Screening of physiological parameters following treatment with 2 mM BCPD and DSF or DSF/Cu

S. mansoni couples were treated with **A** - **E:** 2 mM BCPD and varying concentrations of DSF (1 - 50 µM) and **F** - **J:** 2 mM BCPD, 1 µM $CuCl_2$, and DSF (1 - 50 µM). During treatment, the number of couples (**A**, **F**), the attachment of couples (**B**, **G**), the motility score (**C**, **H**), and egg count for normal (**D**, **I**) and abnormal eggs (**E**, **J**) were assessed every 24 h, n = 3. Each point represents one experiment (average for motility score). Columns represent means with StEM. Statistical analysis (two-tailed t-test) was performed using values after 72 h (treatment vs 2 mM BCPD), $p < 0.05$ (*), $p < 0.01$ (**).
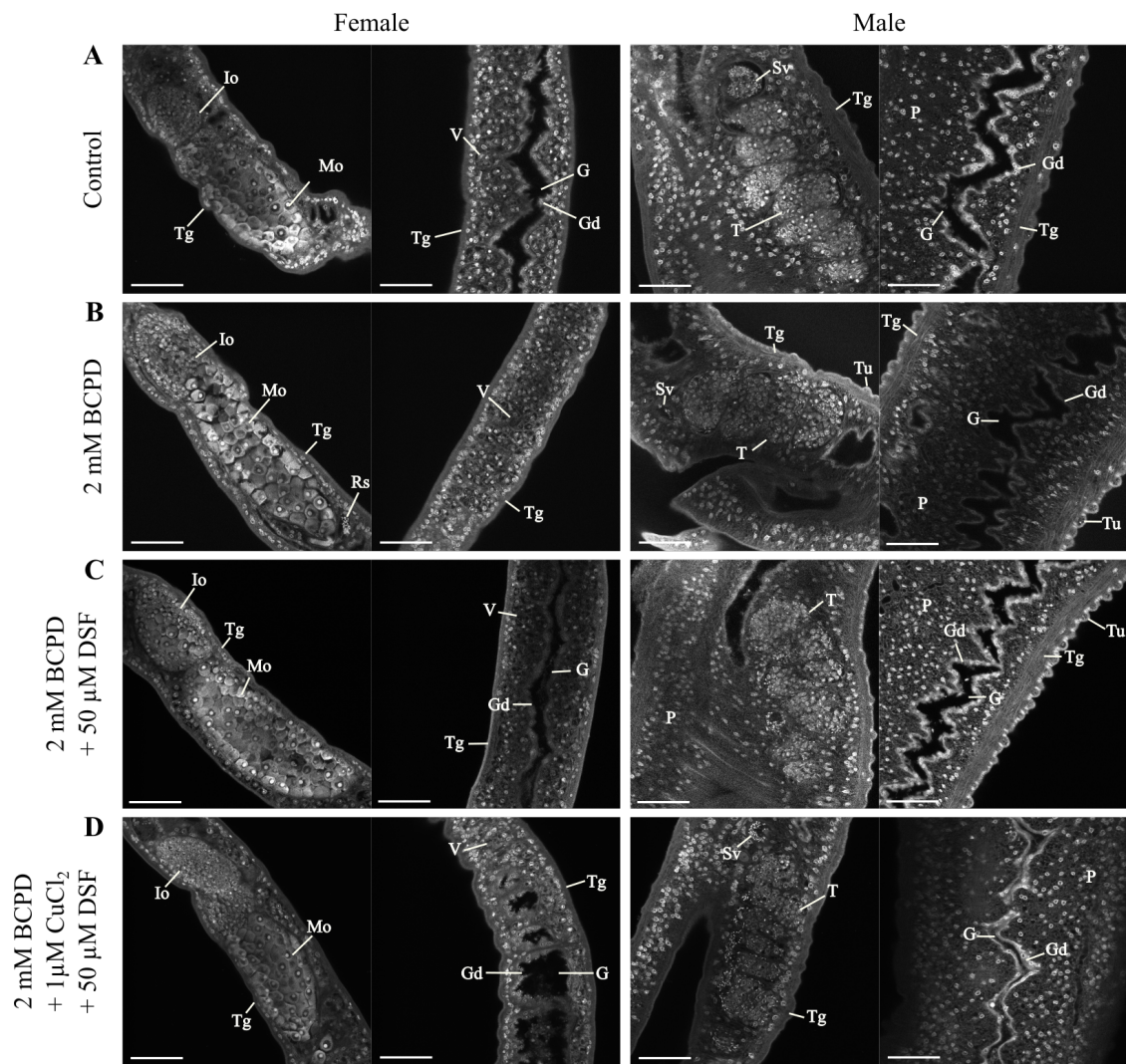
Figure 4.15: Influence of 2 mM BCPD and DSF or DSF/Cu on the morphology of adult *S. mansoni* couples

Couples were treated with **A:** DMSO as control, **B:** 2 mM BCPD, **C:** 2 mM BCPD and 50 µM DSF, and **D:** 2 mM BCPD, 1 µM CuCl$_2$ and 50 µM DSF. Worms were separated for analysis after 72 h. G = gut, Gd = gastrodermis, Io = part of the ovary containing immature oocytes, Mo = part of the ovary containing mature oocytes, P = parenchyma, Rs = *Receptaculum seminis*, Sv = seminal vesicle, T = testis, Tg = tegument, Tu = tubercle, V = vitelline cell. Scale bars represent 50 µm.
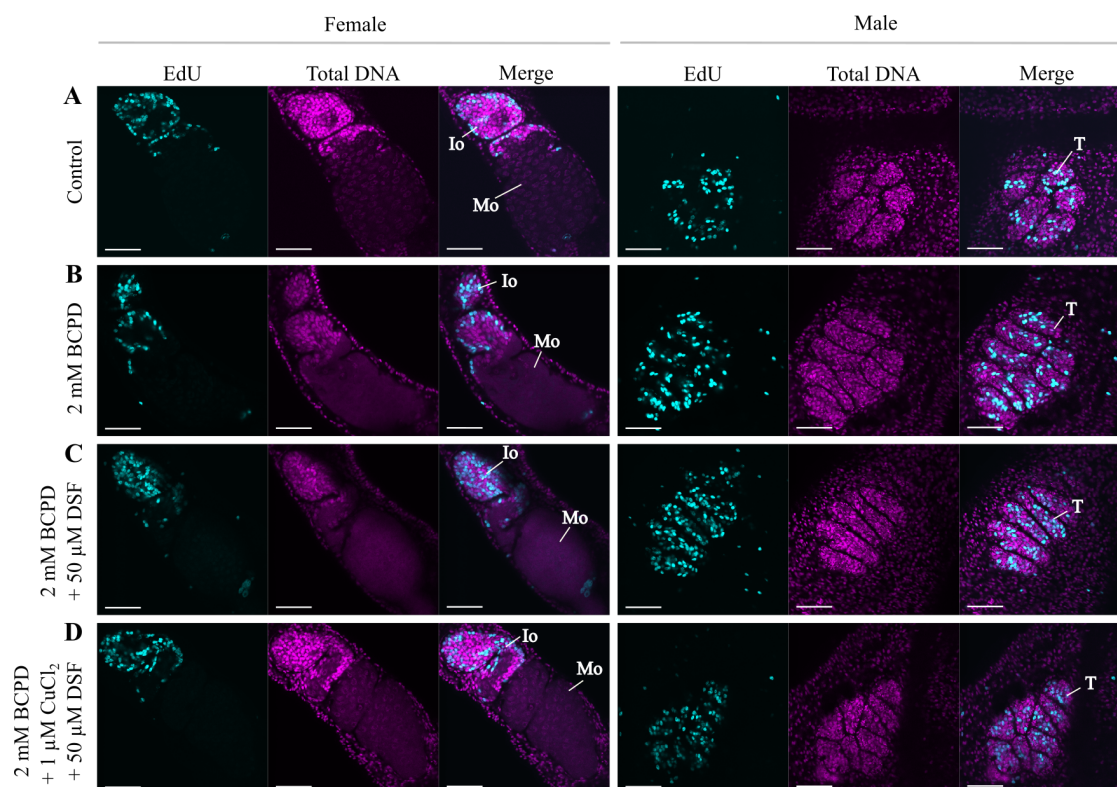
Figure 4.16: Influence of 2 mM BCPD and DSF or DSF/Cu on proliferation in adult *S. mansoni* couples

Schistosome couples were treated with **A:** DMSO as control, **B:** 2 mM BCPD, **C:** 2 mM BCPD and 50 µM DSF, and **D:** 2 mM BCPD, 1 µM CuCl$_2$ + 50 µM DSF. EdU was added 24 h prior separation of the couples for fixation of females and males. EdU-positive cells are shown in cyan and the total DNA in magenta. Io = part of the ovary containing immature oocytes, Mo = part of the ovary containing mature oocytes, T = testis. Scale bars represent 50 µm.

Application of 0.5 mM EDTA and DSF or DSF/Cu showed tremendous effects on worm physiology and cell proliferation

In addition to BCPD, which has already been analyzed for its potential to reverse the effects of DSF and copper before, the potential of EDTA as a chelating agent was also investigated. For this purpose, 0.5 mM EDTA was used as a starting point and administered to the worm cultures in combination with various DSF concentrations (1 - 50 µM) and additionally with 1 µM CuCl$_2$. In the following, the effects of 0.5 mM EDTA in combination with DSF or DSF/Cu are described.

The influence of 0.5 mM EDTA was similar to DMSO or medium alone (data not shown) and served as control during the treatments. While the number of couples appeared to be reduced in a dose-dependent manner by DSF administration after 24 h, the number increased to that of the control after 72 h (**Figure 4.17 A**). In contrast, when 1 µM $CuCl_2$ was added to the culture, nearly 100 % separation of couples occurred (**Figure 4.17 F**). In parallel, the number of attached couples decreased with the separation of the latter (**Figure 4.17 G**). In contrast, in cultures without 1 µM $CuCl_2$, the numbers of attached couples corresponded to the number of total couples in the culture (**Figure 4.17 B**). Worm motility was slightly reduced with a minimum value of 2.3 at 10 µM DSF after 24 h, which increased to 2.7 after 72 h in the double treatment groups (0.5 mM EDTA and DSF) (**Figure 4.17 C**). Worms treated additionally with 1 µM $CuCl_2$ showed a decrease in motility at all DSF concentrations to 1 after 72 h (**Figure 4.17 H**). Determination of the number of eggs revealed a reduction of normal eggs to about one third of the controls at 1 µM DSF in the groups without 1 µM $CuCl_2$, while the number was reduced by almost 94 % when 1 µM $CuCl_2$ was added. But at higher concentrations, the values decreased further in both treatment approaches (**Figure 4.17 D** and **I**). The number of abnormal eggs was comparable to those in the controls for 1 and 10 µM DSF, while higher concentrations decreased the number of eggs (**Figure 4.17 E**). In the presence of 1 µM $CuCl_2$, the number of abnormal eggs was reduced to about one fifth at 1 and 10 µM DSF and an even further reduction was observed at higher concentrations (**Figure 4.17 J**).

Even though no morphological changes were observed in treated worms during the treatment regime, EDTA seemed not to prevent the formation of CuET in cultures when administered as 0.5 mM. For further analysis on morphology, treated worms were analyzed by CLSM. When the 0.5 mM EDTA group was compared with the control group, no changes were observed (**Figure 4.18 A** and **B**). The combined treatment of 0.5 mM EDTA and 50 µM DSF showed no alterations compared to the control worms. The ovaries and testes were structured, displaying normal distribution of oogonia and spermatogonia as well as spermatozoa in the seminal vesicles (**Figure 4.18 C**). The structure of some female ovaries appeared disintegrated, but no further changes were observed in females and males after combined treatment with 0.5 mM EDTA, 50 µM DSF, and 1 µM $CuCl_2$ after 72 h (**Figure 4.18 D**).

Next, the effect on proliferation of oogonia and spermatogonia was evaluated using the EdU assays and CLSM. Administration on 0.5 mM EDTA alone showed signals of

EdU-positive cells comparable with the controls (**Figure 4.19 A** and **B**). When 0.5 mM EDTA and DSF were simultaneously applied, the signals seemed reduced in female ovaries but not in male testes (**Figure 4.19 C**). The presence of 1 µM $CuCl_2$ appeared to have more drastic effects, as the signals were reduced in the gonads of females and males when combined with 0.5 mM EDTA and 50 µM DSF (**Figure 4.19 D**).
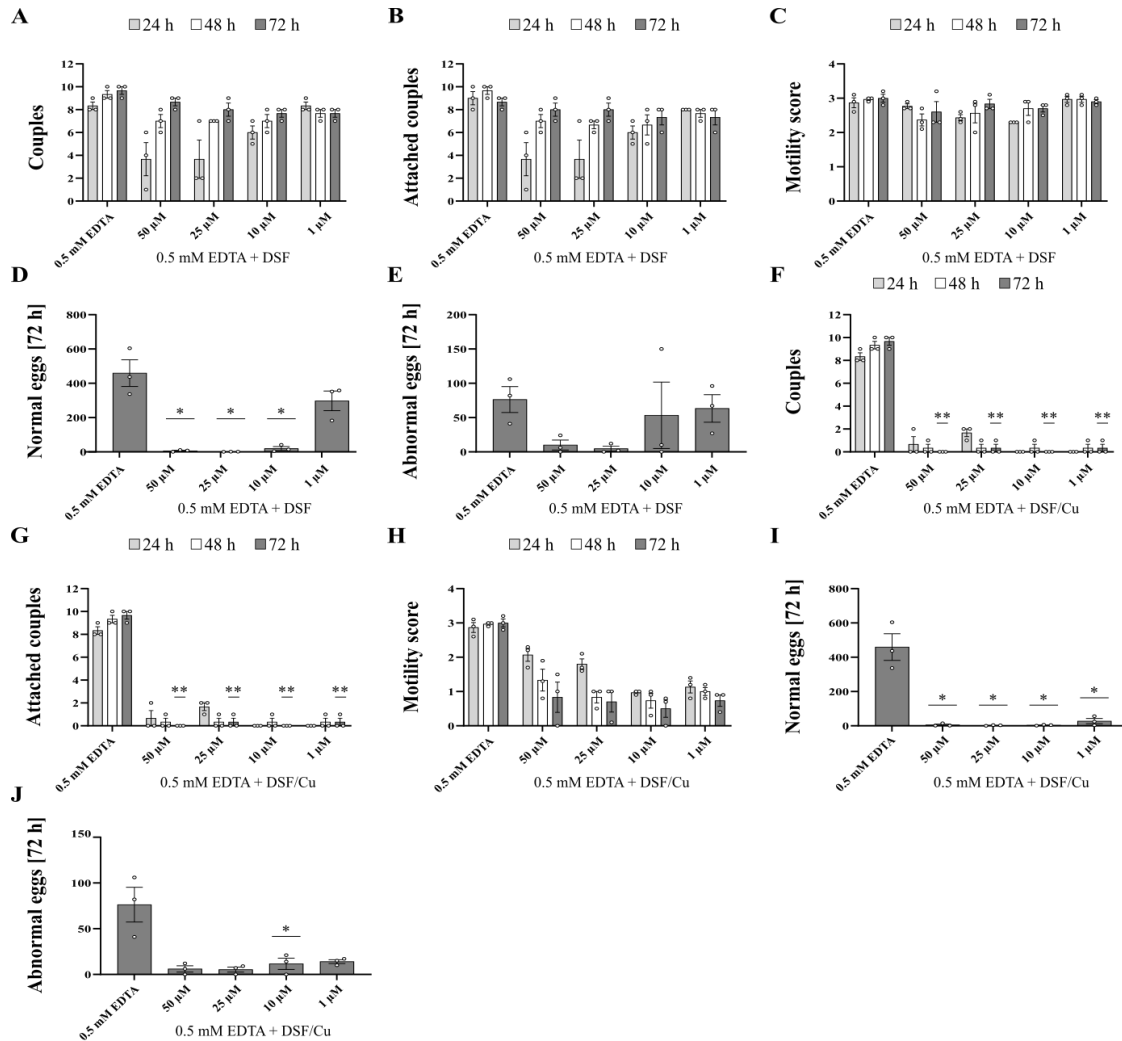
Figure 4.17: Screening of physiological parameters following treatment with 0.5 mM EDTA and DSF or DSF/Cu

S. mansoni couples were treated with **A** - **E:** 0.5 mM EDTA and varying DSF concentrations (1 - 50 µM) and **F** - **J:** 0.5 mM EDTA, 1 µM $CuCl_2$ and varying DSF concentrations (1 - 50 µM). Shown are the assessed number of couples (**A**, **F**), the attachment of couples (**B**, **G**), the motility score (**C**, **H**), and egg count for normal (**D**, **I**) and abnormal eggs (**E**, **J**), n = 3. Each point represents one experiment (average for motility score) with 10 couples each. Columns represent means with StEM. Statistical analysis (two-tailed t-test) was performed using values after 72 h (treatment vs 0.5 mM EDTA), $p < 0.05$ (*), $p < 0.01$ (**).
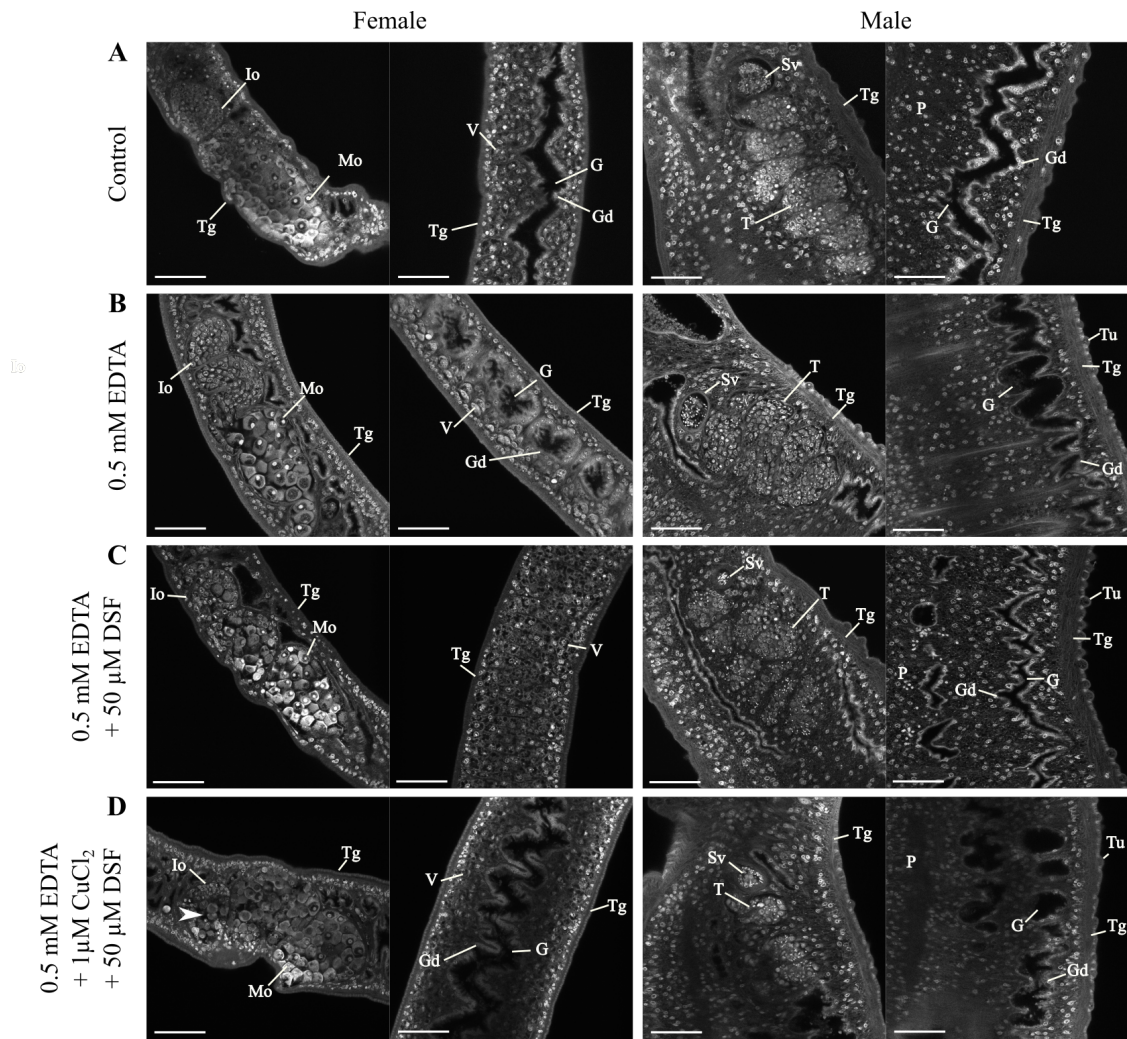
Figure 4.18: Influence of 0.5 mM EDTA and DSF or DSF/Cu on the morphology of adult *S. mansoni* couples

Couples were treated with **A:** DMSO, **B:** 0.5 mM EDTA, **C:** 0.5 mM EDTA and 50 µM DSF, and **D:** 0.5 mM EDTA, 1 µM CuCl$_2$, and 50 µM DSF, where the integrity of female ovaries seemed to be disrupted as indicated by an arrowhead. Worms were analyzed after 72 h. G = gut, Gd = gastrodermis, Io = part of the ovary containing immature oocytes, Mo = part of the ovary containing mature oocytes, P = parenchyma, Sv = seminal vesicle, T = testis, Tg = tegument, Tu = tubercle, V = vitelline cell. Scale bars represent 50 µm.
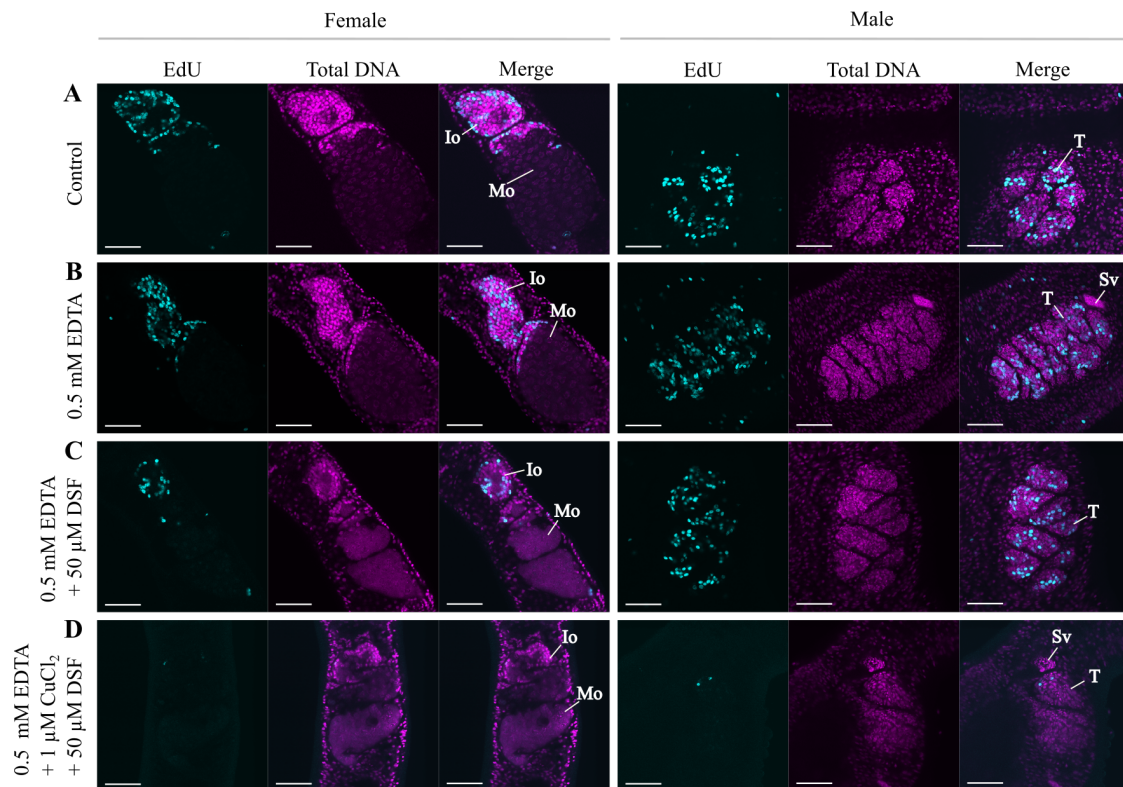
Figure 4.19: Influence of 0.5 mM EDTA and DSF or DSF/Cu on proliferation in adult
***S. mansoni* couples**

Shown are *S. mansoni* couples treated with **A:** DMSO, **B:** 0.5 mM EDTA, **C:** 0.5 mM EDTA and
50 µM DSF, where signals appeared to be reduced, and **D:** 0.5 mM EDTA, 1 µM $CuCl_2$, and
50 µM DSF, where almost no signals were observed in the gonasd in both genders. EdU was
added 24 h prior separation of the couples for fixation of females and males after 72 h. EdU-
positive cells are shown in cyan and the total DNA in magenta. Io = part of the ovary containing
immature oocytes, Mo = part of the ovary containing mature oocytes, Sv = seminal vesicle, T =
testis. Scale bars represent 50 µm.

Application of 2 mM EDTA and DSF or DSF/Cu showed dose-pendent effects

Since 0.5 mM EDTA failed to neutralize the effects of DSF/Cu (see previous section
4.1.3), a higher EDTA concentration (kept constant at 2 mM) was tested. As shown
in **Figure 4.20**, the control (2 mM EDTA itself) showed already an impact on the
evaluated parameters. Furthermore, a dose-dependent effect was observed with increase
in the number of couples when lower doses of DSF were used, while the number of
attached couples also increased with lower DSF concentrations (**Figure 4.20 A** and **B**).

In contrast, in the presence of 1 µM CuCl$_2$, almost all couples were separated and found to be detached after 24 h and remained separated until the end of the observation period (**Figure 4.20 F** and **G**). Motility decreased to 2 in the control group and varied slightly in the double (2 mM EDTA and DSF) and triple (2 mM EDTA and DSF/Cu) treatment approaches, with the highest decrease observed in the triple treatment group after 72 h (**Figure 4.20 C** and **H**). Only few normal and abnormal eggs were found when DSF was administered above 1 µM, but with 1 µM DSF, the numbers of eggs were comparable to those of the control groups (**Figure 4.20 D** and **E**). In triple treatment approaches with DSF/Cu, almost no normal eggs were found, and the number of abnormal eggs was also low with DSF concentrations above 1 µM (**Figure 4.20 I** and **J**). Despite the tremendous effect of 2 mM EDTA alone, the presence of 1 µM CuCl$_2$ worsened the effect of DSF.

Next, the morphology of treated worms was evaluated by CLSM analysis. No changes were observed in organs such as ovaries, testes or gut in the presence of DMSO, which served as a control, or 2 mM EDTA (**Figure 4.21 A** and **B**). Even after addition of 50 µM DSF, no morphological changes were observed (**Figure 4.21 C**). When 50 µM DSF and 1 µM CuCl$_2$ were used, some female ovaries appeared to lose their integrity and revealed empty spaces, which were also observed in some testes of the males (**Figure 4.21 D**).

The effects of 2 mM EDTA and 50 µM DSF and additionally 1 µM CuCl$_2$ on cell proliferation were evaluated next. As shown in **Figure 4.22 A** and **B**, 2 mM EDTA alone displayed signals of EdU-positive cells in the oogonia of ovaries and spermatogonia of testes comparable to the control worms (DMSO-treated). With addition of 50 µM DSF, no signals were observed in the males but in females (**Figure 4.22 C**). Combined treatment of 2 mM EDTA, 50 µM DSF and 1 µM CuCl$_2$ showed no signals in the analyzed worms (**Figure 4.22 D**). The negative effect of DSF and copper on cell proliferation seemed not to be reversible by adding 2 mM EDTA.
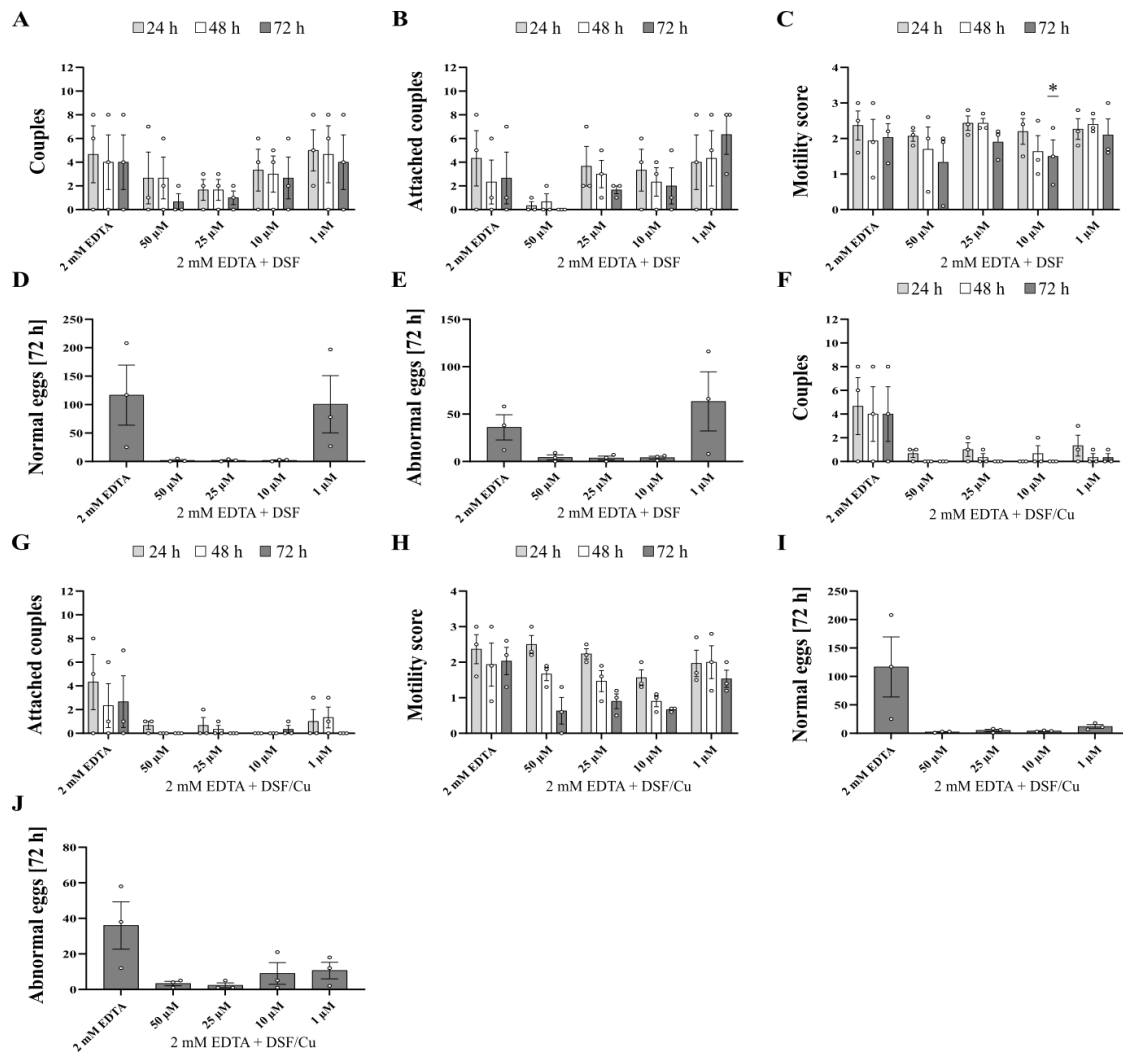
Figure 4.20: Screening of physiological parameters follwoing treatment with 2 mM EDTA and DSF or DSF/Cu

S. mansoni couples were treated with **A** - **E:** 2 mM EDTA and varying concentrations of DSF (1 - 50 µM) and **F** - **J:** 2 mM EDTA, 1 µM CuCl$_2$, and DSF (1 - 50 µM). During treatment, the number of couples (**A**, **F**), the attachment of couples (**B**, **G**), the motility score (**C**, **H**), and egg count for normal (**D**, **I**) and abnormal eggs (**E**, **J**) were assessed every 24 h, n = 3. Each point represents one experiment (average for motility score) with 10 couples each. Columns represent means with StEM. Statistical analysis (two-tailed t-test) was performed using values after 72 h (treatment vs 2 mM EDTA), p < 0.05 (*).
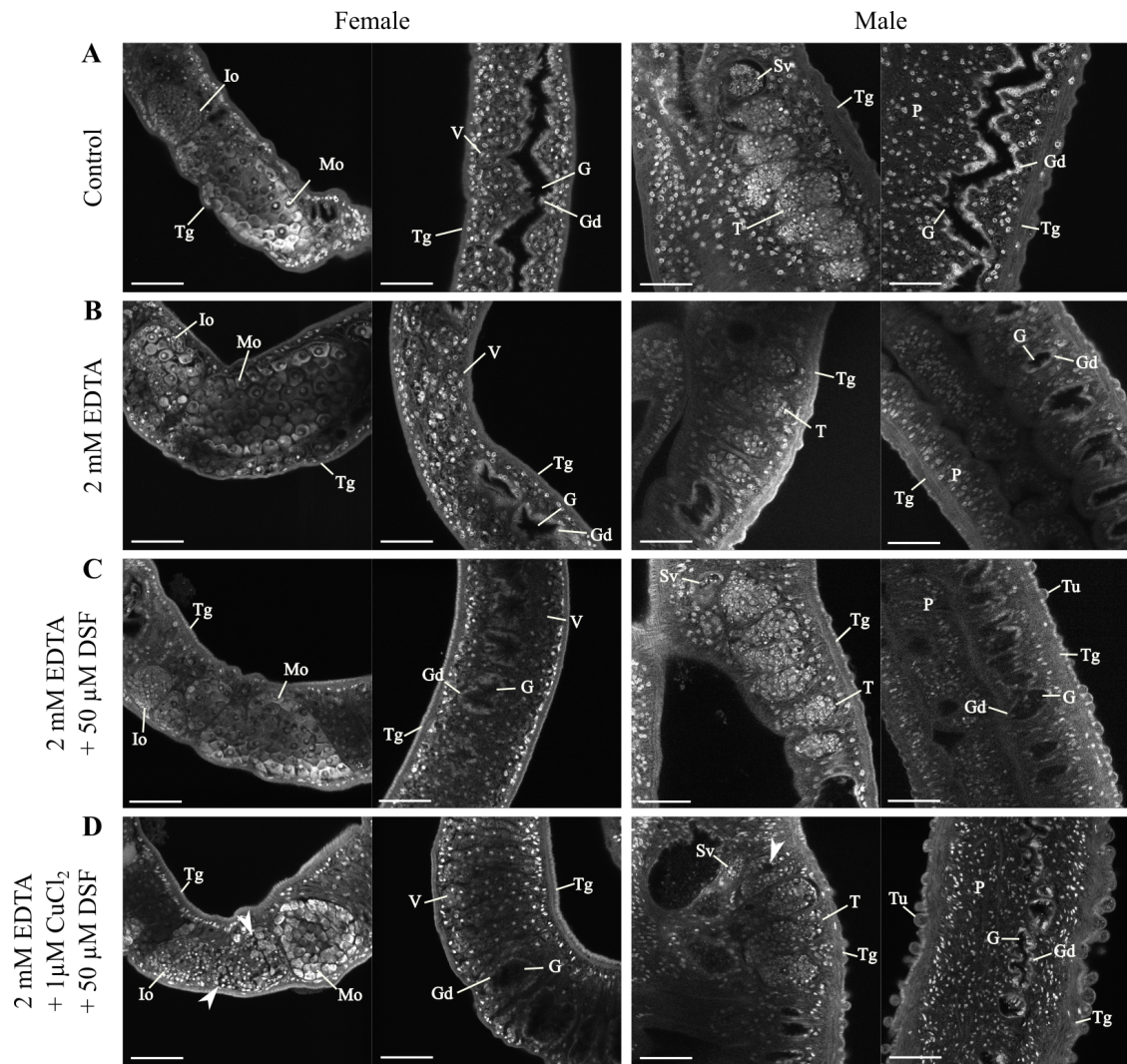
Figure 4.21: Influence of 2 mM EDTA and DSF or DSF/Cu on the morphology of adult *S. mansoni* couples

Couples were treated with **A:** DMSO as control, **B:** 2 mM EDTA, **C:** 2 mM EDTA and 50 µM DSF, and **D:** 2 mM EDTA, 1 µM CuCl$_2$, and 50 µM DSF, where some empty areas occurred in the gonads (indicated by arrowheads). Worms were separated for CLSM analysis after 72 h. G = gut, Gd = gastrodermis, Io = part of the ovary containing immature oocytes, Mo = part of the ovary containing mature oocytes, P = parenchyma, Sv = seminal vesicle, T = testis, Tg = tegument, Tu = tubercle, V = vitelline cell. Scale bars represent 50 µm.
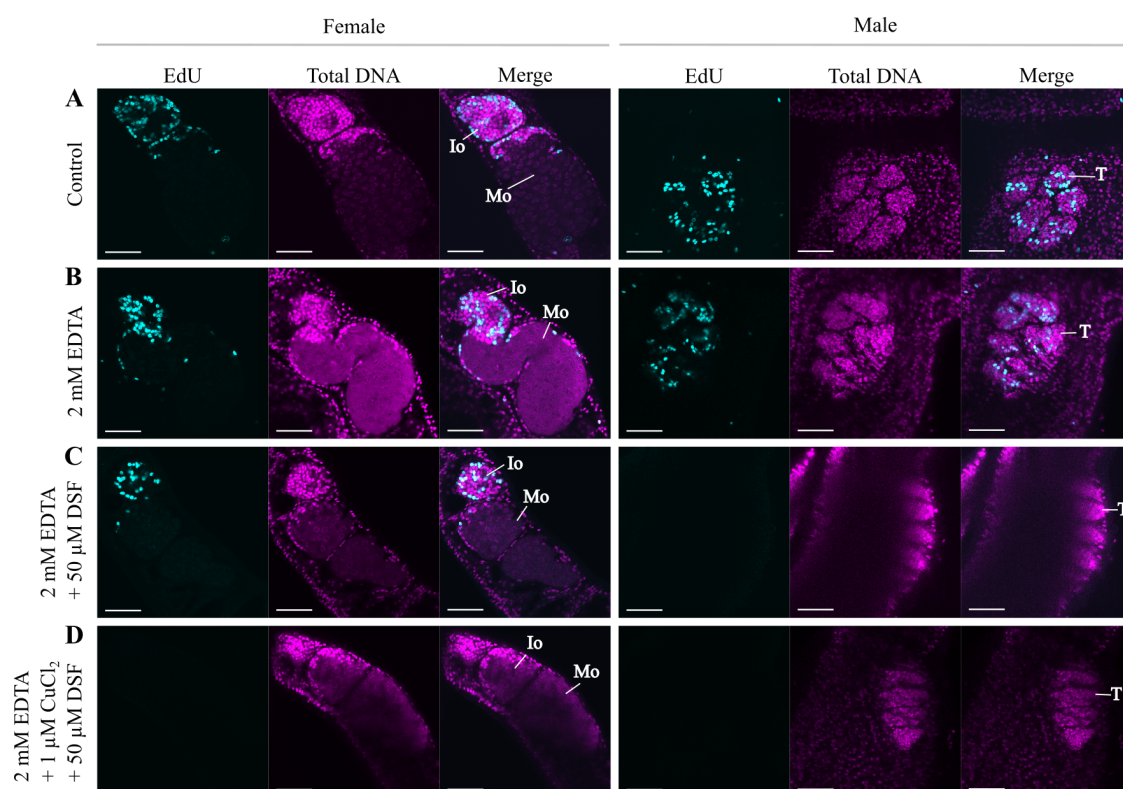
Figure 4.22: Influence of 2 mM EDTA and DSF or DSF/Cu on proliferation in adult *S. mansoni* **couples**

Adult *S. mansoni* couples were treated with **A:** DMSO as control, **B:** 2 mM EDTA, **C:** 2 mM EDTA and 50 µM DSF, where no signals were observed in males, and **D:** 2 mM EDTA, 1 µM CuCl$_2$, and 50 µM DSF, where no signals were observed in both genders. EdU was added 24 h prior separation of the couples for fixation of females and males. EdU-positive cells are shown in cyan and the total DNA in magenta. Io = part of the ovary containing immature oocytes, Mo = part of the ovary containing mature oocytes, T = testis. Scale bars represent 50 µm.

4.1.4 The dithiocarbamate-derivative Schl-32.028 displayed tremendous effects on adult *S. mansoni* couples

In the laboratory of a cooperation partner (Prof. M. Schlitzer), among others, the substance Schl-32.028 was synthesized by Dr. rer. nat. P. Mäder (Mäder, 2016) using DSF as lead structure. Initially, Schl-32.028 was tested by PD S. Häberlein on schistosomula and adult worms. In the juvenile stage, Schl-32.028 showed the abrogation of motility with granulation at 1 µM after 24 h (S. Häberlein, personal communication). In the preliminary experiments on adult worms, effects of Schl-32.028 seemed stronger than

DSF, therefore in the following section, effects of Schl-32.028 on adult schistosomes will be presented.

To get an overview how worm viability will be influenced by Schl-32.028, concentrations ranging from 1 - 30 µM were tested. With concentrations above 5 µM, all couples separated after 24 h, whereas 5 µM showed a reduction of the number of couples by 40 % and 1 µM showed no effect (**Figure 4.23 A**). The number of attached couples was completely reduced with concentrations above 5 µM (**Figure 4.23 B**). At this concentration, the attachment capacity was reduced to about 40 % after 24 h, while no reduction was observed with 1 µM. The motility score was reduced to 0 and below 1 for concentrations above 5 µM after 72 h, while it was reduced to 2.2 with 5 µM after 72 h and remained normal (3.0) with 1 µM (**Figure 4.23 C**). The number of normal and abnormal eggs declined toward 0 at concentrations above 5 µM, but increased at lower concentrations, whereas the highest number of abnormal eggs was observed with 1 µM (**Figure 4.23 D** and **E**).
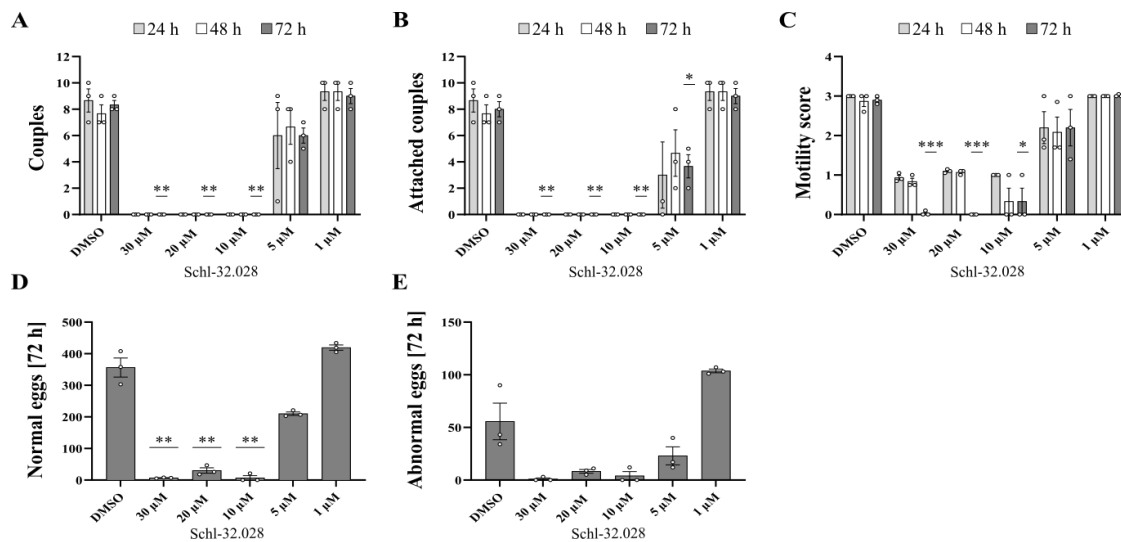
Figure 4.23: Screening of physiological parameters of *S. mansoni* couples following treatment with Schl-32.028
Assessment of physiological parameters during treatment with Schl-32.028 (1 - 30 µM). **A:** number of couples, **B:** attachment of couples, **C:** motility score, and egg count for **D:** normal and **E:** abnormal eggs, n = 3. Each point represents one experiment (average for motility score) with 10 couples each. Columns represent means with StEM. Statistical analysis (two-tailed t-test) was performed using values after 72 h (treatment vs DMSO), $p < 0.05$ (*), $p < 0.01$ (**), $p < 0.001$ (***).

During the treatment regime, worms were also inspected by bright-field microscopy. DMSO, the solvent of Schl-32.028, was used as a control (**Figure 4.24 A**). Most separated female worms were detached from the dish surfaces with 5 µM Schl-32.028. Compared to females, males showed more severe effects such as formation of blebs and detachment of the tegument (**Figure 4.24 B**). Swellings and formation of blebs occurred in females at 10 µM Schl-32.028, while blebs and the dilatation of the gut was observed in males after 72 h (**Figure 4.24 C**).

For further analysis of the effects on the tegument, worms treated with 10 µM Schl-32.028 were used for SEM analysis. Here, treated males showed tegument detachment, swellings, destruction of tubercles, and the formation of vesicles (**Figure 4.25**). Females showed almost no changes except for some swellings (data not shown).

Next, a CLSM-based analysis was performed. Administration of 5 µM Schl-32.028 appeared to have no effect on the organs of the worms compared to the control. This included the gonads and the gut (**Figure 4.26 A** and **B**). With 10 µM Schl-32.028, no changes were found in the ovary, vitellarium or gut of treated females. However, in males, blebs and detachment of the tegument were observed at this concentration, but no changes in the testes were observed (**Figure 4.26 C**). In summary, Schl-32.028 seemed to have no effects on the gonads but destroyed the worm's external surface, the tegument, especially in males.

To determine whether Schl-32.028 has an affect on cell proliferation, an EdU assay was performed. The number of EdU-positive cells was comparable to the control showing no differences in ovary and testis of female and male worms, respectively, with 5 µM Schl-32.028 after 24 h (**Figure 4.27 A** and **B**). Doubling the concentration of Schl-32.028 to 10 µM (**Figure 4.27 C**), however, led to the complete loss of signals in oogonia or spermatogonia, or the rest of the worm bodies, which contains somatic stem cells, the neoblasts.
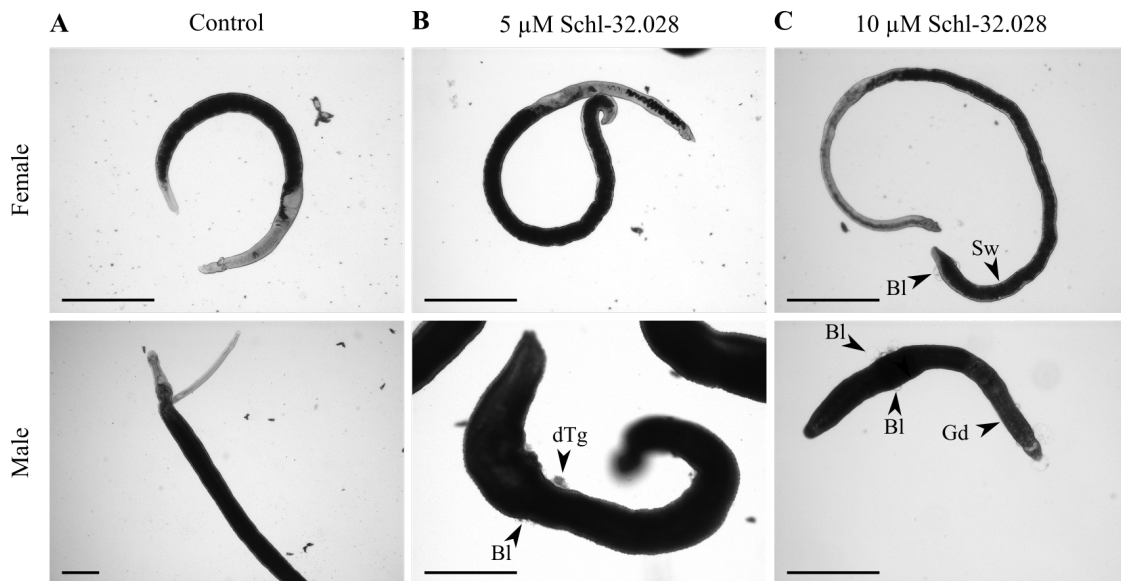
Figure 4.24: Bright-field microscopy of *S. mansoni* couples following Schl-32.028 treatment
S. mansoni couples were treated with **A:** DMSO (control), **B:** 5 µM Schl-32.028, and **C:** 10 µM
Schl-32.028 and cultured for 72 h. Morphological changes such as swellings in females, blebbing
and detachment of the tegument in both genders, as well as gut dilatation in males are indicated
by arrowheads. Bl = bleb, dTg = detached tegument, Gd = gut dilatation, Sw = swelling. Scale
bars represent 500 µm.
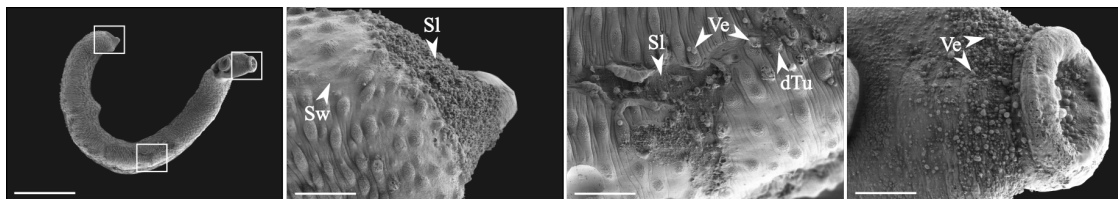
**Figure 4.25: SEM-based analyses of the tegument of adult males following Schl-32.028
treatment**
S. mansoni couples were treated with 10 µM Schl-32.028 and cultured *in vitro* for 72 h. Framed
areas are shown in enlargement. Morphological changes such as swellings, sloughing, disruption
of tubercles, and formation of vesicles were observed in males and indicated by arrowheads. dTu
= disrupted tubercle, Sl = sloughing, Sw = swelling, Ve = vesicle. Scale bars represent 500 µm
(left) and 50 µm (remaining).
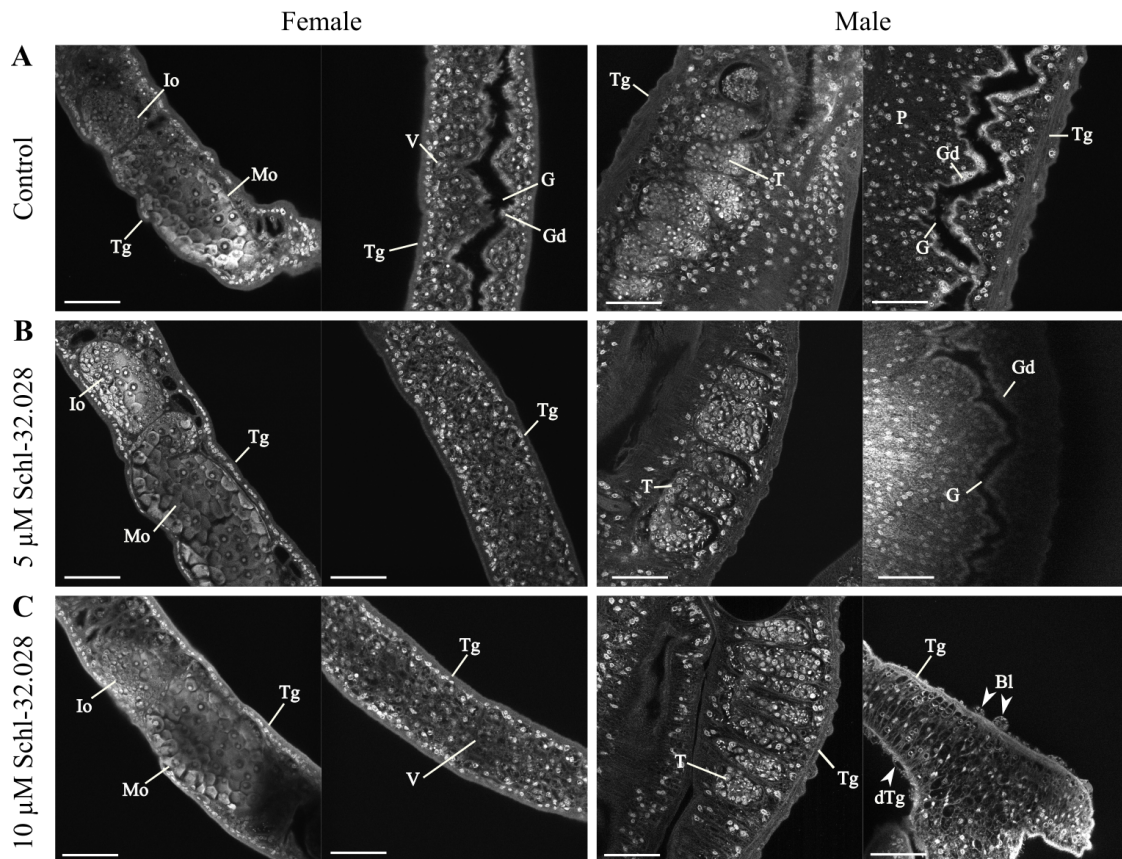
Figure 4.26: Influence of Schl-32.028 on the morphology of adult *S. mansoni* couples
Couples were treated with **A:** DMSO (control), **B:** 5 µM Schl-32.028, and **C:** 10 µM Schl-32.028, before the couples were separated for analysis after 72 h of treatment. Detachment of the tegument and formation of blebs were observed in males after treatment with 10 µM Schl-32.028 (**C**, indicated by arrowheads). Bl = bleb, dTg = detached tegument, G = Gut, Gd = gastrodermis, Io = part of the ovary containing immature oocytes, Mo = part of the ovary containing mature oocytes, P = parenchyma, T = testis, Tg = tegument, V = vitelline cell. Scale bars represent 50 µm.
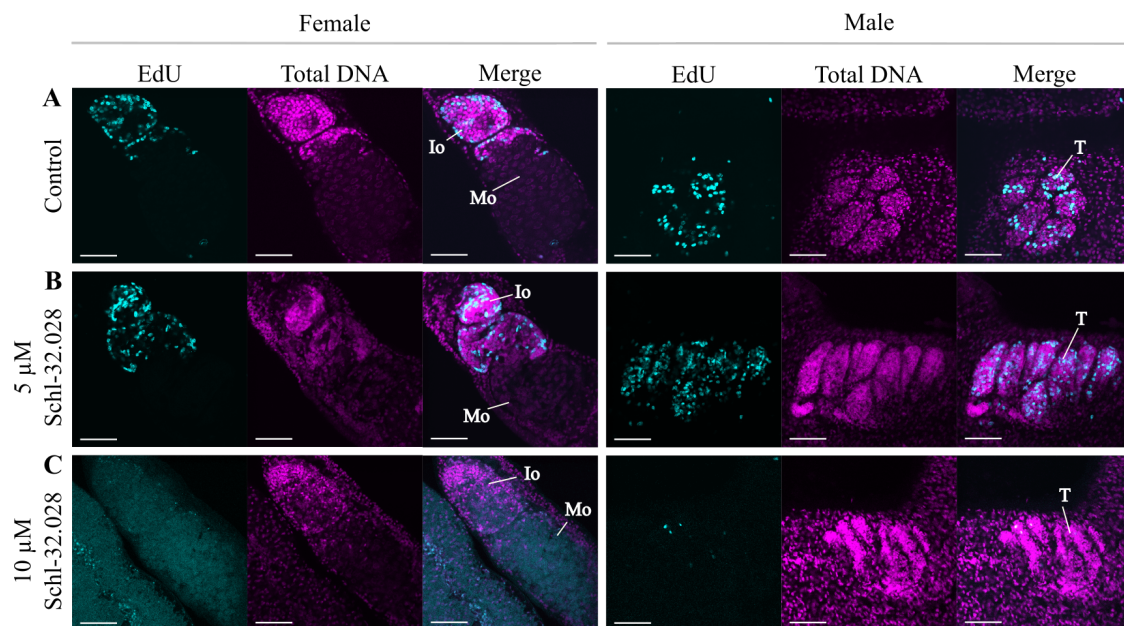
Figure 4.27: Influence of Schl-32.028 on proliferation in adult *S. mansoni* couples
Schistosome couples were treated with **A:** DMSO (control), **B:** 5 µM Schl-32.028, and **C:** 10 µM Schl-32.028. Signals comparable to those in the controls were observed with 5 µM Schl-32.028 (**B**). Almost no signals were observed in both genders at 10 µM Schl-32.028 (**C**). EdU was added 24 h prior separation of the couples for fixation of females and males. EdU-positive cells are shown in cyan and the total DNA in magenta. Io = part of the ovary containing immature oocytes, Mo = part of the ovary containing mature oocytes, T = testis. Scale bars represent 50 µm.

To get a better understanding of the detrimental effects of Schl-32.028, qRT-PCR analyses were performed with RNA/cDNA of treated worms. The selected genes are associated to oxidative stress (Sm*aldh1*, Sm*aldh2*, Sm*ar*, Sm*gpx*, Sm*sod*, and Sm*sodex*), cell cycle (Sm*npl4* and Sm*p53*), apoptosis (Sm*bax* and Sm*bcl-2*), and stem cells (Sm*nanos1* and Sm*nanos2*). For Sm*aldh1*, gene expression was downregulated by one third in females and by two thirds in males, while Sm*aldh2* expression was unaffected (**Figure 4.28 A**). The transcript levels of Sm*ar* appeared to be upregulated by 70 % in females, whereas it remained unchanged in males. No change was observed in gene expression of Sm*gpx* in females, in contrast to males, in which transcription was increased by 50 % (**Figure 4.28 B**). Transcript abundance of Sm*sod* was significantly increased about 10-fold in females, whereas transcript abundance in males was decreased to half of the normal levels. The opposite was observed for Sm*sodex*: in females, transcript abundance was downregulated by about 50 %, whereas in males, a 2.3-fold upregulation was observed. Sm*npl4* gene expression was upregulated in females (1.7-fold), whereas a reduction to 76 % was observed in males (**Figure 4.28 C**). In addition,

a slight reduction in Sm*p53* transcript abundance was found in females (down to 83 %), whereas a slight increase of Sm*p53* transcript abundance was observed in males. Gene expression of Sm*bcl-2* was slightly downregulated in both genders, whereas Sm*bax* was slightly upregulated in females and further increased in males (144 %) (**Figure 4.28 D**). While Sm*nanos1* gene expression appeared unaffected in both genders, Sm*nanos2* gene expression was elevated by one third in females but unaffected in males (**Figure 4.28 E**).
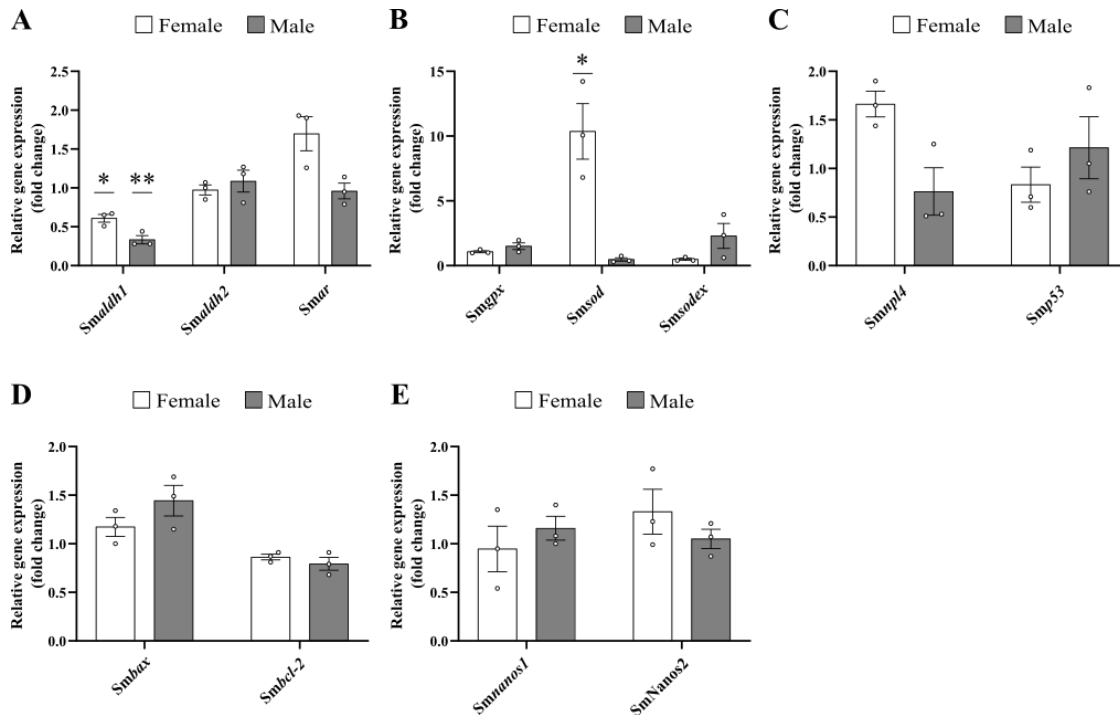
Figure 4.28: qRT-PCR analyses of selected genes following Schl-32.028 treatment
For this analysis, 10 couples each were treated with 10 µM Schl-32.028. Gene expression of **A:** oxidative stress-responsive genes Sm*aldh1,* Sm*aldh2,* and Sm*ar,* **B:** Sm*gpx,* Sm*sod,* Sm*sodex,* **C:** cell cycle-associated genes Sm*npl4* and Sm*p53,* **D:** apoptosis-related genes Sm*bax* and Sm*bcl-2,* and **E:** stem cell-associated genes Sm*nanos1* and Sm*nanos2* were analyzed. Each data point represents one experiment. Columns represent means with StEM, n = 3. Statistical analysis (two-tailed t-test) was performed using treatment vs control (not shown), $p < 0.05$ (*), $p < 0.01$ (**).

4.2 Analyses of target sequences in *S. mansoni*

4.2.1 Comparison of nucleotide and protein sequences from online sources

A first step of this work was the verification of the *S. mansoni* gene sequences that had to be analyzed. Therefore, aa and nt sequences of 2 *aldh* sequences (Smp_022960 and Smp_312440), Sm*tk6,* Sm*abl1,* and Sm*abl2* were obtained from the orthologous sequence of the Puerto Rican strain used for the genome project (Berriman *et al.,* 2009). To this end, *S. mansoni* sequences were retrieved from WormBase ParaSite and NCBI nucleotide, **Table 3.1**), and compared by sequence alignment with Clustal Ω (**Table 3.1**).

Analysis of Sm*aldh* sequences (WormBase ParaSite: Smp_022960, NCBI nucleotide: XM_018798744) showed no alterations when compared to each other (1,560 nt, 519 aa, 57.34 kDa), whereas the other *aldh* sequence (WormBase ParaSite: Smp_312440 (previously Smp_050390), NCBI nucleotide: XM_018791103) had one alteration at nt120, which did not alter the protein sequence (1,476 nt, 491 aa, 53.76 kDa) **Table 4.1**). Comparison of the Sm*abl1* gene and protein sequences retrieved from WormBase ParaSite (Smp_246700, 5,169 nt, 1722 aa, 190.18 kDa), and from NCBI nucleotide (FN582310, 4,992 nt, 1,663 aa, 183.89 kDa) revealed differences in length (59 aa) and MW (6.29 kDa), and alterations at 16 nt positions, leading to synonymous and non-synonymous aa substitutions in the protein sequence (**Table 4.2**). Analysis of the Sm*abl2* sequences from WormBase ParaSite (Smp_128790) and NCBI nucleotide (XP_018650102) revealed a non-synonymous substitution at nt 1,883, which altered Ser to Cys at this position (**Table 4.3**). The overall length of the proteins were identical (3,927 nt, 1,308 aa, 146.63 kDa). Comparison of the Sm*tk6* sequences from WormBase ParaSite (Smp_006920) and NCBI nucleotide (FN397679) showed differences at 7 nt positions that altered the aa composition of the proteins (**Table 4.4**) but not protein length or MW (1,698 nt, 565 aa, 63.64 kDa). Based on these results, primers (**Table 2.12**) were designed to amplify the appropriate full-length sequences according to the sequences from WormBase ParaSite.

Table 4.1: Comparison of Sm*aldh* nt and aa sequences

Sequences were retrieved from WormBase ParaSite (Smp_312440) and → NCBI nucleotide (XM_018791103).

Nucleotide position	Amino acid position
120: G → T	nc[a]

[a] nc = no change

Table 4.2: Comparison of Sm*abl1* nt and aa sequences

Sequences were retrieved from WormBase ParaSite (Smp_246700) and → NCBI nucleotide (FN582310).

Nucleotide position	Amino acid position
1-51: ATG GGA GGA TAT AAT AGT AAA CTG ACA GTG CCA AAA GAT GAA CCA AAT CTC → -	1-17: MGG YNS KLT VPK DEP NL → -
1277: G → A	426: C → Y
1327: T → C	443: S → P
1538: C → T	513: P → L
2041: T → C	681: W → R
2179: - → AAC	728: - → Q
2341: A → G	781: N → D
2487: A → C	817: H → R
2618: A → G	873: D → G
2900: T → C	967: I → T
3140: T → C	1047: I → T
3354: A → G	1117: Q → K
3950: A → G	nc[a]
4518: T → C	nc[a]
4636: C → A	nc[a]
5031-5153: GTA AGT ACT ATC ACC CTC ACC ACT GGT TCT ACA ACA TCT GTT ACT AAT CAA ACT CAT TTA CAT AAT GAT CGA TCG TTT AGT ACT ACT GAT AAT ACT ACT ACT ACT ACT ACT ACC ACT CAT GTA TTT GGC AAA GT → AAT TA	1677-1722: VST ITL TTG STT SVT NQT HLH NDR SFS TTD NTT TTT TTT HVF GKV → NY

[a] nc = no change

Table 4.3: Comparison of Sm*abl2* nt and aa sequences

Sequences were retrieved from WormBase ParaSite (Smp_128790) and → NCBI nucleotide (XP_018650102).

Nucleotide position	Amino acid position
1883: C → G	628: S → C

Table 4.4: Comparison of Sm*tk6* nt and aa sequences

Sequences were retrieved from WormBase ParaSite (Smp_006920) and → NCBI nucleotide (FN397679).

Nucleotide position	Amino acid position
183: A → T	nc[a]
496: C → T	nc[a]
598: A → C	200: K → Q
858-878: ATT TCG TGA TTT TGA AAT TAA → TTT CGT CAT GTT TGC AA TTA T	286-291: QFR DFE IN → HFV MFA II
1126-1127: GG → NN	376: G → X
1231: G → N	411: E → X
1427: T → C	476: V → A

[a] nc = no change

4.2.2 Protein domain analyses of the selected gene sequences

Parts of protein sequences are grouped into functional or structural sections (domains). These contribute to a specific function, e.g., catalytic functions as Aldh or TKD, or interaction with other proteins, e.g., the SH2 domain (Russell *et al.*, 1992; Sadowski *et al.*, 1986). Domains are not restricted to a specific protein family and can occur in different proteins with diverse functions.

So far, *S. mansoni* Aldhs were neither crystallized nor characterized structurally. Domain analysis revealed the typical aldehyde dehydrogenase domains with NAD(P) binding site and catalytic residues (**Figure 4.29**). For SmAldh2, a monotetrameric interface was detected additionally. Diverging statements of occurring domains exist for SmAbl2. Whereas Avelar *et al.* (2011) depicted SmAbl2 harboring only a TKD,

whereas Beckmann *et al.* (2011) reported that besides the TKD there is also a SH2 and a SH3 domain (also for SmTK6). Analyses of the protein domains displayed the structural and functional domains reported as in Beckmann *et al.* (2010) for both SmAbl kinases and SmTK6 (**Figure 4.29**).
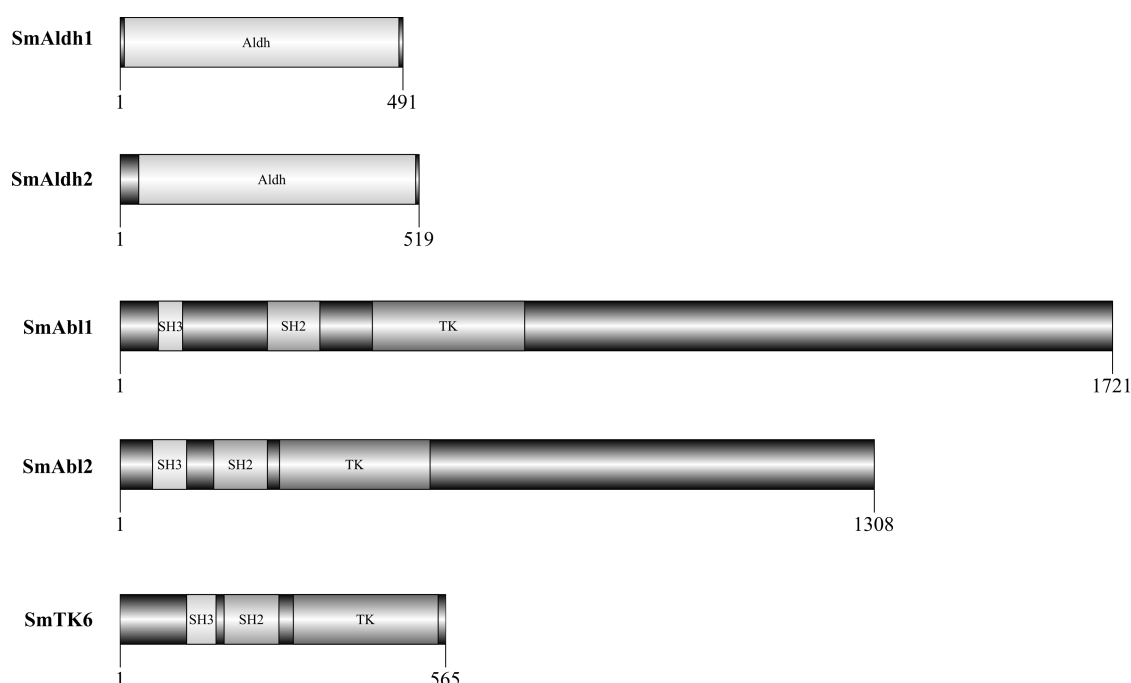
Figure 4.29: Illustration of SmAldh1, SmAldh2, SmAbl1, SmAbl2, and SmTK6 protein domains

Protein sequences were analyzed via CDD on NCBI (**Table 3.1**), start and end of proteins are marked with the respective aa number, domains are highlighted as follows: Aldh = aldehyde dehydrogenase, SH2 = Src homology 2, SH3 = Src homology 3, TK = tyrosine kinase.

4.2.3 Phylogenetic analysis for schistosomal Aldhs Smp_022960 and Smp_312440

There are 19 Aldhs known in humans (Jackson *et al.*, 2011). The nomenclature was established by using Aldh, followed by a number (representing the family), a letter representing the subfamily and a number representing an individual gene within the subfamily (Vasiliou *et al.*, 1999). To analyze to which Aldh family both Aldhs belong, a multiple alignment with other Aldh protein sequences (**Figure 4.30**) and phylogenetic analysis (**Figure 4.31**) were performed.

Both Aldh sequences shared the consensus sequences of other known Aldhs (**Figure 4.30**). Analysis of the given percent identity matrix by Clustal Ω (**Figure A.3**, see appendix) revealed sequence identities of 61 % with HsAldh1A1 and 66.02 % with HsAldh2 for Smp_022960, which makes it likely a member of Aldh family 2, while Smp_312440 shared identities of 54.38 % with HsAldh1A1 and 54.79 % with HsAldh2. No clear statement could be made about the affiliation of Smp_312440. To verify the family memberships, an evolutionary analysis was conducted by maximum likelihood method. As a result, Smp_022960 was classified as a member of Aldh2 and Smp_312440 as an Aldh1 family member (**Figure 4.31**). For this reason, Smp_022960 was designated SmAldh2 and Smp_312440 was designated SmAldh1.

```
conservation
CeAldh1J2       ........MDSSLLRSAVRAS.VQACNGSGLPPGLADFKPKYTSLFINNEFVDAKSGKTFEFVNPANGKLLAKVAEGNRDDVDIAVEAA    80
CsAldh1A1       ...................................MAADLEVKFTQLFINNEFVNSVSGKTFPTINPATEEVTCHVQEGDVEDVKKAVAAA    56
SmedAldh2-like  MSKIMISKKFSILFRPLLLN..SKCFSSLAKPITQNDIKVHYTKIFINNEFVDSVSKCTGPTKNPATGQDTCQVAEGGKEDIDKAVTAA    87
DmAldh1M1       ..............................MADPNAKPKYTKLFINNEFVDSVSGKTFATFWNPATSKEIVQVSEGDKADIDLAVKAA    57
DmAldh1A10      ...MLRVLKTGALLRSQAKNFAAAVANYSSLPQPQTTPDILYTGVFINNEWHKSKSGKITETINPTTAEVTAEIQCADKEDIDIAVQAA    86
HsAldh1A1       .................MSSSGTPDLPVLLTDLKIQYTKIFINNEWHDSVSGKKFPVFWNPATEEELCQVEEGDKEDVDKAVKAA    67
HsAldh2         ...ML...RAAARFGPRLGRRLLSAAATQAVPAPNQQPEVFCNQIFINNEWHDAVSRKTFPTVWNPSTGEVICQVAEGDKEDVDKAVKAA    83
MmAldh1A1       ...................MSSPAQPAVPAPLADLKIQHTKIFINNEWHNSVSGKKFPVLWNPATEEVTCHVEEGDKADVDKAVKAA    67
RnAldh1A1       ...................MSSPAQPAVPAPLANLKIQHTKIFINNEWHDSVSGKKFPVLWNPATEEVTCHVEEGDKADVDKAVKAA    67
Smp_312440      ...............................MTKTYRLPEVKYTQLFIGNEFVDSESKKTGPTINPTLNPATEEVTCHVQEADQNDVNKAVEAA    59
Smp_022960      ...MVFLYSGSKILGAQAITKNI.CKFLGTTVEPILKPEIKRNSIFINNEWVESSSGKTFDTINPATGKVICQVSAGDKADIDKAVKAA    85
consensus                                             *  FI*NE  * S*K F   NP**   ** * **** D **AV AA

conservation
CeAldh1J2       KKAFKIGSEWRRMDASHRGCVLLNRLADLMERDRVILASLESLDNGKPYKEAYNIDLPISIKTFRYYYAGYADKNHGKTIPVGGDYFTYTR    169
CsAldh1A1       KSAFRRDTPWRTMDASKRGLLLCKLASLIVRDAEYIAKLEALDNGKAVSSLL.VDTQFTVDVLRYFAGYADKIHGKVIPIRGDYIGFTR    144
SmedAldh2-like  NKAFQLGSPWRKMDAADRGSLMYKLAQLIRRDADYLAALETLDSCKPVSIRAADVELTIKCYEYYAGWADKNHGKVIPIRGDYIGFTR    176
DmAldh1M1       KKAFHRDSEWRKLSPLQRTNLMNKLCALMDRDKAFLASLETQDNGKPYAEALFDVTYSILTLQYYAGWTDKFFGDFIPAG.GFVSMTR    144
DmAldh1A10      RNAFKLGSPWRRMDASERGRLLYRLADLMERDQVYLASLETLDNGKPYSMSYNVDLPTAIKNLRYFAGWADKNHGKTIPMDGDFFTYTR    175
HsAldh1A1       RQAFQIGSPWRTMDASERGRLLYKLADLIERDRLLLATMESMNGGKLYSNAYLNDLAGCIKTLRYCAGWADKIQGRTIPIDGNFFTYTR    156
HsAldh2         RAAFQLGSPWRRMDASHRGRLLNRLADLIERDRTYLAALETLDNGKPYVISYLVDLDMVLKCLRYYAGWADKYHGKTIPIDGDFFSYTR    172
MmAldh1A1       RQAFQIGSPWRTMDASERGRLLNKLADLMERDRLLLATMEALNGGKVFANAYLSDLGGCIKALKYCAGWADKIHGQTIPSDGDIFTYTR    156
RnAldh1A1       RQAFQIGSPWRTMDASERGRLLNKLADLMERDRLLLATIEAINGGKVFANAYLSDLGGSIKALKYCAGWADKIHGQTIPSDGDIFTFTR    156
Smp_312440      KAAFKTGSTWRTMDASERGVLLYKLADLIEMNAEYIARLEAMDNGKTVESAL.GDVFFAAQTTRYYAGYADKIHGKQLPVDGNMITFTR    147
Smp_022960      RKAFEFGSEWRTMDASHRGVLLNRLADLIERDRVYLASLETLDNGKPFADSYNIDLDDLVLIKCYRYYAGWADKYHGKTIPVNGNYMCFTL    174
consensus            AF  ** WR **** R* L* *L**L *** *A *E * GK  * D   ** Y AG**DK *G **P *   T*

conservation
CeAldh1J2       HEPVGVCGQIIPWNFPLMQAMKLAPALAMGNTVVMKVAVKTPLSALHVASLIKEAQPPEGVVNIIPGRGTDAGEAIASIMDVDKVLFT    258
CsAldh1A1       REPAGVVAGIVPWNYPFFLAVLKLAPALAAGCTIVLKPAEQTPLSGIFLGSLVREAGFPPGVVNIIPGYGETAAGAALSQIPDIRVISFT    233
SmedAldh2-like  HEPVGVCGQIIPWNFPLMQAVKLAPALSMGNTVVLKTAEQTPITANYVASLAAEAGFPPGVVNVVSGGPGTAGAALVTIPKVDKIAFT    265
DmAldh1M1       KEPVGVVGGIIPWNYPLMLAIKWGPALAVSCTIIMKPAEQTPITAIHMAALAKEAGIPAGVINVVNCFGPTAGAAISAIPDIAKVAFT    233
DmAldh1A10      HEPVGVCGQIIPWNFPILMMAVKLGPALATGNTIVLKPAEQTPSTALYIAQLVKEAGFPEGVVNVVPGFGTAGAALANICDVDKVAFT    263
HsAldh1A1       HEPIGVCGQIIPWNFPLLMLIWKIGPALSCGNTVVVKPAEQTPLTALHVASLIKEAGFPPGVVNIVPGFGPTAGAAISSHMDIDKVAFT    245
HsAldh2         HEPVGVCGQIIPWNFPLLMQAWKLGPALATGNVVVMKVAEQTPLTALYVANLIKEAGFPPGVVNIVPGFGPTAGAAIASHEDVDKVAFT    261
MmAldh1A1       REPIGVCGQIIPWNFPMLMFIWKIGPALSCGNTVVVKPAEQTPLTALHLASLIKEAGFPPGVVNIVPGYGPTAGAAISSHMDVDKVAFT    245
RnAldh1A1       REPIGVCGQIIPWNFPLLMFIWKIGPALSCGNTVVVKPAEQTPLTALHMASLIKEAGFPPGVVNIVPGYGPTAGAAISSHMDVDKVAFT    245
Smp_312440      REPVCVACITPWNYPFFLSVLKGTPCLCACCTVVLKPAEQTPLSALYLAALIKEAGFPPGCVFVICGYGETTGEALTHFPDVRAISFT    236
Smp_022960      HEPVGVCGQIIPWNFPLLMQAWKLGPALATGNTVVMKTAEQTPLSANWVAELIKEAGFPPGVVNIVPGFGETAGDALVVIPDVDKIAFT    263
consensus            EP  GV***I*PWN*P ** *K P*L G**** K A**T*L **  * L *EA*FP*GV*N **G G **G*A   H **** *FT

conservation
CeAldh1J2       GSTEVGKTIMKAAAESNVKKVTLELGGKSPNIVFADADLEEAVRQSHALGFNGQGQCCSAGSRTFVGKLYDETVAKAKELVEKTVIGD    347
CsAldh1A1       GSTEVGQLIMKAAA.TNIKQVKLELGGKSPLIIFADADLDKAAAVAHEATMVNHGQGCVAGTRIFVEAPVYEKMVHKLKELAEARKVGD    321
SmedAldh2-like  GSTEVGQILSKHCNENNIKRLTLELGGKSPLSMGNTVVLKTAEQTSYFALFNMGQCCCAGSRIYVEEKIYDKVEAMVAEAKSKVVGN    354
DmAldh1M1       GSVEIGRIVMQAAATSNLKRVSLELGGKSPVVVFDDADIDFAVETTEALFSNHGQSGCAGSRTYVHEKIYDEVAKAAAKAVARKVGN    322
DmAldh1A10      GSTDVGKLIQLASGNTNLKRVTLELGGKSPNIILSDTDMDYAVETAFFGLFFNMGQCCCAGSRTFVEDKIYDEVVERSAERAKRTVGN    352
HsAldh1A1       GSTEVGKLIKEAAGKSNLKRVTLELGGKSPCIVLADADLDNAVEFAHHGVFYHQGQCCIAASRIFVEESIYDEFVRRSVERAKKYILGN    334
HsAldh2         GSTEIGRVIQVAAGSSNLKRVTLELGGKSPNIIMSDADMDWAVEQAHFALFFNLGQCCCAGSRTFVQEDIYDEFVERSVARAKSRVVGN    350
MmAldh1A1       GSTQVGKLIKEAAGKSNLKRVTLELGGKSPCIVLADADLDNAVEFAHHGVFYHQGQCCVAASRIFVEESVYDEFVKRSVERAKKYVLGN    334
RnAldh1A1       GSTQVGKLIKEAAGKSNLKRVTLELGGKSPCIVLADADLDNAVEFAHHGVFYHQGQCCVAASRIFVEESVYDEFVKRSVERAKKYVLGN    334
Smp_312440      GSTEVGQLIMKAAA.TNIKHVKLELGGKSPLIILADADIEKASEVAHEATMVNHGQGCVAGTRIFVQAPIYDQMVEKLKKLAEQRKVGD    324
Smp_022960      GSTAVGRLIGGNAYKHGVKRITLELGGKSPLIIFSDGDFDRAIAASHFGLEFNGQGQCCASSRIFVEESIYDKFVEYSSEEAKKRIVGN    352
consensus       GS* *G  * **  * K***LELGGKSP *   D*D * A*   *  * * GQ*C A *R *V*  *Y* *V     **     G*
```

```
conservation
CeAldh1J2      PFDENTTQGPQIDESQVETIMKYIESGKKEGAQLVTGGVKH.GDQGYYVKPTIFANVNDQMKIAQEEIFGPVMIVIREDSMEELIEKAN   435
CsAldh1A1      PFAPDTVQGPQVDEVQFNKIMSYIESGKKEGARLVTGGCRL.GNKGYYIQPTVFADVTDEMVIAKEEIFGPVQSILKFETIDEVIERAN   409
SmedAldh2-like PFD.NVDQGPQIDEEQMNKILGFLDSGKSEGAQMCTGGKQI.GSKGFIEPTIGTKVEDSRIAKEEIFGPVMQIMKFKDTNEVIARAN    441
DmAldh1M1      PFEQNVQQGPQIDDDMLTKVLGYIESGKKEGAKLQAGGKRI.GNVGFRVEPTVFSDVKDDVRIAQEEIFGPVQSLFKFSSLEEMIDRAN   410
DmAldh1A10     PFDLNTEQGPQVNEEQMEKILGMIKTGKKQGAKLVAGGSRPEGLPCYYVQPTVFADVQDDLTIAREEIFGPVQQLIRFKKLDEVIERAN   441
HsAldh1A1      PLTPGVTQGPQIDKEQYDKILDLIESGKKEGAKLECGGPW.GNKGYYVQPTVFSNVTDEMRIAKEEIFGPVQQIMKFKSLDDVIKRAN   422
HsAldh2        PFDSKTEQGPQVDETQFKKILGYINTCKQEGAKLLCGGGIA.ADRGYYIQPTVFGDVQDGMTIAKEEIFGPVMQILKFKTIEEVVGRAN   438
MmAldh1A1      PLTPGINQGPQIDKBQHDKILDLIESGKKEGAKLECGGRW.GNKGFYVQPTVFSNVTDEMRIAKEEIFGPVQQIMKFKSVDDVIKRAN   422
RnAldh1A1      PLTQGINQGPQIDKBQHDKILDLIESGKKEGAKLECGGRW.GNKGFYVQPTVFSNVTDEMRIAKEEIFGPVQQIMKFKSIDDVIKRAN   422
Smp_312440     PFVSDTIQGPQIDNVQFDKIMSYLEKGKKQGARLVTGGCRI.GEKGYYIQPTVFADVSDEMCIAKEEIFGPVQCILKFNTLEEVIERAN   412
Smp_022960     PFDLNTTQGPQVDEHQFQTVMSYIESGIKEGAKLCTGGKQF.GSDGYYIRPTVFADVQDEMSIAREEIFGPVMQIMKFRSLDELIHRAN   440
consensus      P*    QGPQ * *  **  I**G***GA * GG     * G *  PT*F  V D M IA EEIFGPV * *F    *** *AN

conservation
CeAldh1J2      NTIYGLAAGVVNDLNKALQVANTIRAGSVWVNCYDVFDPAA.PFGGFKQSGIGRELGEYGLAAYTEVKTVTIKVPQKNS   514
CsAldh1A1      SGIYGLGAGVYTSDMDKAMRVAQACEAGSFWINCYNVVYPQAPFGGFKMSCVGRELGKYGLECYLQTKVISMPISLKNS   488
SmedAldh2-like NNEYGLAASIFTQDIDKSLHVTQSLRAGTVWVNCYDVFDAAA.PFGGYKSSCVGRELGEYGLSNYTEVKMVTIKTPSKNS  520
DmAldh1M1      NVQYGLAAGVINDINKALKFANNVDAGSVWINCYDAVLPST.PFGGYKHSCIGRELGKDGLDNYLETKTITMKLL....   485
DmAldh1A10     NSEYGLAAAVFTKDLDKANYIVGGLRAGTVWVNTYNVLAAQAPFGGYKMSCHGRENGFYALSNYTEVKSUIVKVAQKNS   520
HsAldh1A1      NTFYGLSAGVFTKDIDKAITISSALQAGTVWVNCYGVVSAQCPFGGFKMSCNGRELGEYGFHEYTEVKTVTVKISQKNS   501
HsAldh2        NSTYGLAAAVFTKDLDKANYLSQALQAGTVWVNCYDVFGAQSPFGGYKMSCSGRELGEYGLQAYTEVKTVTVKVPQKNS   517
MmAldh1A1      NTTYGLAAGLFTKDLDKAITVSSALQAGTVWVNCYMMLSAQCPFGGFKMSCNGRELGEHGLYEYTELKTVAMKISQKNS   501
RnAldh1A1      NTTYGLAAGVFTKDLDRAITVSSALQAGTVWVNCYMILSAQCPFGGFKMSCNGRELGEHGLYEYTELKTVAMKISQKNS   501
Smp_312440     ATHYGLGAGVFTSDMDKAMRIAQCVEAGSFWINSYNFVSPQTPFGGYKMSCMGREFCKEALDGYLQTKVISMPISVKNS   491
Smp_022960     HTQYGLAAGIFTNNLEKAMHVMQHLQTGTVWINCYDVFDAAA.PFGGYKFSCVGRELGEYSLRNYTEVKTVTTRILQKNS   519
consensus      *   YGL*A***T * ***      *G *W N*Y    PFGG K SG GRE*G* ** Y** K *  *   ***
```

Figure 4.30: Multiple alignment of vertebrate and invertebrate Aldh sequences

Highly conserved residues (≥ 80 %) are shaded gray, and the level of conservation is displayed as bars at the top. The NAD(P)-binding associated residues are shaded blue (as suggested from CDD analysis), and the catalytically active Cys is highlighted by a red frame. At the bottom, the consensus sequence (100 % conservation) is represented by the respective aa, while conservation ≥ 80 % is depicted by asterisks (*). Ce = *C. elegans*, Cs = *C. sinensis*, Smed = *S. mediterranea*, Dm = *D. melanogaster*, Hs = *H. sapiens*, Mm = *M. musculus*, Rn = *R. norvegicus*, Smp = *S. mansoni* protein identifier.
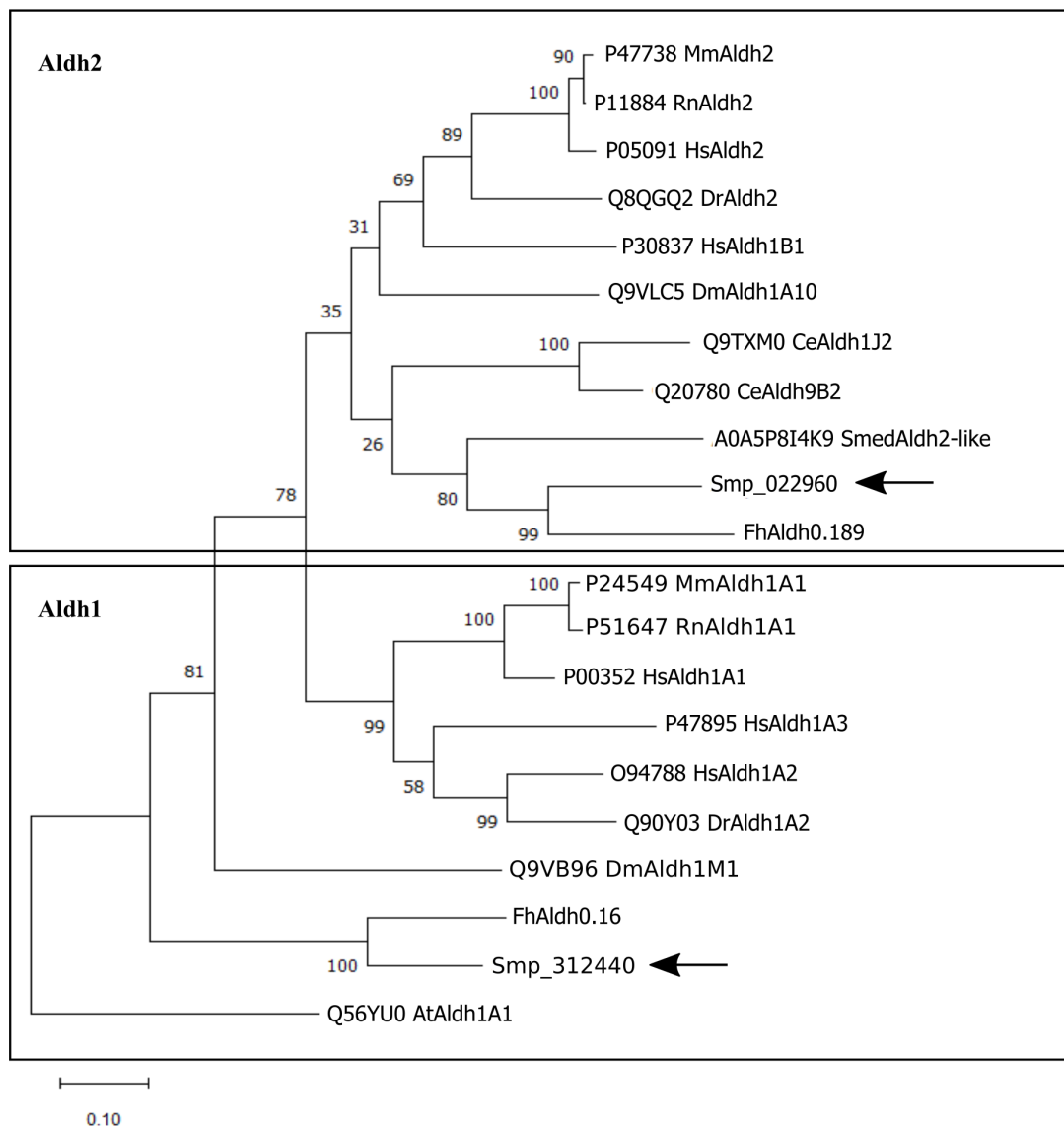
Figure 4.31: Evolutionary analysis by Maximum Likelihood method for Aldhs from verte-brate and invertebrate species

The percentage of trees in which the associated taxa clustered together is shown next to the branches. The tree was drawn to scale, with branch lengths measured in the number of substitutions per site. This analysis involved 21 aa sequences. Boxes cluster members of the respective Aldh families. The UniProt identifier are shown next to the respective Aldh, except for FhAldhs due to space restrictions (WormBase ParaSite identifier: maker-scaffold10x_80_pilon-snap-gene-0.189 (FhAldh0.189) and maker-scaffold10x_208_pilon-snap-gene-0.16 (FhAldh0.16)). At = *A. thaliana*, Ce = *C. elegans*, Cs = *C. sinensis*, Dr = *D. rerio*, Dm = *D. melanogaster*, Fh = *F. hepatica*, Hs = *H. sapiens*, Mm = *M. musculus*, Rn = *R. norvegicus*, and Smed = *S. mediterranea*. Schistosomal Aldh sequences Smp_022960 and Smp_312440 are marked by arrows.

4.2.4 Analysis and prediction of PTMs

PTMs are typically transferred molecules to a protein after translation of the mRNA. They function as regulators of enzyme activity, signal transduction, and mediate protein-protein interactions (Duan and Walther, 2015; Resh, 2006; Seet *et al.*, 2006; Venne *et al.*, 2014; Vu *et al.*, 2018). Well known PTMs among others are acetylation, methylation, phosphorylation, palmitoylation, ubiquitinylation/sumoylation (sumo = small ubiquitin-like modifiers) (Ciechanover, 1998; Kouzarides, 2007), where most experimental observed PTMs were phosphorylation of serine/threonine and N-linked glycosylation (Duan and Walther, 2015; Khoury *et al.*, 2011).

The prediction of PTMs was executed by online tools for acetylation, myristoylation, palmitoylation, and phosphorylation (**Table 3.1**), and the presence of PTMs at the equivalent human protein sequences analyzed at www.uniprot.org. UniProt-Ids of human Aldhs: HsAldh1A1 (8P00352), HsAldh1A2 (O94788), HsAldh1A3 (P47895), HsAldh2 (P05091), and human Abl kinases: HsAbl1 (P00519), HsAbl2 (P42684). Predictions of *S. mansoni* proteins were summarized in **Table 4.5**. Acetylation was predicted for SmAldh1, SmAbl2, and SmTK6, where for HsAldh1A1, HsAldh1A3, and HsAldh2 acetylation sites were annotated at www.uniprot.org. Myristoylation was predicted for both SmAbl kinases at position G2. Palmitoylation was likely to occur in both Aldhs, both SmAbl kinases, and SmTK6. The SmAbl kinases were predicted to be phosphorylated, this is consistent with the phosphorylation of HsAbl kinases. SmTK6 was also predicted to be phosphorylated, but since its Src/Abl hybrid character (Beckmann *et al.*, 2011), there is no direct orthologue in human to compare with. Analyzes of the annotated HsAldh1A1 and HsAldh1A2 revealed phosphorylation sites (www.uniprot.org), and HsAldh2 was shown to be phosphorylated for protein inactivation (Danquah and Gyamfi, 2016). *S. mansoni* Aldhs were predicted to have multiple phosphorylated S/Y residues.

Table 4.5: Predicted post-translational modifications

Modification	Protein	Prediction
Acetylation	SmAldh1	K3
	SmAbl2	K7, K244, K651, K842, K949
	SmTK6	K389
Myristoylation	SmAbl1/2	G2
Palmitoylation	SmAldh1	C292, C293
	SmAldh2	C21, C320, C321
	SmAbl1	C1319, C1320
	SmAbl2	C360, C945
	SmTK6	C4, C6, C270, C271
Phosphorylation	Aldh1/2	
	SmAbl1/2	} multiple S/Y
	SmTK6	

4.2.5 Analysis of the selected *S. mansoni* sequences for codon usage in selected protein expression systems

Each organism has a codon usage bias, which means that there is a preference for certain synonymous codons while protein expression (Ikemura, 1985; Mazumder *et al.*, 2021; Sharp *et al.*, 1988). Usage of highly abundant t-RNAs influences efficiency and translation of gene transcripts (Gouy and Gautier, 1982). This was demonstrated by Hernan *et al.* (1992) when native gene versions of α- and β-globin were not expressed in *E. coli* (DE3) compared to the synthetic (codon optimized) gene versions.

In this work, *E. coli* (pLysS and LOBSTR-RIL strain) and HEK293-6E (EBNA1) cells were available as protein expression systems. To analyze possible bottlenecks in provision of resources for protein expression in the protein expression systems, the online tool Graphical Codon Usage Analyser (**Table 3.1**) was used. After comparison of the target sequences to species-specific codon usage tables, only codons coding leucine were used in the protein expression systems below 20 % (16 % CTA in *E. coli*, 18 % CTA and 20 % TTA in HEK cells), implying that these were a potentially limiting factor while protein expression. The frequencies with which these codons occurred in the target sequences were summarized in **Table 4.6**. After evaluation of these results, the *E. coli*

protein expression system was chosen as main protein expression system due to its lower percentage of codon limitation, and for more convenient handling.

Table 4.6: Codon frequency in *S. mansoni* gene sequences used below 20 % in *E. coli*[a] and HEK293-6E (EBNA1) cells[b]

Gene	Codon CTA[a,b]	Codon TTA[b]
Sm*aldh1*	3x	12x
Sm*aldh2*	2x	16x
Sm*abl1*	13x	58x
Sm*abl2*	13x	56x
Sm*tk6*	1x	15x

4.3 Cloning of the target sequences and comparison of sequences to orthologous sequences retrieved from WormBase ParaSite

All full-length sequences were amplified in PCR reactions with cDNA transcribed from mRNA as template (see sections 3.8.1 and 3.8.2), specific primers (**Table 2.12**) and Q5 High-Fidelity DNA polymerase (see section 3.8.7). After cloning into pDrive (see section 3.8.10), *E. coli* DH5α were transformed and cultured on antibiotic-containing agar plates (see section 3.7.4). After isolation of the plasmids (see section 3.7.6), they were sequenced (see section 3.8.11) and glycerol stocks of the respective bacterial colonies prepared (see section 3.7.2). The recombinant vectors were then used as templates for further amplification and sub-cloning of the insert sequences (see sections 3.8.9 and 3.8.10). Comparisons of the Sm*aldh1* and Sm*aldh2* sequences of the Liberian *S. mansoni* strain used in this work revealed no differences to the orthologous sequences of the Puerto Rican strain (available at WormBase ParaSite, used for the initial sequence analyses (see section 4.2.1)), while comparison of the sequences for Sm*abl1,* Sm*abl2,* and Sm*tk6* revealed changes in the nt sequences, which also altered the protein composition (see sections below).

4.3.1 Cloning of the Sm*aldh1* and Sm*aldh2* full-length sequences into pMal-c5X

The recombinant plasmids pET30a-Sm*aldh1* and pET30a-Sm*aldh2* were provided by a former group member (A. Blohm). Sequencing of both Sm*aldh* sequences, following comparisons of the sequencing results and the orthologous sequences from the Puerto Rican strain (WormBase ParaSite) revealed no changes in the aa sequences. For sub-cloning into pMal-c5X, the vector was prepared by digestion (*Xmn*I, *Nde*I and Quick-CIP), the Sm*aldh1* sequence amplified with primers #190/#191, and the Sm*aldh2* sequence with primer pair #148/#149 followed by clean ups. The cloning reactions assembled the plasmids pMal-c5X-Sm*aldh1* and pMal-c5X-Sm*aldh2*. Expressed proteins were fused to MBP and displayed a small linker region between proteins, and a His_6-tag at the C-terminus of the schistosomal proteins. The recombinant fusion proteins were named MBP:SmAldh1 and MBP:SmAldh2.

4.3.2 Cloning of the Sm*abl1* and Sm*abl2* full-length and TK domain sequences into pET30a+ and pTT

The coding sequence of Sm*abl1* had a length of 5,169 bases and Sm*abl2* 3,927 bases respectively. To minimize errors in the base composition during PCR, the amplification of the sequences was divided into 2 fragments, which were then to be ligated. To do this, the sequences were analyzed for restriction enzyme recognition sites. Primers were designed to amplify approximately half of the gene sequence while overlapping at a *Sal*I recognition site (nt2,399) for Sm*abl1* and a *Bgl*II (nt2,052) for Sm*abl2* (**Figure 4.32 A**).

Therefore, primers #31 and #32 were used to amplify a product named Sm*abl1*p1 (2,407 bp), while #33 and #34 amplified a 2,778 bp product named Sm*abl1*p2 with an additional *Nhe*I recognition site at the 3' end. For Sm*abl2*, primer pair #25/#26 was used to amplify fragment Sm*abl2*p1 (2,038 bp), and #27/#28 for fragment Sm*abl2*p2 (1,885 bp, *Not*I recognition site at 3' end). The amplification results varied throughout the reactions. While only faint bands for Sm*abl1*p1 and Sm*abl2*p2 were detected on an agarose gel, the amplification of Sm*abl*1p2 and Sm*abl*2p1 was more efficient. After purification of the PCR products, the fragments were more concentrated (**Figure 4.32 B**). Subsequently, the fragments were cloned into pDrive and sequenced.

Colony K133 containing pDrive-Sm*abl1*p1 covered the sequence retrieved from WormBase ParaSite despite an additional AAC at nt2,172, which translated in an additional glutamine as predicted from the NCBI nucleotide sequence (**Table 4.2**). Plasmid pDrive-Sm*abl1*p2 (colony K159) showed further deviations compared to the WormBase ParaSite sequence: T2,900 → C2,900 (aa967: I → T), A3,518 → G3,518 (aa1,174: Q → R), C4,636 → A4,636 (aa1,547: Q → K), and a deletion of TAC TAC (aa1,713: TT → –) at nt5,139. To verify these alterations, several parts of the gene sequence were amplified additionally with 2 independent cDNA templates derived from different worm populations. Analyses of sequences confirmed the former stated changes (**Figure 4.33**). Sequencing of Sm*abl2* revealed 100 % sequence identity to the WormBase ParaSite sequence.
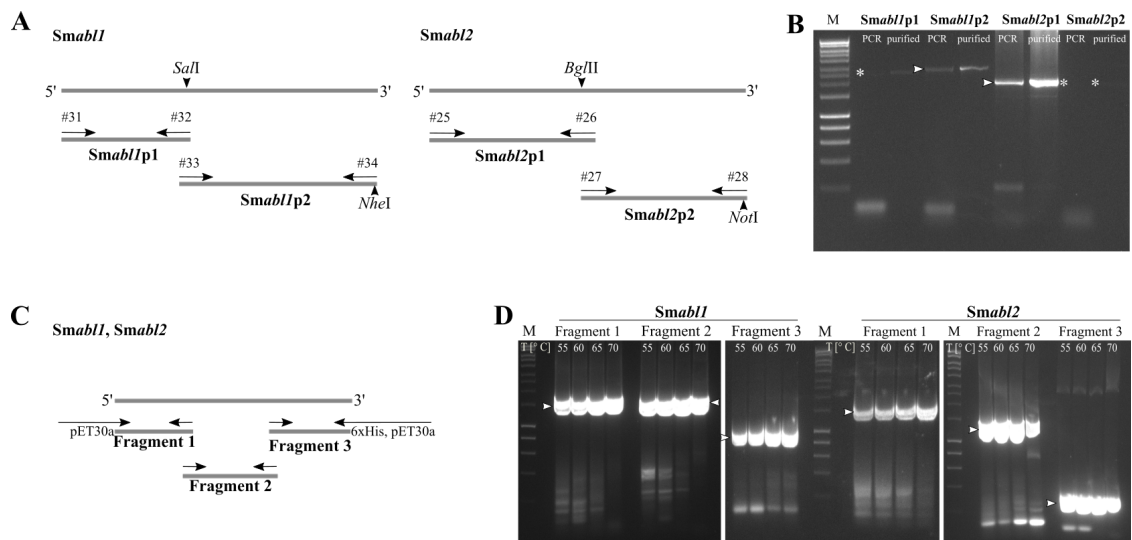
Figure 4.32: Cloning schemes and amplicon analyses for cloning of the Sm*abl* kinase genes
A: overview of the cloning strategies for Sm*abl1* (left) and Sm*abl2* (right), 2 fragments (respective part 1 and part 2 (p1 and p2)) were amplified by PCR, overlapping at the enzyme restriction sites *Sal*I (Sm*abl1*) and *Bgl*II (Sm*abl2*), adding *Nhe*I (Sm*abl1*) and *Not*I (Sm*abl2*) restriction enzyme recognition sites at the 3' end of the sequences to be cloned into vector pDrive. **B:** agarose gel electrophoretic separation of amplicons generated from PCRs for Sm*abl1*p1 (2,407 bp), Sm*abl1*p2 (2,778 bp), Sm*abl2*p1 (2,038 bp), and Sm*abl2*p2 (1,885 bp). Loaded were 2 µl of 50 µl PCR reactions and 2 µl of 20 µl purified fragments. M = 1 kb marker, the asterisks (*) mark the faint bands of Sm*abl1*p1 and Sm*abl2*p2, the arrowheads mark specific products. **C:** overview of the second cloning strategy, respective primers generate 3 specific fragments, which overlap to some extent and with an additional His$_6$-tag at the 3' end of fragment 3. The fragments are used in a DNA assembly reaction to be cloned directly into vector pET30a+. **D:** agarose gel electrophoretic separation of amplified fragments at several extension temperatures during PCR (55 °C - 70 °C) for fragment 1 - 3 of Sm*abl1* (left, fragment 1: 2,051 bp, fragment 2: 1,939 bp, and fragment 3: 1,296 bp) and Sm*abl2* (right, fragment 1: 2,106 bp, fragment 2: 329 bp, and fragment 3: 1,616 bp), specific products are marked by arrowheads, M = 1 kb marker.
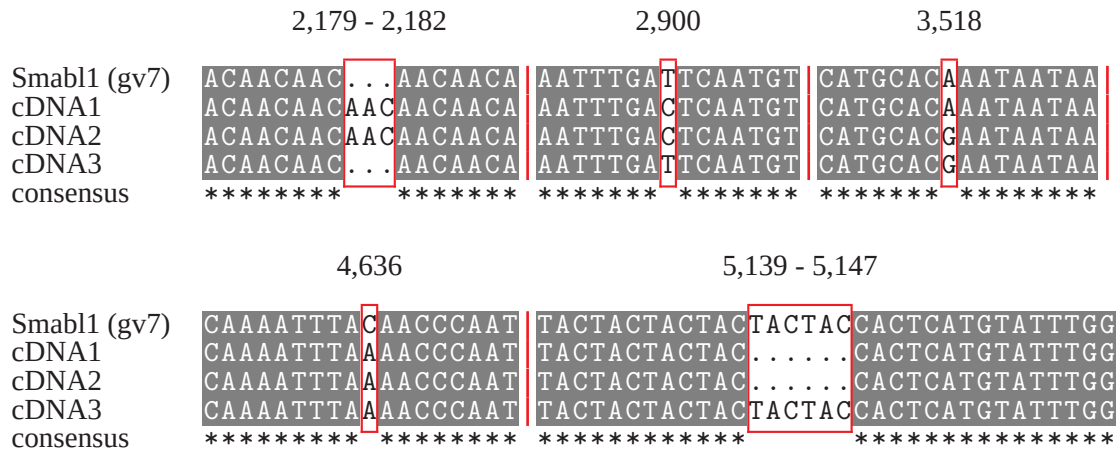
Figure 4.33: Comparison of Sm*abl1* sequences from the Liberian and Puerto Rican *S. mansoni* strain

Sequencing of 3 independently generated cDNAs (Liberian strain) shows the following changes (red boxes) compared to the sequence of the Puerto Rican strain from WormBase ParaSite (gv7): nt2,179-2,182: insertion of AAC (aa: Q), T2,900 → C2,900 (aa967: I → T), A3,518 → G3,518 (aa1,174: Q → R), C4,636 → A4,636 (aa1,547: Q → K), and nt5,139 - 5,147 deletion of TAC TAC (aa1,713: TT → −). The respective nt positions are indicated above the residues, vertical red lines separate individual sections with sequence changes, and equal nt positions are marked by asterisks (*).

The Sm*abl1*p1 and Sm*abl1*p2 products as well as Sm*abl2*p1 and Sm*abl2*p2 could not be successfully cloned by digestion and ligation, leading to a change in cloning strategy. Both sequences were subdivided into 3 fragments (**Figure 4.32 C**), and primers already designed for sequencing and qRT-PCR analysis were used for amplification. For Sm*abl1*, primer pairs #31/#51, #50/#55, and #54/#82 produced 2,024 bp, 1,939 bp, and 2,141 bp amplicons, respectively. Sm*abl2*p2 was subdivided into a 1,404 bp (#27 and #65) and a 1,571 bp PCR product (#7 and #83). All fragments were cloned into pDrive for better template availability in PCRs and check of sequence identities. The final setups for amplification of the 3 fragments used in a DNA assembly reaction with pET30a+ (**Figure 4.32 D**) were fragment 1: #91 and #51 (2,051 bp), fragment 2: #95 and #55 (1,939 bp), and fragment 3: #96 and #92 (1,296 bp, including an additional His$_6$-tag at the 3' end) for Sm*abl1* and fragment1: #93 and #97 (2,106 bp), fragment 2: #27 and #99 (329 bp), and fragment 3: #99 and #94 (1,616 bp with an additional His$_6$-tag at the 3' end) for Sm*abl2*. Via DNA assembly, pET30a-Sm*abl1* and pET30a-Sm*abl2* were created.

Sub-cloning of Sm*abl1* and Sm*abl2* for expression in HEK293-6E (EBNA1) cells

The full-length sequences of Sm*abl1* and Sm*abl2* were sub-cloned into pTT22SSP4, and the respective TKDs into pET30a+ and pTT28. To this end, the full-length sequences were divided into 3 fragments, which were assembled together with pTT22SSP4. Step by step elongation by PCR of the desired TKD was used for cloning the Sm*abl1*-TKD and Sm*abl2*-TKD into the respective vectors (**Table 4.7**). Constructs using pTT22SSP4 and pTT28 were cloned for expression with a secretion signal.

Table 4.7: Overview of amplicons generated for sub-cloning of Sm*abl1* and Sm*abl2* sequences

Name	Primers	Information
pET30a-Sm*abl1*-TKD		
PCR 1	#215, #216	798 bp, Sm*abl1*-TKD
PCR 2	#217, #218	857 bp, pET30a:Sm*abl1*-TKD:pET30a, PCR 1 as template
pET30a-Sm*abl2*-TKD		
PCR 1	#211, #212	785 bp, Sm*abl2*-TKD
PCR 2	#213, #214	848 bp, pET30a:Sm*abl2*-TKD:pET30a, PCR 1 as template
pTT22SSP4-Sm*abl1*, (full-length sequence)		
Fragment 1	#51, #251	2,046 bp, pTT22SSP4:Sm*abl1*
Fragment 2	#55, #95	1,942 bp
Fragment 3	#96, #252	1,256 bp, Sm*abl1*-His$_6$-tag:pTT22SSP4
pTT22SSP4-Sm*abl2*, (full-length sequence)		
Fragment 1	#97, #253	2,103 bp, pTT22SSP4:Sm*abl2*
Fragment 2	#27, #99	329 bp
Fragment 3	#98, #254	1,607 bp, Sm*abl2*-His$_6$-tag:pTT22SSP4
pTT28-Sm*abl1*-TKD		
PCR 1	#216, #241	795 bp, Sm*abl1*-TKD
PCR 2	#246, #247	847 bp, Sm*abl1*-TKD-His$_6$-tag, PCR 1 as template
PCR 3	#246, #248	870 bp, pTT28:Sm*abl1*-TKD-His$_6$-tag:pTT28, PCR 2 as template

Continued on the next page

Table 4.7 – *Continued from previous page*

Name	Primers	Information
pTT28-Sm*abl2*-TKD		
PCR 1	#211, #212	785 bp, Sm*abl2*-TKD
PCR 2	#249, #250	838 bp, Sm*abl2*-TKD-His$_6$-tag, PCR 1 as template
PCR 3	#249, #248	861 bp, pTT28:Sm*abl2*-TKD-His$_6$-tag:pTT28, PCR 2 as template

4.3.3 Cloning of the Sm*tk6* full-length sequence into pDrive, pET30a+, and pMal-c5X

The full-length sequence of Sm*tk6* was amplified with primers #37 and #38, generating a 1,698 bp product (**Figure 4.34 A**), which was cloned into pDrive, resulting in pDrive-Sm*tk6*. Sequencing of 3 clones revealed following alterations compared to the gv7 sequence: T258 → C258 (synonymous aa: T) and C281 → T281 (aa94: A → V). These alterations were confirmed by additional sequencing of PCR products using a total of 3 independently generated cDNAs as templates (**Figure 4.35**). For cloning into pET30a+, primers #104 and #105 were used to generate a 1,762 bp PCR product (**Figure 4.34 B**), which was used for DNA assembly resulting in pET30a-Sm*tk6*. Further cloning of Sm*tk6* was done by assembling a PCR product (primers #150 and #151, 1,765 bp; **Figure 4.34 C**) with pMal-c5X resulting in pMal-c5X-Sm*tk6*.
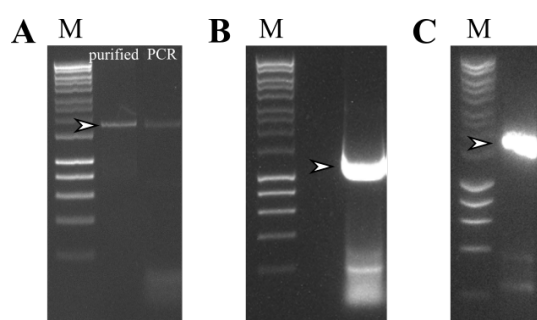

Figure 4.34: Analyses of Sm*tk6* amplicons for cloning purposes
Agarose gel electrophoretic separation of SmTK6 PCR products for cloning into **A:** pDrive (showing purified amplicon and the PCR reaction; 1,698 bp), **B:** pET30a+ (1,762 bp) and **C:** pMal-c5X (1,765 bp). Specific PCR products are marked by arrowheads, M = 1 kb marker.

<div align="center">

258   281

</div>

```
Smtk6 (gv7)  CATATGACTTGTTTAGCTGCCCAAAATGATGCAATCACGTCAGCAATAT
cDNA1        CATATGACCTGTTTAGCTGCCCAAAATGATGTAATCACGTCAGCAATAT
cDNA2        CATATGACCTGTTTAGCTGCCCAAAATGATGTAATCACGTCAGCAATAT
cDNA3        CATATGACCTGTTTAGCTGCCCAAAATGATGTAATCACGTCAGCAATAT
consensus    ******** ********************** *****************
```

Figure 4.35: Comparison of Sm*tk6* sequences from the Liberian and Puerto Rican *S. mansoni* strain
Sequencing of 3 independently generated cDNAs (Liberian strain) shows the following changes (red boxes) compared to the sequence of the Puerto Rican strain from WormBase ParaSite (gv7): T258 → C258 (aa86: T = T) and C281 → T281 (aa94: A → V). The respective nt positions are specified above the residues. Equal nt are shaded gray, and the consensus at the bottom is marked by asterisks (*). Only the section displaying changes is shown.

4.4 Expression of target proteins in pro- and eukaryotic expression systems

For expression of proteins, *E. coli* is a widely used system. The reasons for the success of *E. coli* is due to the easy availability of rich complex media with inexpensive components, the fast transformation of plasmids in only 5 min (Pope and Kent, 1996), and the fast generation time of 20 min (Clark and Maaløe, 1967)) under optimal conditions. The genome is well characterized (Jeong *et al.*, 2009, 2015; Kim *et al.*, 2017; Yoon *et al.*, 2009, 2012), and many strains are available to serve specific needs, among others, the correct folding of disulfide bond in proteins of *E. coli* cytoplasm (Lobstein *et al.*, 2012), over expression of membrane proteins (Wagner *et al.*, 2008), the reduction of lipopolysaccharides in the membrane for expression of membrane proteins (Mamat *et al.*, 2015), reduction of basal expression, codon bias correction (Jia and Jeon, 2016) and many more. It is noteworthy, that *E. coli* was believed to not being able to modify proteins post-translational. But studies showed that the *E. coli* K12 strain does protein tyrosine sulfation (Huang *et al.*, 2017), and *E. coli* B REL606 acetylation and glutamylation (Brown *et al.*, 2017a). However, if PTMs are a requirement, there is a need to switch to other protein expression systems. As eukaryotic expression systems yeast, mammalian and insect cells are widely used (Gray, 1997; McKenzie and Abbott, 2018; Nielsen, 2014).

After cloning of the target sequences (see section 4.3), the constructs were tested for protein expression using *E. coli* strains pLysS and LOBSTR-RIL (**Table 2.11**). Expression was more efficient in *E. coli* LOBSTR-RIL cells than in pLysS (see results below). While full-length proteins of SmAldh1, SmAldh2, and SmTK6 were detected (see sections 4.4.1 and 4.4.3), no expressed proteins of the SmAbl kinases were found in *E. coli* (see section 4.4.2). Therefore, Sm*abl1* and Sm*abl2* were sub-cloned for expression in HEK293-6E (EBNA1) cells. Again, neither full-length nor truncated protein versions were detected (see section 4.4.2).

4.4.1 Expression of recombinant SmAldh1, SmAldh2, MBP:SmAldh1, and MBP:SmAldh2

Expression of SmAldh1 ($\sim$ 54 kDa incl. His$_6$-tag) and SmAldh2 ($\sim$ 58 kDa incl. His$_6$-tag) showed no protein band with increasing intensity at the expected sizes in *E. coli* pLysS cells (**Figure 4.36 A**), not even over night. However, in *E. coli* LOBSTR-RIL cells, an increase of intensity of a protein of the expected size was seen already after 2 h for SmAldh2, and after 4 h for SmAldh1 (**Figure 4.36 B**, left). For a western blot analysis, protein was blotted onto a membrane (**Figure 4.36 B**, middle). The analysis of the expression kinetics in *E. coli* LOBSTR-RIL cells revealed constant rising of both target proteins after already 1 h. For SmAldh1, weak expression started already before induction of protein expression (**Figure 4.36 B**, right). Next to the target proteins, other His-rich proteins increased over time, while the lysate was already less contaminated by His-rich proteins. To analyze if the yield can be increased, expression as fusion protein linked to MBP (MBP:SmAldh1 and MBP:SmAldh2) was tested. As shown by SDS-PAGE (**Figure 4.36 C**, left), the amount of target proteins MBP:SmAldh1 ($\sim$ 96 kDa) and MBP:SmAldh2 ($\sim$ 100 kDa) increased over time. Blotting of the proteins was successful (**Figure 4.36 C**, middle). Western blot analysis revealed low amounts of target proteins already before induction of protein expression for both constructs (**Figure 4.36 C**, right). Overall, more non-specific signals were observed upon expression of MBP:SmAldh2.

Next, SmAldh1 was selected for purification because of its better solubility and higher yield. For analysis, an *E. coli* LOBSTR-RIL culture was harvested 4 h after induction, and SmAldh1 was purified by IMAC followed by SEC to separate the expressed protein from imidazole. At imidazole concentrations below 150 µM, most

non-specific protein was eluted, whereas elution of SmAldh1 was observed at 150 and 300 µM (**Figure 4.37 A**). The eluted protein was already relatively pure (about 83 %). To determine the protein concentration and to perform an activity assay, the imidazole had to be separated from the protein. Using SEC, an even higher degree of purity (94 - 95.5 %) was achieved, while imidazole was separated from the protein (**Figure 4.37 B** and **C**). Thus purified protein could be used for biochemical analyses in an enzyme activity assay.
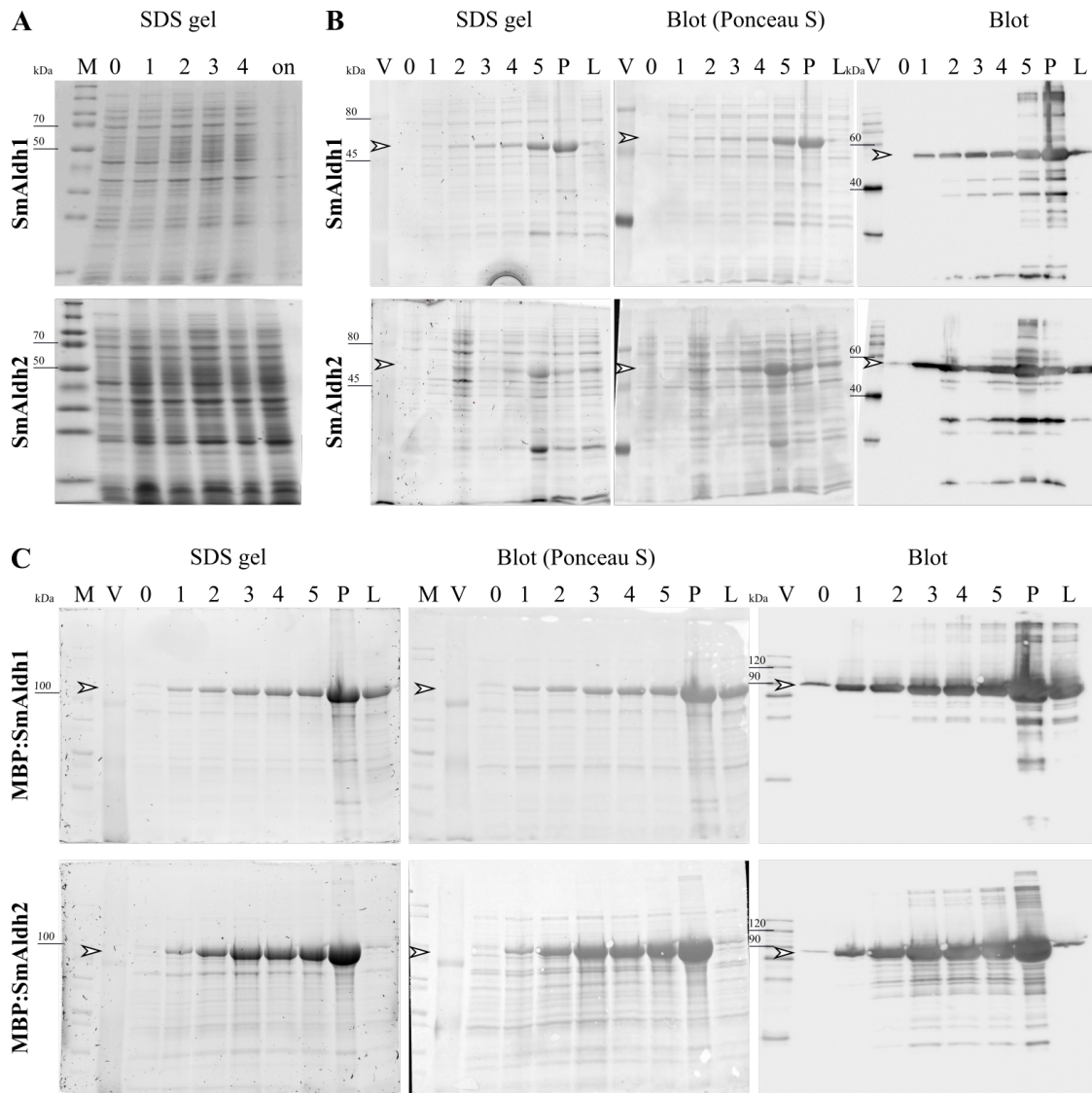
Figure 4.36: Analyses of SmAldh1 and SmAldh2 expressed in *E. coli* alone or as fusion protein (MBP:SmAldh1 and MBP:SmAldh2)

Samples of induced cultures were analyzed via SDS-PAGE for SmAldh1 and SmAldh2 expressed in **A:** *E. coli* pLysS (Coomassie-stained SDS-gel), **B:** *E. coli* LOBSTR-RIL cells followed by a western blot only for SmAldhs expressed in LOBSTR-RIL cells (SmAldh1: $\sim$ 54 kDa and SmAldh2: $\sim$ 58 kDa). **C:** expression analysis for MBP:SmAldh1 ($\sim$ 96 kDa) and MBP:SmAldh2 ($\sim$ 100 kDa) expressed in *E. coli* LOBSTR-RIL cells. Signals of specific protein sizes are marked by arrowheads (**B**, **C**). Numbers (0 - 5) indicate hours after induction of protein expression, on = over night, P = pellet, L = lysate, M = marker, V = marker (VisiBlot).
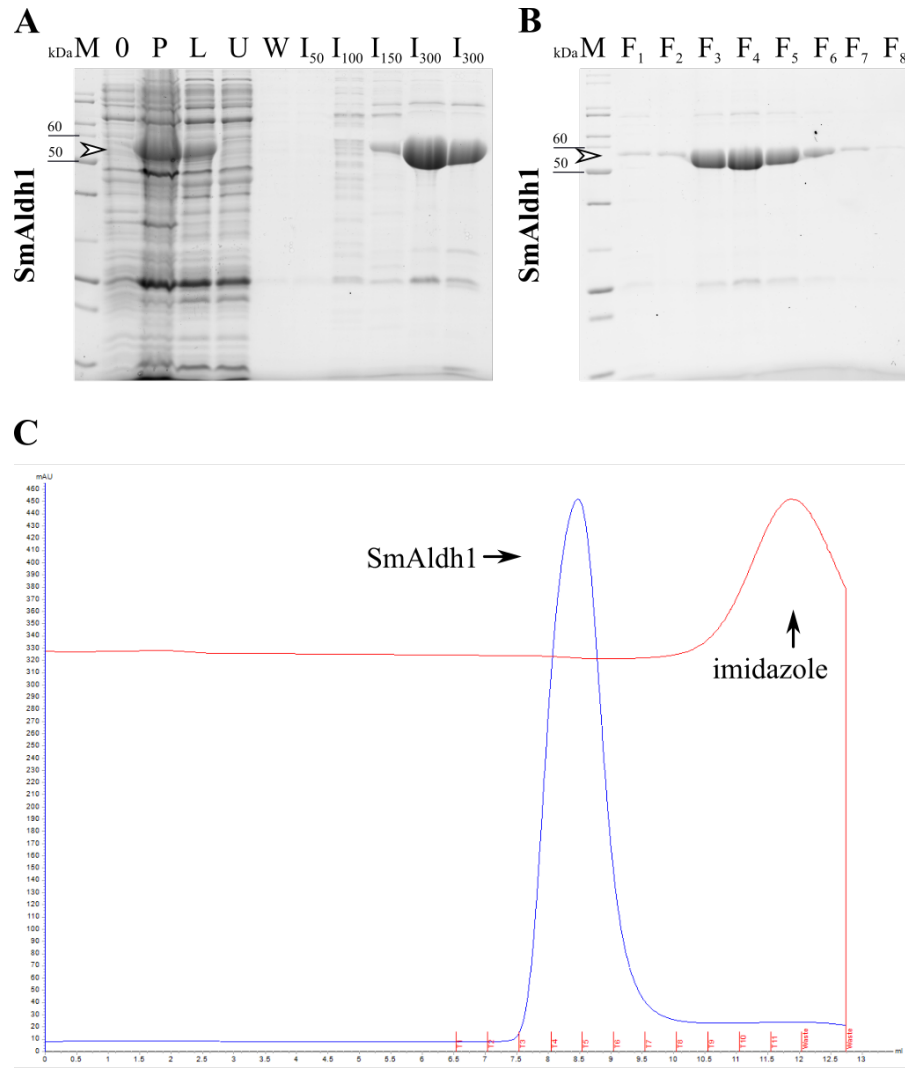
Figure 4.37: Purification of expressed SmAldh1 in *E. coli* LOBSTR-RIL
Protein expression of SmAldh1 was induced in *E. coli* LOBSTR-RIL cells and harvested after
4 h. **A:** SDS-PAGE analysis of SmAldh1 purification by IMAC followed by **C:** SEC to separate
SmAldh1 and imidazole. The fluorescence signal (milli absorbance unit (mAU)) of the protein
is shown in blue and the change in conductivity in red. Fractions of 500 µl each were collected
and analyzed by **B:** SDS-PAGE. Signals of specific protein sizes are indicated by arrowheads (**A**,
B). F_{1-8} (**B**) correspond to T_{1-8} in **C**. 0 = before induction, F_{1-8} = rebuffering fractions 1 - 8, P
= pellet, L = lysate, M = marker, U = unbound protein (flow-through), W = wash fraction, I_x =
elution fraction using x mM imidazole.

4.4.2 Expression of recombinant SmAbl1, SmAbl2, and their respective TKDs

Expression of SmAbl1 ($\sim$ 191 kDa incl. His$_6$-tag) and SmAbl2 ($\sim$ 147 kDa incl. His$_6$-tag) was analyzed in *E. coli* pLysS and *E. coli* LOBSTR-RIL cells (**Figure 4.38 A** and **B**). Neither in *E. coli* pLysS nor in *E. coli* LOBSTR-RIL were SmAbl1 or SmAbl2 detected as full-length proteins. An increased band intensity at $\sim$ 50 kDa was detected by SDS-PAGE for SmAbl1 and SmAbl2 (**Figure 4.38 B**, left). Next to the VisiBlot marker, only in the developed blot for SmAbl1, an increasing signal at $\sim$ 50 kDa was detected (**Figure 4.38 B**, right).

To analyze why full-length proteins were not detectable, protein expression was induced in *E. coli* LOBSTR-RIL and samples were taken after 2 and 4 h each. The cells were centrifuged, RNA isolated (see section 3.8.1) and cDNA synthesized (see section 3.8.2). This served as a template for PCRs to analyze specific Sm*abl1* and Sm*abl2* transcripts (Sm*abl1*p1, primer pair #31/#32 (2,410 bp) and Sm*abl1* 3' end: primer pair #34/#58 (693 bp) as well as Sm*abl2*p1: primer pair #25/#26 (2,061 bp) and Sm*abl2* 3' end: primer pair #28/#66 (609 bp)). By agarose gel electrophoretic analysis, in all cases, bands of 5' and 3' end of Sm*abl1* (**Figure 4.39 A**) and Sm*abl2* (**Figure 4.39 B**) transcripts were detected. Expression of kinases can be toxic to *E. coli* due to phosphorylation of proteins (Kemble *et al.*, 2006; Wang *et al.*, 2006). One way to overcome this effect is to co-express a phosphatase to counteract kinase-induced phosphorylations (Seeliger *et al.*, 2005; Wang *et al.*, 2006). Co-expression of pCDFD Duet-1 (**Table 2.9**; kind gift from Prof. D. Rauh) with pET30a-Sm*abl1* or pET30a-Sm*abl2* for simultaneous expression of YopH did not result in protein detection (data not shown).

To analyze whether the SmAbl proteins can be expressed as truncated versions, the TKDs were cloned. The constructs were tested in *E. coli* LOBSTR-RIL cells, resulting in SmAbl1-TKD as $\sim$ 31.5 kDa (incl. His$_6$-tag) and SmAbl2-TKD $\sim$ 30 kDa (incl. His$_6$-tag) proteins (**Figure 4.38 C**). An increase of protein of the expected sizes was observed by SDS-PAGE and western blot analysis where the latter revealed increasing signals at $\sim$ 25 and 30 kDa. Most signals were observed in the pellet fractions, while a weak, but specific signal was detected in the lysate ($\sim$ 30 kDa).
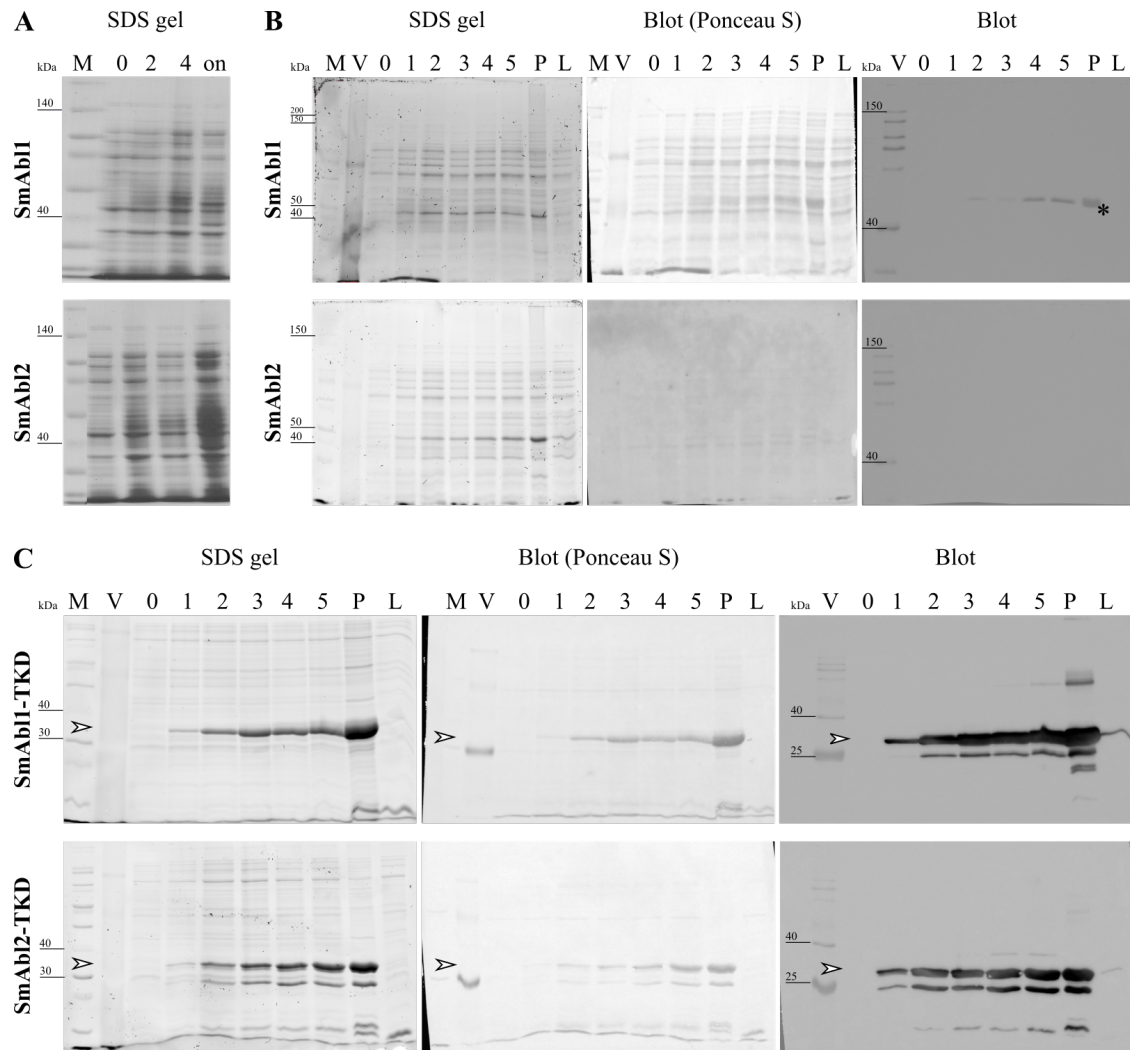
Figure 4.38: Analyses of SmAbl1 and SmAbl2 expressed in *E. coli* as full-length protein or truncated protein with the respective TKDs only

Expression analyses of SmAbl1 ($\sim$ 191 kDa) and SmAbl2 ($\sim$ 147 kDa), expressed in **A:** *E. coli* pLysS (Coomassie-stained SDS-gel) and **B:** *E. coli* LOBSTR-RIL cells followed by a western blot only for SmAbls expressed in LOBSTR-RIL cells. Non-specific signals are marked by an asterisk (*). **C:** expression analysis for SmAbl1-TKD ($\sim$ 30.5 kDa) and SmAbl2-TKD ($\sim$ 30 kDa) expressed in *E. coli* LOBSTR-RIL cells. Signals of specific protein sizes are marked by arrowheads. Numbers (0 - 5) indicate hours after induction of protein expression, on = over night, P = pellet, L = lysate, M = marker, V = marker (VisiBlot).
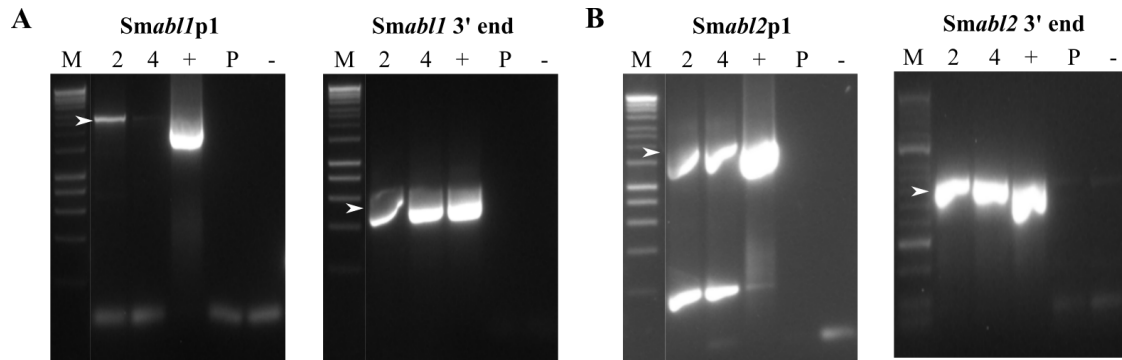
Figure 4.39: Analyses of Sm*abl1* and Sm*abl2* gene transcripts after induction of protein expression in *E. coli* LOBSTR-RIL

Transcript analyses of **A:** Sm*abl1* and **B:** Sm*abl2* after induction of protein expression in *E. coli* LOBSTR-RIL. Specific transcript sizes (Sm*abl1*p1: 2,410 bp, Sm*abl1* 3' end: 693 bp, Sm*abl2*p1: 2,061 bp, and Sm*abl2* 3' end: 609 bp) are marked by arrowheads. Numbers (2 and 4) indicate hours after induction of protein expression, + = recombinant plasmids (pET30a-Sm*abl1* or pET30a-Sm*abl2*), P = plasmid pET30a+, - = water control, M = marker.

Expression of SmAbl1 and SmAbl2 in HEK293-6E (EBNA1) cells

For further expression analysis, the constructs pTT22SSP4-Sm*abl1* and pTT22SSP4-Sm*abl2*, as well as pTT28-Sm*abl1*-TKD and pTT28-Sm*abl2*-TKD were used to transiently transfect HEK293-6E (EBNA1) cells. In addition to the recombinant constructs, a negative control (transfection of cells without DNA) and a positive control (pTTo/GFPq for expression of GFP) were included. Samples were collected every 24 h for 5 d and analyzed via SDS-PAGE and western blot (**Figure 4.40 A**, **B** and **C**). Fractions of the supernatant and cell pellet were loaded. No signals of protein accumulation were observed compared to the negative control. GFP signals were observed 3 d post transfection, confirming successful transfection (data not shown).
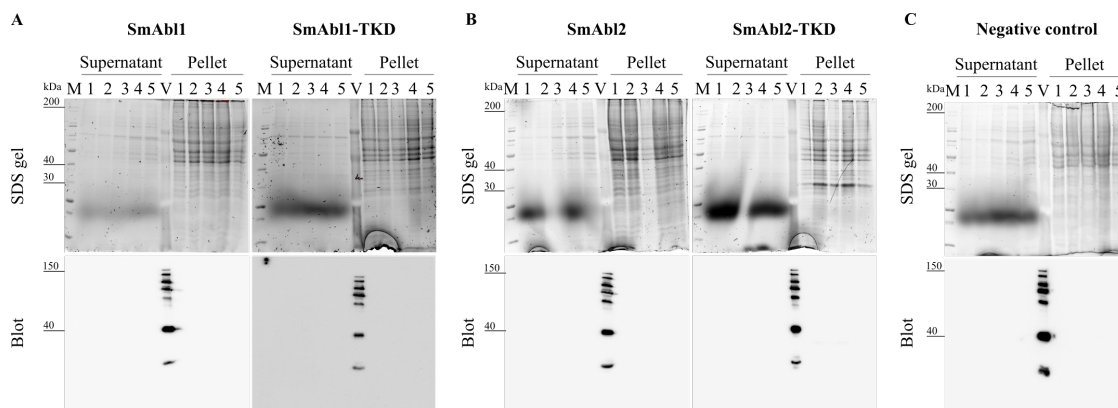
Figure 4.40: Analyses of SmAbl proteins (full-length and TKD) expressed in HEK293-6E (EBNA1) cells

Expression analyses via SDS-PAGE and western blot of **A:** SmAbl1 ($\sim$ 191 kDa) and SmAbl1-TKD ($\sim$ 30.5 kDa), **B:** SmAbl2 ($\sim$ 147 kDa) and SmAbl2-TKD ($\sim$ 30 kDa), expressed in HEK293-6E (EBNA1) cells. **C:** displays the analysis of the negative control (transfection of cells without DNA). Numbers (1 - 5) indicate d for sampling after induction of protein expression, M = marker, V = marker (VisiBlot).

4.4.3 Expression of recombinant SmTK6 and MBP:SmTK6

Protein expression of SmTK6 ($\sim$ 65 kDa incl. His$_6$-tag) was analyzed in *E. coli* pLysS and *E. coli* LOBSTR-RIL cells. No increase of protein signal was observed for recombinant SmTK6 in *E. coli* pLysS (**Figure 4.41 A**). Expression in *E. coli* LOBSTR-RIL analyzed via SDS-PAGE showed an accumulation of protein of the expected size in the pellet fraction (**Figure 4.41 B**, left). The proteins were blotted onto a membrane, which was Ponceau S-stained for analysis following detection of His-rich proteins via His-antibody (**Figure 4.41 B**, middle and right). The blot showed increasing signal intensity at the expected size and additional signals up to 5 h. Most bands were detected in the pellet fraction, while the lysate fraction gave 2 signals, one of them of expected size. The expression of the fusion protein MBP:SmTK6 was analyzed in *E. coli* LOBSTR-RIL cells (**Figure 4.41 C**). An accumulation of protein of the expected size ($\sim$ 107 kDa incl. His$_6$-tag) was detected via SDS-PAGE up to 5 h (**Figure 4.41 C**, left). The blotting success was confirmed by Ponceau S staining of the membrane (**Figure 4.41 C**, middle). Analysis of the developed blot revealed expression of the protein already before protein expression was induced (**Figure 4.41 C**, right). The number of detected bands rose up to 5 h and was highest in the pellet fraction. Analysis of the lysate fraction revealed a strong signal at the expected size and other faint signals. Overall, an increasing amount of protein at $\sim$ 107 kDa was detected over the course of time.
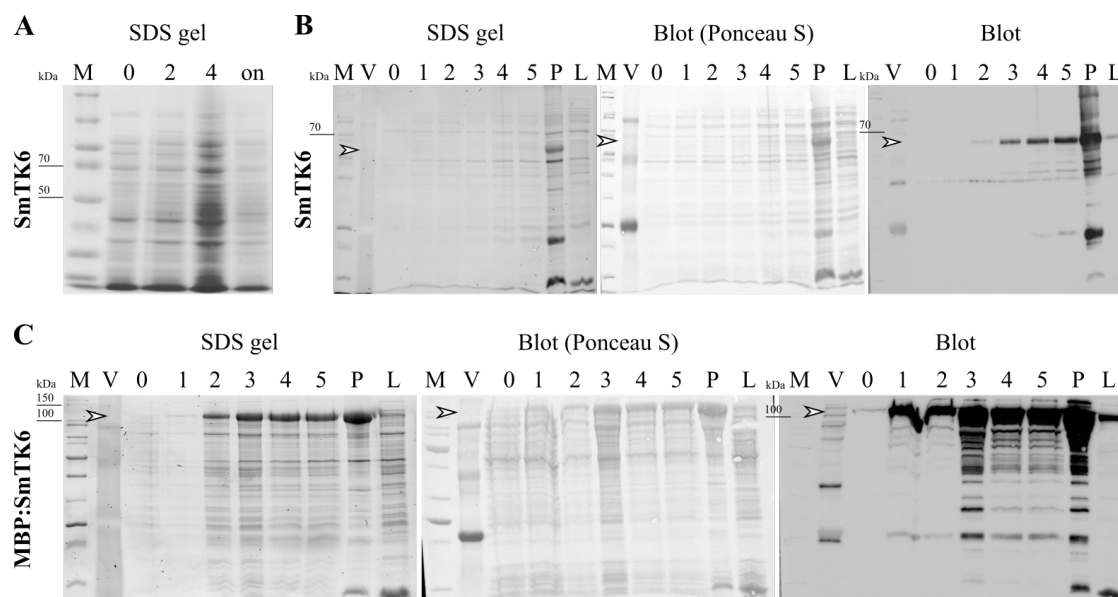
Figure 4.41: Expression analyses of SmTK6 and MBP:SmTK6 expressed in *E. coli*
Expression analyses of SmTK6 ($\sim 65\,$kDa), expressed in **A:** *E. coli* pLysS (Coomassie-stained SDS-gel) and **B:** *E. coli* LOBSTR-RIL cells followed by a western blot analysis only for protein expressed in LOBSTR-RIL cells. **C:** expression analysis for MBP:SmTK6 ($\sim 107\,$kDa) using *E. coli* LOBSTR-RIL cells. Appropriate band sizes are marked by arrowheads. Numbers (0 - 5) indicate hours after induction of protein expression, on = over night, P = pellet, L = lysate, M = marker, V = marker (VisiBlot).

4.5 Biochemical characterization of SmAldh1 revealed increased activity levels in presence of bivalent cations

In collaboration with the working group of Prof. P. Czermak, an enzyme assay was developed, where the activity of SmAldh1 was determined by measurements at 340 nm based on the reduction of NAD^+ to NADH (Harnischfeger, Beutler *et al.*, 2021). In this work, the enzyme activity of recombinantly expressed SmAldh1 in *E. coli* LOBSTR-RIL and in the baculo virus expression system (BEVS) was compared, showing that the enzyme produced in BEVS was more active than its counterpart expressed in *E. coli* LOBSTR-RIL (specific enzyme activity after 2 h for BEVS-derived SmAldh1: 2.11 U mg^{-1} vs *E. coli* LOBSTR-RIL-derived SmAldh1: 0.63 U mg^{-1}) (Harnischfeger,

Beutler *et al.*, 2021). In the following, the influence of 0.5 mM bivalent cations (Ca^{2+} and Mg^{2+}) on SmAldh1 activity was investigated.

The control (without additional ions), showed increasing conversion of NAD^+ to NADH over time (up to 3 h), while the negative control (reaction without DTT) showed a much slower increase during 3 h (**Figure 4.42 A**). The conversion of NAD^+ to NADH appeared to increase when 0.5 mM Ca^{2+} and Mg^{2+} were present. Calculation of specific enzyme activity showed a 1.3-fold increase in the presence of Ca^{2+}, whereas activity increased 1.5-fold with Mg^{2+} (**Figure 4.42 B**).
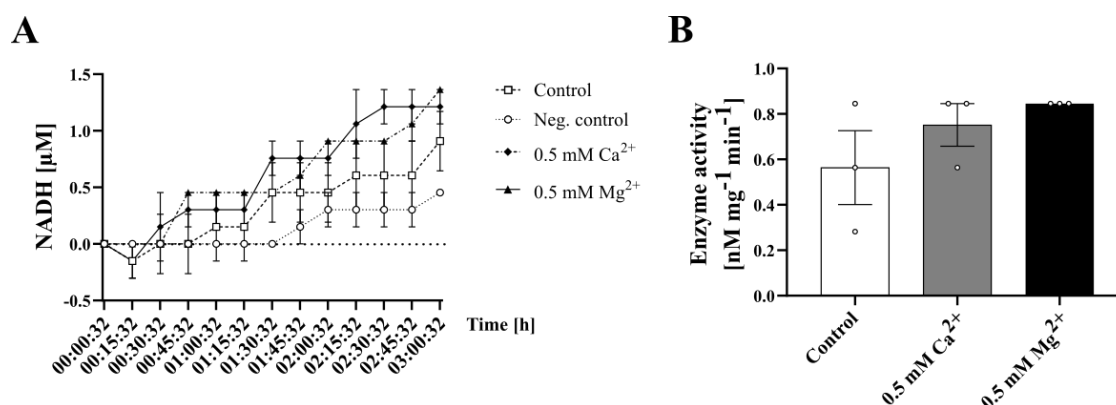
Figure 4.42: Influence of 0.5 mM Ca^{2+} and 0.5 mM Mg^{2+} on the enzymatic activity of SmAldh1
The specific activity of SmAldh1 was determined by measurements of the reduction of NAD^+ to NADH at 340 nm. **A:** The NADH level increased during the activity assay over 3 h, square (□) = control (standard reaction), circle (○) = negative control (standard reaction without DTT), black triangle (▲) = reaction with 0.5 mM Mg^{2+}, black diamond (♦) = reaction with 0.5 mM Ca^{2+}. **B:** Shown is the specific enzymatic activity as reduced nM NADH/mg of enzyme per minute in presence of 0.5 mM Ca^{2+} and Mg^{2+} with the standard reaction as control after 3 h. No statistical significance was found. Data represent technical triplicates with StEM, n = 1.

4.6 Localization analysis by WISH showed a broad distribution of Sm*aldh1* and Sm*aldh2* transcripts in different tissues of both genders

Transcriptomic data generated by Lu *et al*. (2016, 2017) indicated abundant Sm*aldh1* transcripts in males (average expression $\sim$ 3,000 reads per kilobase million (RPKM)) and in their testes ($\sim$ 1,000 RPKM). In contrast, lowest transcript levels were found in females (< 1,000 RPKM). The average expression of Sm*aldh2* was about twice as high in females than in males, with a bias toward the ovary ($\sim$ 15 RPKM). Contrary to these findings, data from a first RNA seq-based single-cell atlas showed a wide distribution of Sm*aldh2* transcripts in adult worms, whereas Sm*aldh1* seemed barely recognized (Wendt *et al.*, 2020). To resolve this discrepancy, localization experiments using WISH were performed.

With each probe, corresponding controls (sense transcripts of Sm*aldh1* and Sm*aldh2*) were included, which showed no signals in females and males (**Figure 4.43 A** and **C**). Localization using the Sm*aldh1* probes revealed a broad distribution of transcripts in adult worms (**Figure 4.43 B**). In females, signals were observed in the ovary, uterus, and gut, whereas no signals were found in the vitellarium. In males, signals were detected in the esophagus, gut, as well as in muscles and the tegument. Sm*aldh2* transcripts were mainly detected in the ovary, uterus, and intestine (**Figure 4.43 D**), whereas no signals were observed in the vitellarium. In males, a broad distribution pattern was observed with signals in the head and ventral sucker, testis, gut, and muscle layers.
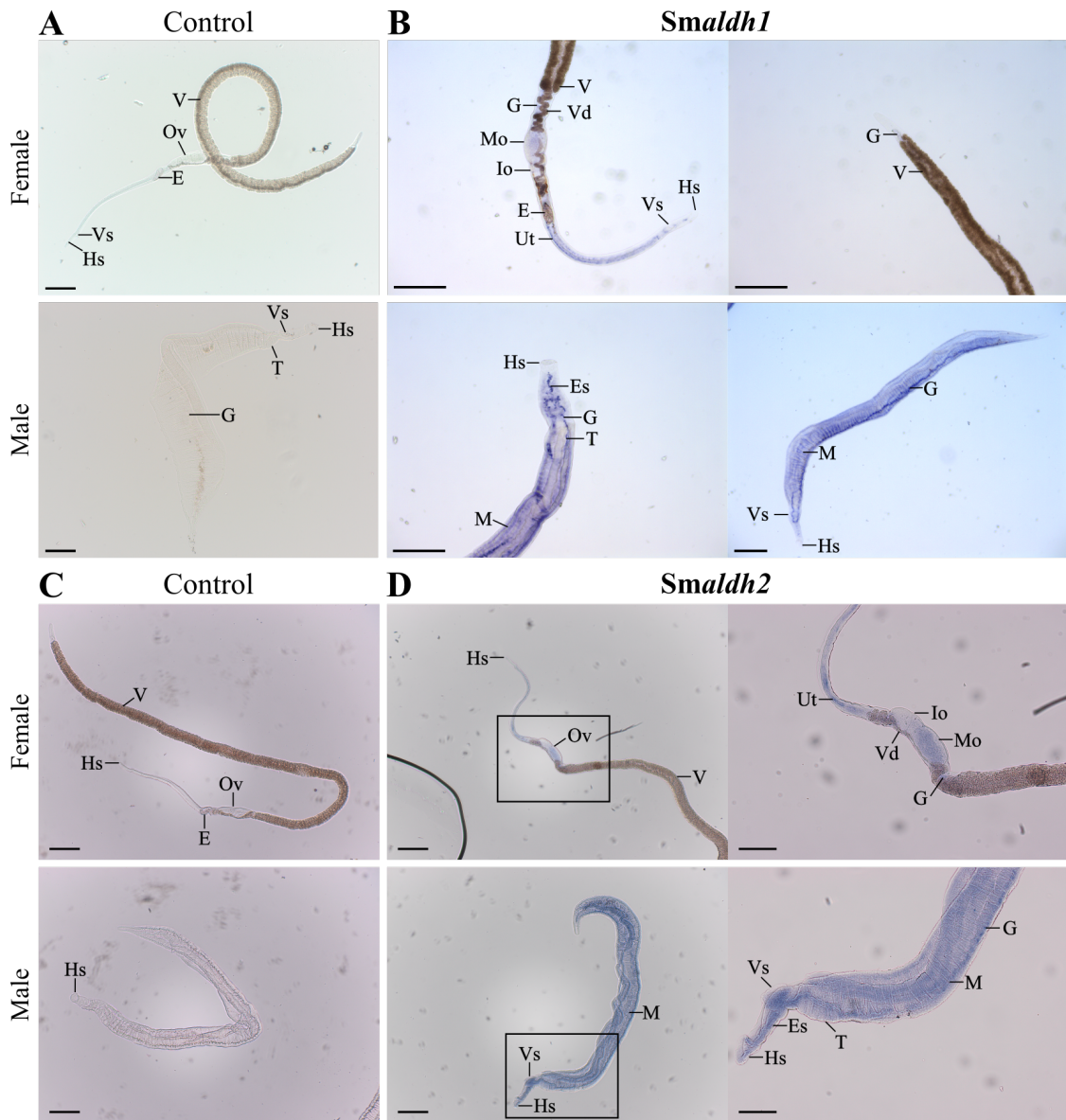
Figure 4.43: Localization of Sm*aldh1* and Sm*aldh2* transcripts in pairing-experienced adult *S. mansoni* couples

Immediately after perfusion, *S. mansoni* couples were separated and fixed for subsequent transcript localization by WISH. Shown are representative images of **A**, **C:** worms treated with sense transcripts as control probes of Sm*aldh1* (**A**) and Sm*aldh2* (**C**). **B**, **D:** worms treated with Sm*aldh1* anti-sense probes (**B**), and Sm*aldh2* anti-sense probes (**D**). Respective transcript signals (blue) are widely distributed in different tissues in both genders including the tegument area. E = egg, Es = esophagus, G = gut, Hs = head sucker, Io = part of the ovary containing immature oocytes, M = muscle, Mo = part of the ovary containing mature oocytes, ov = ovary, T = testis, Ut = uterus, V = vitellarium, Vd = vitelloduct, Vs = ventral sucker. Scale bars represent 250 µm.

4.7 RNAi approaches to unravel the functions of selected genes in adult *S. mansoni* couples

To characterize potential functions of Sm*aldh1*, Sm*aldh2*, Sm*abl1*, Sm*abl2*, and Sm*tk6*, knock down approaches mediated by RNAi were performed on adult *S. mansoni* worms. For each gene, a concentration of $2.5\,\mu g\,ml^{-1}$ specific dsRNA was applied every 3 d for durations of 14 and 21 d. Additionally, $12.5\,\mu g\,ml^{-1}$ dsRNA was applied as a pilot experiment for 14 d to examine if more dsRNA causes more severe effects. Afterwards, the worms were analyzed for changes in their morphology using CLSM, their ability to undergo cell proliferation (EdU assay), and gene transcript analysis (qRT-PCR), which included selected genes associated with oxidative stress (Sm*aldh1*, Sm*aldh2*, Sm*ar*, Sm*gpx*, Sm*sod*, and Sm*sodex*), cell cycle (Sm*npl4* and Sm*p53*), stem cell activity (Sm*nanos1* and Sm*nanos2*), apoptosis (Sm*bax* and Sm*bcl-2*), and differentiation (kinases Sm*abl1*, Sm*abl2*, and Sm*tk6*). In addition to single knock downs targeting a single gene, multiple knock downs using combinations of Sm*aldh1* and Sm*aldh2* as well as Sm*abl1* and Sm*abl2* were performed using $2.5\,\mu g\,ml^{-1}$ and $12.5\,\mu g\,ml^{-1}$ dsRNA, respectively.

4.7.1 Knock down of Sm*aldh1* had no effect on worm physiology

To investigate the relevance of Sm*aldh1* in adult *S. mansoni*, a knock down approach was performed by RNAi using specific Sm*aldh1* dsRNA. For phenotype analysis, physiological parameters were assessed regularly for periods of 14 and 21 d.

To gain an overview to which extent Sm*aldh1* was expressed in female and male worms that were either pairing-experienced (derived from bs infections) or pairing-unexperienced (derived from ss infections), qRT-PCR experiments were performed. A significant difference was observed in bs males (bsM) and ss males (ssM), with ssM showing a higher gene expression level. Transcript abundance was slightly higher in bs females (bsF) than in bsM, whereas expression of Sm*aldh1* was approximately 2.5-fold higher in ssM than in ss females (ssF) (**Figure 4.44**).
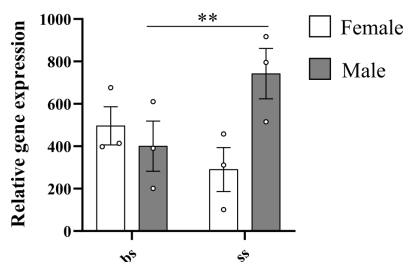
Figure 4.44: Analysis of the transcript profile of Sm*aldh1* in adult *S. mansoni*
Determined relative gene expression of Sm*aldh1* in bsF/M and ssF/M. Each point represents one experiment with 10 worms each, n = 3. Columns represent means with StEM. Statistical analysis was performed as two-tailed t-test, p < 0.01 (**).

Gene expression was examined after Sm*aldh1* knock down. Here, $2.5\,\mu g\,ml^{-1}$ dsRNA was administered for a period of 14 d (**Figure 4.45 A** and **B**) and 21 d (**Figure 4.45 D** and **E**). In addition, gene expression was examined after 14 d of treatment with $12.5\,\mu g\,ml^{-1}$ dsRNA (**Figure 4.45 C**). First, Sm*aldh1* gene expression was significantly downregulated to 7 % and 2 % in females and males, respectively, after 14 d (both p < 0.001; **Figure 4.45 A**), indicating a highly efficient knock down. Sm*aldh2* was upregulated in males by 84 % but was not affected in females, while Sm*ar* expression was not affected in both genders. Gene expression of Sm*gpx* was downregulated to 43 % in females, whereas it was upregulated by 64 % in males (**Figure 4.45 B**). Sm*sod* gene expression was not affected by the knock down approach, whereas Sm*sodex* was downregulated in both genders to 57 % in females and 53 % in males, respectively.

Application of $12.5\,\mu g\,ml^{-1}$ dsRNA reduced expression of Sm*aldh1* to 3 % and 2 % in females and males, respectively (**Figure 4.45 C**). Expression of Sm*gpx* was not affected, while Sm*sod* expression decreased to 44 % in females, and Sm*sodex* increased about 2.9-fold in males. Knock down of Sm*aldh1* was as efficient as before, transcript levels were decreased to 5 % in females and 4 % in males (p < 0.001) after 21 d, **Figure 4.45 D**). Sm*aldh2* was upregulated in males by 50 %, while it was not regulated in females. Gene expression of Sm*ar* was not affected in both genders. Gene expression of Sm*gpx* was downregulated to 42 % and 69 % in females and males, respectively, while Sm*sod* was not affected in both genders. Transcript levels of Sm*sodex* were downregulated to 53 % in females, but were not affected in males (**Figure 4.45 E**).
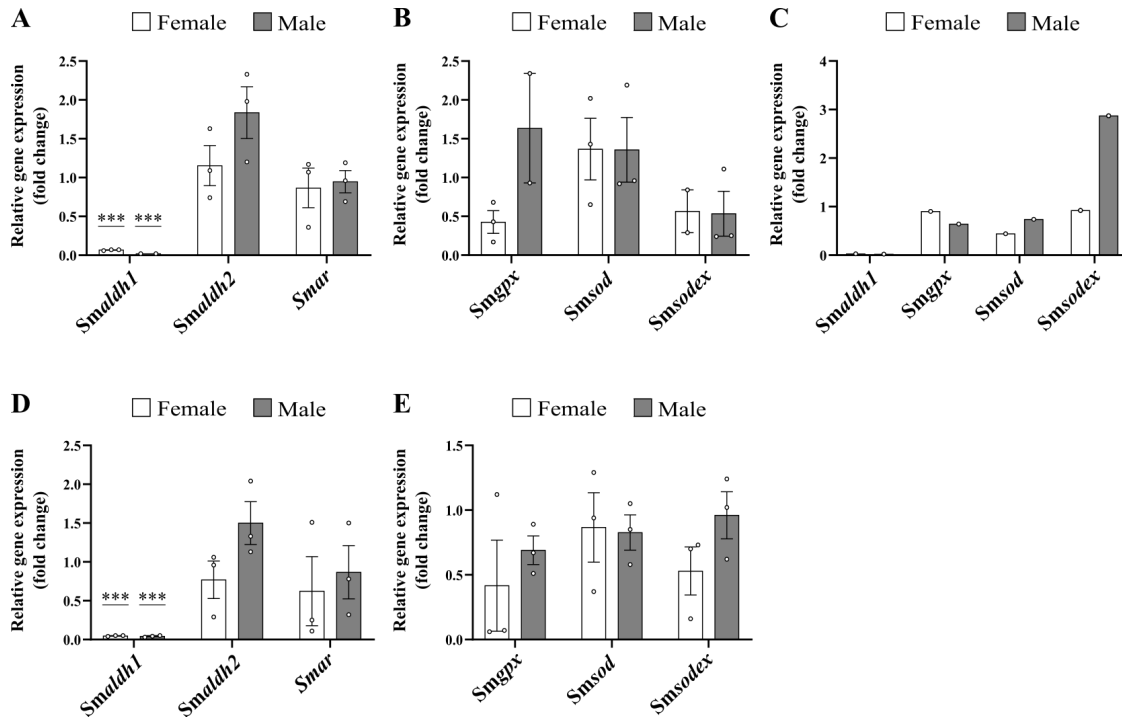
Figure 4.45: qRT-PCR analyses of oxidative stress response gene expression after knock down of Sm*aldh1* in adult *S. mansoni* couples

Relative gene expression was determined after 14 d of 2.5 µg ml^{-1} Sm*aldh1* dsRNA treatment for **A:** Sm*aldh1*, Sm*aldh2*, Sm*ar*, **B:** Sm*gpx*, Sm*sod*, Sm*sodex*, n = 3 (Sm*aldh1* and Sm*gpx* gene expression was determined only 2 times in males). **C:** relative gene expression levels of Sm*aldh1*, Sm*aldh2*, and Sm*ar* after 14 d using 12.5 µg ml^{-1} Sm*aldh1* dsRNA, n = 1. Determined relative gene expression after 21 d for **D:** Sm*aldh1*, Sm*aldh2*, Sm*ar* as well as **E:** Sm*gpx*, Sm*sod*, and Sm*sodex* using 2.5 µg ml^{-1} dsRNA, n = 3 (Sm*sodex* expression was determined in males only 2 times). Each data point represents one qRT-PCR analysis of one independent knock down experiment with 10 couples each. Columns represent means with StEM. Statistical analysis (two-tailed t-test) was performed using treatment vs control (not shown), p < 0.001 (***).

The number of couples (**Figure 4.46 A** and **F**) and their attachment capacity (**Figure 4.46 B** and **G**) in the dsRNA-treated groups (2.5 µg ml^{-1} Sm*aldh1* dsRNA) did not differ significantly from the controls (treated with DEPC-water) during both observation periods. Motility was at a normal level after 14 d (**Figure 4.46 C**), whereas the motility value dropped slightly towards the end of 21 d (control and treatment 2.47, respectively) (**Figure 4.46 H**). The mean values of normally shaped eggs were higher than those from the control groups during the 14 d observation period until day 9, with significant differences at day 6 and day 9 (**Figure 4.46 D**), while the mean values of normal-shaped eggs were insignificant lower compared to the controls during the 21 d treatment interval (**Figure 4.46 I**). The only significant difference in the number of abnormally

formed eggs in the 14 d treatment group was observed at day 6 (control 38 vs treatment group 73, p < 0.05) (**Figure 4.46 E**). The numbers of abnormally formed eggs in the treatment groups were comparable to those in the controls during the 21 d treatment regime (**Figure 4.46 J**).

At higher dsRNA doses (12.5 µg ml^{-1}), the number of couples remained comparable to those of the controls (**Figure 4.46 K**). Moreover, the number of attached couples decreased to a minimum of 5.5 in the treatment groups, while 7 couples were still attached to the dishes in the controls (**Figure 4.46 L**). Worm movements remained normal throughout the treatment period (**Figure 4.46 M**). The number of normal-formed eggs was higher in the treatment groups throughout 9 d (**Figure 4.46 N**), while the number of abnormal-formed eggs was higher in the treatment groups only at day 3 and day 14 (**Figure 4.46 O**).

In addition to the physiological parameters, possible differences in the morphology of the dsRNA-treated worms were examined using CLSM. Analysis of treated worms revealed no morphological changes of the gonads or other organs after treatment with 2.5 µg ml^{-1} and 12.5 µg ml^{-1} dsRNA after 14 d (**Figure 4.47 A - C**). In addition, no changes in the guts or gonads of both genders were observed after 21 d Sm*aldh1* knock down (**Figure 4.47 D** and **E**).

Next, worms were fixed to study a possible effect on proliferating cells after Sm*aldh1* knock down. In an EdU assay to monitor cell proliferation, EdU-positive cells were detected after 14 d of 2.5 µg ml^{-1} dsRNA treatment (**Figure 4.48 B**), as well as after 14 d of 12.5 µg ml^{-1} dsRNA treatment (**Figure 4.48 C**), which were in both cases comparable to the control (**Figure 4.48 A**). Analysis of EdU-positive cells after 21 d revealed signals in the immature part of the ovary (oogonia) and testes (spermatogonia), which were comparable to those of the control groups (**Figure 4.48 D** and **E**).
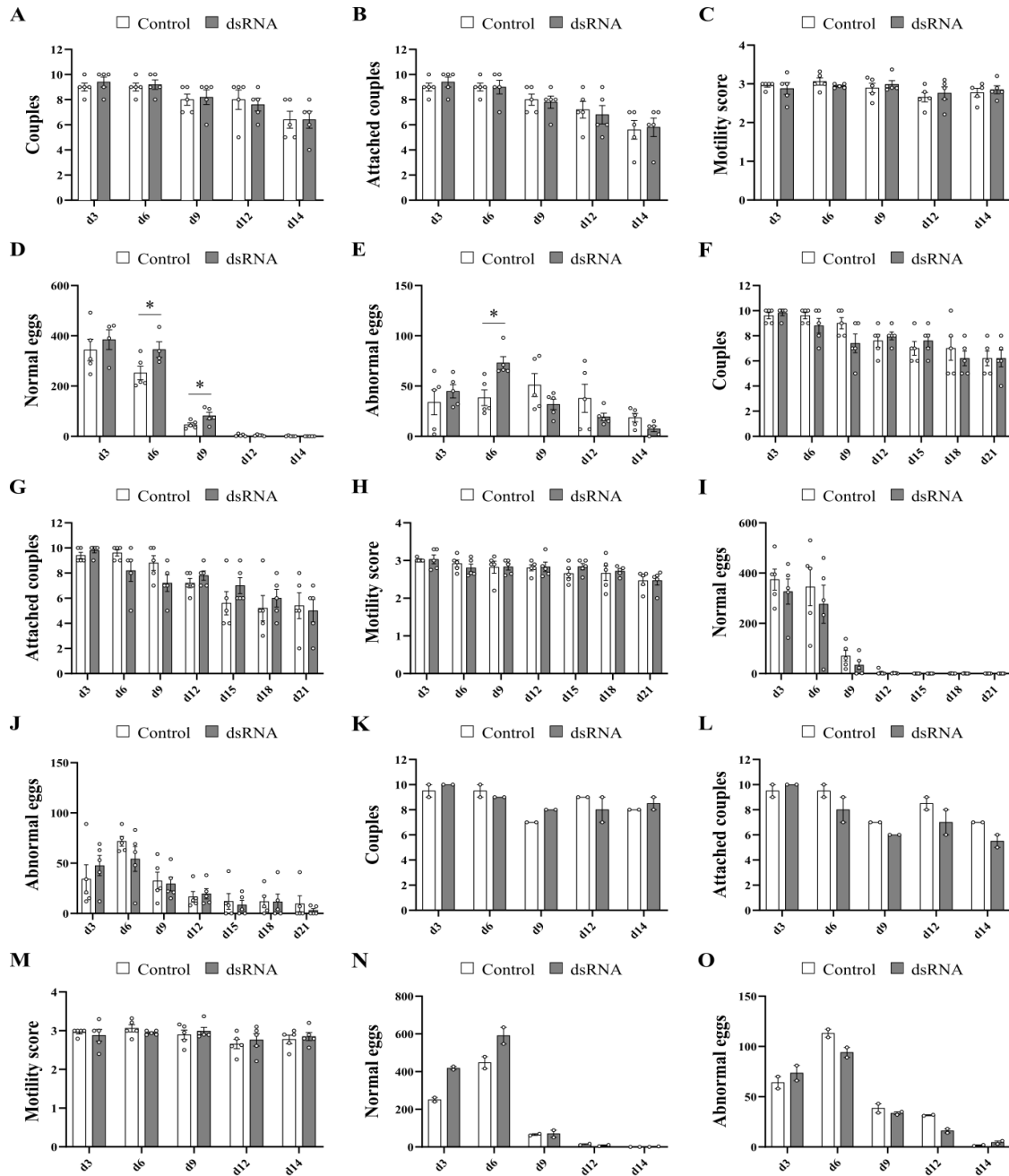
Figure 4.46: Screening of physiological parameters following Sm*aldh1* knock down
Determined number of couples (**A**, **F**, **K**), attachment of couples (**B**, **G**, **L**), motility score (**C**, **H**, **M**), number of normal eggs (**D**, **I**, **N**), and abnormal eggs (**E**, **J**, **O**) during knock down of Sm*aldh1* for **A** - **E:** 14 d (2.5 µg ml^{-1} dsRNA, n = 5), **F** - **J:** 21 d (2.5 µg ml^{-1} dsRNA, n = 5), and **K** - **O:** 14 d (12.5 µg ml^{-1} dsRNA, n = 2). Outliers were removed in D at day 3/6: 984/997. Each point represents a measurement (averaged for motility score) of one experiment with 10 couples each. Columns represent means with StEM. Statistical analysis was performed as two-tailed t-test (treatment vs control), p < 0.05 (*).
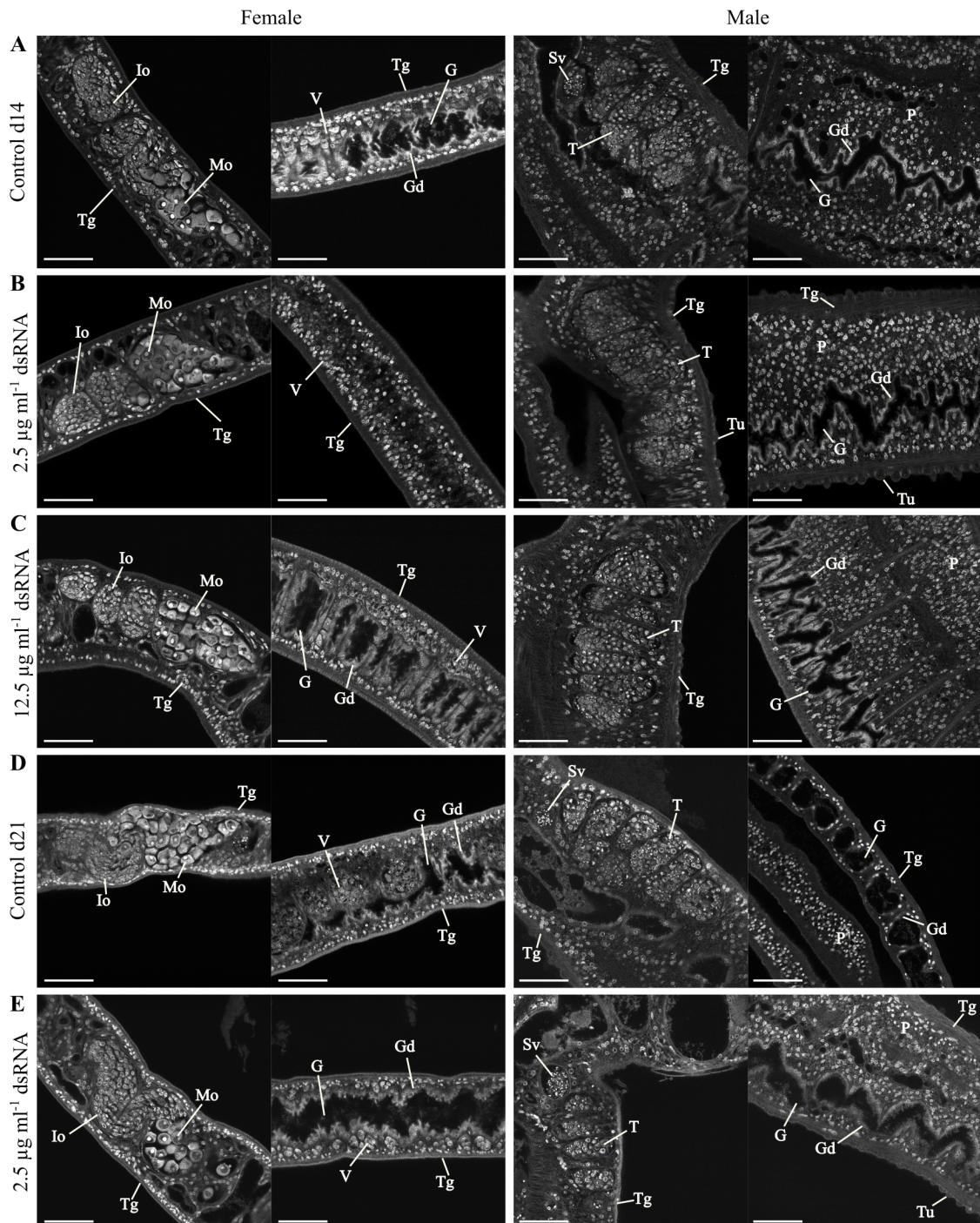
Figure 4.47: Influence of Sm*aldh1* knock down on the morphology of adult *S. mansoni* couples

Images of the control groups after **A:** 14 d and **D:** 21 d. Couples were treated with **B:** 2.5 µg ml^{-1} Sm*aldh1* dsRNA for 14 d, **C:** 12.5 µg ml^{-1} Sm*aldh1* dsRNA for 14 d, and **E:** 2.5 µg ml^{-1} Sm*aldh1* dsRNA for 21 d. Worms of the treatment groups did not differ from the controls. G = gut, Gd = gastrodermis, Io = part of the ovary containing immature oocytes, Mo = part of the ovary containing mature oocytes, P = parenchyma, Sv = seminal vesicle, T = testis, Tg = tegument, Tu = tubercle. Scale bars represent 50 µm.
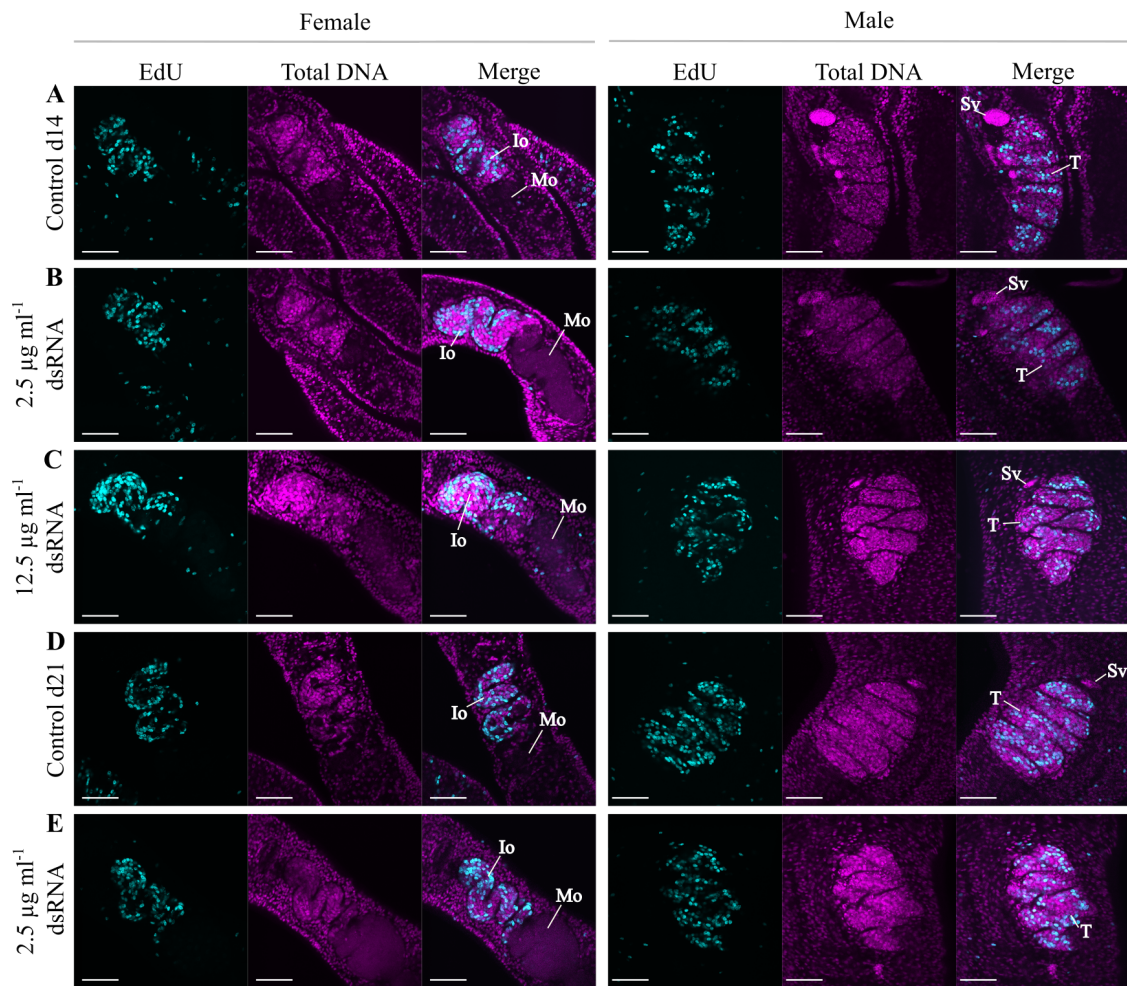
Figure 4.48: Influence of Sm*aldh1* knock down on proliferation in adult *S. mansoni* couples
Representative images of the control groups are shown after experimental durations of **A:** 14 d
and **D:** 21 d. Couples were trated with **B:** 2.5 µg ml^{-1} Sm*aldh1* dsRNA for 14 d, **C:** 12.5 µg ml^{-1}
Sm*aldh1* dsRNA for 14 d, and **E:** 2.5 µg ml^{-1} Sm*aldh1* dsRNA for 21 d. EdU-positive cells are
shown in cyan and the total DNA in magenta. No changes in signals were detected in the treatment
groups. Io = part of the ovary containing immature oocytes, Mo = part of the ovary containing
mature oocytes, Sv = seminal vesicle, T = testis. Scale bars represent 50 µm.

4.7.2 Knock down of Sm*aldh2* induced a loss of mature oocytes after 21d

To evaluate the importance of Sm*aldh2* for *S. mansoni*, a RNAi-mediated knock down
approach was performed. As before, worm couples were treated with either 2.5 µg ml^{-1}
or 12.5 µg ml^{-1} dsRNA for 14 and 21 d.

To gain insight into Sm*aldh2* gene expression, qRT-PCR analysis using bsF/M and ssF/M was performed. Gene expression was approximately 2-fold higher in bsF than in bsM, whereas it was approximately 1.5-fold higher in ssF than ssM (**Figure 4.49**).
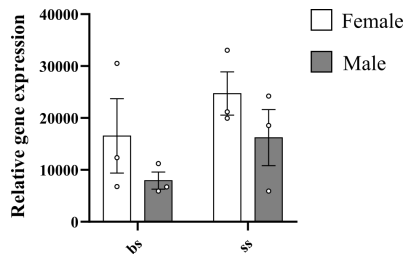
Figure 4.49: Analysis of the transcript profile of Sm*aldh2* in adult *S. mansoni*
Determined relative gene expression of Sm*aldh2* in bsF/M and ssF/M, respectively. Each point represents one experiment with 10 worms each, n = 3. No statistical significance was found. Columns represent means with StEM.

To analyze if the knock down of Sm*aldh2* was efficient, qRT-PCR was performed. Thereby, Sm*aldh2* was downregulated to 61 % in females and even further downregulated in males to 21 % after 14 d treatment with 2.5 µg ml^{-1} Sm*aldh2* dsRNA (**Figure 4.50 A**). While Sm*ar* gene expression was not affected in both genders, gene expression of Sm*aldh1* increased 2.5-fold in females but was not affected in males. Among Sm*gpx*, Sm*sod*, and Sm*sodex* gene expression levels, only Sm*gpx* levels rose 2-fold in males, while the remaining genes were not regulated (**Figure 4.50 B**). Gene expression levels of Sm*aldh2* were significantly decreased to 20 % in females and 28 % in males after 21 d with 2.5 µg ml^{-1} Sm*aldh2* dsRNA (**Figure 4.50 D**). Among the selected genes, only Sm*gpx* expression was downregulated in females by 36 %, while the other analyzed genes were not regulated (**Figure 4.50 E**).

With more Sm*aldh2* dsRNA (12.5 µg ml^{-1}), transcript abundance of Sm*aldh2* decreased to 34 % and 17 % in females and males, respectively, after 14 d of treatment (**Figure 4.50 C**). Analyzed Sm*gpx* and Sm*sod* gene expression did not change, but Sm*sodex* was upregulated 2.3-fold in males, while it was not altered in females.
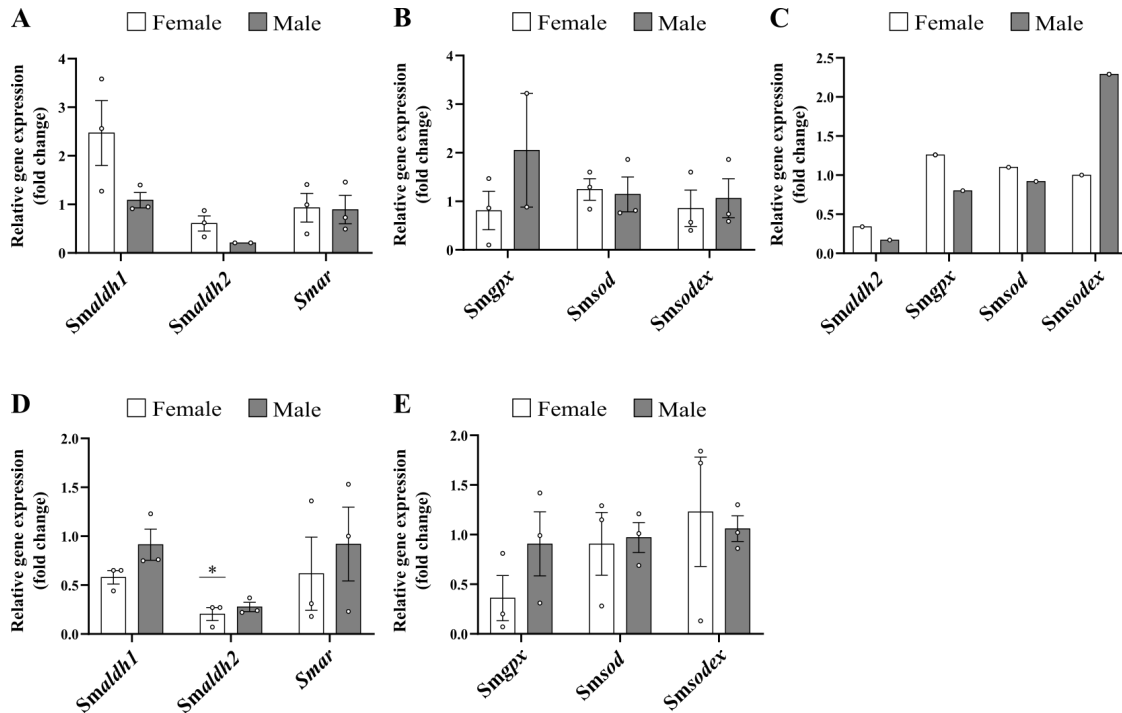
Figure 4.50: qRT-PCR analysis of oxidative stress response gene expression after knock down of Sm*aldh2* in adult *S. mansoni* couples

Relative gene expression of oxidative stress-associated genes was determined after knock down of Sm*aldh1* for 14 d with **A**, **B:** 2.5 µg ml^{-1} Sm*aldh2* dsRNA, n = 3 (determination of Sm*aldh2* and Sm*gpx* gene expression in males was performed only 2 times), **C:** 12.5 µg ml^{-1} Sm*aldh2* dsRNA, n = 1, and **D**, **E:** after 21 d with 2.5 µg ml^{-1} Sm*aldh2* dsRNA, n = 3. Each data point represents one qRT-PCR analysis of one independent knock down experiment with 10 couples. Columns represent means with StEM. Statistical analysis (two-tailed t-test) was performed using treatment vs control (not shown), p < 0.05 (*).

The number of couples did not differ significantly compared to the controls during the 14 and 21 d treatment periods, but the numbers continued to decline the longer the treatment period lasted (**Figure 4.51 A** and **F**). Analysis of attached couples revealed no significant changes compared to the controls during the 14 d observation period (**Figure 4.51 B**), while the number of attached couples was significantly decreased in the treatment groups at day 6 during the longer treatment duration (**Figure 4.51 G**). Average worm movements were normal (value = 3) and dropped slightly towards reduced movement (value = 2) at the end of both observation periods (day 21: control 2.31 vs treatment 2.46) (**Figure 4.51 C** and **H**). In the 14 d treatment groups, the number of normally formed eggs was not significantly higher than in the control groups at day 3, but was significantly higher at day 6 ($\sim$ 71 %) and day 9 ($\sim$ 89 %) (**Figure 4.51 D**). The number of normal-shaped eggs did not differ significantly between the control groups

and the groups treated with Sm*aldh2* dsRNA for 21 d (**Figure 4.51 I**). The number of abnormally shaped eggs peaked in the treatment groups at day 6 and then decreased the following days in both observation periods (**Figure 4.51 E** and **J**). They did not differ at any time from the controls.

To evaluate the possibility of a stronger influence on the worms, $12.5\,\mu\text{g}\,\text{ml}^{-1}$ Sm*aldh2* dsRNA was applied. Worms remained paired comparable to the controls (**Figure 4.51 K**), while the number of couples attached to the dishes were always lower in the treatment groups (**Figure 4.51 L**). Worm movements were normal at all time points except day 12, where movements increased slightly in the control and treatment groups (**Figure 4.51 M**). The number of normal eggs doubled in the treatment groups after 3 d but converged afterwards (**Figure 4.51 N**). At day 3, more abnormal eggs were found in the treatment groups, however, the numbers decreased until the end of the observation period (**Figure 4.51 O**).

Since there were no effects on the physiological parameters, a possible effect on the internal worm structures was analyzed by CLSM. So far, no morphological changes were observed in females or males after 14 d of treatment with $2.5\,\mu\text{g}\,\text{ml}^{-1}$ and $12.5\,\mu\text{g}\,\text{ml}^{-1}$ Sm*aldh2* dsRNA when compared to the controls (**Figure 4.52 A - C**). However, after prolonged treatment, the posterior part of the ovary (harboring the mature oocytes) appeared less tightly in females on day 21 compared with controls (**Figure 4.52 D** and **E**), whereas no changes were observed in the gut. Furthermore, no structural differences were observed in the testes or gut of male worms.

To investigate a possible phenotype in the gonadal cells, an EdU assay was then performed. Analysis of the stained worms by CLSM showed the appearance of signals in the immature part of the ovary as well as in the testes, with no differences between treatments with $2.5\,\mu\text{g}\,\text{ml}^{-1}$ or $12.5\,\mu\text{g}\,\text{ml}^{-1}$ Sm*aldh2* dsRNA and the controls after 14 d (**Figure 4.53 A - C**). The same is true for the application of $2.5\,\mu\text{g}\,\text{ml}^{-1}$ Sm*aldh2* dsRNA for 21 d (**Figure 4.53 D** and **E**).
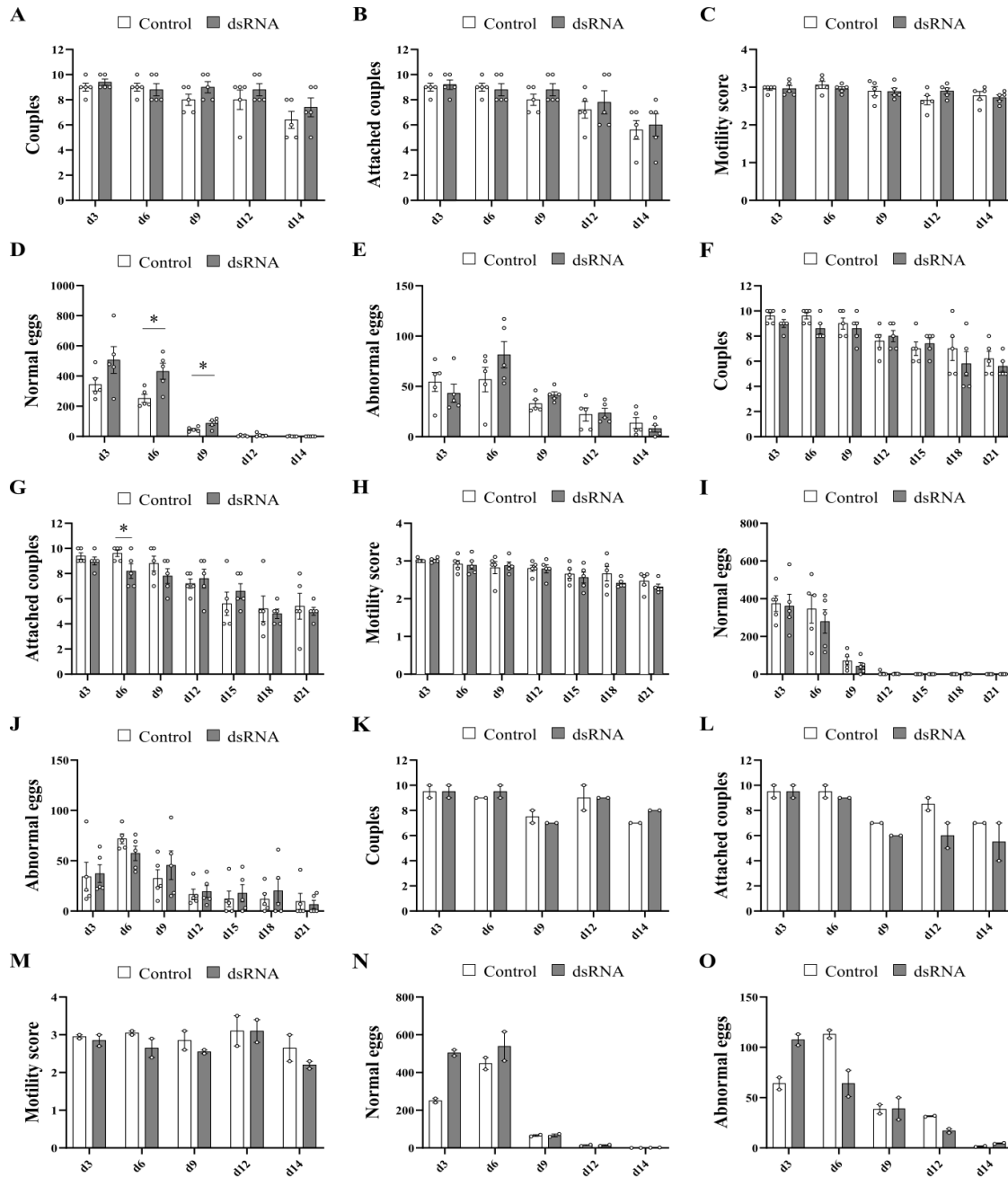
Figure 4.51: Screening of physiological parameters following Sm*aldh2* knock down
The assessed scoring parameters were shown for treatment periods of **A** - **E:** 14 d (n = 5), and **F** - **J:** 21 d with 2.5 µg ml^{-1} Sm*aldh2* dsRNA applied (n = 5), as well as **K** - **O:** 14 d with 12.5 µg ml^{-1} Sm*aldh2* dsRNA (n = 2). The number of couples (**A**, **F**, **K**) and the attachment of couples (**B**, **G**, **L**), motility score (**C**, **H**, **M**), and determined egg numbers for normal (**D**, **I**, **N**) and abnormal eggs (**E**, **J**, **O**) were determined regularly every 3 d. Each point represents a measurement (averaged for motility score) of one experiment with 10 couples each. Columns represent means with StEM. Statistical analysis was performed as two-tailed t-test (treatment vs control), p < 0.05 (*).
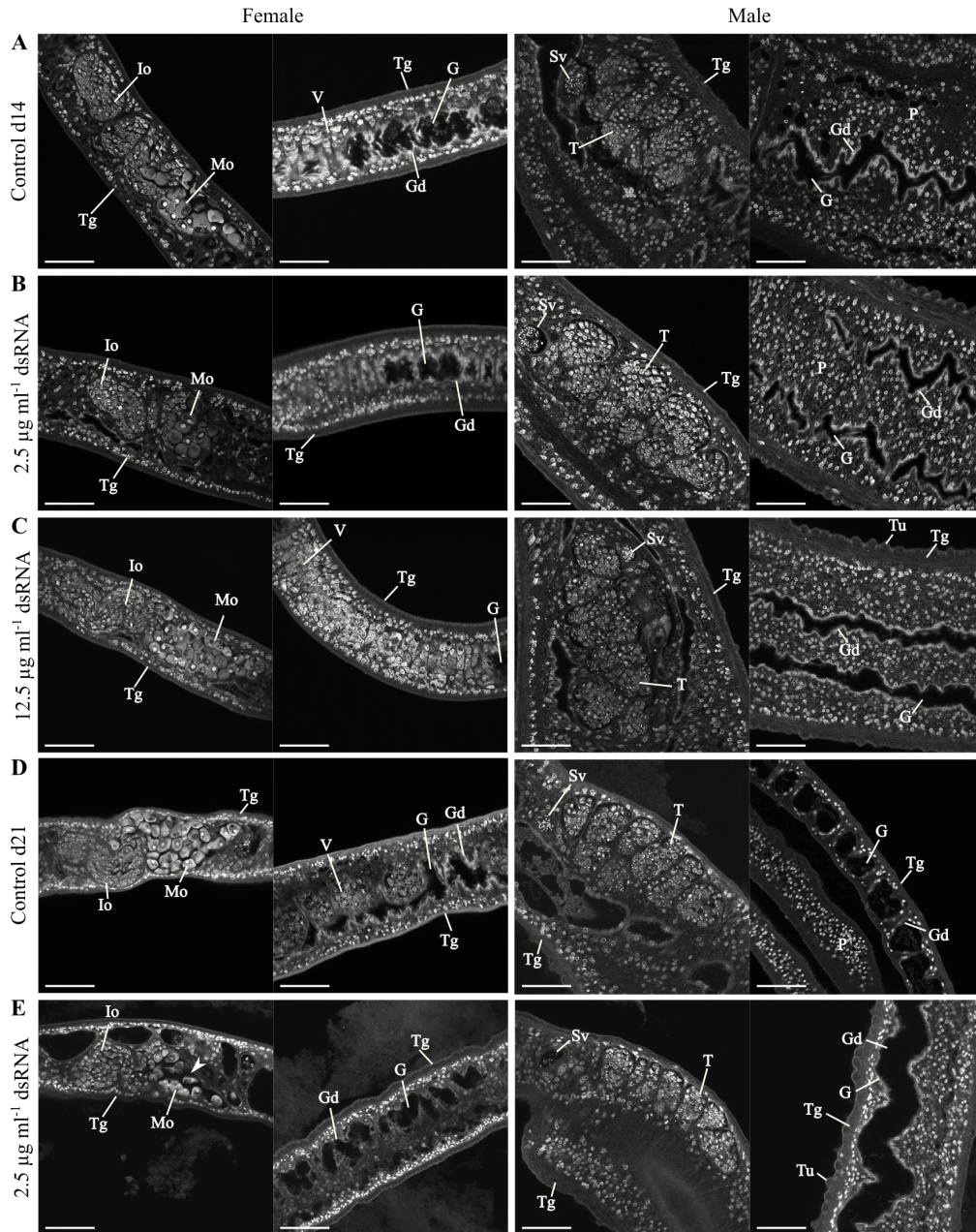
Figure 4.52: Influence of Sm*aldh2* knock down on the morphology of adult *S. mansoni* couples

Couples were treated 2.5 µg ml^{-1} Sm*aldh2* dsRNA for **B:** 14 d and **E:** 21 d. **C:** treatment with 12.5 µg ml^{-1} Sm*aldh2* dsRNA for 14 d. Controls were treated with DEPC-water for **A:** 14 d and **D:** 21 d. The part of the ovary that contains mature oocytes appeared less tightly (marked by an arrowhead). G = gut, Gd = gastrodermis, Io = part of the ovary containing immature oocytes, Mo = part of the ovary containing mature oocytes, P = parenchyma, Sv = seminal vesicle, T = testis, Tg = tegument, Tu = tubercle, V = vitelline cell. Scale bars represent 50 µm.
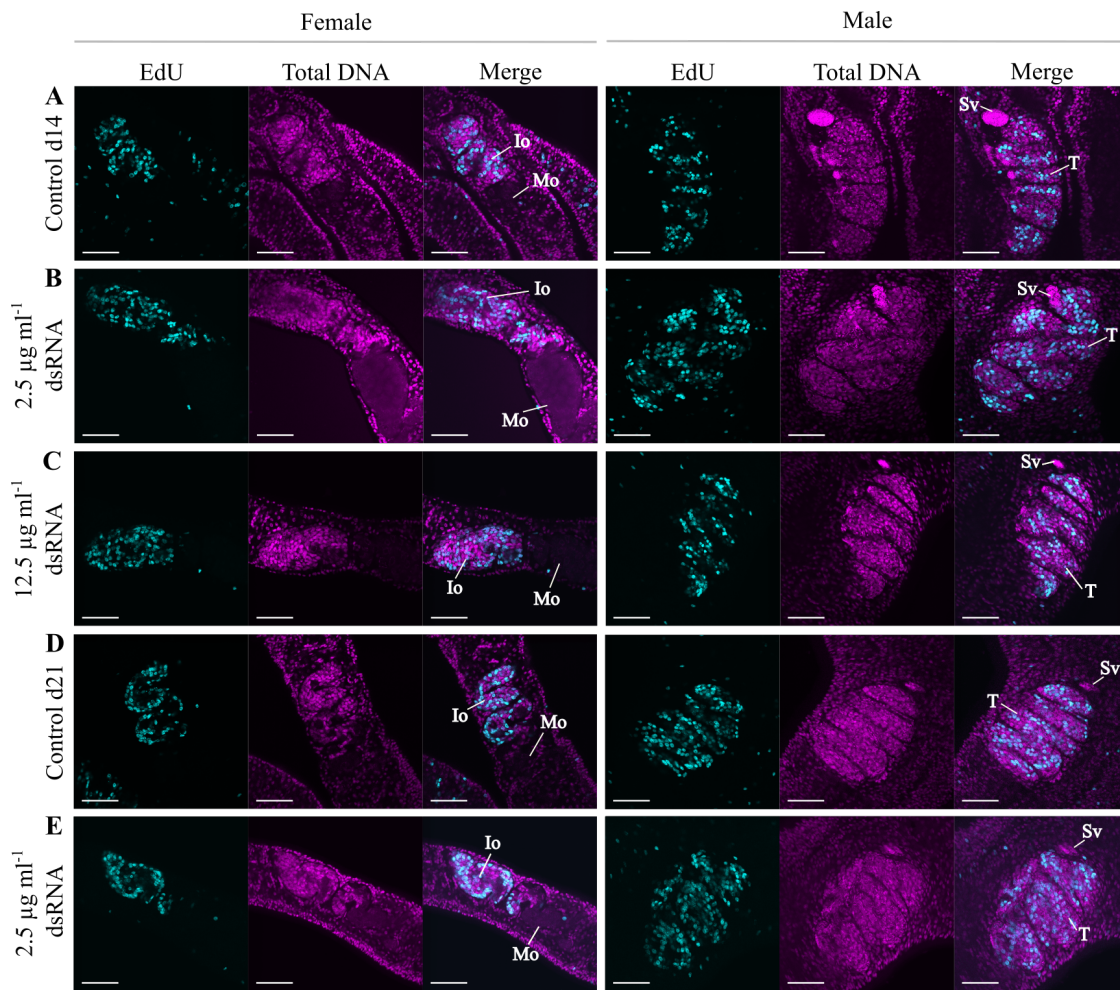
Figure 4.53: Influence of Sm*aldh2* knock down on proliferation in adult *S. mansoni* couples
Couples were treated with 2.5 µg ml^{-1} Sm*aldh2* dsRNA for **B:** 14 d and **E:** 21 d. **C:** treatment of couples with 12.5 µg ml^{-1} Sm*aldh2* dsRNA for 14 d. Controls were treated with DEPC-water for **A:** 14 d and **D:** 21 d. EdU-positive cells are shown in cyan and the total DNA in magenta. Io = part of the ovary containing immature oocytes, Mo = part of the ovary containing mature oocytes, Sv = seminal vesicle, T = testis. Scale bars represent 50 µm.

4.7.3 Simultaneous knock down of Sm*aldh1* and Sm*aldh2* had no clear effects on *S. mansoni* physiology, morphology, and stem cells

Since the knock down of Sm*aldh1* had no effect on worms, while Sm*aldh2* revealed an effect only on ovarian structures after 21 d of RNAi-mediated knock down, attempts were

made to target both Sm*aldh*s simultaneously to analyze possible synergistic knock down effects. Therefore, 2.5 µg ml^{-1} of Sm*aldh1* and Sm*aldh2* dsRNA were added to the worm culture for 14 and 21 d. Additionally, a higher concentration of dsRNA (12.5 µg ml^{-1}) was applied in a pilot experiment to possibly achieve better effects.

To verify the knock down of Sm*aldh1* and Sm*aldh2*, and to analyze further genes possibly involved in oxidative stress response, qRT-PCRs were performed. Expression levels were significantly decreased after 14 d in females and males to 8 % and 4 % for Sm*aldh1* (both p < 0.001) and 22 % (p < 0.01) and 31 % (p < 0.001) for Sm*aldh2* in females and males, respectively (**Figure 4.54 A**). Gene expression was not altered for Sm*ar*, Sm*gpx*, and Sm*sod* in both genders (**Figure 4.54 A** and **B**). In females, expression of Sm*sodex* was increased by 59 %, while the expression in males was not altered. As before, knock down of Sm*aldh1* was significant (p < 0.001). Sm*aldh1* gene expression was significantly downregulated to 5 % in females and 4 % in males, whereas Sm*aldh2* gene expression was significantly reduced to 41 % and 37 % in females and males, respectively, after 21 d (**Figure 4.54 C**). Gene expression of Sm*ar*, Sm*gpx*, and Sm*sod* was not impacted, but Sm*sodex* was upregulated in males (by 54 %) but not in females (**Figure 4.54 C** and **D**).

The number of couples and the attachment rate were significantly higher on day 3, while they did not change during the rest of the 14 d observation period (**Figure 4.55 A** and **B**). The number of couples and the attachment capacity remained comparable to those of the controls, decreasing towards the end of the experimental period (**Figure 4.55 F** and **G**). The motility of the worms remained normal throughout both observation periods (**Figure 4.55 C** and **H**), and decreased slightly after 21 d. The determined number of normal-shaped eggs was comparable to the control groups at day 3 but increased significantly (p < 0.05) by ∼ 56 % and ∼ 87 % in the treatment groups at day 6 and day 9 throughout the 14 d treatment regime (**Figure 4.55 D**), while the egg numbers in the longer treatment groups were slightly increased but not significant (**Figure 4.55 I**). Throughout the 14 d observation period, the number of abnormal formed eggs was significantly increased ∼ 2.2-fold and ∼ 2.1-fold at day 3 and day 6, respectively (**Figure 4.55 E**). The numbers of normal-shaped eggs were comparable with the controls throughout the 21 d period (**Figure 4.55 J**). In the treatment groups, higher levels of abnormally shaped eggs were determined as compared to the control groups throughout the 21 d observation period.

To further investigate whether a higher dsRNA dose would lead to more evident

effects on the worms, 12.5 µg ml^{-1} dsRNA of Sm*aldh1* and Sm*aldh2* was applied for 14 d (**Figure 4.55 C**). As noticed before, the number of couples or the attachment of couples remained comparable to the controls (**Figure 4.55 K** and **L**). In addition, worm motility was comparable to those of the control groups during the observation period but increased slightly in the treatment groups at day 12 before decreasing toward day 14 (**Figure 4.55 M**). The number of normal eggs was 62 % higher compared to the control at day 3, but the values converged again at day 6 (**Figure 4.55 N**). The number of abnormally formed eggs was highest at day 3 ($\sim$ 50 % higher than in the control group) but declined with time (**Figure 4.55 O**).

For examination of the internal worm structures, worms were fixed and stained with carmine for CLSM. Analysis of the worms treated with 2.5 µg ml^{-1} Sm*aldh1* and Sm*aldh2* dsRNA displayed no morphological changes in the gonadal structures nor in the remaining body parts at the observed time points (14 and 21 d, **Figure 4.56 A - E**).

Again, an analysis of proliferating cells was carried out using EdU assays. EdU-positive cells were detected after 14 and 21 d of double treatment with 2.5 µg ml^{-1} Sm*aldh1* and Sm*aldh2* dsRNA, comparable to the appearance of signals in the control groups (**Figure 4.57 A - E**).
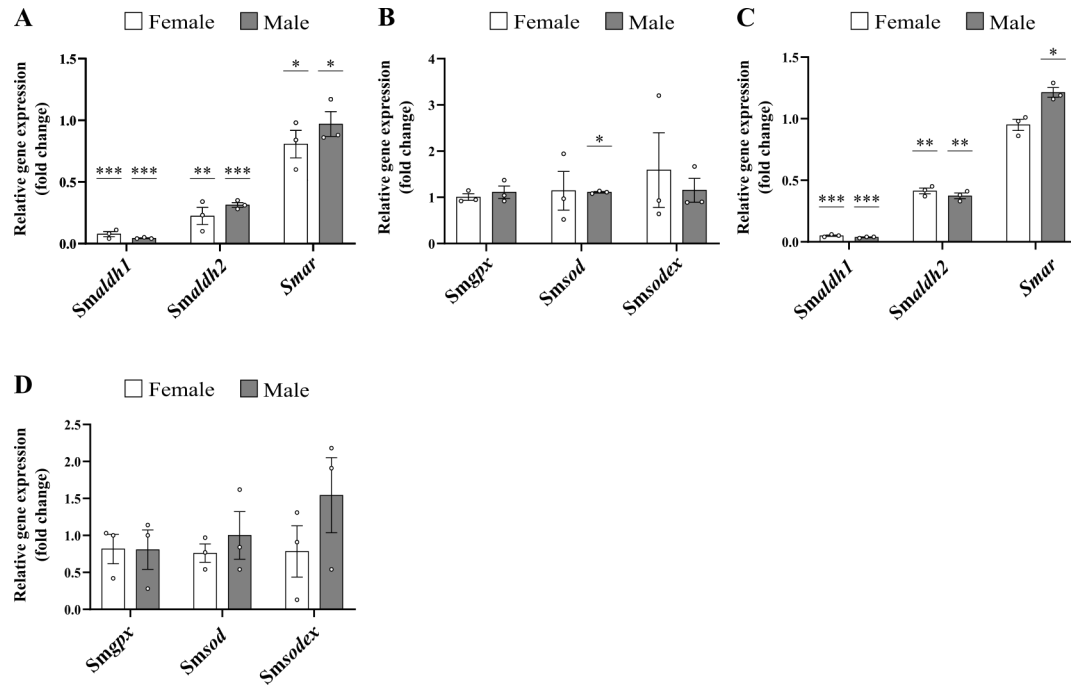
Figure 4.54: qRT-PCR analysis of oxidative stress response gene expression after simultaneous knock down of Sm*aldh1* and Sm*aldh2* in adult *S. mansoni* couples

Treatment durations were **A**, **B:** 14 d ($2.5\,\mu g\,ml^{-1}$ dsRNA, n = 3) and **C**, **D:** 21 d ($2.5\,\mu g\,ml^{-1}$ dsRNA, n = 3). Relative gene expression was determined for Sm*aldh1*, Sm*aldh2*, Sm*ar* (**A**, **C**), Sm*gpx*, Sm*sod*, and Sm*sodex* (**B**, **D**) after double knock down of Sm*aldh1* and Sm*aldh2*. Each data point represents one qRT-PCR analysis of one independent knock down experiment with 10 couples. Columns represent means with StEM. Statistical analysis (two-tailed t-test) was performed using treatment vs control (not shown), $p < 0.05$ (*), $p < 0.01$ (**), $p < 0.001$ (***).
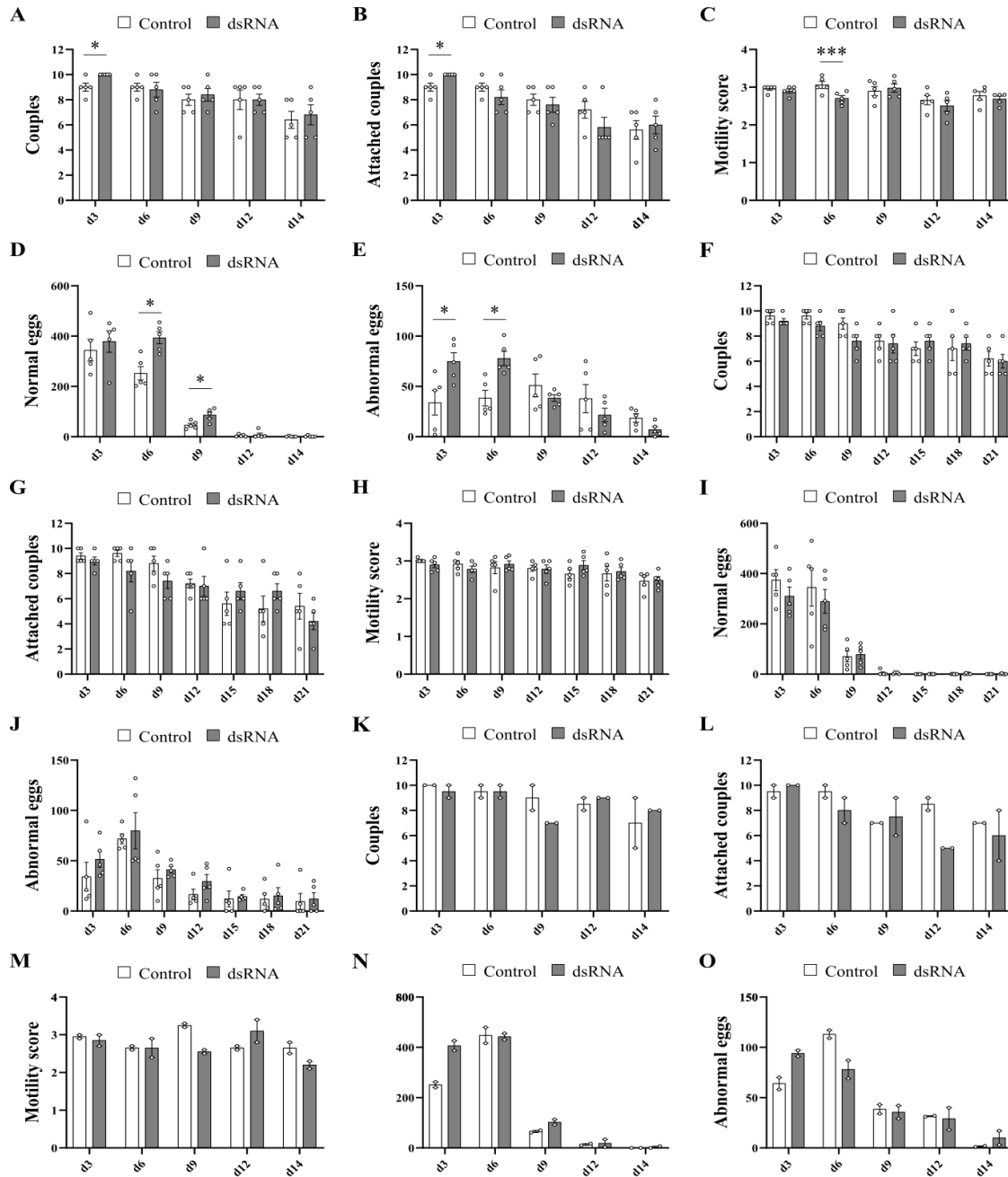
Figure 4.55: Screening of physiological parameters following double knock down of Sm*aldh1* and Sm*aldh2*

Assessed numbers of couples (**A**, **F**, **K**), attachment of couples (**B**, **G**, **L**), motility score (**C**, **H**, **M**), and egg count for normal (**D**, **I**, **N**) and abnormal eggs (**E**, **J**, **O**) while knock down of Sm*aldh1* and Sm*aldh2* with $2.5\,\mu g\,ml^{-1}$ dsRNA each for **A** - **E:** $14\,d$, n = 5, and **F** - **J:** $21\,d$, n = 5. **K** - **O:** administration of $12.5\,\mu g\,ml^{-1}$ Sm*aldh1* and Sm*aldh2* dsRNA each for $14\,d$, n = 2. Each point represents a measurement (averaged for motility score) of one experiment with 10 couples each. Columns represent means with StEM. Statistical analysis was performed as two-tailed t-test (treatment vs control), $p < 0.05$ (*), $p < 0.001$ (***).
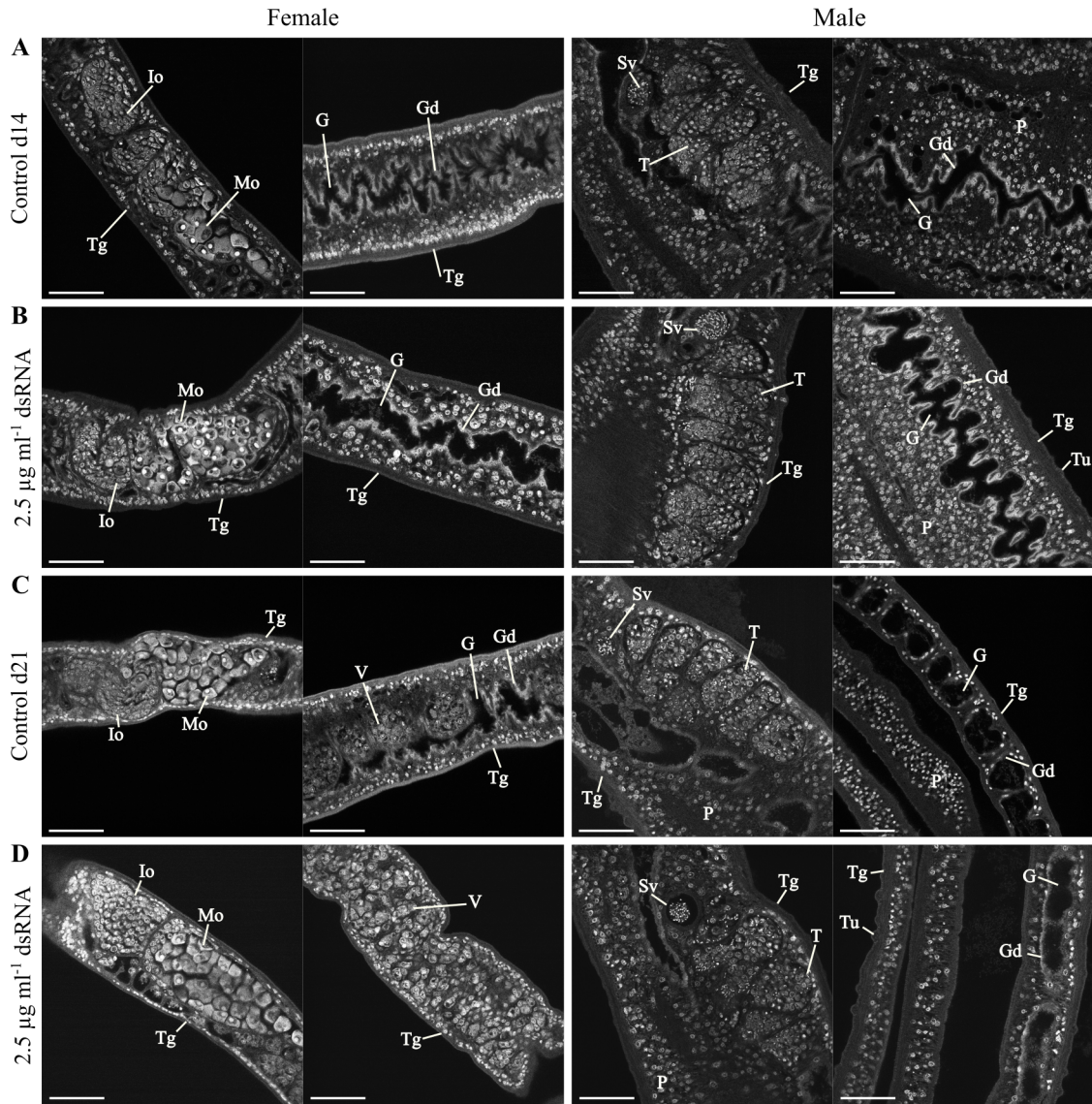
Figure 4.56: Influence of double knock down of Sm*aldh1* and Sm*aldh2* on the morphology of adult *S. mansoni* couples

Couples were treated with 2.5 µg ml^{-1} Sm*aldh1* and Sm*aldh2* dsRNA each for **B:** 14 d and **D:** 21 d. The controls were treated with DEPC-water for **A:** 14 d and **C:** 21 d. Worm couples were separated before staining and microscopy. Worms treated with both dsRNAs displayed no morphological changes when compared to the controls. G = gut, Gd = gastrodermis, Io = part of the ovary containing immature oocyte, Mo = part of the ovary containing mature oocytes, P = parenchyma, Sv = seminal vesicle, T = testis, Tg = tegument, Tu = tubercle. Scale bars represent 50 µm.
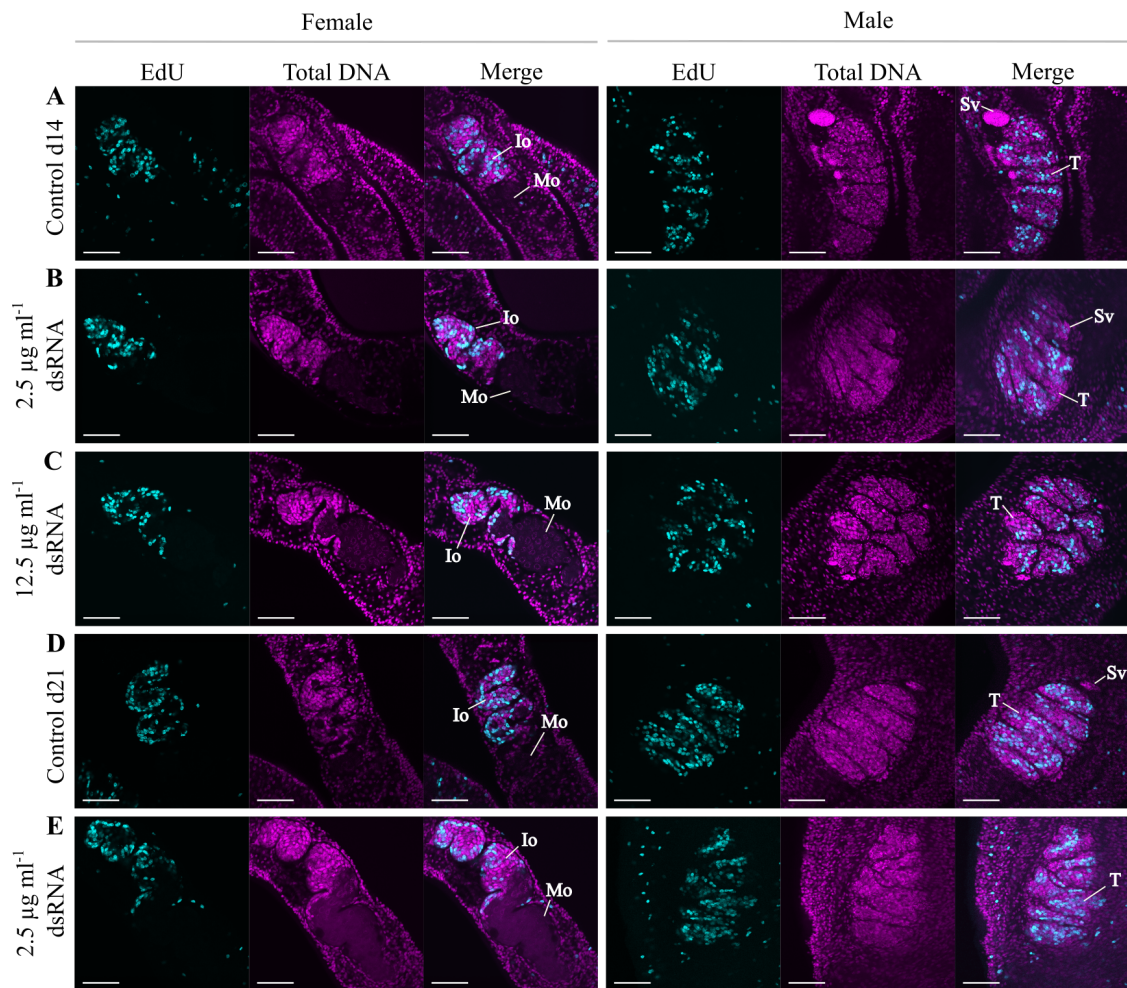
Figure 4.57: Influence of double knock down of Sm*aldh1* and Sm*aldh2* on proliferation in adult *S. mansoni* couples

S. mansoni couples were treated with 2.5 µg ml^{-1} Sm*aldh1* and Sm*aldh2* dsRNA each for **B:** 14 d and **E:** 21 d. **C:** treatment of worms with 12.5 µg ml^{-1} dsRNA (Sm*aldh1* and Sm*aldh2*) for 14 d. Controls were treated with DEPC-water for **A:** 14 d and **D:** 21 d. EdU was added 24 h before fixation and separation of the worms. EdU-positive cells are shown in cyan and the total DNA in magenta. Comparison of treated worms showed no difference in signals when compared to the controls. Io = part of the ovary containing immature oocyte, Mo = part of the ovary containing mature oocytes, T = testis, Sv = seminal vesicle. Scale bars represent 50 µm.

4.7.4 Knock down of Sm*abl1* altered oocyte maturation

SmAbl1 and SmAbl2 were previously classified as Abl kinases (Beckmann *et al.*, 2011). Former analyses of Sm*abl1* and Sm*abl2* revealed their transcript localization in the ovary, ootype, vitelloduct, and oviduct of female worms, and in the testes of males,

while weak signals were also detected in the vitellarium, the gastrodermis, and in some parenchymal cells of both genders (Beckmann and Grevelding, 2010). Analyses whether knocking down Sm*abl1* influences physiology, morphology or proliferation of cells were performed with worms treated regularly with $2.5\,\mu g\,ml^{-1}$ and $12.5\,\mu g\,ml^{-1}$ Sm*abl1* dsRNA for 14 and 21 d.

For Sm*abl1*, gene expression was determined in bsF/M and ssF/M *S. mansoni*. Analysis of qRT-PCR results showed that transcript abundance was slightly higher in bsF than in bsM. However, when the worms had no pairing experience, significant differences were found. Transcript levels were lowest in ssF, while they were increased about 3-fold in ssM, while gene expression was significantly higher in bsF than in ssF (**Figure 4.58**).
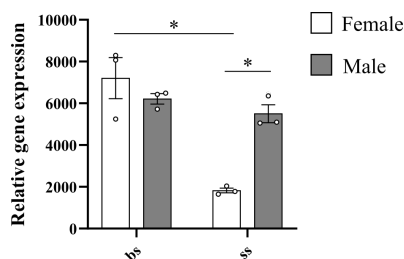
Figure 4.58: Analysis of the transcript profile of Sm*abl1* in adult *S. mansoni*
Results of qRT-PCR analyses to determine the relative gene expression levels of Sm*abl1* in bsF/M and ssF/M, respectively. Each point represents one experiment with 10 worms each, n = 3. Columns represent means with StEM. Statistical analysis was performed as two-tailed t-test, $p < 0.05$ (*).

The knock down efficiencies were determined for all applied conditions. Sm*abl1* was reduced to 79 % in females and significantly reduced to 61 % in males after 14 d (**Figure 4.59 A**). After 21 d, Sm*abl1* was further reduced to 56 % in females but only to 78 % in males (**Figure 4.59 B**). After 14 d, transcript abundance of Sm*abl1* was more efficiently reduced to 45 % in females and 34 % in males when $12.5\,\mu g\,ml^{-1}$ Sm*abl1* dsRNA was used (**Figure 4.59 F**). In addition to Sm*abl1*, transcript levels of Sm*abl2* and Sm*tk6* were determined. Sm*abl2* gene transcripts were not regulated in both genders after 14 and 21 d of Sm*abl1* dsRNA treatment, while Sm*tk6* transcripts were slightly downregulated by 26 % in males but were not affected in females after 14 d (**Figure 4.59 A** and **B**). In contrast, transcripts of Sm*tk6* were downregulated in females by one third, whereas they were upregulated by 2.1-fold in males after 21 d (**Figure 4.59 B**). With

higher Sm*abl1* dsRNA concentrations, Sm*abl2* was downregulated to 52 % in females, while transcript abundance did not change in males (**Figure 4.59 F**). In summary, the knock down became more efficient with increasing time and dsRNA concentration.
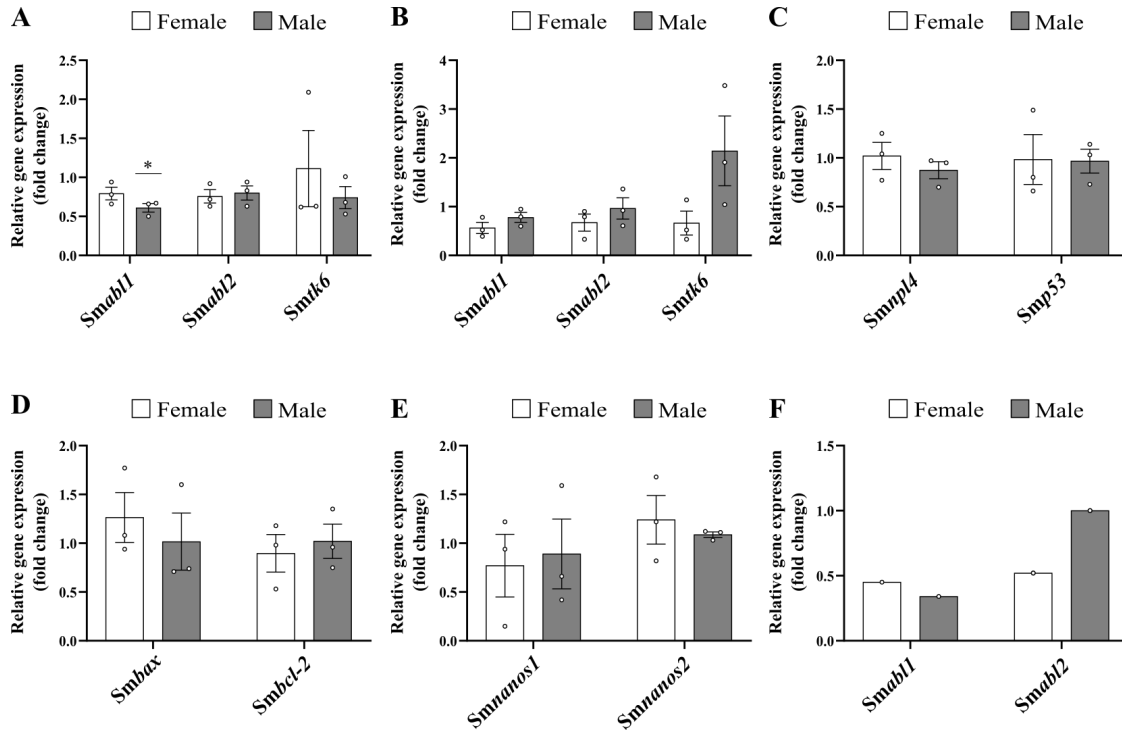
Figure 4.59: qRT-PCR analyses of selected genes after knock down of Sm*abl1* in adult
***S. mansoni* couples**
Relative gene expression was determined after knock down of Sm*abl1* using 2.5 µg ml^{-1} Sm*abl1* dsRNA for **A:** 14 d, n = 3, and **B** - **E:** 21 d, n = 3. **F:** determination of Sm*abl1* and Sm*abl2* transcript levels using 12.5 µg ml^{-1} Sm*abl1* dsRNA after 14 d, n = 1. Next to Sm*abl1*, Sm*abl2*, and Sm*tk6* transcript levels (**A**, **B**), transcript abundance of cell cycle-associated genes Sm*npl4* and Sm*p53* (**C**), apoptosis-related genes Sm*bax* and Sm*bcl-2* (**D**), and stem cell-associated genes Sm*nanos1* and Sm*nanos2* (**E**) were analyzed. Each data point represents one qRT-PCR analysis of one independent knock down experiment with 10 couples. Columns represent means with StEM. Statistical analysis (two-tailed t-test) was performed using treatment vs control (not shown), $p < 0.05$ (*).

Worm physiology was examined regularly during treatment periods (**Figure 4.60**). The number of paired worms did not change significantly in both observation periods compared to the control groups, except during the shorter experimental period at day 12 (**Figure 4.60 A**). The number of couples decreased in both treatment groups with time (**Figure 4.60 A** and **F**). The number of attached couples did not differ significantly

during the 14 d treatment schedule (**Figure 4.60 B**). However, the number was significantly lower at day 9 and higher at day 12 compared to the controls during the longer observation period (**Figure 4.60 G**). Both parameters decreased towards the ends of the experiments. Neither 14 nor 21 d of knock down induced changes in motility, and the worms showed normal movements (**Figure 4.60 C** and **H**). Analysis of egg counts (normal- and abnormal-shaped) revealed no significant changes compared to the control groups. Comparison of the normally shaped egg numbers of both observation periods displayed higher egg numbers in the treatment groups at day 3 and day 6 during the shorter experimental set ups than in the longer ones (**Figure 4.60 D** and **I**). The number of abnormally formed eggs peaked in the treatment groups and controls at both treatment durations at day 6, but the treatment groups never differed significantly from the control groups until the end of the experimental period (**Figure 4.60 E** and **J**).

Application of a 12.5 µg ml^{-1} Sm*abl1* dsRNA (**Figure 4.60 K** - **O**) resulted in values comparable to those of worms treated with 2.5 µg ml^{-1} Sm*abl1* dsRNA for 14 d (**Figure 4.60 A** - **E**). The number of paired worms decreased in the treatment and control groups at day 9 and remained at this level until the end of the experiment (**Figure 4.60 K**), whereas the numbers of attached couples was always lower compared to the controls from day 6 onward (**Figure 4.60 L**). Worm movements decreased slightly toward the end at day 14 (**Figure 4.60 M**). Comparison of normally formed egg numbers determined at day 3 showed a doubling of eggs laid in the treatment groups (**Figure 4.60 N**), however, this difference was no longer observed at later time points. The number of abnormal eggs was highest at day 3 but declined during the rest of the observation period (**Figure 4.60 O**). In total, no unusual changes in worm physiology were noted during the observation periods, indicating that Sm*abl1* did not affect these parameters.

In a next step, possible changes of internal worm structures were analyzed by CLSM after knock down of Sm*abl1* with 2.5 µg ml^{-1} and 12.5 µg ml^{-1} Sm*abl1* dsRNA for 14 d (**Figure 4.61 A** - **C**) and 2.5 µg ml^{-1} dsRNA for 21 d (**Figure 4.61 D** and **E**). Comparison of treatment groups with control groups showed no changes in the guts, vitellaria, or gonads in females or males after application of 2.5 µg ml^{-1} dsRNA for 14 d (**Figure 4.61 A** and **B**). This outcome changed when the knock down duration was prolonged to 21 d. At this time, in some females, maturation of the oocytes appeared to be impaired because the part that normally harbors mature oocytes was full of immature oocytes (**Figure 4.61 E**). In contrast, no changes were observed in the testis of males. Application of 12.5 µg ml^{-1} Sm*abl1* dsRNA showed similar effects in some female ovaries as observed before. The immature oocytes were distributed throughout the ovary, and the number of

immature oocytes appeared to be higher than in the control groups (**Figure 4.61 A** and **C**). As previously observed, no morphological changes were detected in the males.

To analyze whether knock down of Sm*abl1* affects proliferating cells in paired worms, EdU assays were performed. Pairs were treated with 2.5 µg ml^{-1} and 12.5 µg ml^{-1} Sm*abl1* dsRNA for 14 and 21 d, respectively. No decrease or increase of signals in the gonads or the rest of the body was observed at either the lower or higher Sm*abl1* dsRNA concentration (**Figure 4.62 A - E**). Knocking down Sm*abl1* had no effect on proliferating cells.
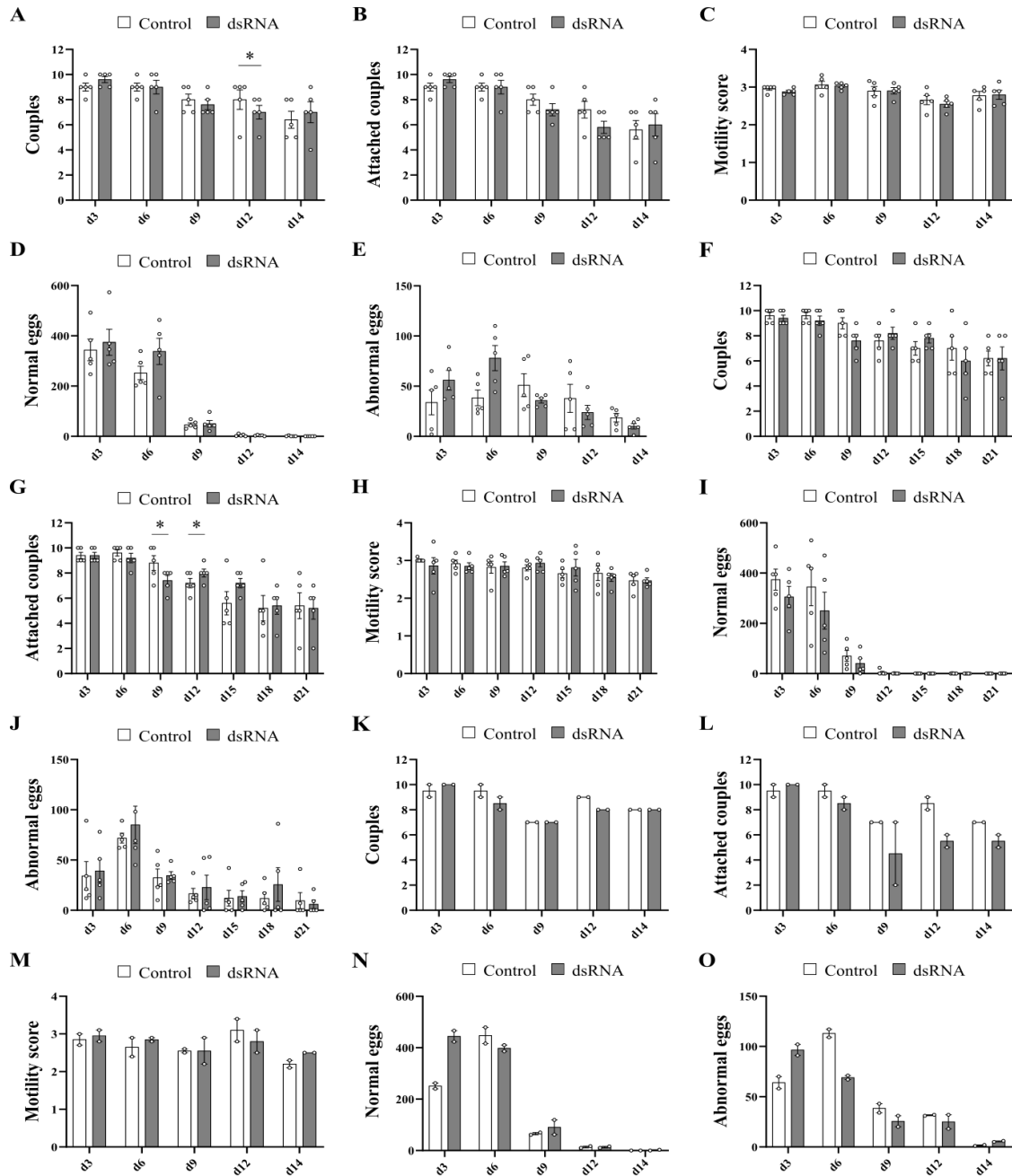
Figure 4.60: Screening of physiological parameters following Sm*abl1* knock down
Assessed numbers of couples (**A**, **F**, **K**), attachment of couples (**B**, **G**, **L**), motility score (**C**, **H**, **M**), and egg count for normal (**D**, **I**, **N**) and abnormal eggs (**E**, **J**, **O**) during Sm*abl1* dsRNA $(2.5\,\mu g\,ml^{-1})$ treatment for **A** - **E:** 14 d, n = 5, and **F** - **J:** 21 d, n = 5. Parameters were also scored during (**K** - **O:**) application of $12.5\,\mu g\,ml^{-1}$ Sm*abl1* dsRNA for 14 d, n = 2. Each point represents a measurement (averaged for motility score) of one experiment with 10 couples each. Columns represent means with StEM. Statistical analysis was performed as two-tailed t-test (treatment vs control), $p < 0.05$ (*).
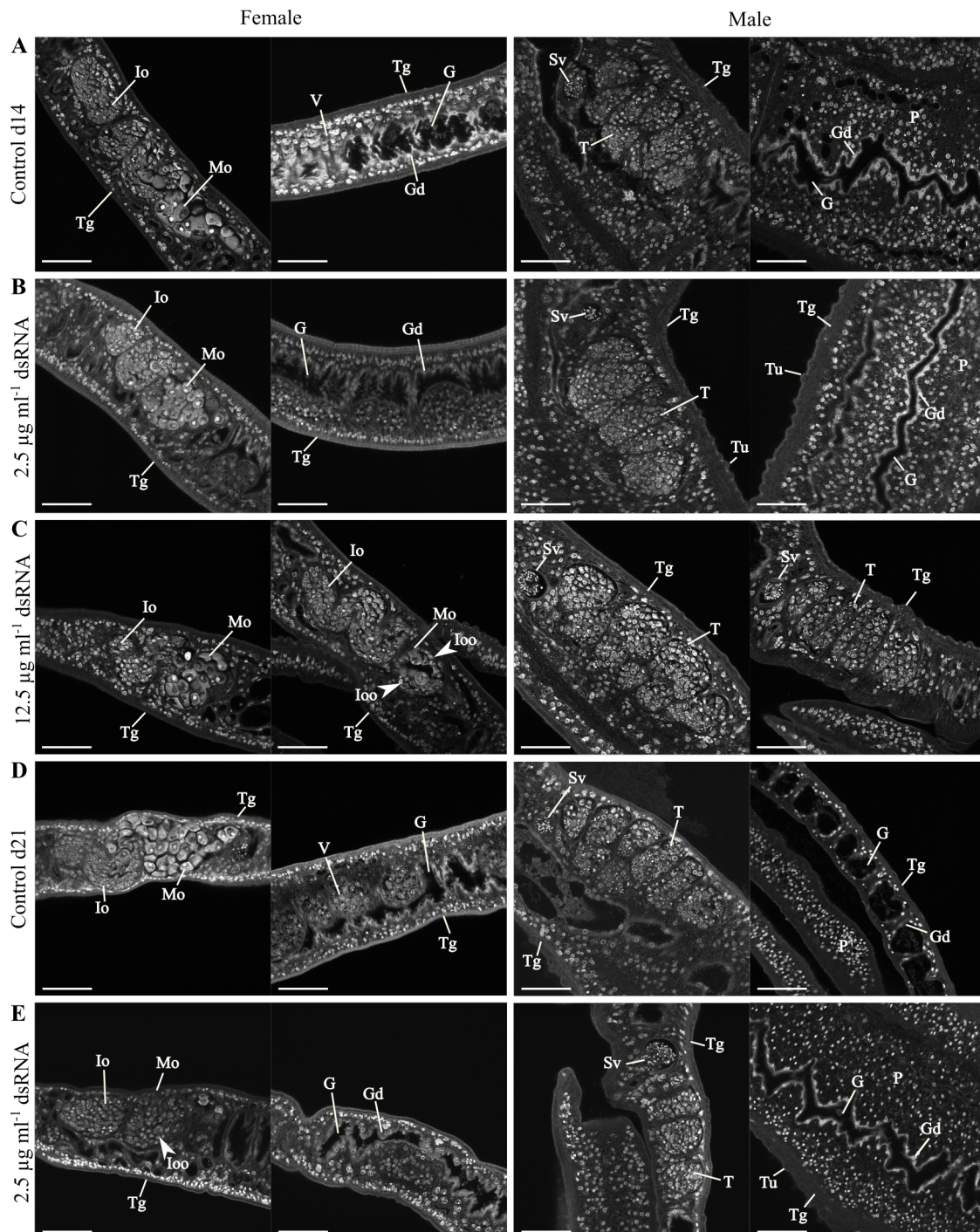
Figure 4.61: Influence of Sm*abl1* knock down on the morphology of adult *S. mansoni* couples

Couples were treated with $2.5\,\mu g\,ml^{-1}$ Sm*abl1* dsRNA for **B:** 14 d (**B**) and **E:** 21 d. **C:** $12.5\,\mu g\,ml^{-1}$ Sm*abl1* dsRNA were applied for 14 d. DEPC-water-treated worms as controls after **A:** 14 d and **D:** 21 d. Couples were separated for staining and microscopy. Over-representation of immature oocytes is indicated by arrowheads. G = gut, Gd = gastrodermis, Io = part of the ovary containing immature oocytes, Ioo = immature oocyte, Mo = part of the ovary containing mature oocytes, P = parenchyma, Sv = seminal vesicle, T = testis, Tg = tegument, Tu = tubercle, V = vitelline cell. Scale bars represent 50 µm.
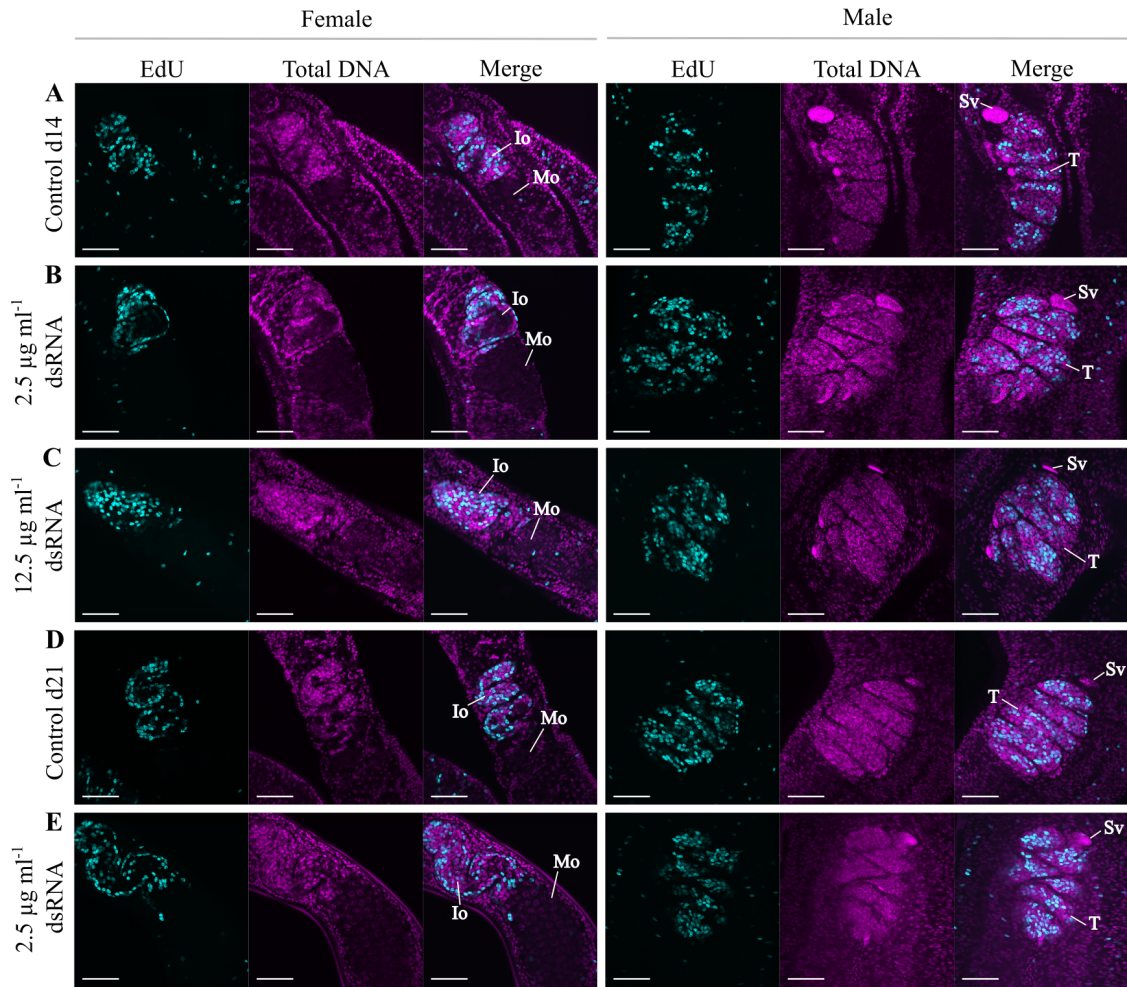
Figure 4.62: Influence of Sm*abl1* knock down on proliferation in *S. mansoni* couples
Worm couples were treated with $2.5\,\mu g\,ml^{-1}$ Sm*abl1* dsRNA for **B:** 14 d and **E:** 21 d and with
C: $12.5\,\mu g\,ml^{-1}$ Sm*abl1* dsRNA for 14 d. **A**, **D:** controls treated with DEPC-water after 14 d (**A**)
and 21 d (**D**). EdU was added 24 h before fixation. EdU-positive cells are shown in cyan and the
total DNA in magenta. Io = part of the ovary containing immature oocyte, Mo = part of the ovary
containing mature oocytes, T = testis, Sv = seminal vesicle. Scale bars represent 50 µm.

4.7.5 Knock down of Sm*abl2* revealed effects on the gonads

As for Sm*abl1*, Sm*abl2* transcripts were localized in the ovary, ootype, vitelloduct,
and oviduct of female worms, and in the testes of males with weak signals in the
vitellarium, the gastrodermis, and in some parenchymal cells of both genders (Beckmann
and Grevelding, 2010). To unravel potential functions of Sm*abl2* in paired worms, knock

down approaches with $2.5\,\mu g\,ml^{-1}$ and $12.5\,\mu g\,ml^{-1}$ dsRNA were performed for 14 and 21 d.

Relative gene expression analysis was also performed for Sm*abl2* using bs and ss females and males, respectively. Transcript abundance was slightly increased in bsF compared to bsM **Figure 4.63**. In contrast, gene expression was lowest in ssF, whereas ssM had comparable gene expression to bsF.
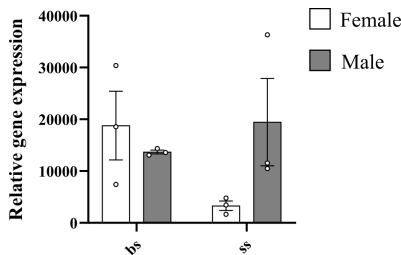
Figure 4.63: Analysis of the transcript profile of Sm*abl2* in adult *S. mansoni*
Relative gene expression of Sm*abl2* was determined by qRT-PCR in bs and ss females and males, respectively. Each point represents one experiment with 10 worms each, n = 3. Columns represent means with StEM. No statistical significance was found.

To determine the knock down efficiencies for Sm*abl2* after 14 and 21 d, qRT-PCR analyses were performed. After 14 d of $2.5\,\mu g\,ml^{-1}$ Sm*abl2* dsRNA application, gene expression of Sm*abl2* was reduced to 68 % in females and even further reduced to 29 % (p < 0.001) in males (**Figure 4.64 A**). In addition, Sm*abl1* was significantly upregulated only in females by 55 %, whereas Sm*tk6* gene expression was not affected in both genders. Gene expression of Sm*abl2* was significantly reduced in females by about two thirds and reduced by about one third in males after 21 d (**Figure 4.64 B**). In addition, transcripts of Sm*tk6* were reduced only in females by about one fourth after 21 d. The other analyzed genes (Sm*npl4*, Sm*p53*, Sm*bax*, Sm*bcl-2*, Sm*nanos1*, and Sm*nanos2*) showed no altered expression (**4.64 C - E**). At the higher dsRNA concentration ($12.5\,\mu g\,ml^{-1}$), gene expression of Sm*abl2* was reduced to 44 % in females and 90 % in males, while Sm*abl1* gene expression was reduced to 52 % and 72 % in females and males, respectively (**Figure 4.64 F**). In summary, knock down of Sm*abl2* was more efficient in male than female worms.
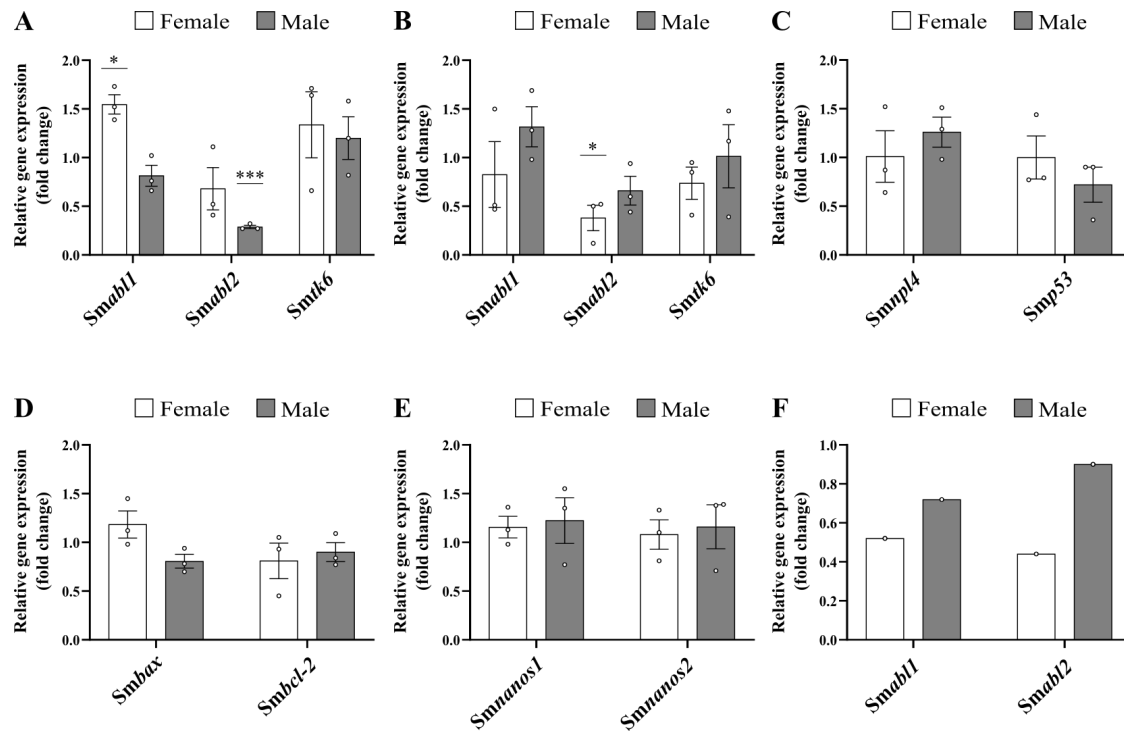
Figure 4.64: qRT-PCR analyses of gene expression after knock down of Sm*abl2* in adult *S. mansoni* couples

Worms were treated with Sm*abl2* dsRNA and relative gene expression determined for **A:** Sm*abl1*, Sm*abl2*, and Sm*tk6* after 14 d (2.5 µg ml^{-1} Sm*abl2* dsRNA, n = 3), **B - E:** Sm*abl1*, Sm*abl2*, and Sm*tk6* (**B**), cell cycle-associated genes Sm*npl4* and Sm*p53* (**C**), apoptosis-related genes Sm*bax* and Sm*bcl-2* (**D**), and stem cell-associated genes Sm*nanos1* and Sm*nanos2* (**E**) after 21 d (12.5 µg ml^{-1}, n = 3), and **F:** Sm*abl1* and Sm*abl2* after 14 d (2.5 µg ml^{-1} Sm*abl2* dsRNA, n = 1). Each data point represents one qRT-PCR analysis of one independent knock down experiment with 10 couples. Columns represent means with StEM. Statistical analysis (two-tailed t-test) was performed using treatment vs control (not shown), p < 0.05 (*), p < 0.001 (***).

Physiological parameters were monitored for both knock down periods (2.5 µg ml^{-1} dsRNA), revealing no significant changes in the number of couples compared to the control groups. The number of couples in the treatment groups was approximately 7 after 14 d and 21 d (**Figure 4.65 A** and **F**). The number of attached couples decreased towards the end of each observation period, with the lowest value after 21 d (**Figure 4.65 B** and **G**). Motility values of the worms did not differ from the controls throughout both observation periods and remained normal with a slight decrease toward the ends (**Figure 4.65 C** and **H**). The production of normal eggs showed no significant differences between treatment group and control during both treatment periods (**Figure 4.65 D** and **I**). Also the comparison of the numbers of abnormal-shaped eggs revealed no differences to the controls after 14 and 21 d (**Figure 4.65 E** and **J**).

Physiological parameters were also determined during the application of a higher concentration of dsRNA (12.5 µg ml^{-1}). During the experiment, the number of couples did not differ from the controls, while the ability to attach to the dishes seemed affected after day 14 (**Figure 4.65 K** and **L**). Worm motility remained normal in the treatment groups, while motility in the control worms varied slightly (**Figure 4.65 M**). In the treatment groups, an approximately 2-fold increase in normally formed eggs was observed on day 3, which was reduced at day 6, while the control groups laid approximately a third more eggs (**Figure 4.65 N**). The number of abnormal-formed eggs was continuously decreasing during the observation period, while the controls showed a peak at day 6 followed by a subsequent decrease (**Figure 4.65 O**). Overall, no remarkable changes in worm physiology were observed during the observation periods, which means that Sm*abl2* had no significant influence on these parameters.

To analyze possible effects on the morphology, treated worms were analyzed by CLSM. Worms treated with 2.5 µg ml^{-1} Sm*abl2* dsRNA showed no morphological changes after 14 d, female and male gonads, vitellarium, gut, and parenchyma were comparable to those of the control worms (**Figure 4.66 A** and **B**). Worms of the longer treatment duration (21 d) showed no differences in females compared with the controls, whereas the testes of males appeared to lose integrity, while the seminal vesicles remained filled with spermatozoa (**Figure 4.66 D** and **E**). When couples were treated with 12.5 µg ml^{-1} Sm*abl2* dsRNA, some female ovaries revealed cell-free spaces indicating a reduced number of mature oocytes (**Figure 4.66 C**).

Afterwards, possible effects on proliferating cells in paired worms were investigated. For each condition (14 d treatment, 2.5 µg ml^{-1} and 12.5 µg ml^{-1} dsRNA, and 21 d 12.5 µg ml^{-1} dsRNA), EdU assays were performed. Neither a reduction nor an increase in EdU-positive cells was observed in any of the experimental set ups compared to the controls (**Figure 4.67**). Therefore, knock down of Sm*abl2* did not appear to affect cell proliferation in paired *S. mansoni*.
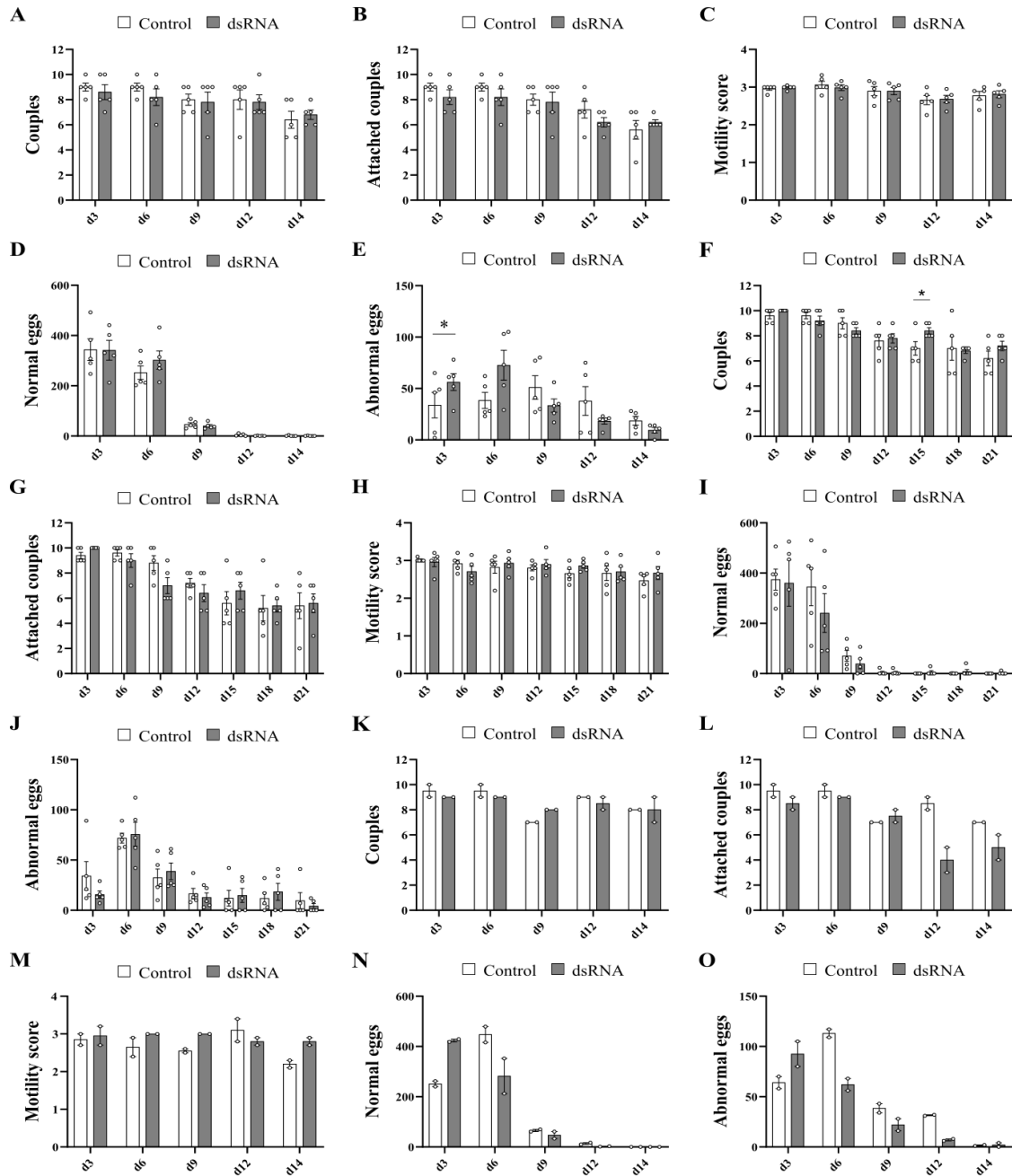
Figure 4.65: Screening of physiological parameters following Sm*abl2* knock down
Assessed number of couples (**A**, **F**, **K**), attachment of couples (**B**, **G**, **L**), motility score (**C**, **H**, **M**), number of normal eggs (**D**, **I**, **N**) and abnormal eggs (**E**, **J**, **O**) during Sm*abl2* dsRNA $(2.5\,\mu g\,ml^{-1})$ treatment for **A** - **E:** 14 d, n = 5, **F** - **J:** 21 d, n = 5. **K** - **O:** Sm*abl2* dsRNA treatment $(12.5\,\mu g\,ml^{-1})$ for 14 d, n = 2. Each point represents a measurement (averaged for motility score) of one experiment of 10 couples each. Coulumns represent means with StEM. Statistical analysis was performed as two-tailed t-test (treatment vs control), p < 0.05 (*).
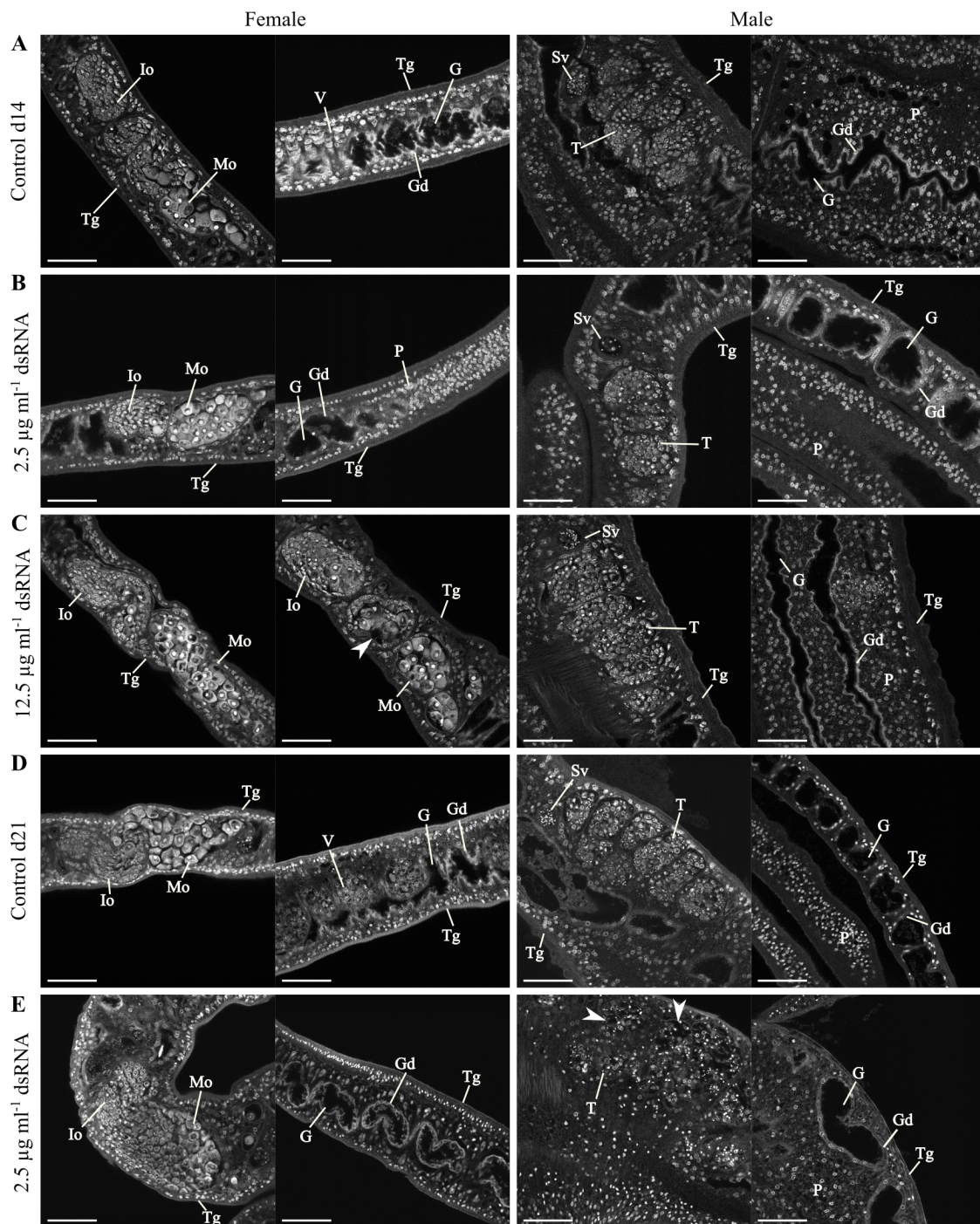
Figure 4.66: Influence of Sm*abl2* knock down on the morphology of adult *S. mansoni* couples

Worm couples were treated with either 2.5 µg ml^{-1} Sm*abl2* dsRNA for **B:** 14 d and **E:** 21 d, or **C:** 12.5 µg ml^{-1} Sm*abl2* dsRNA for 14 d. Controls were treated with DEPC-water for **A:** 14 d and **D:** 21 d before couples were separated for CLSM analysis. Cell-free spaces inside the ovary and testis are indicated by arrowheads. G = gut, Gd = gastrodermis, Io = part of the ovary containing immature oocytes, Mo = part of the ovary containing mature oocytes, P = parenchyma, Sv = seminal vesicle, T = testis, Tg = tegument, V = vitelline cell. Scale bars represent 50 µm.
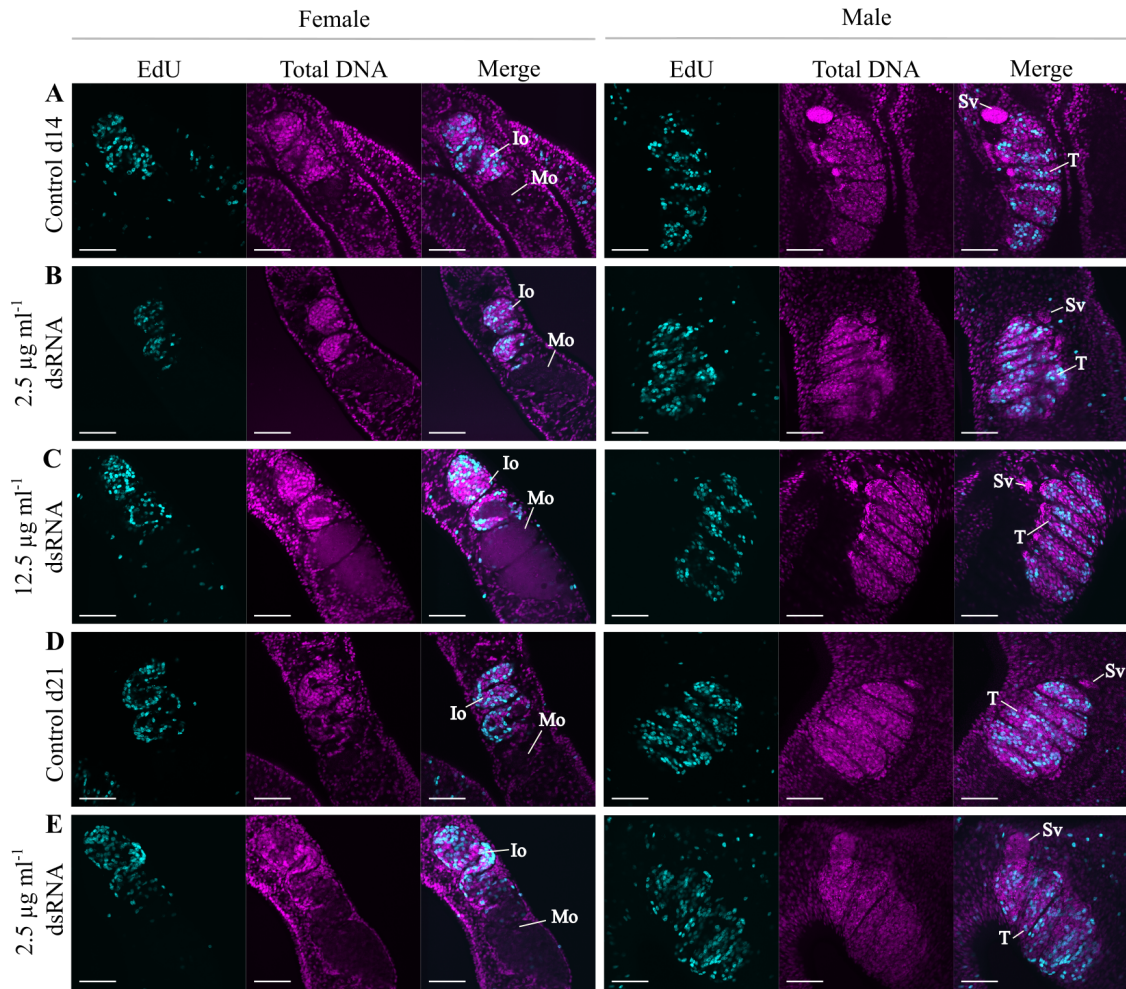
Figure 4.67: Influence of Sm*abl2* knock down on proliferation in adult *S. mansoni* couples
S. mansoni couples were treated with $2.5\,\mu g\,ml^{-1}$ Sm*abl2* dsRNA for **B:** 14 d and **E:** 21 d, and $12.5\,\mu g\,ml^{-1}$ Sm*abl2* dsRNA for **C:** 14 d. Controls were treated with DEPC-water for **A:** 14 d and **D:** 21 d. EdU was added 24 h before fixation. EdU-positive cells are shown in cyan and the total DNA in magenta. Signals in treated groups were similar to those in the controls. Io = part of the ovary containing immature oocyte, Mo = part of the ovary containing mature oocytes, T = testis, Sv = seminal vesicle. Scale bars represent 50 µm.

4.7.6 Simultaneous knock down of Sm*abl1* and Sm*abl2* impaired the integrity of gonads

As summarized in the previous sections (see sections 4.7.4 and 4.7.5), single knock downs of either Sm*abl1* or Sm*abl2* transcripts had slight effects on the gonadal structures of paired female and male worms. Therefore, possible additive effects were investigated

by knocking down both Sm*abl* kinases simultaneously with 2.5 µg ml^{-1} and 12.5 µg ml^{-1} dsRNA for periods of 14 and 21 d.

Analysis for knock down efficiencies was also conducted after the double knock down of Sm*abl1* and Sm*abl2*. After 14 d of 2.5 µg ml^{-1} dsRNA application, almost no reduction of Sm*abl1* was observed in females (95 %), while a moderate gene expression rate was observed in males (55 %, p < 0.05) (**Figure 4.68 A**). Downregulation of Sm*abl2* was more efficient in males than females (transcript levels of 63 % vs 34 %, respectively, p < 0.01). Expression of Sm*tk6* increased by 50 % in females and 45 % in males, respectively. A downregulation was observed for Sm*abl1* by one fourth and Sm*abl2* about one third in females, while Sm*tk6* was slightly downregulated to 60 % after 21 d (**Figure 4.68 B**). In males, expression rates of Sm*abl1* and Sm*abl2* were significantly downregulated to 70 % and 50 %, respectively, whereas Sm*tk6* transcript levels were upregulated about one third after 21 d. Cell cycle-associated genes Sm*npl4* and Sm*p53* and apoptosis-related genes Sm*bax* and Sm*bcl-2* were not affected in both genders (**Figure 4.68 C** and **D**). The stem cell marker Sm*nanos1* was slightly downregulated by about one third in females, while it was not influenced in males. Sm*nanos2* was not affected in both genders (**Figure 4.68 E**). In general, Sm*abl* kinase gene expression was downregulated more efficiently in males than in females.

As before, physiological parameters were examined regularly during both observation periods (**Figure 4.69**). Application of both dsRNAs had no effect on the rate of paired worms during the shorter experimental set up (14 d, 2.5 µg ml^{-1} dsRNA each) (**Figure 4.69 A**). The only significant change in the number of couples was observed during the longer treatment period at day 12 (**Figure 4.69 F**). The ability to attach to dishes did not vary significantly during both periods but decreased with time (**Figure 4.69 B** and **G**). Worm movements were evaluated as normal during both examination periods in the treatment and control groups (**Figure 4.69 C** and **H**). The longer the *in vitro* experiment lasted, the more likely was a slight reduction in movements. The number of normal eggs was higher in the treatment groups than in the control groups at day 3, but was not significantly different from the control groups at either time period (**Figure 4.69 D** and **I**). Analysis of the number of abnormally formed eggs showed a significant increase in the treatment groups (more than twice as high as in the controls) at day 3 during the 14 d knock down period (**Figure 4.69 E**), whereas the numbers did not significantly differ from the controls after 21 d dsRNA treatment (**Figure 4.69 J**). The number of abnormally formed eggs peaked in the treatment group at day 6 during

the longer treatment period, but was not significantly different from the control groups (**Figure 4.69 J**).

When more dsRNA ($12.5\,\mu g\,ml^{-1}$ each) was applied, the number of couples decreased with time in the treatment groups (**Figure 4.69 K**). The attachment rate was affected towards the end of the observation period (**Figure 4.69 L**). Worm movement was not affected in the treatment groups and remained normal (**Figure 4.69 M**), whereas the controls had reduced movements at day 14 (controls 2.2 vs treatment groups 2.9). The number of normally formed eggs was highest at day 3 and decreased gradually with time, while the numbers of normal eggs in the control groups peaked at day 6 (**Figure 4.69 N**). Similar patterns were observed for the abnormally shaped eggs (**Figure 4.69 O**). Altogether, no unusual changes in worm physiology were observed during the treatment periods. Knock down of Sm*abl1* and Sm*abl2* seemed to have no impact on these parameters.

After knocking down both Sm*abl* kinases, couples were separated and stained with carmine for CLSM analysis. Worms treated for 14 d showed no morphological changes compared to the control (**Figure 4.70 A** and **B**). After 21 d, effects were observed in the gonads of female and male worms, whereas the other tissues remained comparable to the controls. In some females, ovary integrity appeared to be disrupted, while oocyte maturation seemed to be impeded. Mature oocytes appeared reduced in size compared to those of the control groups (**Figure 4.70 C** and **D**). In some males, the integrity of the testes appeared to be disturbed, as evidenced by inseparable lobes and the appearance of cavities (**Figure 4.70 D**). Nevertheless, the seminal vesicles were still filled with spermatozoa.

Next, dsRNA-treated worms were used in an EdU assay to analyze cell proliferation. After 14 d of treatment with $2.5\,\mu g\,ml^{-1}$ and $12.5\,\mu g\,ml^{-1}$ Sm*abl1* and Sm*abl2* dsRNA, signals in female ovaries (immature oocytes) and in male's testes were observed comparable to those of the controls (**Figure 4.71 A - C**). Similar signal patterns were observed when treatment groups and control groups were compared after 21 d (**Figure 4.71 D** and **E**). Therefore, double knock down of Sm*abl1* and Sm*abl2* did not appear to affect proliferating cells in *S. mansoni*.
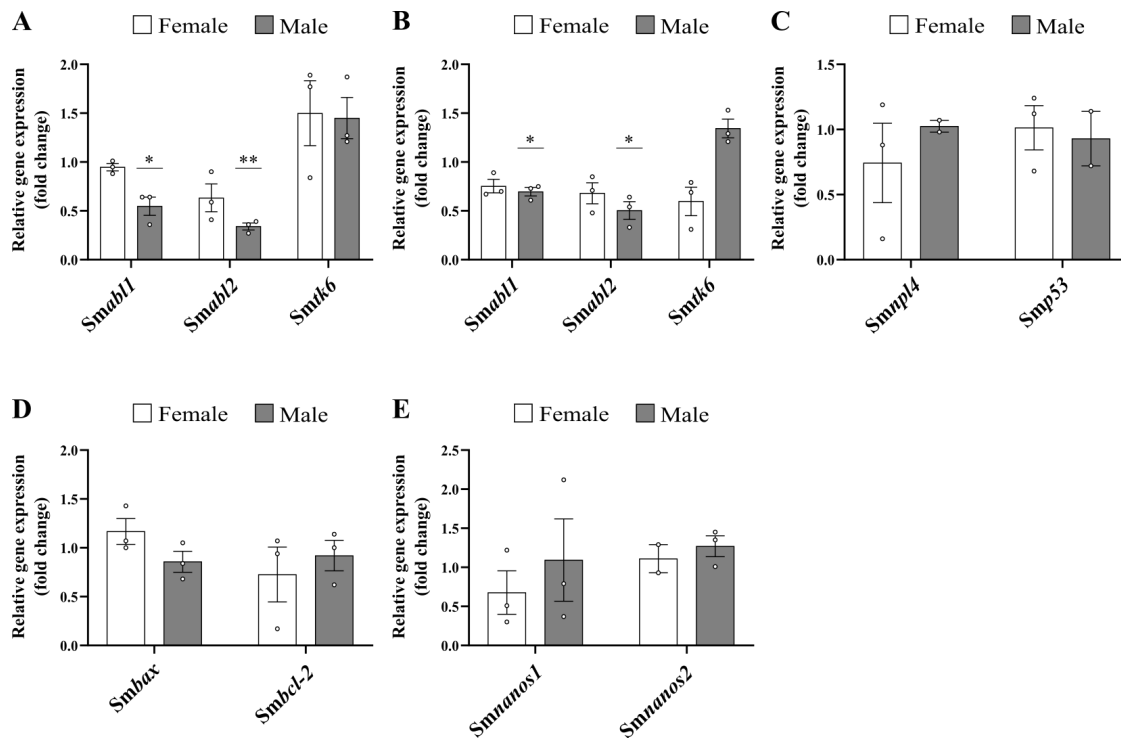
Figure 4.68: qRT-PCR analyses of selected genes after simultaneous knock down of Sm*abl1* and Sm*abl2* in adult *S. mansoni* couples

Relative gene expression was determined after knock down of Sm*abl1* and Sm*abl2* with 2.5 µg ml^{-1} dsRNA for **A:** Sm*abl1*, Sm*abl2*, and Sm*tk6* after 14 d, n = 3. The following gene transcript levels were determined after 21 d of RNAi (2.5 µg ml^{-1} dsRNA each, n = 3): **B:** Sm*abl1*, Sm*abl2*, and Sm*tk6*, **C:** cell cycle-associated genes Sm*npl4* and Sm*p53* (determined only 2 times in males), **D:** apoptosis-related genes Sm*bax* and Sm*bcl-2*, and **E:** stem cell-associated genes Sm*nanos1* and Sm*nanos2*. Each data point represents one qRT-PCR analysis of one independent knock down experiment with 10 couples. Columns represent means with StEM. Statistical analysis (two-tailed t-test) was performed using treatment vs control (not shown), p < 0.05 (*), p < 0.01 (**).
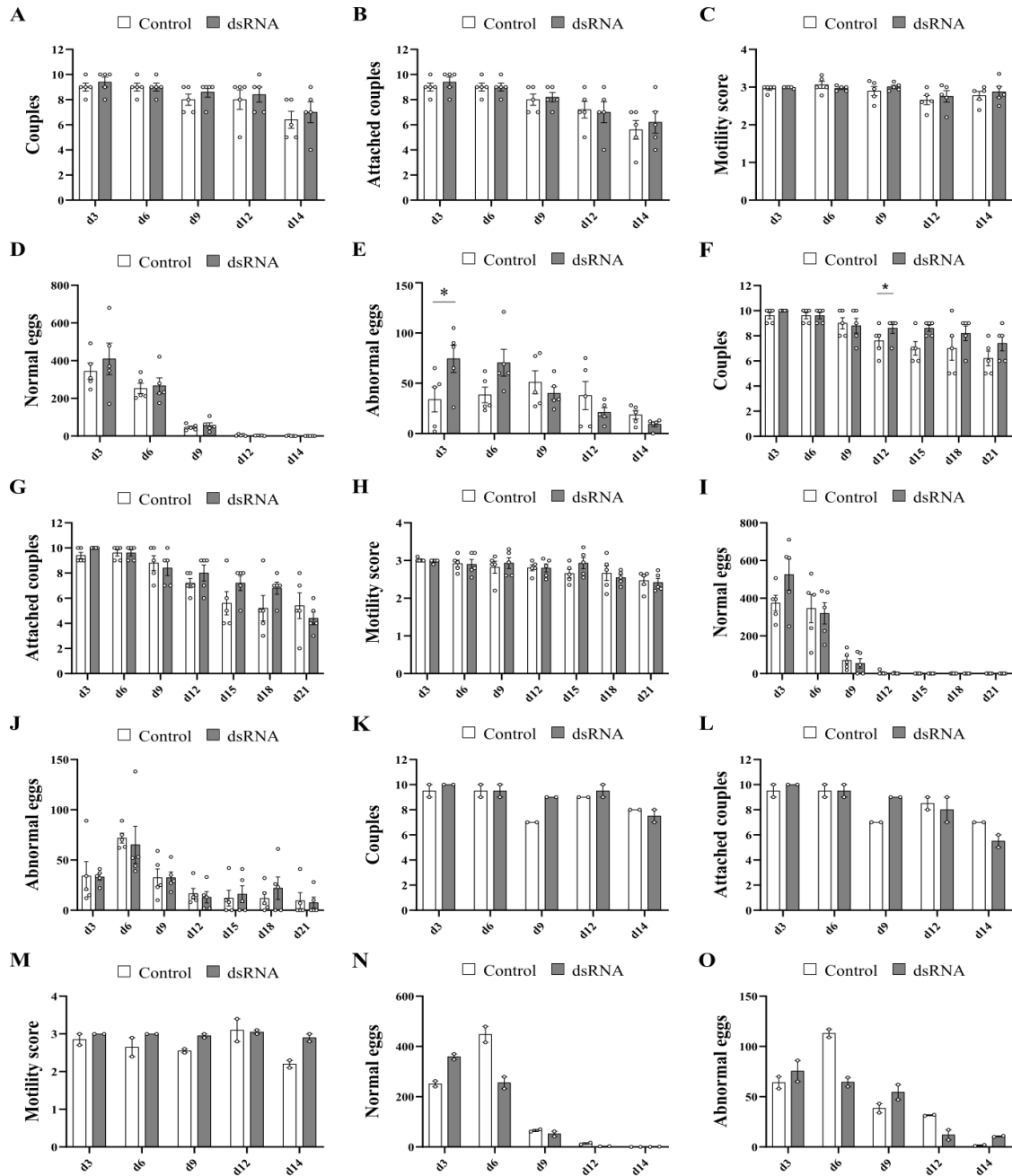
Figure 4.69: Screening of physiological parameters following double knock down of Sm*abl1* and Sm*abl2*

S. mansoni couples were treated with both Sm*abl1* and Sm*abl2* dsRNAs ($2.5\,\mu g\,ml^{-1}$ dsRNA each) for durations of **A - E:** 14 d, n = 5, **F - J:** 21 d, n = 5. **K - O:** treatment with $12.5\,\mu g\,ml^{-1}$ Sm*abl1* and Sm*abl2* dsRNA each for 14 d, n = 2. Shown are the assessed number of couples (**A**, **F**, **K**), number of attached couples (**B**, **G**, **L**), motility score (**C**, **H**, **M**), number of normal (**D**, **I**, **N**) and abnormal eggs (**E**, **J**, **O**). Each data point represents a measurement (averaged for motility score) of one experiment with 10 couples each. Columns represent means with StEM. Statistical analysis was performed as two-tailed t-test (treatment vs control), p < 0.05 (*).
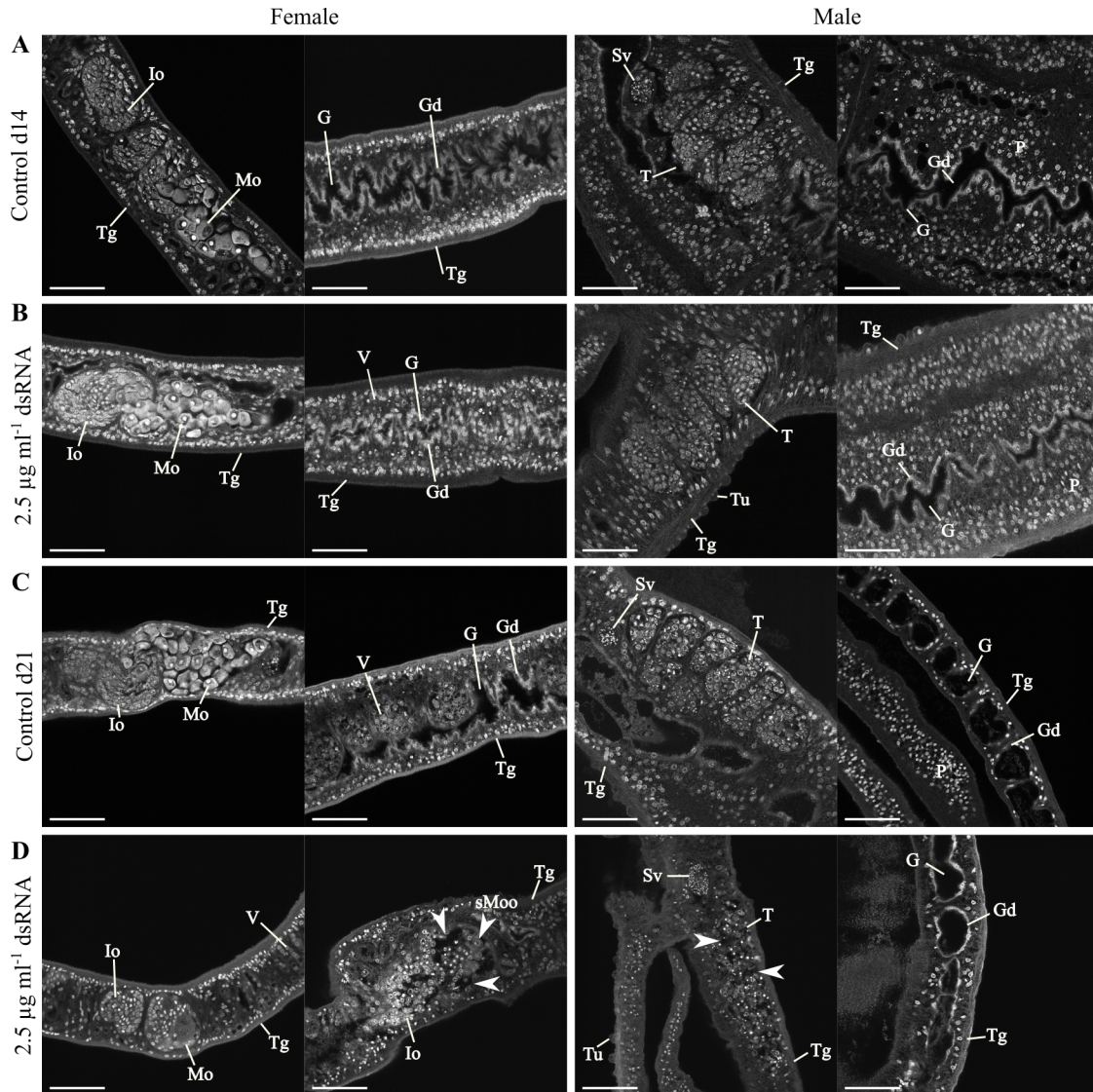
Figure 4.70: Influence of double knock down of Sm*abl1* and Sm*abl2* on the morphology of adult *S. mansoni* couples

S. mansoni couples were treated **A**, **B:** for 14 d and **C**, **D:** for 21 d with DEPC-water as control (**A**, **C**) and $12.5 \, \mu g \, ml^{-1}$ Sm*abl1* and Sm*abl2* dsRNA each (**B**, **D**). Structural changes such as the formation of cavities and small-sized mature oocytes in the ovaries and impairments of the testes are indicated by arrowheads. G = gut, Gd = gastrodermis, Io = part of the ovary containing immature oocytes, sMoo = small mature oocyte, Mo = part of the ovary containing mature oocytes, P = parenchyma, Sv = seminal vesicle, T = testis, Tg = tegument, Tu = tubercle, V = vitelline cell. Scale bars represent $50 \, \mu m$.
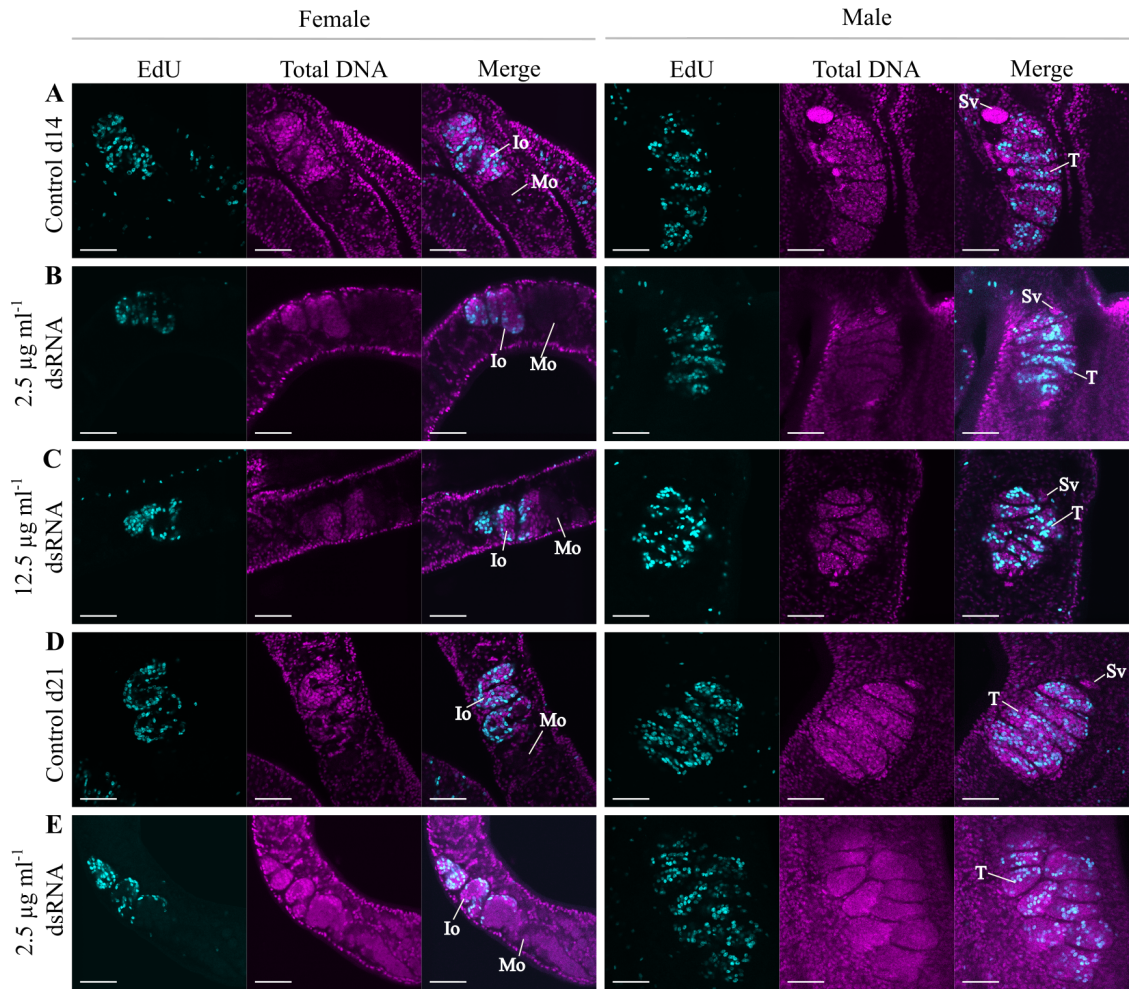
Figure 4.71: Influence of double knock down of Sm*abl1* and Sm*abl2* on proliferation in adult
***S. mansoni* couples**

A - C: treatment of adult *S. mansoni* couples for 14 d and **D**, **E:** for 21 d. Couples were treated
with DEPC-water as control (**A**, **D**), 2.5 µg ml^{-1} Sm*abl1* and Sm*abl2* dsRNA each (**B**, **E**), and
12.5 µg ml^{-1} Sm*abl1* and Sm*abl2* dsRNA each (**C**). EdU-positive cells are shown in cyan and
the total DNA in magenta. Similar signals were found in the gonads of both genders in treatment
and control groups after 14 and 21 d. Io = part of the ovary containing immature oocyte, Mo =
part of the ovary containing mature oocytes, T = testis, Sv = seminal vesicle. Scale bars represent
50 µm.

4.7.7 Knock down of Sm*tk6* impaired the gonads in both genders

Previous studies have shown that Sm*tk6* localized in the parenchyma and gonads of both genders (Beckmann *et al.,* 2010). This kinase was proposed to function in a SmVKR1 complex with SmTK3 and SmTK4 (Beckmann *et al.,* 2010, 2011) and to be involved in processes such as cytoskeleton reorganization, mitosis, cell growth, and proliferation through different down-stream interaction partners (Beckmann *et al.,* 2011). Furthermore, it was shown that interactions of the SmVKR1 complex with Smβ-Int1 inhibited apoptosis in primary oocytes in *S. mansoni* couples (Gelmedin *et al.,* 2017). To analyze the role of Sm*tk6* in more detail, knock down approaches with $2.5\,\mu g\,ml^{-1}$ and $12.5\,\mu g\,ml^{-1}$ dsRNA on adult worms were performed for 14 and 21 d.

To analyze to which extend Sm*tk6* was expressed in female and male worms, qRT-PCRs were performed. For this purpose, either bsF/M or ssF/M were used for analyses. Transcript abundance was similar in bsF and ssF, whereas transcript abundance was slightly lower in bsM and ssM compared to respective female gene expression (**Figure 4.72**).
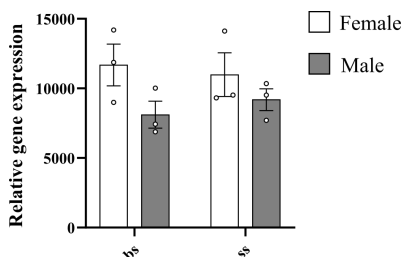
Figure 4.72: Analysis of the transcript profile of Sm*tk6* in adult *S. mansoni*
qRT-PCR analyses to determine the relative gene expression of Sm*tk6* in bsF/M and ssF/M, respectively. Each data point represents one experiment with 10 worms each, n = 3. Columns represent means with StEM. No statistical significance was found.

Analysis by qRT-PCR revealed a moderate knock down for Sm*tk6* to 53 % in females and 37 % in males (both $p < 0.05$) after 14 d of $2.5\,\mu g\,ml^{-1}$ dsRNA treatment (**Figure 4.73 A**). Gene expression of Sm*abl1* increased by approximately 2-fold in females and males, respectively, whereas Sm*abl2* increased by 41 % in females and 90 % in males. Sm*tk6* was significantly reduced by 82 % in females and by 60 % in males after 21 d knock

down with 2.5 µg ml^{-1} Sm*tk6* dsRNA (**Figure 4.73 B**). Sm*abl1* transcripts were reduced to 61 %, while the expression did not change in males. The opposite was observed for gene expression of Sm*abl2*. Here, gene transcripts were slightly upregulated by 18 % in females, while transcript abundance was upregulated by 40 % in females. Sm*npl4* gene expression was not affected in both genders, but Sm*p53* was downregulated in females, while transcript levels did not change in males after 21 d (**Figure 4.73 C**). Apoptosis markers Sm*bax* and Sm*bcl-2* were not affected (**Figure 4.73 D**). The stem cell marker Sm*nanos1* was slightly upregulated in males but not in females (**Figure 4.73 E**). Moreover, Sm*nanos2* expression was not altered after 21 d treatment. With 12.5 µg ml^{-1} Sm*tk6* dsRNA, the Sm*tk6* transcript level was reduced to 44 % and 29 % in females and males, respectively, while expression levels of Sm*abl1* and Sm*abl2* were not affected after 14 d (**Figure 4.73 C**). Overall, knock down efficiency of Sm*tk6* was more efficient in males than in females.
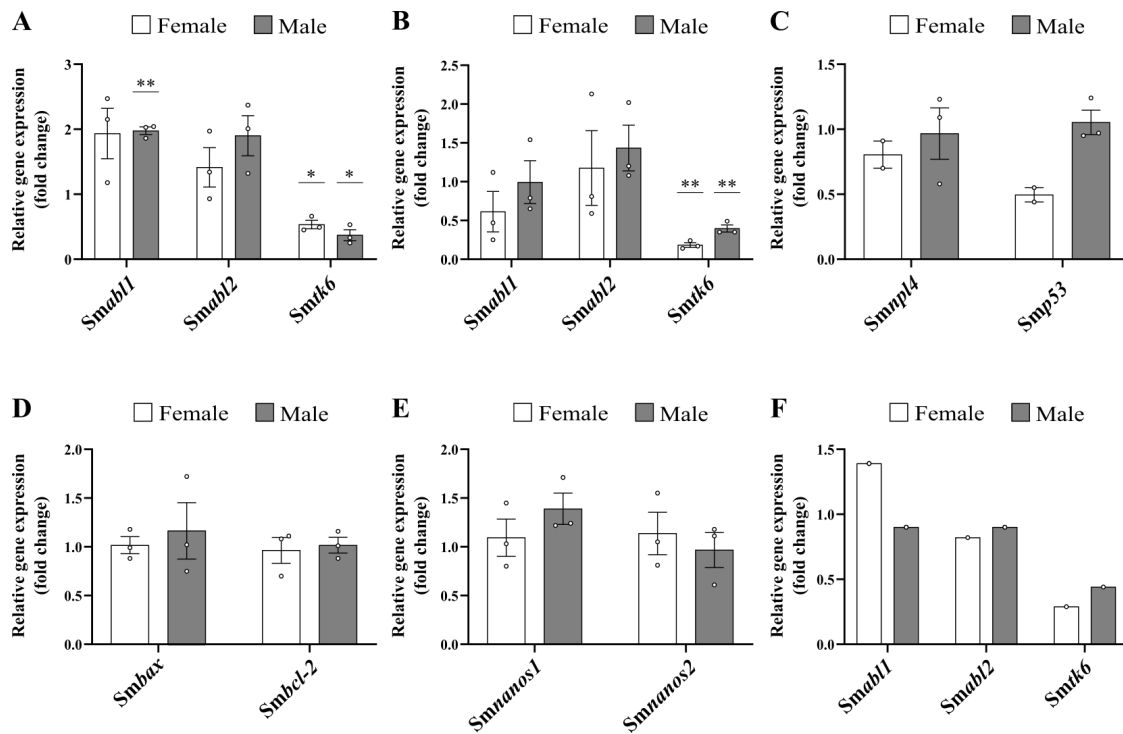
Figure 4.73: qRT-PCR analyses of selected genes after knock down of Sm*tk6* in adult *S. mansoni* couples

The relative gene expression was determined after knock down of Sm*tk6* with 2.5 µg ml^{-1} dsRNA **A:** for Sm*abl1*, Sm*abl2*, and Sm*tk6* after 14 d, n = 3, **B - E**: for Sm*abl1*, Sm*abl2*, and Sm*tk6* after 21 d, n = 3, (**B**), Sm*npl4* and Sm*p53* after 21 d (determined only two times in females) (**C**), Sm*bax* and Sm*bcl-2* after 21 d (**D**), as well as Sm*nanos1* and Sm*nanos2* after 21 d (**E**). **F:** Gene expression for Sm*abl1*, Sm*abl2*, and Sm*tk6* after 14 d using 12.5 µg ml^{-1} Sm*tk6* dsRNA, n = 1. Each data point represents one qRT-PCR analysis of one independent knock down experiment with 10 couples. Columns represent means with StEM. Statistical analysis (two-tailed t-test) was performed using treatment vs control (not shown), $p < 0.05$ (*), $p < 0.01$ (**).

Physiological parameters were observed during the knock down periods (**Figure 4.74**). It was found that the number of couples did not change significantly during the knock down approaches lasting 14 and 21 d, while the number of paired worms decreased towards the respective ends (**Figure 4.74 A** and **F**). The attachment capacity of couples did not significantly change compared to the controls and decreased gradually with time during the 14 and 21 d treatment periods (**Figure 4.74 B** and **G**). Knock down of Sm*tk6* showed no effect on worm motility, movements were evaluated as being normal during both observation periods (**Figure 4.74 C** and **H**). No effect on the number of normal eggs was detected (**Figure 4.74 D** and **I**). The number of eggs of the treatment groups was comparable to that of the control groups, with the highest numbers detected at day

3 after 14 and 21 d. The egg numbers decreased as the experiments progressed during both experimental set ups. The number of abnormally formed eggs was significantly increased by $\sim$ 71 % and 92 % at day 3 and day 6 during the shorter knock down period (**Figure 4.74 E**), while the numbers of abnormally formed eggs remained comparable to those of the control groups during the 21 d period, peaking at day 6, followed by a consistently low number until the end (**Figure 4.74 J**).

Application of a higher dsRNA concentration (12.5 µg ml^{-1}) led to separation of couples and reduction of the attachment rate comparable to the control groups after 14 d (**Figure 4.74 K** and **L**). The motility of the worms remained normal throughout the observation period (**Figure 4.74 M**). The number of normally shaped eggs increased by $\sim$ 2-fold compared to the controls at day 3, whereas the number lowered at day 6 (**Figure 4.74 N**). Most abnormally shaped eggs were observed at day 3, with their number decreasing over time (**Figure 4.74 O**). In short, knock down of Sm*tk6* did not alter physiological parameters drastically.

Next, morphological structures were investigated. To this end, 2.5 µg ml^{-1} and 12.5 µg ml^{-1} dsRNA were administered to couples for 14 and 21 d, respectively, before analysis was done using CLSM. All worm tissues of the treatment groups (2.5 µg ml^{-1} and 12.5 µg ml^{-1} Sm*tk6* dsRNA) were comparable in their integrity to those of the controls during 14 d (**Figure 4.75 A** - **C**). However, changes in the gonads of both genders were observed after administration of 2.5 µg ml^{-1} dsRNA for 21 d (**Figure 4.75 E**). In some females, the number of immature oocytes appeared to increase while the number of mature oocytes appeared to decrease. In other females, the part of the ovary that harbors the mature oocytes appeared to lose its integrity, while oocytes appeared granulated. Testicular disruption was observed in males, forming cavities in the lobe structures, while seminal vesicles were partly filled.

To analyze a possible impact on proliferating cells in paired *S. mansoni*, an EdU assay was performed after Sm*tk6* knock down with 2.5 µg ml^{-1} and 12.5 µg ml^{-1} dsRNA for 14 and 21 d. EdU positive cells were detected in the controls as well as in the treatment groups (**Figure 4.76 A** - **E**). Neither treatment with 2.5 µg ml^{-1} dsRNA for 14 and 21 d nor treatment with 12.5 µg ml^{-1} for 14 d appeared to alter the signal appearance of EdU-positive cells.
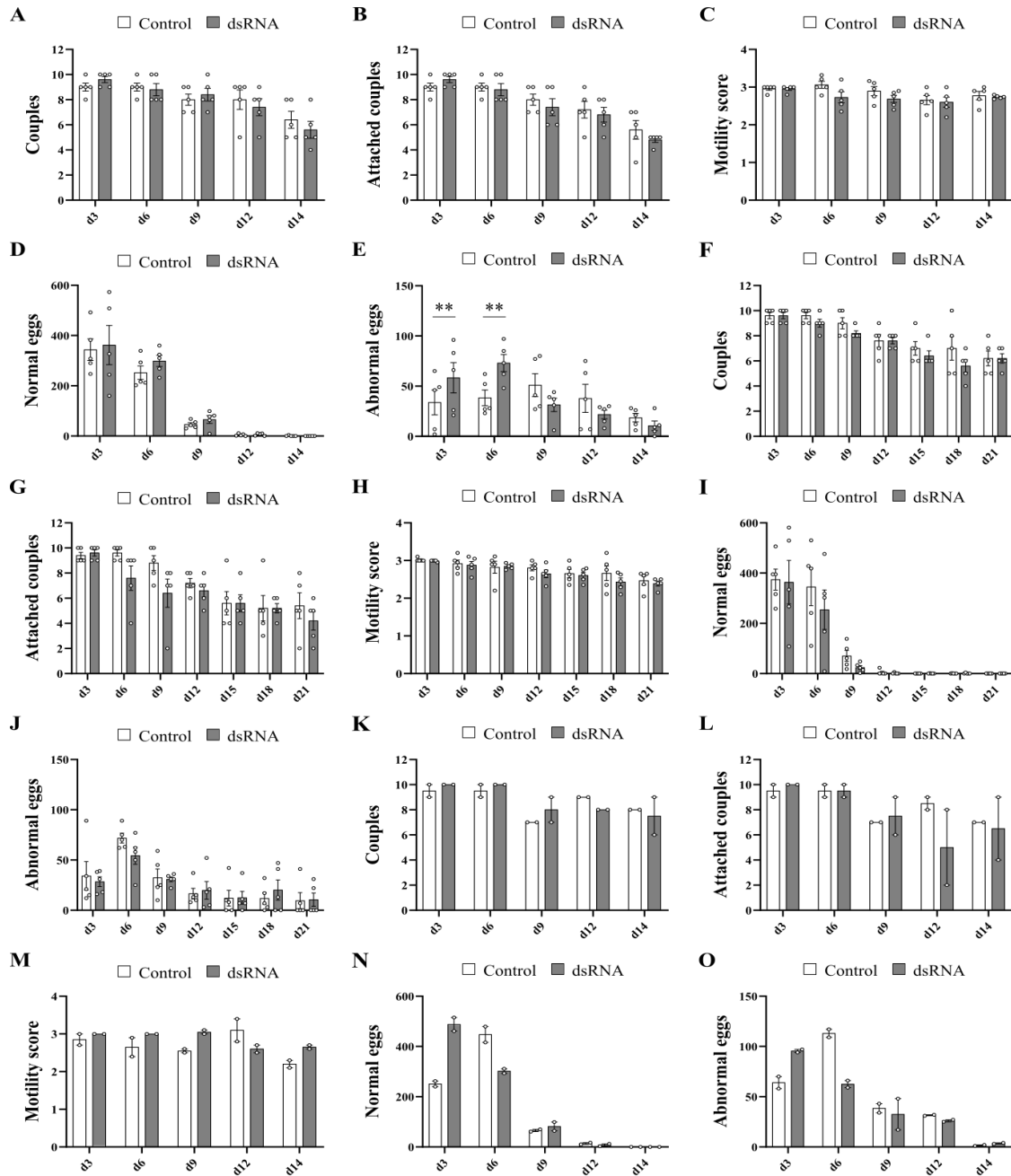
Figure 4.74: Screening of physiological parameters following Sm*tk6* knock down

Assessed number of couples (**A**, **F**, **K**), attachment of couples (**B**, **G**, **L**), motility score (**C**, **H**, **M**), number of normal eggs (**D**, **I**, **N**) and abnormal eggs (**E**, **J**, **O**) during Sm*tk6* knock down ($2.5\,\mu g\,ml^{-1}$ dsRNA) for **A** - **E:** 14 d, n = 5, and **F** - **J:** 21 d, n = 5. **K** - **O:** Sm*tk6* dsRNA treatment ($12.5\,\mu g\,ml^{-1}$) for 14 d, n = 2. Each point represents a measurement (averaged for motility score) of one experiment with 10 couples each. Columns represent means with StEM. Statistical analysis was performed as two-tailed t-test (treatment vs control), $p < 0.01$ (**).
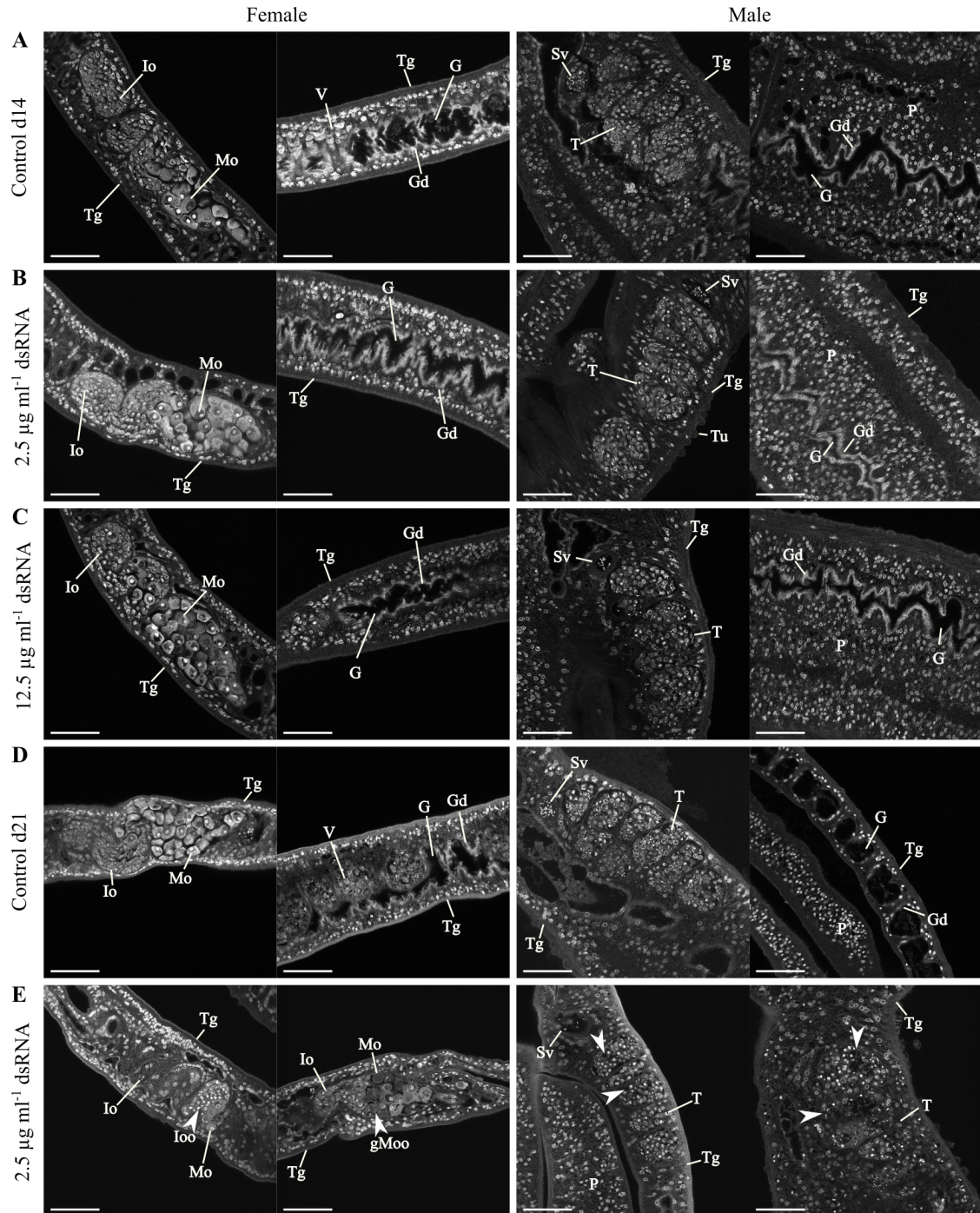
Figure 4.75: Influence of Sm*tk6* knock down on the morphology of adult *S. mansoni* couples
A - **C:** treatment duration of 14 d and **D**, **E:** 21 d. Treatments were as follows: DEPC-water as control (**A**, **D**), 2.5 µg ml^{-1} Sm*tk6* dsRNA (**B**, **E**) and 12.5 µg ml^{-1} Sm*tk6* dsRNA (**C**). Morphological changes as impairment of the gonads and granulated mature oocytes are indicated by arrowheads. G = gut, Gd = gastrodermis, gMoo = granulated mature oocyte, Io = part of the ovary containing immature oocytes, Ioo = immature oocyte, Mo = part of the ovary containing mature oocytes, P = parenchyma, Sv = seminal vesicle, T = testis, Tg = tegument, Tu = tubercle. Scale bars represent 50 µm.
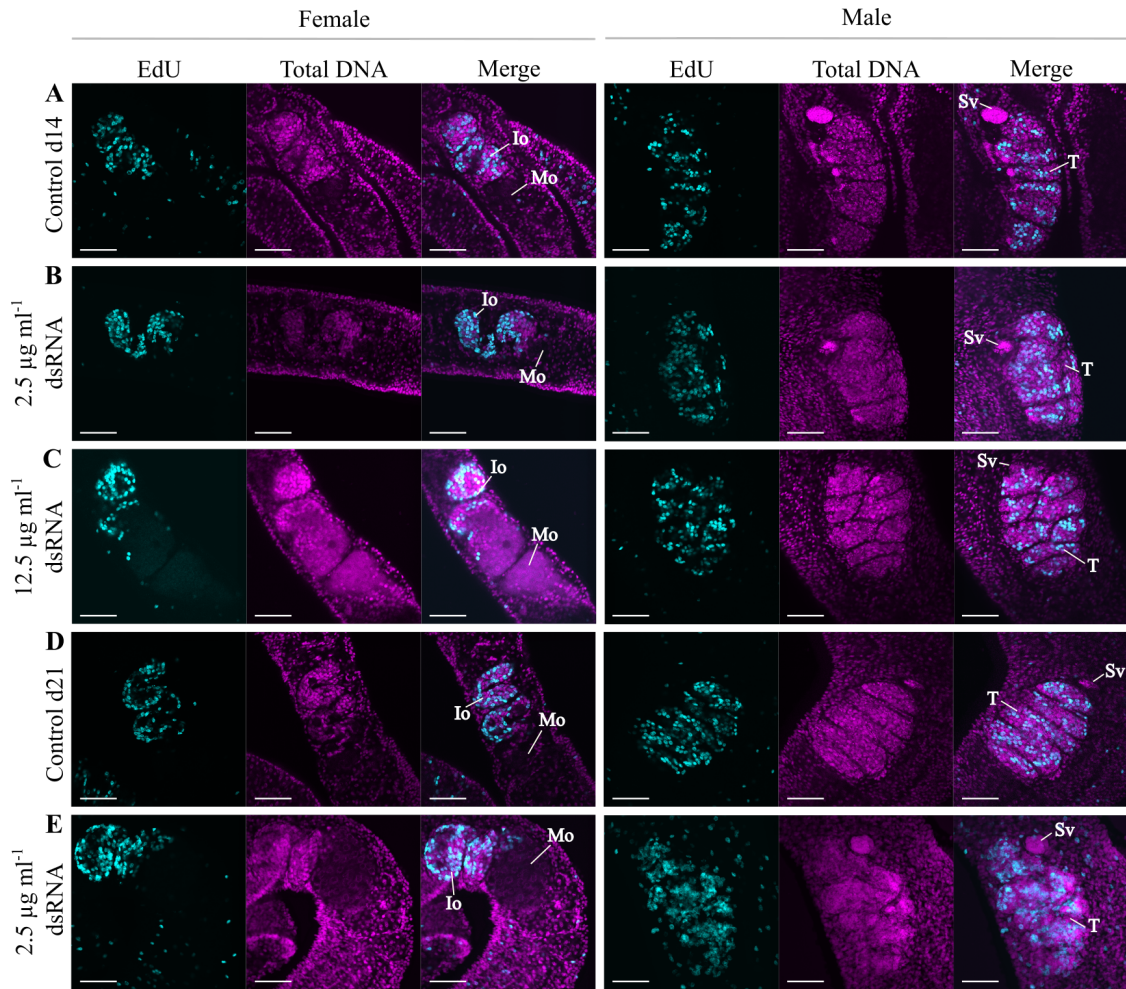
Figure 4.76: Influence of Sm*tk6* knock down on proliferation in adult *S. mansoni* couples
A - C: representative images of *S. mansoni* couples after a 14 d treatment regime with DEPC-water as control (**A**), 2.5 µg ml^{-1} Sm*tk6* dsRNA (**B**), and 12.5 µg ml^{-1} Sm*tk6* dsRNA (**C**). **D, E:** treatment of *S. mansoni* couples with DEPC-water as control after 21 d (**D**) and 2.5 µg ml^{-1} Sm*tk6* dsRNA after 21 d (**E**). EdU was added 24 h before fixation. EdU-positive cells are shown in cyan and the total DNA in magenta. Signals of EdU-positive cells were comparable between all treatment groups and the controls. Io = part of the ovary containing immature oocyte, Mo = part of the ovary containing mature oocytes, T = testis, Sv = seminal vesicle. Scale bars represent 50 µm.

4.8 Functional analyses of SmAldh1 and SmAldh2 with RNAi and oxidative stress conditions

In previous studies in *S. mansoni*, H_2O_2 was shown to be useful for the induction of oxidative stress (Aragon *et al.*, 2008; De Paula *et al.*, 2014). In a pilot experiment, worms were treated with 20 - 400 µM H_2O_2 (data not shown) and the effects on worm physiology were analyzed. The use of 150 µM H_2O_2 showed no obvious effects on *S. mansoni* couples and was chosen to study possible morphological changes induced by RNAi and oxidative stress treatment. To analyze to which extend 150 µM H_2O_2 influences transcript levels of Sm*aldh1*, Sm*aldh2*, and Sm*ar*, qRT-PCR was performed.

Motility and pairing stability of treated worms were determined after 72 h (**Figure 4.77 A**). No effect on motility, the number of couples, or attachment capacity were observed with 150 µM H_2O_2. Next, the possibility of elevating transcript levels of the oxidative stress-responsive genes Sm*aldh1*, Sm*aldh2*, and Sm*ar* was analyzed. While gene expression of Sm*aldh1* was upregulated in females, no effect was observed in males (**Figure 4.77 B**). Transcript levels of Sm*aldh2* did not seem to be altered in either gender, whereas transcript levels of Sm*ar* increased slightly in females but not in males. According to these results, 150 µM H_2O_2 induced an oxidative stress-responsive gene (Sm*aldh1*) without influencing worm physiology. To specify the possible involvement in the oxidative stress response of *S. mansoni*, experiments were performed with knock down of Sm*aldh1* and Sm*aldh2* for 14 d followed by 150 µM H_2O_2 administration for 3 consecutive d. To this end, worms were first treated with 2.5 µg ml^{-1} dsRNA for 14 d while physiological parameters (viability and egg shedding) were evaluated every 3 d. After this "pre-knock down" period, a daily application of 150 µM H_2O_2 followed for further three days. With this strategy, a more severe effect of H_2O_2 on *aldh*-knock down worms was expected.
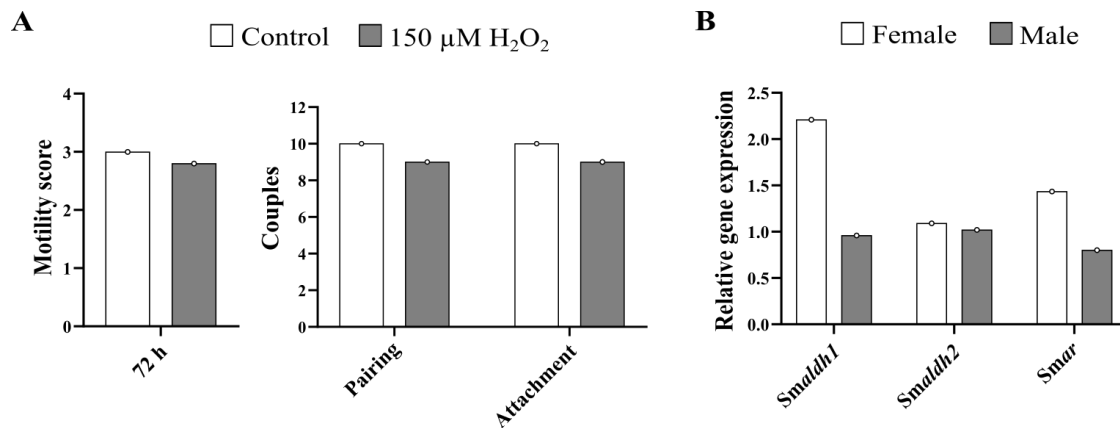
Figure 4.77: Effects of H₂O₂ on worm viability and gene expression of selected oxidative stress-responsive genes

S. mansoni couples were treated with 150 μM H_2O_2 and cultured for 72 h. Thereafter, worms were used for **A:** evaluation of motility and number of paired and attached couples, and **B:** qRT-PCR analysis of Sm*aldh1*, Sm*aldh2*, and Sm*ar*. Relative gene expression of H_2O_2-treated worms vs control worms is depicted (B). Data represent a single experiment.

In the controls (untreated for 14 d then 150 μM H_2O_2 daily), the number of worm couples was slightly reduced by d 14, remained stable for 2 d, and decreased again slightly on d 17, the last day of the observation period. For the Sm*aldh1* and Sm*aldh2* dsRNA treatment groups, the number of couples also decreased until d 14 but remained stable throughout the subsequent H_2O_2 treatment (**Figure 4.78 A** and **F**). The number of attached couples decreased during the Sm*aldh1* dsRNA treatments to 6 and continued to decrease until the end of the experiment, while in the control groups, the number of couples also decreased slightly until d 14 and continued to decrease until d 17 (**Figure 4.78 B**). The number of attached couples during Sm*aldh2* dsRNA treatment remained stable with only a slight decrease until d 17 (**Figure 4.78 G**). Motility values in both dsRNA-treatment groups were comparable to those of the control groups, whereas motility in Sm*aldh1* dsRNA-treated groups was reduced to 2 at d 17 (**Figure 4.78 C** and **H**). The impact of H_2O_2 treatment on the number of normally and abnormally formed eggs could not be determined because of the late application time points. Normally and abnormally shaped eggs were most frequently observed in both treatment groups after 3 d with continuous declines until the end of the experiment (**Figure 4.78 D** - **E** and **I** - **J**).
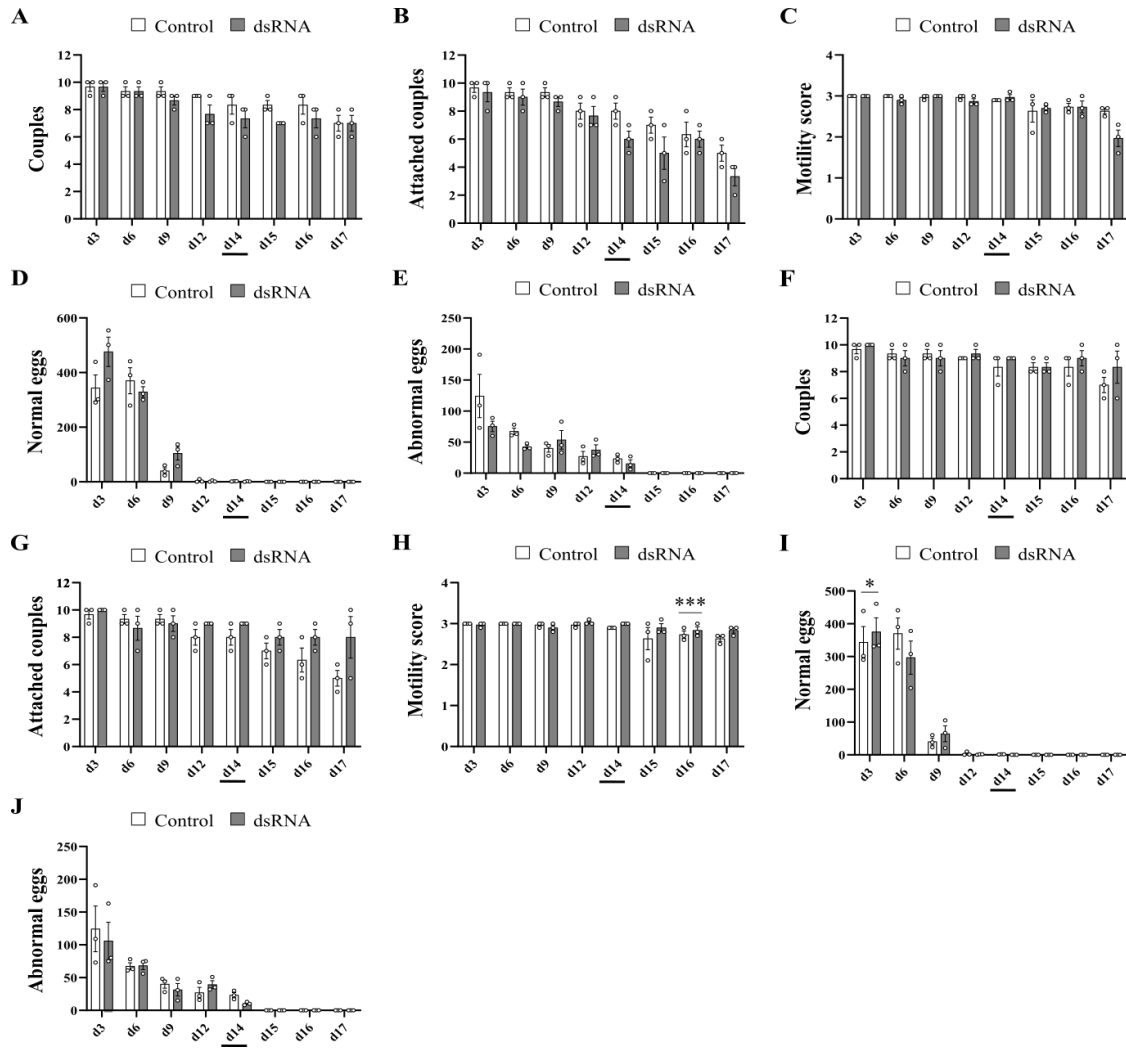
Figure 4.78: Screening of physiological parameters following knock down of Sm*aldh1* or Sm*aldh2* and induction of oxidative stress by H$_2$O$_2$

Physiological parameters such as the number of couples (**A**, **F**), the attachment of couples (**B**, **G**), motility score (**C**, **H**), and egg count for normal (**D**, **I**) and abnormal eggs (**E**, **J**) were assessed during a 14 d knock down of **A** - **E:** Sm*aldh1* or **F** - **J:** Sm*aldh2* followed by induction of oxidative stress with 150 µM H$_2$O$_2$ for further 3 d. The starting point for H$_2$O$_2$ treatment is underlined. Each point represents a measurement (average for motility score) of one experiment, n = 3. Columns represent means with StEM. Statistical analysis (two-tailed t-test) was performed using treatment vs control, p < 0.05 (*), p < 0.001 (***).

Observation of the worms by bright-field microscopy revealed some degeneration in the regions between the head and ventral suckers of the females and the posterior parts of both genders at d 17 (**Figure 4.79 B** and **C**). These effects could not be attributed as a response to the previous knock downs of Sm*aldh1* or Sm*aldh2* as they were also evident

in the control group (**Figure 4.79 A**).
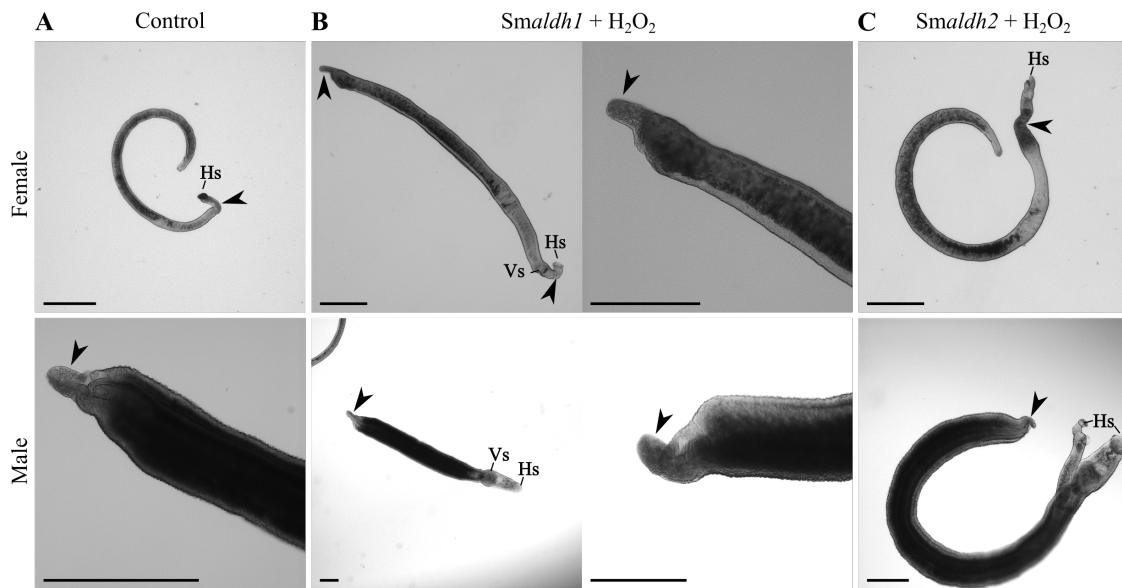
Figure 4.79: Bright-field microscopy of *S. mansoni* couples after knock down of Sm*aldh1* or Sm*aldh2* and H$_2$O$_2$ treatment
Presented are images of **A:** control worms, untreated for 14 d, then treated with 150 µM H$_2$O$_2$ (daily for 3 d), **B:** *S. mansoni* couples treated with Sm*aldh1* dsRNA (including close-ups), or **C:** Sm*aldh2* dsRNA for 14 d, followed by administration of 150 µM H$_2$O$_2$ (daily, 3 d). The observed degenerations on several worm bodies are marked by arrowheads. Hs = head sucker, Vs = ventral sucker. Scale bars represent 250 µm.

Next, gene expression analysis of oxidative stress-responsive genes (Sm*aldh1*, Sm*aldh2*, Sm*ar*, Sm*gpx*, Sm*sod*, and Sm*sodex*) and cell cycle-associated genes (Sm*npl4* and Sm*p53*) was performed. In the two knock down groups, the respective transcript levels of the knocked down Sm*aldh* were significantly reduced without affecting the transcript levels of the other Sm*aldh* or Sm*ar* (**Figure 4.80 A** and **D**). However, Sm*gpx* was slightly and Sm*sod* significantly downregulated in females, whereas Sm*sodex* appeared slightly upregulated in males after Sm*aldh1* knock down and H$_2$O$_2$ stress (**Figure 4.80 B**), while only Sm*sod* appeared slightly downregulated in females after Sm*aldh2* knock down and oxidative stress induction (**Figure 4.80 E**). The transcript levels of Sm*npl4* and Sm*p53* were not significantly affected in both treatment groups (**Figure 4.80 C** and **F**).
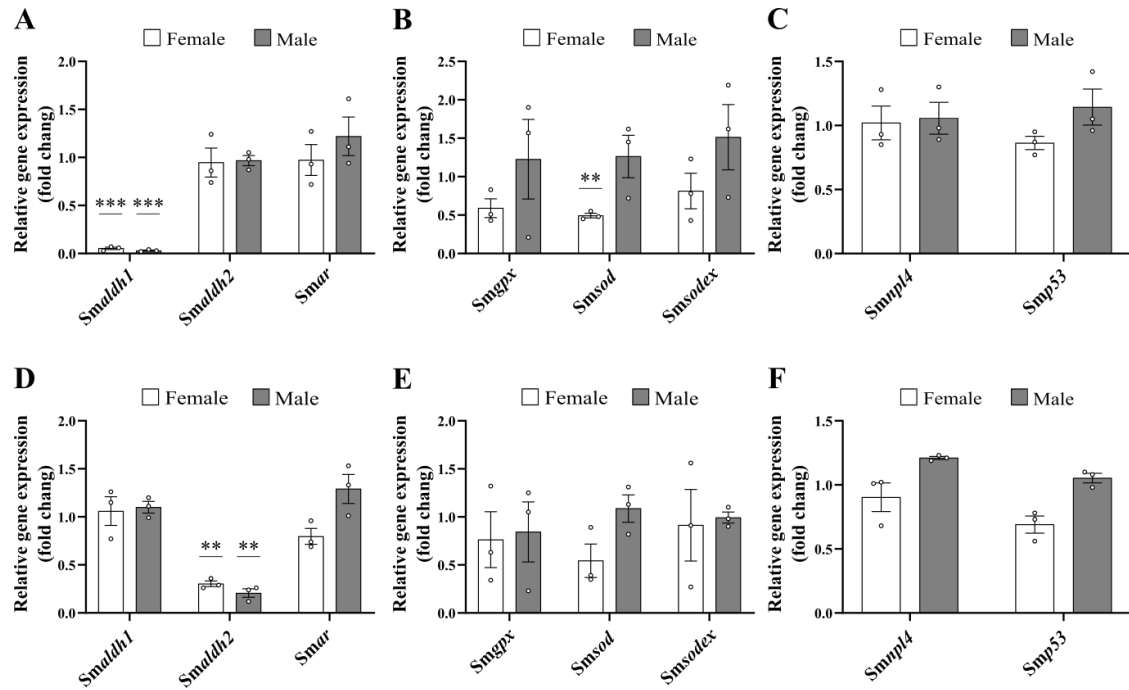
Figure 4.80: qRT-PCR analyses of selected genes after knock down of Sm*aldh1* and Sm*aldh2* and H₂O₂ treatment in adult *S. mansoni* couples

S. mansoni couples were treated with **A** - **C:** $2.5\,\mu g\,ml^{-1}$ Sm*aldh1* dsRNA or **D** - **F:** $2.5\,\mu g\,ml^{-1}$ Sm*aldh2* dsRNA for 14 d, followed by 150 µM H₂O₂ for further 3 d (daily application). Relative transcript levels of H₂O₂ and dsRNA-treated vs H₂O₂-treated control worms are shown and analyzed for oxidative stress-response genes Sm*aldh1*, Sm*aldh2*, and Sm*ar*, (**A**, **D**), Sm*gpx*, Sm*sod*, and Sm*sodex* (**B**, **E**), and the cell cycle-associated genes Sm*npl4* and Sm*p53* (**C**, **F**). Each data point represents one experiment, n = 3. Columns represent means with StEM. Statistical analysis (two-tailed t-test) was performed using treatment vs control (not shown), p < 0.01 (**), p < 0.001 (***).

5 Discussion

5.1 Drug repurposing: DSF as schistosomicide

In this work, the anti-parasitic efficacy of DSF on adult *S. mansoni* was investigated. This included analyses whether DSF or its copper metabolite CuET causes effects on *in vitro*-cultured *S. mansoni*. DSF is able to complex copper and form CuET (Lewis *et al.*, 2014). The complex was also shown to form in medium *in vitro* (Skrott *et al.*, 2019). In this work, the complex formation was interrupted by the addition of copper chelating agents (BCPD and EDTA), and the influence on adult *S. mansoni* worms was determined. To this end, *S. mansoni* couples were cultured in different conditions:

- DSF alone
- DSF and 1 µM CuCl$_2$ (DSF/Cu)
- CuET
- BCPD, DSF, and 1 µM CuCl$_2$
- EDTA, DSF, and 1 µM CuCl$_2$

The worms were examined every 24 h for their physiological parameters (motility, pairing status (number of couples and their attachment ability), and the number of normal and abnormal eggs). After 3 d, the treatment effects on morphology, proliferating cells, and gene expression were analyzed by CLSM (and partly SEM), EdU assay, and qRT-PCR.

5.1.1 Effects of DSF on adult *S. mansoni* couples

DSF's ability against several tumor species in humans has been investigated (Cen *et al.*, 2002; Schmidtova *et al.*, 2019). However, it has been shown to be active against different bacteria, oomycetes, and protozoa (Castillo-Villanueva *et al.*, 2017; Gordon and Seaton, 1942; Krajaejun *et al.*, 2019; Liegner, 2019; Phillips *et al.*, 1991) and was proposed as anti-parasitic drug (Shirley *et al.*, 2021). In this work, the effect on adult *S. mansoni* was investigated.

DSF affected viability in a dose-dependent manner

DSF was administered at a range of 1 - 200 µM to adult *S. mansoni* couples, and the worms were examined for their ability to maintain their pairing status and attachment capacity to the dishes, their overall motility, and the number of normal and abnormal eggs (**Figure 4.1**). Application of DSF showed a dose-dependent effect with highest influence on the screened parameters at 200 µM. Separation of 50 % of the couples were observed at 25 µM DSF, while 50 % of the couples were not longer attached to the dishes at 10 µM DSF. The number of eggs decreased already at 1 µM DSF after 72 h. Worm's motility decreased to almost no movements at 200 µM. Dose-dependent effects of the metabolite DETC and DSF were observed when Khouri *et al.* (2010) and Peniche *et al.* (2015) explored the anti-parasitic properties against *Leishmania* species. No parasitic viability was observed after 48 h of treatment with 250 µM DSF in infected hamster spleen cells (Peniche *et al.*, 2015), while 2 mM DETC were needed to clear parasites in human macrophages after 48 h (Khouri *et al.*, 2010).

The effective dose needed for killing *S. mansoni* worms was not determined, but worms exposed to 200 µM DSF displayed 100 % separation and detachment from the dishes with drastically reduced movements. Weaker dose-dependent effects on the motility were observed when immature and adult *F. hepatica* flukes were exposed to DSF (Houhou, 2022). The youngest juvenile worm stages (schistosomula and newly excysted juveniles (NEJs)) of *S. mansoni* and *F. hepatica* were found to be most susceptible against DSF with doses as low as 0.5 µM and 20 µM, respectively, after 72 h (Beutler, Harnischfeger *et al.*, 2022, manuscript in preparation; Houhou, 2022). In contrast, Lalli *et al.* (2015) screened schistosomula after treatment with 10 µM DSF and observed no toxicity including no tegument damage after 24 h. This discrepancy

in observed phenotypes after DSF treatment could be a time-dependent effect, as Lalli *et al.* (2015) examined schistosomula after 24 h, whereas Beutler, Harnischfeger *et al.* (2022, manuscript in preparation) examined the effects after 72 h.

Another effect of DSF was to reduce worm burden and alter egg case formation in *Trichuris*-infected mice (Hill and Fetterer, 1997). A further consideration that needs to be made concerns the stability of the drug. DSF was found to be stable in aquatic solutions (Das Gupta, 1981), but the influence of additives such as FCS, temperature, and pH of the medium could alter its availability or metabolization.

DSF disrupted the tegument in both genders

Using bright-field microscopy to evaluate the overall status of *S. mansoni* revealed effects such as muscle constrictions, detachment of the tegument, and blebbing at higher doses (100 and 200 µM DSF) (**Figure 4.2**), while in-depth analyses of the tegument by SEM revealed changes such as swelling, sloughing, and destruction of tubercles at 10 µM DSF after 72 h (**Figure 4.3 B**). Tegument destruction occurred with higher frequency at 25 and 50 µM DSF (**Figure 4.3 C** and **D**), resulting in sloughing and blebbing in both genders as well as vesicle formation in males. The destructive effects on the tegument (detachment and bubble formation) was likewise observed at a low frequency by CLSM analysis at 25 µM DSF (**Figure 4.4 C**).

As an external barrier, the tegument is susceptible to the influences of its environment and the first encounter when worms are exposed to drugs (Skelly and Wilson, 2006). The tegument of the controls was intact, while disruptions, blebbing, and vesicle formation were observed after DSF treatment. Voge and Bueding (1980) treated *S. mansoni* worms with a sub-curative dose of the schistosomicide amoscanate and analyzed the tegument by SEM, revealing swellings and erosion of the tegument and ruptured tubercles in males, while females additionally showed enlarged pores. Leitch and Probert (1984) confirmed the ultrastructural tegument changes by SEM analysis in amoscanate-treated *S. haematobium*. Vesicles were also observed when De Paula *et al.* (2014) treated *S. mansoni* worms with H_2O_2, indicating that vesicle formation is a response to oxidative stress. Moreover, DSF was shown to induce oxidative stress and apoptosis, resulting in necrosis of human melanoma cells (Cen *et al.*, 2002). This could be induced by DSF's ability to form intramolecular disulfide bonds with various proteins (Lipsky *et al.*, 2001) or its metabolite MeDETC-SO, which forms protein-

adducts (Shen *et al.,* 2001). This way, proteins involved in apoptosis or redox-balancing pathways may be influenced by DSF. It was demonstrated by Cocco *et al.* (1981) that DETC inhibits copper/zinc-dependent SOD (Cu/Zn-SOD) isolated from bovine erythrocytes *in vitro.* SOD is an enzyme involved in the conversion of superoxide anions to hydrogen peroxide. In *S. mansoni,* Sm*sod* transcripts were identified and localized in the tegument (Hong *et al.,* 1992a, 1993), indicating that SmSOD is a first-line enzyme of defense against oxidative stress. In addition, SmAldh1 and SmAldh2 were identified in tegument fractions of *S. mansoni* worms (Beutler, Harnischfeger *et al.,* 2022, manuscript in preparation; Ludolf *et al.,* 2014; Winkelmann *et al.,* 2022), suggesting a detoxifying role in the tegument. DSF as Aldh inhibitor seemed to inhibit this process by targeting both Aldhs.

The observed tegumental alterations after DSF treatment were more pronounced in males than in females. An explanation for this could be the differences in the size of the worms as well as the residence of the females in the gynaecophoric canal, which leads to a kind of shielding of the female from the environment. Mokosch *et al.* (2021) showed by atmospheric-pressure scanning microprobe matrix-assisted laser desorption/ionization mass spectrometry imaging that imatinib accumulated in males earlier than in females when *S. mansoni* couples were exposed to the drug *in vitro.* When Woolhouse and Kaye (1977) examined the ability of female and male worms to take up OXA *in vitro* and *in vivo,* they found that both genders took up the drug at comparable concentrations, leaving the size difference as poor explanation. They also observed that pairs separated rapidly after drug administration (Woolhouse and Kaye, 1977), which subsequently exposes both genders similarly to the drug. DSF resulted in 50 % of separated couples at 25 µM, the concentration at which the frequency of tegument changes also increased in females (**Figure 4.3**). Therefore, the efficacy of the drug seemed to be dependent on the exposure to both genders.

DSF impaired the structure of ovaries and testes in both genders

Dose-dependent inhibition of proliferating gonadal cells (oogonia and spermatogonia) was observed when the DSF dose was increased from 10 to 25 µM (**Figure 4.5**), corresponding to structural decay of the gonads (**Figure 4.4**) and vitelline cells. DSF has been shown to induce apoptosis and cell death (Cen *et al.,* 2002; Choi *et al.,* 2015), while O'Brien *et al.* (2019) demonstrated the inhibition of cell proliferation of oral squamous

cell carcinoma cells by DSF and the ability to induce ER stress. The observed granulation of mature oocytes and cavities in ovaries and testes could be the result of apoptotic cells followed by necrosis upon oxidative and ER stress induction (Chaube *et al.*, 2005; Iurlaro and Muñoz-Pinedo, 2015). Inhibition of gonadal stem cell proliferation likewise results in a reduction of mature gonadal cells. The observed cavities remain visible when the remaining mature cells undergo apoptosis and necrosis without being displaced by new maturing cells. This, in addition to the separation of the worms, could explain the observed decrease in egg laying. Aldh has been identified as a stem cell marker (Cai *et al.*, 2004; Choi *et al.*, 2014, 2015; Corti *et al.*, 2006; Storms *et al.*, 1999). Choi *et al.* (2014) knocked down HsAldh1 in brain tumor-initiating cells and found decreased proliferative capacity and cell viability. Since DSF inhibits recombinant SmAldh1 (Beutler, Harnischfeger *et al.*, 2022, manuscript in preparation), this could be another mechanism for the observed reductions in proliferative capacity of gonadal stem cells. To further clarify whether less or no EdU was taken up due to induced cell death or a temporary arrest of proliferation, wash out experiments should be performed. If increased signal strength would be detected in the treated cells after DSF wash out, this would indicate that the cells were merely arrested and are still capable of proliferation.

DSF altered gene expression of stem cell markers and response to oxidative stress

Considering the observed alterations in worm morphology and proliferation capacity, induction of selected genes related to oxidative stress response (Sm*aldh1*, Sm*aldh2*, Sm*ar*, Sm*gpx*, Sm*sod*, and Sm*sodex*), cell cycle regulation (Sm*npl4* and Sm*p53*), apoptosis (Sm*bcl-2* and Sm*bax*), and stemness (Sm*nanos1* and Sm*nanos2*) was expected. Exposure of 10 µM DSF did not induce any of the analyzed genes in females (**Figure 4.6 A - E**), while Sm*gpx* was upregulated in males, indicating a response to oxidative stress. In addition, under the same conditions, Sm*nanos1* gene expression was downregulated in males, whereas Sm*nanos2* was upregulated. When 25 µM DSF were administered (**Figure 4.6 F - J**), transcripts of Sm*sodex* were increased and Sm*nanos1* decreased in females, while Sm*gpx* and Sm*sodex* expression levels were increased in males, indicating a response to oxidative stress caused by DSF. Furthermore, transcript levels of cell cycle-regulator Sm*p53* were upregulated and Sm*nanos1* downregulated, respectively, whereas the transcript level of Sm*nanos2* was upregulated in males.

Nanos proteins are RNA-binding proteins with post-transcriptional regulatory function associated with germline and somatic development (Asaoka-Taguchi *et al.,* 1999; Irish *et al.,* 1989; Janic *et al.,* 2010; Lee *et al.,* 2017; Mochizuki *et al.,* 2000; Rabinowitz *et al.,* 2008; Tsuda *et al.,* 2003; Wharton and Struhl, 1989). Sm*nanos1* is mainly expressed in the gonadal stem cells of females and males (Wendt *et al.,* 2020). The decrease in transcript abundance is consistent with the observed reduced number of gonadal stem cells and impairment of gonads with formation of cavities (**Figure 4.4**), and with the reduction in the ability to proliferate in both genders (**Figure 4.5**). Sm*nanos2* was identified in somatic stem cells along with Sm*p53* (Collins *et al.,* 2013). Transcript abundance of both genes was increased in males at 25 µM DSF. In *S. mediterranea,* a *p53* homologue (Smed*p53*) was identified and associated with the self-renewal capacity of early progeny cells (Pearson *et al.,* 2009). Collins *et al.* (2013) associated Sm*p53* as well as Sm*nanos2* itself to a proliferating somatic cell population, which in a follow-up study was shown to be neoblasts possibly involved in the tegument renewal (Collins *et al.,* 2016). After radiation treatment, both genes were downregulated after 2 d and even further after 15 d (Collins *et al.,* 2016), indicating the loss of stem cell ability in the cells studied. In comparison, Pearson *et al.* (2009) detected increased cell division after 3 d and a depletion at d 15 after Smed*p53* RNAi treatment. They also confirmed the involvement of Smed*p53* in the DNA damage response (Pearson *et al.,* 2009). The induction of Sm*nanos2* and Sm*p53* in males may be due to a higher requirement for tegument renewal and initiation of repair mechanisms as 25 µM DSF already caused tremendous damage to the tegument, possibly due to its ability to induce oxidative stress (Cen *et al.,* 2002) and as observed by SEM analysis (**Figure 4.3**). It cannot be excluded that the induction of both genes is reduced at later time points.

Although DSF induces apoptosis (Cen *et al.,* 2002; Choi *et al.,* 2015) and empty spaces were observed in the gonads of *S. mansoni,* which may be explained by apoptosis, expression of the apoptosis markers Sm*bcl-2* and Sm*bax* was not altered. Apoptosis (autophagy) can be inhibited by the interaction of the anti-apoptotic protein BCL-2 with a BH3-like domain of Beclin 1 (Maiuri *et al.,* 2007). Pro-apoptotic initiator proteins inhibit the BCL family proteins and stimulate pro-apoptotic effectors such as BAX (Oltvai *et al.,* 1993), leading to mitochondrial outer membrane permeabilization (MOMP) (Adams *et al.,* 2019). MOMP enables the release of apoptotic factors, initiating cell death mediated by the caspase cascade (Adams *et al.,* 2019).

Both Sm*aldhs* and Sm*ar* were not induced upon DSF treatment, suggesting that they are not involved in the response after 10 µM DSF treatment. A trainee of the group of Prof. C. G. Grevelding (S. Müller) determined an upregulation of Sm*aldh1* in males up

to 3-fold after 25 and 50 µM DSF application, respectively, whereas gene expression was downregulated in females by about 80 % and 50 % at 25 and 50 µM DSF, respectively. He also found an increase in transcript abundance of Sm*aldh2* by about 50 % only in males after 50 µM DSF, while Sm*gpx* transcripts were increased about 2-fold in females after 50 µM DSF (Müller, 2019). These data suggest that higher DSF concentrations are necessary to induce *aldh* gene expression. In contrast, it has been shown that DSF downregulated the expression of HsAldh1A1 and HsAldh2 in a dose-dependent manner (Jia *et al.*, 2019; Mittal *et al.*, 2014).

It seems that the principle of how a substance acts differs between organisms and their ability to respond to different stimuli. In *F. hepatica*, the orthologous Fh*aldh1*, Fh*sod*, and FH*sodex* were upregulated after sub-lethal doses of DSF (Houhou, 2022). Although Sm*sod* is also associated with the schistosomal tegument (Hong *et al.*, 1993; Mei and LoVerde, 1997) and has a broad distribution pattern in both genders according to a single-cell transcriptome atlas (Wendt *et al.*, 2020), no induction was observed. Cocco *et al.* (1981) showed inhibition of a bovine Cu/Zn-SOD by DETC due to its copper-chelating ability. The same effect might be active here. The extent, to which Sm*sod* expression is regulated after inhibition, is not known, but there is evidence that in case of HsAldh1A1, gene expression is also downregulated by DSF (which also inhibits the protein) (Liu *et al.*, 2016). Furthermore, three SOD enzymes exist in humans, being attributed to the mitochondrium, cytoplasm, or extracellular compartment (Crapo *et al.*, 1992; Marklund, 1984; Weisiger and Fridovich, 1973). Since *S. mansoni* does not possess a catalase (cat) gene (Mkoji *et al.*, 1988), detoxification of H_2O_2 relies on other enzymes such as SmGPx. Transcripts of Sm*gpx* were localized in eggs, vitellocytes, and vitelloduct of females (Roche *et al.*, 1996), but according to the single-cell transcriptome atlas, it is also widely distributed in males (Wendt *et al.*, 2020). The observed more frequent gene expression of Sm*gpx* and Sm*sodex* in males is also an indicator of oxidative stress. The differential induction of Sm*sod* and Sm*sodex* suggests that SmSODex is the enzyme responsible for antioxidant defense in the tegument, whereas SmSOD is associated with the cytoplasm (Hong *et al.*, 1992a; Hong *et al.*, 1992b). Sm*sodex* has been analyzed by RNA-seq studies and single-cell transcriptome atlas, and was found highly expressed in males, particularly in the tegument (Lu *et al.*, 2016; Wendt *et al.*, 2020). A lower frequency of tegument damage was observed in females, which may be due to the protection provided by being in the gynaecophoric canal. It is to note that there is also a female-specific Sm*sodex* (f-Sm*sodex*; Smp_095980) (Simurda *et al.*, 1988), which average expression is 8,000 RPKM (compared to the other Sm*sodex*: < 10

RPKM in females but mainly expressed in the tegument) and is ubiquitously distributed with a bias towards late vitellocytes (Lu *et al.*, 2016; Wendt *et al.*, 2020). Therefore, the analyzed Sm*sodex* (used in the present study) seems to be the one involved upon oxidative stress on the tegument. In *Leishmania*, SOD was linked to parasite survival in macrophages, showing the importance to respond to oxidative stress. That less oxidative stress response genes were induced in females at the observed time point does not exclude the possibility that an induction of stress response genes occurs at a later time point after DSF exposure or becomes more dominant after administration of higher doses. As only a small set of genes was analyzed using qRT-PCR, it is proposed to perform further analyses using microarrays to analyze a broader range of genes.

5.1.2 DSF/Cu multiplied the effects of DSF observed in *S. mansoni* couples

Combination treatment of DSF and $1\,\mu M$ CuCl$_2$ showed severe effects even at $1\,\mu M$ DSF, where $100\,\%$ of the couples separated and detached after $24\,h$ and remained separated until the end of the observation period ($72\,h$) (**Figure 4.7 A** and **B**). Moreover, worm motility as well as egg laying were drastically reduced (**Figure 4.7 C - E**). Similar effects were observed when $1\,\mu M$ CuET was applied (**Figure 4.7 F - J**). At $0.25\,\mu M$ CuET, viability parameters (number and attachment capacity of couples and motility) were comparable to the controls, while the shedding of normal eggs was reduced at $0.1\,\mu M$, and the number of abnormal eggs increased above that of the control.

The higher toxicity of DSF/Cu, when compared to DSF alone, was also observed in tumor cells (Li *et al.*, 2018b; Morrison *et al.*, 2010; Safi *et al.*, 2014; Tawari *et al.*, 2015). These results suggest that the effects of the combined treatment of DSF/Cu on worm viability are due to the formation of CuET, as DSF alone shows weaker effects at the same concentrations (**Figure 4.1**). DSF in combination with Cu^{2+} was shown to inhibit the growth of various cancer cell types *in vitro* and *in vivo* (Brar *et al.*, 2004; Chen *et al.*, 2006; Hassan *et al.*, 2018; Morrison *et al.*, 2010; Viola-Rhenals *et al.*, 2007). Brar *et al.* (2004) analyzed the effects of DSF alone, DSF/Cu and DSF/Zn on CRL1619 human melanoma cells supplemented with $10\,\%$ FCS and found a reduction in proliferation of the cells when DSF alone was administered. The effect was multiplied in a dose-dependent manner by the addition of bivalent ions, with Cu^{2+} showing a stronger anti-proliferative effect than Zn^{2+} (Brar *et al.*, 2004). In breast cancer cells, the

combination of DSF/Cu rapidly inhibited the 20S proteasome (as early as 30 min after application), leading to accumulation of ubiquitinylated proteins, induction of caspase-mediated apoptosis, and accumulation of the pro-apoptotic protein BAX (Chen *et al.*, 2006). Viola-Rhenals *et al.* (2007) also linked the toxicity of CuET to melanoma and carcinoma cells to an induction of BAX and a decrease in cell cycle-associated protein Cyclin A, resulting in DNA condensation. They also noted a higher requirement for ROS-degrading enzymes (Cat, GPx, and mitochondrial manganese-dependent SOD), suggesting that CuET induces oxidative stress in cells and mediates apoptosis due to mitochondrial impairment (Viola-Rhenals *et al.*, 2007). Butcher *et al.* (2018) examined the induction of apoptosis in NSCLC after combination treatments of DSF metabolites and copper, showing that only DETC/Cu, DSF/Cu, and CuET were able to induce apoptosis as evidenced by poly-ADP-ribose-polymerase-1 cleavage, increase of BAX, and decrease of BCL-2. Wu *et al.* (2018) also showed that DSF/Cu induced autophagy in NSCLC and autophagy inhibition enhanced apoptosis.

Yip *et al.* (2011) performed experiments with DSF in combination with and without FCS on human breast cancer cell lines and found no toxic effects on the cell lines when DSF was administered in medium without FCS, even at higher DSF concentrations. DSF in combination with serum was shown to be more toxic to breast cancer cells than without (Yip *et al.*, 2011). BSA as part of FCS (Francis, 2010) forms rapidly and reversibly a non-covalent adduct with DSF followed by the unimolecular reduction of DSF to two molecules of DETC (one free molecule of DETC and a mixed disulfide of DETC-BSA) (Agarwal *et al.*, 1986). As DSF can be reduced to DETC in FCS-containing medium, and FCS contains various amounts of metals (Glassman *et al.*, 1980), it can be assumed that the observed effects on *S. mansoni* couples are not solely due to the action of DSF. Chen *et al.* (2006) and Dalecki *et al.* (2015) recognized a color change when DSF was mixed with copper. This is in line with observations made during DSF/Cu experiments, where a rapid formation of a dark brown precipitate was observed when high concentrations of DSF were added to 1 µM $CuCl_2$-containing medium. The precipitate disappeared after shaking the plates to distribute the additives evenly in the wells. The formation of CuET (dark brown powder) by DSF and copper was even shown *in vitro* and *in vivo* (Skrott *et al.*, 2017, 2019).

The formation of blebs on *S. mansoni* was observed by bright-field microscopy with 1 µM DSF and 1 µM $CuCl_2$ after 72 h, whereas no changes were observed with 1 µM CuET (data not shown). However, drastic effects on the tegument were found with 5 µM

CuET (**Figure 4.8**). Morphological analyses of treated worms revealed the detachment of the tegument with 1 µM DSF and 1 µM $CuCl_2$, and, moreover, impairment of the gonads with 10 µM DSF and 1 µM $CuCl_2$ (**Figure 4.9**). The opposite was observed with CuET: 1 µM affected the gonads of both genders but left the tegument intact, whereas 5 µM CuET affected the gonads, vitellarium, and tegument. Consistent with the structural changes was the reduction in cell-proliferative capacity. No EdU-positive cells were detected after treatment with 1 µM DSF and 1 µM $CuCl_2$, while 1 µM CuET showed reduced signals, and 5 µM CuET no signals anymore (**Figure 4.10**).

DSF/Cu and CuET were shown to induce oxidative stress and apoptosis (Brar *et al.*, 2004; Calderon-Aparicio *et al.*, 2015; Chen *et al.*, 2006; Morrison *et al.*, 2010; Tawari *et al.*, 2015; Viola-Rhenals *et al.*, 2007). Gene expression levels of oxidative stress-associated genes were not determined after DSF/Cu or CuET treatment, but it seems likely that both Sm*aldhs,* Sm*gpx,* as well as Sm*sod* and Sm*sodex* were induced to respond to the oxidative stress (and likely ROS formation) by DSF/Cu. ROS also serve as signaling molecules required for cell survival and mitosis (Finkel, 2011; Groeger *et al.*, 2009), and excessive ROS cause single- and double-strand DNA (ss/dsDNA) breaks, leading to apoptosis, disease, and tumor growth (Halliwell and Aruoma, 1991; Kaina, 2003; Luo *et al.*, 2019; Simon *et al.*, 2000). The ability of DSF to induce oxidative stress and to trigger apoptosis has been linked to copper availability (Morrison *et al.*, 2010; Tawari *et al.*, 2015; Viola-Rhenals *et al.*, 2007). Excess copper increases ROS production through Fenton-Haber Weiss redox reactions (Fenton, 1894; Haber and Weiss, 1934) and lipid peroxidation, and it impairs the mitochondrial membrane potential (Hosseini *et al.*, 2014; Mehta *et al.*, 2006). To investigate whether high copper concentrations and subsequent ROS formation in the worm could be responsible for the observed phenotypes, ROS formation should be measured. In addition, Calderon-Aparicio *et al.* (2015) showed that DSF in combination with exogenous H_2O_2 induced apoptosis (Calderon-Aparicio *et al.*, 2015), underpinning the importance of oxidative stress in the context of apoptosis.

A proposed mechanism of action for DSF/Cu is based on the complexation of copper, with an increase in intracellular copper levels inducing the former stated reactions, while DSF-metabolites (such as Me-DETC sulfoxide as formed in humans) forms irreversible thiol complexes with Cys residues of proteins (Koppaka *et al.*, 2012), leading to their inactivation, more oxidative stress, and subsequently apoptosis. The accumulation of copper in redox-sensitive tissues of *S. mansoni* such as the gonads would then undergo apoptosis and necrosis, as probably observed in *S. mansoni* ovaries and testes (**Figure 4.9**), while the tegument is damaged as the first barrier. Metabolization of DSF enhances

its anti-tumor properties (Allensworth *et al.*, 2015; Cao *et al.*, 2022; Park *et al.*, 2018). How DSF and its metabolites (DETC/CuET) are metabolized in *S. mansoni* is not known. Several methyltransferases can be found on WormBase ParaSite in the *S. mansoni* genome, one of them is the putative S-adenosyl-methyltransferase (Smp_053120), which might introduce a methyl group to DETC. In addition, the *S. mansoni* genome harbors several monooxygenases as found on WormBase ParaSite, which may confer Me-DETC metabolization into Me-DETC sulfoxides and sulfonoxides. Unlike DETC, which is loosely adsorbed to protein SH groups but not chemically bound to them, Me-DETC sulfoxide and sulfonoxide can irreversibly form mixed thiol groups with other proteins (such as HsAldh2) (Hart and Faiman, 1993; Mays *et al.*, 1995). Therefore, it seems likely that proteins in *S. mansoni* are bound and/or inactivated by DSF or its metabolites, affecting viability.

5.1.3 The enhanced effect of DSF relied on the addition of copper

The ability to enhance the toxic effects of DSF by addition of copper was shown in the previous section (see section 5.1.2). DSF and copper form the copper-containing complex CuET *in vitro* and *in vivo* (Skrott *et al.*, 2017; Skrott *et al.*, 2019). This substance appeared to exert the anti-schistosomal effect. To elucidate the underlying mechanism, copper-chelating agents (EDTA and BCPD) were added to the culture medium, and the toxicity of DSF/Cu to adult *S. mansoni* was examined. EDTA effectively and stably chelates Cu^{2+} at a molar ratio of 1:1 and other divalent metals such as Ca^{2+}, Mg^{2+}, and Zn^{2+} (Blaedel and Knight, 1954), and BCPD forms stable complexes with Cu^{+} at a molar ratio of 2:1 (Bruyninckx *et al.*, 1978; Campos *et al.*, 2009).

Upon the addition of 0.5 mM BCPD to the *in vitro* culture (**Figure 4.11 A - E**), the assessed physiological parameters such as pairing status (number of couples and their attachment capacity), motility, and oviposition, increased compared to the values obtained by DSF alone (**Figure 4.1**). The viability parameters of the worms were comparable to those of 0.5 mM BCPD and DSF when 1 μM $CuCl_2$ was added to the medium (**Figure 4.11 F - J**). Moreover, no morphological changes were observed when carmine red-stained worms were analyzed by CLSM after treatment with 0.5 mM BCPD and DSF or DSF/Cu (**Figure 4.12**). The ability of gonadal stem cells to proliferate

was also not altered when compared to the controls (**Figure 4.13**). Increasing BCPD concentration to 2 mM increased the overall worm viability assessed above, which was observed with 0.5 mM BCPD (**Figure 4.14 A - E**). Again, the assessed parameters after additional $CuCl_2$ (1 µM) treatment were comparable to those assessed with 2 mM BCPD and DSF alone (**Figure 4.14 F - J**) and showed no effects on morphology (**Figure 4.15**) or proliferation (**Figure 4.16**). The application of 0.5 mM EDTA and DSF resulted in slightly higher scores of the physiological parameters (**Figure 4.17 A - E**) compared with those assessed with 0.5 mM BCPD and DSF (**Figure 4.11 A - E**), while the combination of 0.5 mM EDTA and DSF/Cu (**Figure 4.17 F - J**) resulted in a similar decrease in worm viability as observed with DSF/Cu (**Figure 4.7 A - E**). In the absence of 1 µM $CuCl_2$, no morphological changes were observed, but with 1 µM $CuCl_2$, the ovaries of females appeared to be affected, as the typical structural division with immature and mature oocytes was lost and cavities appeared inside the ovaries (**Figure 4.18 D**). The proliferative ability of cells appeared to be lost when 0.5 mM EDTA and DSF/Cu were administered (**Figure 4.19 D**). A higher EDTA concentration (2 mM) reduced the viability parameters drastically, and in combination with DSF, EDTA failed to restore the values of the pairing parameters to those of the controls at DSF concentrations above 25 µM (**Figure 4.20 A** and **B**). Addition of 2 mM EDTA and DSF/Cu had the same tremendous effects as DSF/Cu on worm's viability, morphology, and proliferative capacity (**Figure 4.20 F - J**, **Figure 4.21 D**, and **Figure 4.22 D**).

Application of 0.5 mM EDTA and DSF seemed to reverse DSF's toxicity, while 0.5 mM EDTA and DSF/Cu did not. With the latter, the effects worsened after 72 h, indicating that autophagy and apoptosis induction after DSF/Cu treatment could not be prevented efficiently (Chen *et al.,* 2006; Han *et al.,* 2013; Morrison *et al.,* 2010; Viola-Rhenals *et al.,* 2007). EDTA is a strong chelator for divalent cations such as Cu^{2+}, Ca^{2+}, and Mg^{2+} (Blaedel and Knight, 1954), while BCPD specifically chelates Cu^+ (Bruyninckx *et al.,* 1978; Campos *et al.,* 2009; Morera *et al.,* 2003). Both agents are non-permeable substances, but EDTA is able to destabilize membranes (Barton, 2014; Cen *et al.,* 2004; Prachayasittikul *et al.,* 2007). In theory, it was expected that EDTA would be able to invert the effects of DSF/Cu because copper was added to the culture as divalent ions ($CuCl_2$), whereas BCPD was expected not to be able to reverse the effects of DSF/Cu due to its specificity to bind Cu^+. The opposite was observed when DSF in combination with EDTA was applied. The toxic effects of DSF alone were reversed suggesting that the amount of free copper in the medium derived from FCS supplementation was bound by EDTA. The used medium, M199, is

supplemented with Earle's salts, (M199 formulation can be studied in detail online at www.thermofisher.com/de/de/home/technical-resources/media-formulation.294.html), containing 1.8 mM $CaCl_2$, 0.8 mM $MgSO_4$, 5.3 mM KCl, and 117.2 mM Nacl, where the additional Ca^{2+} and Mg^{2+} will be complexed by EDTA, too. In addition, it was shown that FCS also contains ions such as Ca^{2+} and Mg^{2+} in the mM range (Glassman *et al.*, 1980), to which EDTA can bind to. The amounts may fluctuate from batch to batch making it hard to predict the exact amounts. When 0.5 mM EDTA and DSF were applied to the *S. mansoni* culture, the chelating capacity seemed not to be exceeded. When DSF was given the chance to form CuET after copper administration in addition to 0.5 mM EDTA, it seemed that the kinetics of CuET formation was faster than that of copper chelation by EDTA. This resulted in the lethal effects observed when DSF/Cu was used alone.

Lewinska *et al.* (2007) showed that different media containing supplements such as phenol red and FCS have antioxidant properties. This would lead to a reduction of Cu^{2+} to Cu^+ in the media. The reduction of Cu^{2+} to Cu^+ and subsequent binding by BCPD is used to measure the total antioxidant capacity (TAC) of aqueous solutions (Campos *et al.*, 2009) and was used by Apak *et al.* (2008) to measure the non-enzymatic antioxidant capacity of vitamins, polyphenols, and flavonoids. In addition, BSA is present in FCS at approximately 50 mg ml^{-1} (Francis, 2010). BSA complexes copper (Hazra *et al.*, 2017; Sarkar and Das, 2014) and reduces it under alkaline conditions, making it a standard in protein determination assays (Chen *et al.*, 2016). FCS has also been used as a protein supplement for analysis of *in vitro* fertilization (Leibfried-Rutledge *et al.*, 1986). Bump and Reed (1977) showed that FCS contained protein-glutathione mixed disulfides and small amounts of free glutathione that can affect the redox potential of the solution with which it is supplemented. It is not known to what extend FCS is able to modulate the redox status of copper, but depending on the oxidation status of copper, complex formation with different chelators may be preferred. For the analysis to interrupt CuET formation, this would imply that some copper molecules would not be chelated by EDTA or BCPD and may form CuET after chelation with DETC. DETC itself was shown to complex both Cu^+ and Cu^{2+}, respectively (Han *et al.*, 2013). Whether DETC has a preference for the redox state of chelated copper is not known. Interruption of the negative effects of DSF/Cu was observed with addition of BCPD, whereas EDTA was not able to reverse the tremendous effects of DSF/Cu administration. This leads to the following assumptions: Cu^{2+} was reduced to Cu^+ by the antioxidant capacity of the medium and its additives. Therefore, Cu^+ complexed by BCPD may prevent the formation of CuET. In contrast, EDTA appeared to be unable to chelate copper, or at

least not as rapidly and sufficiently prior to reduction. This in turn led to the formation of CuET, which was detrimental to the worms.

For both BCPD concentrations, a time-dependent increase in the examined viability parameters was observed with DSF and DSF/Cu at DSF doses of 25 µM and 50 µM, suggesting recovery of the worms after the initial treatment. Several studies have shown that the addition of BCPD abrogates the toxic effects of DSF/Cu on tumor cells by preventing the induction of apoptosis (Brar *et al.*, 2004; Morrison *et al.*, 2010; Safi *et al.*, 2014; Skrott *et al.*, 2019; all studies used Cu^{2+} sources - either $CuCl_2$ or $CuSO_4$). To test whether copper will be reduced in the medium, experiments with both copper sources ($Cu^{+/2+}$) and chelators would have to be repeated using a minimal medium without antioxidant capacity. Since *S. mansoni* are blood-feeding parasites that reside in veins, creating such conditions seems rather problematic. Another option would be to determine the TAC of the medium to draw conclusions about the oxidation state of the copper and analyze CuET formation with DETC and both copper variants, followed by high-pressure liquid chromatography and mass spectrometric analysis to determine the composition of CuET.

An alternative scenario is that EDTA altered the medium composition by chelating divalent ions or destabilized the tegument membrane (Prachayasittikul *et al.*, 2007), allowing copper to enter the worm bodies in addition to the influx mediated by copper transporters, placing copper ions beyond the reach of EDTA for complexation. Analysis of the presence of copper transporters in *S. mansoni* using WormBase ParaSite revealed the existence of a conserved copper transporter (Smp_048230) (Dumay *et al.*, 2006) and a putative transporter for divalent metals (Smp_099850) (Gunshin *et al.*, 1997), suggesting that both oxidation states of copper (Cu^+ and Cu^{2+}) can be transported across *S. mansoni* membranes. DSF is lipophilic and readily transits through membranes (Viola-Rhenals *et al.*, 2018) and could form CuET in the body of the worm to exert its tremendous effects. Tegument destabilization could explain the observed effects of 2 mM EDTA on adult *S. mansoni* physiology, leading to separation of couples and reduced motility (**Figure 4.20 A - C**) without apparent tegument damage or effects on proliferation. To test this hypothesis, trypan blue staining or another viability assay would be required to test the integrity of the tegument. Considering the size of the tegument and parenchyma compared with the gonads, it was less likely that any effect on these tissues would be observed when EDTA and DSF/Cu were administered at the concentrations used.

5.1.4 Is DSF a suitable schistosomicide?

As evident from the present study, DSF alone and in combination with copper has effects on *S. mansoni* adult couples. It was also shown that DSF is active against schistosomula (Beutler, Harnischfeger *et al.*, 2022, manuscript in preparation). In contrast, PZQ is not effective against this juvenile worm stage (Caffrey, 2007). The enhanced effects of DSF and copper can likely be attributed to the chelation of copper with the reduced form of DSF, DETC, which is then called CuET (**Figure 1.3**). The lipophilic nature of CuET (Johansson, 1992) allows it to cross membranes and increases intracellular copper levels. In fact, the combination of DSF/Cu has been shown to transport copper across the blood-brain barrier in copper transporter-deficient mice (Bhadhprasit *et al.*, 2012) and probably also transports copper across the tegument of *S. mansoni*. Elevated copper levels induce oxidative stress and initiate apoptosis, as observed in breast cancer cells (Allensworth *et al.*, 2015). As observed during the present study, the combination of DSF/Cu led to cell-free spaces inside the gonads of both genders (**Figure 4.9**) and reduced proliferation (**Figure 4.10**) probably due to the formation of CuET and high intracellular copper levels. This could be an attractive and lucrative motivator for pharmaceutical companies to invest capital and move forward with the development of a drug with DSF/Cu as the active ingredient. Recently, a phase 1 trial of DSF/Cu in patients with solid tumors metastasized to the liver was conducted, demonstrating the safety and tolerability of DSF with a maximum of 8 mg of elemental copper without dose limiting toxicity (Kelley *et al.*, 2021).

DETC and other DSF metabolites have been shown to be active *in vitro* against various organisms such as bacteria, oomycetes, and protozoa such as *Staphylococcus aureus, Pythium insidiosum, Babesia, Borrelia, Giardia, Leishmania, Plasmodium, Sarcoptes*, and *Trypanosoma* (Castillo-Villanueva *et al.*, 2017; De Freitas Oliveira *et al.*, 2019; Frazier *et al.*, 2019; Gordon and Seaton, 1942; Krajaejun *et al.*, 2019; Liegner, 2019; Peniche *et al.*, 2015; Phillips *et al.*, 1991; Scheibel *et al.*, 1979). Some DSF targets are known, such as SmAldh1 as shown by *in vitro* studies (Beutler, Harnischfeger *et al.*, 2022, manuscript in preparation). However, additional targets have been identified over time. Among the confirmed DSF/DETC targets (*in vitro*) are: bovine Cu/Zn-SOD (Cocco *et al.*, 1981), dopamine-β-hydroxylase from beef adrenal glands (Goldstein *et al.*, 1964), monoamine oxidase of rat liver (Schurr *et al.*, 1978), human DNA topoisomerase (Yakisich *et al.*, 2001), phosphoinositide 3-kinase in human breast cancer cells (Zhang *et al.*, 2010), inosine 5-monophosphate dehydrogenase of *Cryptosporidium parvum* (Sarwono *et al.*, 2018), rat and human glutathione S-transferase (GST) (Ploemen *et al.*,

1996), human NPL4 (Skrott *et al.*, 2017, 2019), and triosephosphate isomerase of *Giardia lamblia* (Castillo-Villanueva *et al.*, 2017). This suggests that the reuse of DSF as an anti-parasitic against a variety of pathogens appears promising. Given this broad spectrum of potential DSF/DETC targets, it seems likely that inhibition of SmAldh1 alone (Beutler, Harnischfeger *et al.*, 2022, manuscript in preparation) may not be the only reason why DSF (or its copper metabolite) is active against *S. mansoni*. On the other hand, simultaneous inhibition of multiple targets reduces the risk of resistance development. A single nucleotide polymorphism can lead to a change in the drug binding site of the target or to truncated protein versions that do not harbor/present the drug binding site (Kotze and Prichard, 2016; Le Clec'h *et al.*, 2021). As observed with OXA and PZQ, resistance can be introduced by repeated treatments *in vivo* and *in vitro* (Coelho *et al.*, 1997; Fallon and Doenhoff, 1994; Li *et al.*, 2011). It is unlikely that multiple targets will simultaneously develop mutations leading to resistance to a multi-targeting drug and this represents a major plus for DSF as a potential schistosomicide. Since DSF is an approved drug, repurposing could be a cost-effective and efficient way to expand the range of drugs against schistosomes.

5.2 Evaluation of a drug candidate: a dithiocarbamate-derivative showed anti-schistosomal properties

The search for new drugs against *S. mansoni* is important. Here, the anti-schistosomal properties of a dithiocarbamate-derivative Schl-32.028 (Mäder, 2016) were evaluated. Previous studies showed that Schl-32.028 was not toxic against HepG2 and LS174T cells up to 100 µM (Mäder, 2016), making it a promising candidate for drug development. In addition, Schl-32.028 was also tested on *F. hepatica* and showed promising effects against the fluke (Houhou, 2022).

5.2.1 Schl-32.028 affected the tegument of *S. mansoni* males

The compound Schl-32.028 proved to be active against *S. mansoni* with 5 µM, with the highest efficacy at 10 µM. The complete separation of couples was observed at 10 µM already after 24 h and motility as well as oviposition were almost completely reduced to 0 after 72 h (**Figure 4.23**). In contrast, CuET reduced almost all scored parameters to 0 with 1 µM (**Figure 4.7 F - J**). In *F. hepatica*, the motility of adult flukes was reduced by about 90 % with 100 µM and in immature flukes with 20 µM, whereas NEJs died with 2 µM (Houhou, 2022). Morphological changes such as swellings, blebbing, and tegument detachment were observed only in the tegument of *S. mansoni* (**Figure 4.24**), while the gonads of both genders were not affected (**Figure 4.26**). Males appeared to be more affected than females. This was confirmed by SEM analysis, in which male worms exhibited tegument damage such as sloughing, swelling, vesicle formation, and destroyed tubercles (**Figure 4.25**). Houhou (2022) also observed blebbing on juvenile *F. hepatica* flukes after treatment with 20 µM Schl-32.028, while NEJs showed severe tegumental damage with darkening of their bodies after treatment with 2 µM.

An attempt was made to analyze the uptake pathway of Schl-32.028. To this end, Gallinger (2022) coupled a fluorescent dye to Schl-32.028, resulting in the compound Schl-37.066. Using Schl-37.066, strong signals were detected in the esophagus, gut, muscles, and tegument of schistosomes, as well as in the gut and vitellarium of adult *F. hepatica* treated with the compound for 1 h (Gallinger, 2022). Uptake of Schl-32.028 by the tegument could explain the observed damage of this tissue and the high separation rate of *S. mansoni* couples. Comparing the results obtained for both parasites also showed that the absorption of this compound and its action can differ among organisms.

5.2.2 Schl-32.028 induces, among others, genes that respond to oxidative stress

Analysis of oxidative stress-responsive genes in *S. mansoni* (**Figure 4.28 A** and **B**) clearly showed the induction of oxidative stress in treated worms, although the exact mechanisms appeared to differ between males and females. As previously observed, the tegument of males was highly damaged, possibly due to oxidative stress and ROS formation, which is in line with the observed DSF (**Figure 4.3** and **Figure 4.4**) and CuET damages (**Figure 4.8** and **Figure 4.9**), including upregulation of Sm*sodex* and

Sm*gpx* as ROS-detoxifying enzymes in males after application of 10 µM Schl-32.028. In contrast, females showed almost no tegument damage and a lower expression of Sm*sodex* but increased Sm*ar* and 10-fold higher Sm*sod* transcript levels, also indicating a strong detoxification response to generated ROS. ROS can induce ss/dsDNA breaks (Halliwell and Aruoma, 1991). Gene expression of Sm*npl4* was upregulated in females, suggesting a higher requirement for proteasomal protein degradation because NPL4 functions as adaptor protein to p97, which transports ubiquitinylated proteins to the 26s proteasome (Isaacson *et al.*, 2007; Skrott *et al.*, 2017; Torrecilla *et al.*, 2017; Vaz *et al.*, 2013). Since Sm*p53* is not upregulated in females, it appears that the anti-oxidative stress response is either efficient enough, or the damages not yet severe enough. Transcript levels of Sm*bcl-2* were slightly downregulated, whereas transcript levels of Sm*bax* were increased in both genders, suggesting a shift toward apoptosis in both genders. In contrast to the effects observed on the gonads after DSF and DSF/Cu treatments, no disorganization or disruption was observed after 10 µM Schl-32.028 treatment, as confirmed by the stable expression of Sm*nanos1* in both genders. In addition, no signal was observed in *S. mansoni* gonads when Schl-37.066 was used to determine the uptake pathway of Schl-32.028 (Gallinger, 2022). This suggests that using 10 µM Schl-32.028 might have a delayed effect on the gonads since the compound fails to accumulate in these organs in the first place (Gallinger, 2022). Analysis of the gonadal proliferative capacity in adult *S. mansoni* revealed no effects with 5 µM, whereas 10 µM almost completely abolished the EdU-positive signals (**Figure 4.27**). No EdU-positive signals were observed in juvenile *F. hepatica* after treatment with 1 µM Schl-32.028 (Houhou, 2022). The stem cell marker Sm*nanos2* was slightly upregulated in females, suggesting an effect on somatic stem cells. In adult *F. hepatica,* Fh*sodex* was upregulated 4-fold, whereas the expression of Fh*sod* and Fh*aldh1* was not induced after 72 h treatment with 20 µM Schl-32.028. Induction of oxidative stress was observed in both flukes, but neither in *S. mansoni* nor in *F. hepatica* was Sm*aldh1* upregulated. On the contrary, Sm*aldh1* was downregulated in *S. mansoni*. As described by Huang *et al.* (2021), expression of the micro RNAs miR-15b-5p and miR-16-5p was induced in HCT116 and LoVo cells, binding to the 3'UTR of Aldh1A3 inducing gene silencing via the RISC complex after CuET treatment. In addition, DSF and CuET have been shown to downregulate the expression of HsAldhs in a dose-dependent manner (Jia *et al.*, 2019; Liu *et al.*, 2016); Mittal *et al.*, 2014.

A gene expression analysis was not performed through the high impacts on vitality with already low doses of DSF/Cu and CuET. It might be possible that Schl-32.028

regulates the expression of Sm*aldh1* in a similar way compared to DSF or CuET. For further analysis to what extend oxidative stress was induced, the formation of ROS (such as H_2O_2) should be measured and western blot analysis should be performed to determine the expression of enzymes associated with oxidative stress. To get a better insight into the regulation of genes, a microarray analysis should be performed. Here, many genes are analyzed simultaneously, in contrast to the smaller number of genes that can be analyzed in a qRT-PCR run.

5.2.3 Is Schl-32.028 a drug candidate?

The uptake of Schl-32.028 was studied as fluorescently-labeled compound Schl-37.066 in adult *S. mansoni* and *F. hepatica* (Gallinger, 2022). The accumulation in esophagus, gut, muscles, and tegument proposed an efficient uptake of the substance in *S. mansoni* with a broad distribution in different organs. The mechanism by which Schl-32.028 works is unknown, but it might be due to the formation of adducts or altered transcript regulation, as observed with DSF and its metabolites (Cao *et al.*, 2022; Erve *et al.*, 2000; Huang *et al.*, 2021; Mittal *et al.*, 2014; Shen *et al.*, 2001; Tonkin *et al.*, 2000), leading to apoptosis and subsequent cell death. It is not known, if Schl-32.028 undergoes metabolization in *S. mansoni*. As for DSF, metabolization enhances its anti-tumor properties (Allensworth *et al.*, 2015; Cao *et al.*, 2022; Park *et al.*, 2018) and, as shown by this study, the anti-schistosomal effects.

In addition, the company MERCK determined solubility, microsomal clearance, and human ether-à-go-go-related gene (hERG) inhibition parameters (Gallinger, 2022). A good solubility was determined (128 µM), which was confirmed using the compound for *S. mansoni in vitro* experiments. The value for microsomal clearance was low, indicating a slow degradation of the compound *in vivo* resulting in a slow loss of efficacy. To test the capacity of a drug to inhibit hERG is important since it is a cardiac potassium channel (Garrido *et al.*, 2020), Schl-32.028 showed no inhibition. Since Schl-32.028 had a promising toxicity profile, the compound was tested in a mouse *in vivo* infection model by the group of Prof. J. Keiser (Swiss Tropical and Public Health Institute, Allschwil, Switzerland). Here, administration of 3x 50 mg kg^{-1} per 24 h showed moderate activity with a reduction in worm burden of about 48 %, while 100 mg kg^{-1} were toxic leading to the death of some mice (Gallinger, 2022). Because Schl-32.028 was the most promising candidate among the dithiocarbamate-derived compounds synthesized by Mäder (2016),

Gallinger (2022) concluded that there was no further potential for optimization of this class of derivatives. Nevertheless, Schl-32.028 showed potential against *S. mansoni*, but unfortunately, as with many other substances, the path to an official drug ended before it could be completed.

5.3 Basic analysis of the selected genes as a starting point for follow-up characterizations

Before any characterizations could be made, basic analyses of the selected genes had to be performed. Therefore, the selected sequences of Sm*aldh1*, Sm*aldh2*, Sm*abl1*, Sm*abl2*, and Sm*tk6* were compared with the published sequences of the Puerto Rican *S. mansoni* strain (Berriman *et al.*, 2009) and primers were designed for cloning and subsequent validation of the sequences. The next step was the analysis of protein structures, including phylogenetic analyses for SmAldh1 and SmAldh2, and prediction of possible PTMs (acetylation, myristoylation, palmitoylation, and phosphorylation). After these basic analyses, the selected sequences were cloned into two *E. coli* strains (pLysS and LOBSTR-RIL) and into HEK293-6E (EBNA1) cells with the aim of protein expression. Since SmAldh1 was produced in sufficient amounts, an assay of enzyme activity was performed.

5.3.1 Structural analysis of two putative SmAldhs proved their affiliation with the Aldh family

At the beginning, the schistosomal *aldh* sequences found online on WormBase ParaSite and NCBI nucleotide were compared. While the Sm*aldh1* sequence from WormBase ParaSite differed at nt120 (G $\rightarrow$ T), resulting in a synonymous aa when compared with the NCBI sequence (**Table 4.1**), the sequences of Sm*aldh2* were identical from both online sources. To verify the schistosomal *aldh* sequences, recombinant plasmids pET30a-Sm*aldh1* and pET30a-Sm*aldh2*, provided by a former group member (A. Blohm), were sequenced. Analysis of the results revealed 100 % sequence identities with the WormBase ParaSite sequences. With these verified sequences, protein domain

analysis, multiple alignment, and phylogenetic tree analysis were performed to analyze the affiliation of the two schistosomal Aldh sequences.

Domain analysis of both SmAldhs using the CDD revealed the presence of the Aldh domain. Within this domain, catalytic residues and NAD(P)-binding sites were localized. For proper function, the correct positioning of NAD^+ is important. Moore *et al.* (1998) showed that positioning of NAD^+ in Aldh1 of sheep and Aldh2 of cattle is mediated by the same aas but by different mechanisms. For SmAldh1 and SmAldh2, the $NAD(P)^+$-binding site was found to be highly conserved ($> 80\%$ in comparison with 9 additional Aldh sequences) (**Figure 4.30**). Furthermore, the catalytic active Cys302 (HsAldh2 numeration) is essential for binding the aldehyde and for transfer of the hydride to NAD^+ (Moore *et al.*, 1998; Steinmetz *et al.*, 1997). The catalytically important aas were also found to be 100% conserved among the schistosomal and other Aldh sequences.

When both schistosomal Aldh sequences were compared based on their respective sequence identities (**Table A.3**, see appendix), SmAldh1 shared identities between 54 and 55% with HsAldh1 and HsAldh2, whereas SmAldh2 shared the highest similarity with HsAldh2 (66%). However, it should be noted that the matrix values only reflect the percentage of identical aa, but do not take into account the percentage of aa with strongly similar properties.

To gain a deeper insight into the affiliation of the SmAldhs, a phylogenetic tree analysis was performed with Aldh1 and Aldh2 sequences from vertebrate and invertebrate species. Evaluation of evolutionary analysis revealed that Smp_312440 (SmAldh1) clustered with other Aldh1 members, whereas Smp_022960 (SmAldh2) clustered within Aldh2 members of other species (**Figure 4.31**).

5.3.2 Prediction of PTMs revealed possible functions and localizations for the selected enzymes

Prior to protein expression, a prediction for selected PTMs (acetylation, myristoylation, palmitoylation, and phosphorylation) of the selected proteins was carried out to gain insight into possible activation mechanisms and localizations in the cell (**Table 4.5**). *S. mansoni* is capable of post-translationally modifying proteins with a wide range of modifications (Costa *et al.*, 2015; De Moraes Maciel *et al.*, 2008; Fu *et al.*, 2004; Hirst *et al.*, 2020; Osman *et al.*, 1999; Pereira *et al.*, 2011, 2012, 2013; Roger *et al.*,

2008; Smit *et al.*, 2015). PTMs regulate apoptosis, cellular growth, signal transduction, protein interaction, protein translocation, as well as enzyme activation/silencing (Duan and Walther, 2015; Resh, 2006; Seet *et al.*, 2006; Venne *et al.*, 2014; Vu *et al.*, 2018). When the selected genes were analyzed for their predicted PTMs, SmAldh1, SmAbl2 and SmTK6 were predicted to get acetylated, the SmAbl kinases myristoylated and all enzymes were predicted to get palmitoylated and phosphorylated (**Table 4.5**).

Acetylation of Lys was associated with the modifications of histones and the regulation of gene expression (Allfrey *et al.*, 1964; Braunstein *et al.*, 1993; Loidl, 1994). But acetylation of enzymes is also important for cell metabolism (Zhao *et al.*, 2010), enzyme activity (Xue *et al.*, 2012; Zhao *et al.*, 2014), protein stabilization (Fan *et al.*, 2022; Ito *et al.*, 2001) or cell fate (Caslini *et al.*, 2019; Ito *et al.*, 2001). The tumor suppressor p53 gets acetylated and stabilized upon exposure of UV-B radiation, oxidative stress (H_2O_2 treatment) and blocking of nuclear export by leptomycin B (Ito *et al.*, 2001). In terms of enzyme activation, Zhao *et al.* (2014) determined decreasing activity for HsAldh1A1 with an acetylated K363 to 50 % of the wild type enzyme, while the activity was partly reconstituted after deacetylation mediated by NAD^+-dependent sirtuin deacetylase 3 (Sirt3). In contrast, HsAldh2 was found to be activated upon hyper-acetylation caused by ethanol treatment of human aortic endothelial cells and inactivated by Sirt3-mediated deacetylation (Xue *et al.*, 2012). Acetylation of a c-Abl kinase regulates its localization from the nucleus to the cytoplasm without altering the activity (Di Bari *et al.*, 2006). It may be that SmAldh1 activity is similarly regulated by acetylation, whereas SmAbl1 and SmTK6 may migrate to the cytoplasm instead.

Next, myristoylation of the proteins was predicted. Myristoylation is the process of irreversibly transferring a myristate (C14:0) to the N-terminus of proteins mediated by the myristoyl CoA:protein N-myristoyl transferase (Cross *et al.*, 1984; Henderson *et al.*, 1983; Kamps *et al.*, 1985; Marchildon *et al.*, 1984; Towler *et al.*, 1987) and occurs during protein synthesis after the initial cleavage of Met1 (Buss *et al.*, 1984; Olson and Spizz, 1986). When Kamps *et al.* (1985) changed the transforming gene, the tyrosine-specific protein kinase (p60Src), of Rous sarcoma virus via point mutations, less p60Src was bound to membranes and the transforming ability was lost, while the intrinsic kinase activity of non-myristoylated p60Src was unaffected in comparison to the wild type p60Src. Similar observations were made, when parts of the N-terminus of p60Src were deleted and the respective proteins screened for their ability to attach to membranes (Cross *et al.*, 1984) showing that the myristoylation site is harbored N-

terminally and myristate gets linked to Gly2 (Goddard *et al.*, 1989; Towler and Glaser, 1986; Towler *et al.*, 1987, 1988). Both SmAbl kinases and SmTK6 each have a Gly2, but the myristoylation motif in SmTK6 is not fully conserved (Beckmann *et al.*, 2011). c-Abl was shown to be myristoylated (Jackson and Baltimore, 1989). Mutational studies on the myristoylation site of c-Abl revealed an overly active enzyme, which localized together with the wild type enzyme mainly in the cytoplasm and to a minor extend in the nucleus, leading to the conclusion that myristate inhibits the c-Abl enzyme and is not necessary for its translocation (Hantschel *et al.*, 2003). Indeed, via crystallization analysis of c-Abl, Hantschel *et al.* (2003) and Nagar *et al.* (2003) were able to reveal the binding of myristate in a hydrophobic pocket of the kinase domain, which adopts a conformation in which the SH2 and SH3 domains remain tightly linked. Therefore, it seems likely that the activity of both SmAbl kinases is also inhibited by this mechanism.

Another fatty acid, palmitic acid (C16:0), was found to be reversibly linked N-terminally through a thioester with Cys3, Cys5, or Cys6 (Jing and Trowbridge, 1987; Rodgers *et al.*, 1994; Rose *et al.*, 1984; Shenoy-Scaria *et al.*, 1993, 1994; Staufenbiel and Lazarides, 1986; Zlatkine *et al.*, 1997) and occurs, in contrast to myristoylation, after protein synthesis (Magee *et al.*, 1987; Olson and Spizz, 1986; Omary and Trowbridge, 1981; Sefton *et al.*, 1982). Palmitoylation was linked to protein interaction (Cao *et al.*, 2016), protein sorting, axonal development, pre-synaptic signaling, G-protein signaling, and ion channel clustering (El-Husseini and Bredt, 2002). It was shown that myristoylation of p60Src and palmitoylation of p21 are required for binding to membranes (Buss *et al.*, 1986; Kamps *et al.*, 1985; Willumsen *et al.*, 1984). In addition, Robbins *et al.* (1995) have shown that myristoylation of Src kinases is a pre-requisite for palmitoylation, and other research groups verified the simultaneous occurrence of myristoylation and palmitoylation on proteins (Buss *et al.*, 1984; Kamps *et al.*, 1985; Milligan *et al.*, 1995; Robbins *et al.*, 1995; Sefton *et al.*, 1982). Upon double acylation, cytosolic proteins were directed to membranes and anchored within one minute (Van't Hof and Resh, 1997). Modification with myristate alone is too weak to bind efficiently to the membrane, while double acylation leads to complete membrane binding (Silvius, 2002).

Src family members are myristoylated and (except Src and BLK) also palmitoylated (Alland *et al.*, 1994; Patwardhan and Resh, 2010; Resh, 1994, 2006). These modifications direct them to the membrane. Furthermore, Src, Fyn, Hck, and Lck kinases have been found in calveolae (Anderson, 1998; Li *et al.*, 1996). Calveolae

are specialized invaginations of the plasma membrane (Anderson, 1993; Rothberg *et al.*, 1992). That SmTK6 is predicted to be palmitoylated but not myristoylated was surprising, as myristoylation was found to be a pre-requisite for Src kinases to become palmitoylated (Buss *et al.*, 1984; Kamps *et al.*, 1985; Milligan *et al.*, 1995; Robbins *et al.*, 1995; Sefton *et al.*, 1982). However, it is unknown if SmTK6 gets myristoylated and/or palmitoylated *in vivo*, but the kinase was associated with the membrane-associated SmVKR1 complex (Beckmann *et al.*, 2011). Both SmAbl kinases were predicted to be dually acylated (**Table 4.5**). This suggests that they might be inhibited by myristoylation, as was shown for HsAbl1b and HsAbl2b. Palmitoylation could promote association with the membrane or mediate further protein interactions. In humans, Abl isoforms 1a and 2a are not acylated by myristate or palmitate, whereas Abl isoforms 1b and 2b have myristoylation sites (Hantschel *et al.*, 2003; Hantschel and Superti-Furga, 2004; Nagar *et al.*, 2003).

In schistosomes, palmitoylation of proteins was verified when cercariae and adult schistosomes were incubated with [^{3}H] palmitate for 3 - 24 h and modified proteins with [^{3}H] palmitate were detected (Pearce *et al.*, 1991; Wiest *et al.*, 1988). Among others, palmitoylated Sm25 (a major antigen of *S. mansoni*) appeared to be anchored in the surface of the tegument (Pearce *et al.*, 1991), whereas Farias *et al.* (2010) detected palmitoylated stomatin-like protein-2 localized in mitochondria and tegument. Proteins associated to process both acyl modifications were found in the genome of *S. mansoni*. When searching the *S. mansoni* gene expression atlas, a N-myristoyl transferase (Smp_121420) and several palmitoyl transferases were found. Therefore, acylation of proteins with palmitic acid is feasible, while acylation with myristate seems possible but needs to be validated experimentally.

That both SmAbl kinases and SmTK6 may be phosphorylated has already been assumed based on their property as kinases (Brasher and Van Etten, 2000; Dorey *et al.*, 2001; Hunter, 1995; Neet and Hunter, 1996). Domain analysis of both enzymes revealed the presence of one SH2, SH3, and kinase domain, respectively (**Figure 4.29**). Phylogenetic analysis performed by Beckmann *et al.* (2011) revealed the membership in the Abl family, with SmTK6 being a hybrid of Src/Abl kinases. Approximately 1.9 % of the schistosome proteome is composed of eukaryotic protein kinases that phosphorylate proteins, with Hirst *et al.* (2020) noting a phosphorylation bias toward female worm proteins. Activation of mitochondrial HsAldh2 occurred after phosphorylation by ϵ protein kinase C (ϵPKC) (Nene *et al.*, 2017) and ϵPKC was translocated to mitochondria

after ethanol treatment (Chen *et al.,* 1999). Whether phosphorylation of SmAldhs increases or decreases activity is not known.

The similarities of the predicted PTMs compared with their human counterparts raise the possibility that the enzymes may be regulated by the same mechanisms. The extent of the influence of PTMs on recombinantly expressed schistosomal enzymes is still largely unknown and provides a broad area for exploration. Nevertheless, further analysis of the influence of PTMs on the selected enzymes is not an objective of this work. However, it is noteworthy that similar enzymes are differentially affected by the same PTM (as previously discussed for activation or inhibition of HsAldh1A1 and HsAldh2 by acetylation).

5.3.3 Selection of *E. coli* over HEK293-6E (EBNA1) cells as protein expression system due to easier handling and faster protein over-expression

The next step after verification of the sequences, was the selection of a protein expression system. As prokaryotic expression system, *E. coli* strains pLysS and LOBSTR-RIL were chosen, while HEK293-6E (EBNA1) cells were available at the lab of a collaboration partner (research group of Prof. F. H. Falcone, Justus-Liebig-University Giessen) as eukaryotic expression system. To name the advantages of *E. coli*: the genome of *E. coli* is well studied (Jeong *et al.,* 2009, 2015; Kim *et al.,* 2017; Yoon *et al.,* 2009, 2012), and meanwhile a lot of strains are available for specific needs during protein expression such as expression of membrane proteins (Wagner *et al.,* 2008), folding of disulfide bonds in proteins (Lobstein *et al.,* 2012), reduction of basal expression, codon bias correction (Jia and Jeon, 2016). The culture of bacteria is easy and media can be enriched with inexpensive components, and *E. coli* is easy to transform with plasmids and fast growing under optimal conditions (Clark and Maaløe, 1967; Pope and Kent, 1996). Besides these advantages, *E. coli* often fails to express the preferred protein (Büssow *et al.,* 2005; Langlais *et al.,* 2007; Pacheco *et al.,* 2012) or forms inclusion bodies (Gräslund *et al.,* 2008; Strandberg and Enfors, 1991; Williams *et al.,* 1982). It is possible to recover protein from inclusion bodies, but the experimental procedure must be carefully tested and may still end in low yield and inactive protein forms (Burgess, 1996, 2009; Singh *et al.,* 2015). Despite the fact that some *E. coli* strains (K12)

were shown to modify proteins post-translationally (acetylation, acylation, carboxylation, glutamylation, phosphorylation, sulfation) (Brown *et al.,* 2017a; Huang *et al.,* 2017; Macek *et al.,* 2008; Sun *et al.,* 2003; Thao *et al.,* 2010; Tu *et al.,* 2015; Xu *et al.,* 2018), these modifications are only a fraction of what eukaryotic cells are capable of modifying.

In contrast, HEK293-6E (EBNA1) cells are efficient in carboxylation, N-glycosylation, lipidation, phosphorylation, and sulfation (Berkner, 1993; Croset *et al.,* 2012; Østergaard *et al.,* 2021; Peters *et al.,* 2013; Sandwall *et al.,* 2009). HEK293-6E (EBNA1) cells can be grown in serum-free medium, can be easily manipulated and used for transient and stable production of recombinant proteins (Loignon *et al.,* 2008; Meissner *et al.,* 2001; Thomas and Smart, 2005). A disadvantage is the longer culture time, which leads to a higher risk of potential contamination.

To determine the specific codon usage of the selected genes in the two available expression systems, the graphical codon usage analyzer was used. Analysis revealed that the codons CTA and TTA, both coding for Leu, were used least frequently in both expression systems (CTA < 16 % in *E. coli,* CTA and TTA < 20 % in HEK293-6E (EBNA1) cells) (**Table 4.6**).

To sum this section up, schistosomal proteins expressed in *E. coli* lack typical PTMs. It is not known if the selected enzymes are post-translationally modified in *S. mansoni* and if, to which extent, but bioinformatical predictions suggested a variety of PTMs. It is noteworthy that similar enzymes are influenced differently by the same PTM (as discussed before for the activation or inhibition of human Aldh). Analysis of the specific codon usages in *E. coli* and HEK293-6E (EBNA1) cells revealed a lower number of codon restrictions and lower frequency for only one Leu-coding codon (CTA) in *E. coli.* Due to the lower restrictive codon usage, the easier handling and faster growth, *E. coli* was chosen as the primary expression system for the selected target genes.

5.4 Cloning and expression of selected genes

One objective of this work was to characterize the selected proteins. Therefore, the cloned sequences were first confirmed by sequencing. The published *S. mansoni* genome of the Puerto Rican strain (Berriman *et al.,* 2009) was used as a template for the cloning strategy (primer design) of the selected genes of the Liberian strain used in this work.

After sequence verification, the constructs were tested for their expression capacity in the prokaryotic expression system *E. coli* and the eukaryotic expression system HEK293-6E (EBNA1) cells.

5.4.1 Cloning and expression of SmAldh1 and SmAldh2

The cloned constructs of pET30a-Sm*aldh1* and pET30a-Sm*aldh2* were provided by a A. Blohm and used for protein expression in *E. coli* pLysS and *E. coli* LOBSTR-RIL. No protein expression signal was observed for SmAldh1 and SmAldh2 when *E. coli* pLysS was used (**Figure 4.36** A). This indicated that the expression of these proteins was strain-dependent. In contrast, SmAldh1 and SmAldh2 were successfully expressed using *E. coli* LOBSTR-RIL (**Figure 4.36** B). This *E. coli* strain possesses additional t-RNA genes coding for Asp, Ile, and Leu. As discussed previously, *E. coli*'s lower probability to use Leu might be a bottleneck for protein synthesis (**Table 4.6**). Although only two to three Leu are required for one molecule of SmAldh1 or SmAldh2, respectively, *E. coli* synthesizes an excessive amount of these proteins. Thus, a deficiency of Leu is likely to inhibit protein expression. It seems that the additional equipment of aas enables *E. coli* LOBSTR-RIL to successfully synthesize the expected proteins in a sufficient amount that is detectable by analysis by SDS-PAGE after induction of protein expression.

In addition, expression of the respective enzymes was confirmed by western blot analysis, which showed an increase of signals at the expected sizes and additional signals after induction. Compared with the pellet fractions, the lysates were relatively pure and showed signals of the expected size for SmAldh2 and SmAldh1 and an additional signal for SmAldh1. Because the lysate represents the crude extract of soluble *E. coli* protein, detection of some additional proteins was expected. Consistent with this, the lysate fractions analyzed by SDS-PAGE showed a variety of protein bands, most of which were subsequently removed by IMAC. Bolanos-Garcia and Davies (2006) analyzed proteins co-purified by IMAC and showed that they cluster into four different categories: stress-responsive proteins, native metal-binding proteins, His-rich proteins and proteins of different binding mechanism. Most of these co-purified proteins were separated from SmAldh1 using imidazole concentrations $\leq 100\,\mu\text{M}$ (**Figure 4.37 A**) and by using the *E. coli* LOBSTR-RIL strain with modified genes for lower co-purification of His-rich proteins (Andersen *et al.*, 2013).

The amount of protein in the lysate fraction of SmAldh2 appeared to be much lower than that of SmAldh1 with an increased protein signal in the pellet fraction. This indicated that SmAldh2 formed insoluble inclusion bodies, which is a well-known disadvantage of protein expression using *E. coli* (Gräslund *et al.*, 2008; Strandberg and Enfors, 1991; Williams *et al.*, 1982). Moreover, *E. coli* sometimes does not express proteins efficiently (Büssow *et al.*, 2005; Langlais *et al.*, 2007; Pacheco *et al.*, 2012), or degrades recombinant proteins depending on where the His-tag is located (C-terminal or N-terminal) (Liobikas *et al.*, 2006). There are protocols for refolding procedures, but they must be carefully tested to restore the structure and catalytic activity of the enzyme (Burgess, 1996, 2009; Singh *et al.*, 2015). Another option to reduce the formation of inclusion bodies might be the co-expression of chaperones to help with proper folding (De Marco *et al.*, 2007; Haacke *et al.*, 2009).

Moreover, solubility of proteins can be increased by fusing them with more soluble proteins such as GST or MBP (Harper and Speicher, 2011; Lebendiker and Danieli, 2011; Liobikas *et al.*, 2006). To test this, SmAldh1 and SmAldh2 were cloned for expression as MBP fusion proteins. Both constructs were successfully expressed (**Figure 4.36 C**). MBP:SmAldh1 was even expressed at higher levels than SmAldh1 alone, whereas MBP:SmAldh2 did not appear to be present in the lysate fraction at higher levels than SmAldh2 alone. Consideration of additional steps for the affinity purification (amylose resin, MBP-tag) and cleavage of MBP with factor Xa, followed by a second round of affinity purification (Ni-NTA resin, His-tag) and SEC, made the use of MBP:SmAldh1 disadvantageous because of longer processing times and a higher probability of protein loss and loss of protein activity. Because SmAldh1 could be expressed in sufficient amounts, it was used to determine its specific activity in an enzyme activity assay.

5.4.2 Cloning and expression of SmAbl1, SmAbl2, and SmTK6

Cloning of the Sm*abl* kinases was challenging because the sequences are relatively long (5,169 bp for Sm*abl1* and 3,927 bp for Sm*abl2*). The first cloning strategy, amplification of the sequences to naturally occurring restriction enzyme sites in the middle of the gene sequences followed by ligation, failed (**Figure 4.32 A** and **B**). PCR reactions did not yield sufficient amounts of amplicons for Sm*abl1*p1 and Sm*abl2*p2. Switching to a different cloning strategy, splitting the sequences into three fragments that were then amplified and joined by recombination-based assembly, was successful because sufficient amplicons were generated (**Figure 4.32 C** and **D**). Cloning of Sm*tk6* (1,698 bp) was performed

according to the latter strategy, with only one PCR fragment joined to a respective plasmid (**Figure 4.34**).

Due to predetermined base composition of the gene sequence to be amplified, the choice in primer design is limited if the full-length sequence is to be amplified. Therefore, sometimes primers have to be designed that do not correspond to the theoretically optimal properties for primer design. The use of sub-optimal primers can lead to less efficient amplifications, while longer PCR products are more difficult to amplify (Rychlik, 1993). Moreover, template integrity is an important factor, templates up to 30 kb can be amplified successfully with a sufficient amount of good quality cDNA (Cheng *et al.*, 1995). In addition, ligation of previously digested PCR fragments can be challenging, as digestion efficiency is difficult to predict when only a few bases are removed to create overhangs. This could be overcome by digesting fragments based on recombinant plasmids amplified in bacteria. However, the amplification process is then less controllable, since in a PCR reaction the accuracy can be adjusted by changing the concentrations of reaction components such as K^+ and Mg^{2+}, dNTPs, template amounts, or by using a high-fidelity polymerase (Barnes, 1992; Batra *et al.*, 2006; Cheng *et al.*, 1995; Joyce and Benkovic, 2004; Yang *et al.*, 2004).

After successful cloning, sequencing confirmed the correctness of the cloned genes. Sm*abl2* showed 100 % identity to the published *S. mansoni* genome of the Puerto Rican strain (Berriman *et al.*, 2009), while Sm*abl1* and Sm*tk6* showed non-synonymous alterations (**Figure 4.33** and **Figure 4.35**).

Next, the cloned full-length constructs (in pET30a+) were used to express SmAbl1, SmAbl2, and SmTK6 in *E. coli* pLysS and *E. coli* LOBSTR-RIL to characterize them in subsequent enzyme assays. As previously noted for SmAldh1 and SmAldh2, when *E. coli* pLysS cells were used, no obvious increase in the intensity of protein bands for SmAbl1 and SmAbl2 of the expected sizes was observed by SDS-PAGE (**Figure 4.38 A**). Analysis of protein expression in *E. coli* LOBSTR-RIL also showed no increase in protein signals of the expected sizes by SDS-PAGE (**Figure 4.38 B**), whereas an increase of non-specific signals was observed for SmAbl1 after western blot analysis.

As no specific protein signals were observed, *E. coli* LOBSTR-RIL cells were examined 2 and 4 h after induction for specific Sm*abl1* and Sm*abl2* transcripts (**Figure 4.39**). Specific Sm*abl1* and Sm*abl2* transcripts covering half of the sequence and the 3' ends, respectively, were detected. High transcript amounts were found for Sm*abl2,* whereas Sm*abl1* transcripts were found in lower amounts, especially Sm*abl1*p1. This observation was explained by less efficient primer binding for amplification of Sm*abl1*p1

as observed during the cloning process (**Figure 4.32 B**).

One explanation why no protein was expressed could be the size of the kinases (SmAbl1: 191 kDa, SmAbl2: 147 kDa). Most *E. coli* proteins are multiples of the size of 14 kDa (n = 1, 2, 3, ...), with high abundances of sizes < 70 kDa (Savageau, 1986). Most *E. coli* proteins are in the range of 25 - 120 kDa, as determined by 2D gel electrophoresis, but signals from proteins up to 500 kDa were also observed by matrix-associated laser desorption/ionization time-of-flight mass spectrometry (Chong *et al.*, 1997). Bhattacharyya *et al.* (2021) successfully expressed spider silk protein up to 150 kDa but also observed truncated versions. Furthermore, expression of a 200 kDa wheat protein was successfully demonstrated (Ouellet *et al.*, 1993). Successful expression of kinases in *E. coli* was demonstrated (Caspers *et al.*, 1994; Dodson, 2017; Haacke *et al.*, 2009; Klein *et al.*, 2005; Sunderhaus *et al.*, 2022). Klein *et al.* (2005) used a co-expression approach to phosphorylate protein kinase B by phosphoinositol-dependent kinase resulting in an active expressed enzyme. Others used the co-expression of chaperones to express kinases (Caspers *et al.*, 1994). There are opposing statements that chaperone co-expression is protein-specific and not a general strategy for all (Gräslund *et al.*, 2008; Haacke *et al.*, 2009; Sunderhaus *et al.*, 2022; Wall and Plückthun, 1995). Co-expression of chaperones was not tested in this work, so this might be an option to express full-length SmAbl kinases. Another option is the co-expression of phosphatases to inhibit kinase activity (Haacke *et al.*, 2009; Seeliger *et al.*, 2005), which phosphorylates *E. coli* proteins and is therefore toxic for its host. Co-expression attempts of YopH with SmAbl1 and SmAbl2 were performed but resulted in no detectable protein after western blot analysis (data not shown). Some proteins are just not expressed by *E. coli* (Büssow *et al.*, 2005; Langlais *et al.*, 2007).

In a next step, expression of truncated protein versions (TKD only) was tested. Signals of expected protein sizes (both TKDs approximately 31 kDa) were detected 2 h after protein induction (**Figure 4.38 C**). Corresponding signals were also observed by western blot. As with SmAldh2, strong signals were detected in the pellet fractions and only weak signals in the lysate fractions. Expression of SmAbl-TKDs finally succeeded, probably because of their smaller size but appeared to be trapped in inclusion bodies. To prevent the formation of inclusion bodies and increase solubility, protein can be fused to affinity tags (GST or MBP) (Harper and Speicher, 2011; Lebendiker and Danieli, 2011; Liobikas *et al.*, 2006). Fusion of c-Abl-TKD to MBP and co-expression of chaperones increased the solubility of the recombinant protein (Xue *et al.*, 2012). This strategy might also work for the expression of SmAbl-TKDs.

To test whether an eukaryotic expression system might be able to express the SmAbl kinases as full-length or yielding higher protein amounts of the truncated versions, respective Sm*abl1* and Sm*abl2* versions were sub-cloned for expression in HEK293-6E (EBNA1) cells. Neither signals of full-length protein nor truncated TKD versions were found when compared to a negative control (transfection of cells without DNA) (**Figure 4.40**). HEK293 cells were shown to successfully express kinases (Fraser *et al.*, 1998; Giraud *et al.*, 2004; Klein *et al.*, 2005; Nettleship *et al.*, 2015). Co-expression of kinase interacting partners as well as Ebola virus protein 35 enhanced the expression of an active kinase complex in HEK-293 cells by 10-fold (Gantke *et al.*, 2013). For expression in HEK293-6E (EBNA1) cells, no co-expression approach with interacting partners was used but might be considered in future expression experiments. Maybe this method yields stably expressed kinases in good amounts.

Increasing signals corresponding to the expected size of SmTK6 were also not observed by SDS-PAGE with either *E. coli* strain. However, western blot analysis showed increasing signals of the expected size from 2 h onward (**Figure 4.41 B**). As with SmAldh2, most of the protein was precipitated as inclusion bodies, as indicated by an intense band in the pellet fraction and a less intense band in the lysate fraction. To address this solubility issue, Sm*tk6* was sub-cloned into pMal-c5X for expression of MBP:SmTK6. Solubility increased slightly compared with SmTK6 alone (**Figure 4.41 C**). To increase soluble protein levels, protein expression conditions may be altered (e.g., lower expression temperature to slow protein expression, lower IPTG concentrations to induce protein expression, different culture media, or different *E. coli* strains overexpressing chaperones), buffers may be changed (e.g., HEPES buffer, pH, or different salt concentrations), or a method to refold misfolded proteins may need to be established.

In summary, *E. coli* LOBSTR-RIL cells already showed expression of the respective enzymes upon SDS-PAGE analysis only for the SmAbl-TKDs. Expression of the full-length SmAbl kinases failed, possibly because of their high MW. Expression of their truncated versions as TKD succeeded in *E. coli* LOBSTR-RIL, but the yield of soluble proteins was low. The assumption of achieving higher protein yields with HEK293-6E (EBNA1) cells was not confirmed, as this expression system could not produce any of the SmAbl versions (full-length or as TKD). Expression of SmTK6 was successful in *E. coli* LOBSTR-RIL, but the amount of soluble protein was low. When MBP:SmTK6 was expressed, the amount of soluble protein appeared to increase slightly. Further efforts

are required to increase the soluble amounts of SmAbl-TKDs and SmTK6, and to express sufficient amounts of protein to perform enzyme assays.

5.5 Bivalent cations enhanced the enzymatic activity of SmAldh1

After structural analysis and successful expression of SmAldh1 in *E. coli* LOBSTR-RIL, analysis for the enzyme's specific activity followed. To this end, together with the group of Prof. P. Czermak, an Aldh activity assay using SmAldh1 derived from either *E. coli* LOBSTR-RIL or BEVS was developed (Harnischfeger, Beutler *et al.*, 2021). The criterion for the setup was the suitability for screening potential inhibitory compounds at high throughput while being cost effective. For this purpose, the assay was optimized to function with as little as 167 nM enzyme and acetaldehyde as favorable substrate. In direct comparison, BEVS-derived SmAldh1 seemed more active than the one derived from *E. coli* LOBSTR-RIL. To optimize the assay conditions, BEVS-derived SmAldh1 was used and found to have 1.3-fold with 0.5 mM $CaCl_2$ and 1.5-fold elevated activity with 0.5 mM $MgCl_2$ (Harnischfeger, Beutler *et al.*, 2021). In this work, the same results were achieved when using *E. coli* LOBSTR-RIL-derived SmAldh1 in combination with 0.5 mM $CaCl_2$ and 0.5 mM $MgCl_2$ (**Figure 4.42**).

In contrast, previous studies with cytosolic Aldh1 from rat, cattle, and horse showed that enzymatic activity was inhibited by the presence of Ca^{2+} and Mg^{2+} *in vitro*, while Aldh2 enzyme activity was elevated (Takahashi *et al.*, 1980; Vallari and Pietruszko, 1984a; Weiner and Takahashi, 1983). The existence of several conformational states and relative mobility of the co-factor NAD^+/NADH was demonstrated previously (Gonnella *et al.*, 2011; Hammen *et al.*, 2002; Moretti *et al.*, 2016; Perez-Miller and Hurley, 2003) and shown to be important when bound to HsAldh2 (Hammen *et al.*, 2002; Perez-Miller and Hurley, 2003): dependent on the conformation, the nicotinamide ring is in close proximity to Cys302 for hydride transfer (hydride transfer conformation) or the nicotinamide ribose turned by 80 ° to allow Glu286 to act as general base for deacylation of the enzyme-substrate adduct (hydrolysis conformation). Mg^{2+} and other metals were co-crystallized located at the phosphate oxygen of the co-factor (Morgan and Hurley, 2015; Steinmetz *et al.*, 1997). In presence of Mg^{2+}, the co-factor favored the hydrolysis conformation (Hammen *et al.*, 2002).

To further resolve the mechanism of co-factor binding and stabilization, crystal-

lization attempts of wildtype HsAldh2 and a Ser302 mutant, in combination with the oxidized and reduced co-factor (NAD^+/NADH) as well as in the absence or presence of Mg^{2+} were conducted by Perez-Miller and Hurley (2003). When they compared oxidized and reduced co-factors complexed with a Ser302 mutant protein, they found NAD^+ in the hydride transfer position and NADH in the hydrolysis position. Crystallization of enzyme and co-factor with and without Mg^{2+} revealed increased mobility of NAD^+ in the absence of Mg^{2+}, whereas high Mg^{2+} concentrations (10 mM) stabilized the conformations (Perez-Miller and Hurley, 2003). Addition of Mg^{2+} appears to increase the rate of deacylation (the rate-determining step for Aldh2) due to isomerization of the cofactor toward the hydrolysis position thus accelerating the kinetics, but to decrease the rate of NADH release (rate-determining step for Aldh1) by causing tighter binding of NADH to the enzyme, which has an inhibitory effect on Aldh1 (Gonnella *et al.*, 2011; Ho *et al.*, 2005; Vallari and Pietruszko, 1984a, 1984b). The amount of free Mg^{2+} in mitochondria was determined to be 0.4 mM by Corkey *et al.* (1986), which coincides with the activation of Aldh2 in the presence of Mg^{2+} (Takahashi *et al.*, 1980; Vallari and Pietruszko, 1984a; Weiner and Takahashi, 1983).

Despite studies showing the contrary effect of the influence of divalent ions on Aldh activity, the Mg^{2+}-stimulated increase of enzyme activity of SmAldh1, gives this schistosomal enzyme a unique position with characteristics of both, Aldh1 and Aldh2 (**Table A.3**, see appendix): higher structural similarities to the Aldh1 class (**Figure 4.31**) and at the same time enzymatic activation by Ca^{2+} and Mg^{2+}, which is typical for members of Aldh2 (**Figure 4.42**). Further studies are needed to unravel the enzymatic mysteries of SmAldh1.

For further characterizing of SmAldh1, substrate specificity should be determined. Substrates should be selected according to the family member's affiliation and their respective substrate preferences (Ambroziak and Pietruszko, 1991; Riveros-Rosas *et al.*, 2013; Yoshida *et al.*, 1992). Studies by Ambroziak and Pietruszko (1991) showed that HsAldh1 and HsAldh2 were active with all-*trans* and 13-*cis* retinal, and acetaldehyde, whereas the affinity for acetaldehyde was 50-fold higher for HsAldh2 than HsAldh1. In contrast, Yoshida *et al.* (1992) found HsAldh1 being active with all-*trans* retinal, whereas HsAldh2 was not but showing a 10-fold higher affinity for acetaldehyde compared to HsAldh1. Moreover, Moretti *et al.* (2016) determined a 258-fold decreased Km for all-*trans* retinal compared to acetaldehyde when HsAldh1A3 was assayed. Crystallization studies of sheep Aldh1 in comparison to the bovine Aldh2 crystal structure explained the substrate specificity for sheep Aldh1 towards retinal as bulky substrate for a relatively

big substrate tunnel (solvent-accessible volume of the tunnel: $150\,\text{Å}^3$), whereas bovine Aldh2 displayed a narrow substrate tunnel of $20\,\text{Å}^3$ solvent-accessible volume, appropriate for acetaldehyde (Moore *et al.*, 1998). Therefore, the use of all-*trans* retinal as an alternative substrate should provide a deeper insight into the biochemical substrate preference of SmAldh1. A conclusive statement can be made when crystal structures with acetaldehyde or all-*trans* retinal in combination with Ca^{2+} or Mg^{2+} are available.

5.6 Characterization of alternative drug targets for approved drugs

A good drug target should have the following characteristics (Gashaw *et al.*, 2011; Gilbert, 2014):

1) it essentially modifies a disease or has an established role in the pathophysiology of a disease

2) it should have a druggable active site, and the effects should be monitorable (e.g., by biomarkers)

3) it is easily testable and allows high-throughput screening

4) it has no competitors on the target itself

5) side effects should be reduced and predictable, e.g., by knock-out data

6) resistance potential should be low

The target might also alter gene expression or regulatory factors to exert its effects (Rang and Hill, 2013). Ideally, the target in parasites is specific to the organism and should play an important role in maintaining its viability. Therefore, metabolically and structurally active enzymes, enzymes involved in stress responses or signal transduction, became the focus of interest (Bernhardt *et al.*, 2009; Davies *et al.*, 2020; Doerig *et al.*, 2002; Gelmedin *et al.*, 2015; Hitz *et al.*, 2021; Maurya and Namdeo, 2021; Santi and Murta, 2022; Tyagi *et al.*, 2019; Wu *et al.*, 2021). In the following sections, the potential of two Aldhs and three cytosolic kinases as drug targets will be discussed.

To analyze the importance and potential functions of the selected genes in *S. mansoni*, RNAi approaches were performed to knock down Sm*aldh1*, Sm*aldh2*, Sm*abl1*, Sm*abl2*, and Sm*tk6*, as well as both Sm*aldh* and Sm*abl* kinases simultaneously using $2.5\,\mu\text{g}\,\text{ml}^{-1}$ or $12.5\,\mu\text{g}\,\text{ml}^{-1}$ of the respective dsRNA for a duration of 14 and 21 d. During these

experiments, worms were examined every 3 d for their pairing status (number of couples), ability to attach to petri dishes, motility, and oviposition. At the end of each experiment, worms were examined for their cell proliferation ability and possible morphological changes using CLSM. In addition, qRT-PCR analyses of selected, putative oxidative stress-responsive genes (Sm*aldh1*, Sm*aldh2*, Sm*ar*, Sm*gpx*, Sm*sod*, and Sm*sodex*), cell cycle regulatory genes (Sm*npl4* and Sm*p53*), apoptosis-associated genes (Sm*bax* and Sm*bcl-2*), and stem cell-associated genes (Sm*nanos1* and Sm*nanos2*) were performed. In addition, the distribution of Sm*aldh1* and Sm*aldh2* transcripts in adult *S. mansoni* was analyzed by WISH. To investigate whether Sm*aldh1* or Sm*aldh2* play a role in the response to oxidative stress, each gene was knocked down for a period of 14 d, followed by treatments with fresh dsRNA (to keep gene transcripts low) and H_2O_2 (to induce oxidative stress) for another 3 d.

5.6.1 Analyses of Aldhs as potential drug targets

Sm*aldh1* and Sm*aldh2* showed a broad transcript distribution

Analyses of transcripts in adult *S. mansoni* revealed different expression levels of the respective *aldh* genes, with Sm*aldh1* being a low-abundantly expressed gene, whereas Sm*aldh2* is high-abundantly expressed (**Figure 4.44** and **Figure 4.49**). This is in contrast to the data obtained by RNA-seq analyses, in which Sm*aldh1* showed high expression levels in the following order: bsM > ssM > ssF > bsF and Sm*aldh2* low expression levels with the highest transcript levels in bsF, followed by ssF > ssM > bsM (Lu *et al.*, 2016). When the total soluble protein of *S. mansoni* worms was examined, SmAldh1 accounted for 2.5 % of the total protein analyzed. Moreover, SmAldh2 was also found in the tegument of bsF/M and ssF/M, respectively, with only half the peptide count found for SmAldh1 by LC–MS/MS analysis (Winkelmann *et al.*, 2022). There may be a discrepancy between the transcript abundance and the amount of protein expressed. To test this, western blot analysis should be performed using SmAldh1 and SmAldh2-specific antibodies (which do not yet exist). Nevertheless, expression of the Sm*aldh* genes appeared to be pairing-influenced. In males, a lower transcript abundance of Sm*aldh1* was observed in bsM compared to ssM (**Figure 4.44**). Sm*aldh2* gene expression was always lower in bsF and bsM, respectively, compared to their ss counterparts and showed the highest overall expression in females (**Figure 4.49**).

According to a single-cell transcriptome atlas, Sm*aldh1* is expressed in some clusters of neoblasts, tegument, and neurons of both genders, and additionally in the vitellarium of females (Wendt *et al.*, 2020). In contrast, Sm*aldh2* appeared to be preferentially expressed in the tegument, neurons, and neoblasts in males, whereas higher expression was observed in the vitellarium, parenchyma, and germ stem cells (GSCs) in females (Wendt *et al.*, 2020). These data suggest that both SmAldhs may be primarily involved in stem cell activities and possibly defense mechanisms (within the tegument). In addition, Aldhs appear to be involved in vitellarium developmental processes in females, which could explain the tendency of higher expression in females. Transcript localization of Sm*aldh1* and Sm*aldh2* by WISH (**Figure 4.43**) revealed a broad distribution pattern for both Sm*aldh* gene transcripts. In contrast to the single-cell transcriptome atlas (Wendt *et al.*, 2020), no signals of Sm*aldh1* or Sm*aldh2* were observed in the vitellarium. It is possible that the signal is shadowed by the brown vitellocyte color. In this case, repeating the experiments with a prolonged bleaching step would clarify this issue. Looking at the stage-dependent gene expression analysis (Lu *et al.*, 2018; Lu and Berriman, 2018), it seems likely that the observed results are influenced by the age of the worms used for analysis. Sm*aldh1* gene expression peaked between day 35 and day 38 before decreasing 10-fold in adult males, while expression peaked in juvenile worms (day 28) and then decreased 20-fold until it was almost non-existent in adult females (> day 42). The highest transcript level of Sm*aldh2* was found in miracidia and sporocysts, followed by low expression until the juvenile worm stage with similar expression in adult males and slightly higher expression in adult females. This suggests a role for SmAldhs in developmental processes, as high levels of Sm*aldh* were found in juvenile stages compared with adult stages and in stem cells (Lu *et al.*, 2018; Lu and Berriman, 2018; Wendt *et al.*, 2020).

Knock down efficacy varied between the Sm*aldh* genes

Knock down of Sm*aldh1* was very efficient (> 93 %) with 2.5 µg ml^{-1} Sm*aldh1* dsRNA after 14 and 21 d (**Figure 4.45**). For 12.5 µg ml^{-1} dsRNA, the efficacy was similar. For Sm*aldh2*, knock down was less efficient in females (remaining transcript levels of 61 %) than in males (remaining transcript levels of 21 %) after 14 d of Sm*aldh2* dsRNA treatment (**Figure 4.50**). Knock down efficiency varied after 21 d RNAi treatment, with a downregulation of 80 % in females, whereas it was downregulated by 72 % in males. More dsRNA did not result in better efficacy. RNAi has been successfully applied to

knock down genes in schistosomes (Correnti *et al.,* 2005; Kalinna and Brindley, 2007; Moguel *et al.,* 2015; Skelly *et al.,* 2003) and, as seen with Sm*aldh1*, it can be very efficient. Another way to approach RNAi is the direct use of siRNA instead of dsRNA. But as observed in *S. japonicum*, knock down of two tyrosinase genes with siRNAs resulted in only moderate knock down efficiency (He *et al.,* 2012). Continuous exposure to dsRNA may result in higher efficiencies as observed in pollen beetles (Willow *et al.,* 2021). However, efficacy also depends on the application method. While worms were drenched with dsRNA during culture, there is also the option for electroporation, which can lead to higher RNAi efficiencies. Krautz-Peterson *et al.* (2007) showed by knock down of *cathepsin B* in *S. mansoni* that in their case electroporation was more efficient than soaking and that the efficacy depended on the sequence and amount of siRNAs used. In addition, there are RNAi approaches based on plasmid vectors and retroviral vectors, expressing siRNAs and hairpin RNAs (hpRNAs) (Sliva and Schnierle, 2010). Zhao *et al.* (2008) demonstrated knock down of the *Mago nashi* gene by 81 % after 5 d of electroporation of *S. japonicum* schistosomula with plasmid-based expression of a 19 nt−long siRNA.

Variation of knock down efficiencies may be due to mixtures of worms from different hamsters in each biological replicate, resulting in worms exposed to different host environments, e.g., a host-specific effect on the egg-laying capacity was observed in *S. mansoni* females (El Ridi *et al.,* 1997). Moreover, it was shown that host-specific sera can also modulate schistosomal development and survival (Anisuzzaman *et al.,* 2021). Analysis of the effects of non-specific dsRNA on schistosomula revealed more differences in gene regulation between biological replicates compared to the effect of treatments with non-specific dsRNAs (Gava *et al.,* 2017). A variance of transcript amounts was also found when Buro *et al.* (2013) compared gene expression analyzed by qRT-PCR and microarray. This indicates that in addition to the methodological approach, the biology of each individual has a major impact on the outcome. Additionally, there is no one-size-fits-all strategy for silencing a gene, so the appropriate approach for each gene must be validated individually to maximize RNAi efficacy.

RNAi effects on physiology, morphology, and cell proliferation

Knock down of Sm*aldh1* or Sm*aldh2* alone or simultaneously showed no drastic effects on worm physiology (**Figure 4.46**, **Figure 4.51**, and **Figure 4.55**). Significantly higher numbers of normal and abnormal eggs were observed on the first 9 d of the 14 d treatment,

which was not the case when treatment was extended to 21 d. Female *S. mansoni* lay up to 300 eggs per day (Moore and Sandground, 1956). The observed numbers in the treatment and control groups were in this range before egg numbers decreased after day 9, probably due to the *in vitro* culture environment. Barth *et al.* (1996) examined individual couples for their oviposition in various serum-supplemented media and found a peak in oviposition after 6 d *in vitro* culture, which was also mostly observed during this study. They also observed a serum-dependent effect on the number of eggs laid (Barth *et al.*, 1996). Variation in observed egg numbers may also be due to varying numbers of females laying eggs (El Ridi *et al.*, 1997). The effect of decreasing egg production can be overcome when the medium is supplemented with additives such as bile salts (taurochenodeoxycholic acid and tauroursodeoxycholic acid), red blood cells, low density lipids, and ascorbic acid, as the blood of a host is usually highly nutritious (Badr *et al.*, 1999; Wang *et al.*, 2019). A late effect on oviposition by RNAi cannot be discussed, as egg production decreased with the duration of *in vitro* culture. Since most experiments were started with M199(3+), it was maintained throughout all experiments for better comparability. It seems that both SmAldh enzymes are not directly involved in the maintenance of pairing status, attachment ability, or motility, at least under *in vitro* conditions.

Following Sm*aldh2* knock down, morphological changes in female ovaries were detected after 21 d (**Figure 4.52 E**). This seemed plausible because highest Sm*aldh2* expression was found in bsF ovaries (Lu *et al.*, 2017) and the vitellarium (Wendt *et al.*, 2020). It seemed that the establishment of this phenotype was slow as it was not observed after 14 d, possibly due to insufficient knock down efficacy or compensatory effects of other enzymes (such as SmAldh1). The vitellarium loses its ability to produce vital vitellocytes during *in vitro* culture (Irie *et al.*, 1987; Wang *et al.*, 2019). Nethertheless, when the treatment groups were compared with controls, no visible effect on the vitellarium caused by Sm*aldh* knock down was detected. However, the previously observed female-specific ovary phenotype was not observed following a double knock down approach, leaving the question of the role of Sm*aldh2* in modulating *S. mansoni* reproductive biology unanswered. It was found that HsAldh1 stabilizes mitogen-activated protein kinase kinase-1 (MEK-1) mRNA followed by increased MEK-1 protein expression when non-small cell lung cancer cells (NSCLC) were investigated for their apoptotic potential (Tian *et al.*, 2018). MEK is part of the MEK/extracellular signal-regulated kinase (ERK) signaling pathway and its activation leads to gene expression involved in cell proliferation and apoptosis through a phosphorylation cascade (McCubrey *et al.*,

2007). In NSCLC, stabilization of MEK-1 by Aldh1 led to increased expression of death receptors that promoted apoptosis after TRAIL exposure. The observed ovarian phenotype after Sm*aldh2* RNAi may not necessarily be due to reduced oxidative stress-defense mechanisms as no stressor was applied but might suggest a role of SmAldh2 during stem cell differentiation and cell survival.

To gain further insight into their functions, analyses should be performed to clarify whether apoptotic genes are induced after knock down of Sm*aldh*. Because knock down efficacy varied between approaches and treatment durations, it is unclear whether the lack of effect was due to a reduced knock down efficacy. In addition, it is unclear whether knock down lowered protein concentration and during what time period. Whether Sm*aldh1* or Sm*aldh2* gene products have an effect on the vitality of the vitellarium or the egg-laying capacity should be studied using improved culture conditions as suggested by (Wang *et al.*, 2019). Aldh enzymes also catalyze the oxidation of retinaldehyde to RA (Duester, 2000; Huang *et al.*, 2009; Tomita *et al.*, 2016), which is involved in developmental processes (Kam *et al.*, 2012). Therefore, an additional approach to elucidate the roles of SmAldh1 and SmAldh2 proteins is to knock down the corresponding genes in schistosomula to observe the effects on their development.

No effect on the proliferative capacity of stem cells was observed for a single or double Sm*aldh* knock down (**Figure 4.48**, **Figure 4.53**, and **Figure 4.57**). As discussed before, Sm*aldh1* and Sm*aldh2* transcripts have been found in neoblasts and GSC (Wendt *et al.*, 2020). It was therefore assumed that they play a role in maintaining stemness or influence cells with stem cell characteristics. High Aldh expression was linked to normal and cancer stem cells, while HsAldh1A1 was specifically proposed as a marker for tissues normally expressing low Aldh1A1 levels (Douville *et al.*, 2009; Huang *et al.*, 2009; Tomita *et al.*, 2016). Several Aldhs metabolize retinaldehyde to RA (Huang *et al.*, 2009; Tomita *et al.*, 2016). RA regulates cell differentiation, proliferation, and apoptosis through interactions with retinoic acid receptors (RAR), retinoid x receptors (RXR), and estrogen receptor α (ERα) and subsequently retinoic acid response elements. Expression of c-Myc and Cyclin D1 is induced by the interaction of RA with ERα and RARα, leading to an anti-apoptotic pathway and cell proliferation (including tumor growth). In contrast, interaction of RA with RXR and RARα leads to induction and expression of RARβ, resulting in differentiation, growth inhibition, and induction of apoptotic pathways (Tomita *et al.*, 2016). No estrogen receptor homolog was annotated yet in the schistosome genome. But it cannot be excluded that homologs are present. That knocking down Sm*aldh1* and Sm*aldh2* had no effects on GSC of *S. mansoni* suggests

that both SmAldhs may not be the important factor in maintaining cells' proliferative activity.

Influence of Sm*aldh* RNAi on putative oxidative stress genes

To analyze whether knock down of Sm*aldh1* or Sm*aldh2* has effects on putative oxidative stress genes, transcription of Sm*aldh1*, Sm*aldh2*, Sm*ar*, Sm*gpx*, Sm*sod*, and Sm*sodex* was examined. Upregulation of Sm*aldh2* was observed in males after Sm*aldh1* was knocked down for 14 and 21 d. When Sm*aldh2* was knocked down, up to 2.5-fold upregulation of Sm*aldh1* was observed in females after 14 d but not after 21 d. It seems that the other Aldh may exert transient compensatory effects in different organs of females and males. According to these results, Sm*aldh1* seems to play a more important role in males, whereas Sm*aldh2* seems to be more important for biological functions of females. During the single knock down approaches, Sm*gpx* and Sm*sod* gene transcripts were slightly upregulated after 14 d but not after 21 d or after double knock down. This observation might have been only a temporary effect or due to biological variance (Gava *et al.*, 2017), where some worms experienced oxidative stress.

Possible roles of Sm*aldh1* and Sm*aldh2* after RNAi and induction of oxidative stress by H$_2$O$_2$

To elucidate whether SmAldh1 and SmAldh2 may play a role in detoxification processes after oxidative stress in *S. mansoni*, Sm*aldh1* and Sm*aldh2* were knocked down for 14 d. Subsequently, couples were treated daily with 150 µM H$_2$O$_2$ for further 3 d. Worms of all groups showed some degeneration in the anterior part in both genders and between head and ventral suckers of females (**Figure 4.79**). Knock down of Sm*aldh1* followed by treatment with H$_2$O$_2$ resulted only in a decrease in the attachment ability and motility observed at the last day of the experiment, whereas no effects on physiological parameters were observed for Sm*aldh2* RNAi (**Figure 4.78**). Because the control worms also exhibited degeneration during the observation period, no knock down-specific phenotype was detected. Transcript level analysis showed that both knock down efficiencies were as good as previously observed, and oxidative stress-associated gene transcripts increased only in males after Sm*aldh1* RNAi (**Figure 4.80**). Assuming

that knock down at the protein level was equally efficient, these results suggest that males are more susceptible to oxidative stress than females (as long as they are a couple), perhaps because they protect the female in the gynaecophoric canal from environmental influences. In addition, it seemed that a higher oxidative stress response was triggered after previous Sm*aldh1* knock down, suggesting a more important role of Sm*aldh1* than Sm*aldh2* in the oxidative stress response. Jean *et al.* (2011) found that human myoblasts (which express Aldh1A1 almost exclusively) were more susceptible to H_2O_2 treatment when cells were incubated with N,N-diethylaminobenzaldehyde (DEAB; an Aldh inhibitor). When unpaired female and male *S. mansoni* were separately exposed to 100 µM H_2O_2 for 4 h, Sm*aldh1*, Sm*gpx*, and f-Sm*sodex* were found upregulated by up to 5-fold (Aragon *et al.,* 2008). In a preliminary experiment, upregulation of Sm*aldh1* was observed after treatment of *S. mansoni* couples with 150 µM H_2O_2 after 3 d (**Figure 4.77**). Upregulation of each of the other Sm*aldh* was not observed in this experiment, suggesting that either sufficient detoxifying proteins were present or the oxidative stress stimulus was not sufficient to induce gene expression. Degeneration appeared to occur only in certain parts of the worm body. It is possible that these parts are more sensitive, or at least more exposed, because there is no surrounding tissue in the anterior part (the end of the worm body). In contrast, when couples of the Luis Evangelista *S. mansoni* strain were exposed to H_2O_2, no tegument changes were observed below 800 µM H_2O_2 after 24 h (De Paula *et al.,* 2014). Because the control showed the same degeneration phenotype in the experiments presented here, the role of Sm*aldh1* and Sm*aldh2* in the response of *S. mansoni* to oxidative stress remains unclear, although there is an indication that SmAldh1 appears to be more important. It cannot be excluded that the functions are compensated by the presence of other SmAldh enzymes in *S. mansoni*. Meanwhile, there are 10 putative Sm*aldh* genes listed at WormBase ParaSite (based on gv9) transcribing 11 enzyme variants. These putative Sm*aldh* genes are listed in **Table A.2** (see appendix).

Cancer stem cells and Hodgkin lymphoma cells (both exert high Aldh expression) have been linked to possess lower ROS levels through higher expression of antioxidant enzymes (Ikeda *et al.,* 2012; Mizuno *et al.,* 2015). On one hand, elevated ROS levels induce apoptosis (Simon *et al.,* 2000; Su *et al.,* 2019), while on the other hand, ROS at low levels promote cell growth and survival (Day and Suzuki, 2006; Finkel, 2011; Groeger *et al.,* 2009). Additionally, Aldh1A1 expression has been associated to increased human myoblast survival after H_2O_2 exposure by prevention of Caspase3/7-mediated apoptosis (Jean *et al.,* 2011). The degeneration phenotype might be explained by low Sm*aldh* expression, although it is not enhanced after Sm*aldh* knock down. One

option to analyze the role in oxidative stress defense would be the induction of Sm*aldhs* by the Aldh activator Alda-1 (Belmont-Díaz *et al.*, 2016; Kotraiah *et al.*, 2012; Li *et al.*, 2018a) before induction of oxidative stress (e.g., by direct H_2O_2 application or supplementation of glucose oxidase, which constantly generates H_2O_2). Analysis should include tegument structure, possible morphological changes of gonads, and proliferative capacity of stem cells should be analyzed (in case of previous SmAldh knock down and induction of oxidative stress and in case of previous application of Alda-1 before induction of oxidative stress). In addition, changes in gene transcription should be analyzed by microarrays instead of qRT-PCRs. Because of the amount of genes analyzed simultaneously, a better conclusion can be made about the role of the two SmAldhs.

Are SmAldh1 and SmAldh2 good drug targets?

According to Crowther *et al.* (2010), no Aldh was ranked as possible good drug target in *S. mansoni* as resulted by *in silico* analyses, whereas they were for *T. brucei* (rank 25). No changes in physiology, morphology, or cell proliferation were observed when Sm*aldh1* was knocked down. Only when Sm*aldh2* was knocked down for 21 d, alterations in the ovary structures were observed, which did not occur after a double knock down. It is not known whether knock down was as efficient at the protein level as at the transcriptional level. This needs to be analyzed by western blot in future studies. Therefore, a final conclusion on the suitability of SmAldhs cannot yet be drawn.

In the case of good knock down efficacy at the protein level, knocking down both SmAldhs does not appear to have a significant effect on *S. mansoni*. The analyzed SmAldhs as such do not seem to be a suitable sole target, and combination treatment with other targets is suggested (Gouveia *et al.*, 2018). In cancer cells, high Aldh activity indicates chemotherapeutic resistance, and its inhibition leads to restoration of sensitivity to chemotherapeutic agents in resistant cancer cells (Cortes-Dericks *et al.*, 2014; Croker and Allan, 2012; Darooee *et al.*, 2021; Moreb *et al.*, 2000). In *Plasmodium berghei*- or *P. vinckei petteri*-infected mice, concomitant treatment of chloroquine and other drugs known to reduce cellular glutathione levels (acetaminophen, DSF) potentiated the effects of sub-curative chloroquine doses (Deharo *et al.*, 2003). DSF has shown tremendous effects on adult schistosomes but does not seem to solely inhibit SmAldhs. Further confirmed DSF targets are bovine Cu/Zn-SOD, bovine dopamine-β-hydroxylase, rat monoamine oxidase, human DNA topoisomerase, human phosphoinositide 3-kinase, *Cryptosporidium* inosine 5-monophosphate dehydrogenase, rat and human GST, human

NPL4, and *Giardia* triosephosphate isomerase (Castillo-Villanueva *et al.,* 2017; Cocco *et al.,* 1981; Goldstein *et al.,* 1964; Ploemen *et al.,* 1996; Sarwono *et al.,* 2018; Schurr *et al.,* 1978; Skrott *et al.,* 2017; Yakisich *et al.,* 2001; Zhang *et al.,* 2010).

Both SmAldh enzymes are highly conserved, as revealed by alignment analysis (**Figure 4.30** and **Table A.3**, see appendix). Neither Sm*aldh* is pathogen-specific, as the number of *aldh* genes is generally highly variable and conserved among archaea, prokaryotes, and eukaryotes (Jackson *et al.,* 2011; Sophos and Vasiliou, 2003). The bacterium *Pseudomonas pseudo-alcaligenes* harbors 49 *aldh* genes (Riveros-Rosas *et al.,* 2019), the plant model organism *A. thaliana* harbors 16 *aldh* genes (Tola *et al.,* 2020), soybean (*Glycine max*) harbors 53 *aldh* genes (Tola *et al.,* 2020), *C. elegans* harbors 13 *aldh* genes (Singh *et al.,* 2013), and humans harbor 19 *aldh* genes (Black *et al.,* 2009). They are considerably important enzymes, as suggested by the high redundancy of genes and their protective roles due to the detoxification of reactive aldehydes resulting from oxidative stress (Choudhary *et al.,* 2005; Marchitti *et al.,* 2008; Singh *et al.,* 2013).

SmAldhs do have druggable target sites, and SmAldh1 was used in an enzyme activity assay, which can be used in future studies to analyze further compounds for their inhibiting potential. Side effects caused by inhibition of Aldhs were tolerable in humans, as demonstrated by DSF treatment of recovering alcoholics. Therefore, treatments targeting SmAldhs in schistosomiasis seem feasible, but of course need to be validated.

Aldhs are involved in the response to oxidative stress, and inhibition of the oxidative defense system renders *S. mansoni* susceptible to host defense mechanisms. Because knock down of both SmAldhs appeared to have little effect on H_2O_2-treated adults, their role may not be an exclusive one. In comparison to adult worms, schistosomula are more susceptible to oxidative stress such as H_2O_2 and contain less protein (Mkoji *et al.,* 1988). The juvenile stage expresses less oxidatively active protein than adults (LoVerde, 1998; Mei and LoVerde, 1997; Nare *et al.,* 1990). Additionally, schistosomula were shown to have a higher survival rate when in close proximity to adults due to the H_2O_2 removal ability of adults (Mkoji *et al.,* 1988). Therefore, after knocking down SmAldh, the juvenile stages might show a different phenotype than the adults. Furthermore, Aldhs are involved in developmental processes due to RA metabolism (Duester, 2000; Huang *et al.,* 2009; Kam *et al.,* 2012) and are also expressed in young schistosomula (Lu and Berriman, 2018). Treatment with drugs that inhibit SmAldhs and additionally SmGST and/or SmSOD appear to be promising in eliminating the major antioxidant defense capacity of *S. mansoni,* as the latter are the most abundant enzymes in adults (LoVerde, 1998). Interrupting development and reducing defense mechanism in oxidative stress

may be a good strategy to act on juvenile and adult worms simultaneously and is worth further investigation.

5.6.2 Analyses of kinases as potential drug targets

Expression pattern of selected kinases in *S. mansoni*

Expression of Sm*abl1* and Sm*abl2* appeared to be induced in a pairing-dependent manner (**Figure 4.58** and **Figure 4.63**). Approximately 2.5-fold higher expression of Sm*abl1* was observed in bsF compared with ssF, whereas expression in ssM and bsM appeared comparable. In pairing-experienced *S. mansoni*, transcript levels did not differ significantly, whereas ssM had approximately 3-fold higher Sm*abl1* transcript levels than ssF. The ratios are consistent with those of Lu *et al.* (2016). A similar transcript distribution was observed for Sm*abl2*, with approximately 4.5-fold higher expression in bsF than ssF. A slightly higher transcript abundance of Sm*tk6* was observed in ssF and bsF compared to ssM and bsM (**Figure 4.72**). This describes the expression pattern in the opposite direction compared with the data of Lu *et al.* (2016). All three genes seemed to be highly expressed in *S. mansoni* adults. Transcripts of Sm*abl1* were mainly found in neurons, neoblasts, and their progeny of both genders, as well as in parenchyma, muscles, GSC and their progeny, as well as in the tegument of females (Wendt *et al.*, 2020). Sm*abl2* gene expression seemed to be higher in females when compared to males with ubiquitous distribution in both genders, and enrichment in neurons, vitelline cells, muscles, and parenchyma of females (Wendt *et al.*, 2020). Both Sm*abl* transcripts were found by *in situ* hybridization in ovary, ootype, vitellarium, testes, gastrodermis, and parenchyma (Beckmann and Grevelding, 2010). Sm*tk6* transcripts were found ubiquitously, with higher expression in neoblasts and GSC of both genders, in vitelline cells, GSC progeny, and parenchyma in females, and in neurons as well as in the tegument of males (Wendt *et al.*, 2020). This corresponds to Sm*tk6* localization analyses by Beckmann *et al.* (2010), where transcripts were found in parenchyma and gonads of both genders.

Knock down efficacy varied between the selected kinase genes

Knock down efficiency varied greatly between approaches and genders. Knock down of Sm*abl1* resulted in moderate transcript levels ranging from 56 - 79 % in both genders after 14 and 21 d (**Figure 4.59**). Knock down of Sm*abl1* also appeared to induce expression of Sm*tk6* after 14 and 21 d. Knock down of Sm*abl2* was more efficient with remaining transcript levels ranging from 29 - 68 % in both genders after 14 and 21 d. Gene expression of Sm*abl1* appeared to be upregulated at both time points in females (**Figure 4.64**). When both Sm*abl* kinases were knocked down, the efficacy for Sm*abl2* was of the same order of magnitude as when knocked down alone, whereas Sm*abl1* transcript levels were on average 18 % higher than when knocked down alone in females. An increase of Sm*tk6* transcript was observed, too. This could be due to the observed upregulation of Sm*abl1* when Sm*abl2* was knocked down alone and to the less efficient knock down of Sm*abl1* itself. It seemed that Sm*abl2* exerted some function that can be compensated by Sm*abl1* and Sm*tk6*. On the other hand, knock down of Sm*tk6* resulted in up to 2-fold higher transcript levels of Sm*abl1* and Sm*abl2* after 14 d, with elevated transcript levels for Sm*abl2* only after 21 d. This further suggests compensatory effects of the SmAbl kinases in a time-dependent manner.

In general, more dsRNA seemed to lead to higher efficiencies, but this needs to be validated as the determination was performed only once. In addition, the exact amounts needed for gene knock down should be determined individually for each gene beforehand, as the application of more dsRNA may lead to a higher number of off-target cross-hybridization events, as observed with siRNA on NSCLC cells (Semizarov *et al.*, 2003). Furthermore, different application methods such as electroporation or use of si/hpRNA may yield higher efficiencies (Krautz-Peterson *et al.*, 2007; Sliva and Schnierle, 2010; Zhao *et al.*, 2008). To analyze the extent to which the kinases contribute to worm survival or development, approaches such as knock-out/knock-in to generate transgenic *S. mansoni* worms could be a possibility (Beckmann and Grevelding, 2012; Du *et al.*, 2021; Ittiprasert *et al.*, 2019; Mann *et al.*, 2011).

Another important factor to consider is biological variation. Each hamster may have a different impact on worm development. It has been shown in Swiss-Webster mice that when infected with cercariae, only about one third of adult worms can be recovered, compared to about half of worms when *in vitro* transformed schistosomula were injected subcutaneously (Vilar and Pinto, 2005). As observed with perfusion, worm recovery was different for each individual hamster although hamsters have been infected with the same amount of cercariae.

RNAi effects on physiology, morphology, and cell proliferation

No obvious effects were observed on the physiological parameters determined during the two knock down periods. Since all three gene transcripts were localized in the gonads, an effect on egg laying capacity was expected. A peak of abnormal eggs was observed at d 6 during oviposition, which also occurred during knock down of both Sm*aldhs*. Numbers for normal and abnormal eggs varied in both groups, as suggested by El Ridi *et al.* (1997), possibly due to the fact that not all females lay eggs in the same manner. M199(3+) does not appear to be the correct medium to study egg laying effects because it lacks important supplements such as bile salts, red blood cells, low-density lipids, and ascorbic acid to maintain viability of the vitellarium (Badr *et al.*, 1999; Wang *et al.*, 2019). As with M199(3+), egg numbers reduced dramatically after 9 d, and no effect of RNAi treatment was detected. It is possible that there are early effects on egg laying when the selected kinases are knocked down, but because the knock down efficiencies were only moderate, this remains unclear. To overcome these obstacles, a more appropriate medium composition should be used.

When Beckmann and Grevelding (2010) treated *S. mansoni* couples with the Abl kinase inhibitor imatinib, they observed a separation of 85 % of couples after 24 h using 50 µM and less than 40 % of worms still alive after 3 d. It was shown that even lower concentrations of imatinib (20 µM) resulted in 90 % separation after 24 h (Mughal *et al.*, 2022). Gut dilatation was observed in both studies (Beckmann and Grevelding, 2010; Mughal *et al.*, 2022). None of these observations were made in this work, suggesting that either imatinib has multiple drug targets despite SmAbl kinases in *S. mansoni*, or the knock down effect was not sufficient to cause any of the expected phenotypes. It is unlikely that the observed phenotypes following imatinib treatment are only due to inhibition of SmAbl kinases. Further imatinib targets are the transmembrane receptor c-KIT and the platelet-derived growth factor receptor kinase (Manley *et al.*, 2002; Pardanani and Tefferi, 2004). Orthologs of these targets have not been found yet in *S. mansoni* and, therefore, imatinib was considered SmAbl kinase specific for *S. mansoni* (Beckmann and Grevelding, 2010). However, there are more known targets to imatinib such as the NAD(P)H:quinone oxidoreductase 2 (NQO2) or the RTK: discoidin domain receptor 1 (DDR1) (Hantschel *et al.*, 2008; Rix *et al.*, 2007). Using NCBI's blastp and WormBase ParaSite, NQO sequences (NQO1 UniProt ID: P15559, NQO2 UniProt ID: P16083) showed no significant similarity compared to the schistosome taxid. Searching WormBase ParaSite, a DDR1 ortholog was found in *S. mansoni* (annotated as F5/8 type C domain-containing protein, Smp_244370). This suggests more potential targets for

imatinib, which could contribute to the observed phenotype spectrum in *S. mansoni*.

However, to achieve higher knock down efficiencies and maybe more severe phenotypes associated, a different RNAi approach should be considered, e.g., using siRNA or multiple ds/siRNAs targeting one gene. Furthermore, it would be interesting to knock down Sm*abl* kinases in schistosomula to study their development into adult worms as the *abl1/abl2* knock out phenotype is lethal in mice (Koleske *et al.*, 1998). Because transcript levels of Sm*abl1* and Sm*abl2* increase in bsF (**Figure 4.58** and **Figure 4.63**), another study approach would be to use RNAi-treated ssF to examine pairing-dependent vitellarium and ovarian development after mating with males.

RNAi-treated worms showed gonad-specific effects after 21 d. While Sm*abl1* transcripts were reduced with $2.5\,\mu g\,ml^{-1}$ dsRNA, the number of immature oocytes appeared to increase and expand to the part of the ovary that normally harbors mature oocytes in females, whereas no effects on the testes were observed (**Figure 4.61**). A similar phenotype was obtained earlier (14 d) when more dsRNA ($12.5\,\mu g\,ml^{-1}$) was used. This suggested that the transcript amount may be linked to the fast development of the observed phenotype. Knock down of Sm*abl2* with $2.5\,\mu g\,ml^{-1}$ dsRNA resulted in the occurrence of cell-free spaces in the testes and inseparable testicular lobes without clear epithelium after 21 d, whereas the ovaries showed cell-free spaces after 14 d with $12.5\,\mu g\,ml^{-1}$ dsRNA (**Figure 4.66**). When Sm*abl1* and Sm*abl2* were simultaneously knocked down, the observed phenotypes were confirmed. Mature oocytes appeared smaller in females, while testes showed some cavities and inseparable lobes (**Figure 4.70**). When Sm*tk6* was knocked down for 21 d, more immature oocytes were observed than mature oocytes in females compared to the control, whereas males showed some cavities in the testes (**Figure 4.75**).

In eukaryotes, Abl kinases regulate cytoskeletal reorganization, cell proliferation, survival, and stress responses (Pendergast, 2002), and they are activated by RTKs, adhesion receptors (integrins and cadherins), and immunoreceptors (B cell antigen receptor and T cell receptor) (Gu *et al.*, 2009). Abl kinases were linked to possess an important role in epithelial-mesenchymal transition (EMT) in invasion and metastasis of cancer (Luttman *et al.*, 2021). HsAbl1 and HsAbl2 are important for maintaining adherens junctions in epithelial cells, as inhibition of HsAbl kinases led to activation of a Rho-ROCK-myosin signaling pathway that disrupted intercellular adhesions (Zandy *et al.*, 2007). Inhibition of Abl kinases may lead to reduced tumor growth and affect the spread of metastases (Luttman *et al.*, 2021). When *abl2* was knocked down in fibroblasts, they showed decreased adhesion turnover and detached from the extracellular matrix

(ECM) (Peacock *et al.*, 2007).

SmAbl kinases appear to elicit gender-specific effects in *S. mansoni*. Knock down of Sm*abl1* appeared to affect cell adhesion as well as proliferation and impair cell differentiation in females, whereas knock down of Sm*abl2* appeared to impair cell connectivity in male testes. Over expression of BCR-Abl resulted in differentiation and decreased self-renewal capacity in hematopoietic stem cells in a mouse model (Schemionek *et al.*, 2010). In turn, knock down of Sm*abl* kinases may lead to increased proliferation of immature oocytes, as has been observed after RNAi.

SmTK6 as a Src/Abl hybrid (Beckmann *et al.*, 2011) may have a role in EMT, as both Abl and Src kinases are involved in EMT (Luttman *et al.*, 2021; Ortiz *et al.*, 2021). Because Src kinases also interact with Abelson interactor 1 (Abi-1) through their SH2 domain, and since Abi-1 modulates actin cytoskeletal dynamics by regulating kinases and actin nucleation-promoting factors (Ortiz *et al.*, 2021), it seems likely that their signaling pathways are connected, leading to interchangeable results when a participating kinase is inhibited. As determined by qRT-PCR analyses, after knock down of Sm*tk6*, both Sm*abl* transcripts were increased, highlighting their potential to compensate for the loss of function of the other.

Treatment of *S. mansoni* with imatinib resulted in the loss of immature oocytes as well as vitelline cells, while the cells appeared partially apoptotic (Beckmann and Grevelding, 2010). Parts of these observations were confirmed in this study, linking the functions of SmAbl kinases to the development and maintenance of gonadal structures. After knock down of Sm*abl1* or Sm*abl2* alone, Sm*bax* was upregulated in females, indicating a shift toward apoptosis after 21 d (**Figure 4.59** and **Figure 4.64**). This may explain why higher numbers of immature oocytes were observed, while mature oocytes underwent apoptosis, immature oocytes took their place in the ovary. In contrast, when both Sm*abl1* and Sm*abl2* were knocked down simultaneously, less Sm*nanos1* transcripts were found, while gene regulation of Sm*bax* and Sm*bcl-2* shifted towards an anti-apoptotic response in females. Sm*nanos1* is a stem cell marker (Suzuki *et al.*, 2009; Tsuda *et al.*, 2003) and reduction of its transcript level indicates that there are either less cells expressing the gene (as there were less cells through cavity formation) or gene expression was negatively influenced by a mechanism involving the SmAbl kinases. Although male testes were affected by the double knock down, no alterations in the analyzed transcript amounts were observed, indicating that regulation of Sm*abl* transcripts does not provoke cell cycle regulation or apoptosis through the observed genes in males at the observed time point sufficiently (maybe due to its low knock down efficacy).

On the other hand, BCR-Abl was shown to regulate *bcl-2* gene expression (Sánchez-García and Martín-Zanca, 1997). Brown *et al.* (2017b) showed that constitutively active BCR-Abl activates the Ras/Raf/MEK/ERK pathway, resulting in gene expression of *bcl-2*. High BCL-2 levels are usually associated with anti-apoptotic properties, but this is not always the case (Ruvolo *et al.*, 2001). Phosphorylation of the latter at Ser70 mediated by the JNK/SAPK kinase p54-SAPKβ, PKCα, ERK1, or ERK2 has been associated with its pro-survival function (Ruvolo *et al.*, 2001).

It cannot be excluded that the selected genes are regulated in a time-dependent manner, suggesting that no extraordinary response to the knock down was required at the observed time point, maybe also due to the compensating functions of Sm*tk6*.

PTKs such as FAK, Src, and Abl have been shown to be induced by transforming growth factor β (TGFβ) resulting in highly amplified TGFβ signaling in mesenchymal or dedifferentiated epithelial cells (Wendt *et al.*, 2009). TGFβ is involved in almost every cell process such as apoptosis, cell growth and motility, differentiation, ECM production, EMT, and early embryonic development via binding to dimers of TβRI/II (Massagué, 1998; Roberts and Sporn, 1993; Tzavlaki and Moustakas, 2020; Yue and Mulder, 2001). Effects of TGFβ signaling are highly dependent on cell type, growth conditions, and presence of other growth and transcription factors (Kubiczkova *et al.*, 2012). It was shown that integrin β3 interacts with TβRII and promotes EMT after Src kinase-mediated phosphorylation of TβRII in mammary epithelial cells (Galliher and Schiemann, 2006).

Furthermore, Buro *et al.* (2013) postulated a cooperative involvement of TGFβ and Src kinase signaling to promote gene expression involved in eggshell formation in *S. mansoni*. Members of the TGFβ pathway (SmTβRI/II, activin receptor of type IIb (SmActRIIb), suppressor of mothers against decapentaplegic (SMAD) 4 (SmSMAD4), SmSMAD2, and FK506-binding protein 12) were identified in *S. mansoni* (Beall *et al.*, 2000; Davies *et al.*, 1998; Forrester *et al.*, 2004; Osman *et al.*, 2004; Rossi *et al.*, 2002). In addition, BCR-Abl was shown to increase the levels of SMADs, thereby enhancing TGFβ signaling activity as shown in fibroblasts of African green monkey kidneys (Møller *et al.*, 2007). On the other hand, inactivation of c-Abl in mammary epithelial cells induced EMT (Allington *et al.*, 2009). Maybe compensating (over) expression of Sm*abl* kinases and Sm*tk6* influences TGFβ signaling to further promote EMT and subsequent loss of adhesions as their downstream interacting partners may differ trough altered signaling. Horowitz *et al.* (2007) showed that lung myofibroblasts undergo anoikis (a special kind of apoptosis mediated by the loss of adhesion signals

(Frisch and Screaton, 2001)) when adhesion signaling was disrupted. TGFβ can inhibit growth of epithelial cells (Yue and Mulder, 2001). Wilkes and Leof (2006) showed that TGFβ stimulated c-Abl activity in murine and human fibroblasts but not in mink, canine, or human (HeLa) epithelial cultures. Additionally, they provided evidence for c-Abl being a target downstream of phosphatidylinositol 3-kinase and p21-activated kinase 2 in fibroblasts promoting their transformation (Wilkes and Leof, 2006). However, TGFβ induced growth inhibition is cell type-dependent (Atfi *et al.*, 2005; Møller *et al.*, 2007).

BCR-Abl suppresses cell growth arrest and apoptosis without interfering in the TGFβ-activated SMAD-mediated signaling pathway via activation of the AKT/FoxO3 pathway leading to inactivation of FoxO3 (Atfi *et al.*, 2005). FoxO3 is a transcription factor mediating growth inhibition and apoptosis in response to TGFβ, and if not inactivated by phosphorylation (Accili and Arden, 2004). In addition, BCR-Abl kinase activates CDKs and cell cycle progression by downregulating p27 protein expression (which is a CDK inhibitor) in murine and human hematopoietic cells (Jonuleit *et al.*, 2000). Less SmAbl may lead to minor activation of the AKT/FoxO3 pathway, promoting growth inhibition and apoptosis in *S. mansoni* gonads, as observed by RNAi, and may downregulate TGFβ signaling and subsequent pathways involved in gonadal maintenance and differentiation. The latter processes could also be affected in a kinase-dependent manner, as knock down of Sm*abl1* and Sm*abl2* resulted in differential effects in the gonads of *S. mansoni* females and males.

SmTK6 interacts in a complex with SmTK3 and SmTK4 with SmVKR1 (Beckmann *et al.*, 2010, 2011). This complex induces the ERK2/JNK/AKT pathway (Gelmedin *et al.*, 2017), which in turn may lead to inactivation of FoxO3 and subsequent growth and anti-apoptotic effects as rescuing response upon Sm*abl* RNAi. Knocking down Sm*tk6* resulted in lower transcript levels of cell cycle-associated genes (Sm*npl4* and Sm*p53*) in females. This may be due to the disturbed signaling pathway involving SmTK6 as a link. Moreover, Gelmedin *et al.* (2017) found that the Smβ-Int1/SmVKR1 complex is important for maintaining oocyte differentiation status and survival. As mentioned before, intβ was shown to interact with TβRII in mammary epithelial cells (Galliher and Schiemann, 2006). Targeting the SmVKR1 complex via Sm*tk6* knock down may lead to the reduction and subsequent loss of mature oocytes through disordered TGFβ signaling. This might explain the observed degeneration of mature oocytes (granulation) after knock down of Sm*tk6* for 21 d.

Although Sm*abl1*, Sm*abl2*, and Sm*tk6* transcripts were found in the gonads (Beckmann and Grevelding, 2010; Beckmann *et al.*, 2011), no effect on cell proliferation was

observed after RNAi treatment using EdU assays. It might be that the kinases do not exclusively affect proliferating cells and are more likely to be expressed in meiotic and differentiated cells. To test this, specific antibodies (which do not yet exist) could be used to detect both SmAbls and SmTK6 in isolated gonads. Other possible explanations include the involvement in other processes than proliferation (such as the maintenance of the tissue structure by maintaining the adhesive junctions), moderate knock down efficiency and compensatory functions of other kinases, as upregulation of Sm*tk6* was observed after knock down of Sm*abl* and *vice versa*. A triple knock down with higher efficiency could lead to a better understanding of the role that the selected kinases play in these processes.

Wang *et al.* (2021) showed phosphorylation of four-and-a-half-LIM-only protein 2 (FHL2) by c-Abl, thus repressing cell-proliferation in MCF-7 cells. In contrast, FHL2 promotes proliferation of glioblastoma cells and cervical cancer (Jin *et al.*, 2018; Sun *et al.*, 2018). In addition, knock down of FHL2 induced apoptosis via BAX/BCL-2 in cervical cancer cells (Jin *et al.*, 2018). FHL2 has many interacting partners such as structural proteins, signal transducers, transcription factors and co-factors, splicing factors, DNA replication and repair enzymes, and metabolic enzymes (Johannessen *et al.*, 2006), therefore its activation and cellular function depends strongly on the cell type of its expression. Using NCBI's blastp suite, a FHL2 (UniProt ID: Q14192) ortholog was found in *S. mansoni* (Smp_048560), showing a broad distribution pattern including muscles as well as GSC and their progeny in both genders (Lu *et al.*, 2016, 2017; Wendt *et al.*, 2020). Searching WormBase ParaSite, two additional putative FHL proteins (Smp_012810 and Smp_143130) were identified, which are dominantly expressed in neurons and muscles of both genders and showing broader expression levels in male somatic tissues (Lu *et al.*, 2016, 2017; Wendt *et al.*, 2020). FHL2 has been shown to interact with c-Jun and c-Fos to modulate transcription (Morlon and Sassone-Corsi, 2003). Respective orthologs were found in *S. mansoni* using WormBase ParaSite (Jun orthologs: Smp_067520, Smp_335650, Smp_080420, c-Fos ortholog: Smp_333300). Therefore, a regulation of proliferation might be possible through phosphorylation of SmFHL2 and subsequent interaction with SmJun and SmFos by the SmAbl kinases.

Are *S. mansoni* kinases good drug targets?

Kinases represent a class of highly conserved proteins in metazoans. Humans, fly, nematodes, and yeast share 53 kinase subfamilies, while except yeast, the metazoans

share 91 kinase subfamilies, including TKs and TKLs (Manning, 2005). In *S. mansoni*, 252 ePKs were annotated, accounting for 1.9 % of the proteome (Andrade *et al.*, 2011). Stroehlein *et al.* (2015) found 272 kinase-encoding genes in *S. haematobium* (ePKs and PKLs), of which 267 were orthologs to *S. mansoni*. Later studies based on an updated *S. mansoni* genome version (gv7) suggested the existence of 357 kinases (Grevelding *et al.*, 2018). Kinase activation can be mediated by RTKs, integrins, cadherins, and immunoreceptors (Gu *et al.*, 2009). Kinases are involved in cytoskeletal reorganization, cell proliferation, metabolism, transcription, and survival and stress responses (Manning *et al.*, 2002a; Pendergast, 2002). Phosphorylation of proteins may lead to their activation or deactivation, can alter protein interactions, can direct them to subcellular locations or target them for degradation (Pawson and Scott, 2005).

Dysfunction of kinases has been linked to developmental and metabolic disorders as well as various cancers (Lahiry *et al.*, 2010). Since many kinases are targeted in various diseases, there is an opportunity to consider drug repurposing to combat parasitic organisms (Beckmann *et al.*, 2012; Dissous *et al.*, 2007; Doerig, 2004; Doerig and Grevelding, 2015; Morel *et al.*, 2014; Pereira Moreira *et al.*, 2022; Wu *et al.*, 2021). Since knock down of both SmAbl kinases and SmTK6 showed effects on the gonads in both genders, although the knock downs were only moderately effective, they appear to play a role in the structure and organization of these organs. Inhibition of parts of the egg production apparatus helps to contain the symptoms of the disease and its spread. Small molecule PK inhibitors such as imatinib were shown to be potent compounds against *S. mansoni* and *S. japonicum* (Beckmann and Grevelding, 2010; Li *et al.*, 2019; Mughal *et al.*, 2022) but also against other parasites (Chien *et al.*, 2021; Hemer and Brehm, 2012; Kesely *et al.*, 2016; O'Connell *et al.*, 2015, 2017). So far, the expression of full-length of SmTK6 and the SmAbl-TKDs were successful in *E. coli*. These proteins can be used as a starting point for the development of enzyme assays to test the inhibition of SmAbl-TKDs and SmTK6 by various kinase inhibitors.

Stroehlein *et al.* (2015) associated imatinib with 30 kinases as potential targets *in silico*. Targeting more than one enzyme is a good strategy to avoid resistances. Thereby, drugs with different inhibiting mechanisms should be preferred as Burgess *et al.* (Burgess *et al.*, 2005) showed that the Src/Abl kinase inhibitor BMS-354825 induced mutations in BCR-Abl changing structural contact points to provide resistance. HsAbl binds imatinib preferentially through its kinked P-loop conformation and more Van Der Waals contacts than HsSrc and blocks ATP binding, leaving HsAbl in an inactive conformation (Lin *et al.*, 2013; Nagar, 2007). Change of Thr315 to Ile315 (T315I) confers imatinib insensitivity (Azam *et al.*, 2008; Hochhaus *et al.*, 2002; Reddy and Aggarwal, 2012; Shah

et al., 2002). On the other hand, the allosteric inhibitor GNF-2 binds to the hydrophobic myristate pocket, leading to a conformational change that imatinib tolerates a T315I mutation (Reddy and Aggarwal, 2012).

Targeting enzymes involved in a variety of processes offers the opportunity to interrupt multiple processes simultaneously. Recently, Mughal *et al.* (2022) found evidence that imatinib induces autophagy in *S. mansoni*, suggesting that the drug exerts its anti-schistosomal effects through lysosomal functions next to potentially inhibiting SmAbl kinases. Imatinib showed no activity against *S. mansoni* in infected mice (Katz *et al.*, 2013). This discrepancy with previous *in vitro* data (Beckmann and Grevelding, 2010) was explained by Beckmann *et al.* (2014) due to the high content of imatinib-binding proteins in mice such as AGP and serum albumin. As has been shown with other drugs, the use of nanotechnology to encapsulate drugs for targeted delivery (Patra *et al.*, 2018) could be an option to overcome early drug metabolism and increase bioavailability by preventing binding to blood components.

The use of imatinib against SmAblkinases seems feasible, as patients with chronic myeloid leukemia take this drug for a period of weeks to months (or as long as side effects worsen) (Druker *et al.*, 1996).

Combined inhibition with other important drug targets such as enzymes involved in defense mechanisms of the parasite or altering survival mechanisms could be a promising treatment regime (Gouveia *et al.*, 2018). Carter *et al.* (2016) showed that concurrent inhibition of BCL-2 and Abl kinases is a good way to improve chronic myeloid leukemia in mice. Concomitant application of a sub-lethal dose of PZQ and CAMK inhibitors showed promising effects on adult *S. mansoni in vitro* with less effects *in vivo* but reducing liver egg burden by 47 - 68 % compared to PZQ alone (Nawaratna *et al.*, 2020). Analysis of existing kinase-specific drugs for their repurposing potential against schistosomes would be a good way to expand the range of drugs against schistosomes. In this regard, parasite-specific targets would be the optimum. VKRs are specific to schistosomes (and some protostomes) but are not present in the human genome (Vanderstraete *et al.*, 2013; Vicogne *et al.*, 2003). In *S. mansoni*, two *vkr* genes were identified (Gouignard *et al.*, 2012; Vicogne *et al.*, 2003). Transcripts of Sm*vkr1* were detected in mature oocytes and Sm*vkr2* transcripts were detected in immature oocytes (Vanderstraete *et al.*, 2014). When both gene transcripts were targeted by RNAi, disorganized ovaries and a reduction of size of the ovary and testes lobes were observed (Vanderstraete *et al.*, 2014). SmTK6 is involved in the signaling complex formed by SmTK3, SmTK4, and SmVKR1 (Beckmann *et al.*, 2010, 2011). In addition, it was found

that Smβ-Int1 interacts with the SmVKR1 complex maintaining oocyte differentiation status and survival (Gelmedin *et al., 2017*). Targeting SmVKRs may lead to the loss of egg production thus reducing the pathogenicity of the parasites. Additional treatment to target other kinases involved in muscular and neuronal signaling (e.g., PKA) (De Saram *et al., 2013*) seems also feasible. In this work, the effects of knocking down kinases in adult *S. mansoni* were investigated. The treatment of schistosomula should be considered in future studies, as kinases are important signaling molecules that are also involved in developmental processes.

However, further existing kinase inhibitors should also be considered for drug repurposing. Third generation tyrosine kinase inhibitor (TKI) ponatinib (AP24534) and other approved TKI were used in *in vitro* and *in vivo* studies in mice against *S. mansoni* (Cowan and Keiser, 2015). The *in vitro* experiments were performed with and without physiological amounts of human serum albumin (HSA; $45\,\mathrm{g\,l^{-1}}$; Fasano *et al.*, 2005) and showed that HSA could increase the half-maximal inhibitory concentrations (IC_{50}) by more than 33-fold. Drugs showing HSA-adjusted IC_{50} (HSA-IC_{50}) values $< 33.3\,\mathrm{\mu M}$ were used for *in vivo* screening. Afatinib (TKI) and sunitinib (receptor tyrosine kinase inhibitor) with the lowest HSA-IC_{50} values (both $\sim 10\,\mathrm{\mu M}$) showed low to very low worm burden reduction (WBR) rates *in vivo* (27.5 % and 2.2 %, respectively). With HSA-IC_{50} values of $\sim 21\,\mathrm{\mu M}$, ponatinib showed a low WBR rate (18.6 %), while trametinib (MEK inhibitor) showed a WBR rate of 63.6 % *in vivo* (Cowan and Keiser, 2015). Imatinib was not tested *in vivo* by the authors due to its effect-neutralizing binding capacity to serum components such as AGP, which occurs in high concentrations in rodent infection models, and serum albumin protein (Beckmann *et al.*, 2014). Here, a change to another model organism closer to humans, e.g., non-human primates, was suggested. Thorough investigation and comparison of *in vitro* and *in vivo* data is necessary to make meaningful statements. The variety of known kinase inhibitors make schistosomal kinases promising targets.

References

Abdullah, L. N. and Chow, E. K.-H. (2013). "Mechanisms of chemoresistance in cancer stem cells". In: *Clinical and Translational Medicine*. Vol. 2 (1), art. no. e3. DOI: 10.1186/2001-1326-2-3.

Abelson, H. T. and Rabstein, L. S. (1970). "Lymphosarcoma: virus-induced thymic-independent disease in mice". In: *Cancer Research*. Vol. 30 (8), pp. 2213–2222. PMID: 4318922.

Accili, D. and Arden, K. C. (2004). "FoxOs at the crossroads of cellular metabolism, differentiation, and transformation". In: *Cell*. Vol. 117 (4), pp. 421–426. DOI: 10.1016/s0092-8674(04)00452-0.

Adams, C. M., Clark-Garvey, S., Porcu, P., and Eischen, C. M. (2019). "Targeting the BCL-2 family in B cell lymphoma". In: *Frontiers in Oncology*. Vol. 8 (8), art. no. 636. DOI: 10.3389/fonc.2018.00636.

Adeyemo, P., Léger, E., Hollenberg, E., Diouf, N., Sène, M., Webster, J. P., and Häsler, B. (2022). "Estimating the financial impact of livestock schistosomiasis on traditional subsistence and transhumance farmers keeping cattle, sheep and goats in northern Senegal". In: *Parasites & Vectors*. Vol. 15 (1), art. no. 101. DOI: 10.1186/s13071-021-05147-w.

Agarwal, R. P., Phillips, M., McPherson, R. A., and Hensley, P. (1986). "Serum albumin and the metabolism of disulfiram". In: *Biochemical Pharmacology*. Vol. 35 (19), pp. 3341–3347. DOI: 10.1016/0006-2952(86)90433-8.

Alland, L., Peseckis, S. M., Atherton, R. E., Berthiaume, L., and Resh, M. D. (1994). "Dual myristylation and palmitylation of Src family member p59Fyn affects subcellular localization". In: *The Journal of Biological Chemistry*. Vol. 269 (24), pp. 16701–16705. DOI: 10.1016/s0021-9258(19)89447-4.

Allensworth, J. L., Evans, M. K., Bertucci, F., Aldrich, A. J., Festa, R. A., Finetti, P., Ueno, N. T., Safi, R., McDonnell, D. P., Thiele, D. J., Van Laere, S., and Devi, G. R. (2015). "Disulfiram (DSF) acts as a copper ionophore to induce copper-dependent oxidative stress and mediate anti-tumor efficacy in inflammatory breast cancer". In: *Molecular Oncology*. Vol. 9 (6), pp. 1155–1168. DOI: 10.1016/j.molonc.2015.02. 007.

Allfrey, V. G., Faulkner, R., and Mirsky, A. E. (1964). "Acetylation and methylation of histones and their possible role in the regulation of RNA synthesis". In: *Proceedings of the National Academy of Sciences of the United States of America*. Vol. 51 (5), pp. 786–794. DOI: 10.1073/pnas.51.5.786.

Allington, T. M., Galliher-Beckley, A. J., and Schiemann, W. P. (2009). "Activated Abl kinase inhibits oncogenic transforming growth factor-β signaling and tumorigenesis in mammary tumors". In: *FASEB Journal: Official Publication of the Federation of American Societies for Experimental Biology*. Vol. 23 (12), pp. 4231–4243. DOI: 10.1096/fj.09-138412.

Altschul, S. F., Gish, W., Miller, W., Myers, E. W., and Lipman, D. J. (1990). "Basic local alignment search tool". In: *Journal of Molecular Biology*. Vol. 215 (3), pp. 403–410. DOI: 10.1016/S0022-2836(05)80360-2.

Ambroziak, W. and Pietruszko, R. (1991). "Human aldehyde dehydrogenase. Activity with aldehyde metabolites of monoamines, diamines, and polyamines". In: *The Journal of Biological Chemistry*. Vol. 266 (20), pp. 13011–13018. DOI: 10.1016/ s0021-9258(18)98796-x.

Andersen, K. R., Leksa, N. C., and Schwartz, T. U. (2013). "Optimized *E. coli* expression strain LOBSTR eliminates common contaminants from His-tag purification". In: *Proteins*. Vol. 81 (11), pp. 1857–1861. DOI: 10.1002/prot.24364.

Anderson, R. G. (1993). "Caveolae: where incoming and outgoing messengers meet". In: *Proceedings of the National Academy of Sciences of the United States of America*. Vol. 90 (23), pp. 10909–10913. DOI: 10.1073/pnas.90.23.10909.

Anderson, R. G. W. (1998). "The caveolae membrane system". In: *Annual Review of Biochemistry*. Vol. 67, pp. 199–225. DOI: 10.1146/annurev.biochem.67.1.199.

Andrade, L. F., Nahum, L. A., Avelar, L. G. A., Silva, L. L., Zerlotini, A., Ruiz, J. C., and Oliveira, G. (2011). "Eukaryotic protein kinases (ePKs) of the helminth parasite *Schistosoma mansoni*". In: *BMC Genomics*. Vol. 12, art. no. 215. DOI: 10.1186/ 1471-2164-12-215.

Andrews, P. and Harder, A. (1989). "Membrane changes induced by praziquantel". In: *Perspectives in Antiinfective Therapy. Current Topics in Infectious Diseases and Clinical Microbiology*. Ed. by G. G. Jackson, H. D. Schlumberger, and H. J. Zeiler. Vieweg+Teubner, pp. 68–75. DOI: 10.1007/978-3-322-86064-4_10.

Andrews, K. T., Fisher, G., and Skinner-Adams, T. S. (2014). "Drug repurposing and human parasitic protozoan diseases". In: *International Journal for Parasitology: Drugs and Drug Resistance*. Vol. 4 (2), pp. 95–111. DOI: 10.1016/j.ijpddr.2014.02.002.

Anisuzzaman, D. V. M., Frahm, S., Prodjinotho, U. F., Bhattacharjee, S., Verschoor, A., and Prazeres Da Costa, C. (2021). "Host-specific serum factors control the development and survival of *Schistosoma mansoni*". In: *Frontiers in Immunology*. Vol. 12, art. no. 635622. DOI: 10.3389/fimmu.2021.635622.

Apak, R., Güçlü, K., Özyürek, M., Bektaşoğlu, B., and Bener, M. (2008). "Cupric ion reducing antioxidant capacity assay for food antioxidants: vitamins, polyphenolics, and flavonoids in food extracts". In: *Advanced Protocols in Oxidative Stress I*. Ed. by D. Armstrong. Humana Press, pp. 163–193. DOI: 10.1007/978-1-60327-517-0_14.

Aragon, A. D., Imani, R. A., Blackburn, V. R., and Cunningham, C. (2008). "Microarray based analysis of temperature and oxidative stress induced messenger RNA in *Schistosoma mansoni*". In: *Molecular and Biochemical Parasitology*. Vol. 162 (2), pp. 134–141. DOI: 10.1016/j.molbiopara.2008.08.004.

Aruleba, R. T., Adekiya, T. A., Oyinloye, B. E., Masamba, P., Mbatha, L. S., Pretorius, A., and Kappo, A. P. (2019). "PZQ therapy: how close are we in the development of effective alternative anti-schistosomal drugs?" In: *Infectious Disorders - Drug Targets*. Vol. 19 (4), pp. 337–349. DOI: 10.2174/1871526519666181231153139.

Asaoka-Taguchi, M., Yamada, M., Nakamura, A., Hanyu, K., and Kobayashi, S. (1999). "Maternal Pumilio acts together with Nanos in germline development in *Drosophila* embryos". In: *Nature Cell Biology*. Vol. 1 (7), pp. 431–437. DOI: 10.1038/15666.

Atfi, A., Abécassis, L., and Bourgeade, M.-F. (2005). "Bcr-Abl activates the AKT/FoxO3 signalling pathway to restrict transforming growth factor-β-mediated cytostatic signals". In: *EMBO Reports*. Vol. 6 (10), pp. 985–991. DOI: 10.1038/sj.embor.7400501.

Avelar, L. G. A., Nahum, L. A., Andrade, L. F., and Oliveira, G. (2011). "Functional diversity of the *Schistosoma mansoni* tyrosine kinases". In: *Journal of Signal Transduction*. Vol. 2011, art. no. 603290. DOI: 10.1155/2011/603290.

References

Azam, M., Seeliger, M. A., Gray, N. S., Kuriyan, J., and Daley, G. Q. (2008). "Activation of tyrosine kinases by mutation of the gatekeeper threonine". In: *Nature Structural & Molecular Biology*. Vol. 15 (10), pp. 1109–1118. DOI: 10.1038/nsmb.1486.

Badr, S. G., Pica-Mattoccia, L., Moroni, R., Angelico, M., and Cioli, D. (1999). "Effect of bile salts on oviposition *in vitro* by *Schistosoma mansoni*". In: *Parasitology Research*. Vol. 85 (5), pp. 421–423. DOI: 10.1007/s004360050570.

Bahia, D., Andrade, L. F., Ludolf, F., Mortara, R. A., and Oliveira, G. (2006). "Protein tyrosine kinases in *Schistosoma mansoni*". In: *Memórias do Instituto Oswaldo Cruz*. Vol. 101 (1), pp. 137–143. DOI: 10.1590/S0074-02762006000900022.

Barnes, W. M. (1992). "The fidelity of *Taq* polymerase catalyzing PCR is improved by an N-terminal deletion". In: *Gene*. Vol. 112 (1), pp. 29–35. DOI: 10.1016/0378-1119(92)90299-5.

Barth, L. R., Fernandes, A. P., and Rodrigues, V. (1996). "Oviposition by *Schistosoma mansoni* during *in vitro* cultivation". In: *Revista do Instituto de Medicina Tropical de Sao Paulo*. Vol. 38 (6), pp. 423–426. DOI: 10.1590/s0036-46651996000600006.

Barton, C. (2014). "EDTA (ethylenediaminetetraacetic acid)". In: *Encyclopedia of Toxicology*. Ed. by P. Wexler. Academic Press, pp. 310–311. DOI: 10.1016/B978-0-12-386454-3.00309-2.

Batra, V. K., Beard, W. A., Shock, D. D., Krahn, J. M., Pedersen, L. C., and Wilson, S. H. (2006). "Magnesium-induced assembly of a complete DNA polymerase catalytic complex". In: *Structure (London, England: 1993)*. Vol. 14 (4), pp. 757–766. DOI: 10.1016/j.str.2006.01.011.

Beall, M. J., McGonigle, S., and Pearce, E. J. (2000). "Functional conservation of *Schistosoma mansoni* SMADs in TGF-β signaling". In: *Molecular and Biochemical Parasitology*. Vol. 111 (1), pp. 131–142. DOI: 10.1016/s0166-6851(00)00307-8.

Beckmann, S. and Grevelding, C. G. (2010). "Imatinib has a fatal impact on morphology, pairing stability and survival of adult *Schistosoma mansoni in vitro*". In: *International Journal for Parasitology*. Vol. 40 (5), pp. 521–526. DOI: 10.1016/j.ijpara.2010.01.007.

Beckmann, S., Buro, C., Dissous, C., Hirzmann, J., and Grevelding, C. G. (2010). "The SYK kinase SmTK4 of *Schistosoma mansoni* is involved in the regulation of spermatogenesis and oogenesis". In: *PLoS Pathogens*. Vol. 6 (2), art. no. e1000769. DOI: 10.1371/journal.ppat.1000769.

Beckmann, S., Hahnel, S., Cailliau, K., Vanderstraete, M., Browaeys, E., Dissous, C., and Grevelding, C. G. (2011). "Characterization of the Src/Abl hybrid kinase SmTK6 of *Schistosoma mansoni*". In: *Journal of Biological Chemistry*. Vol. 286 (49), pp. 42325–42336. DOI: 10.1074/jbc.M110.210336.

Beckmann, S. and Grevelding, C. G. (2012). "Paving the way for transgenic schistosomes". In: *Parasitology*. Vol. 139 (5), pp. 651–668. DOI: 10.1017/S0031182011001466.

Beckmann, S., Leutner, S., Gouignard, N., Dissous, C., and Grevelding, C. G. (2012). "Protein kinases as potential targets for novel anti-schistosomal strategies". In: *Current Pharmaceutical Design*. Vol. 18 (24), pp. 3579–3594. DOI: 10.2174/138161212801327310.

Beckmann, S., Long, T., Scheld, C., Geyer, R., Caffrey, C. R., and Grevelding, C. G. (2014). "Serum albumin and α-1 acid glycoprotein impede the killing of *Schistosoma mansoni* by the tyrosine kinase inhibitor imatinib". In: *International Journal for Parasitology: Drugs and Drug Resistance*. Vol. 4 (3), pp. 287–295. DOI: 10.1016/j.ijpddr.2014.07.005.

Beitz, E. (2000). "TEXshade: shading and labeling of multiple sequence alignments using LATEX2e". In: *Bioinformatics*. Vol. 16 (2), pp. 135–139. DOI: 10.1093/bioinformatics/16.2.135.

Belmont-Díaz, J. A., Yoval-Sánchez, B., Calleja-Castañeda, L. F., Pardo Vázquez, J. P., and Rodríguez-Zavala, J. S. (2016). "Alda-1 modulates the kinetic properties of mitochondrial aldehyde dehydrogenase (Aldh2)". In: *The FEBS Journal*. Vol. 283 (19), pp. 3637–3650. DOI: 10.1111/febs.13833.

Benedetti, A., Comporti, M., and Esterbauer, H. (1980). "Identification of 4-hydroxynonenal as a cytotoxic product originating from the peroxidation of liver microsomal lipids". In: *Biochimica et Biophysica Acta (BBA) - Lipids and Lipid Metabolism*. Vol. 620 (2), pp. 281–296. DOI: 10.1016/0005-2760(80)90209-x.

Benson, D. A., Cavanaugh, M., Clark, K., Karsch-Mizrachi, I., Lipman, D. J., Ostell, J., and Sayers, E. W. (2013). "GenBank". In: *Nucleic Acids Research*. Vol. 41 (Database issue), pp. 36–42. DOI: 10.1093/nar/gks1195.

Berkner, K. L. (1993). "Expression of recombinant vitamin K-dependent proteins in mammalian cells: factors IX and VII". In: *Methods in Enzymology*. Vol. 222, pp. 450–477. DOI: 10.1016/0076-6879(93)22029-f.

References

Bernhardt, V. G., Pinto, J. R. T., and Pai, V. R. (2009). "Superoxide dismutase: an alternate target for *Plasmodium*". In: *Biomedical Research*. Vol. 20 (2), pp. 127–135. URL: https://www.alliedacademies.org/articles/superoxide-dismutase--an-alternate-target-for-plasmodium.html (visited on Aug. 8, 2022).

Berriman, M., Haas, B. J., LoVerde, P. T., Wilson, R. A., Dillon, G. P., Cerqueira, G. C., Mashiyama, S. T., Al-Lazikani, B., Andrade, L. F., Ashton, P. D., Aslett, M. A., Bartholomeu, D. C., Blandin, G., Caffrey, C. R., Coghlan, A., Coulson, R., Day, T. A., Delcher, A., DeMarco, R., Djikeng, A., Eyre, T., Gamble, J. A., Ghedin, E., Gu, Y., Hertz-Fowler, C., Hirai, H., Hirai, Y., Houston, R., Ivens, A., Johnston, D. A., Lacerda, D., Macedo, C. D., McVeigh, P., Ning, Z., Oliveira, G., Overington, J. P., Parkhill, J., Pertea, M., Pierce, R. J., Protasio, A. V., Quail, M. A., Rajandream, M.-A., Rogers, J., Sajid, M., Salzberg, S. L., Stanke, M., Tivey, A. R., White, O., Williams, D. L., Wortman, J., Wu, W., Zamanian, M., Zerlotini, A., Fraser-Liggett, C. M., Barrell, B. G., and El-Sayed, N. M. (2009). "The genome of the blood fluke *Schistosoma mansoni*". In: *Nature*. Vol. 460 (7253), pp. 352–358. DOI: 10.1038/nature08160.

Bhadhprasit, W., Kodama, H., Fujisawa, C., Hiroki, T., and Ogawa, E. (2012). "Effect of copper and disulfiram combination therapy on the macular mouse, a model of Menkes disease". In: *Journal of Trace Elements in Medicine and Biology*. Vol. 26 (2-3), pp. 105–108. DOI: 10.1016/j.jtemb.2012.05.002.

Bhattacharyya, G., Oliveira, P., Krishnaji, S. T., Chen, D., Hinman, M., Bell, B., Harris, T. I., Ghazitabatabaei, A., Lewis, R. V., and Jones, J. A. (2021). "Large scale production of synthetic spider silk proteins in *Escherichia coli*". In: *Protein Expression and Purification*. Vol. 183, art. no. 105839. DOI: 10.1016/j.pep.2021.105839.

Black, W. J., Stagos, D., Marchitti, S. A., Nebert, D. W., Tipton, K. F., Bairoch, A., and Vasiliou, V. (2009). "Human aldehyde dehydrogenase genes: alternatively spliced transcriptional variants and their suggested nomenclature". In: *Pharmacogenetics and Genomics*. Vol. 19 (11), pp. 893–902. DOI: 10.1097/FPC.0b013e3283329023.

Blaedel, W. J. and Knight, H. T. (1954). "Stoichiometry of titration of metal ions with disodium salt of ethylenediaminetetraacetic acid using high frequency technique". In: *Analytical Chemistry*. Vol. 26 (4), pp. 743–746. DOI: 10.1021/ac60088a041.

Blair, K. L., Bennett, J. L., and Pax, R. A. (1992). "Praziquantel: physiological evidence for its site(s) of action in magnesium-paralysed *Schistosoma mansoni*". In: *Parasitology*. Vol. 104 (1), pp. 59–66. DOI: 10.1017/s0031182000060807.

Blohm, A. S., Mäder, P., Quack, T., Lu, Z., Hahnel, S., Schlitzer, M., and Grevelding, C. G. (2016). "Derivatives of biarylalkyl carboxylic acid induce pleiotropic phenotypes in adult *Schistosoma mansoni in vitro*". In: *Parasitology Research*. Vol. 115 (10), pp. 3831–3842. DOI: 10.1007/s00436-016-5146-7.

Blume-Jensen, P. and Hunter, T. (2001). "Oncogenic kinase signalling". In: *Nature*. Vol. 411 (6835), pp. 355–365. DOI: 10.1038/35077225.

Boissier, J., Grech-Angelini, S., Webster, B. L., Allienne, J.-F., Huyse, T., Mas-Coma, S., Toulza, E., Barré-Cardi, H., Rollinson, D., Kincaid-Smith, J., Oleaga, A., Galinier, R., Foata, J., Rognon, A., Berry, A., Mouahid, G., Henneron, R., Moné, H., Noel, H., and Mitta, G. (2016). "Outbreak of urogenital schistosomiasis in Corsica (France): an epidemiological case study". In: *The Lancet. Infectious Diseases*. Vol. 16 (8), pp. 971–979. DOI: 10.1016/S1473-3099(16)00175-4.

Bolanos-Garcia, V. M. and Davies, O. R. (2006). "Structural analysis and classification of native proteins from *E. coli* commonly co-purified by immobilised metal affinity chromatography". In: *Biochimica et Biophysica Acta (BBA) - General Subjects*. Vol. 1760 (9), pp. 1304–1313. DOI: 10.1016/j.bbagen.2006.03.027.

Bologna, G., Yvon, C., Duvaud, S., and Veuthey, A.-L. (2004). "N-Terminal myristoylation predictions by ensembles of neural networks". In: *Proteomics*. Vol. 4 (6), pp. 1626–1632. DOI: 10.1002/PMIC.200300783.

Boukriche, Y., Weisser, I., Aubert, P., and Masson, C. (2000). "MRI findings in a case of late onset disulfiram-induced neurotoxicity". In: *Journal of Neurology*. Vol. 247 (9), pp. 714–715. DOI: 10.1007/s004150070119.

Brar, S. S., Grigg, C., Wilson, K. S., Holder Jr., W. D., Dreau, D., Austin, C., Foster, M., Ghio, A. J., Whorton, A. R., Stowell, G. W., Whittall, L. B., Whittle, R. R., White, D. P., and Kennedy, T. P. (2004). "Disulfiram inhibits activating transcription factor/cyclic AMP-responsive element binding protein and human melanoma growth in a metal-dependent manner *in vitro*, in mice and in a patient with metastatic disease". In: *Molecular Cancer Therapeutics*. Vol. 3 (9), pp. 1049–1060. DOI: 10.1158/1535-7163.1049.3.9.

Brasher, B. B. and Van Etten, R. V. (2000). "c-Abl has high intrinsic tyrosine kinase activity that is stimulated by mutation of the Src homology 3 domain and by autophosphorylation at two distinct regulatory tyrosines". In: *The Journal of Biological Chemistry*. Vol. 275 (45), pp. 35631–35637. DOI: 10.1074/jbc.M005401200.

Braunstein, M., Rose, A. B., Holmes, S. G., Allis, C. D., and Broach, J. R. (1993). "Transcriptional silencing in yeast is associated with reduced nucleosome acetylation". In: *Genes & Development*. Vol. 7 (4), pp. 592–604. DOI: 10.1101/gad.7.4.592.

Brehm, K. (2009). "*Echinococcus multilocularis* as an experimental model in stem cell research and molecular host-parasite interaction". In: *Parasitology*. Vol. 137 (3), pp. 537–555. DOI: 10.1017/S0031182009991727.

Brown, C. W., Sridhara, V., Boutz, D. R., Person, M. D., Marcotte, E. M., Barrick, J. E., and Wilke, C. O. (2017a). "Large-scale analysis of post-translational modifications in *E. coli* under glucose-limiting conditions". In: *BMC Genomics*. Vol. 18 (1), art. no. 301. DOI: 10.1186/s12864-017-3676-8.

Brown, L. M., Hanna, D. T., Khaw, S. L., and Ekert, P. G. (2017b). "Dysregulation of BCL-2 family proteins by leukemia fusion genes". In: *Journal of Biological Chemistry*. Vol. 292 (35), pp. 14325–14333. DOI: 10.1074/jbc.R117.799056.

Bruyninckx, W. J., Gutteridge, S., and Mason, H. S. (1978). "Detection of copper on polyacrylamide gels". In: *Analytical Biochemistry*. Vol. 89 (1), pp. 174–177. DOI: 10.1016/0003-2697(78)90738-8.

Buljan, M., Ciuffa, R., Van Drogen, A., Vichalkovski, A., Mehnert, M., Rosenberger, G., Lee, S., Varjosalo, M., Pernas, L. E., Spegg, V., Snijder, B., Aebersold, R., and Gstaiger, M. (2020). "Kinase interaction network expands functional and disease roles of human kinases". In: *Molecular Cell*. Vol. 79 (3), pp. 504–520, e9. DOI: 10.1016/j.molcel.2020.07.001.

Bump, E. A. and Reed, D. J. (1977). "A unique property of fetal bovine serum: high levels of protein-glutathione mixed disulfides". In: *In Vitro*. Vol. 13 (2), pp. 115–118. DOI: 10.1007/BF02615075.

Burgess, R. R. (1996). "Purification of overproduced *Escherichia coli* RNA polymerase σ factors by solubilizing inclusion bodies and refolding from sarkosyl". In: *Methods in Enzymology. RNA Polymerase and Associated Factors Part A*. Ed. by R. R. Burgess and M. P. Deutscher. Academic Press, pp. 145–149. DOI: 10.1016/S0076-6879(96)73014-8.

Burgess, M. R., Skaggs, B. J., Shah, N. P., Lee, F. Y., and Sawyers, C. L. (2005). "Comparative analysis of two clinically active BCR-Abl kinase inhibitors reveals the role of conformation-specific binding in resistance". In: *Proceedings of the National Academy of Sciences of the United States of America*. Vol. 102 (9), pp. 3395–3400. DOI: 10.1073/pnas.0409770102.

Burgess, R. R. (2009). "Refolding solubilized inclusion body proteins". In: *Methods in Enzymology. Guide to Protein Purification*. Ed. by R. R. Burgess and M. P. Deutscher. Academic Press, pp. 259–282. DOI: 10.1016/S0076-6879(09)63017-2.

Buro, C., Oliveira, K. C., Lu, Z., Leutner, S., Beckmann, S., Dissous, C., Cailliau, K., Verjovski-Almeida, S., and Grevelding, C. G. (2013). "Transcriptome analyses of inhibitor-treated schistosome females provide evidence for cooperating Src-kinase and TGFβ receptor pathways controlling mitosis and eggshell formation". In: *PLoS Pathogens*. Vol. 9 (6), art. no. e1003448. DOI: 10.1371/journal.ppat.1003448.

Buro, C., Beckmann, S., Oliveira, K. C., Dissous, C., Cailliau, K., Marhöfer, R. J., Selzer, P. M., Verjovski-Almeida, S., and Grevelding, C. G. (2014). "Imatinib treatment causes substantial transcriptional changes in adult *Schistosoma mansoni in vitro* exhibiting pleiotropic effects". In: *PLoS Neglected Tropical Diseases*. Vol. 8 (6), art. no. e2923. DOI: 10.1371/journal.pntd.0002923.

Buss, J. E., Kamps, M. P., and Sefton, B. M. (1984). "Myristic acid is attached to the transforming protein of Rous sarcoma virus during or immediately after synthesis and is present in both soluble and membrane-bound forms of the protein". In: *Molecular and Cellular Biology*. Vol. 4 (12), pp. 2697–2704. DOI: 10.1128/mcb.4.12.2697-2704.1984.

Buss, J. E., Kamps, M. P., Gould, K., and Sefton, B. M. (1986). "The absence of myristic acid decreases membrane binding of p60Src but does not affect tyrosine protein kinase activity". In: *Journal of Virology*. Vol. 58 (2), pp. 468–474. DOI: 10.1128/jvi.58.2.468-474.1986.

Büssow, K., Scheich, C., Sievert, V., Harttig, U., Schultz, J., Simon, B., Bork, P., Lehrach, H., and Heinemann, U. (2005). "Structural genomics of human proteins – target selection and generation of a public catalogue of expression clones". In: *Microbial Cell Factories*. Vol. 4, art. no. 21. DOI: 10.1186/1475-2859-4-21.

Butcher, K., Kannappan, V., Kilari, R. S., Morris, M. R., McConville, C., Armesilla, A. L., and Wang, W. (2018). "Investigation of the key chemical structures involved in the anticancer activity of disulfiram in A549 non-small cell lung cancer cell line". In: *BMC Cancer*. Vol. 18 (1), art. no. 753. DOI: 10.1186/s12885-018-4617-x.

Caffrey, C. R. (2007). "Chemotherapy of schistosomiasis: present and future". In: *Current Opinion in Chemical Biology*. Vol. 11 (4), pp. 433–439. DOI: 10.1016/j.cbpa.2007.05.031.

Cai, J., Weiss, M. L., and Rao, M. S. (2004). "In search of "stemness"". In: *Experimental Hematology*. Vol. 32 (7), pp. 585–598. DOI: 10.1016/j.exphem.2004.03.013.

Calderon-Aparicio, A., Strasberg-Rieber, M., and Rieber, M. (2015). "Disulfiram anticancer efficacy without copper overload is enhanced by extracellular H_2O_2 generation: antagonism by tetrathiomolybdate". In: *Oncotarget*. Vol. 6 (30), pp. 29771–29781. DOI: 10.18632/oncotarget.4833.

References

Campos, C., Guzmán, R., López-Fernández, E., and Casado, A. (2009). "Evaluation of the copper(II) reduction assay using bathocuproinedisulfonic acid disodium salt for the total antioxidant capacity assessment: the CUPRAC-BCS assay". In: *Analytical Biochemistry*. Vol. 392 (1), pp. 37–44. DOI: 10.1016/j.ab.2009.05.024.

Cao, N., Li, J.-K., Rao, Y.-Q., Liu, H., Wu, J., Li, B., Zhao, P., Zeng, L., and Li, J. (2016). "A potential role for protein palmitoylation and zDHHC16 in DNA damage response". In: *BMC Molecular Biology*. Vol. 17 (1), art. no. 12. DOI: 10.1186/s12867-016-0065-9.

Cao, H.-Z., Yang, W.-T., and Zheng, P.-S. (2022). "Cytotoxic effect of disulfiram/copper on human cervical cancer cell lines and LGR5-positive cancer stem-like cells". In: *BMC Cancer*. Vol. 22 (1), art. no. 521. DOI: 10.1186/s12885-022-09574-5.

Carter, B. Z., Mak, P. Y., Mu, H., Zhou, H., Mak, D. H., Schober, W., Leverson, J. D., Zhang, B., Bhatia, R., Huang, X., Cortes, J., Kantarjian, H., Konopleva, M., and Andreeff, M. (2016). "Combined targeting of BCL-2 and BCR-Abl tyrosine kinase eradicates chronic myeloid leukemia stem cells". In: *Science Translational Medicine*. Vol. 8 (355), art. no. 355ra117, 355ra117. DOI: 10.1126/scitranslmed.aag1180.

Caslini, C., Hong, S., Ban, Y. J., Chen, X. S., and Ince, T. A. (2019). "HDAC7 regulates histone 3 lysine 27 acetylation and transcriptional activity at super-enhancer-associated genes in breast cancer stem cells". In: *Oncogene*. Vol. 38 (39), pp. 6599–6614. DOI: 10.1038/s41388-019-0897-0.

Caspers, P., Stieger, M., and Burn, P. (1994). "Overproduction of bacterial chaperones improves the solubility of recombinant protein tyrosine kinases in *Escherichia coli*". In: *Cellular and Molecular Biology (Noisy-le-grand, France)*. Vol. 40 (5), pp. 635–644. PMID: 7981620.

Castillo-Villanueva, A., Rufino-González, Y., Méndez, S.-T., Torres-Arroyo, A., Ponce-Macotela, M., Martínez-Gordillo, M. N., Reyes-Vivas, H., and Oria-Hernández, J. (2017). "Disulfiram as a novel inactivator of *Giardia lamblia* triosephosphate isomerase with antigiardial potential". In: *International Journal for Parasitology: Drugs and Drug Resistance*. Vol. 7 (3), pp. 425–432. DOI: 10.1016/j.ijpddr.2017.11.003.

CDC - Centers for Disease Control and Prevention DPDx (2019). "Schistosomiasis Infection". Online. URL: https://www.cdc.gov/dpdx/schistosomiasis/index.html (visited on Sept. 1, 2022).

Cen, D., Gonzalez, R. I., Buckmeier, J. A., Kahlon, R. S., Tohidian, N. B., and Meyskens, F. L. (2002). "Disulfiram induces apoptosis in human melanoma cells: a redox-related process". In: *Molecular Cancer Therapeutics*. Vol. 1 (3), pp. 197–204. PMID: 12467214.

Cen, D., Brayton, D., Shahandeh, B., Meyskens, F. L., and Farmer, P. J. (2004). "Disulfiram facilitates intracellular Cu uptake and induces apoptosis in human melanoma cells". In: *Journal of Medicinal Chemistry*. Vol. 47 (27), pp. 6914–6920. DOI: 10. 1021/jm049568z.

Chaube, S. K., Prasad, P. V., Thakur, S. C., and Shrivastav, T. G. (2005). "Hydrogen peroxide modulates meiotic cell cycle and induces morphological features characteristic of apoptosis in rat oocytes cultured *in vitro*". In: *Apoptosis*. Vol. 10 (4), pp. 863–874. DOI: 10.1007/s10495-005-0367-8.

Cheever, A. W., Macedonia, J. G., Mosimann, J. E., and Cheever, E. A. (1994). "Kinetics of egg production and egg excretion by *Schistosoma mansoni* and *S. japonicum* in mice infected with a single pair of worms". In: *The American Journal of Tropical Medicine and Hygiene*. Vol. 50 (3), pp. 281–295. DOI: 10.4269/ajtmh.1994.50.281.

Chen, C. H., Gray, M. O., and Mochly-Rosen, D. (1999). "Cardioprotection from ischemia by a brief exposure to physiological levels of ethanol: role of ϵ protein kinase C". In: *Proceedings of the National Academy of Sciences of the United States of America*. Vol. 96 (22), pp. 12784–12789. DOI: 10.1073/pnas.96.22.12784.

Chen, D., Cui, Q. C., Yang, H., and Dou, Q. P. (2006). "Disulfiram, a clinically used anti-alcoholism drug and copper-binding agent, induces apoptotic cell death in breast cancer cultures and xenografts via inhibition of the proteasome activity". In: *Cancer Research*. Vol. 66 (21), pp. 10425–10433. DOI: 10.1158/0008-5472.CAN-06-2126.

Chen, L., Xue, X., Jiang, D., Yang, J., Zhao, B., Han, X. X., and Jung, Y. M. (2016). "A turn-on resonance raman scattering (BCS/Cu$^+$) sensor for quantitative determination of proteins". In: *Applied Spectroscopy*. Vol. 70 (2), pp. 355–362. DOI: 10.1177/0003702815620560.

Chen, J., Li, Y., Zhang, K., and Wang, H. (2018). "Whole-genome sequence of phage-resistant strain *Escherichia coli* DH5α". In: *Genome Announcements*. Vol. 6 (10), art. no. e00097-18. DOI: 10.1128/genomeA.00097-18.

Chen, R., Wang, J., Gradinaru, I., Vu, H. S., Geboers, S., Naidoo, J., Ready, J. M., Williams, N. S., DeBerardinis, R. J., Ross, E. M., and Collins, J. J. (2022). "A male-derived nonribosomal peptide pheromone controls female schistosome development". In: *Cell*. Vol. 185 (9), pp. 1506–1520, e17. DOI: 10.1016/j.cell.2022.03.017.

Cheng, S., Chen, Y., Monforte, J. A., Higuchi, R., and Van Houten, B. (1995). "Template integrity is essential for PCR amplification of 20- to 30-kb sequences from genomic DNA". In: *PCR Methods and Applications*. Vol. 4 (5), pp. 294–298. DOI: 10.1101/gr.4.5.294.

Chien, H. D., Pantaleo, A., Kesely, K. R., Noomuna, P., Putt, K. S., Tuan, T. A., Low, P. S., and Turrini, F. M. (2021). "Imatinib augments standard malaria combination therapy without added toxicity". In: *The Journal of Experimental Medicine*. Vol. 218 (10), art. no. e20210724. DOI: 10.1084/jem.20210724.

Choi, S. A., Lee, J. Y., Phi, J. H., Wang, K.-C., Park, C.-K., Park, S.-H., and Kim, S.-K. (2014). "Identification of brain tumour initiating cells using the stem cell marker aldehyde dehydrogenase". In: *European Journal of Cancer (Oxford, England: 1990)*. Vol. 50 (1), pp. 137–149. DOI: 10.1016/j.ejca.2013.09.004.

Choi, S. A., Choi, J. W., Wang, K.-C., Phi, J. H., Lee, J. Y., Park, K. D., Eum, D., Park, S.-H., Kim, I. H., and Kim, S.-K. (2015). "Disulfiram modulates stemness and metabolism of brain tumor initiating cells in atypical teratoid/rhabdoid tumors". In: *Neuro-Oncology*. Vol. 17 (6), pp. 810–821. DOI: 10.1093/neuonc/nou305.

Chong, B. E., Wall, D. B., Lubman, D. M., and Flynn, S. J. (1997). "Rapid profiling of *E. coli* proteins up to 500 kDa from whole cell lysates using matrix-assisted laser desorption/ionization time-of-flight mass spectrometry". In: *Rapid Communications in Mass Spectrometry*. Vol. 11 (17), pp. 1900–1908. DOI: 10.1002/(sici)1097-0231(199711)11:17<1900::aid-rcm95>3.0.co;2-k.

Choudhary, S., Xiao, T., Vergara, L. A., Srivastava, S., Nees, D., Piatigorsky, J., and Ansari, N. H. (2005). "Role of aldehyde dehydrogenase isozymes in the defense of rat lens and human lens epithelial cells against oxidative stress". In: *Investigative Opthalmology & Visual Science*. Vol. 46 (1), pp. 259–267. DOI: 10.1167/iovs.04-0120.

Christopherson, J. B. (1918). "Intravenous injections of antimonium tartaratum in bilharziosis". In: *The British Medical Journal*. Vol. 2 (3024), pp. 652–653. DOI: 10.1136/bmj.2.3024.652.

Ciechanover, A. (1998). "The ubiquitin-proteasome pathway: on protein death and cell life". In: *The EMBO Journal*. Vol. 17 (24), pp. 7151–7160. DOI: 10.1093/emboj/17.24.7151.

Cioli, D., Pica-Mattoccia, L., Rosenberg, S., and Archer, S. (1985). "Evidence for the mode of antischistosomal action of hycanthone". In: *Life Sciences*. Vol. 37 (2), pp. 161–167. DOI: 10.1016/0024-3205(85)90419-9.

Cioli, D., Pica-Mattoccia, L., and Moroni, R. (1992). "*Schistosoma mansoni*: hycanthone/oxamniquine resistance is controlled by a single autosomal recessive gene". In: *Experimental Parasitology*. Vol. 75 (4), pp. 425–432. DOI: 10.1016/0014-4894(92)90255-9.

Cioli, D., Pica-Mattoccia, L., and Archer, S. (1995). "Antischistosomal drugs: past, present ... and future?" In: *Pharmacology & Therapeutics*. Vol. 68 (1), pp. 35–85. DOI: 10.1016/0163-7258(95)00026-7.

Clark, D. J. and Maaløe, O. (1967). "DNA replication and the division cycle in *Escherichia coli*". In: *Journal of Molecular Biology*. Vol. 23 (1), pp. 99–112. DOI: 10.1016/S0022-2836(67)80070-6.

Clark, D. W. and Palle, K. (2016). "Aldehyde dehydrogenases in cancer stem cells: potential as therapeutic targets". In: *Annals of Translational Medicine*. Vol. 4 (24), art. no. 518. DOI: 10.21037/atm.2016.11.82.

Cocco, D., Calabrese, L., Rigo, A., Argese, E., and Rotilio, G. (1981). "Re-examination of the reaction of diethyldithiocarbamate with the copper of superoxide dismutase". In: *The Journal of Biological Chemistry*. Vol. 256 (17), pp. 8983–8986. DOI: 10.1016/s0021-9258(19)52496-6.

Coelho, P. M., Lima e Silva, F. C., and Nogueira-Machado, J. A. (1997). "Resistance to oxamniquine of a *Schistosoma mansoni* strain isolated from patient submitted to repeated treatments". In: *Revista do Instituto de Medicina Tropical de Sao Paulo*. Vol. 39 (2), pp. 101–106. DOI: 10.1590/s0036-46651997000200007.

Colicelli, J. (2010). "Abl tyrosine kinases: evolution of function, regulation, and specificity". In: *Science Signaling*. Vol. 3 (139), art. no. re6. DOI: 10.1126/scisignal.3139re6.

Collins, J. J., Hou, X., Romanova, E. V., Lambrus, B. G., Miller, C. M., Saberi, A., Sweedler, J. V., and Newmark, P. A. (2010). "Genome-wide analyses reveal a role for peptide hormones in planarian germline development". In: *PLoS Biology*. Vol. 8 (10), art. no. e1000509. DOI: 10.1371/journal.pbio.1000509.

Collins, J. J., Wang, B., Lambrus, B. G., Tharp, M. E., Iyer, H., and Newmark, P. A. (2013). "Adult somatic stem cells in the human parasite, *Schistosoma mansoni*". In: *Nature*. Vol. 494 (7438), pp. 476–479. DOI: 10.1038/nature11924.

Collins, J. J., Wendt, G. R., Iyer, H., and Newmark, P. A. (2016). "Stem cell progeny contribute to the schistosome host-parasite interface". In: *eLife*. Vol. 5, art. no. e12473. DOI: 10.7554/eLife.12473.

Collins, J. N. R. and Collins, J. J. (2017). "Methods for studying the germline of the human parasite *Schistosoma mansoni*". In: *Germline Stem Cells. Methods in Molecular Biology*. Ed. by M. Buszczak. Humana press, pp. 35–47. DOI: 10.1007/ 978-1-4939-4017-2_2.

Corkey, B. E., Duszyński, J., Rich, T. L., Matschinsky, B., and Williamson, J. R. (1986). "Regulation of free and bound magnesium in rat hepatocytes and isolated mitochondria". In: *The Journal of Biological Chemistry*. Vol. 261 (6), pp. 2567–2574. DOI: 10.1016/s0021-9258(17)35825-8.

Correnti, J. M., Brindley, P. J., and Pearce, E. J. (2005). "Long-term suppression of *cathepsin B* levels by RNA interference retards schistosome growth". In: *Molecular and Biochemical Parasitology*. Vol. 143 (2), pp. 209–215. DOI: 10 . 1016 / j . molbiopara.2005.06.007.

Cortes-Dericks, L., Froment, L., Boesch, R., Schmid, R. A., and Karoubi, G. (2014). "Cisplatin-resistant cells in malignant pleural mesothelioma cell lines show Aldh^{high} CD44$^+$ phenotype and sphere-forming capacity". In: *BMC Cancer*. Vol. 14, art. no. 304. DOI: 10.1186/1471-2407-14-304.

Corti, S., Locatelli, F., Papadimitriou, D., Donadoni, C., Salani, S., Del Bo, R., Strazzer, S., Bresolin, N., and Comi, G. P. (2006). "Identification of a primitive brain–derived neural stem cell population based on aldehyde dehydrogenase activity". In: *Stem Cells*. Vol. 24 (4), pp. 975–985. DOI: 10.1634/stemcells.2005-0217.

Costa, M. P., Oliveira, V. F., Pereira, R. V., De Abreu, F. C. P., Jannotti-Passos, L. K., Borges, W. C., and Guerra-Sá, R. (2015). "*In silico* analysis and developmental expression of ubiquitin-conjugating enzymes in *Schistosoma mansoni*". In: *Parasitology Research*. Vol. 114 (5), pp. 1769–1777. DOI: 10.1007/s00436-015-4362-x.

Cowan, N. and Keiser, J. (2015). "Repurposing of anticancer drugs: *in vitro* and *in vivo* activities against *Schistosoma mansoni*". In: *Parasites & Vectors*. Vol. 8, art. no. 417. DOI: 10.1186/s13071-015-1023-y.

Crapo, J. D., Oury, T., Rabouille, C., Slot, J. W., and Chang, L. Y. (1992). "Copper, zinc superoxide dismutase is primarily a cytosolic protein in human cells". In: *Proceedings of the National Academy of Sciences of the United States of America*. Vol. 89 (21), pp. 10405–10409. DOI: 10.1073/pnas.89.21.10405.

Croker, A. K. and Allan, A. L. (2012). "Inhibition of aldehyde dehydrogenase (Aldh) activity reduces chemotherapy and radiation resistance of stem-like Aldh^{hi}CD44$^+$ human breast cancer cells". In: *Breast Cancer Research and Treatment*. Vol. 133 (1), pp. 75–87. DOI: 10.1007/s10549-011-1692-y.

Croset, A., Delafosse, L., Gaudry, J.-P., Arod, C., Glez, L., Losberger, C., Begue, D., Krstanovic, A., Robert, F., Vilbois, F., Chevalet, L., and Antonsson, B. (2012). "Differences in the glycosylation of recombinant proteins expressed in HEK and CHO cells". In: *Journal of Biotechnology*. Vol. 161 (3), pp. 336–348. DOI: 10.1016/j.jbiotec.2012.06.038.

Cross, F. R., Garber, E. A., Pellman, D., and Hanafusa, H. (1984). "A short sequence in the p60Src N terminus is required for p60Src myristylation and membrane association and for cell transformation". In: *Molecular and Cellular Biology*. Vol. 4 (9), pp. 1834–1842. DOI: 10.1128/mcb.4.9.1834-1842.1984.

Crowther, G. J., Shanmugam, D., Carmona, S. J., Doyle, M. A., Hertz-Fowler, C., Berriman, M., Nwaka, S., Ralph, S. A., Roos, D. S., Van Voorhis, W. C., and Agüero, F. (2010). "Identification of attractive drug targets in neglected-disease pathogens using an *in silico* approach". In: *PLoS Neglected Tropical Diseases*. Vol. 4 (8), art. no. e804. DOI: 10.1371/journal.pntd.0000804.

Da Silva, L. C., Chieffi, P. P., and Carrilho, F. J. (2005). "Schistosomiasis mansoni – clinical features". In: *Gastroenterología y Hepatología*. Vol. 28 (1), pp. 30–39. DOI: 10.1157/13070382.

Dalecki, A. G., Haeili, M., Shah, S., Speer, A., Niederweis, M., Kutsch, O., and Wolschendorf, F. (2015). "Disulfiram and copper ions kill *Mycobacterium tuberculosis* in a synergistic manner". In: *Antimicrobial Agents and Chemotherapy*. Vol. 59 (8), pp. 4835–4844. DOI: 10.1128/AAC.00692-15.

Danquah, K. O. and Gyamfi, D. (2016). "Alcohol and aldehyde dehydrogenases: molecular aspects". In: *Molecular Aspects of Alcohol and Nutrition*. Ed. by V. B. Patel. Academic Press, pp. 25–43. DOI: 10.1016/B978-0-12-800773-0.00003-3.

Darooee, M., Akbari, V., and Taheri, A. (2021). "Inhibition of aldehyde dehydrogenase by furazolidone nanoemulsion to decrease cisplatin resistance in lung cancer cells". In: *Therapeutic Delivery*. Vol. 12 (8), pp. 611–625. DOI: 10.4155/tde-2020-0130.

Das Gupta, V. (1981). "Stability of aqueous suspensions of disulfiram". In: *American Journal of Hospital Pharmacy*. Vol. 38 (3), pp. 363–364. DOI: 10.1093/ajhp/38.3.363.

Davies, S. J., Shoemaker, C. B., and Pearce, E. J. (1998). "A divergent member of the transforming growth factor β receptor family from *Schistosoma mansoni* is expressed on the parasite surface membrane". In: *The Journal of Biological Chemistry*. Vol. 273 (18), pp. 11234–11240. DOI: 10.1074/jbc.273.18.11234.

Davies, H., Belda, H., Broncel, M., Ye, X., Bisson, C., Introini, V., Dorin-Semblat, D., Semblat, J.-P., Tibúrcio, M., Gamain, B., Kaforou, M., and Treeck, M. (2020). "An exported kinase family mediates species-specific erythrocyte remodelling and virulence in human malaria". In: *Nature Microbiology*. Vol. 5 (6), pp. 848–863. DOI: 10.1038/s41564-020-0702-4.

Davis, M. W. and Jorgensen, E. M. (2022). "ApE, a plasmid editor: a freely available DNA manipulation and visualization program". In: *Frontiers in Bioinformatics*. Vol. 2, art. no. 818619. DOI: 10.3389/fbinf.2022.818619.

Day, T. A., Bennett, J. L., and Pax, R. A. (1992). "Praziquantel: the enigmatic antiparasitic". In: *Parasitology Today*. Vol. 8 (10), pp. 342–344. DOI: 10.1016/0169-4758(92)90070-I.

Day, R. M. and Suzuki, Y. J. (2006). "Cell proliferation, reactive oxygen and cellular glutathione". In: *Dose-Response*. Vol. 3 (3), pp. 425–442. DOI: 10.2203/dose-response.003.03.010.

De Freitas Oliveira, J. W., Rocha, H. A. O., De Medeiros, W. M. T. Q., and Silva, M. S. (2019). "Application of dithiocarbamates as potential new antitrypanosomatids-drugs: approach chemistry, functional and biological". In: *Molecules (Basel, Switzerland)*. Vol. 24 (15), art. no. 2806. DOI: 10.3390/molecules24152806.

De Marco, A., Deuerling, E., Mogk, A., Tomoyasu, T., and Bukau, B. (2007). "Chaperone-based procedure to increase yields of soluble recombinant proteins produced in *E. coli*". In: *BMC Biotechnology*. Vol. 7 (1), art. no. 32. DOI: 10.1186/1472-6750-7-32.

De Moraes Maciel, R., Da Costa, R. F. M., De Oliveira, F. M. B., Rumjanek, F. D., and Fantappié, M. R. (2008). "Protein acetylation sites mediated by *Schistosoma mansoni* GCN5". In: *Biochemical and Biophysical Research Communications*. Vol. 370 (1), pp. 53–56. DOI: 10.1016/j.bbrc.2008.03.022.

De Paula, R. G., De Magalhães Ornelas, A. M., Morais, E. R., De Castro Borges, W., Natale, M., Magalhães, L. G., and Rodrigues, V. (2014). "Biochemical characterization and role of the proteasome in the oxidative stress response of adult *Schistosoma mansoni* worms". In: *Parasitology Research*. Vol. 113 (8), pp. 2887–2897. DOI: 10.1007/s00436-014-3950-5.

De Saram, P. S. R., Ressurreição, M., Davies, A. J., Rollinson, D., Emery, A. M., and Walker, A. J. (2013). "Functional mapping of protein kinase A reveals its importance in adult *Schistosoma mansoni* motor activity". In: *PLoS Neglected Tropical Diseases*. Vol. 7 (1), art. no. e1988. DOI: 10.1371/journal.pntd.0001988.

Deharo, E., Barkan, D., Krugliak, M., Golenser, J., and Ginsburg, H. (2003). "Potentiation of the antimalarial action of chloroquine in rodent malaria by drugs known to reduce cellular glutathione levels". In: *Biochemical Pharmacology*. Vol. 66 (5), pp. 809–817. DOI: 10.1016/s0006-2952(03)00396-4.

Dettman, C. D., Higgins-Opitz, S. B., and Saikoolal, A. (1989). "Enhanced efficacy of the paddling method for schistosome infection of rodents by a four-step pre-soaking procedure". In: *Parasitology Research*. Vol. 76 (2), pp. 183–184. DOI: 10.1007/BF00930846.

Deutsche Hauptstelle für Suchtfragen e.V. (2019). "Medikamente zur Behandlung der Alkoholabhängigkeit". Online. URL: https://www.dhs.de/fileadmin/user_upload/pdf/dhs-stellungnahmen/DHS_Stellungnahme_Medikamente_zur_Behandlung_der_Alkoholabhaengigkeit.pdf (visited on Sept. 9, 2022).

Di Bari, M. G., Ciuffini, L., Mingardi, M., Testi, R., Soddu, S., and Barilà, D. (2006). "c-Abl acetylation by histone acetyltransferases regulates its nuclear-cytoplasmic localization". In: *EMBO Reports*. Vol. 7 (7), pp. 727–733. DOI: 10.1038/sj.embor.7400700.

Di Bella, S., Riccardi, N., Giacobbe, D. R., and Luzzati, R. (2018). "History of schistosomiasis (bilharziasis) in humans: from Egyptian medical papyri to molecular biology on mummies". In: *Pathogens and Global Health*. Vol. 112 (5), pp. 268–273. DOI: 10.1080/20477724.2018.1495357.

Dimasi, J. A., Grabowski, H. G., and Hansen, R. W. (2016). "Innovation in the pharmaceutical industry: new estimates of R&D costs". In: *Journal of Health Economics*. Vol. 47, pp. 20–33. DOI: 10.1016/j.jhealeco.2016.01.012.

Dissous, C., Ahier, A., and Khayath, N. (2007). "Protein tyrosine kinases as new potential targets against human schistosomiasis". In: *BioEssays*. Vol. 29 (12), pp. 1281–1288. DOI: 10.1002/bies.20662.

Do Nascimento, M. F. A., Borgati, T. F., De Souza, L. C. R., Tagliati, C. A., and De Oliveira, A. B. (2020). "*In silico, in vitro* and *in vivo* evaluation of natural Bignoniaceous naphthoquinones in comparison with atovaquone targeting the selection of potential antimalarial candidates". In: *Toxicology and Applied Pharmacology*. Vol. 401, art. no. 115074. DOI: 10.1016/j.taap.2020.115074.

Dodson, C. A. (2017). "Production of protein kinases in *E. coli*". In: *Heterologous Gene Expression in E.coli. Methods in Molecular Biology*. Ed. by N. Burgess-Brown. Humana Press, pp. 251–264. DOI: 10.1007/978-1-4939-6887-9_16.

Doerig, C., Meijer, L., and Mottram, J. C. (2002). "Protein kinases as drug targets in parasitic protozoa". In: *Trends in Parasitology*. Vol. 18 (8), pp. 366–371. DOI: 10. 1016/s1471-4922(02)02321-8.

Doerig, C. (2004). "Protein kinases as targets for anti-parasitic chemotherapy". In: *Biochimica et Biophysica Acta (BBA) - Proteins and Proteomics*. Vol. 1697 (1-2), pp. 155–168. DOI: 10.1016/j.bbapap.2003.11.021.

Doerig, C. and Grevelding, C. G. (2015). "Targeting kinases in *Plasmodium* and *Schisto-soma*: same goals, different challenges". In: *Biochimica et Biophysica Acta (BBA) - Proteins and Proteomics*. Vol. 1854 (10), pp. 1637–1643. DOI: 10.1016/j.bbapap. 2015.03.002.

Dorey, K., Engen, J. R., Kretzschmar, J., Wilm, M., Neubauer, G., Schindler, T., and Superti-Furga, G. (2001). "Phosphorylation and structure-based functional studies reveal a positive and a negative role for the activation loop of the c-Abl tyrosine kinase". In: *Oncogene*. Vol. 20 (56), pp. 8075–8084. DOI: 10.1038/sj.onc.1205017.

Douville, J., Beaulieu, R., and Balicki, D. (2009). "Aldh1 as a functional marker of cancer stem and progenitor cells". In: *Stem Cells and Development*. Vol. 18 (1), pp. 17–25. DOI: 10.1089/scd.2008.0055.

Doyle, L. A., Yang, W., Abruzzo, L. V., Krogmann, T., Gao, Y., Rishi, A. K., and Ross, D. D. (1998). "A multidrug resistance transporter from human MCF-7 breast cancer cells". In: *Proceedings of the National Academy of Sciences of the United States of America*. Vol. 95 (26), pp. 15665–15670. DOI: 10.1073/pnas.95.26.15665.

Druker, B. J., Tamura, S., Buchdunger, E., Ohno, S., Segal, G. M., Fanning, S., Zim-mermann, J., and Lydon, N. B. (1996). "Effects of a selective inhibitor of the Abl tyrosine kinase on the growth of BCR–Abl positive cells". In: *Nature Medicine*. Vol. 2 (5), pp. 561–566. DOI: 10.1038/nm0596-561.

Du, X., McManus, D. P., French, J. D., Jones, M. K., and You, H. (2021). "CRISPR/Cas9: a new tool for the study and control of helminth parasites". In: *BioEssays: News and Reviews in Molecular, Cellular and Developmental Biology*. Vol. 43 (1), art. no. e2000185. DOI: 10.1002/bies.202000185.

Duan, G. and Walther, D. (2015). "The roles of post-translational modifications in the context of protein interaction networks". In: *PLoS Computational Biology*. Vol. 11 (2), art. no. e1004049. DOI: 10.1371/journal.pcbi.1004049.

Duester, G. (2000). "Families of retinoid dehydrogenases regulating vitamin A function". In: *European Journal of Biochemistry*. Vol. 267 (14), pp. 4315–4324. DOI: 10.1046/ j.1432-1327.2000.01497.x.

Dumay, Q. C., Debut, A. J., Mansour, N. M., and Saier, M. H. (2006). "The copper transporter (Ctr) family of Cu^+ uptake systems". In: *Journal of Molecular Microbiology and Biotechnology*. Vol. 11 (1-2), pp. 10–19. DOI: 10.1159/000092815.

Duvall, R. H. and DeWitt, W. B. (1967). "An improved perfusion technique for recovering adult schistosomes from laboratory animals". In: *The American Journal of Tropical Medicine and Hygiene*. Vol. 16 (4), pp. 483–486. DOI: 10.4269/ajtmh.1967.16.483.

Egner, U., Krätzschmar, J., Kreft, B., Pohlenz, H.-D., and Schneider, M. (2005). "The target discovery process". In: *Chembiochem: a European Journal of Chemical Biology*. Vol. 6 (3), pp. 468–479. DOI: 10.1002/cbic.200400158.

El Ridi, R., Ozaki, T., Inaba, T., Ito, M., and Kamiya, H. (1997). "*Schistosoma mansoni* oviposition *in vitro* reflects worm fecundity *in vivo*: individual-, parasite age- and host-dependent variations". In: *International Journal for Parasitology*. Vol. 27 (4), pp. 381–387. DOI: 10.1016/S0020-7519(96)00191-9.

Emadi, A., Jones, R. J., and Brodsky, R. A. (2009). "Cyclophosphamide and cancer: golden anniversary". In: *Nature Reviews Clinical Oncology*. Vol. 6 (11), pp. 638–647. DOI: 10.1038/nrclinonc.2009.146.

Erko, B., Degarege, A., Tadesse, K., Mathiwos, A., and Legesse, M. (2012). "Efficacy and side effects of praziquantel in the treatment of *Schistosomiasis mansoni* in schoolchildren in Shesha Kekele elementary school, Wondo Genet, Southern Ethiopia". In: *Asian Pacific Journal of Tropical Biomedicine*. Vol. 2 (3), pp. 235–239. DOI: 10.1016/S2221-1691(12)60049-5.

Erve, J. C., Jensen, O. N., Valentine, H. S., Amarnath, V., and Valentine, W. M. (2000). "Disulfiram generates a stable N,N-diethylcarbamoyl adduct on Cys-125 of rat hemo-globin β-chains *in vivo*". In: *Chemical Research in Toxicology*. Vol. 13 (4), pp. 237–244. DOI: 10.1021/tx990191n.

Fabbro, D., Cowan-Jacob, S. W., Möbitz, H., and Martiny-Baron, G. (2012). "Targeting cancer with small-molecular-weight kinase inhibitors". In: *Kinase Inhibitors. Methods in Molecular Biology*. Ed. by B. Kuster. Humana Press, pp. 1–34. DOI: 10.1007/978-1-61779-337-0_1.

Fallon, P. G. and Doenhoff, M. J. (1994). "Drug-resistant schistosomiasis: resistance to praziquantel and oxamniquine induced in *Schistosoma mansoni* in mice is drug specific". In: *The American Journal of Tropical Medicine and Hygiene*. Vol. 51 (1), pp. 83–88. DOI: 10.4269/ajtmh.1994.51.83.

References

Fan, K., Ni, X., Shen, S., Gong, Z., Wang, J., Xin, Y., Zheng, B., Sun, W., Liu, H., Suo, T., Ni, X., and Liu, H. (2022). "Acetylation stabilizes Stathmin1 and promotes its activity contributing to gallbladder cancer metastasis". In: *Cell Death Discovery*. Vol. 8 (1), art. no. 265. DOI: 10.1038/s41420-022-01051-z.

Fang, X., Yu, S. X., Lu, Y., Bast, R. C., Woodgett, J. R., and Mills, G. B. (2000). "Phosphorylation and inactivation of glycogen synthase kinase 3 by protein kinase A". In: *Proceedings of the National Academy of Sciences of the United States of America*. Vol. 97 (22), pp. 11960–11965. DOI: 10.1073/pnas.220413597.

Farias, L. P., Cardoso, F. C., Miyasato, P. A., Montoya, B. O., Tararam, C. A., Roffato, H. K., Kawano, T., Gazzinelli, A., Correa-Oliveira, R., Coulson, P. S., Wilson, R. A., Oliveira, S. C., and Leite, L. C. C. (2010). "*Schistosoma mansoni* stomatin like protein-2 is located in the tegument and induces partial protection against challenge infection". In: *PLoS Neglected Tropical Diseases*. Vol. 4 (2), e597. DOI: 10.1371/journal.pntd.0000597.

Fasano, M., Curry, S., Terreno, E., Galliano, M., Fanali, G., Narciso, P., Notari, S., and Ascenzi, P. (2005). "The extraordinary ligand binding properties of human serum albumin". In: *IUBMB Life*. Vol. 57 (12), pp. 787–796. DOI: 10.1080/15216540500404093.

Fasehee, H., Dinarvand, R., Ghavamzadeh, A., Esfandyari-Manesh, M., Moradian, H., Faghihi, S., and Ghaffari, S. H. (2016). "Delivery of disulfiram into breast cancer cells using folate-receptor-targeted PLGA-PEG nanoparticles: *in vitro* and *in vivo* investigations". In: *Journal of Nanobiotechnology*. Vol. 14, art. no. 32. DOI: 10.1186/s12951-016-0183-z.

Fasolo, J., Sboner, A., Sun, M. G. F., Yu, H., Chen, R., Sharon, D., Kim, P. M., Gerstein, M., and Snyder, M. (2011). "Diverse protein kinase interactions identified by protein microarrays reveal novel connections between cellular processes". In: *Genes & Development*. Vol. 25 (7), pp. 767–778. DOI: 10.1101/gad.1998811.

Fenton, H. J. H. (1894). "Oxidation of tartaric acid in presence of iron". In: *Journal of the Chemical Society, Transactions*. Vol. 65, pp. 899–910. DOI: 10.1039/CT8946500899.

Finkel, T. (2011). "Signal transduction by reactive oxygen species". In: *The Journal of Cell Biology*. Vol. 194 (1), pp. 7–15. DOI: 10.1083/jcb.201102095.

Forrester, S. G., Warfel, P. W., and Pearce, E. J. (2004). "Tegumental expression of a novel type II receptor serine/threonine kinase (SmRK2) in *Schistosoma mansoni*". In: *Molecular and Biochemical Parasitology*. Vol. 136 (2), pp. 149–156. DOI: 10.1016/j.molbiopara.2004.03.007.

Foster, R., Cheetham, B. L., and King, D. F. (1973). "Studies with the schistosomicide oxamniquine (uk-4271) II. Activity in primates". In: *Transactions of the Royal Society of Tropical Medicine and Hygiene*. Vol. 67 (5), pp. 685–693. DOI: 10.1016/0035-9203(73)90039-4.

Francis, G. L. (2010). "Albumin and mammalian cell culture: implications for biotechnology applications". In: *Cytotechnology*. Vol. 62 (1), pp. 1–16. DOI: 10.1007/s10616-010-9263-3.

Fraser, I. D. C., Tavalin, S. J., Lester, L. B., Langeberg, L. K., Westphal, A. M., Dean, R. A., Marrion, N. V., and Scott, J. D. (1998). "A novel lipid-anchored A-kinase anchoring protein facilitates cAMP-responsive membrane events". In: *The EMBO Journal*. Vol. 17 (8), pp. 2261–2272. DOI: 10.1093/emboj/17.8.2261.

Frazier, K. R., Moore, J. A., and Long, T. E. (2019). "Antibacterial activity of disulfiram and its metabolites". In: *Journal of Applied Microbiology*. Vol. 126 (1), pp. 79–86. DOI: 10.1111/jam.14094.

Frisch, S. M. and Screaton, R. A. (2001). "Anoikis mechanisms". In: *Current Opinion in Cell Biology*. Vol. 13 (5), pp. 555–562. DOI: 10.1016/s0955-0674(00)00251-9.

Fu, M., Wang, C., Zhang, X., and Pestell, R. G. (2004). "Acetylation of nuclear receptors in cellular growth and apoptosis". In: *Biochemical Pharmacology*. Vol. 68 (6), pp. 1199–1208. DOI: 10.1016/j.bcp.2004.05.037.

Galliher, A. J. and Schiemann, W. P. (2006). "β_3 integrin and SRC facilitate transforming growth factor-β mediated induction of epithelial-mesenchymal transition in mammary epithelial cells". In: *Breast Cancer Research*. Vol. 8 (4), art. no. R42. DOI: 10.1186/bcr1524.

Gallinger, T. L., Aboagye, S. Y., Obermann, W., Weiss, M., Grünweller, A., Unverzagt, C., Williams, D. L., Schlitzer, M., and Häberlein, S. (2022). "First *in* silico screening of insect molecules for identification of novel anti-parasitic compounds". In: *Pharmaceuticals*. Vol. 15 (2), art. no. 119. DOI: 10.3390/ph15020119.

Gallinger, T. L. (2022). "Entwicklung von Dithiocarbazat- und Dithiocarbamat-Derivaten als potenzielle Anthelminthik agegen *Schistosoma mansoni*". PhD thesis. Philipps-Universität Marburg. URL: https://archiv.ub.uni-marburg.de/diss/z2022/0233/pdf/dtlg.pdf.

Gamo, F.-J., Sanz, L. M., Vidal, J., De Cozar, C., Alvarez, E., Lavandera, J.-L., Vanderwall, D. E., Green, D. V. S., Kumar, V., Hasan, S., Brown, J. R., Peishoff, C. E., Cardon, L. R., and Garcia-Bustos, J. F. (2010). "Thousands of chemical starting points for antimalarial lead identification". In: *Nature*. Vol. 465 (7296), pp. 305–310. DOI: 10.1038/nature09107.

Gantke, T., Boussouf, S., Janzen, J., Morrice, N., Howell, S., Mühlberger, E., and Ley, S. C. (2013). "Ebola virus VP35 induces high-level production of recombinant TPL-2-ABIN-2-NF-κB1 p105 complex in co-transfected HEK-293 cells". In: *The Biochemical Journal*. Vol. 452 (2), pp. 359–365. DOI: 10.1042/BJ20121873.

Garrido, A., Lepailleur, A., Mignani, S. M., Dallemagne, P., and Rochais, C. (2020). "hERG toxicity assessment: useful guidelines for drug design". In: *European Journal of Medicinal Chemistry*. Vol. 195, art. no. 112290. DOI: 10.1016/j.ejmech.2020.112290.

Gashaw, I., Ellinghaus, P., Sommer, A., and Asadullah, K. (2011). "What makes a good drug target?" In: *Drug Discovery Today*. Vol. 16 (23-24), pp. 1037–1043. DOI: 10.1016/j.drudis.2011.09.007.

Gava, S. G., Tavares, N. C., De Matos Salim, A. C., De Araújo, F. M. G., Oliveira, G., and Mourão, M. M. (2017). "*Schistosoma mansoni*: off-target analyses using nonspecific double-stranded RNAs as control for RNAi experiments in schistosomula". In: *Experimental Parasitology*. Vol. 177, pp. 98–103. DOI: 10.1016/j.exppara.2017.04.011.

Gelmedin, V., Dissous, C., and Grevelding, C. G. (2015). "Re-positioning protein-kinase inhibitors against schistosomiasis". In: *Future Medicinal Chemistry*. Vol. 7 (6), pp. 737–752. DOI: 10.4155/fmc.15.31.

Gelmedin, V., Morel, M., Hahnel, S., Cailliau, K., Dissous, C., and Grevelding, C. G. (2017). "Evidence for integrin – venus kinase receptor 1 alliance in the ovary of *Schistosoma mansoni* females controlling cell survival". In: *PLoS Pathogens*. Vol. 13 (1), art. no. e1006147. DOI: 10.1371/journal.ppat.1006147.

Gilbert, I. H. (2014). "Target-based drug discovery for human African trypanosomiasis: selection of molecular target and chemical matter". In: *Parasitology*. Vol. 141 (1), pp. 28–36. DOI: 10.1017/S0031182013001017.

Ginestier, C., Hur, M. H., Charafe-Jauffret, E., Monville, F., Dutcher, J., Brown, M., Jacquemier, J., Viens, P., Kleer, C. G., Liu, S., Schott, A., Hayes, D., Birnbaum, D., Wicha, M. S., and Dontu, G. (2007). "Aldh1 is a marker of normal and malignant human mammary stem cells and a predictor of poor clinical outcome". In: *Cell Stem Cell*. Vol. 1 (5), pp. 555–567. DOI: 10.1016/j.stem.2007.08.014.

Giraud, S., Diaz-Latoud, C., Hacot, S., Textoris, J., Bourette, R. P., and Diaz, J.-J. (2004). "US11 of Herpes Simplex Virus type 1 interacts with HIPK2 and antagonizes HIPK2-induced cell growth arrest". In: *Journal of Virology*. Vol. 78 (6), pp. 2984–2993. DOI: 10.1128/JVI.78.6.2984-2993.2004.

280

Glassman, A. B., Rydzewski, R. S., and Bennett, C. E. (1980). "Trace metal levels in commercially prepared tissue culture media". In: *Tissue and Cell*. Vol. 12 (4), pp. 613–617. DOI: 10.1016/0040-8166(80)90016-6.

Goddard, C., Arnold, S. T., and Felsted, R. L. (1989). "High affinity binding of an N-terminal myristoylated p60Src peptide". In: *Journal of Biological Chemistry*. Vol. 264 (26), pp. 15173–15176. DOI: 10.1016/S0021-9258(19)84805-6.

Goff, S. P., Gilboa, E., Witte, O. N., and Baltimore, D. (1980). "Structure of the Abelson murine leukemia virus genome and the homologous cellular gene: studies with cloned viral DNA". In: *Cell*. Vol. 22 (3), pp. 777–785. DOI: 10.1016/0092-8674(80)90554-1.

Goldstein, M., Anagnoste, B., Lauber, E., and McKereghan, M. R. (1964). "Inhibition of dopamine-β-hydroxylase by disulfiram". In: *Life Sciences*. Vol. 3 (7), pp. 763–767. DOI: 10.1016/0024-3205(64)90031-1.

Gonnella, T. P., Leedahl, T. S., Karlstad, J. P., and Picklo, M. J. (2011). "NADH fluorescence lifetime analysis of the effect of magnesium ions on Aldh2". In: *Chemico-Biological Interactions*. Enzymology and Molecular Biology of Carbonyl Metabolism Vol. 191 (1-3), pp. 147–152. DOI: 10.1016/j.cbi.2011.01.023.

Gönnert, R. (1955). "Schistosomiasis-Studien I. Beitrage zur Anatomie und Histologie von *Schistosoma mansoni*". In: *Zeitschrift für Tropenmedizin und Parasitologie*. Vol. 6 (1), pp. 18–33. PMID: 14387064.

Gönnert, R. and Andrews, P. (1977). "Praziquantel, a new board-spectrum antischistosomal agent". In: *Zeitschrift für Parasitenkunde (Berlin, Germany)*. Vol. 52, pp. 129–150. DOI: 10.1007/BF00389899.

Gordon, R. M. and Seaton, D. R. (1942). "Observations on the treatment of scabies". In: *British Medical Journal*. Vol. 1, pp. 685–687. DOI: 10.1136/bmj.1.4248.685.

Gouignard, N., Vanderstraete, M., Cailliau, K., Lescuyer, A., Browaeys, E., and Dissous, C. (2012). "*Schistosoma mansoni*: structural and biochemical characterization of two distinct venus kinase receptors". In: *Experimental Parasitology*. Vol. 132 (1), pp. 32–39. DOI: 10.1016/j.exppara.2011.05.007.

Gouveia, M. J., Brindley, P. J., Gärtner, F., Da Costa, J. M. C., and Vale, N. (2018). "Drug repurposing for schistosomiasis: combinations of drugs or biomolecules". In: *Pharmaceuticals*. Vol. 11 (1), art. no. 15. DOI: 10.3390/ph11010015.

Gouy, M. and Gautier, C. (1982). "Codon usage in bacteria: correlation with gene expressivity". In: *Nucleic Acids Research*. Vol. 10 (22), pp. 7055–7074. DOI: 10.1093/nar/10.22.7055.

Gräslund, S., Nordlund, P., Weigelt, J., Hallberg, B. M., Bray, J., Gileadi, O., Knapp, S., Oppermann, U., Arrowsmith, C., Hui, R., Ming, J., dhe-Paganon, S., Park, H.-w., Savchenko, A., Yee, A., Edwards, A., Vincentelli, R., Cambillau, C., Kim, R., Kim, S.-H., Rao, Z., Shi, Y., Terwilliger, T. C., Kim, C.-Y., Hung, L.-W., Waldo, G. S., Peleg, Y., Albeck, S., Unger, T., Dym, O., Prilusky, J., Sussman, J. L., Stevens, R. C., Lesley, S. A., Wilson, I. A., Joachimiak, A., Collart, F., Dementieva, I., Donnelly, M. I., Eschenfeldt, W. H., Kim, Y., Stols, L., Wu, R., Zhou, M., Burley, S. K., Emtage, J. S., Sauder, J. M., Thompson, D., Bain, K., Luz, J., Gheyi, T., Zhang, F., Atwell, S., Almo, S. C., Bonanno, J. B., Fiser, A., Swaminathan, S., Studier, F. W., Chance, M. R., Sali, A., Acton, T. B., Xiao, R., Zhao, L., Ma, L. C., Hunt, J. F., Tong, L., Cunningham, K., Inouye, M., Anderson, S., Janjua, H., Shastry, R., Ho, C. K., Wang, D., Wang, H., Jiang, M., Montelione, G. T., Stuart, D. I., Owens, R. J., Daenke, S., Schütz, A., Heinemann, U., Yokoyama, S., Büssow, K., and Gunsalus, K. C. (2008). "Protein production and purification". In: *Nature Methods*. Vol. 5 (2), pp. 135–146. DOI: 10.1038/nmeth.f.202.

Gray, D. (1997). "Overview of protein expression by mammalian cells". In: *Current Protocols in Protein Science*. Vol. 10 (1), pp. 591–5918. DOI: 10.1002/0471140864. ps0509s10.

Grevelding, C. G. (1995). "The female-specific W1 sequence of the Puerto Rican strain of *Schistosoma mansoni* occurs in both genders of a Liberian strain". In: *Molecular and Biochemical Parasitology*. Vol. 71 (2), pp. 269–272. DOI: 10.1016/0166-6851 (94)00058-U.

Grevelding, C. G., Kampkötter, A., and Kunz, W. (1997). "*Schistosoma mansoni*: sexing cercariae by PCR without DNA extraction". In: *Experimental Parasitology*. Vol. 85 (1), pp. 99–100. DOI: 10.1006/expr.1996.4129.

Grevelding, C. G., Langner, S., and Dissous, C. (2018). "Kinases: molecular stage directors for schistosome development and differentiation". In: *Trends in Parasitology*. Vol. 34 (3), pp. 246–260. DOI: 10.1016/j.pt.2017.12.001.

Groeger, G., Quiney, C., and Cotter, T. G. (2009). "Hydrogen peroxide as a cell-survival signaling molecule". In: *Antioxidants & Redox Signaling*. Vol. 11 (11), pp. 2655–2671. DOI: 10.1089/ars.2009.2728.

Gu, J. J., Ryu, J. R., and Pendergast, A. M. (2009). "Abl tyrosine kinases in T-cell signaling". In: *Immunological Reviews*. Vol. 228 (1), pp. 170–183. DOI: 10.1111/j. 1600-065X.2008.00751.x.

Gunshin, H., Mackenzie, B., Berger, U. V., Gunshin, Y., Romero, M. F., Boron, W. F., Nussberger, S., Gollan, J. L., and Hediger, M. A. (1997). "Cloning and characterization of a mammalian proton-coupled metal-ion transporter". In: *Nature*. Vol. 388 (6641), pp. 482–488. DOI: 10.1038/41343.

Haacke, A., Fendrich, G., Ramage, P., and Geiser, M. (2009). "Chaperone over-expression in *Escherichia coli*: apparent increased yields of soluble recombinant protein kinases are due mainly to soluble aggregates". In: *Protein Expression and Purification*. Vol. 64 (2), pp. 185–193. DOI: 10.1016/j.pep.2008.10.022.

Haber, F. and Weiss, J. (15, 1934). "The catalytic decomposition of hydrogen peroxide by iron salts". In: *Proceedings of the Royal Society A: Mathematical, Physical and Engineering Sciences*. Vol. 147 (861), pp. 332–351. DOI: 10.1098/rspa.1934.0221.

Häberlein, S., Angrisano, A., Quack, T., Lu, Z., Kellershohn, J., Blohm, A., Grevelding, C. G., and Hahnel, S. R. (2019). "Identification of a new panel of reference genes to study pairing-dependent gene expression in *Schistosoma mansoni*". In: *International Journal for Parasitology*. Vol. 49 (8), pp. 615–624. DOI: 10.1016/j.ijpara.2019.01.006.

Hald, J. and Jacobsen, E. (1948). "The formation of acetaldehyde in the organism after ingestion of Antabuse (tetraethylthiuramdisulphide) and alcohol". In: *Acta Pharmacologica et Toxicologica*. Vol. 4 (3-4), pp. 305–310. DOI: 10.1111/j.1600-0773.1948.tb03352.x.

Halliwell, B. and Aruoma, O. I. (1991). "DNA damage by oxygen-derived species. Its mechanism and measurement in mammalian systems". In: *FEBS Letters*. Vol. 281 (1-2), pp. 9–19. DOI: 10.1016/0014-5793(91)80347-6.

Hammen, P. K., Allali-Hassani, A., Hallenga, K., Hurley, T. D., and Weiner, H. (2002). "Multiple conformations of NAD and NADH when bound to human cytosolic and mitochondrial aldehyde dehydrogenase". In: *Biochemistry*. Vol. 41 (22), pp. 7156–7168. DOI: 10.1021/bi012197t.

Han, J., Liu, L., Yue, X., Chang, J., Shi, W., and Hua, Y. (2013). "A binuclear complex constituted by diethyldithiocarbamate and copper(I) functions as a proteasome activity inhibitor in pancreatic cancer cultures and xenografts". In: *Toxicology and Applied Pharmacology*. Vol. 273 (3), pp. 477–483. DOI: 10.1016/j.taap.2013.09.009.

Hanks, S. K., Quinn, A. M., and Hunter, T. (1988). "The protein kinase family: conserved features and deduced phylogeny of the catalytic domains". In: *Science (New York, N. Y.)*. Vol. 241 (4861), pp. 42–52. DOI: 10.1126/science.3291115.

References

Hantschel, O., Nagar, B., Guettler, S., Kretzschmar, J., Dorey, K., Kuriyan, J., and Superti-Furga, G. (2003). "A myristoyl/phosphotyrosine switch regulates c-Abl". In: *Cell*. Vol. 112 (6), pp. 845–857. DOI: 10.1016/s0092-8674(03)00191-0.

Hantschel, O. and Superti-Furga, G. (2004). "Regulation of the c-Abl and Bcr–Abl tyrosine kinases". In: *Nature Reviews Molecular Cell Biology*. Vol. 5 (1), pp. 33–44. DOI: 10.1038/nrm1280.

Hantschel, O. and Superti-Furga, G. (2006). "Mechanisms of activation of Abl family kinases". In: *Abl Family Kinases in Development and Disease. Molecular Biology Intelligence Unit*. Ed. by A. J. Koleske. Springer, pp. 1–10. DOI: 10.1007/978-0-387-68744-5_1.

Hantschel, O., Rix, U., and Superti-Furga, G. (2008). "Target spectrum of the BCR-Abl inhibitors imatinib, nilotinib and dasatinib". In: *Leukemia & Lymphoma*. Vol. 49 (4), pp. 615–619. DOI: 10.1080/10428190801896103.

Harnischfeger, J., Beutler, M., Salzig, D., Rahlfs, S., Becker, K., Grevelding, C. G., and Czermak, P. (2021). "Biochemical characterization of the recombinant schistosome tegumental protein SmAldh_312 produced in *E. coli* and baculovirus expression vector system". In: *Electronic Journal of Biotechnology*. Vol. 54, pp. 26–36. DOI: 10.1016/j.ejbt.2021.08.002.

Harper, S. and Speicher, D. W. (2011). "Purification of proteins fused to glutathione S-tranferase". In: *Protein Chromatography. Methods in Molecular Biology book series*. Ed. by D. Walls and S. Loughran. Humana Press, pp. 259–280. DOI: 10.1007/978-1-60761-913-0_14.

Hart, B. W. and Faiman, M. D. (1993). "Bioactivation of S-methyl N,N-diethylthiolcarbamate to S-methyl N,N-diethylthiolcarbamate sulfoxide: implications for the role of cytochrome P450". In: *Biochemical Pharmacology*. Vol. 46 (12), pp. 2285–2290. DOI: 10.1016/0006-2952(93)90619-8.

Hassan, I., Khan, A. A., Aman, S., Qamar, W., Ebaid, H., Al-Tamimi, J., Alhazza, I. M., and Rady, A. M. (2018). "Restrained management of copper level enhances the antineoplastic activity of imatinib *in vitro* and *in vivo*". In: *Scientific Reports*. Vol. 8 (1), art. no. 1682. DOI: 10.1038/s41598-018-19410-1.

Hazra, M., Dolai, T., Pandey, A., Dey, S. K., and Patra, A. (2017). "Fluorescent copper(II) complexes: the electron transfer mechanism, interaction with bovine serum albumin (BSA) and antibacterial activity". In: *Journal of Saudi Chemical Society*. Vol. 21 (1), pp. 240–247. DOI: 10.1016/j.jscs.2014.02.009.

He, Y., Cai, G., Ni, Y., Li, Y., Zong, H., and He, L. (2012). "siRNA-mediated knock-down of two tyrosinase genes from *Schistosoma japonicum* cultured *in vitro*". In: *Experimental Parasitology*. Vol. 132 (4), pp. 394–402. DOI: 10.1016/j.exppara.2012.10.001.

Hemer, S. and Brehm, K. (2012). *"In vitro* efficacy of the anticancer drug imatinib on *Echinococcus multilocularis* larvae". In: *International Journal of Antimicrobial Agents*. Vol. 40 (5), pp. 458–462. DOI: 10.1016/j.ijantimicag.2012.07.007.

Henderson, L. E., Krutzsch, H. C., and Oroszlan, S. (1983). "Myristyl amino-terminal acylation of murine retrovirus proteins: an unusual post-translational proteins modification". In: *Proceedings of the National Academy of Sciences of the United States of America*. Vol. 80 (2), pp. 339–343. DOI: 10.1073/pnas.80.2.339.

Hernan, R. A., Hui, H. L., Andracki, M. E., Noble, R. W., Sligar, S. G., Walder, J. A., and Walder, R. Y. (1992). "Human hemoglobin expression in *Escherichia coli*: importance of optimal codon usage". In: *Biochemistry*. Vol. 31 (36), pp. 8619–8628. DOI: 10.1021/bi00151a032.

Hill, D. E. and Fetterer, R. H. (1997). "The effect of disulfiram on egg shell formation in adult *Trichuris muris*". In: *The Journal of Parasitology*. Vol. 83 (5), pp. 938–942. DOI: 10.2307/3284293.

Hirst, N. L., Nebel, J.-C., Lawton, S. P., and Walker, A. J. (2020). "Deep phosphoproteome analysis of *Schistosoma mansoni* leads development of a kinomic array that highlights sex-biased differences in adult worm protein phosphorylation". In: *PLoS Neglected Tropical Diseases*. Vol. 14 (3), art. no. e0008115. DOI: 10.1371/journal.pntd.0008115.

Hitz, E., Wiedemar, N., Passecker, A., Graça, B. A. S., Scheurer, C., Wittlin, S., Brancucci, N. M. B., Vakonakis, I., Mäser, P., and Voss, T. S. (2021). "The 3-phosphoinositide–dependent protein kinase 1 is an essential upstream activator of protein kinase A in malaria parasites". In: *PLoS Biology*. Vol. 19 (12), art. no. e3001483. DOI: 10.1371/journal.pbio.3001483.

Ho, K. K., Allali-Hassani, A., Hurley, T. D., and Weiner, H. (2005). "Differential effects of Mg^{2+} ions on the individual kinetic steps of human cytosolic and mitochondrial aldehyde dehydrogenases". In: *Biochemistry*. Vol. 44 (22), pp. 8022–8029. DOI: 10.1021/bi050038u.

Hochhaus, A., Kreil, S., Corbin, A. S., La Rosée, P., Müller, M. C., Lahaye, T., Hanfstein, B., Schoch, C., Cross, N. C. P., Berger, U., Gschaidmeier, H., Druker, B. J., and Hehlmann, R. (2002). "Molecular and chromosomal mechanisms of resistance to imatinib (STI571) therapy". In: *Leukemia*. Vol. 16 (11), pp. 2190–2196. DOI: 10. 1038/sj.leu.2402741.

Hong, Z., Kosman, D. J., Thakur, A., Rekosh, D., and LoVerde, P. T. (1992a). "Identification and purification of a second form of Cu/Zn superoxide dismutase from *Schistosoma mansoni*". In: *Infection and Immunity*. Vol. 60 (9), pp. 3641–3651. DOI: 10.1128/iai.60.9.3641-3651.1992.

Hong, Z., LoVerde, P. T., Hammarskjöld, M. L., and Rekosh, D. (1992b). "*Schistosoma mansoni*: cloning of a complementary DNA encoding a cytosolic Cu/Zn superoxide dismutase and high-yield expression of the enzymatically active gene product in *Escherichia coli*". In: *Experimental Parasitology*. Vol. 75 (3), pp. 308–322. DOI: 10.1016/0014-4894(92)90216-w.

Hong, Z., LoVerde, P. T., Thakur, A., Hammarskjöld, M. L., and Rekosh, D. (1993). "*Schistosoma mansoni*: a Cu/Zn superoxide dismutase is glycosylated when expressed in mammalian cells and localizes to a subtegumental region in adult schistosomes". In: *Experimental Parasitology*. Vol. 76 (2), pp. 101–114. DOI: 10.1006/expr.1993.1012.

Horowitz, J. C., Rogers, D. S., Sharma, V., Vittal, R., White, E. S., Cui, Z., and Thannickal, V. J. (2007). "Combinatorial activation of FAK and AKT by transforming growth factor-β1 confers an anoikis-resistant phenotype to myofibroblasts". In: *Cellular Signalling*. Vol. 19 (4), pp. 761–771. DOI: 10.1016/j.cellsig.2006.10.001.

Hosseini, M.-J., Shaki, F., Ghazi-Khansari, M., and Pourahmad, J. (2014). "Toxicity of copper on isolated liver mitochondria: impairment at complexes I, II, and IV leads to increased ROS production". In: *Cell Biochemistry and Biophysics*. Vol. 70 (1), pp. 367–381. DOI: 10.1007/s12013-014-9922-7.

Hotez, P. J. and Kamath, A. (2009). "Neglected tropical diseases in Sub-Saharan Africa: review of their prevalence, distribution, and disease burden". In: *PLoS Neglected Tropical Diseases*. Vol. 3 (8), art. no. e412. DOI: 10.1371/journal.pntd.0000412.

Houhou, H. (2022). "Identification and characterization of aldehyde dehydrogenases (Aldhs) and their suitability as drug targets against the liver fluke *Fasciola hepatica*". PhD thesis. Justus-Liebig-University.

Howe, K. L., Bolt, B. J., Cain, S., Chan, J., Chen, W. J., Davis, P., Done, J., Down, T., Gao, S., Grove, C., Harris, T. W., Kishore, R., Lee, R., Lomax, J., Li, Y., Muller, H.-M., Nakamura, C., Nuin, P., Paulini, M., Raciti, D., Schindelman, G., Stanley, E., Tuli, M. A., Van Auken, K., Wang, D., Wang, X., Williams, G., Wright, A., Yook, K., Berriman, M., Kersey, P., Schedl, T., Stein, L., and Sternberg, P. W. (2016). "WormBase 2016: expanding to enable helminth genomic research". In: *Nucleic Acids Research*. Vol. 44 (1), pp. 774–780. DOI: 10.1093/nar/gkv1217.

Howe, K. L., Bolt, B. J., Shafie, M., Kersey, P., and Berriman, M. (2017). "WormBase ParaSite − a comprehensive resource for helminth genomics". In: *Molecular and Biochemical Parasitology*. Vol. 215, pp. 2–10. DOI: 10.1016/j.molbiopara.2016.11.005.

Huang, E. H., Hynes, M. J., Zhang, T., Ginestier, C., Dontu, G., Appelman, H., Fields, J. Z., Wicha, M. S., and Boman, B. M. (2009). "Aldehyde dehydrogenase 1 is a marker for normal and malignant human colonic stem cells (SC) and tracks SC overpopulation during colon tumorigenesis". In: *Cancer Research*. Vol. 69 (8), pp. 3382–3389. DOI: 10.1158/0008-5472.CAN-08-4418.

Huang, B.-Y., Chen, P.-C., Chen, B.-H., Wang, C.-C., Liu, H.-F., Chen, Y.-Z., Chen, C.-S., and Yang, Y.-S. (2017). "High-throughput screening of sulfated proteins by using a genome-wide proteome microarray and protein tyrosine sulfation system". In: *Analytical Chemistry*. Vol. 89 (6), pp. 3278–3284. DOI: 10.1021/acs.analchem.6b02853.

Huang, X., Hou, Y., Weng, X., Pang, W., Hou, L., Liang, Y., Wang, Y., Du, L., Wu, T., Yao, M., Wang, J., and Meng, X. (2021). "Diethyldithiocarbamate-copper complex (CuET) inhibits colorectal cancer progression via miR-16-5p and 15b-5p/Aldh1A3/PKM2 axis-mediated aerobic glycolysis pathway". In: *Oncogenesis*. Vol. 10 (1), art. no. 4. DOI: 10.1038/s41389-020-00295-7.

Hunter, T. (1995). "Protein kinases and phosphatases: the yin and yang of protein phosphorylation and signaling". In: *Cell*. Vol. 80 (2), pp. 225–236. DOI: 10.1016/0092-8674(95)90405-0.

El-Husseini, A. E.-D. and Bredt, D. S. (2002). "Protein palmitoylation: a regulator of neuronal development and function". In: *Nature Reviews. Neuroscience*. Vol. 3 (10), pp. 791–802. DOI: 10.1038/nrn940.

Ikeda, J.-I., Mamat, S., Tian, T., Wang, Y., Luo, W., Rahadiani, N., Aozasa, K., and Morii, E. (2012). "Reactive oxygen species and aldehyde dehydrogenase activity in Hodgkin lymphoma cells". In: *Laboratory Investigation*. Vol. 92 (4), pp. 606–614. DOI: 10.1038/labinvest.2012.4.

References

Ikemura, T. (1985). "Codon usage and tRNA content in unicellular and multicellular organisms". In: *Molecular Biology and Evolution*. Vol. 2 (1), pp. 13–34. DOI: 10.1093/oxfordjournals.molbev.a040335.

Irie, Y., Tanaka, M., and Yasuraoka, K. (1987). "Degenerative changes in the reproductive organs of female schistosomes during maintenance *in vitro*". In: *The Journal of Parasitology*. Vol. 73 (4), pp. 829–835. PMID: 3625433.

Irish, V., Lehmann, R., and Akam, M. (1989). "The *Drosophila* posterior-group gene *nanos* functions by repressing hunchback activity". In: *Nature*. Vol. 338 (6217), pp. 646–648. DOI: 10.1038/338646a0.

Isaacson, R. L., Pye, V. E., Simpson, P., Meyer, H. H., Zhang, X., Freemont, P. S., and Matthews, S. (2007). "Detailed structural insights into the p97-NPL4-Ufd1 interface". In: *Journal of Biological Chemistry*. Vol. 282 (29), pp. 21361–21369. DOI: 10.1074/jbc.M610069200.

Ishizaki, T., Kamo, E., and Boehme, K. (1979). "Double-blind studies of tolerance to praziquantel in Japanese patients with *Schistosoma japonicum* infections". In: *Bulletin of the World Health Organization*. Vol. 57 (5), pp. 787–791. PMID: 396055.

Islam, M. S. and Ghosh, A. (2022). "Evolution, family expansion, and functional diversification of plant aldehyde dehydrogenases". In: *Gene*. Vol. 829, art. no. 146522. DOI: 10.1016/j.gene.2022.146522.

Ismail, M., Metwally, A., Farghaly, A., Bruce, J., Tao, L. F., and Bennett, J. L. (1996). "Characterization of isolates of *Schistosoma mansoni* from Egyptian villagers that tolerate high doses of praziquantel". In: *The American Journal of Tropical Medicine and Hygiene*. Vol. 55 (2), pp. 214–218. DOI: 10.4269/ajtmh.1996.55.214.

Ito, A., Lai, C. H., Zhao, X., Saito, S., Hamilton, M. H., Appella, E., and Yao, T. P. (2001). "p300/CBP-mediated p53 acetylation is commonly induced by p53-activating agents and inhibited by MDM2". In: *The EMBO Journal*. Vol. 20 (6), pp. 1331–1340. DOI: 10.1093/emboj/20.6.1331.

Ittiprasert, W., Mann, V. H., Karinshak, S. E., Coghlan, A., Rinaldi, G., Sankaranarayanan, G., Chaidee, A., Tanno, T., Kumkhaek, C., Prangtaworn, P., Mentink-Kane, M. M., Cochran, C. J., Driguez, P., Holroyd, N., Tracey, A., Rodpai, R., Everts, B., Hokke, C. H., Hoffmann, K. F., Berriman, M., and Brindley, P. J. (2019). "Programmed genome editing of the ω-1 ribonuclease of the blood fluke, *Schistosoma mansoni*". In: *eLife*. Vol. 8, art. no. e41337. DOI: 10.7554/eLife.41337.

Iurlaro, R. and Muñoz-Pinedo, C. (2015). "Cell death induced by endoplasmic reticulum stress". In: *The FEBS Journal*. Vol. 283 (14), pp. 2640–2652. DOI: 10.1111/febs.13598.

Jackson, P. and Baltimore, D. (1989). "N-terminal mutations activate the leukemogenic potential of the myristoylated form of c-Abl". In: *The EMBO Journal*. Vol. 8 (2), pp. 449–456. DOI: 10.1002/j.1460-2075.1989.tb03397.x.

Jackson, B., Brocker, C., Thompson, D. C., Black, W., Vasiliou, K., Nebert, D. W., and Vasiliou, V. (2011). "Update on the aldehyde dehydrogenase gene (Aldh) superfamily". In: *Human Genomics*. Vol. 5 (4), pp. 283–303. DOI: 10.1186/1479-7364-5-4-283.

Janic, A., Mendizabal, L., Llamazares, S., Rossell, D., and Gonzalez, C. (2010). "Ectopic expression of germline genes drives malignant brain tumor growth in *Drosophila*". In: *Science (New York, N. Y.)*. Vol. 330 (6012), pp. 1824–1827. DOI: 10.1126/science.1195481.

Jean, E., Laoudj-Chenivesse, D., Notarnicola, C., Rouger, K., Serratrice, N., Bonnieu, A., Gay, S., Bacou, F., Duret, C., and Carnac, G. (2011). "Aldehyde dehydrogenase activity promotes survival of human muscle precursor cells". In: *Journal of Cellular and Molecular Medicine*. Vol. 15 (1), pp. 119–133. DOI: 10.1111/j.1582-4934.2009.00942.x.

Jeong, H., Barbe, V., Lee, C. H., Vallenet, D., Yu, D. S., Choi, S.-H., Couloux, A., Lee, S.-W., Yoon, S. H., Cattolico, L., Hur, C.-G., Park, H.-S., Ségurens, B., Kim, S. C., Oh, T. K., Lenski, R. E., Studier, F. W., Daegelen, P., and Kim, J. F. (2009). "Genome sequences of *Escherichia coli* B strains REL606 and BL21(DE3)". In: *Journal of Molecular Biology*. Vol. 394 (4), pp. 644–652. DOI: 10.1016/j.jmb.2009.09.052.

Jeong, H., Kim, H. J., and Lee, S. J. (2015). "Complete genome sequence of *Escherichia coli* strain BL21". In: *Genome Announcements*. Vol. 3 (2), art. no. e00134–15. DOI: 10.1128/genomeA.00134-15.

Jia, B. and Jeon, C. O. (2016). "High-throughput recombinant protein expression in *Escherichia coli*: current status and future perspectives". In: *Open Biology*. Vol. 6 (8), art.no. 160196. DOI: 10.1098/rsob.160196.

Jia, Y., Jiang, J., Zhao, K., Zhang, T., Sun, P., Peng, J., Yang, Q., and Qian, Y. (2019). "Disulfiram suppressed ethanol promoted RANKL-induced osteoclastogenesis *in vitro* and ethanol-induced osteoporosis *in vivo* via Aldh1A1-NFATc1 axis". In: *Aging*. Vol. 11 (19), pp. 8103–8119. DOI: 10.18632/aging.102279.

Jin, X., Jiao, X., Jiao, J., Zhang, T., and Cui, B. (2018). "Increased expression of FHL2 promotes tumorigenesis in cervical cancer and is correlated with poor prognosis". In: *Gene*. Vol. 669, pp. 99–106. DOI: 10.1016/j.gene.2018.05.087.

Jing, S. Q. and Trowbridge, I. S. (1987). "Identification of the intermolecular disulfide bonds of the human transferrin receptor and its lipid-attachment site". In: *The EMBO Journal*. Vol. 6 (2), pp. 327–331. DOI: 10.1002/j.1460-2075.1987.tb04758.x.

Johannessen, M., Møller, S., Hansen, T., Moens, U., and Van Ghelue, M. (2006). "The multifunctional roles of the four-and-a-half-LIM only protein FHL2". In: *Cellular and Molecular Life Sciences: CMLS*. Vol. 63 (3), pp. 268–284. DOI: 10.1007/s000 18-005-5438-z.

Johansson, B. (1992). "A review of the pharmacokinetics and pharmacodynamics of disulfiram and its metabolites". In: *Acta Psychiatrica Scandinavica. Supplementum*. Vol. 86 (369), pp. 15–26. DOI: 10.1111/j.1600-0447.1992.tb03310.x.

Jonuleit, T., Van Der Kuip, H., Miething, C., Michels, H., Hallek, M., Duyster, J., and Aulitzky, W. E. (2000). "BCR-Abl kinase down-regulates cyclin-dependent kinase inhibitor p27 in human and murine cell lines". In: *Blood*. Vol. 96 (5), pp. 1933–1939. DOI: 10.1182/blood.V96.5.1933.

Joyce, C. M. and Benkovic, S. J. (2004). "DNA polymerase fidelity: kinetics, structure, and checkpoints". In: *Biochemistry*. Vol. 43 (45), pp. 14317–14324. DOI: 10.1021/ bi048422z.

Juliano, R. L. and Ling, V. (1976). "A surface glycoprotein modulating drug permeability in Chinese hamster ovary cell mutants". In: *Biochimica et Biophysica Acta (BBA) - Biomembranes*. Vol. 455 (1), pp. 152–162. DOI: 10.1016/0005-2736(76)90160-7.

Kaina, B. (2003). "DNA damage-triggered apoptosis: critical role of DNA repair, double-strand breaks, cell proliferation and signaling". In: *Biochemical Pharmacology*. Vol. 66 (8), pp. 1547–1554. DOI: 10.1016/s0006-2952(03)00510-0.

Kalinna, B. H. and Brindley, P. J. (2007). "Manipulating the manipulators: advances in parasitic helminth transgenesis and RNAi". In: *Trends in Parasitology*. Vol. 23 (5), pp. 197–204. DOI: 10.1016/j.pt.2007.03.007.

Kam, R. K. T., Deng, Y., Chen, Y., and Zhao, H. (2012). "Retinoic acid synthesis and functions in early embryonic development". In: *Cell & Bioscience*. Vol. 2 (1), art. no. 11. DOI: 10.1186/2045-3701-2-11.

Kampkötter, A., Ridgers, I., Johnston, D. A., Rollinson, D., Kunz, W., and Grevelding, C. G. (1999). "*Schistosoma mansoni*: cloning and characterization of the Ras homologue". In: *Experimental Parasitology*. Vol. 91 (3), pp. 280–283. DOI: 10. 1006/expr.1998.4377.

Kamps, M., Buss, J., and Sefton, B. (1985). "Mutation of NH$_2$-terminal glycine of p60Src prevents both myristoylation and morphological transformation". In: *Proceedings of the National Academy of Sciences of the United States of America*. Vol. 82 (14), pp. 4625–4628. DOI: 10.1073/PNAS.82.14.4625.

Kannappan, V., Ali, M., Small, B., Rajendran, G., Elzhenni, S., Taj, H., Wang, W., and Dou, Q. P. (2021). "Recent advances in repurposing disulfiram and disulfiram derivatives as copper-dependent anticancer agents". In: *Frontiers in Molecular Biosciences*. Vol. 8, art. no. 741316. DOI: 10.3389/fmolb.2021.741316.

Kapp, K., Schüssler, P., Kunz, W., and Grevelding, C. G. (2001). "Identification, isolation and characterization of a Fyn-like tyrosine kinase from *Schistosoma mansoni*". In: *Parasitology*. Vol. 122 (3), pp. 317–327. DOI: 10.1017/s0031182001007430.

Kapp, K., Knobloch, J., Schüssler, P., Sroka, S., Lammers, R., Kunz, W., and Grevelding, C. G. (2004). "The *Schistosoma mansoni* Src kinase TK3 is expressed in the gonads and likely involved in cytoskeletal organization". In: *Molecular and Biochemical Parasitology*. Vol. 138 (2), pp. 171–182. DOI: 10.1016/j.molbiopara.2004.07.010.

Katz, N., Rocha, R. S., and Chaves, A. (1979). "Preliminary trials with praziquantel in human infections due to *Schistosoma mansoni*". In: *Bulletin of the World Health Organization*. Vol. 57 (5), pp. 781–785. PMID: 396054.

Katz, N., Couto, F. F. B., and Araújo, N. (2013). "Imatinib activity on *Schistosoma mansoni*". In: *Memórias do Instituto Oswaldo Cruz*. Vol. 108 (7), pp. 850–853. DOI: 10.1590/0074-0276130207.

Kelley, K. C., Grossman, K. F., Brittain-Blankenship, M., Thorne, K. M., Akerley, W. L., Terrazas, M. C., Kosak, K. M., Boucher, K. M., Buys, S. S., McGregor, K. A., Werner, T. L., Agarwal, N., Weis, J. R., Sharma, S., Ward, J. H., Kennedy, T. P., Sborov, D. W., and Shami, P. J. (2021). "A phase 1 dose-escalation study of disulfiram and copper gluconate in patients with advanced solid tumors involving the liver using S-glutathionylation as a biomarker". In: *BMC Cancer*. Vol. 21 (1), art. no. 510. DOI: 10.1186/s12885-021-08242-4.

Kemble, D. J., Wang, Y.-H., and Gongqin, S. (2006). "Bacterial expression and characterization of catalytic loop mutants of Src protein tyrosine kinase". In: *Biochemistry*. Vol. 45 (49), pp. 14749–14754. DOI: 10.1021/bi061664+.

Kesely, K. R., Pantaleo, A., Turrini, F. M., Olupot-Olupot, P., and Low, P. S. (2016). "Inhibition of an erythrocyte tyrosine kinase with imatinib prevents *Plasmodium falciparum* egress and terminates parasitemia". In: *PloS One*. Vol. 11 (10), art. no. e0164895. DOI: 10.1371/journal.pone.0164895.

References

Khouri, R., Novais, F., Santana, G., De Oliveira, C. I., Vannier Dos Santos, M. A., Barral, A., Barral-Netto, M., and Van Weyenbergh, J. (2010). "DETC induces *Leishmania* parasite killing in human *in vitro* and murine *in vivo* models: a promising therapeutic alternative in leishmaniasis". In: *PLoS One*. Vol. 5 (12), art. no. e14394. DOI: 10.1371/journal.pone.0014394.

Khoury, G. A., Baliban, R. C., and Floudas, C. A. (2011). "Proteome-wide post-translational modification statistics: frequency analysis and curation of the swiss-prot database". In: *Scientific Reports*. Vol. 1, art. no. 90. DOI: 10.1038%2Fsrep00090.

Kibbe, W. A. (2007). "OligoCalc: an online oligonucleotide properties calculator". In: *Nucleic Acids Research*. Vol. 35 (Web Server Issue), pp. 43–46. DOI: 10.1093/nar/gkm234.

Kiernan, J. A. (2007). "Indigogenic substrates for detection and localization of enzymes". In: *Biotechnic & Histochemistry*. Vol. 82 (2), pp. 73–103. DOI: 10.1080/10520290701375278.

Kim, S., Jeong, H., Kim, E.-Y., Kim, J. F., Lee, S. Y., and Yoon, S. H. (2017). "Genomic and transcriptomic landscape of *Escherichia coli* BL21(DE3)". In: *Nucleic Acids Research*. Vol. 45 (9), pp. 5285–5293. DOI: 10.1093/nar/gkx228.

King, R. S. and Newmark, P. A. (2013). "*In situ* hybridization protocol for enhanced detection of gene expression in the planarian *Schmidtea mediterranea*". In: *BMC Developmental Biology*. Vol. 13, art. no. 8. DOI: 10.1186/1471-213X-13-8.

Klein, S., Geiger, T., Linchevski, I., Lebendiker, M., Itkin, A., Assayag, K., and Levitzki, A. (2005). "Expression and purification of active PKB kinase from *Escherichia coli*". In: *Protein Expression and Purification*. Vol. 41 (1), pp. 162–169. DOI: 10.1016/j.pep.2005.01.003.

Knobloch, J., Winnen, R., Quack, M., Kunz, W., and Grevelding, C. G. (2002). "A novel SYK-family tyrosine kinase from *Schistosoma mansoni* which is preferentially transcribed in reproductive organs". In: *Gene*. Vol. 294 (1-2), pp. 87–97. DOI: 10.1016/s0378-1119(02)00760-6.

Knobloch, J., Kunz, W., and Grevelding, C. G. (2006). "Herbimycin A suppresses mitotic activity and egg production of female *Schistosoma mansoni*". In: *International Journal for Parasitology*. Vol. 36 (12), pp. 1261–1272. DOI: 10.1016/j.ijpara.2006.06.004.

Knobloch, J., Beckmann, S., Burmeister, C., Quack, T., and Grevelding, C. G. (2007). "Tyrosine kinase and cooperative TGFβ signaling in the reproductive organs of *Schistosoma mansoni*". In: *Experimental Parasitology*. Vol. 117 (3), pp. 318–336. DOI: 10.1016/j.exppara.2007.04.006.

Koleske, A. J., Gifford, A. M., Scott, M. L., Nee, M., Bronson, R. T., Miczek, K. A., and Baltimore, D. (1998). "Essential roles for the Abl and Arg tyrosine kinases in neurulation". In: *Neuron*. Vol. 21 (6), pp. 1259–1272. DOI: 10.1016/s0896-6273(00) 80646-7.

Koppaka, V., Thompson, D. C., Chen, Y., Ellermann, M., Nicolaou, K. C., Juvonen, R. O., Petersen, D., Deitrich, R. A., Hurley, T. D., and Vasiliou, V. (2012). "Aldehyde dehydrogenase inhibitors: a comprehensive review of the pharmacology, mechanism of action, substrate specificity, and clinical application". In: *Pharmacological Reviews*. Vol. 64 (3), pp. 520–539. DOI: 10.1124/pr.111.005538.

Kotraiah, V., Pallares, D., Toema, D., Kong, D., and Beausoleil, E. (2012). "Identification of aldehyde dehydrogenase 1A1 modulators using virtual screening". In: *Journal of Enzyme Inhibition and Medicinal Chemistry*. Vol. 28 (3), pp. 489–494. DOI: 10. 3109/14756366.2011.653353.

Kotze, A. C. and Prichard, R. K. (2016). "Anthelmintic resistance in *Haemonchus contortus*: history, mechanisms and diagnosis". In: *Advances in Parasitology. Haemonchus contortus and haemonchosis – past, present and future trends*. Ed. by R. B. Gasser and G. Von Samson-Himmelstjerna. Elsevier, pp. 397–428. DOI: 10.1016/bs.apar. 2016.02.012.

Kouzarides, T. (2007). "Chromatin modifications and their function". In: *Cell*. Vol. 128 (4), pp. 693–705. DOI: 10.1016/j.cell.2007.02.005.

Kraft, R. and Harteneck, C. (2005). "The mammalian melastatin-related transient receptor potential cation channels: an overview". In: *Pflügers Archiv: European Journal of Physiology*. Vol. 451 (1), pp. 204–211. DOI: 10.1007/s00424-005-1428-0.

Kragh, H. (2008). "From disulfiram to Antabuse: the invention of a drug". Online. URL: https://www.semanticscholar.org/paper/FROM-DISULFIRAM-TO-ANTABUSE :-THE-INVENTION-OF-A-Kragh/f30ff3ad1251d78de43405a3065edab712cac8d 6 (visited on Aug. 9, 2022).

Krajaejun, T., Lohnoo, T., Yingyong, W., Rujirawat, T., Kumsang, Y., Jongkhajornpong, P., Theerawatanasirikul, S., Kittichotirat, W., Reamtong, O., and Yolanda, H. (2019). "The repurposed drug disulfiram inhibits urease and aldehyde dehydrogenase and prevents *in vitro* growth of the oomycete *Pythium insidiosum*". In: *Antimicrobial Agents and Chemotherapy*. Vol. 63 (8), art. no. e00609–19. DOI: 10.1128/AAC. 00609-19.

References

Krautz-Peterson, G., Radwanska, M., Ndegwa, D., Shoemaker, C. B., and Skelly, P. J. (2007). "Optimizing gene suppression in schistosomes using RNA interference". In: *Molecular and Biochemical Parasitology*. Vol. 153 (2), pp. 194–202. DOI: 10.1016/j.molbiopara.2007.03.006.

Kruh, G. D., King, C. R., Kraus, M. H., Popescu, N. C., Amsbaugh, S. C., McBride, W. O., and Aaronson, S. A. (1986). "A novel human gene closely related to the Abl proto-oncogene". In: *Science (New York, N. Y.)*. Vol. 234 (4783), pp. 1545–1548. DOI: 10.1126/science.3787260.

Kubiczkova, L., Sedlarikova, L., Hajek, R., and Sevcikova, S. (2012). "TGF-β – an excellent servant but a bad master". In: *Journal of Translational Medicine*. Vol. 10, art. no. 183. DOI: 10.1186/1479-5876-10-183.

Kumar, S., Stecher, G., Li, M., Knyaz, C., and Tamura, K. (2018). "MEGA X: molecular evolutionary genetics analysis across computing platforms". In: *Molecular Biology and Evolution*. Vol. 35 (6), pp. 1547–1549. DOI: 10.1093/molbev/msy096.

Kunz, W. (2001). "Schistosome male–female interaction: induction of germ-cell differentiation". In: *Trends in Parasitology*. Vol. 17 (5), pp. 227–231. DOI: 10.1016/S1471-4922(01)01893-1.

L'Abbé, D., Bisson, L., Gervais, C., Grazzini, E., and Durocher, Y. (2018). "Transient gene expression in suspension HEK293-EBNA1 cells". In: *Recombinant Protein Expression in Mammalian Cells. Methods in Molecular Biology*. Ed. by D. L. Hacker. Humana Press, pp. 1–16. DOI: 10.1007/978-1-4939-8730-6_1.

Laemmli, U. K. (1970). "Cleavage of structural proteins during the assembly of the head of bacteriophage T4". In: *Nature*. Vol. 227 (5259), pp. 680–685. DOI: 10.1038/227680a0.

Lahiry, P., Torkamani, A., Schork, N. J., and Hegele, R. A. (2010). "Kinase mutations in human disease: interpreting genotype–phenotype relationships". In: *Nature Reviews Genetics*. Vol. 11 (1), pp. 60–74. DOI: 10.1038/nrg2707.

Lalli, C., Guidi, A., Gennari, N., Altamura, S., Bresciani, A., and Ruberti, G. (2015). "Development and validation of a luminescence-based, medium-throughput assay for drug screening in *Schistosoma mansoni*". In: *PLoS Neglected Tropical Diseases*. Vol. 9 (1), art. no. e0003484. DOI: 10.1371/journal.pntd.0003484.

Langlais, C., Guilleaume, B., Wermke, N., Scheuermann, T., Ebert, L., LaBaer, J., and Korn, B. (2007). "A systematic approach for testing expression of human full-length proteins in cell-free expression systems". In: *BMC Biotechnology*. Vol. 7, art. no. 64. DOI: 10.1186/1472-6750-7-64.

Lassen, N., Bateman, J. B., Estey, T., Kuszak, J. R., Nees, D. W., Piatigorsky, J., Duester, G., Day, B. J., Huang, J., Hines, L. M., and Vasiliou, V. (2007). "Multiple and additive functions of Aldh3A1 and Aldh1A1: cataract phenotype and ocular oxidative damage in *aldh3a1$^{(-/-)}$/aldh1a1$^{(-/-)}$* knock-out mice". In: *The Journal of Biological Chemistry*. Vol. 282 (35), pp. 25668–25676. DOI: 10.1074/jbc.M702076200.

Le Clec'h, W., Chevalier, F. D., Mattos, A. C. A., Strickland, A., Diaz, R., McDew-White, M., Rohr, C. M., Kinung'hi, S., Allan, F., Webster, B. L., Webster, J. P., Emery, A. M., Rollinson, D., Djirmay, A. G., Al Mashikhi, K. M., Al Yafae, S., Idris, M. A., Moné, H., Mouahid, G., LoVerde, P., Marchant, J. S., and Anderson, T. J. C. (2021). "Genetic analysis of praziquantel response in schistosome parasites implicates a transient receptor potential channel". In: *Science Translational Medicine*. Vol. 13 (625), art. no. eabj9114. DOI: 10.1126/scitranslmed.abj9114.

Lebendiker, M. and Danieli, T. (2011). "Purification of proteins fused to maltose-binding protein". In: *Protein Chromatography. Methods in Molecular Biology*. Ed. by D. Walls and S. Loughran. Humana Press, pp. 281–293. DOI: 10.1007/978-1-60761-913-0_15.

Lee, C.-Y. S., Lu, T., and Seydoux, G. (2017). "Nanos promotes epigenetic reprograming of the germline by down-regulation of the THAP transcription factor LIN-15B". In: *eLife*. Vol. 6, art. no. e30201. DOI: 10.7554/eLife.30201.

Leibfried-Rutledge, M. L., Critser, E. S., and First, N. L. (1986). "Effects of fetal calf serum and bovine serum albumin on *in vitro* maturation and fertilization of bovine and hamster cumulus-oocyte complexes". In: *Biology of Reproduction*. Vol. 35 (4), pp. 850–857. DOI: 10.1095/biolreprod35.4.850.

Leitch, B. and Probert, A. J. (1984). "*Schistosoma haematobium*: amoscanate and adult worm ultrastructure". In: *Experimental Parasitology*. Vol. 58 (3), pp. 278–289. DOI: 10.1016/0014-4894(84)90045-6.

Lemmon, M. A. and Schlessinger, J. (2010). "Cell signaling by receptor-tyrosine kinases". In: *Cell*. Vol. 141 (7), pp. 1117–1134. DOI: 10.1016/j.cell.2010.06.011.

Lewinska, A., Wnuk, M., Slota, E., and Bartosz, G. (2007). "Total anti-oxidant capacity of cell culture media". In: *Clinical and Experimental Pharmacology and Physiology*. Vol. 34 (8), pp. 781–786. DOI: 10.1111/j.1440-1681.2007.04637.x.

Lewis, D. J., Deshmukh, P., Tedstone, A. A., Tuna, F., and O'Brien, P. (2014). "On the interaction of copper(II) with disulfiram". In: *Chemical Communications*. Vol. 50 (87), pp. 13334–13337. DOI: 10.1039/C4CC04767B.

Li, S., Couet, J., and Lisanti, M. P. (1996). "Src tyrosine kinases, G_α subunits, and H-Ras share a common membrane-anchored scaffolding protein, caveolin". In: *The Journal of Biological Chemistry*. Vol. 271 (46), pp. 29182–29190. DOI: 10.1074/jbc.271.46.29182.

Li, A., Xue, Y., Jin, C., Wang, M., and Yao, X. (2006). "Prediction of N^ϵ-acetylation on internal lysines implemented in Bayesian discriminant method". In: *Biochemical and Biophysical Research Communications*. Vol. 350 (4), pp. 818–824. DOI: 10.1016/j.bbrc.2006.08.199.

Li, H.-J., Liang, Y.-S., Dai, J.-R., Wang, W., Qu, G.-L., Li, Y.-Z., Xing, Y.-T., Tao, Y.-H., Qian, K., Jia, Y., Yang, Z.-K., and Wei, J.-Y. (2011). "Studies on resistance of *Schistosoma* to praziquantel XIV experimental comparison of susceptibility to praziquantel between PZQ-resistant isolates and PZQ-susceptible isolates of *Schistosoma japonicum* in stages of adult worms, miracidia and cercariae". In: *Zhongguo Xue Xi Chong Bing Fang Zhi Za Zhi = Chinese Journal of Schistosomiasis Control*. Vol. 23 (6), pp. 611–619. PMID: 22379813.

Li, M., Xu, M., Li, J., Chen, L., Xu, D., Tong, Y., Zhang, J., Wu, H., Kong, X., and Xia, Q. (2018a). "Alda-1 ameliorates liver Ischemia-reperfusion injury by activating aldehyde dehydrogenase 2 and enhancing autophagy in mice". In: *Journal of Immunology Research*. Vol. 2018, art. no 9807139. DOI: 10.1155/2018/9807139.

Li, Y., Wang, L.-H., Zhang, H.-T., Wang, Y.-T., Liu, S., Zhou, W.-L., Yuan, X.-Z., Li, T.-Y., Wu, C.-F., and Yang, J.-Y. (2018b). "Disulfiram combined with copper inhibits metastasis and epithelial-mesenchymal transition in hepatocellular carcinoma through the NF-κB and TGF-β pathways". In: *Journal of Cellular and Molecular Medicine*. Vol. 22 (1), pp. 439–451. DOI: 10.1111/jcmm.13334.

Li, X., Häberlein, S., Zhao, L., Mughal, M., Zhu, T., Liu, L., Fang, R., Zhou, Y., Zhao, J., Grevelding, C., and Hu, M. (2019). "The Abl kinase inhibitor imatinib causes phenotypic changes and lethality in adult *Schistosoma japonicum*". In: *Parasitology Research*. Vol. 118 (3), pp. 1–10. DOI: 10.1007/s00436-019-06224-x.

Li, P., Sarfati, D. N., Xue, Y., Yu, X., Tarashansky, A. J., Quake, S. R., and Wang, B. (2021). "Single-cell analysis of *Schistosoma mansoni* identifies a conserved genetic program controlling germline stem cell fate". In: *Nature Communications*. Vol. 12 (1), art. no. 485. DOI: 10.1038/s41467-020-20794-w.

Liang, Y.-S., Coles, G., Dai, J.-R., Zhu, Y.-C., and Doenhoff, M. (2002). "Adult worm tegumental damage and egg-granulomas in praziquantel-resistant and -susceptible *Schistosoma mansoni* treated *in vivo*". In: *Journal of Helminthology*. Vol. 76 (4), pp. 327–333. DOI: 10.1079/joh2002135.

Liegner, K. B. (2019). "Disulfiram tetraethylthiuram disulfide in the treatment of Lyme disease and babesiosis: report of experience in three cases". In: *Antibiotics (Basel, Switzerland)*. Vol. 8 (2), art. no. 72. DOI: 10.3390/antibiotics8020072.

Lin, Y.-L., Meng, Y., Jiang, W., and Roux, B. (2013). "Explaining why Gleevec is a specific and potent inhibitor of Abl kinase". In: *Proceedings of the National Academy of Sciences of the United States of America*. Vol. 110 (5), pp. 1664–1669. DOI: 10.1073/pnas.1214330110.

Liobikas, J., Polianskyte, Z., Speer, O., Thompson, J., Alakoskela, J. M., Peitsaro, N., Franck, M., Whitehead, M. A., Kinnunen, P. J. K., and Eriksson, O. (2006). "Expression and purification of the mitochondrial serine protease LACTB as an N-terminal GST fusion protein in *Escherichia coli*". In: *Protein Expression and Purification*. Vol. 45 (2), pp. 335–342. DOI: 10.1016/j.pep.2005.08.006.

Lipsky, J. J., Shen, M. L., and Naylor, S. (2001). "Overview–*in vitro* inhibition of aldehyde dehydrogenase by disulfiram and metabolites". In: *Chemico-Biological Interactions*. Vol. 130-132 (1-3), pp. 81–91. DOI: 10.1016/s0009-2797(00)00224-6.

Liu, Z. J., Sun, Y. J., Rose, J., Chung, Y. J., Hsiao, C. D., Chang, W. R., Kuo, I., Perozich, J., Lindahl, R., Hempel, J., and Wang, B. C. (1997). "The first structure of an aldehyde dehydrogenase reveals novel interactions between NAD and the Rossmann fold". In: *Nature Structural Biology*. Vol. 4 (4), pp. 317–326. DOI: 10.1038/nsb0497-317.

Liu, X., Wang, L., Cui, W., Yuan, X., Lin, L., Cao, Q., Wang, N., Li, Y., Guo, W., Zhang, X., Wu, C., and Yang, J. (2016). "Targeting Aldh1A1 by disulfiram/copper complex inhibits non-small cell lung cancer recurrence driven by Aldh-positive cancer stem cells". In: *Oncotarget*. Vol. 7 (36), pp. 58516–58530. DOI: 10.18632/oncotarget.11305.

Lobstein, J., Emrich, C. A., Jeans, C., Faulkner, M., Riggs, P., and Berkmen, M. (2012). "SHuffle, a novel *Escherichia coli* protein expression strain capable of correctly folding disulfide bonded proteins in its cytoplasm". In: *Microbial Cell Factories*. Vol. 11, art. no. 56. DOI: 10.1186/1475-2859-11-56.

Loeffler, I. K. and Bennett, J. L. (1996). "A rab-related GTP-binding protein in *Schistosoma mansoni*". In: *Molecular and Biochemical Parasitology*. Vol. 77 (1), pp. 31–40. DOI: 10.1016/0166-6851(96)02579-0.

Loidl, P. (1994). "Histone acetylation: facts and questions". In: *Chromosoma*. Vol. 103 (7), pp. 441–449. DOI: 10.1007/BF00337382.

Loignon, M., Perret, S., Kelly, J., Boulais, D., Cass, B., Bisson, L., Afkhamizarreh, F., and Durocher, Y. (2008). "Stable high volumetric production of glycosylated human recombinant IFNα2b in HEK293 cells". In: *BMC Biotechnology*. Vol. 8, art. no. 65. DOI: 10.1186/1472-6750-8-65.

Lorette, G., Jaafar, M. R., Grojean, M. F., and Duong, T. (1983). "Schistosomiasis mekongi diagnosed by rectal biopsy". In: *British Medical Journal (Clinical Research Edition)*. Vol. 286 (6383), pp. 2012–2013. DOI: 10.1136/bmj.286.6383.2012.

LoVerde, P. T. and Chen, L. (1991). "Schistosome female reproductive development". In: *Parasitology Today*. Vol. 7 (11), pp. 303–308. DOI: 10.1016/0169-4758(91)90263-N.

LoVerde, P. T. (1998). "Do antioxidants play a role in schistosome host-parasite interactions?" In: *Parasitology Today (Personal Edition)*. Vol. 14 (7), pp. 284–289. DOI: 10.1016/s0169-4758(98)01261-7.

LoVerde, P. T. (2019). "Schistosomiasis". In: *Digenetic Trematodes. Advances in Experimental Medicine and Biology*. Ed. by R. Toledo and B. Fried. Springer, pp. 45–70. DOI: 10.1007/978-3-030-18616-6_3.

Low, G. C. (1916). "The history of the use of intravenous injections of tartar emetic (antimonium tartaratum) in tropical medicine". In: *Transactions of the Royal Society of Tropical Medicine and Hygiene*. Vol. 10 (2), pp. 37–42. DOI: 10.1016/S0035-9203(16)90068-3.

Lu, Z., Sessler, F., Holroyd, N., Hahnel, S., Quack, T., Berriman, M., and Grevelding, C. G. (2016). "Schistosome sex matters: a deep view into gonad-specific and pairing-dependent transcriptomes reveals a complex gender interplay". In: *Scientific Reports*. Vol. 6, art. no. 31150. DOI: 10.1038/srep31150.

Lu, Z., Sessler, F., Holroyd, N., Hahnel, S., Quack, T., Berriman, M., and Grevelding, C. G. (2017). "A gene expression atlas of adult *Schistosoma mansoni* and their gonads". In: *Scientific Data*. Vol. 4, art. no. 170118. DOI: 10.1038/sdata.2017.118.

Lu, Z., Zhang, Y., and Berriman, M. (2018). "A web portal for gene expression across all life stages of *Schistosoma mansoni*". In: *BioRxiv.*, art. no. 308213. DOI: 10.1101/308213.

Lu, Z. and Berriman, M. (2018). "Meta-analysis of RNA-seq studies reveals genes responsible for life stage-dominant functions in *Schistosoma mansoni*". In: *BioRxiv.*, art. no. 308189. DOI: 10.1101/308189.

Lu, S., Wang, J., Chitsaz, F., Derbyshire, M. K., Geer, R. C., Gonzales, N. R., Gwadz, M., Hurwitz, D. I., Marchler, G. H., Song, J. S., Thanki, N., Yamashita, R. A., Yang, M., Zhang, D., Zheng, C., Lanczycki, C. J., and Marchler-Bauer, A. (2020). "CDD/SPARCLE: the conserved domain database in 2020". In: *Nucleic Acids Research*. Vol. 48 (1), pp. 265–268. DOI: 10.1093/nar/gkz991.

Ludolf, F., Patrocínio, P. R., Corrêa-Oliveira, R., Gazzinelli, A., Falcone, F. H., Teixeira-Ferreira, A., Perales, J., Oliveira, G. C., and Silva-Pereira, R. A. (2014). "Serological screening of the *Schistosoma mansoni* adult worm proteome". In: *PLoS Neglected Tropical Diseases*. Vol. 8 (3), art. no. e2745. DOI: 10.1371/journal.pntd.0002745.

Luo, Z., Xu, X., Sho, T., Zhang, J., Xu, W., Yao, J., and Xu, J. (2019). "ROS-induced autophagy regulates porcine trophectoderm cell apoptosis, proliferation, and differentiation". In: *American Journal of Physiology. Cell Physiology*. Vol. 316 (2), pp. 198–209. DOI: 10.1152/ajpcell.00256.2018.

Luttman, J. H., Colemon, A., Mayro, B., and Pendergast, A. M. (2021). "Role of the Abl tyrosine kinases in the epithelial–mesenchymal transition and the metastatic cascade". In: *Cell Communication and Signaling*. Vol. 19 (1), art. no. 59. DOI: 10.1186/s12964-021-00739-6.

Macek, B., Gnad, F., Soufi, B., Kumar, C., Olsen, J. V., Mijakovic, I., and Mann, M. (2008). "Phosphoproteome analysis of *E. coli* reveals evolutionary conservation of bacterial Ser/Thr/Tyr phosphorylation". In: *Molecular & Cellular Proteomics: MCP*. Vol. 7 (2), pp. 299–307. DOI: 10.1074/mcp.M700311-MCP200.

Mäder, P., Blohm, A. S., Quack, T., Lange-Grünweller, K., Grünweller, A., Hartmann, R. K., Grevelding, C. G., and Schlitzer, M. (2016). "Biarylalkyl carboxylic acid derivatives as novel antischistosomal agents". In: *ChemMedChem*. Vol. 11 (13), pp. 1459–1468. DOI: 10.1002/cmdc.201600127.

Mäder, P., Rennar, G. A., Peter Ventura, A. M., Grevelding, C. G., and Schlitzer, M. (2018). "Chemotherapy for fighting schistosomiasis: past, present and future". In: *ChemMedChem*. Vol. 13 (22), pp. 2374–2389. DOI: 10.1002/cmdc.201800572.

Mäder, P. (2016). "Synthese und biologische Testung von Biarylalkylcarbonsäure-Derivaten und Dithiocarbamat-Derivaten als potentielle anthelmintische Wirkstoffe gegen *Schistosoma mansoni*". PhD thesis. Philipps-University Marburg. URL: https://archiv.ub.uni-marburg.de/diss/z2016/0231/.

Magee, A., Gutiérrez, L., McKay, I., Marshall, C., and Hall, A. (1987). "Dynamic fatty acylation of p21N-Ras". In: *The EMBO Journal*. Vol. 6 (11), pp. 3353–3357. DOI: 10.1002/j.1460-2075.1987.tb02656.x.

Maiuri, M. C., Toumelin, G. L., Criollo, A., Rain, J.-C., Gautier, F., Juin, P., Tasdemir, E., Pierron, G., Troulinaki, K., Tavernarakis, N., Hickman, J. A., Geneste, O., and Kroemer, G. (2007). "Functional and physical interaction between BCL-X(L) and a BH3-like domain in Beclin-1". In: *The EMBO Journal*. Vol. 26 (10), pp. 2527–2539. DOI: 10.1038/sj.emboj.7601689.

Mamat, U., Wilke, K., Bramhill, D., Schromm, A. B., Lindner, B., Kohl, T. A., Corchero, J. L., Villaverde, A., Schaffer, L., Head, S. R., Souvignier, C., Meredith, T. C., and Woodard, R. W. (2015). "Detoxifying *Escherichia coli* for endotoxin-free production of recombinant proteins". In: *Microbial Cell Factories*. Vol. 14, art. no. 57. DOI: 10.1186/s12934-015-0241-5.

Manley, P. W., Cowan-Jacob, S. W., Buchdunger, E., Fabbro, D., Fendrich, G., Furet, P., Meyer, T., and Zimmermann, J. (2002). "Imatinib: a selective tyrosine kinase inhibitor". In: *European Journal of Cancer (Oxford, England: 1990)*. Vol. 38 (5), pp. 19–27. DOI: 10.1016/s0959-8049(02)80599-8.

Mann, V. H., Suttiprapa, S., Rinaldi, G., and Brindley, P. J. (2011). "Establishing transgenic schistosomes". In: *PLoS Neglected Tropical Diseases*. Vol. 5 (8), art. no. e1230. DOI: 10.1371/journal.pntd.0001230.

Manning, G., Plowman, G. D., Hunter, T., and Sudarsanam, S. (2002a). "Evolution of protein kinase signaling from yeast to man". In: *Trends in Biochemical Sciences*. Vol. 27 (10), pp. 514–520. DOI: 10.1016/s0968-0004(02)02179-5.

Manning, G., Whyte, D. B., Martinez, R., Hunter, T., and Sudarsanam, S. (2002b). "The protein kinase complement of the human genome". In: *Science (New York, N. Y.)*. Vol. 298 (5600), pp. 1912–1934. DOI: 10.1126/science.1075762.

Manning, G. (2005). "Genomic overview of protein kinases". In: *The C. elegans Research Community*. Ed. by WormBook. WormBook, pp. 1–19. DOI: 10.1895/wormbook.1.60.1.

Marchildon, G. A., Casnellie, J. E., Walsh, K. A., and Krebs, E. G. (1984). "Covalently bound myristate in a lymphoma tyrosine protein kinase". In: *Proceedings of the National Academy of Sciences of the United States of America*. Vol. 81 (24), pp. 7679–7682. DOI: 10.1073/pnas.81.24.7679.

Marchitti, S. A., Brocker, C., Stagos, D., and Vasiliou, V. (2008). "Non-P450 aldehyde oxidizing enzymes: the aldehyde dehydrogenase superfamily". In: *Expert Opinion on Drug Metabolism & Toxicology*. Vol. 4 (6), pp. 697–720. DOI: 10.1517/17425255.4.6.697.

Marchitti, S. A., Deitrich, R. A., and Vasiliou, V. (2007). "Neurotoxicity and metabolism of the catecholamine-derived 3,4-dihydroxyphenylacetaldehyde and 3,4-dihydroxy-phenylglycolaldehyde: the role of aldehyde dehydrogenase". In: *Pharmacological Reviews*. Vol. 59 (2), pp. 125–150. DOI: 10.1124/pr.59.2.1.

Marklund, S. L. (1984). "Extracellular superoxide dismutase and other superoxide dismutase isoenzymes in tissues from nine mammalian species". In: *Biochemical Journal*. Vol. 222 (3), pp. 649–655. DOI: 10.1042/bj2220649.

Massagué, J. (1998). "TGF-β signal transduction". In: *Annual Review of Biochemistry*. Vol. 67, pp. 753–791. DOI: 10.1146/annurev.biochem.67.1.753.

Matte, A., Tari, L. W., and Delbaere, L. T. J. (1998). "How do kinases transfer phosphoryl groups?" In: *Structure (London, England: 1993)*. Vol. 6 (4), pp. 413–419. DOI: 10.1016/S0969-2126(98)00043-4.

Maurya, R. and Namdeo, M. (2021). "Superoxide dismutase: a key enzyme for the survival of intracellular pathogens in host". In: *Reactive Oxygen Species*. Ed. by R. Ahmad. IntechOpen, pp. 1–25. DOI: 10.5772/intechopen.100322.

Mays, D. C., Nelson, A. N., Fauq, A. H., Shriver, Z. H., Veverka, K. A., Naylor, S., and Lipsky, J. J. (1995). "S-methyl N,N-diethylthiocarbamate sulfone, a potential metabolite of disulfiram and potent inhibitor of low Km mitochondrial aldehyde dehydrogenase". In: *Biochemical Pharmacology*. Vol. 49 (5), pp. 693–700. DOI: 10.1016/0006-2952(94)00504-F.

Mazumder, T. H., Alqahtani, A. M., Alqahtani, T., Emran, T. B., A. Aldahish, A., and Uddin, A. (2021). "Analysis of codon usage of speech gene *FoxP2* among animals". In: *Biology*. Vol. 10 (11), art. no. 1078. DOI: 10.3390/biology10111078.

McCubrey, J. A., Steelman, L. S., Chappell, W. H., Abrams, S. L., Wong, E. W. T., Chang, F., Lehmann, B., Terrian, D. M., Milella, M., Tafuri, A., Stivala, F., Libra, M., Basecke, J., Evangelisti, C., Martelli, A. M., and Franklin, R. A. (2007). "Roles of the Raf/MEK/ERK pathway in cell growth, malignant transformation and drug resistance". In: *Biochimica et Biophysica Acta (BBA) - Molecular Cell Research*. Vol. 1773 (8), pp. 1263–1284. DOI: 10.1016/j.bbamcr.2006.10.001.

McKenzie, E. A. and Abbott, W. M. (2018). "Expression of recombinant proteins in insect and mammalian cells". In: *Methods (San Diego, California)*. Vol. 147, pp. 40–49. DOI: 10.1016/j.ymeth.2018.05.013.

McMahon, J. E. and Kolstrup, N. (1979). "Praziquantel: a new schistosomicide against *Schistosoma haematobium*". In: *British Medical Journal*. Vol. 2 (6202), pp. 1396–1398. DOI: 10.1136/bmj.2.6202.1396.

References

Meggyesy, P. M., Masaldan, S., Clatworthy, S. A. S., Volitakis, I., Eyckens, D. J., Aston-Mourney, K., and Cater, M. A. (2020). "Copper ionophores as novel antiobesity therapeutics". In: *Molecules (Basel, Switzerland)*. Vol. 25 (21), art. no. 4957. DOI: 10.3390/molecules25214957.

Mehta, R., Templeton, D. M., and O'Brien, P. J. (2006). "Mitochondrial involvement in genetically determined transition metal toxicity II. Copper toxicity". In: *Chemico-Biological Interactions*. Vol. 163 (1-2), pp. 77–85. DOI: 10.1016/j.cbi.2006.05.011.

Mei, H. and LoVerde, P. T. (1997). "*Schistosoma mansoni*: the developmental regulation and immunolocalization of antioxidant enzymes". In: *Experimental Parasitology*. Vol. 86 (1), pp. 69–78. DOI: 10.1006/expr.1997.4150.

Meissner, P., Pick, H., Kulangara, A., Chatellard, P., Friedrich, K., and Wurm, F. M. (2001). "Transient gene expression: recombinant protein production with suspension-adapted HEK293-EBNA cells". In: *Biotechnology and Bioengineering*. Vol. 75 (2), pp. 197–203. DOI: 10.1002/bit.1179.

Meraz-Torres, F., Plöger, S., Garbe, C., Niessner, H., and Sinnberg, T. (2020). "Disulfiram as a therapeutic agent for metastatic malignant melanoma—old myth or new logos?" In: *Cancers*. Vol. 12 (12), art. no. 3538. DOI: 10.3390/cancers12123538.

Messing, J., Gronenborn, B., Müller-Hill, B., and Hans Hopschneider, P. (1977). "Filamentous coliphage M13 as a cloning vehicle: insertion of a *Hind*II fragment of the lac regulatory region in M13 replicative form *in vitro*". In: *Proceedings of the National Academy of Sciences of the United States of America*. Vol. 74 (9), pp. 3642–3646. DOI: 10.1073/pnas.74.9.3642.

Milligan, G., Parenti, M., and Magee, A. I. (1995). "The dynamic role of palmitoylation in signal transduction". In: *Trends in Biochemical Sciences*. Vol. 20 (5), pp. 181–187. DOI: 10.1016/s0968-0004(00)89004-0.

Mitta, G., Adema, C. M., Gourbal, B., Loker, E. S., and Theron, A. (2012). "Compatibility polymorphism in snail/schistosome interactions: from field to theory to molecular mechanisms". In: *Developmental and Comparative Immunology*. Vol. 37 (1), pp. 1–8. DOI: 10.1016/j.dci.2011.09.002.

Mittal, M., Khan, K., Pal, S., Porwal, K., China, S. P., Barbhuyan, T. K., Baghel, K. S., Rawat, T., Sanyal, S., Bhadauria, S., Sharma, V. L., and Chattopadhyay, N. (2014). "The thiocarbamate disulphide drug, disulfiram induces osteopenia in rats by inhibition of osteoblast function due to suppression of acetaldehyde dehydrogenase activity". In: *Toxicological Sciences: an Official Journal of the Society of Toxicology*. Vol. 139 (1), pp. 257–270. DOI: 10.1093/toxsci/kfu020.

Mizuno, T., Suzuki, N., Makino, H., Furui, T., Morii, E., Aoki, H., Kunisada, T., Yano, M., Kuji, S., Hirashima, Y., Arakawa, A., Nishio, S., Ushijima, K., Ito, K., Itani, Y., and Morishige, K. (2015). "Cancer stem-like cells of ovarian clear cell carcinoma are enriched in the Aldh-high population associated with an accelerated scavenging system in reactive oxygen species". In: *Gynecologic Oncology*. Vol. 137 (2), pp. 299–305. DOI: 10.1016/j.ygyno.2014.12.005.

Mkoji, G. M., Smith, J. M., and Prichard, R. K. (1988). "Antioxidant systems in *Schistosoma mansoni*: correlation between susceptibility to oxidant killing and the levels of scavengers of hydrogen peroxide and oxygen free radicals". In: *International Journal for Parasitology*. Vol. 18 (5), pp. 661–666. DOI: 10.1016/0020-7519(88)90101-4.

Mochizuki, K., Sano, H., Kobayashi, S., Nishimiya-Fujisawa, C., and Fujisawa, T. (2000). "Expression and evolutionary conservation of *nanos*-related genes in *Hydra*". In: *Development Genes and Evolution*. Vol. 210 (12), pp. 591–602. DOI: 10.1007/s004270000105.

Moguel, B., Bobes, R. J., Carrero, J. C., and Laclette, J. P. (2015). "Transfection of platyhelminthes". In: *BioMed Research International*. Vol. 2015, art. no. 206161. DOI: 10.1155/2015/206161.

Moine, E., Denevault-Sabourin, C., Debierre-Grockiego, F., Silpa, L., Gorgette, O., Barale, J.-C., Jacquiet, P., Brossier, F., Gueiffier, A., Dimier-Poisson, I., and Enguehard-Gueiffier, C. (2015). "A small-molecule cell-based screen led to the identification of biphenylimidazoazines with highly potent and broad-spectrum anti-apicomplexan activity". In: *European Journal of Medicinal Chemistry*. Vol. 89, pp. 386–400. DOI: 10.1016/j.ejmech.2014.10.057.

Mokosch, A. S., Gerbig, S., Grevelding, C. G., Häberlein, S., and Spengler, B. (2021). "High-resolution AP-SMALDI MSI as a tool for drug imaging in *Schistosoma mansoni*". In: *Analytical and Bioanalytical Chemistry*. Vol. 413 (10), pp. 2755–2766. DOI: 10.1007/s00216-021-03230-w.

Molla, G., Tintagu, T., Yasin, A., Alemu, B., Assen, A. A., and Tadesse, K. (2022). "Bovine schistosomiasis in some selected areas of South Wollo and Oromia zones of Amhara region, North-East Ethiopia". In: *PLoS One*. Vol. 17 (6), art. no. e0259787. DOI: 10.1371/journal.pone.0259787.

Møller, G. M. O., Frost, V., Melo, J. V., and Chantry, A. (2007). "Upregulation of the TGFβ signalling pathway by BCR-Abl: implications for haemopoietic cell growth and chronic myeloid leukaemia". In: *FEBS Letters*. Vol. 581 (7), pp. 1329–1334. DOI: 10.1016/j.febslet.2007.02.048.

Molyneux, D. (2013). "Neglected tropical diseases". In: *Community Eye Health*. Vol. 26 (82), pp. 21–24. PMID: 24023397.

Moné, H. and Boissier, J. (2004). "Sexual biology of schistosomes". In: *Advances in Parasitology*. Vol. 57, pp. 89–189. DOI: 10.1016/S0065-308X(04)57002-1.

Moore, D. V. and Sandground, J. H. (1956). "The relative egg producing capacity of *Schistosoma mansoni* and *Schistosoma japonicum*". In: *The American Journal of Tropical Medicine and Hygiene*. Vol. 5 (5), pp. 831–840. DOI: 10.4269/ajtmh.1956. 5.831.

Moore, S., Baker, H., Blythe, T. J., Kitson, K., Kitson, T., and Baker, E. (1998). "Sheep liver cytosolic aldehyde dehydrogenase: the structure reveals the basis for the retinal specificity of class 1 aldehyde dehydrogenases". In: *Structure (London, England: 1993)*. Vol. 6 (12), pp. 1541–1551. DOI: 10.1016/S0969-2126(98)00152-X.

Moreb, J. S., Maccow, C., Schweder, M., and Hecomovich, J. (2000). "Expression of antisense RNA to aldehyde dehydrogenase class-1 sensitizes tumor cells to 4-hydroperoxycy-clophosphamide *in vitro*". In: *The Journal of Pharmacology and Experimental Therapeutics*. Vol. 293 (2), pp. 390–396. PMID: 10773007.

Morel, M., Vanderstraete, M., Hahnel, S., Grevelding, C. G., and Dissous, C. (2014). "Receptor tyrosine kinases and schistosome reproduction: new targets for chemotherapy". In: *Frontiers in Genetics*. Vol. 5, art. no. 238. DOI: 10.3389/fgene.2014.00238.

Morera, F. J., Wolff, D., and Vergara, C. (2003). "External copper inhibits the activity of the large-conductance calcium- and voltage-sensitive potassium channel from skeletal muscle". In: *The Journal of Membrane Biology*. Vol. 192 (1), pp. 65–72. DOI: 10.1007/s00232-002-1064-y.

Moretti, A., Li, J., Donini, S., Sobol, R. W., Rizzi, M., and Garavaglia, S. (2016). "Crystal structure of human aldehyde dehydrogenase 1A3 complexed with NAD$^+$ and retinoic acid". In: *Scientific Reports*. Vol. 6, art. no. 35710. DOI: 10.1038/ srep35710.

Morgan, C. and Hurley, T. (2015). "Development of a high-throughput *in vitro* assay to identify selective inhibitors for human Aldh1A1". In: *Chemico-Biological Interactions*. Vol. 234, pp. 29–37. DOI: 10.1016/j.cbi.2014.10.028.

Morlon, A. and Sassone-Corsi, P. (2003). "The LIM-only protein FHL2 is a serum-inducible transcriptional coactivator of AP-1". In: *Proceedings of the National Academy of Sciences of the United States of America*. Vol. 100 (7), pp. 3977–3982. DOI: 10.1073/pnas.0735923100.

Morrison, T. B., Weis, J. J., and Wittwer, C. T. (1998). "Quantification of low-copy transcripts by continuous SYBR Green I monitoring during amplification". In: *BioTechniques*. Vol. 24 (6), 954-958, 960, 962. PMID: 9631186.

Morrison, B. W., Doudican, N. A., Patel, K. R., and Orlow, S. J. (2010). "Disulfiram induces copper-dependent stimulation of reactive oxygen species and activation of the extrinsic apoptotic pathway in melanoma". In: *Melanoma Research*. Vol. 20 (1), pp. 11–20. DOI: 10.1097/CMR.0b013e328334131d.

Mughal, M. N., Grevelding, C. G., and Häberlein, S. (2022). "The anticancer drug imatinib induces autophagy in *Schistosoma mansoni*". In: *International Journal for Parasitology*. Vol. 52 (4), pp. 211–215. DOI: 10.1016/j.ijpara.2021.10.008.

Müller, S. (2019). *Erste Untersuchungen zur Wirkung von Disulfiram gegen Schistosoma mansoni*. Internship report. Justus-Liebig-University Giessen.

Mullis, K. B. (1990). "The unusual origin of the polymerase chain reaction". In: *Scientific American*. Vol. 262 (4), pp. 56–61, 64–65. DOI: 10.1038/scientificamerican0490-56.

Mutschler, J. and Grosshans, M. (2016). "Stellenwert der Disulfiramtherapie heute?" In: *Nervenheilkunde*. Vol. 35 (11), pp. 748–751. DOI: 10.1055/s-0037-1616446.

Muzio, G., Maggiora, M., Paiuzzi, E., Oraldi, M., and Canuto, R. A. (2012). "Aldehyde dehydrogenases and cell proliferation". In: *Free Radical Biology & Medicine*. Vol. 52 (4), pp. 735–746. DOI: 10.1016/j.freeradbiomed.2011.11.033.

Nagar, B., Hantschel, O., Young, M. A., Scheffzek, K., Veach, D., Bornmann, W., Clarkson, B., Superti-Furga, G., and Kuriyan, J. (2003). "Structural basis for the autoinhibition of c-Abl tyrosine kinase". In: *Cell*. Vol. 112 (6), pp. 859–871. DOI: 10.1016/s0092-8674(03)00194-6.

Nagar, B. (2007). "c-Abl tyrosine kinase and inhibition by the cancer drug imatinib (Gleevec/STI-571)". In: *The Journal of Nutrition*. Vol. 137 (6), pp. 1518–1523. DOI: 10.1093/jn/137.6.1518S.

Nare, B., Smith, J. M., and Prichard, R. K. (1990). "*Schistosoma mansoni*: levels of antioxidants and resistance to oxidants increase during development". In: *Experimental Parasitology*. Vol. 70 (4), pp. 389–397. DOI: 10.1016/0014-4894(90)90122-s.

Nawaratna, S. S. K., McManus, D. P., Gasser, R. B., Brindley, P. J., Boyle, G. M., Rivera, V., Ranasinghe, S. L., Jones, M. K., You, H., and Gobert, G. N. (2020). "Use of kinase inhibitors against schistosomes to improve and broaden praziquantel efficacy". In: *Parasitology*. Vol. 147 (13), pp. 1488–1498. DOI: 10.1017/S0031182020001250.

Neet, K. and Hunter, T. (1996). "Vertebrate non-receptor protein–tyrosine kinase families". In: *Genes to Cells: Devoted to Molecular & Cellular Mechanisms*. Vol. 1 (2), pp. 147–169. DOI: 10.1046/j.1365-2443.1996.d01-234.x.

Nene, A., Chen, C.-H., Disatnik, M.-H., Cruz, L., and Mochly-Rosen, D. (2017). "Aldehyde dehydrogenase 2 activation and coevolution of its εPKC-mediated phosphorylation sites". In: *Journal of Biomedical Science*. Vol. 24 (1), art. no. 3. DOI: 10.1186/s12929-016-0312-x.

Nettleship, J. E., Watson, P. J., Rahman-Huq, N., Fairall, L., Posner, M. G., Upadhyay, A., Reddivari, Y., Chamberlain, J. M. G., Kolstoe, S. E., Bagby, S., Schwabe, J. W. R., and Owens, R. J. (2015). "Transient expression in HEK 293 cells: an alternative to *E. coli* for the production of secreted and intracellular mammalian proteins". In: *Insoluble Proteins. Methods in Molecular Biology*. Ed. by E. García-Fruitós. Humana Press, pp. 209–222. DOI: 10.1007/978-1-4939-2205-5_11.

Neves, R. H., Lamare Biolchini, C. de, Machado-Silva, J. R., Carvalho, J. J., Branquinho, T. B., Lenzi, H. L., Hulstijn, M., and Gomes, D. C. (2005). "A new description of the reproductive system of *Schistosoma mansoni* (Trematoda: Schistosomatidae) analyzed by confocal laser scanning microscopy". In: *Parasitology Research*. Vol. 95 (1), pp. 43–49. DOI: 10.1007/s00436-004-1241-2.

Newmark, P. A. and Sánchez Alvarado, A. (2002). "Not your father's planarian: a classic model enters the era of functional genomics". In: *Nature Reviews Genetics*. Vol. 3 (3), pp. 210–219. DOI: 10.1038/nrg759.

Nielsen, K. H. (2014). "Protein expression-yeast". In: *Methods in Enzymology*. Vol. 536. Ed. by J. Lorsch, pp. 133–147. DOI: 10.1016/B978-0-12-420070-8.00012-X.

Nishi, H., Hashimoto, K., and Panchenko, A. R. (2011). "Phosphorylation in protein-protein binding: effect on stability and function". In: *Structure (London, England: 1993)*. Vol. 19 (12), pp. 1807–1815. DOI: 10.1016/j.str.2011.09.021.

O'Brien, P. S., Xi, Y., Miller, J. R., Brownell, A. L., Zeng, Q., Yoo, G. H., Garshott, D. M., O'Brien, M. B., Galinato, A. E., Cai, P., Narula, N., Callaghan, M. U., Kaufman, R. J., and Fribley, A. M. (2019). "Disulfiram (Antabuse) activates ROS-dependent ER-stress and apoptosis in oral cavity squamous cell carcinoma". In: *Journal of Clinical Medicine*. Vol. 8 (5), art. no. 611. DOI: 10.3390/jcm8050611.

O'Connell, E. M., Bennuru, S., Steel, C., Dolan, M. A., and Nutman, T. B. (2015). "Targeting filarial Abl-like kinases: orally available, food and drug administration-approved tyrosine kinase inhibitors are microfilaricidal and macrofilaricidal". In: *The Journal of Infectious Diseases*. Vol. 212 (5), pp. 684–693. DOI: 10.1093/infdis/jiv065.

O'Connell, E. M., Kamenyeva, O., Lustigman, S., Bell, A., and Nutman, T. B. (2017). "Defining the target and the effect of imatinib on the filarial c-Abl homologue". In: *PLoS Neglected Tropical Diseases*. Vol. 11 (7), art. no. e0005690. DOI: 10.1371/journal.pntd.0005690.

Olson, E. N. and Spizz, G. (1986). "Fatty acylation of cellular proteins. Temporal and subcellular differences between palmitate and myristate acylation". In: *The Journal of Biological Chemistry*. Vol. 261 (5), pp. 2458–2466. DOI: 10.1016/s0021-9258(17)35957-4.

Oltvai, Z. N., Milliman, C. L., and Korsmeyer, S. J. (1993). "BCL-2 heterodimerizes *in vivo* with a conserved homolog, BAX, that accelerates programmed cell death". In: *Cell*. Vol. 74 (4), pp. 609–619. DOI: 10.1016/0092-8674(93)90509-o.

Omary, M. and Trowbridge, I. (1981). "Biosynthesis of the human transferrin receptor in cultured cells". In: *The Journal of Biological Chemistry*. Vol. 256 (24), pp. 12888–12892. DOI: 10.1016/s0021-9258(18)42979-1.

Ortiz, M. A., Mikhailova, T., Li, X., Porter, B. A., Bah, A., and Kotula, L. (2021). "Src family kinases, adaptor proteins and the actin cytoskeleton in epithelial-to-mesenchymal transition". In: *Cell Communication and Signaling: CCS*. Vol. 19, art. no. 67. DOI: 10.1186/s12964-021-00750-x.

Osman, A., Niles, E. G., and LoVerde, P. T. (1999). "Characterization of the Ras homologue of *Schistosoma mansoni*". In: *Molecular and Biochemical Parasitology*. Vol. 100 (1), pp. 27–41. DOI: 10.1016/s0166-6851(99)00029-8.

Osman, A., Niles, E. G., and LoVerde, P. T. (2004). "Expression of functional *Schistosoma mansoni* SMAD4: role in ERK-mediated transforming growth factor β (TGF-β) down-regulation". In: *The Journal of Biological Chemistry*. Vol. 279 (8), pp. 6474–6486. DOI: 10.1074/jbc.M310949200.

Østergaard, S., Paulsson, J. F., Kofoed, J., Zosel, F., Olsen, J., Jeppesen, C. B., Spetzler, J., Ynddal, L., Schleiss, L. G., Christoffersen, B. Ø., Raun, K., Sensfuss, U., Nielsen, F. S., Jørgensen, R., and Wulff, B. S. (2021). "The effect of fatty diacid acylation of human PYY$_{3\text{-}36}$ on Y$_2$ receptor potency and half-life in minipigs". In: *Scientific Reports*. Vol. 11 (1), art. no. 21179. DOI: 10.1038/s41598-021-00654-3.

Ouellet, F., Houde, M., and Sarhan, F. (1993). "Purification, characterization and cDNA cloning of the 200 kDa protein induced by cold acclimation in wheat". In: *Plant & Cell Physiology*. Vol. 34 (1), pp. 59–65. PMID: 8025821.

Overington, J. P., Al-Lazikani, B., and Hopkins, A. L. (2006). "How many drug targets are there?" In: *Nature Reviews. Drug Discovery*. Vol. 5 (12), pp. 993–996. DOI: 10.1038/nrd2199.

Pacheco, B., Crombet, L., Loppnau, P., and Cossar, D. (2012). "A screening strategy for heterologous protein expression in *Escherichia coli* with the highest return of investment". In: *Protein Expression and Purification*. Vol. 81 (1), pp. 33–41. DOI: 10.1016/j.pep.2011.08.030.

Pardanani, A. and Tefferi, A. (2004). "Imatinib targets other than BCR/Abl and their clinical relevance in myeloid disorders". In: *Blood*. Vol. 104 (7), pp. 1931–1939. DOI: 10.1182/blood-2004-01-0246.

Park, Y. M., Go, Y. Y., Shin, S. H., Cho, J.-G., Woo, J.-S., and Song, J.-J. (2018). "Anti-cancer effects of disulfiram in head and neck squamous cell carcinoma via autophagic cell death". In: *PLoS One*. Vol. 13 (9), art. no. e0203069. DOI: 10.1371/journal.pone.0203069.

Park, S.-K., Gunaratne, G. S., Chulkov, E. G., Moehring, F., McCusker, P., Dosa, P. I., Chan, J. D., Stucky, C. L., and Marchant, J. S. (2019). "The anthelmintic drug praziquantel activates a schistosome transient receptor potential channel". In: *Journal of Biological Chemistry*. Vol. 294 (49), pp. 18873–18880. DOI: 10.1074/jbc.AC119.011093.

Park, S.-K. and Marchant, J. S. (2020). "The journey to discovering a flatworm target of praziquantel: a long TRP". In: *Trends in Parasitology*. Vol. 36 (2), pp. 182–194. DOI: 10.1016/j.pt.2019.11.002.

Park, S.-K., Friedrich, L., Yahya, N. A., Rohr, C. M., Chulkov, E. G., Maillard, D., Rippmann, F., Spangenberg, T., and Marchant, J. S. (2021). "Mechanism of praziquantel action at a parasitic flatworm ion channel". In: *Science Translational Medicine*. Vol. 13 (625), art. no. eabj5832. DOI: 10.1126/scitranslmed.abj5832.

Pasche, V., Laleu, B., and Keiser, J. (2019). "Early antischistosomal leads identified from *in vitro* and *in vivo* screening of the medicines for Malaria Venture Pathogen box". In: *ACS Infectious Diseases*. Vol. 5 (1), pp. 102–110. DOI: 10.1021/acsinfecdis.8b00220.

Patra, J. K., Das, G., Fraceto, L. F., Campos, E. V. R., Rodriguez-Torres, M. d. P., Acosta-Torres, L. S., Diaz-Torres, L. A., Grillo, R., Swamy, M. K., Sharma, S., Habtemariam, S., and Shin, H.-S. (2018). "Nano based drug delivery systems: recent developments and future prospects". In: *Journal of Nanobiotechnology*. Vol. 16, art. no. 71. DOI: 10.1186/s12951-018-0392-8.

Patwardhan, P. and Resh, M. D. (2010). "Myristoylation and membrane binding regulate c-Src stability and kinase activity". In: *Molecular and Cellular Biology*. Vol. 30 (17), pp. 4094–4107. DOI: 10.1128/MCB.00246-10.

Pawson, T. and Nash, P. (2003). "Assembly of cell regulatory systems through protein interaction domains". In: *Science (New York, N. Y.).* Vol. 300 (5618), pp. 445–452. DOI: 10.1126/science.1083653.

Pawson, T. and Scott, J. D. (2005). "Protein phosphorylation in signaling–50 years and counting". In: *Trends in Biochemical Sciences.* Vol. 30 (6), pp. 286–290. DOI: 10.1016/j.tibs.2005.04.013.

Peacock, J. G., Miller, A. L., Bradley, W. D., Rodriguez, O. C., Webb, D. J., and Koleske, A. J. (2007). "The Abl-related gene tyrosine kinase acts through p190RhoGAP to inhibit actomyosin contractility and regulate focal adhesion dynamics upon adhesion to fibronectin". In: *Molecular Biology of the Cell.* Vol. 18 (10), pp. 3860–3872. DOI: 10.1091/mbc.E07-01-0075.

Pearce, E. J., Magee, A. I., Smithers, S. R., and Simpson, A. J. (1991). "Sm25, a major schistosome tegumental glycoprotein, is dependent on palmitic acid for membrane attachment". In: *The EMBO Journal.* Vol. 10 (10), pp. 2741–2746. DOI: 10.1002/j.1460-2075.1991.tb07822.x.

Pearson, B. J., Eisenhoffer, G. T., Gurley, K. A., Rink, J. C., Miller, D. E., and Sánchez Alvarado, A. (2009). "Formaldehyde-based whole-mount *in situ* hybridization method for planarians". In: *Developmental Dynamics: an Official Publication of the American Association of Anatomists.* Vol. 238 (2), pp. 443–450. DOI: 10.1002/dvdy.21849.

Pendergast, A. M. (2002). "The Abl family kinases: mechanisms of regulation and signaling". In: *Advances in Cancer Research.* Vol. 85, pp. 51–100. DOI: 10.1016/s0065-230x(02)85003-5.

Peniche, A. G., Renslo, A. R., Melby, P. C., and Travi, B. L. (2015). "Antileishmanial activity of disulfiram and thiuram disulfide analogs in an *ex vivo* model system is selectively enhanced by the addition of divalent metal ions". In: *Antimicrobial Agents and Chemotherapy.* Vol. 59 (10), pp. 6463–6470. DOI: 10.1128/AAC.05131-14.

Pereira, R. V., Cabral, F. J., De Souza Gomes, M., Baba, E. H., Jannotti-Passos, L. K., Carvalho, O., Rodrigues, V., Afonso, R. J. C. F., Castro-Borges, W., and Guerra-Sá, R. (2011). "Molecular characterization of SUMO E2 conjugation enzyme: differential expression profile in *Schistosoma mansoni*". In: *Parasitology Research.* Vol. 109 (6), pp. 1537–1546. DOI: 10.1007/s00436-011-2394-4.

Pereira, R. V., Cabral, F. J., De Souza Gomes, M., Jannotti-Passos, L. K., Castro-Borges, W., and Guerra-Sá, R. (2012). "Transcriptional profile and astructural conservation of SUMO-specific proteases in *Schistosoma mansoni*". In: *Journal of Parasitology Research*. Vol. 2012, art. no. 480824. DOI: 10.1155/2012/480824.

Pereira, R. V., De Souza Gomes, M., Olmo, R. P., Souza, D. M., Jannotti-Passos, L. K., Baba, E. H., Castro-Borges, W., and Guerra-Sá, R. (2013). "NEDD8 conjugation in *Schistosoma mansoni*: genome analysis and expression profiles". In: *Parasitology International*. Vol. 62 (2), pp. 199–207. DOI: 10.1016/j.parint.2012.12.009.

Pereira Moreira, B., Weber, M. H. W., Häberlein, S., Mokosch, A. S., Spengler, B., Grevelding, C. G., and Falcone, F. H. (2022). "Drug repurposing and *de novo* drug discovery of protein kinase inhibitors as new drugs against schistosomiasis". In: *Molecules (Basel, Switzerland)*. Vol. 27 (4), art. no. 1414. DOI: 10.3390/molecules27041414.

Perez-Miller, S. J. and Hurley, T. D. (2003). "Coenzyme isomerization is integral to catalysis in aldehyde dehydrogenase". In: *Biochemistry*. Vol. 42 (23), pp. 7100–7109. DOI: 10.1021/bi034182w.

Perozich, J., Nicholas, H., Wang, B. C., Lindahl, R., and Hempel, J. (1999). "Relationships within the aldehyde dehydrogenase extended family". In: *Protein Science: a Publication of the Protein Society*. Vol. 8 (1), pp. 137–146. DOI: 10.1110/ps.8.1.137.

Peter Ventura, A. M., Häberlein, S., Lange-Grünweller, K., Grünweller, A., Hartmann, R. K., Grevelding, C. G., and Schlitzer, M. (2019). "Development of biarylalkyl carboxylic acid amides with improved anti-schistosomal activity". In: *ChemMedChem*. Vol. 14 (21), pp. 1856–1862. DOI: 10.1002/cmdc.201900423.

Peters, R. T., Toby, G., Lu, Q., Liu, T., Kulman, J. D., Low, S. C., Bitonti, A. J., and Pierce, G. F. (2013). "Biochemical and functional characterization of a recombinant monomeric factor VIII-Fc fusion protein". In: *Journal of Thrombosis and Haemostasis: JTH*. Vol. 11 (1), pp. 132–141. DOI: 10.1111/jth.12076.

Pfaffl, M. W. (2001). "A new mathematical model for relative quantification in real-time RT–PCR". In: *Nucleic Acids Research*. Vol. 29 (9), art. no. e45. DOI: 10.1093/nar/29.9.e45.

Phillips, M., Malloy, G., Nedunchezian, D., Lukrec, A., and Howard, R. G. (1991). "Disulfiram inhibits the *in vitro* growth of methicillin-resistant *Staphylococcus aureus*". In: *Antimicrobial Agents and Chemotherapy*. Vol. 35 (4), pp. 785–787. DOI: 10.1128/aac.35.4.785.

Pica-Mattoccia, L., Dias, L. C. D., Moroni, R., and Cioli, D. (1993). "*Schistosoma mansoni:* genetic complementation analysis shows that two independent hycanthone/oxamniquine-resistant strains are mutated in the same gene". In: *Experimental Parasitology*. Vol. 77 (4), pp. 445–449. DOI: 10.1006/expr.1993.1104.

Pica-Mattoccia, L., Novi, A., and Cioli, D. (1997). "Enzymatic basis for the lack of oxamniquine activity in *Schistosoma haematobium* infections". In: *Parasitology Research*. Vol. 83 (7), pp. 687–689. DOI: 10.1007/s004360050320.

Pica-Mattoccia, L. and Cioli, D. (2004). "Sex- and stage-related sensitivity of *Schistosoma mansoni* to *in vivo* and *in vitro* praziquantel treatment". In: *International Journal for Parasitology*. Vol. 34 (4), pp. 527–533. DOI: 10.1016/j.ijpara.2003.12.003.

Ploemen, J.-P. H. T. M., Van Iersel, M. L., Wormhoudt, L. W., Commandeur, J. N., Vermeulen, N. P., and Van Bladeren, P. J. (1996). "*In vitro* inhibition of rat and human glutathione S-transferase isoenzymes by disulfiram and diethyldithiocarbamate". In: *Biochemical Pharmacology*. Vol. 52 (2), pp. 197–204. DOI: 10.1016/0006-2952(96)00142-6.

Pope, B. and Kent, H. M. (1996). "High efficiency 5 min transformation of *Escherichia coli*". In: *Nucleic Acids Research*. Vol. 24 (3), pp. 536–537. DOI: 10.1093/nar/24.3.536.

Popiel, I. and Basch, P. F. (1984). "Reproductive development of female *Schistosoma mansoni* (Digenea: Schistosomatidae) following bisexual pairing of worms and worm segments". In: *The Journal of Experimental Zoology*. Vol. 232 (1), pp. 141–150. DOI: 10.1002/jez.1402320117.

Popiel, I., Cioli, D., and Erasmus, D. A. (1984). "The morphology and reproductive status of female *Schistosoma mansoni* following separation from male worms". In: *International Journal for Parasitology*. Vol. 14 (2), pp. 183–190. DOI: 10.1016/0020-7519(84)90047-X.

Popiel, I. (1986). "Male-stimulated female maturation in *Schistosoma*: a review". In: *Journal of Chemical Ecology*. Vol. 12 (8), pp. 1745–1754. DOI: 10.1007/BF01022380.

Prachayasittikul, V., Isarankura-Na-Ayudhya, C., Tantimongcolwat, T., Nantasenamat, C., and Galla, H.-J. (2007). "EDTA-induced membrane fluidization and destabilization: biophysical studies on artificial lipid membranes". In: *Acta Biochimica et Biophysica Sinica (Shanghai)*. Vol. 39 (11), pp. 901–913. DOI: 10.1111/j.1745-7270.2007.00350.x.

Quack, T., Knobloch, J., Beckmann, S., Vicogne, J., Dissous, C., and Grevelding, C. G. (2009). "The formin-homology protein SmDia interacts with the Src kinase SmTK and the GTPase SmRho1 in the gonads of *Schistosoma mansoni*". In: *PLoS One*. Vol. 4 (9), art. no. e6998. DOI: 10.1371/journal.pone.0006998.

Rabinowitz, J. S., Chan, X. Y., Kingsley, E. P., Duan, Y., and Lambert, J. D. (2008). "Nanos is required in somatic blast cell lineages in the posterior of a mollusk embryo". In: *Current Biology*. Vol. 18 (5), pp. 331–336. DOI: 10.1016/j.cub.2008.01.055.

Ramirez, B., Bickle, Q., Yousif, F., Fakorede, F., Mouries, M.-A., and Nwaka, S. (2007). "Schistosomes: challenges in compound screening". In: *Expert Opinion on Drug Discovery*. Vol. 2 (1), pp. 53–61. DOI: 10.1517/17460441.2.S1.S53.

Rang, H. P. and Hill, R. G. (2013). "Choosing the target". In: *Drug Discovery and Development*. Ed. by R. G. Hill and H. P. Rang. Churchill Livingstone, pp. 63–76. DOI: 10.1016/B978-0-7020-4299-7.00006-8.

Rauch, J., Volinsky, N., Romano, D., and Kolch, W. (2011). "The secret life of kinases: functions beyond catalysis". In: *Cell Communication and Signaling*. Vol. 9, art. no. 23. DOI: 10.1186/1478-811X-9-23.

Reddy, E. P. and Aggarwal, A. K. (2012). "The ins and outs of BCR-Abl inhibition". In: *Genes & Cancer*. Vol. 3 (5-6), pp. 447–454. DOI: 10.1177/1947601912462126.

Reimers, N., Homann, A., Höschler, B., Langhans, K., Wilson, R. A., Pierrot, C., Khalife, J., Grevelding, C. G., Chalmers, I. W., Yazdanbakhsh, M., Hoffmann, K. F., Hokke, C. H., Haas, H., and Schramm, G. (2015). "Drug-induced exposure of *Schistosoma mansoni* antigens SmCD59a and SmKK7". In: *PLoS Neglected Tropical Diseases*. Vol. 9 (3), art. no. e0003593. DOI: 10.1371/journal.pntd.0003593.

Ren, J., Wen, L., Gao, X., Jin, C., Xue, Y., and Yao, X. (2008). "CSS-Palm 2.0: an updated software for palmitoylation sites prediction". In: *Protein Engineering, Design and Selection*. Vol. 21 (11), pp. 639–644. DOI: 10.1093/protein/gzn039.

Ren, J., Wen, L., Gao, X., Jin, C., Xue, Y., and Yao, X. (2009). "DOG 1.0: illustrator of protein domain structures". In: *Cell Research*. Vol. 19 (2), pp. 271–273. DOI: 10.1038/cr.2009.6.

Rennar, G. A., Gallinger, T. L., Mäder, P., Lange-Grünweller, K., Häberlein, S., Grünweller, A., Grevelding, C. G., and Schlitzer, M. (2022). "Disulfiram and dithiocarbamate analogues demonstrate promising antischistosomal effects". In: *European Journal of Medicinal Chemistry*. Vol. 242, art. no. 114641. DOI: 10.1016/j.ejmech.2022.114641.

Resh, M. D. (1994). "Myristylation and palmitylation of Src family members: the fats of the matter". In: *Cell*. Vol. 76 (3), pp. 411–413. DOI: 10.1016/0092-8674(94)90104-x.

Resh, M. D. (2006). "Palmitoylation of ligands, receptors, and intracellular signaling molecules". In: *Science's STKE: Signal Transduction Knowledge Environment*. Vol. 2006 (359), art. no. re14. DOI: 10.1126/stke.3592006re14.

Riveros-Rosas, H., González-Segura, L., Julián-Sánchez, A., Díaz-Sánchez, Á. G., and Muñoz-Clares, R. A. (2013). "Structural determinants of substrate specificity in aldehyde dehydrogenases". In: *Chemico-Biological Interactions*. Vol. 202 (1-3), pp. 51–61. DOI: 10.1016/j.cbi.2012.11.015.

Riveros-Rosas, H., Julián-Sánchez, A., Moreno-Hagelsieb, G., and Muñoz-Clares, R. A. (2019). "Aldehyde dehydrogenase diversity in bacteria of the *Pseudomonas* genus". In: *Chemico-Biological Interactions*. Vol. 304, pp. 83–87. DOI: 10.1016/j.cbi.2019.03.006.

Rix, U., Hantschel, O., Dürnberger, G., Remsing Rix, L. L., Planyavsky, M., Fernbach, N. V., Kaupe, I., Bennett, K. L., Valent, P., Colinge, J., Köcher, T., and Superti-Furga, G. (2007). "Chemical proteomic profiles of the BCR-Abl inhibitors imatinib, nilotinib, and dasatinib reveal novel kinase and nonkinase targets". In: *Blood*. Vol. 110 (12), pp. 4055–4063. DOI: 10.1182/blood-2007-07-102061.

Robbins, S., Quintrell, N., and Bishop, J. (1995). "Myristoylation and differential palmitoylation of the Hck protein-tyrosine kinases govern their attachment to membranes and association with caveolae". In: *Molecular and Cellular Biology*. Vol. 15 (7), pp. 3507–3515. DOI: 10.1128/MCB.15.7.3507.

Roberts, A. B. and Sporn, M. B. (1993). "Physiological actions and clinical applications of transforming growth factor-β (TGF-β)". In: *Growth Factors (Chur, Switzerland)*. Vol. 8 (1), pp. 1–9. DOI: 10.3109/08977199309029129.

Roche, C., Liu, J. L., LePresle, T., Capron, A., and Pierce, R. J. (1996). "Tissue localization and stage-specific expression of the phospholipid hydroperoxide glutathione peroxidase of *Schistosoma mansoni*". In: *Molecular and Biochemical Parasitology*. Vol. 75 (2), pp. 187–195. DOI: 10.1016/0166-6851(95)02523-5.

Rodgers, W., Crise, B., and Rose, J. K. (1994). "Signals determining protein tyrosine kinase and glycosyl-phosphatidylinositol-anchored protein targeting to a glycolipid-enriched membrane fraction". In: *Molecular and Cellular Biology*. Vol. 14 (8), pp. 5384–5391. DOI: 10.1128/mcb.14.8.5384-5391.1994.

Rodrigues, T. and Schneider, G. (2015). "*In silico* screening: hit finding from database mining". In: *The Practice of Medicinal Chemistry*. Ed. by C. G. Wermuth, D. Aldous, P. Raboisson, and D. Rognan. Academic Press, pp. 141–160. DOI: 10.1016/B978-0-12-417205-0.00006-7.

Rodriguez, E. L., Poddar, S., Iftekhar, S., Suh, K., Woolfork, A. G., Ovbude, S., Pekarek, A., Walters, M., Lott, S., and Hage, D. S. (2020). "Affinity chromatography: a review of trends and developments over the past 50 years". In: *Journal of Chromatography. B, Analytical Technologies in the Biomedical and Life Sciences*. Vol. 1157, art. no. 122332. DOI: 10.1016/j.jchromb.2020.122332.

Roger, E., Gourbal, B., Grunau, C., Pierce, R. J., Galinier, R., and Mitta, G. (2008). "Expression analysis of highly polymorphic mucin proteins (SmPoMuc) from the parasite *Schistosoma mansoni*". In: *Molecular and Biochemical Parasitology*. Vol. 157 (2), pp. 217–227. DOI: 10.1016/j.molbiopara.2007.11.015.

Rognan, D. (2017). "The impact of *in silico* screening in the discovery of novel and safer drug candidates". In: *Pharmacology & Therapeutics*. Vol. 175, pp. 47–66. DOI: 10.1016/j.pharmthera.2017.02.034.

Rose, J. K., Adams, G. A., and Gallione, C. J. (1984). "The presence of cysteine in the cytoplasmic domain of the vesicular stomatitis virus glycoprotein is required for palmitate addition". In: *Proceedings of the National Academy of Sciences of the United States of America*. Vol. 81 (7), pp. 2050–2054. PMID: 6326102.

Roskoski, R. (2015). "A historical overview of protein kinases and their targeted small molecule inhibitors". In: *Pharmacological Research*. Vol. 100, pp. 1–23. DOI: 10.1016/j.phrs.2015.07.010.

Ross, A. G., Vickers, D., Olds, G. R., Shah, S. M., and McManus, D. P. (2007). "Katayama syndrome". In: *The Lancet. Infectious Diseases*. Vol. 7 (3), pp. 218–224. DOI: 10.1016/S1473-3099(07)70053-1.

Rossi, A., Pica-Mattoccia, L., Cioli, D., and Klinkert, M.-Q. (2002). "Rapamycin insensitivity in *Schistosoma mansoni* is not due to FKBP12 functionality". In: *Molecular and Biochemical Parasitology*. Vol. 125 (1-2), pp. 1–9. DOI: 10.1016/s0166-6851(02)00207-4.

Rothberg, K. G., Heuser, J. E., Donzell, W. C., Ying, Y. S., Glenney, J. R., and Anderson, R. G. (1992). "Caveolin, a protein component of caveolae membrane coats". In: *Cell*. Vol. 68 (4), pp. 673–682. DOI: 10.1016/0092-8674(92)90143-z.

Rugel, A. R., Guzman, M. A., Taylor, A. B., Chevalier, F. D., Tarpley, R. S., McHardy, S. F., Cao, X., Holloway, S. P., Anderson, T. J. C., Hart, P. J., and LoVerde, P. T. (2020). "Why does oxamniquine kill *Schistosoma mansoni* and not *S. haematobium* and *S. japonicum*?" In: *International Journal for Parasitology: Drugs and Drug Resistance*. Vol. 13, pp. 8–15. DOI: 10.1016/j.ijpddr.2020.04.001.

Russell, R. B., Breed, J., and Barton, G. J. (1992). "Conservation analysis and structure prediction of the SH2 family of phosphotyrosine binding domains". In: *FEBS Letters*. Vol. 304 (1), pp. 15–20. DOI: 10.1016/0014-5793(92)80579-6.

Ruvolo, P. P., Deng, X., and May, W. S. (2001). "Phosphorylation of BCL-2 and regulation of apoptosis". In: *Leukemia*. Vol. 15 (4), pp. 515–522. DOI: 10.1038/sj.leu.2402090.

Rychlik, W. (1993). "Selection of primers for polymerase chain reaction". In: *PCR Protocols. Methods in Molecular Biology*. Ed. by B. A. White. Humana Press, pp. 31–40. DOI: 10.1385/0-89603-244-2:31.

Ryter, S. W., Kim, H. P., Hoetzel, A., Park, J. W., Nakahira, K., Wang, X., and Choi, A. M. K. (2007). "Mechanisms of cell death in oxidative stress". In: *Antioxidants & Redox Signaling*. Vol. 9 (1), pp. 49–89. DOI: 10.1089/ars.2007.9.49.

Sabah, A. A., Fletcher, C., Webbe, G., and Doenhoff, M. J. (1986). "*Schistosoma mansoni*: chemotherapy of infections of different ages". In: *Experimental Parasitology*. Vol. 61 (3), pp. 294–303. DOI: 10.1016/0014-4894(86)90184-0.

Sadowski, I., Stone, J. C., and Pawson, T. (1986). "A noncatalytic domain conserved among cytoplasmic protein-tyrosine kinases modifies the kinase function and transforming activity of Fujinami sarcoma virus p130gag-fps". In: *Molecular and Cellular Biology*. Vol. 6 (12), pp. 4396–4408. DOI: 10.1128/mcb.6.12.4396-4408.1986.

Safi, R., Nelson, E. R., Chitneni, S. K., Franz, K. J., George, D. J., Zalutsky, M. R., and McDonnell, D. P. (2014). "Copper signaling axis as a target for prostate cancer therapeutics". In: *Cancer Research*. Vol. 74 (20), pp. 5819–5831. DOI: 10.1158/0008-5472.CAN-13-3527.

Saitoh, A., Nagayama, Y., Yamada, D., Makino, K., Yoshioka, T., Yamanaka, N., Nakatani, M., Takahashi, Y., Yamazaki, M., Shigemoto, C., Ohashi, M., Okano, K., Omata, T., Toda, E., Sano, Y., Takahashi, H., Matsushima, K., and Terashima, Y. (2022). "Disulfiram produces potent anxiolytic-like effects without benzodiazepine anxi-olytics-related adverse effects in mice". In: *Frontiers in Pharmacology*. Vol. 13, art. no. 826783. DOI: 10.3389/fphar.2022.826783.

Salas-Coronas, J., Bargues, M. D., Lozano-Serrano, A. B., Artigas, P., Martínez-Ortí, A., Mas-Coma, S., Merino-Salas, S., and Abad Vivas-Pérez, J. I. (2021). "Evidence of autochthonous transmission of urinary schistosomiasis in Almeria (Southeast Spain): an outbreak analysis". In: *Travel Medicine and Infectious Disease*. Vol. 44, art. no. 102165. DOI: 10.1016/j.tmaid.2021.102165.

Sánchez-García, I. and Martín-Zanca, D. (1997). "Regulation of *bcl-2* gene expression by BCR-Abl is mediated by Ras". In: *Journal of Molecular Biology*. Vol. 267 (2), pp. 225–228. DOI: 10.1006/jmbi.1996.0779.

Sandwall, E., Bodevin, S., Nasser, N. J., Nevo, E., Avivi, A., Vlodavsky, I., and Li, J.-P. (2009). "Molecular structure of heparan sulfate from Spalax: implications of heparanase and hypoxia". In: *Journal of Biological Chemistry*. Vol. 284 (6), pp. 3814–3822. DOI: 10.1074/jbc.M802196200.

Santi, A. M. M. and Murta, S. M. F. (2022). "Antioxidant defence system as a rational target for Chagas disease and leishmaniasis chemotherapy". In: *Memórias do Instituto Oswaldo Cruz*. Vol. 117, art. no. e210401. DOI: 10.1590/0074-02760210401.

Santos, R., Ursu, O., Gaulton, A., Bento, A. P., Donadi, R. S., Bologa, C. G., Karlsson, A., Al-Lazikani, B., Hersey, A., Oprea, T. I., and Overington, J. P. (2017). "A comprehensive map of molecular drug targets". In: *Nature Reviews Drug Discovery*. Vol. 16 (1), pp. 19–34. DOI: 10.1038/nrd.2016.230.

Sarkar, S. and Das, B. (2014). "Synthesis and characterization of mononuclear copper(II) complex of tetradentate N2S2 donor set and the study of DNA and bovine serum albumin binding". In: *Complex Metals*. Vol. 1 (1), pp. 80–87. DOI: 10.1080/2164232X.2014.887448.

Sarwono, A. E. Y., Mitsuhashi, S., Kabir, M. H. B., Shigetomi, K., Okada, T., Ohsaka, F., Otsuguro, S., Maenaka, K., Igarashi, M., Kato, K., and Ubukata, M. (2018). "Repurposing existing drugs: identification of irreversible IMPDH inhibitors by high-throughput screening". In: *Journal of Enzyme Inhibition and Medicinal Chemistry*. Vol. 34 (1), pp. 171–178. DOI: 10.1080/14756366.2018.1540474.

Savageau, M. A. (1986). "Proteins of *Escherichia coli* come in sizes that are multiples of 14 kDa: domain concepts and evolutionary implications". In: *Proceedings of the National Academy of Sciences of the United States of America*. Vol. 83 (5), pp. 1198–1202. DOI: 10.1073/pnas.83.5.1198.

Scheibel, L. W., Adler, A., and Trager, W. (1979). "Tetraethylthiuram disulfide (Antabuse) inhibits the human malaria parasite *Plasmodium falciparum*". In: *Proceedings of the National Academy of Sciences of the United States of America*. Vol. 76 (10), pp. 5303–5307. DOI: 10.1073/pnas.76.10.5303.

Schemionek, M., Elling, C., Steidl, U., Bäumer, N., Hamilton, A., Spieker, T., Göthert, J. R., Stehling, M., Wagers, A., Huettner, C. S., Tenen, D. G., Tickenbrock, L., Berdel, W. E., Serve, H., Holyoake, T. L., Müller-Tidow, C., and Koschmieder, S. (2010). "BCR-Abl enhances differentiation of long-term repopulating hematopoietic stem cells". In: *Blood.* Vol. 115 (16), pp. 3185–3195. DOI: 10.1182/blood-2009-04-215376.

Schmidtova, S., Kalavska, K., Gercakova, K., Cierna, Z., Miklikova, S., Smolkova, B., Buocikova, V., Miskovska, V., Durinikova, E., Burikova, M., Chovanec, M., Matuskova, M., Mego, M., and Kucerova, L. (2019). "Disulfiram overcomes cisplatin resistance in human embryonal carcinoma cells". In: *Cancers.* Vol. 11 (9), art. no. 1224. DOI: 10.3390/cancers11091224.

Schurr, A., Ho, B. T., and Schoolar, J. C. (1978). "The effects of disulfiram on rat liver mitochondrial monoamine oxidase". In: *Life Sciences.* Vol. 22 (22), pp. 1979–1984. DOI: 10.1016/0024-3205(78)90542-8.

Schwarz, R. and Dayhoff, M. (1979). "Matrices for detecting distant relationships". In: *Atlas of Protein Sequences.* Ed. by M. Dayhoff. National Biomedical Research Foundation, pp. 353–358.

Seeliger, M., Young, M., Henderson, M., Pellicena, P., King, D., Falick, A., and Kuriyan, J. (2005). "High yield bacterial expression of active c-Abl and c-Src tyrosine kinases". In: *Protein Science: a Publication of the Protein Society.* Vol. 14 (12), pp. 3135–3139. DOI: 10.1110/ps.051750905.

Seet, B. T., Dikic, I., Zhou, M.-M., and Pawson, T. (2006). "Reading protein modifications with interaction domains". In: *Nature Reviews Molecular Cell Biology.* Vol. 7 (7), pp. 473–483. DOI: 10.1038/nrm1960.

Sefton, B. M., Trowbridge, I. S., Cooper, J. A., and Scolnick, E. M. (1982). "The transforming proteins of Rous sarcoma virus, Harvey sarcoma virus and Abelson virus contain tightly bound lipid". In: *Cell.* Vol. 31 (2), pp. 465–474. DOI: 10.1016/0092-8674(82)90139-8.

Semizarov, D., Frost, L., Sarthy, A., Kroeger, P., Halbert, D. N., and Fesik, S. W. (2003). "Specificity of short interfering RNA determined through gene expression signatures". In: *Proceedings of the National Academy of Sciences of the United States of America.* Vol. 100 (11), pp. 6347–6352. DOI: 10.1073/pnas.1131959100.

Seubert, J., Pohlke, R., and Loebich, F. (1977). "Synthesis and properties of praziquantel, a novel broad spectrum anthelmintic with excellent activity against schistosomes and cestodes". In: *Experientia.* Vol. 33 (8), pp. 1036–1037. DOI: 10.1007/BF01945954.

References

Shah, N. P., Nicoll, J. M., Nagar, B., Gorre, M. E., Paquette, R. L., Kuriyan, J., and Sawyers, C. L. (2002). "Multiple BCR-Abl kinase domain mutations confer polyclonal resistance to the tyrosine kinase inhibitor imatinib (STI571) in chronic phase and blast crisis chronic myeloid leukemia". In: *Cancer Cell*. Vol. 2 (2), pp. 117–125. DOI: 10.1016/S1535-6108(02)00096-X.

Sharp, P. M., Cowe, E., Higgins, D. G., Shields, D. C., Wolfe, K. H., and Wright, F. (1988). "Codon usage patterns in *Escherichia coli*, *Bacillus subtilis*, *Saccharomyces cerevisiae*, *Schizosaccharomyces pombe*, *Drosophila melanogaster* and *Homo sapiens*; a review of the considerable within-species diversity". In: *Nucleic Acids Research*. Vol. 16 (17), pp. 8207–8211. DOI: 10.1093/nar/16.17.8207.

Shen, M. L., Johnson, K. L., Mays, D. C., Lipsky, J. J., and Naylor, S. (2001). "Determination of *in vivo* adducts of disulfiram with mitochondrial aldehyde dehydrogenase". In: *Biochemical Pharmacology*. Vol. 61 (5), pp. 537–545. DOI: 10.1016/s0006-2952(00)00586-4.

Shenoy-Scaria, A. M., Gauen, L. K., Kwong, J., Shaw, A. S., and Lublin, D. M. (1993). "Palmitylation of an amino-terminal cysteine motif of protein tyrosine kinases p56Lck and p59Fyn mediates interaction with glycosyl-phosphatidylinositol-anchored proteins". In: *Molecular and Cellular Biology*. Vol. 13 (10), pp. 6385–6392. DOI: 10.1128/mcb.13.10.6385-6392.1993.

Shenoy-Scaria, A. M., Dietzen, D., Kwong, J., Link, D., and Lublin, D. M. (1994). "Cysteine3 of Src family protein tyrosine kinase determines palmitoylation and localization in caveolae". In: *The Journal of Cell Biology*. Vol. 126 (2), pp. 353–363. DOI: 10.1083/JCB.126.2.353.

Shirley, D.-A., Sharma, I., Warren, C. A., and Moonah, S. (2021). "Drug repurposing of the alcohol abuse medication disulfiram as an anti-parasitic agent". In: *Frontiers in Cellular and Infection Microbiology*. Vol. 11, art. no. 633194. DOI: 10.3389/fcimb.2021.633194.

Shortall, K., Djeghader, A., Magner, E., and Soulimane, T. (2021). "Insights into aldehyde dehydrogenase enzymes: a structural perspective". In: *Frontiers in Molecular Biosciences*. Vol. 8, art. no. 659550. DOI: 10.3389/fmolb.2021.659550.

Sibomana, J. P., Campeche, A., Carvalho-Filho, R. J., Correa, R. A., Duani, H., Pacheco Guimaraes, V., Hilton, J. F., Kassa, B., Kumar, R., Lee, M. H., Loureiro, C. M. C., Mazimba, S., Mickael, C., Oliveira, R. K. F., Ota-Arakaki, J. S., Rezende, C. F., Silva, L. C. S., Sinkala, E., Ahmed, H. Y., and Graham, B. B. (2020). "Schistosomiasis pulmonary arterial hypertension". In: *Frontiers in Immunology*. Vol. 11, art. no. 608883. DOI: 10.3389/fimmu.2020.608883.

318

Sievers, F. and Higgins, D. G. (2018). "Clustal omega for making accurate alignments of many protein sequences". In: *Protein Science: a Publication of the Protein Society*. Vol. 27 (1), pp. 135–145. DOI: 10.1002/pro.3290.

Silvius, J. R. (2002). "Lipidated peptides as tools for understanding the membrane interactions of lipid-modified proteins". In: *Current Topics in Membranes*. Vol. 52, pp. 371–395. DOI: 10.1016/S1063-5823(02)52015-9.

Simon, H. U., Haj-Yehia, A., and Levi-Schaffer, F. (2000). "Role of reactive oxygen species (ROS) in apoptosis induction". In: *Apoptosis: an International Journal on Programmed Cell Death*. Vol. 5 (5), pp. 415–418. DOI: 10.1023/a:1009616228304.

Simurda, M. C., Van Keulen, H., Rekosh, D. M., and LoVerde, P. T. (1988). "*Schistosoma mansoni*: identification and analysis of an mRNA and a gene encoding superoxide dismutase (Cu/Zn)". In: *Experimental Parasitology*. Vol. 67 (1), pp. 73–84. DOI: 10.1016/0014-4894(88)90010-0.

Singh, S., Brocker, C., Koppaka, V., Chen, Y., Jackson, B. C., Matsumoto, A., Thompson, D. C., and Vasiliou, V. (2013). "Aldehyde dehydrogenases in cellular responses to oxidative/electrophilic stress". In: *Free Radical Biology & Medicine*. Vol. 56, pp. 89–101. DOI: 10.1016/j.freeradbiomed.2012.11.010.

Singh, A., Upadhyay, V., Upadhyay, A. K., Singh, S. M., and Panda, A. K. (2015). "Protein recovery from inclusion bodies of *Escherichia coli* using mild solubilization process". In: *Microbial Cell Factories*. Vol. 14, art. no. 41. DOI: 10.1186/s12934-015-0222-8.

Skelly, P. J., Da'dara, A., and Harn, D. A. (2003). "Suppression of cathepsin B expression in *Schistosoma mansoni* by RNA interference". In: *International Journal for Parasitology*. Vol. 33 (4), pp. 363–369. DOI: 10.1016/S0020-7519(03)00030-4.

Skelly, P. J. and Wilson, R. A. (2006). "Making sense of the schistosome surface". In: *Advances in Parasitology*. Vol. 63, pp. 185–284. DOI: 10.1016/S0065-308X(06)63003-0.

Skrott, Z., Mistrik, M., Andersen, K. K., Friis, S., Majera, D., Gursky, J., Ozdian, T., Bartkova, J., Turi, Z., Moudry, P., Kraus, M., Michalova, M., Vaclavkova, J., Dzubak, P., Vrobel, I., Pouckova, P., Sedlacek, J., Miklovicova, A., Kutt, A., Li, J., Mattova, J., Driessen, C., Dou, Q. P., Olsen, J., Hajduch, M., Cvek, B., Deshaies, R., and Bartek, J. (2017). "Alcohol-abuse drug disulfiram targets cancer via p97 segregase adaptor NPL4". In: *Nature*. Vol. 552 (7684), pp. 194–199. DOI: 10.1038/nature25016.

Skrott, Z., Majera, D., Gursky, J., Buchtova, T., Hajduch, M., Mistrik, M., and Bartek, J. (2019). "Disulfiram's anti-cancer activity reflects targeting NPL4, not inhibition of aldehyde dehydrogenase". In: *Oncogene*. Vol. 38 (40), pp. 6711–6722. DOI: 10.1038/s41388-019-0915-2.

Sliva, K. and Schnierle, B. S. (2010). "Selective gene silencing by viral delivery of short hairpin RNA". In: *Virology Journal*. Vol. 7, art. no. 248. DOI: 10.1186/1743-422X-7-248.

Smit, C. H., Van Diepen, A., Nguyen, D. L., Wuhrer, M., Hoffmann, K. F., Deelder, A. M., and Hokke, C. H. (2015). "Glycomic analysis of life stages of the human parasite *Schistosoma mansoni* reveals developmental expression profiles of functional and antigenic glycan motifs". In: *Molecular & Cellular Proteomics: MCP*. Vol. 14 (7), pp. 1750–1769. DOI: 10.1074/mcp.M115.048280.

Smithers, S. R. and Terry, R. J. (1965). "The infection of laboratory hosts with cercariae of *Schistosoma mansoni* and the recovery of the adult worms". In: *Parasitology*. Vol. 55 (4), pp. 695–700. DOI: 10.1017/s0031182000086248.

Sophos, N. A. and Vasiliou, V. (2003). "Aldehyde dehydrogenase gene superfamily: the 2002 update". In: *Chemico-Biological Interactions*. Vol. 143-144, pp. 5–22. DOI: 10.1016/S0009-2797(02)00163-1.

Standley, C. J., Dobson, A. P., and Stothard, J. R. (2012). "Out of animals and back again: schistosomiasis as a zoonosis in Africa". In: *Schistosomiasis*. Ed. by M. B. Rokni. IntechOpen, pp. 209–230. DOI: 10.5772/25567.

Staufenbiel, M. and Lazarides, E. (1986). "Ankyrin is fatty acid acylated in erythrocytes". In: *Proceedings of the National Academy of Sciences of the United States of America*. Vol. 83 (2), pp. 318–322. DOI: 10.1073/pnas.83.2.318.

Steinmetz, C. G., Xie, P., Weiner, H., and Hurley, T. D. (1997). "Structure of mitochondrial aldehyde dehydrogenase: the genetic component of ethanol aversion". In: *Structure*. Vol. 5 (5), pp. 701–711. DOI: 10.1016/S0969-2126(97)00224-4.

Stelma, F. F., Sall, S., Daff, B., Sow, S., Niang, M., and Gryseels, B. (1997). "Oxamniquine cures *Schistosoma mansoni* infection in a focus in which cure rates with praziquantel are unusually low". In: *The Journal of Infectious Diseases*. Vol. 176 (1), pp. 304–307. DOI: 10.1086/517273.

Stokes, M. and Abdijadid, S. (2022). "Disulfiram". In: *StatPearls [Internet]*. URL: http://www.ncbi.nlm.nih.gov/books/NBK459340/ (visited on Sept. 8, 2022).

Storms, R. W., Trujillo, A. P., Springer, J. B., Shah, L., Colvin, O. M., Ludeman, S. M., and Smith, C. (1999). "Isolation of primitive human hematopoietic progenitors on the basis of aldehyde dehydrogenase activity". In: *Proceedings of the National Academy of Sciences of the United States of America*. Vol. 96 (16), pp. 9118–9123. DOI: 10.1073/pnas.96.16.9118.

Strandberg, L. and Enfors, S. O. (1991). "Factors influencing inclusion body formation in the production of a fused protein in *Escherichia coli*". In: *Applied and Environmental Microbiology*. Vol. 57 (6), pp. 1669–1674. DOI: 10.1128/aem.57.6.1669-1674.1991.

Stroehlein, A. J., Young, N. D., Jex, A. R., Sternberg, P. W., Tan, P., Boag, P. R., Hofmann, A., and Gasser, R. B. (2015). "Defining the *Schistosoma haematobium* kinome enables the prediction of essential kinases as anti-schistosome drug targets". In: *Scientific Reports*. Vol. 5, art. no. 17759. DOI: 10.1038/srep17759.

Studier, F. W. and Moffatt, B. A. (1986). "Use of bacteriophage T7 RNA polymerase to direct selective high-level expression of cloned genes". In: *Journal of Molecular Biology*. Vol. 189 (1), pp. 113–130. DOI: 10.1016/0022-2836(86)90385-2.

Su, L.-J., Zhang, J.-H., Gomez, H., Murugan, R., Hong, X., Xu, D., Jiang, F., and Peng, Z.-Y. (2019). "Reactive oxygen species-induced lipid peroxidation in apoptosis, autophagy, and ferroptosis". In: *Oxidative Medicine and Cellular Longevity*. Vol. 2019, art. no. e5080843. DOI: 10.1155/2019/5080843.

Sugawara, I. (1990). "Expression and functions of P-glycoprotein (*mdr1* gene product) in normal and malignant tissues". In: *Acta Pathologica Japonica*. Vol. 40 (8), pp. 545–553. DOI: 10.1111/j.1440-1827.1990.tb01598.x.

Suh, J. J., Pettinati, H. M., Kampman, K. M., and O'Brien, C. P. (2006). "The status of disulfiram: a half of a century later". In: *Journal of Clinical Psychopharmacology*. Vol. 26 (3), pp. 290–302. DOI: 10.1097/01.jcp.0000222512.25649.08.

Sun, T., Nukaga, M., Mayama, K., Braswell, E. H., and Knox, J. R. (2003). "Comparison of β-lactamases of classes A and D: 1.5-Å crystallographic structure of the class D OXA-1 oxacillinase". In: *Protein Science: a Publication of the Protein Society*. Vol. 12 (1), pp. 82–91. DOI: 10.1110/ps.0224303.

Sun, L., Yu, S., Xu, H., Zheng, Y., Lin, J., Wu, M., Wang, J., Wang, A., Lan, Q., Furnari, F., Cavenee, W., Purow, B., and Li, M. (2018). "FHL2 interacts with EGFR to promote glioblastoma growth". In: *Oncogene*. Vol. 37 (10), pp. 1386–1398. DOI: 10.1038/s41388-017-0068-0.

References

Sun, D., Gao, W., Hu, H., and Zhou, S. (2022). "Why 90 % of clinical drug development fails and how to improve it?" In: *Acta Pharmaceutica Sinica B*. Vol. 12 (7), pp. 3049–3062. DOI: 10.1016/j.apsb.2022.02.002.

Sunderhaus, A., Imran, R., Enoh, E., Adedeji, A., Obafemi, T., and Abdel Aziz, M. H. (2022). "Comparative expression of soluble, active human kinases in specialized bacterial strains". In: *PLoS One*. Vol. 17 (4), art. no. e0267226. DOI: 10.1371/journal.pone.0267226.

Suzuki, H., Sada, A., Yoshida, S., and Saga, Y. (2009). "The heterogeneity of spermatogonia is revealed by their topology and expression of marker proteins including the germ cell-specific proteins Nanos2 and Nanos3". In: *Developmental Biology*. Vol. 336 (2), pp. 222–231. DOI: 10.1016/j.ydbio.2009.10.002.

Takahashi, K., Brown, C. S., and Weiner, H. (1980). "Mechanism of the magnesium ion activation of the catalytic activity of horse liver aldehyde dehydrogenase". In: *Alcohol and Aldehyde Metabolizing Systems-IV*. Ed. by R. G. Thurman. Springer, pp. 181–188. DOI: 10.1007/978-1-4757-1419-7_19.

Tawari, P. E., Wang, Z., Najlah, M., Tsang, C. W., Kannappan, V., Liu, P., McConville, C., He, B., Armesilla, A. L., and Wang, W. (2015). "The cytotoxic mechanisms of disulfiram and copper(II) in cancer cells". In: *Toxicology Research*. Vol. 4 (6), pp. 1439–1442. DOI: 10.1039/C5TX00210A.

Taylor, R. G., Walker, D. C., and McInnes, R. R. (1993). "*E. coli* host strains significantly affect the quality of small scale plasmid DNA preparations used for sequencing". In: *Nucleic Acids Research*. Vol. 21 (7), pp. 1677–1678. DOI: 10.1093/nar/21.7.1677.

Thao, S., Chen, C.-S., Zhu, H., and Escalante-Semerena, J. C. (2010). "N^ϵ−lysine acetylation of a bacterial transcription factor inhibits its DNA-binding activity". In: *PLoS One*. Vol. 5 (12), art. no. e15123. DOI: 10.1371/journal.pone.0015123.

The UniProt Consortium (2021). "UniProt: the universal protein knowledgebase in 2021". In: *Nucleic Acids Research*. Vol. 49 (1), pp. 480–489. DOI: 10.1093/nar/gkaa1100.

ThermoFisher (2022). "Technical resources - media formulations". Online. URL: https://www.thermofisher.com/de/de/home/technical-resources/media-formulation.294.html (visited on Aug. 12, 2022).

Thomas, P. and Smart, T. G. (2005). "HEK293 cell line: a vehicle for the expression of recombinant proteins". In: *Journal of Pharmacological and Toxicological Methods*. Vol. 51 (3), pp. 187–200. DOI: 10.1016/j.vascn.2004.08.014.

Tian, S., Liu, D.-H., Wang, D., Ren, F., and Xia, P. (2018). "Aldehyde dehydrogenase 1 (Aldh1) promotes the toxicity of TRAIL in non-small cell lung cancer cells via post-transcriptional regulation of MEK-1 expression". In: *Cellular Physiology and Biochemistry*. Vol. 51 (1), pp. 217–227. DOI: 10.1159/000495202.

Tola, A. J., Jaballi, A., Germain, H., and Missihoun, T. D. (2020). "Recent development on plant aldehyde dehydrogenase enzymes and their functions in plant development and stress signaling". In: *Genes (Basel)*. Vol. 12 (1), art. no. 51. DOI: 10.3390/genes12010051.

Tomita, H., Tanaka, K., Tanaka, T., and Hara, A. (2016). "Aldehyde dehydrogenase 1A1 in stem cells and cancer". In: *Oncotarget*. Vol. 7 (10), pp. 11018–11032. DOI: 10.18632/oncotarget.6920.

Tonkin, E. G., Erve, J. C. L., and Valentine, W. M. (2000). "Disulfiram produces a non-carbon disulfide-dependent schwannopathy in the rat". In: *Journal of Neuropathology and Experimental Neurology*. Vol. 59 (9), pp. 786–797. DOI: 10.1093/jnen/59.9.786.

Torrecilla, I., Oehler, J., and Ramadan, K. (2017). "The role of ubiquitin-dependent segregase p97 (VCP or Cdc48) in chromatin dynamics after DNA double strand breaks". In: *Philosophical Transactions of the Royal Society of London. Series B, Biological Sciences*. Vol. 372 (1731), art. no. 20160282. DOI: 10.1098/rstb.2016.0282.

Towler, D. A. and Glaser, L. (1986). "Protein fatty acid acylation: enzymatic synthesis of an N-myristoylglycyl peptide". In: *Proceedings of the National Academy of Sciences of the United States of America*. Vol. 83 (9), pp. 2812–2816. DOI: 10.1073/pnas.83.9.2812.

Towler, D. A., Adams, S. P., Eubanks, S. R., Towery, D. S., Jackson-Machelski, E., Glaser, L., and Gordon, J. I. (1987). "Purification and characterization of yeast myristoyl CoA:protein N-myristoyltransferase". In: *Proceedings of the National Academy of Sciences of the United States of America*. Vol. 84 (9), pp. 2708–2712. DOI: 10.1073/pnas.84.9.2708.

Towler, D. A., Adams, S. P., Eubanks, S. R., Towery, D. S., Jackson-Machelski, E., Glaser, L., and Gordon, J. I. (1988). "Myristoyl CoA:protein N-myristoyltransferase activities from rat liver and yeast possess overlapping yet distinct peptide substrate specificities". In: *Journal of Biological Chemistry*. Vol. 263 (4), pp. 1784–1790. DOI: 10.1016/S0021-9258(19)77945-9.

Tsuda, M., Sasaoka, Y., Kiso, M., Abe, K., Haraguchi, S., Kobayashi, S., and Saga, Y. (2003). "Conserved role of Nanos proteins in germ cell development". In: *Science (New York, N. Y.)*. Vol. 301 (5637), pp. 1239–1241. DOI: 10.1126/science.1085222.

Tu, S., Guo, S.-J., Chen, C.-S., Liu, C.-X., Jiang, H.-W., Ge, F., Deng, J.-Y., Zhou, Y.-M., Czajkowsky, D. M., Li, Y., Qi, B.-R., Ahn, Y.-H., Cole, P. A., Zhu, H., and Tao, S.-C. (2015). "YcgC represents a new protein deacetylase family in prokaryotes". In: *eLife*. Vol. 4, art. no. e05322. DOI: 10.7554/eLife.05322.

Tyagi, R., Elfawal, M. A., Wildman, S. A., Helander, J., Bulman, C. A., Sakanari, J., Rosa, B. A., Brindley, P. J., Janetka, J. W., Aroian, R. V., and Mitreva, M. (2019). "Identification of small molecule enzyme inhibitors as broad-spectrum anthelmintics". In: *Scientific Reports*. Vol. 9 (1), art. no. 9085. DOI: 10.1038/s41598-019-45548-7.

Tzavlaki, K. and Moustakas, A. (2020). "TGF-β signaling". In: *Biomolecules*. Vol. 10 (3), art. no. 487. DOI: 10.3390/biom10030487.

Ullmann, A., Jacob, F., and Monod, J. (1967). "Characterization by *in vitro* complementation of a peptide corresponding to an operator-proximal segment of the β-galactosidase structural gene of *Escherichia* coli". In: *Journal of Molecular Biology*. Vol. 24 (2), pp. 339–343. DOI: 10.1016/0022-2836(67)90341-5.

Utzinger, J., Keiser, J., Shuhua, X., Tanner, M., and Singer, B. H. (2003). "Combination chemotherapy of schistosomiasis in laboratory studies and clinical trials". In: *Antimicrobial Agents and Chemotherapy*. Vol. 47 (5), pp. 1487–1495. DOI: 10.1128/AAC.47.5.1487-1495.2003.

Valentim, C. L. L., Cioli, D., Chevalier, F. D., Cao, X., Taylor, A. B., Holloway, S. P., Pica-Mattoccia, L., Guidi, A., Basso, A., Tsai, I. J., Berriman, M., Carvalho-Queiroz, C., Almeida, M., Aguilar, H., Frantz, D. E., Hart, P. J., LoVerde, P. T., and Anderson, T. J. C. (2013). "Genetic and molecular basis of drug resistance and species-specific drug action in schistosome parasites". In: *Science (New York, N. Y.)*. Vol. 342 (6164), pp. 1385–1389. DOI: 10.1126/science.1243106.

Vallari, R. C. and Pietruszko, R. (1984a). "Interaction of Mg^{2+} with human liver aldehyde dehydrogenase. I. Species difference in the mitochondrial isozyme". In: *The Journal of Biological Chemistry*. Vol. 259 (8), pp. 4922–4926. DOI: 10.1016/s0021-9258(17)42934-6.

Vallari, R. C. and Pietruszko, R. (1984b). "Interaction of Mg^{2+} with human liver aldehyde dehydrogenase. II. Mechanism and site of interaction". In: *The Journal of Biological Chemistry*. Vol. 259 (8), pp. 4927–4933. DOI: 10.1016/S0021-9258(17)42935-8.

Van't Hof, W. and Resh, M. D. (1997). "Rapid plasma membrane anchoring of newly synthesized p59Fyn: selective requirement for NH_2-terminal myristoylation and palmitoylation at cysteine-3". In: *The Journal of Cell Biology*. Vol. 136 (5), pp. 1023–1035. DOI: 10.1083/jcb.136.5.1023.

Vanderstraete, M., Gouignard, N., Ahier, A., Morel, M., Vicogne, J., and Dissous, C. (2013). "The venus kinase receptor (VKR) family: structure and evolution". In: *BMC Genomics*. Vol. 14, art. no. 361. DOI: 10.1186/1471-2164-14-361.

Vanderstraete, M., Gouignard, N., Cailliau, K., Morel, M., Hahnel, S., Leutner, S., Beckmann, S., Grevelding, C. G., and Dissous, C. (2014). "Venus kinase receptors control reproduction in the platyhelminth parasite *Schistosoma mansoni*". In: *PLoS Pathogens*. Vol. 10 (5), art. no. e1004138. DOI: 10.1371/journal.ppat.1004138.

Vasiliou, V., Bairoch, A., Tipton, K. F., and Nebert, D. W. (1999). "Eukaryotic aldehyde dehydrogenase (*aldh*) genes: human polymorphisms, and recommended nomenclature based on divergent evolution and chromosomal mapping". In: *Pharmacogenetics*. Vol. 9 (4), pp. 421–434. PMID: 10780262.

Vaz, B., Halder, S., and Ramadan, K. (2013). "Role of p97/VCP (CDC48) in genome stability". In: *Frontiers in Genetics*. Vol. 4, art. no. 60. DOI: 10.3389/fgene.2013.00060.

Venne, A. S., Kollipara, L., and Zahedi, R. P. (2014). "The next level of complexity: crosstalk of posttranslational modifications". In: *Proteomics*. Vol. 14 (4-5), pp. 513–524. DOI: 10.1002/pmic.201300344.

Verma, S. and Prabhakar, Y. S. (2015). "Target based drug design - a reality in virtual sphere". In: *Current Medicinal Chemistry*. Vol. 22 (13), pp. 1603–1630. DOI: 10.2174/0929867322666150209151209.

Vicogne, J., Pin, J. P., Lardans, V., Capron, M., Noël, C., and Dissous, C. (2003). "An unusual receptor tyrosine kinase of *Schistosoma mansoni* contains a venus flytrap module". In: *Molecular and Biochemical Parasitology*. Vol. 126 (1), pp. 51–62. DOI: 10.1016/s0166-6851(02)00249-9.

Vilar, M. M. and Pinto, R. M. (2005). "Reappraisal of experimental infections with cercariae and schistosomula of a brazilian strain of *Schistosoma mansoni* in mice". In: *Brazilian Journal of Biology*. Vol. 65 (4), pp. 729–733. DOI: 10.1590/S1519-69842005000400020.

Viola-Rhenals, M., Rieber, M. S., and Rieber, M. (2007). "Role of peroxidases, thiols and BAK/BAX in tumor cell susceptibility to $Cu[DEDTC]_2$". In: *Biochemical Pharmacology*. Vol. 74 (6), pp. 841–850. DOI: 10.1016/j.bcp.2007.06.048.

Viola-Rhenals, M., Patel, K. R., Jaimes-Santamaria, L., Wu, G., Liu, J., and Dou, Q. P. (2018). "Recent advances in Antabuse (disulfiram): the importance of its metal-binding ability to its anticancer activity". In: *Current Medicinal Chemistry*. Vol. 25 (4), pp. 506–524. DOI: 10.2174/0929867324666171023161121.

Voge, M. and Bueding, E. (1980). "*Schistosoma mansoni*: tegumental surface alterations induced by subcurative doses of the schistosomicide amoscanate". In: *Experimental Parasitology*. Vol. 50 (2), pp. 251–259. DOI: 10.1016/0014-4894(80)90026-0.

Vu, L. D., Gevaert, K., and De Smet, I. (2018). "Protein language: post-translational modifications talking to each other". In: *Trends in Plant Science*. Vol. 23 (12), pp. 1068–1080. DOI: 10.1016/j.tplants.2018.09.004.

Wagner, S., Klepsch, M. M., Schlegel, S., Appel, A., Draheim, R., Tarry, M., Högbom, M., Wijk, K. J. van, Slotboom, D. J., Persson, J. O., and De Gier, J.-W. (2008). "Tuning *Escherichia coli* for membrane protein overexpression". In: *Proceedings of the National Academy of Sciences of the United States of America*. Vol. 105 (38), pp. 14371–14376. DOI: 10.1073/pnas.0804090105.

Wall, J. and Plückthun, A. (1995). "Effects of overexpressing folding modulators on the *in vivo* folding of heterologous proteins in *Escherichia coli*". In: *Current Opinion in Biotechnology*. Vol. 6 (5), pp. 507–516. DOI: 10.1016/0958-1669(95)80084-0.

Wang, Y.-H., Ayrapetov, M. K., Lin, X., and Sun, G. (2006). "A new strategy to produce active human Src from bacteria for biochemical study of its regulation". In: *Biochemical and Biophysical Research Communications*. Vol. 346 (2), pp. 606–611. DOI: 10.1016/j.bbrc.2006.05.180.

Wang, B., Lee, J., Li, P., Saberi, A., Yang, H., Liu, C., Zhao, M., and Newmark, P. A. (2018). "Stem cell heterogeneity drives the parasitic life cycle of *Schistosoma mansoni*". In: *eLife*. Vol. 7, art. no. e35449. DOI: 10.7554/eLife.35449.

Wang, J., Chen, R., and Collins, J. J. (2019). "Systematically improved *in vitro* culture conditions reveal new insights into the reproductive biology of the human parasite *Schistosoma mansoni*". In: *PLoS Biology*. Vol. 17 (5), art. no. e3000254. DOI: 10.1371/journal.pbio.3000254.

Wang, C., Xu, H., Lin, S., Deng, W., Zhou, J., Zhang, Y., Shi, Y., Peng, D., and Xue, Y. (2020). "GPS 5.0: an update on the prediction of kinase-specific phosphorylation sites in proteins". In: *Genomics, Proteomics & Bioinformatics*. Vol. 18 (1), pp. 72–80. DOI: 10.1016/j.gpb.2020.01.001.

Wang, G.-F., Niu, X., Liu, H., Dong, Q., Yao, Y., Wang, D., Liu, X., and Cao, C. (2021). "c-Abl kinase regulates cell proliferation and ionizing radiation-induced G2/M arrest via phosphorylation of FHL2". In: *FEBS Open Bio*. Vol. 11 (6), pp. 1731–1738. DOI: 10.1002/2211-5463.13177.

Watson, C. P., Ashby, P., and Bilbao, J. M. (1980). "Disulfiram neuropathy". In: *Canadian Medical Association Journal*. Vol. 123 (2), pp. 123–126. PMID: 6266628.

Webbe, G. and James, C. (1977). "A comparison of the susceptibility to praziquantel of *Schistosoma haematobium*, *S. japonicum*, *S. mansoni*, *S. intercalatum* and *S. mattheei* in hamsters". In: *Zeitschrift für Parasitenkunde (Berlin, Germany)*. Vol. 52 (2), pp. 169–177. DOI: 10.1007/BF00389901.

Weiner, H. and Takahashi, K. (1983). "Effects of magnesium and calcium on mitochondrial and cytosolic liver aldehyde dehydrogenases". In: *Pharmacology Biochemistry and Behavior*. Vol. 18 (1), pp. 109–112. DOI: 10.1016/0091-3057(83)90155-7.

Weisiger, R. A. and Fridovich, I. (1973). "Mitochondrial superoxide dimutase. Site of synthesis and intramitochondrial localization". In: *The Journal of Biological Chemistry*. Vol. 248 (13), pp. 4793–4796. PMID: 4578091.

Weiss, S. and Hatcher, R. A. (1923). "The mechanism of the vomiting induced by antimony and potassium tartrate (tartar emetic)". In: *Journal of Experimental Medicine*. Vol. 37 (1), pp. 97–111. DOI: 10.1084/jem.37.1.97.

Wendt, M. K., Allington, T. M., and Schiemann, W. P. (2009). "Mechanisms of epithelial-mesenchymal transition by TGF-β". In: *Future Oncology*. Vol. 5 (8), pp. 1145–1168. DOI: 10.2217/fon.09.90.

Wendt, G. R. and Collins, J. J. (2016). "Schistosomiasis as a disease of stem cells". In: *Current Opinion in Genetics & Development*. Vol. 40, pp. 95–102. DOI: 10.1016/j.gde.2016.06.010.

Wendt, G., Zhao, L., Chen, R., Liu, C., O'Donoghue, A. J., Caffrey, C. R., Reese, M. L., and Collins, J. J. (2020). "A single-cell RNA-seq atlas of *Schistosoma mansoni* identifies a key regulator of blood feeding". In: *Science (New York, N. Y.)*. Vol. 369 (6511), pp. 1644–1649. DOI: 10.1126/science.abb7709.

Wharton, R. P. and Struhl, G. (1989). "Structure of the *Drosophila* BicaudalD protein and its role in localizing the posterior determinant nanos". In: *Cell*. Vol. 59 (5), pp. 881–892. DOI: 10.1016/0092-8674(89)90611-9.

WHO (2021). "Model list of essential medicines - 22nd list". Online. URL: https://www.who.int/publications-detail-redirect/WHO-MHP-HPS-EML-2021.02 (visited on Sept. 8, 2022).

References

WHO (2022). "Schistosomiasis". Online. URL: https://www.who.int/news-room/fact-sheets/detail/schistosomiasis (visited on Aug. 24, 2022).

Wiest, P. M., Tisdale, E. J., Roberts, W. L., Rosenberry, T. L., Mahmoud, A. A., and Tartakoff, A. M. (1988). "Characterization of [^{3}H] palmitate- and [^{3}H] ethanolamine-labelled proteins in the multicellular parasitic trematode *Schistosoma mansoni*". In: *Biochemical Journal*. Vol. 254 (2), pp. 419–426. DOI: 10.1042/bj2540419.

Wilkes, M. C. and Leof, E. B. (2006). "Transforming growth factor β activation of c-Abl is independent of receptor internalization and regulated by phosphatidylinositol 3-kinase and PAK2 in mesenchymal cultures". In: *The Journal of Biological Chemistry*. Vol. 281 (38), pp. 27846–27854. DOI: 10.1074/jbc.M603721200.

Williams, D. C., Van Frank, R. M., Muth, W. L., and Burnett, J. P. (1982). "Cytoplasmic inclusion bodies in *Escherichia coli* producing biosynthetic human insulin proteins". In: *Science (New York, N. Y.)*. Vol. 215 (4533), pp. 687–689. DOI: 10.1126/science.7036343.

Willow, J., Soonvald, L., Sulg, S., Kaasik, R., Silva, A. I., Taning, C. N. T., Christiaens, O., Smagghe, G., and Veromann, E. (2021). "RNAi efficacy is enhanced by chronic dsRNA feeding in pollen beetle". In: *Communications Biology*. Vol. 4, art. no. 444. DOI: 10.1038/s42003-021-01975-9.

Willumsen, B., Norris, K., Papageorge, A., Hubbert, N., and Lowy, D. (1984). "Harvey murine sarcoma virus p21 Ras protein: biological and biochemical significance of the cysteine nearest the carboxy terminus". In: *The EMBO Journal*. Vol. 3 (11), pp. 2581–2585. DOI: 10.1002/j.1460-2075.1984.tb02177.x.

Winkelmann, F., Gesell Salazar, M., Hentschker, C., Michalik, S., Macháček, T., Scharf, C., Reisinger, E. C., Völker, U., and Sombetzki, M. (2022). "Comparative proteome analysis of the tegument of male and female adult *Schistosoma mansoni*". In: *Scientific Reports*. Vol. 12 (1), art. no. 7569. DOI: 10.1038/s41598-022-11645-3.

Wiseman, H. and Halliwell, B. (1996). "Damage to DNA by reactive oxygen and nitrogen species: role in inflammatory disease and progression to cancer". In: *The Biochemical Journal*. Vol. 313 (1), pp. 17–29. DOI: 10.1042/bj3130017.

Wong, S. and Witte, O. N. (2004). "The BCR-Abl story: bench to bedside and back". In: *Annual Review of Immunology*. Vol. 22, pp. 247–306. DOI: 10.1146/annurev.immunol.22.012703.104753.

Woo, H. A., Yim, S. H., Shin, D. H., Kang, D., Yu, D.-Y., and Rhee, S. G. (2010). "Inactivation of peroxiredoxin I by phosphorylation allows localized H_2O_2 accumulation for cell signaling". In: *Cell*. Vol. 140 (4), pp. 517–528. DOI: 10.1016/j.cell.2010.01.009.

Woolhouse, N. M. and Kaye, B. (1977). "Uptake of [^{14}C] oxamniquine by *Schistosoma mansoni*". In: *Parasitology*. Vol. 75 (1), pp. 111–118. DOI: 10.1017/s00311820000 4837x.

Wu, X., Xue, X., Wang, L., Wang, W., Han, J., Sun, X., Zhang, H., Liu, Y., Che, X., Yang, J., and Wu, C. (2018). "Suppressing autophagy enhances disulfiram/copper-induced apoptosis in non-small cell lung cancer". In: *European Journal of Pharmacology*. Vol. 827, pp. 1–12. DOI: 10.1016/j.ejphar.2018.02.039.

Wu, K., Zhai, X., Huang, S., Jiang, L., Yu, Z., and Huang, J. (2021). "Protein kinases: potential drug targets against *Schistosoma japonicum*". In: *Frontiers in Cellular and Infection Microbiology*. Vol. 11, art. no. 691757. DOI: 10.3389/fcimb.2021.691757.

Xiao, S.-H., Friedman, P. A., Catto, B. A., and Webster, L. T. J. (1984). "Praziquantel-induced vesicle formation in the tegument of male *Schistosoma mansoni* is calcium dependent". In: *The Journal of Parasitology*. Vol. 70 (1), pp. 177–179. DOI: 10. 2307/3281955.

Xiao, S. H., Yue, W. J., Yang, Y. Q., and You, J. Q. (1987). "Susceptibility of *Schistosoma japonicum* to different developmental stages to praziquantel". In: *Chinese Medical Journal (English)*. Vol. 100 (9), pp. 759–768. PMID: 3127152.

Xiao, S.-H. (2005). "Development of antischistosomal drugs in China, with particular consideration to praziquantel and the artemisinins". In: *Acta Tropica*. Vol. 96 (2-3), pp. 153–167. DOI: 10.1016/j.actatropica.2005.07.010.

Xu, J.-Y., Xu, Y., Chu, X., Tan, M., and Ye, B.-C. (2018). "Protein acylation affects the artificial biosynthetic pathway for pinosylvin production in engineered *E. coli*". In: *ACS Chemical Biology*. Vol. 13 (5), pp. 1200–1208. DOI: 10.1021/acschembio. 7b01068.

Xue, L., Xu, F., Meng, L., Wei, S., Wang, J., Hao, P., Bian, Y., Zhang, Y., and Chen, Y. (2012). "Acetylation-dependent regulation of mitochondrial Aldh2 activation by Sirt3 mediates acute ethanol-induced eNOS activation". In: *FEBS Letters*. Vol. 586 (2), pp. 137–142. DOI: 10.1016/j.febslet.2011.11.031.

Yakisich, J. S., Sidén, Å., Eneroth, P., and Cruz, M. (2001). "Disulfiram is a potent *in vitro* inhibitor of DNA topoisomerases". In: *Biochemical and Biophysical Research Communications*. Vol. 289 (2), pp. 586–590. DOI: 10.1006/bbrc.2001.6027.

Yang, L., Arora, K., Beard, W. A., Wilson, S. H., and Schlick, T. (2004). "Critical role of magnesium ions in DNA polymerase β's closing and active site assembly". In: *Journal of the American Chemical Society*. Vol. 126 (27), pp. 8441–8453. DOI: 10. 1021/ja049412o.

Yip, K. W. and Reed, J. C. (2008). "BCL-2 family proteins and cancer". In: *Oncogene*. Vol. 27 (50), pp. 6398–6406. DOI: 10.1038/onc.2008.307.

Yip, N. C., Fombon, I. S., Liu, P., Brown, S., Kannappan, V., Armesilla, A. L., Xu, B., Cassidy, J., Darling, J. L., and Wang, W. (2011). "Disulfiram modulated ROS-MAPK and NFκB pathways and targeted breast cancer cells with cancer stem cell-like properties". In: *British Journal of Cancer*. Vol. 104 (10), pp. 1564–1574. DOI: 10.1038/bjc.2011.126.

Yoon, S. H., Jeong, H., Kwon, S.-K., and Kim, J. F. (2009). "Genomics, biological features, and biotechnological applications of *Escherichia coli* B: "Is B for better?!"". In: *Systems Biology and Biotechnology of Escherichia coli*. Ed. by S. Y. Lee. Springer, pp. 1–17. DOI: 10.1007/978-1-4020-9394-4_1.

Yoon, S. H., Han, M.-J., Jeong, H., Lee, C. H., Xia, X.-X., Lee, D.-H., Shim, J. H., Lee, S. Y., Oh, T. K., and Kim, J. F. (2012). "Comparative multi-omics systems analysis of *Escherichia coli* strains B and K-12". In: *Genome Biology*. Vol. 13 (5), art. no. R37. DOI: 10.1186/gb-2012-13-5-r37.

Yoshida, A., Hsu, L. C., and Davé, V. (1992). "Retinal oxidation activity and biological role of human cytosolic aldehyde dehydrogenase". In: *Enzyme*. Vol. 46 (4-5), pp. 239–244. DOI: 10.1159/000468794.

Yue, J. and Mulder, K. M. (2001). "Transforming growth factor-β signal transduction in epithelial cells". In: *Pharmacology & Therapeutics*. Vol. 91 (1), pp. 1–34. DOI: 10.1016/s0163-7258(01)00143-7.

Zandy, N. L., Playford, M., and Pendergast, A. M. (2007). "Abl tyrosine kinases regulate cell-cell adhesion through Rho GTPases". In: *Proceedings of the National Academy of Sciences of the United States of America*. Vol. 104 (45), pp. 17686–17691. DOI: 10.1073/pnas.0703077104.

Zhang, H., Chen, D., Ringler, J., Chen, W., Cui, Q. C., Ethier, S. P., Dou, Q. P., and Wu, G. (2010). "Disulfiram treatment facilitates phosphoinositide 3-kinase inhibition in human breast cancer cells *in vitro* and *in vivo*". In: *Cancer Research*. Vol. 70 (10), pp. 3996–4004. DOI: 10.1158/0008-5472.CAN-09-3752.

Zhao, Z.-R., Lei, L., Liu, M., Zhu, S.-C., Ren, C.-P., Wang, X.-N., and Shen, J.-J. (2008). "*Schistosoma japonicum*: inhibition of *Mago nashi* gene expression by shRNA-mediated RNA interference". In: *Experimental Parasitology*. Vol. 119 (3), pp. 379–384. DOI: 10.1016/j.exppara.2008.03.015.

Zhao, S., Xu, W., Jiang, W., Yu, W., Lin, Y., Zhang, T., Yao, J., Zhou, L., Zeng, Y., Li, H., Li, Y., Shi, J., An, W., Hancock, S. M., He, F., Qin, L., Chin, J., Yang, P., Chen, X., Lei, Q., Xiong, Y., and Guan, K.-L. (2010). "Regulation of cellular metabolism by protein lysine acetylation". In: *Science (New York, N. Y.)*. Vol. 327 (5968), pp. 1000–1004. DOI: 10.1126/science.1179689.

Zhao, D., Mo, Y., Li, M.-T., Zou, S.-W., Cheng, Z.-L., Sun, Y.-P., Xiong, Y., Guan, K.-L., and Lei, Q.-Y. (2014). "NOTCH-induced aldehyde dehydrogenase 1A1 deacetylation promotes breast cancer stem cells". In: *The Journal of Clinical Investigation*. Vol. 124 (12), pp. 5453–5465. DOI: 10.1172/JCI76611.

Zipper, H., Brunner, H., Bernhagen, J., and Vitzthum, F. (2004). "Investigations on DNA intercalation and surface binding by SYBR Green I, its structure determination and methodological implications". In: *Nucleic Acids Research*. Vol. 32 (12), art. no. e103. DOI: 10.1093/nar/gnh101.

Zlatkine, P., Mehul, B., and Magee, A. I. (1997). "Retargeting of cytosolic proteins to the plasma membrane by the Lck protein tyrosine kinase dual acylation motif". In: *Journal of Cell Science*. Vol. 110 (5), pp. 673–679. DOI: 10.1242/jcs.110.5.673.

Zuker, M. and Stiegler, P. (1981). "Optimal computer folding of large RNA sequences using thermodynamics and auxiliary information". In: *Nucleic Acids Research*. Vol. 9 (1), pp. 133–148. DOI: 10.1093/nar/9.1.133.

Appendix

Table A.1: GeneIDs of used genes for analysis

Name	Gene ID	Abbreviation
Abelson-like kinase	Smp_246700	Sm*abl1*
	Smp_128790	Sm*abl2*
Aldehye dehydrogenase	Smp_312440	Sm*aldh1*
	Smp_022960	Sm*aldh2*
Aldose reductase	Smp_053220	Sm*ar*
B-cell lymphoma-2	Smp_072180	Sm*bcl-2*
Bcl-2 associated X protein	Smp_095190	Sm*bax*
Glutathione peroxidase	Smp_058690	Sm*gpx*
Leucine zipper-EF-hand-containing transmembrane protein 1	Smp_310820	Sm*letm1*
Nanos	Smp_055740	Sm*nanos1*
	Smp_051920	Sm*nanos2*
Nuclear protein localization protein 4	Smp_039180	Sm*npl4*
Tumor protein p53	Smp_139530	Sm*p53*
Superoxide dismutase	Smp_176200	Sm*sod*
Superoxide dismutase, extracellular	Smp_174810	Sm*sodex*
Tyrosine kinase 6	Smp_006920	Sm*tk6*

Table A.2: Putative *aldh* genes in *S. mansoni*
Gene IDs of putative Sm*aldh* genes found on WormBase ParaSite using gv9 as of 15th August 2022.

Gene ID	Annotation	Location
Smp_022960	Putative Aldh	SM_V9_7: 12,927,894 - 12,949,557
Smp_036950	not availabe	SM_V9_4: 4,327,260 - 4,330,122
Smp_065060	Multifunctional fusion protein L-glutamate γ-semialdehyde dehydrogenase δ-1-pyrroline-5-carboxylate dehydrogenase	SM_V9_2: 15,921,529 - 15,946,428
Smp_145020	δ-1-pyrroline-5-carboxylate synthase Glutamate 5-kinase γ-glutamyl phosphate reductase	SM_V9_4: 35,582,477 - 35,613,413
Smp_161350	Putative succinate semialdehyde dehydrogenase	SM_V9_1: 69,104,425 - 69,119,608
Smp_172730	Aldh	SM_V9_ZSR: 12,886,829 - 12,909,368
Smp_210440	Aldh domain-containing protein	SM_V9_1: 40,478,984 - 40,493,661
Smp_312440	putative Aldh	SM_V9_4: 7,300,729 - 7,320,787
Smp_312450	Aldh domain-containing protein	SM_V9_4: 7387,102 - 7,399,563
Smp_312460	putative Aldh	SM_V9_4: 7,405,962 - 7,428,478

Table A.3: Percent identity matrix of Aldhs from vertebrate and invertebrate species

	HsAldh1A1	HsAldh1A2	HsAldh1A3	HsAldh2	DmAldh1M1	DmAldh1A10	CeAldh1J2	CeAldh9B2	MmAldh1A1	MmAldh2	DrAldh1A2	DrAldh2	Smp_022960	Smp_312440
HsAldh1A1	100.00	72.06	69.86	68.06	57.53	64.20	60.88	63.07	87.03	67.66	71.06	65.47	61.00	54.38
HsAldh1A2	72.06	100.00	69.73	65.31	56.08	62.48	59.38	60.31	71.46	65.57	79.34	63.23	59.50	54.18
HsAldh1A3	69.86	69.73	100.00	64.06	56.49	59.49	56.72	58.33	68.46	67.38	63.50	62.99	58.51	54.18
HsAldh2	68.06	65.31	64.06	100.00	57.73	69.77	58.56	67.06	67.27	65.50	57.38	66.02	54.79	54.79
DmAldh1M1	57.53	56.08	56.49	57.73	100.00	55.17	58.56	58.56	56.08	57.94	58.35	56.61	56.61	52.69
DmAldh1A10	64.20	62.48	59.49	69.77	55.17	100.00	61.21	64.05	62.40	62.48	69.51	61.78	61.78	54.29
CeAldh1J2	60.88	59.38	56.72	58.56	58.56	61.21	100.00	82.35	59.68	56.84	56.84	61.99	61.91	53.36
CeAldh9B2	63.07	60.31	58.33	67.06	58.56	64.05	82.35	100.00	61.68	65.62	59.92	64.24	62.99	52.75
MmAldh1A1	87.03	71.46	68.46	67.27	56.08	62.40	59.68	61.68	100.00	66.67	70.06	63.27	60.80	54.79
MmAldh2	67.66	65.57	67.38	65.50	57.94	62.48	56.84	65.62	66.67	100.00	66.15	64.98	59.30	55.60
DrAldh1A2	71.06	79.34	63.50	57.38	58.35	69.51	56.84	59.92	70.06	66.15	100.00	64.98	65.18	56.01
DrAldh2	65.47	63.23	62.99	66.02	56.61	61.78	61.99	64.24	63.27	64.98	64.98	100.00	65.30	54.29
Smp_022960	61.00	59.50	58.51	54.79	56.61	61.78	61.91	62.99	60.80	59.30	65.18	65.30	100.00	54.29
Smp_312440	54.38	54.18	54.18	54.79	52.69	54.29	53.36	52.75	54.79	55.60	56.01	54.29	54.29	100.00

Contributions

Publications

Beutler, M., Harnischfeger, J., Hahnel, S. R., Quack, T., Blohm, A., Weber, M. H. W., Überall, M. E., Häberlein, S., Timm, T., Lochnit, G., Rennar, G. A., Gallinger, T. L., Rahlfs, S., Schlitzer, M., Falcone, F. H., Becker, K., Czermak, P., Salzig, D., Grevelding, C. G. (2022). "Identification and characterization of the tegument-expressed aldehyde dehydrogenase SmALDH_312 of *Schistosoma mansoni*, a target of disulfiram". Manuscript in preparation.

Harnischfeger, J., **Beutler, M.**, Salzig, D., Rahlfs, S., Becker, K., Grevelding, C. G., Czermak, P. (2021). "Biochemical characterization of the recombinant schistosome tegumental protein SmALDH_312 produced in *E. coli* and baculovirus expression vector system". In: *Electronic Journal of Biotechnology*. Vol. 54, pp. 26–36. DOI: 10.1016/j.ejbt.2021.08.002

Conferences

2021/11 - **4th DRUID Retreat**, Giessen
Talk: ALDH_312 in *Schistosoma mansoni*: A potential drug target?

2021/09 - **14th Annual GGL Conference**, Giessen
Talk: Expression of *Schistosoma mansoni* proteins in *E. coli* and HEK cells

2020/10 - **3rd DRUID Retreat**, Giessen
Talk: Project B4: Differentiation of *Schistosoma mansoni,* biological targets for anti-parasitic agents

2020/09 - **First Digital GGL Annual Conference**, Giessen
Talk: Characterization of an aldehyde dehydrogenase as a potential drug target in *Schistosoma mansoni*

2020/04 - **DRUID Spring Symposium**, Marburg
Poster: Protein expression of SmALDHs, SmAR, and SmTK6 of *Schistosoma mansoni*

2019/11 – **2nd DRUID Retreat**, Rauischholzhausen
Talk: Comparison of the production of schistosomal enzymes using *E. coli* and BEVS

2019/09 - **12th Annual GGL Conference**, Giessen
Poster: Protein expression of SmALDH1&2, SmAR, and SmTK6 of *Schistosoma mansoni*

2019/03 - **20th Anniversary Drug Design & Development Seminar (DDDS) of the German Society for Parasitology**, Giessen
Poster: Expression cloning of potential target molecules of *Schistosoma mansoni*

2019/02 - **DRUID Spring Symposium**, Frankfurt (Main)
Poster: Expression cloning of potential target molecules of *Schistosoma mansoni*

2018/11 - **1st DRUID Retreat**, Rauischholzhausen
Poster: Characterization of potential target molecules to fight schistosomiasis

2018/09 - **11th Annual GGL Conference**, Giessen
Poster: Fighting schistosomiasis - Characterisation of potential target molecules

Acknowledgement

Selbstständigkeitserklärung

Ich erkläre: Ich habe die vorgelegte Dissertation selbstständig und ohne unerlaubte fremde Hilfe und nur mit den Hilfen angefertigt, die ich in der Dissertation angegeben habe. Alle Textstellen, die wörtlich oder sinngemäß aus veröffentlichten Schriften entnommen sind, und alle Angaben, die auf mündlichen Auskünften beruhen, sind als solche kenntlich gemacht. Ich stimme einer evtl. Überprüfung meiner Dissertation durch eine Antiplagiat-Software zu. Bei den von mir durchgeführten und in der Dissertation erwähnten Untersuchungen habe ich die Grundsätze guter wissenschaftlicher Praxis, wie sie in der „Satzung der Justus-Liebig-Universität Gießen zur Sicherung guter wissenschaftlicher Praxis" niedergelegt sind, eingehalten.

_____   _____

Datum   Unterschrift